COMPUTATIONAL METHODS FOR SOUND TRANSMISSION IN NONUNIFORM WAVEGUIDES

A THESIS
PRESENTED FOR THE
DEGREE OF DOCTOR OF PHILOSOPHY
IN MECHANICAL ENGINEERING
IN THE UNIVERSITY OF CANTERBURY,
CHRISTCHURCH, NEW ZEALAND

BY

VO PHU THANH
B.E. (honours)

UNIVERSITY OF CANTERBURY
JUNE, 1979

ERRATA

Page	Line number or Equation number	Original Text	Corrected Text
29	6	$\left\{b_n^+\right\}$ [TRAN] $\left\{a_n^+\right\}$	$\left\{b_n^+\right\}$ = [TRAN] $\left\{a_n^+\right\}$
46	Equation (3.2.19)	$\sum_{i=n}$	$\sum_{i=1}$
54	3	1,2,4,5,6,7	1,2,3,4,5,6,7
59	9	The convergence trend	The converging trend of solutions
67	Equation (4.2.27)	$\cos K_m r$	$\cos (K_m r)$
73	23	the high-order mode pair	the highest calculated mode pair
96	18	little discrepancies	small discrepancy
98	5	Refer [104]	Refer to [104]
107	4	(2.2.30)	(2.2.20)
109	5	u-nomentum	u-momentum
114	5	$\sin k_n R$	$\sin K_n R$
116	Equation (5.1.55)	$\sum_{m-1}$	$\sum_{m=1}$
116	Equation (5.1.56)	$K_m R J'_{m_o} (\bar{K}_m R)$	$\bar{K}_m R J'_{m_o} (\bar{K}_m R)$
123	Equation (5.1.75)	$\left\{a^+ \atop a^-\right\}_{z=\ell}$	$\left\{a^+ \atop a^-\right\}_{z=0}$

Cont'd....

Page	Line number or Equation number	Original Text	Corrected Text
126	11	Compability	Comparability
129	Last line	more highly cut-off than the hardwall ones	highly attenuated
136	11	This is looked after	This is taken care of
141	5	$b_n^+ J_{w_2}^+$	$b_n^+ J_{w_2 n}^+$
179	18	the number of incident, reflected and transmitted	the number of incident reflected and transmitted modes
232	14...	(matrix equation is not numbered)	(matrix equation is numbered (7.2.2))
234	10...	(matrix equation is not numbered)	(matrix equation is numbered (7.2.3))
237	4	supercrips	supercripts
258	13	previous discussed	previously discussed
263	6	Tables 8.18 - 8.17	Tables 8.18 - 8.19
280	7	1.080 - 0.397i	-1.080 - 0.397i
280	13	1.092 - 0.413i	-1.092 - 0.413i
334	3	PEUBE, J.L.	PUEBE, J.L.

ACKNOWLEDGEMENTS

The support and guidance provided by my supervisor, Professor W. Eversman, is gratefully acknowledged. His suggestions and time spent in discussion have been deeply appreciated.

I am also indebted to Dr. R.J. Astley, my associate supervisor, for valuable suggestions.

My great gratitude is extended to Professor D.C. Stevenson, Head of the Department of Mechanical Engineering, for the use of departmental resources and facilities in this study.

The research programme has been supported by The National Aeronautics and Space Administration, Lewis Research Center in the United States of America under Grant NSG 7192 awarded to the University of Canterbury. The University of Canterbury's University Grants Committee Postgraduate Scholarship awarded to the author for the last two years is also acknowledged.

I also wish to thank the Computer Centre staff for their assistance in computer programming, Mrs. J. Ritchie and Mr. T. Bird for their help and care in preparing the diagrams, and Mrs. J. Percival for her perseverance and meticulous typing.

Finally, my deepest gratitude is extended to my family, especially sister Loan, for their continual encouragement and sacrifice, which have enabled me to undertake and complete this study programme.

ABSTRACT

The Method of Weighted Residuals in the form of a Modified Galerkin Method with boundary residuals and the Finite Element Method in a Galerkin implementation are developed for the study of the sound transmission in nonuniform axisymmetric ducts carrying a steady, compressible flow. In this investigation the mean flow is modelled as essentially one-dimensional but with a kinematic modification to force tangency of the flow and the wall.

The Method of Weighted Residuals uses trigonometric basis functions which are derived from an equivalent problem in a two-dimensional duct. The Finite Element Method formulation is based on a weighted residuals approach, and uses eight-node isoparametric rectangular elements. The two computational methods are developed through three stages : eigenproblem, no-flow case and flow case with designed testing cases or alternative checkouts.

Data presented for various circular duct configurations include eigenvalues for uniform ducts, modal coefficients of transmitted and reflected waves, acoustic efficiencies and acoustic field for non-uniform ducts. The quantitative results obtained by the two methods are of comparable accuracy for the eigenproblem and the no-flow transmission problem. For the flow case with moderate Mach numbers good agreements are achieved. When the flow attains the subsonic non-linear regime the Finite Element Method suffers the difficulty of high dimensionality, however, correlations are still observed. Numerical simulations revealed no traces of the subsonic acoustic choking phenomenon.

LIST OF CONTENTS

PAGE

PAGE

LIST OF TABLES

LIST OF FIGURES

LIST OF SYMBOLS

Unless defined otherwise the symbols used in the text have the following meanings :

SYMBOL	DEFINITION
A	Specific Admittance to Reference State of Duct Section (B)
$\hat{A}$	Reduced 2D Domain
A	Cross-Sectional Area
A	Coefficient Matrix
(A)	Uniform Duct Section ($z < 0$)
A_1	Specific Admittance to Reference State of Duct Section (A)
A_2	Specific Admittance to Reference State of Duct Section (C)
A_c	Local Cross-Sectional Area
A_ℓ	Local Specific Admittance
A_f	Specific Admittance of Uniform Duct
A_o^*	Local Specific Admittance
A_{ij}	Block Submatrices
a_i	Modal Coefficient in Mode i
B	Coefficient Matrix
(B)	Nonuniform Duct Section
B_{ij}	Block Submatrices
b_i	Modal Coefficient in Mode i
C	2D Boundary
C	Coefficient Matrix
(C)	Uniform Duct Section ($z > \ell$)
C_1, C_2, C_3	2D Contours in Figure 3.6
c	Speed of Sound
c_o	Nondimensional Local Speed of Sound in Mean Flow Medium
c_r	Speed of Sound in Reference State
c_o^*	Local Speed of Sound in Mean Flow Medium
D	3D Domain
D	Coefficient Matrix
div	Divergence Operator
E	Coefficient Matrix
E_1, E_2	Absolute Error Squares in End-Matching
e	Exponential Function
e	A Diagonal Matrix

SYMBOL	DEFINITION
F,f	Functions
F,f	Load Vectors
G,g	Functions
grad	Gradient Operator
H	Half Height of 2D Duct
H_i	Gaussian Quadrature Weights
I	Identity Matrix
I	Acoustic Intensity
I	Velocity Functional
I_e	2D Element Integral
I'_e	Line Element Integral
i	$\sqrt{-1}$
i	An Index
J	Eigenfunction for Uniform Axisymmetric Duct
J	Jacobian Matrix
J_{m_o}	Bessel Function of Order m_o
j	An Index
$\mathcal{K}$	Coefficient Matrix
$K(=k_z/k)$	Nondimensional Axial Propagation Coefficient
K	System Matrix (Excluding Contribution by End Matching)
K_{nm}	Integrals
K_p	Modified System Matrix (Excluding Contribution by End Matching)
k	Free-Space Wave Number in Ambient State for No-Flow Duct
k	Free-Space Wave Number in Flow Medium for Uniform Flow Duct
k	An Index
k_ℓ	Local Free-Space Wave Number
k_r	Free-Space Wave Number in Reference State
k_z	Axial Propagation Coefficient
$\mathscr{L}$	Differential Operator
$\mathcal{L}$	Coefficient Matrix
L_{nm}	Matrix Coefficients
L_{nm}	Integrals
ℓ	Duct Length
ℓ	An Index
$\mathcal{M}$	Coefficient Matrix
M	Coefficient Matrix
M	Modal Matrix
M_o	Local Mach Number or Mach Number in Uniform Duct

SYMBOL	DEFINITION
M_1	Mach Number in Uniform Duct Section (A)
M_2	Mach Number in Uniform Duct Section (C)
M_{nm}	Matrix Coefficients
M_{nm}	Integrals
M_r	Mach Number in Reference State
M_t	Local Mach Number at the Throat
m	An Index
m_o	Angular Mode Number
$\mathcal{N}$	Coefficient Matrix
N	Coefficient Matrix
N	Number of Basis Functions used in MWR
N	Global Shape Function Matrix
N^e	Element Shape Function Matrix
N_i	Shape Function Corresponding to Node i
N_{nm}	Matrix Coefficients
N_{nm}	Integrals
n	An Index
n_a	Number of Incident or Reflected Acoustic Modes at $z = 0$
n_a	Total Number of Acoustic and Hydrodynamic Modes at $z = 0$
n_{a^+}, n_{b^+}	Numbers of Positively Running Modes for $z < 0$ and $z > \ell$ Respectively
n_{a^-}, n_{b^-}	Numbers of Negatively Running Modes for $z < 0$ and $z > \ell$ Respectively
n_{aH}, n_{bH}	Numbers of Hydrodynamic Modes for $z < 0$ and $z > \ell$ Respectively
n_b	Number of Transmitted Acoustic Modes at $z = \ell$
n_b	Total Number of Acoustic and Hydrodynamic Modes at $z = \ell$
n_e	Total Number of Elements
n_{e_1}	Number of Elements Across a Duct (on C_1 in Figure 3.6)
n_{e_3}	Number of Elements Along a Duct (on C_3 in Figure 3.6)
n_H	Number of Hydrodynamic Modes
n_ℓ	Number of Load Vectors (in Multiple Load)
n_n	Total Number of Nodes
n_{n_1}	Number of Nodes Across a Duct at $z = 0$ (on C_1 in Figure 3.6)
$n_{n_2} (=n_{n_1})$	Number of Nodes Across a Duct at $z = \ell$ (on C_2 in Figure 3.6)
$n_r (=n_{n_1})$	Number of Corner and Mid-Side Nodes Across a Duct

SYMBOL	DEFINITION
n_{rm}	Number of Mid-Side Nodes Across a Duct
n_v	Number of Dependent Variables (Generally $n_v = 4$)
n_w	Bandwidth of System Matrix (Excluding Contribution by End Matching)
n_z	Number of Corner and Mid-Side Nodes Along Duct Centreline
n_{zm}	Number of Mid-Side Nodes Along a Duct
P	Modal Coefficient
P	Coefficient Matrix
P_a	Power Matrix at z = 0
P_b	Power Matrix at z = ℓ
p	Nondimensional Acoustic Particle Pressure
p'	Total Fluid Perturbation Pressure
P*	Acoustic Particle Pressure
p_o^*	Mean Flow Pressure
$\tilde{p}$	Acoustic Particle Pressure in FEM Approximation
p_m	Coefficients in MWR Expansion for Pressure
p_N	Acoustic Particle Pressure in MWR Approximation
Q	Coefficient Matrix
q_i	Modal Coefficient in Mode i
R	Termination Matrix
R	Residual Error
R	Radius of Nonuniform Duct Section (B)
R_1	Radius of Uniform Duct Section (A)
R_2	Radius of Uniform Duct Section (C)
R_i	Residuals
R_B	Boundary Residual
REFL	Reflection Matrix
R_t	Radius at the Throat
r	Radial Coordinate in Cylindrical System (r,θ,z)
$\underline{r}$	Position Vector
S	3D Boundary
S	Cross-Sectional Area
S	Coefficient Matrix
s	Arc Length on 2D Contours
$S_1, S_1', S_2, S_2', S_3$	Boundary Surfaces in Figure 2.4
S_A, S_B, S_C	Cross-Sectional Areas of Duct Sections (A), (B), (C) Respectively

SYMBOL	DEFINITION
T	Transformation Matrix
TF	Transfer Matrix
TRAN	Transmission Matrix
TS	Transition Matrix
t	Time
U	Modal Coefficient
U_o	Transverse Component of Nondimensional Mean Flow Velocity
u	Transverse Component of Nondimensional Acoustic Particle Velocity
$\tilde{u}$	Transverse Component of Acoustic Particle Velocity in FEM Approximation
u_m	Coefficients in MWR Expansion for Transverse Velocity Component
u_N	Transverse Component of Acoustic Particle Velocity in MWR Approximation
V	Modal Coefficient
$\underline{V}$	Nondimensional Acoustic Particle Velocity
$\underline{V}^*$	Acoustic Particle Velocity
$\underline{V}'$	Total Fluid Perturbation Velocity
$\underline{V}_o$	Nondimensional Mean Flow Velocity
$\underline{V}^*_o$	Mean Flow Velocity
$\underline{V}_{o1}$	Mean Flow Velocity in Uniform Duct Section (A)
$\underline{V}_{o2}$	Mean Flow Velocity in Uniform Duct Section (C)
$V_{o\tau}$	Nondimensional Mean Flow Velocity Component in Direction Tangential to Duct Wall
$V^*_{o\tau}$	Mean Flow Velocity Component in Direction Tangential to Duct Wall
V_ν	Nondimensional Acoustic Particle Velocity Component in Direction Normal to Duct Wall
V^*_ν	Acoustic Particle Velocity Component in Direction Normal to Duct Wall
V_θ	Angular Component of Mean Flow Velocity
V_r	Radial Component of Mean Flow Velocity
V_z	Axial Component of Mean Flow Velocity
v	Angular Component of Nondimensional Acoustic Particle Velocity
$\tilde{v}$	Angular Component of Acoustic Particle Velocity in FEM Approximation
v_m	Coefficients in MWR Expansion for Angular Velocity Component.
v_N	Angular Component of Acoustic Particle Velocity in MWR Approximation
W	Modal Coefficient
W	Acoustic Power

SYMBOL	DEFINITION
W_o	Axial Component of Nondimensional Mean Flow Velocity
W_o^*	Axial Component of Mean Flow Velocity
W_i	Weighting Functions
W_i	Incident Acoustic Power
W_r	Reflected Acoustic Power
W_t	Transmitted Acoustic Power
w	Axial Component of Nondimensional Acoustic Particle Velocity
$\tilde{w}$	Axial Component of Acoustic Particle Velocity in FEM Approximation
w_m	Coefficients in MWR Expansion for Axial Velocity Component
w_N	Axial Component of Acoustic Particle Velocity in MWR Approximation
X,Y	Column Vector of Unknowns
x	Coordinate in Cartesian System (x,y,z)
x_1	Eigenvector
x_2	Eigenvector
Y_{m_o}	Newmann Function of Order m_o
y	Coordinate in Cartesian System (x,y,z)
Z	Impedance of Duct Wall
Z_A, Z_B, Z_C	Impedances of Duct Wall in Duct Sections (A), (B), (C) Respectively
z	Coordinate in Cartesian System (x,y,z) or Axial Coordinate in Cylindrical System (r,θ,z)
z	Function Argument
α	Angle between Axial Direction and Direction Tangential to Duct Wall or Taper Angle
α_k	Block Submatrices
α_n	Modal Coefficients
α_{nm}	Matrix Coefficients
β_k	Block Submatrices
β_n	Modal Coefficients
β_{nm}	Matrix Coefficients
γ	Ratio of Specific Heats
γ_k	Block Submatrices
γ_n	Modal Coefficients
$\underline{\nabla}$	Gradient Operator
∇^2	Laplacian Operator
δ	Column Vector of Unknowns or Eigenvector

SYMBOL	DEFINITION
$\delta_1, \delta_2, \delta_{in}$	Column Vectors of Nodal Values
δ_{nm}	Kronecker Delta
$\sum$	Summation Symbol
ε	Arbitrarily Small Constant
η	Dummy Variable
η	Local Coordinate in (η,ξ) Systems
η_a	Absorption Efficiency
η_r	Reflection Efficiency
η_t	Transmission Efficiency
θ	Angular Coordinate in Cylindrical System (r,θ,z)
θ_m	Basis Functions
κ	Transverse Propagation Coefficient for Uniform 2D or Axisymmetric Duct
λ	Function Argument
λ_r	Free-Space Wavelength in Reference State
$\underline{\nu}$	Unit Outward Normal Vector at Boundary
ξ	Local Coordinate in (η,ξ) System
ξ	Acoustic Particle Displacement
π	Pi = 3.1415926535
ρ	Nondimensional Acoustic Particle Density
ρ'	Total Fluid Perturbation Density
ρ^*	Acoustic Particle Density
ρ_o	Nondimensional Mean Flow Density
ρ_o^*	Mean Flow Density
ρ_r	Acoustic Particle Density in Reference State
$\underline{\tau}$	Unit Tangential Vector at Duct Wall
ϕ	Mean Flow Potential Function
ϕ_m	Basis Functions
χ	Function Argument
χ_m	Basis Functions
ψ_m	Basis Functions
ω	Frequency in Radians per Second
$\cdot$	Denotes Inner Product Operation or Multiplication
[ ]	Denotes Matrix or Row Vector or Brackets
{ }	Denotes Column Vector or Brackets
$\lceil\ \rfloor$	Denotes Diagonal Matrix

Subscripts

o	Denotes Mean Flow Condition
o,1	Refer to z = 0

SYMBOL	DEFINITION
$1, 1', 2, 2'$	Refers to Surfaces S_1, S_1', S_2, S_2' in Figure 2.4 Respectively
2	Refers to $z = \ell$
a	Refers to $z = 0$
b	Refers to $z = \ell$
e	Refers to Element
i	An Index
j	An Index
k	An Index
ℓ	Refers to $z = \ell$
ℓ	An Index
m	An Index
n	An Index
p	Refers to Pressure
r	Refers to Reference State
r,θ,z	Denote Derivatives with Respect to r,θ,z Respectively or Components in Radial, Angular and Axial Directions Respectively
u,v,w	Refer to Radial, Angular and Axial Velocity Components Respectively
ν,τ	Denote Components in Normal and Tangential Directions Respectively

Superscripts

- (minus)	Refers to Negatively Running Mode
- (bar)	Denotes One-Dimensional Solution for Mean Flow or a Variant
+	Refers to Positively Running Mode
*	Denotes Complex Conjugate or a Variant
'	Denotes 1st. Derivative or a Variant
''	Denotes 2nd. Derivative or a Variant
^	Denotes a Variant
~	Denotes Approximate Variant
e	Refers to Element
H	Refers to Hydrodynamic Mode
p, (p)	Refer to Pressure
u, (u)	Refer to Transverse Velocity Component
v, (v)	Refer to Angular Velocity Component
w, (w)	Refer to Axial Velocity Component
T	Denotes Transpose

SYMBOL	DEFINITION
Abbreviations	
BC	Boundary Condition
BF	Basis Function
EIGEN	Eigenfunction
FDM	Finite Difference Method
FEM	Finite Element Method
FEM (n)	Finite Element Method with n Line Elements
FEM (nxm)	Finite Element Method with n Elements Across and m Elements Along a Duct
FIG.	Figure
LSQ	Least-Square (Matching)
MWR	Method of Weighted Residuals
MWR (nBF)	Method of Weighted Residuals Using n Basis Functions
PM	Point Matching
SDM	Stepped Duct Method
1D	One-Dimensional
2D	Two-Dimensional
3D	Three-Dimensional
Eigenproblem	Algebraic Eigenvalue Problem

CHAPTER 1

INTRODUCTION

1.1 PROBLEM IN DUCT ACOUSTICS

The science of acoustics has long been a traditional subject of classical physics with many important applications in such diverse fields as auditorium design, sound insulation and machinery noise. In the past few decades advancing technology in the air transport industry has brought with it the problems of production of noise by jets and other aerodynamic disturbances. Today the science and technology of aeroacoustics has become an important branch of acoustics and a matter of great importance for the future of air transportation.

In the aircraft industry noise suppression is now an integral part of aeroengine design and installation. As a consequence, extensive research programmes have been conducted with the aim of developing efficient design techniques. Recently, the introduction of high bypass ratio fan jet engines, primarily for the purpose of increasing propulsive efficiency, incidentally has led to a reduction in jet noise. The rotating machinery, fan and compressor, then becomes the primary noise source, particularly during approach and landing, which are critical phases of aircraft operations as far as community noise exposure is concerned. The reduction of fan and compressor noise is attacked from two directions, (a) suppression at the source by the development of quiet rotating machinery, and (b) attenuation along the propagation path by the incorporation of suppression techniques in the engine nacelle. It is the second approach with which this study is concerned.

Acoustic lining design requires analytical methods for predicting the effects of acoustic absorption on propagated noise. This has

resulted in a resurgence of interest in the classical problem of acoustic wave propagation in ducts. Substantial advances in the state of the art of modelling duct sound transmission and attenuation characteristics have been made in recent years. As a result, it is now routine to design acoustic linings for maximum attenuation of given modes using the theory of acoustic wave propagation in uniform, infinite ducts. However, there are still many unsolved problems which complicate the task of incorporating such linings in an actual engine nacelle. Among the most important factors is the problem of duct nonuniformities.

In a typical jet engine nacelle the flow passages are not uniform and infinitely long. This departure from the mathematically tractable idealized model creates several practical implications, which include the following :

(a) The environment in which the sound source operates can significantly affect the nature and the magnitude of the sound radiation. The acoustic impedance modelled by the finite-length, nonuniform nacelle may diverge substantially from that of the ideal duct.

(b) Sound reflections from discontinuities and changes of cross section of the nacelle set up standing waves which may seriously alter the performance of an acoustic liner. In addition the transmitted modes generated at the nonuniformity might be less successfully attenuated by the lining which is primarily designed for incident modes.

(c) Radial splitters and annular rings placed in a duct to provide more surface area for the lining material might be used to further advantage by being positioned in the

nacelle in such a manner as to redistribute the acoustic energy incident on the lining. Thus it is possible to increase lining effectiveness, to decrease sound radiation efficiency, or to alter the directivity of the radiated sound by a judicious choice of duct geometry.

(d) Experimentally it has been found that a useful attenuation of fan and compressor noise is possible by the use of an inlet throat operating at a high subsonic flow Mach number. Inlet noise suppression by choking at a sonic throat is well known, but suppression of noise by "subsonic choking" is less well understood. A theory of acoustically treated inhomogeneous ducts is essential for the understanding of the mechanism of subsonic choking.

Apart from the aircraft engine duct system, an accurate theory of wave propagation in nonuniform ducts would find applications to the design of numerous facilities such as air conditioning and heating installations, high-speed wind tunnels, and rocket nozzles.

1.2 LITERATURE REVIEW

The classical problem of sound propagation in ducts was presented by Lord Rayleigh [1] about a century ago, but rapid progress in the field has been made recently. Rayleigh's approach by a ray treatment of propagation was not generally adequate for lined ducts [1]. A more rigorous theory of acoustic disturbance propagation, a wave approach valid for all frequencies, in both axisymmetric and rectangular, infinite, unlined or lined ducts without flow, was established by Morse [2,3,4], with solutions in the form of graphs [4] for softwalled ducts. The problem of optimum attenuation in lined ducts was studied by Cremer [5].

Most of the early researchers were primarily interested in the plane wave mode, however, it was first shown by Ingard [6] and later by

Tyler and Sofrin [7], Morfey [8], and Rice [9] that in order to treat the duct propagation in its entirety, by accounting for a sound source and duct terminating impedance, the high-order modes must be considered.

By taking into account the increased wave length of sound propagated in the flow direction Lambert [10] was able to calculate and experimentally verify the insertion loss due to a single resonator in a duct as a function of the duct flow velocity. Thereafter Ingard [11], Miles [12], Ribner [13], Morfey [14], Rice [15], Ko [16], Eversman [17] and Tester [18], among others, made contributions to the study of the effects of uniform flow on sound propagation in both hardwalled and softwalled uniform infinite ducts. The method of solution used was analytical in a classical sense. From these studies one was able to conclude that the effect of convection flow in a lined duct is to decrease the attenuation of the downstream propagating modes and to increase the attenuation of the modes propagating upstream. The Cremer approach [5] was still widely used to determine an optimum wall admittance for a particular mode of propagation, even in the presence of flow. The basic assumption is that the optimum attenuation occurs when the two lowest modes have the same attenuation rate, which occurs when they have the same eigenvalue. Although this criterion is not always valid [18] it is still used as a practical rule many years later [19].

The state of the art in uniform duct acoustics was further refined with consideration of the problem of flow nonuniformity in the form of a boundary layer in the mean flow field. Pridmore-Brown [20] introduced a sophisticated mathematical model of sound transmission in a duct with uniform viscous flow involving the influence of the boundary layer. This flow model approximated the boundary layer with an inviscid sheared flow with a characteristic velocity profile. Pridmore-Brown employed an asymptotic solution for high frequencies in a hardwalled two-dimensional channel. Tack and Lambert [21] made use of a power series in Pridmore-

Brown's two-dimensional formulation to generate an approximate solution valid for single mode propagation at lower frequencies. Mungur and Gladwell [22] used a Runge-Kutta numerical scheme to treat the transmission problem in a hardwalled channel and presented an extension of the method to the softwall case. Following these initial studies, Pridmore-Brown's mathematical model was thoroughly investigated by Runge-Kutta [22,23], finite difference [24], and Galerkin [25,26] methods and extended to different geometries such as annular [23] and circular [27] ducts. The Runge-Kutta scheme yields the most accurate results to date and serves as a standard of comparison for other approaches. It has also been proposed for the problem with helical ducted flow [28]. These studies assumed that, for the duct size, flow speed and frequency range of interest, mode attenuation due to scattering by turbulent flow in the boundary layer is insignificant in comparison to the effect of shear layer, and found that the effect of refraction by the inviscid shear layer for downstream propagation is to turn wavefronts into the softwall and thus increase the attenuation of sound waves and for upstream propagation the effect is to turn the wavefront away from the softwall thereby decreasing the attenuation.

The consideration of propagation in ducts with flow brought with it the problem of boundary conditions at the lining. For a no-slip mean flow continuity of normal particle velocity and continuity of normal particle displacement are equivalent. But considerable discussion has appeared in the literature as to whether continuity of normal particle velocity or continuity of particle displacement is the appropriate boundary condition for flow with slip at the wall. Tack and Lambert [21], Munger and Plumblee [23], Savkar [29] made experimental and theoretical investigations in detail. The consensus is that generally the continuity of particle displacement is valid although

Tack and Lambert's observation showed that the continuity of normal particle velocity is reasonably accurate and more useful over a certain range of forced frequency. Eversman and Beckemeyer [30] and Tester [31] used the method of matched asymptotic expansions to show that the shear-profile results approach, in the limit of vanishing boundary-layer thickness, the results of a uniform profile continuity of particle displacement at the wall. Nayfeh, Kaiser and Shaker [32] confirmed numerically the conclusion and emphasized that the conclusion that the continuity of particle displacement is the appropriate boundary condition is based on the assumption that the acoustic boundary-layer thickness vanishes faster than the mean flow boundary thickness. If they are of the same order the appropriate boundary condition is still an open question [33].

The problem of flow gradients leads naturally to the consideration of mean temperature gradients. Kapur, Cummings, and Mungur [34] analyzed the wave propagation in a combustion can with no mean flow, taking into account axial temperature and density gradients. Their solution was found to be very sensitive to the acoustic transfer impedance of the system at the burner. Mungur and Tree [35] derived an equation describing the acoustic pressure in a duct with flow, considering both the mean flow velocity and temperature gradients. Their results show that temperature gradients have refractive effects similar to those for sheared flow. Using a forward integration scheme Nayfeh and Sun [36] evaluated numerically the effects of transverse temperature gradients in two-dimensional ducts carrying mean flow. They concluded that, for downstream propagation in softwall cases, cooling the duct wall leads to a shift in the peak attenuation rate to a lower flow resistance. For upstream propagation heating the duct wall leads to a decrease in the attenuation rate, and furthermore, the rate of decrease of the attenuation rate with wall temperature decreases as the mode number increases.

The present research programme has as its principal focus the study of nonuniformities in the form of duct area variation. A number of studies of historical interest appeared prior to the aeroengine noise problem but the major advances have been fairly recent. The classical work is that of Webster [37] who combined the linearized acoustic equations for ducts of variable cross-section to obtain Webster's horn equation, of which extensive studies have appeared in the literature [38,39]. Closed-form solutions for single mode propagation have been found for conical, exponential and catenoidal horns. A novel application is that of Cummings [40] who studied the acoustics of a wine bottle. The wine bottle is a nonuniform finite-length duct without flow and the acoustic field is approximated by a Runge-Kutta integration scheme based on Webster's horn equation.

Practical calculations for acoustic propagation in nonuniform ducts without flow seem to have begun with a stepped duct approximation. Zorumski and Clark [41] introduced this method to study ducts of uniform area with lining variations. It was subsequently implemented by Alfredson [42] for the study of hardwalled ducts of varying cross-sectional area. This method, originally used by Miles [43] for the analysis of reflection and transmission of sound as it propagates past a single area discontinuity consists of representing the duct by a series of uniform stepped ducts and systematically matching the pressure and velocity at the intersections of the duct elements.

A second multimodal approach is the variational method of Beckemeyer and Eversman [44], in which the acoustic problem becomes a Rayleigh-Ritz minimization of a certain functional. This process determines the coefficients of the trial solutions in terms of basis functions which do not necessarily satisfy the boundary conditions and need not be generated for each duct geometry. Another method of this category is the Modified Galerkin Method used successfully by Eversman

(et al) [45] for the two-dimensional no-flow problem. In this approach the Galerkin minimization of residuals transforms the problem into a system of ordinary differential equations in the form of Telegraphist's equations which can be solved by an integration scheme. The Galerkin approach in the form of a method of weighted residuals was first employed in electromagnetic waveguide problems by Schelkunoff [46,47]. Stevenson appears to be the first to suggest the method of this type to acoustic horn problems [48,49].

Approximations based on perturbation methods offer useful solutions under appropriate circumstances. Nayfeh and Telionis [50] used the method of multiple scales to determine the propagation of a wave packet in rectangular and circular ducts with slowly varying cross-sections and slowly varying wall admittance. The solution is limited to one mode of propagation and for hardwalled ducts it becomes equivalent to that of Stevenson for slowly varying area. Isakovitch [51], Samuels [52] and Salant [53] obtained perturbation solutions for wave propagation in ducts whose rigid walls have sinusoidal variations of small amplitude.

In aeroengine acoustics the presence of high speed flows complicates the acoustics problem in the nonuniform duct. Propagation through this type of nonuniform flow has received considerable attention. Many studies appearing have been based on a one-dimensional theory which treats the wave propagation as plane waves moving in a one-dimensional nozzle flow. King and Karamcheti [54] applied the method of characteristics to solve the quasi-one-dimensional acoustic equations in the x-t plane. Powell [55] used a method of multiple reflection to develop a one-dimensional treatment of the propagation of a pressure pulse through a variable cross-section channel carrying a compressible flow. Eisenberg and Kao [56] analyzed the linear quasi-one-dimensional wave

propagation by transforming the governing equations into a pair of coupled second-order ordinary differential equations with variable coefficients, which can be solved by numerical techniques. Huerre and Karamcheti [57] analyzed the propagation of the lowest mode for the same problem using a WKB approximation to solve a derived acoustic velocity potential equation, which is a generalization of Webster's horn equation to the case of compressible mean flow. Davis and Johnson [58] used a forward-integration, shooting technique to obtain solutions to the one-dimensional acoustic equations for travelling waves in several duct-nozzle configurations. Kooker and Zinn [59] used a relaxation technique to solve for standing waves in a combustion chamber choked-nozzle configuration.

In what appears to be the first published computations on multimodal propagation in nonuniform ducts in the presence of flow, Tam [60] considered hardwalled circular ducts with slowly varying cross-section and used the Born first-order approximation and the Fourier transform method to determine the backscattering of a spinning acoustic wave mode when it is incident in the upstream direction on a throat or constriction in the duct. His results show a substantial attenuation of acoustic energy for an axial inlet flow Mach number of about 0.6 with throats of reasonable area reduction, which is in qualitative agreement with the observed subsonic acoustic choking phenomenon [61].

Nayfeh, Telionis and Lekoudis [62,63] extended the method of multiple scales to the flow problem to analyze the propagation of all acoustic modes in a two-dimensional channel and in annular ducts with a slowly varying cross-section that carry an incompressible, sheared flow. For a general mean flow there is no analytical solution and numerical techniques were used. The study evaluated the effects of variations of duct cross-section and growing boundary layers on different acoustic modes.

Recently, Eversman (et al) [64,65] have successfully extended the Modified Galerkin method to the 2D flow problem with hydrodynamic modes included in the acoustic solution. An approximation was used for the nonuniform steady flow field based on one-dimensional compressible flow with a kinematic modification to allow for flow tangency at the duct wall. The results obtained for transmission loss in hard-walled converging-diverging or simply converging ducts carrying inlet flow of Mach numbers up to 0.81 at the throat, do not show substantial evidence of subsonic choking.

The concept of forward radiated sound suppression using an inlet operating with a throat Mach number at sonic condition is appealing and has been investigated experimentally, for example, see [66]. So called "sonic choking" does, in fact occur, but even under fully sonic conditions complete attenuation is not achieved [67], a phenomenon probably attributable to subsonic regions in the boundary-layer through which propagation occurs. Of perhaps greater interest is the phenomenon of significant choking at subsonic Mach numbers, "subsonic choking". The physics of this occurrence are not altogether clear and possible explanations include linear effects of flow gradients and duct geometry and non-linear effects associated with finite amplitude waves in transonic flow.

Tam's theoretical study [68] by a perturbation procedure on finite amplitude spinning acoustic modes and subsonic choking concluded that non-linear effects are not negligible for wave modes of moderate amplitude. In linear theory, the presence of axial flow can cause the group velocity of the acoustic wave mode in a flow duct to become zero when the flow Mach number is unity, resulting in the well known phenomenon of sonic choking. Tam showed that for a subsonic axial flow when weak-nonlinearity is included, the characteristic velocity of propagation becomes smaller and dependent upon the amplitude of the

waves. As a consequence, it is not necessary for the axial flow to reach sonic condition before the acoustic waves stop propagating in the upstream direction. This may be the most significant feature of subsonic choking.

The linear aspect of the phenomenon is still unsettled. The study by Eversman (et al) [64,65] on hardwalled two-dimensional channels reveals little evidence of subsonic choking, but Tam's [60] study of spinning acoustic modes in a slightly nonuniform circular flow duct reveals a mechanism for its occurrence, though probably not to the extent observed. At this time the theoretical basis for "subsonic choking" is not complete and further development is required. In particular, the linear theory in axisymmetric ducts must be developed to provide a rigorous mathematical model against which to compare approximate theories and experimental results.

The present research programme has as its primary goal the development of numerical techniques suitable for the study of sound transmission in nonuniform axisymmetric ducts carrying high speed flow. It is desired to develop the capability to study sound propagation in nonuniform flow ducts and the linear aspects of subsonic choking. Hence, we are interested in methods for the no-flow case which appear to be extendable to the case with flow and for two-dimensional techniques extendable to axisymmetric problems.

Of the approaches to duct acoustics problems in the literature review four appear to be promising for solving problems with reasonably realistic physical description. These methods are the Stepped Duct Method (SDM), the Method of Weighted Residuals (MWR) in form of Modified Galerkin Method, the Finite Difference Method (FDM), and the Finite Element Method (FEM).

The SDM [42], with success in no-flow problems may find its use

in the flow problem but, in addition to its high dimensionality, it is questionable whether the nonuniform form flow field can be represented in sufficient detail in a series of stepped segments.

The extension of the MWR by Eversman (et al) [65] includes nonuniform flow in the two-dimensional channel. Evidence has been presented indicating the suitability of the method for extension to axisymmetric ducts [69]. Kaiser and Nayfeh [70] adopted what is essentially a MWR and introduced a refinement, the "Wave Envelope Technique", due in its original form to Baumeister [71], into the formulation. This may have some benefit in the computational phase, but the utility of the method is likely to be similar to the previously noted MWR.

Direct application of purely numerical techniques such as the FDM or the FEM to the acoustic equation, are still in their early development. Such a method has the advantage of flexibility in varying physical description. In addition, the steady flow field can be solved by the same technique on a similar scale of dimensionality, as the solution can be used as input data for acoustic problems. The FDM has been proposed and investigated by Baumeister [71] and Quinn [72] and successful trials have been made on problems of simple geometry. An assessment of FDM for more general configurations has not as yet appeared. The FEM is the most recently introduced technique. It has achieved prominence in other fields, notably continuum mechanics. Recently it has been used to approach the sound transmission problem. Sigman, Majjigi and Zinn [73] applied FEM with triangular elements to acoustic velocity potential equations using an approximate solution for the irrotational steady potential flow field. Abrahamson [74] employed rectangular finite elements in a similar geometrical model with test cases showing a trend of convergence in uniform ducts. The

finite-length model used is sophisticated enough to represent the turbo-fan inlet geometry but the analysis is limited to one mode of propagation. Recently Eversman (et al) [65,75] have made numerical comparisons between FEM and MWR for the multimodal transmission problem in uniform and nonuniform ducts with or without flow, showing good quantitative agreements for two-dimensional cases with an approximation to the compressible steady flow field.

Of the several methods available for propagation problems in nonuniform axisymmetric ducts MWR, FEM and FDM are considered to be the most suitable for further development. Each method has its own advantages for a specific problem. The MWR offers low dimensionality but is not suitable for irregular boundary geometry. For a wide variety of problems the FEM has promise of offering the flexibility of the FDM at a reduced dimensionality and at a lower degree of effort involved in formulation. In the present research programme attention is focused on the Method of Weighted Residuals in the form of a Modified Galerkin Method and in a Galerkin implementation of the Finite Element Method

1.3 PROPOSED SCOPE OF STUDY

In the study reported here the MWR and the FEM are chosen for investigating the problem of multimodal sound wave propagation in axisymmetric ducts.

In order to test the numerical implementations three stages of development are considered: eigenproblem, no-flow case and flow case. Test cases and comparisons with alternative schemes are shown. Subsequently the two methods are evaluated and applied in configurations which simulate numerically the subsonic choking environment.

The following chapters are devoted to such work. In Chapter 2 governing acoustic equations are derived from the linear theory and the mathematical modelling is specified for study. Chapter 3 details the proposed methods. The eigenproblem in uniform ducts is solved in Chapter 4 to serve as a first checkout of the methods. In Chapter 5 the multimodal sound transmission problem in nonuniform ducts without flow is studied in detail. Chapters 6, 7 and 8 deal with the problem in nonuniform ducts with flow. Chapter 9 concludes the research programme with general discussions and suggestions for future work.

CHAPTER 2

MATHEMATICAL MODELLING AND GOVERNING EQUATIONS

2.1 GEOMETRY

2.1.1 Geometry and Coordinates

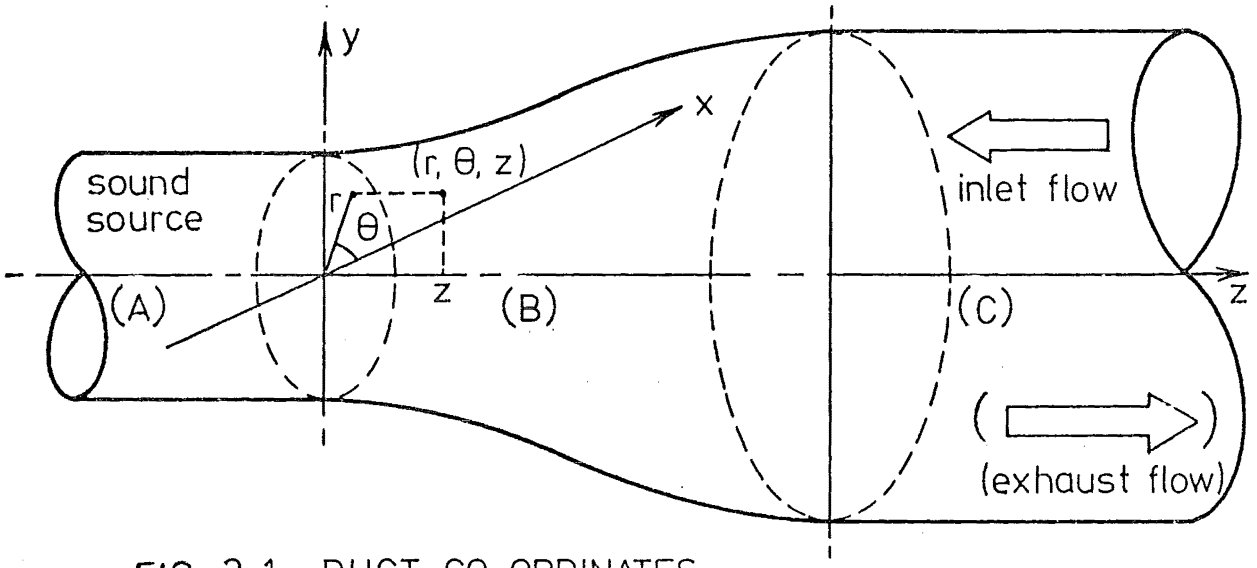

FIG. 2·1 DUCT CO-ORDINATES

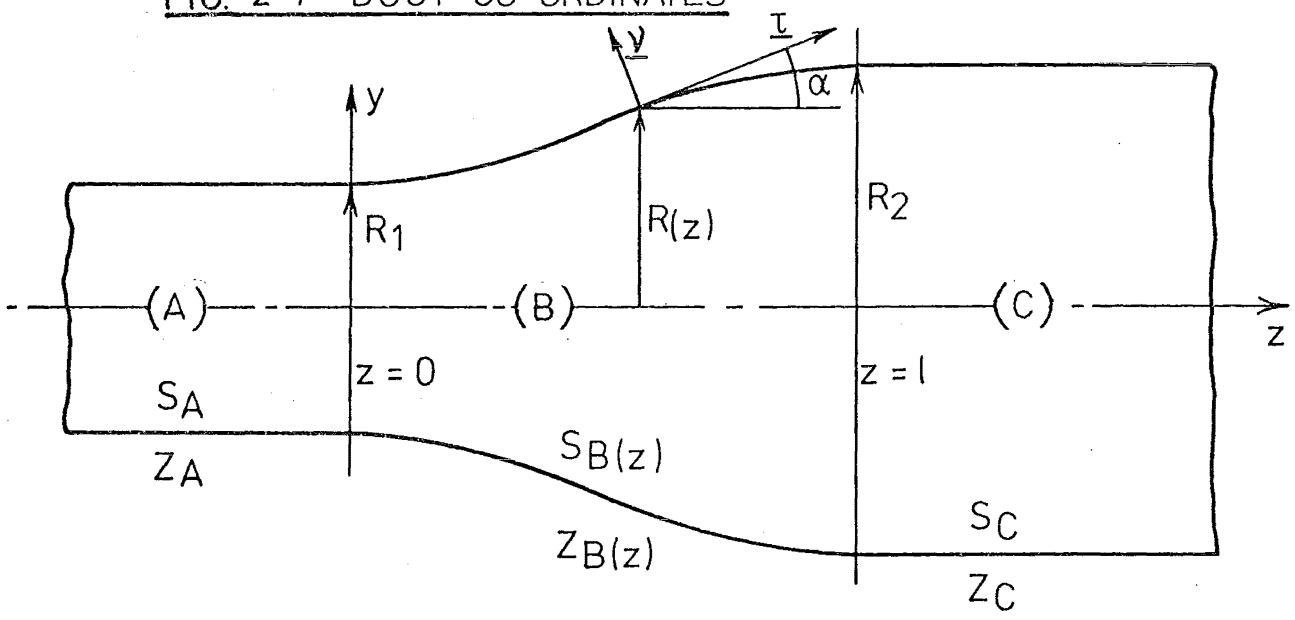

FIG. 2·2 DUCT CONFIGURATION

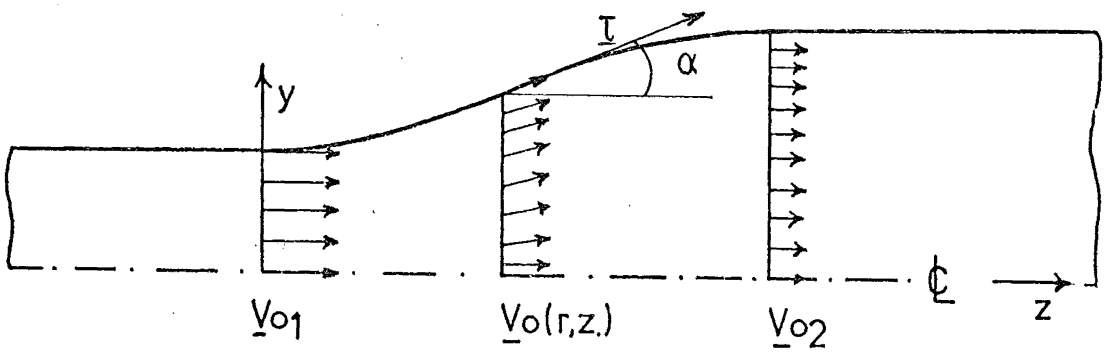

FIG. 2·3 KINEMATIC MEAN FLOW APPROXIMATION

In this analysis axisymmetric ducts of infinite length are considered. The extension to include a finite duct termination is possible in the present formulations provided reflection and transmission characteristics of the termination are specified.

Figure 2.1 shows the duct configuration under study in which two semi-infinite circular uniform sections of wall impedance Z_A and Z_C and area S_A and S_C are joined by an axisymmetric transition section of length ℓ, variable area $S_B(z)$ and variable impedance $Z_B(z)$ where z is the axial coordinate. In the study the area variation is restricted to be continuous, but the lining variation can be discontinuous at the ends of nonuniformity.

In order to specify boundary conditions at the duct wall, a cylindrical coordinate system is introduced as shown in Figure 2.2

The mathematical model is chosen to permit an investigation of linear effects on propagation due to the nonuniformity in area, impedance, and flow apart from the terminating end conditions in a finite duct.

2.1.2 Boundary Conditions

(i) At the duct wall.

In Figure 2.1 the duct-wall boundary condition used is characteristic of a normally reacting lining in the presence of a harmonic pressure variation

$$p^* = Z V_\nu^*$$

where V_ν^* is the particle velocity in the acoustic lining at the wall, assumed in the direction of the outward normal $\underline{\nu}$. Z is the wall specific acoustic impedance defined as the ratio of pressure to wall normal velocity, which is dependent upon the forcing frequency. For a variation of lining Z may be taken as a function of axial position.

In nondimensional form the boundary condition becomes

$$p = \frac{Z}{\rho_r c_r} V_\nu$$

or
$$V_\nu = Ap \tag{2.1.1}$$

where $A = \rho_r c_r / Z$ is the specific acoustic admittance of the lining based on the reference admittance $1/\rho_r c_r$.

To derive the acoustic boundary condition for a fluid moving past a lined wall continuity of the particle displacement is assumed. This condition in harmonic motion gives rise to the relation between the components of fluid particle velocity at the wall and particle velocity in the lining at the surface (see Appendix A)

$$\underline{V}^* \cdot \underline{\nu} = V_\nu^* + V_{o\tau}^* \frac{\partial}{\partial \tau} \left(\frac{V_\nu^*}{i\omega} \right) \tag{2.1.2}$$

where $V_{o\tau}^*$ is the fluid velocity tangent to the wall and $\frac{\partial}{\partial \tau}$ is the directional derivative along the wall. In nondimensional form equation (2.1.2) can be written as

$$\underline{V} \cdot \underline{\nu} = V_\nu + \frac{V_{o\tau}}{ik_r} \frac{\partial V_\nu}{\partial \tau} \tag{2.1.3}$$

With a time dependence $e^{i\omega t}$ assumed equations (2.1.1) and (2.1.3) can be combined to give the boundary condition at the duct wall

$$\underline{V} \cdot \underline{\nu} = Ap - i \frac{V_{o\tau}}{k_r} \frac{\partial}{\partial \tau} (Ap) \tag{2.1.4}$$

(ii) At the ends of the nonuniformity.

The governing equations (derived in the next section) together with the boundary condition (2.1.4) specify a boundary problem for sound wave propagation in the described geometry. The problem is still not well posed unless the end conditions are specified. The solutions in the uniform semi-infinite ducts are not defined unless the solution in the non-uniform field has been represented. Consequently, a matching procedure at the ends of the nonuniformity is to be used.

In the following study the least-square matching, the weighted residual matching and the collocation or point matching are considered accordingly to a specific problem.

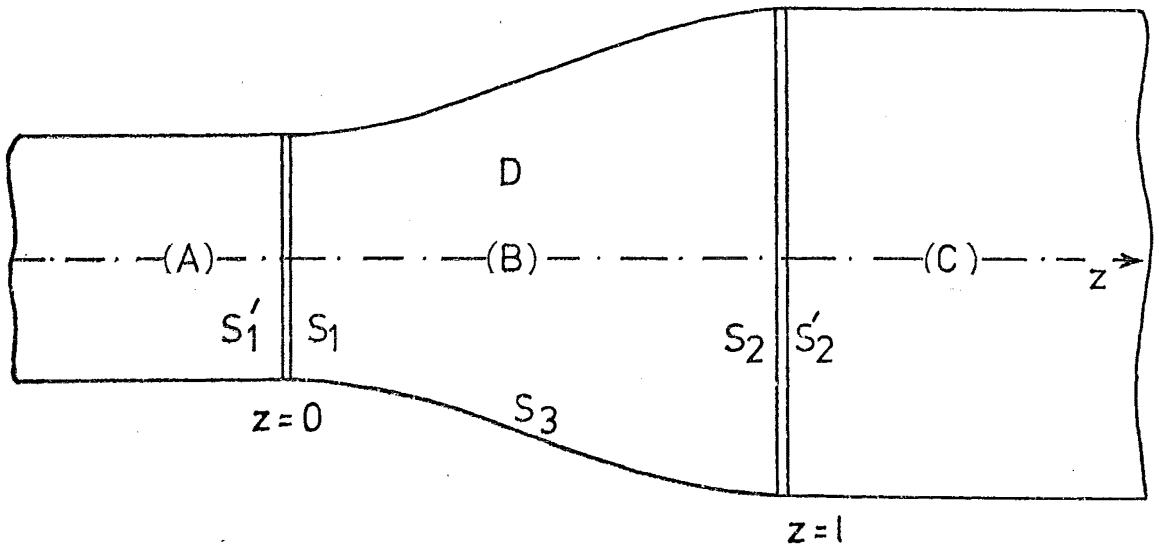

FIG. 2·4 DUCT GEOMETRY WITH DOMAIN AND BOUNDARIES.

Consider the domain D inside a nonuniform duct section (B) (as shown in Figure 2.4) bounded by surfaces S_1, S_2 and S_3 forming the boundary $S = S_1 + S_2 + S_3$ and the semi-infinite ducts (A) and (C) terminated by surfaces S_1' and S_2' respectively at the junctions $z = 0$ and $z = \ell$. Suppose the solutions for acoustic velocity components u,v,w, and acoustic pressure p satisfy the governing equations (derived in Section 2.2)in D and the duct-wall boundary condition (2.1.4) and furthermore u_1, v_1, w_1 and p_1 are the solution values in the uniform duct (A) on S_1' and similarly u_2, v_2, w_2 and p_2 in (C) on S_2'. Through the interfaces at $z = 0$ and $z = \ell$ the acoustic energy and momentum are continuous and conserved. These quantities: energy and momentum at the interfaces are basically dependent on the variables u, v, w and p over the boundary surfaces. Therefore it is equivalent to require

that the variables u, v, w and p be continuous and conserved at the junctions. Hence, the matching based on the acoustic velocity and pressure at the interfaces is derived in this sense.

So, to formalize the matching at the ends of the nonuniformity, the differences or the errors in the values of respective dependent variables at the interfaces are minimized in an average sense by standard procedures. For instance, at $z = \ell$ on the surface S_2', the solution p_2 in the uniform duct (C) can be approximated in the form of a truncated series :

$$p_2 = \sum_{n=1}^{N} a_n J_n(r)$$

where a_n are unknown constants and J_n are eigenfunctions appropriate to the geometry [Appendix C]. N coefficients a_n are to be determined so that the minimization process is chosen so as to yield N equations in a_n.

(a) For the least-square method the quantity $\int_{S_2} |p_2 - p|^2 \, dS$ is minimized with respect to a_i giving N relations :

$$\frac{\partial}{\partial a_i} \int_{S_2} |p_2 - p|^2 \, dS = 0 \ , \ i = 1,2...N$$

or for the sum of errors to be minimal

$$\frac{\partial}{\partial a_i} \int_{S_2} \left(|p_2 - p|^2 + |u_2 - u|^2 + |v_2 - v|^2 + |w_2 - w|^2 \right) dS = 0 \ , \quad i = 1,2...N$$

(b) For the weighted residual method the error $(p_2 - p)$ is forced to be orthogonal to a complete set of linearly independent functions, which is truncated to a finite series for practical purposes, that is

$$\int_{S_2} W_i (p_2 - p) \, dS = 0 \ , \ i = 1,2,..N \ ,$$

W_i are weighting functions, if $W_i \equiv J_i$ that is a Galerkin procedure. The concept of the method of weighted residuals will be discussed in Chapter 3.

(c) For the collocation or point matching method it requires that, for the difference between p_2 and p to be minimal in the average, $p = p_2$ at N locations r_i on S_2.

The same concept of matching is also applied for the other dependent variables, u, v, w and similarly at the interface z = 0.

The formulations of these matching methods will be elaborated in specific problems.

2.2 GOVERNING ACOUSTIC EQUATIONS

In this study the acoustic propagation is considered as small perturbations on the duct flow. It is assumed that the fluid motion is non-viscous and isentropic and the mean flow is steady. The equations of continuity, momentum, energy and state in dimensional form are used to derive the acoustic equations :

Conservation of mass

$$\frac{\partial \rho'}{\partial t} + \operatorname{div}(\rho' \underline{V}') = 0 \qquad (2.2.1)$$

Conservation of momentum

$$\rho' \frac{\partial \underline{V}'}{\partial t} + \rho' \underline{V}' \cdot \operatorname{grad} \underline{V}' = - \operatorname{grad} p' \qquad (2.2.2)$$

Conservation of energy

$$\frac{\partial p'}{\partial t} + \underline{V}' \cdot \operatorname{grad} p' + \gamma p' \operatorname{div} \underline{V}' = 0 \qquad (2.2.3)$$

Equation of state

$$p' = K\rho'^{\gamma} \tag{2.2.4}$$

where K is a constant. The fluid state variables density, ρ', pressure, p', and velocity, $\underline{V}'$ are made up of small acoustic perturbations on the steady mean flow, so that

$$\rho' = \rho_o^* + \rho^* \tag{2.2.5}$$

$$p' = p_o^* + p^* \tag{2.2.6}$$

$$\underline{V}' = \underline{V}_o^* + \underline{V}^* \tag{2.2.7}$$

where ρ_o^* , p_o^*, $\underline{V}_o^*$ are the steady mean flow conditions defined by

$$\text{div } (\rho_o^* \underline{V}_o^*) = 0 \tag{2.2.8}$$

$$\rho_o^* \underline{V}_o^* \cdot \text{grad } \underline{V}_o^* = - \text{grad } p_o^* \tag{2.2.9}$$

$$\underline{V}_o^* \cdot \text{grad } p_o^* + \gamma p_o^* \text{ div } \underline{V}_o^* = 0 \tag{2.2.10}$$

$$p_o^* = K\rho_o^{*\gamma} \tag{2.2.11}$$

Because of the isentropic assumption the energy equation is directly derivable from the continuity equation. The energy equation does not contain the density and is more convenient to use.

By substituting equations (2.2.5) - (2.2.7) into equation (2.2.2) - (2.2.4) and making use of the assumption of small acoustic perturbations on the steady mean flow, the dimensional acoustic momentum, energy and state equations are derived :

$$\rho_o^* \frac{\partial \underline{V}^*}{\partial t} + \rho_o^* \underline{V}^* \cdot \text{grad } \underline{V}_o^* + \rho^* \underline{V}_o^* \cdot \text{grad } \underline{V}_o^* + \rho_o^* \underline{V}_o^* \cdot \text{grad } \underline{V}^*$$

$$= - \text{grad } p^* \tag{2.2.12}$$

$$\frac{\partial p^*}{\partial t} + \underline{V}_o^* \cdot \text{grad } p^* + \gamma p_o^* \text{ div } \underline{V}^* + \underline{V}^* \cdot \text{grad } p_o^* + \gamma p^* \text{ div } \underline{V}_o^* = 0 \tag{2.2.13}$$

$$p^* = \gamma \frac{p_o^*}{\rho_o^*} \rho^* = c_o^{*2} \rho^* \tag{2.2.14}$$

Equations (2.2.9) and (2.2.10) were used to eliminate the steady mean flow terms in equations (2.2.12) and (2.2.13). The term in equation (2.2.12) containing ρ^* can be rewritten by using equations (2.2.14) and (2.2.9) :

$$\rho^* \underline{V}_o^* \cdot \text{grad } \underline{V}_o^* = - \frac{1}{\gamma} \frac{p^*}{p_o^*} \text{grad } p_o^*$$

The modified momentum equation is then

$$\rho_o^* \frac{\partial \underline{V}^*}{\partial t} + \rho_o^* \underline{V}^* \cdot \text{grad } \underline{V}_o^* + \rho_o^* \underline{V}_o^* \cdot \text{grad } \underline{V}^* + \text{grad } p^* - \frac{p^*}{\gamma p_o^*} \text{grad } p_o^* = 0 \tag{2.2.15}$$

The governing acoustic equations can be nondimensionalized in the standard way by defining the nondimensional variables :

$$p = \frac{p^*}{\rho_r c_r^2} \quad , \quad \underline{V} = \frac{\underline{V}^*}{c_r} \quad , \quad \rho = \frac{\rho^*}{\rho_r}$$

$$p_o = \frac{p_o^*}{\rho_r c_r^2} \quad , \quad \underline{V}_o = \frac{\underline{V}_o^*}{c_r} \quad , \quad \rho_o = \frac{\rho_o^*}{\rho_r}$$

The reference state variables ρ_r, c_r are arbitrary values of density and speed of sound. They can be conveniently chosen as the state which exists in the flow incident on the nonuniformity. The nondimensional equations of momentum, energy and state are then :

$$\frac{1}{c_r} \frac{\partial \underline{V}}{\partial t} + \underline{V} \cdot \text{grad } \underline{V}_o + \underline{V}_o \cdot \text{grad } \underline{V} - \frac{1}{\gamma} \frac{p}{p_o \rho_o} \text{grad } p_o = 0 \tag{2.2.16}$$

$$\frac{1}{c_r} \frac{\partial p}{\partial t} + \underline{V}_o \cdot \text{grad } p + \gamma p_o \text{ div } \underline{V} + \underline{V} \cdot \text{grad } p_o + \gamma p \text{ div } \underline{V}_o = 0 \tag{2.2.17}$$

$$p = \gamma \frac{p_o}{\rho_o} \rho \tag{2.2.18}$$

When a harmonic time dependence of the form $e^{i\omega t}$ is assumed for acoustic perturbation quantities where ω is the forced frequency in rad/s, equations (2.2.16) and (2.2.17) become

$$ik_r \underline{V} + \underline{V} \cdot \text{grad } \underline{V}_o + \underline{V}_o \cdot \text{grad } \underline{V} + \frac{1}{\rho_o} \text{grad } p - \frac{1}{\gamma} \frac{p}{p_o \rho_o} \text{grad } p_o = 0 \quad (2.2.19)$$

$$ik_r p + \underline{V}_o \cdot \text{grad } p + \gamma p_o \text{ div } \underline{V} + \underline{V} \cdot \text{grad } p_o + \gamma p \text{ div } \underline{V}_o = 0 \quad (2.2.20)$$

where $k_r = \frac{\omega}{c_r} = \frac{2\pi}{\lambda_r}$ and λ_r is the free space wavelength in the reference state. Equations (2.2.19) and (2.2.20) are basic equations on which mathematical formulations in the following work are established.

2.3 APPROXIMATION TO STEADY MEAN FLOW

2.3.1 Approximate Flow Model

The introduction of steady mean flow into the study of nonuniform duct propagation complicates the problem in two ways. The acoustic field equations can no longer be reduced to either the simple wave equation of the no-flow case or the convected wave equation of the uniform flow case. In addition, the steady nonuniform flow field itself is difficult to be described.

The flow field would be defined by the solution of equations (2.2.8) - (2.2.11) plus suitable boundary conditions. Even for simple duct geometries this requires sophisticated numerical techniques and only rarely in highly specialized cases could one hope to generate an exact closed-form solution. For detailed studies a fairly exact description of the flow field may be required. However, in order to study the effect of duct nonuniformities on wave propagation with a certain degree of generality an approximation to the steady flow field will be used.

The most common approximate description of the steady mean flow field is the one-dimensional theory, which is an elementary topic in

gasdynamics. This theory proves to be very useful for a wide range of duct contours when the area change is gradual.

In the one-dimensional theory the variation of the Mach number, nondimensional density and pressure with axial position are given by

$$M_o = M_o(z)$$

$$\frac{dM_o}{dz} = -\frac{M_o}{1-M_o^2}\left[1 + \frac{\gamma-1}{2} M_o^2\right] \frac{1}{A_c} \frac{dA_c}{dz} \tag{2.3.1}$$

$$\rho_o = \frac{\rho_o^*}{\rho_r} = \frac{\left[1 + \frac{\gamma-1}{2} M_r^2\right]^{\frac{1}{\gamma-1}}}{\left[1 + \frac{\gamma-1}{2} M_o^2\right]^{\frac{1}{\gamma-1}}} \tag{2.3.2}$$

$$p_o = \frac{p_o^*}{\rho_r c_r^2} = \frac{1}{\gamma} \frac{\left[1 + \frac{\gamma-1}{2} M_r^2\right]^{\frac{\gamma}{\gamma-1}}}{\left[1 + \frac{\gamma-1}{2} M_o^2\right]^{\frac{\gamma}{\gamma-1}}} \tag{2.3.3}$$

where A_c is the local cross-sectional area of a flow duct. In addition, the local nondimensional speed of sound and the local nondimensional flow velocity are given by

$$c_o = \frac{c_o^*}{c_r} = \frac{\left[1 + \frac{\gamma-1}{2} M_r^2\right]^{\frac{1}{2}}}{\left[1 + \frac{\gamma-1}{2} M_o^2\right]^{\frac{1}{2}}} \tag{2.3.4}$$

$$W_o = \frac{W_o^*}{c_r} = M_o \frac{\left[1 + \frac{\gamma-1}{2} M_r^2\right]^{\frac{1}{2}}}{\left[1 + \frac{\gamma-1}{2} M_o^2\right]^{\frac{1}{2}}} \tag{2.3.5}$$

$$= M_o c_o$$

where W_o is the local axial velocity component of steady flow, the radial and whirling components being assumed zero in the one-dimensional approximation.

The acoustic problem, equations (2.2.19) and (2.2.20), involves mean flow pressure and axial, radial and angular velocity components as well as axial, radial and angular gradients. Furthermore, for an ideal

fluid, the boundary condition requires the velocity tangent to the wall. This velocity field could be approximated simply by using the one-dimensional theory and ignoring the radial and angular velocity components and the radial and angular gradients. But the solution to equations (2.2.8) - (2.2.11) is taken to include some measure of the effect of radial velocity and its gradient. The steady flow field variables in nondimensional form for the axisymmetric duct, are :

$$\left.\begin{aligned} \underline{V}_o &= (U_o, V_o, W_o) \\ W_o\,(r,\theta,z) &= \bar{W}_o(z) \\ U_o\,(r,\theta,z) &= U_o(r,z) = \bar{W}_o(z)\,\frac{r}{R}\,\frac{dR}{dz} \\ V_o\,(r,\theta,z) &= 0 \\ p_o\,(r,\theta,z) &= \bar{p}_o(z) \\ c_o\,(r,\theta,z) &= \bar{c}_o(z) \end{aligned}\right\} \qquad (2.3.6)$$

where the bar notation denotes the one-dimensional solution.

2.3.2 Discussion and FEM Flow Model

The flow model given by equation (2.3.6) must be recognized as approximate, but it is considered to be a reasonable approximation, in that it exactly satisfies the continuity equation, equation (2.2.8) and the θ and z components of the momentum equation, equation (2.2.9). The r component of equation (2.2.9) is not satisfied exactly, but is satisfied on the average basis over the cross-section of a duct symmetric with respect to the z axis. In addition, the solution satifies the requirement of flow tangency at the duct wall. Based on the success of one-dimensional nozzle theory the axial velocity component, pressure and density variations should be acceptable over a fairly wide range of duct shapes. The assumption for the radial velocity component is on a less firm basis, and more accurate for gradual area changes.

An attempt has been made to obtain the flow field by the FEM to give comparisons to the one-dimensional model. The governing equations (2.2.8) - (2.2.11) for an irrotational steady flow are solved by the nodal FEM using an appropriate potential function (see Appendix B). The problem is nonlinear, consequently an iterative method together with nodal interpolations is employed to yield the flow field solution. Results in Appendix B compare the velocity field for nonuniform ducts, showing discrepancies between the rotational and irrotational flow models.

In the analysis of the acoustic problem it is believed that the approximate flow field will be useful for developing mathematical methods and identifying some important general properties of the sound transmission in nonuniform ducts with flow.

2.4 EQUATIONS IN CYLINDRICAL COORDINATES

With the described approximation to the steady mean flow in Section 2.3, the governing acoustic field equations (2.2.19) and (2.2.20) can be expanded in cylindrical coordinates, for use in axi-symmetric duct problems, to give four partial differential equations.

By assuming the solution is of the angular harmonic form $e^{-im_o\theta}$ where m_o is the angular mode number and using

$$\underline{V}_o = (V_r, V_\theta, V_z)$$

$$V_r = U_o(r,z)$$

$$V_\theta \equiv 0 \text{ , i.e. the mean flow is unwhirling}$$

$$V_z = \bar{W}_o(z)$$

$$\underline{V} = (u,v,w): \text{ acoustic particle velocity}$$

in cylindrical coordinates (r,θ,z) one can write the field equations as follows :

$$\left(ik_r + \frac{\partial U_o}{\partial r}\right) u + \frac{\partial U_o}{\partial z}\, w + U_o \frac{\partial u}{\partial r} + \bar{W}_o \frac{\partial u}{\partial z} + \frac{1}{\bar{\rho}_o} \frac{\partial p}{\partial r} = 0 \qquad (2.4.1)$$

$$\left(ik_r + \frac{U_o}{r}\right) v + U_o \frac{\partial v}{\partial r} + \bar{W}_o \frac{\partial v}{\partial z} - \frac{im_o}{\bar{\rho}_o r} p = 0 \qquad (2.4.2)$$

$$\left(ik_r + \frac{\partial \bar{W}_o}{\partial z}\right) w + U_o \frac{\partial w}{\partial r} + \bar{W}_o \frac{\partial w}{\partial z} + \frac{1}{\bar{\rho}_o} \frac{\partial p}{\partial z} - \frac{\partial \bar{p}_o/\partial z}{\gamma \bar{p}_o \bar{\rho}_o}\, p = 0 \qquad (2.4.3)$$

$$ik_r p + U_o \frac{\partial p}{\partial r} + \bar{W}_o \frac{\partial p}{\partial z} + \gamma \bar{p}_o \left[\frac{1}{r} \frac{\partial}{\partial r}(ru) - \frac{im_o}{r} v + \frac{\partial w}{\partial z}\right] + w \frac{\partial \bar{p}_o}{\partial z}$$

$$+ \gamma p \left[\frac{1}{r} \frac{\partial (rU_o)}{\partial r} + \frac{\partial \bar{W}_o}{\partial z}\right] = 0 \qquad (2.4.4)$$

Also, the boundary condition (2.1.3) can be expanded by noting that, at the duct wall in Figure 2.2

$$V_{o\tau} = W_o \cos \alpha + U_o \sin \alpha$$

$$\frac{\partial}{\partial \tau} (Ap) = \cos \alpha \frac{\partial}{\partial z} (Ap) + \sin \alpha\, A \frac{\partial p}{\partial r}$$

Thus

$$V_{o\tau} \frac{\partial}{\partial \tau} (Ap) = \left(W_o \cos^2 \alpha + U_o \sin \alpha \cos \alpha\right) \frac{\partial}{\partial z} (Ap)$$

$$+ \left(W_o \cos \alpha \sin \alpha + U_o \sin^2 \alpha\right) A \frac{\partial p}{\partial r}$$

The boundary condition at the wall for the steady mean flow is that the normal velocity must vanish

$$U_o \cos \alpha - W_o \sin \alpha = 0$$

or

$$U_o = W_o \tan \alpha = W_o \frac{dR}{dz}$$

Thus, at the duct wall

$$V_{o\tau} \frac{\partial}{\partial \tau} (Ap) = \left[W_o \frac{\partial}{\partial z} (Ap) + W_o \frac{dR}{dz}\, A \frac{\partial p}{\partial r}\right]$$

Furthermore,

$$\underline{V} \cdot \underline{\nu} = u \cos \alpha - w \sin \alpha$$

Equation (2.1.3) together with the approximation for the steady mean flow becomes, at a duct wall

$$\underline{V} \cdot \underline{\nu} = u \cos \alpha - w \sin \alpha = Ap - \frac{i\bar{W}_o}{k_r} \left[\frac{\partial (Ap)}{\partial z} + A \frac{dR}{dz} \frac{\partial p}{\partial r} \right] \quad (2.4.5)$$

2.5 OBJECTIVE IN SOUND TRANSMISSION PROBLEMS

In the mathematical model, Figures 2.1 - 2.3, the acoustic field in the nonuniform section will be defined only if the initial and terminating conditions are specified at the interfaces $z = 0$ and $z = \ell$. In this analysis the far-field is assumed to be incident from the left (Figure 2.1), or $z < 0$ and the uniform acoustic field for $z < 0$ consists of incident and reflected sound waves up to the start of the nonuniformity. For $z > \ell$ it is also assumed that the transmitted sound propagates to the right in a semi-infinite duct and, hence, consists only of waves propagating away from the end of the nonuniformity. So in the two uniform sections (A) and (C) the acoustic eigenproblem is encountered in a classical sense.

In general, to compute the transmission loss through the nonuniform duct section (B), the following relation is sought:

$$\begin{Bmatrix} b_n^+ \\ - - \\ b_n^- \end{Bmatrix} = [TF] \begin{Bmatrix} a_n^+ \\ - - \\ a_n^- \end{Bmatrix}, \quad n = 1,2,3,\ldots N \quad (2.5.1)$$

where a_n^+, a_n^- are incident and reflection amplitude coefficients of propagation modes in section (A), and b_n^+, b_n^- in (C), and [TF] is a transfer matrix derived from the solution in the nonuniform duct and matching at the interfaces.

Thus, if $b_n^- \equiv 0$, i.e. there is no reflection in (C), one can compute reflected and transmitted mode amplitudes a_n^-, b_n^+ from and through the nonuniform duct in terms of incident amplitudes a_n^+, in the following matrix form

$$\left\{a_n^-\right\} = [\text{REFL}] \quad \left\{a_n^+\right\} \tag{2.5.2}$$

and

$$\left\{b_n^+\right\} \quad [\text{TRAN}] \quad \left\{a_n^+\right\} \tag{2.5.3}$$

where [REFL] and [TRAN] are the reflection and transmission matrices respectively. The physical significance of the elements of these matrices is as follows :

(a) REFL_{ij} is the amplitude of reflected mode i excited by incident mode j forced with unit amplitude.

(b) TRAN_{ij} is the amplitude of transmitted mode i excited by incident mode j forced with unit amplitude.

Termination conditions for $z > \ell$ can be accounted for in case of other than semi-infinite ducts employed in this analysis. If a relationship is known between b_n^+ and b_n^- at the end of a finite uniform duct, i.e.

$$\left\{b_n^-\right\} = [R] \quad \left\{b_n^+\right\} \tag{2.5.4}$$

where [R] is the termination matrix, then equation (2.5.1) can be written:

$$\begin{bmatrix} I \\ \hline R \end{bmatrix} \quad \{b_n^+\} \quad = \quad [\text{TF}] \quad \begin{Bmatrix} a_n^+ \\ \hline a_n^- \end{Bmatrix}$$

where [I] is the identity matrix.

The transmission and reflection coefficients of [TRAN] and [REFL] together with the eigenfunctions in the two semi-infinite ducts enable computations of the transmitted and reflected acoustic energy,

hence assessment of the performance of the nonuniform acoustic element.

For the problem of acoustic transmission in a duct with flow there exist coupled hydrodynamic modes. The problem will be discussed further in Chapter 4 and the modified form of the transfer matrix [TF] involving hydrodynamic modes will be established for the flow case.

In the following study a number of test cases consider the geometries described in Figure 2.5.

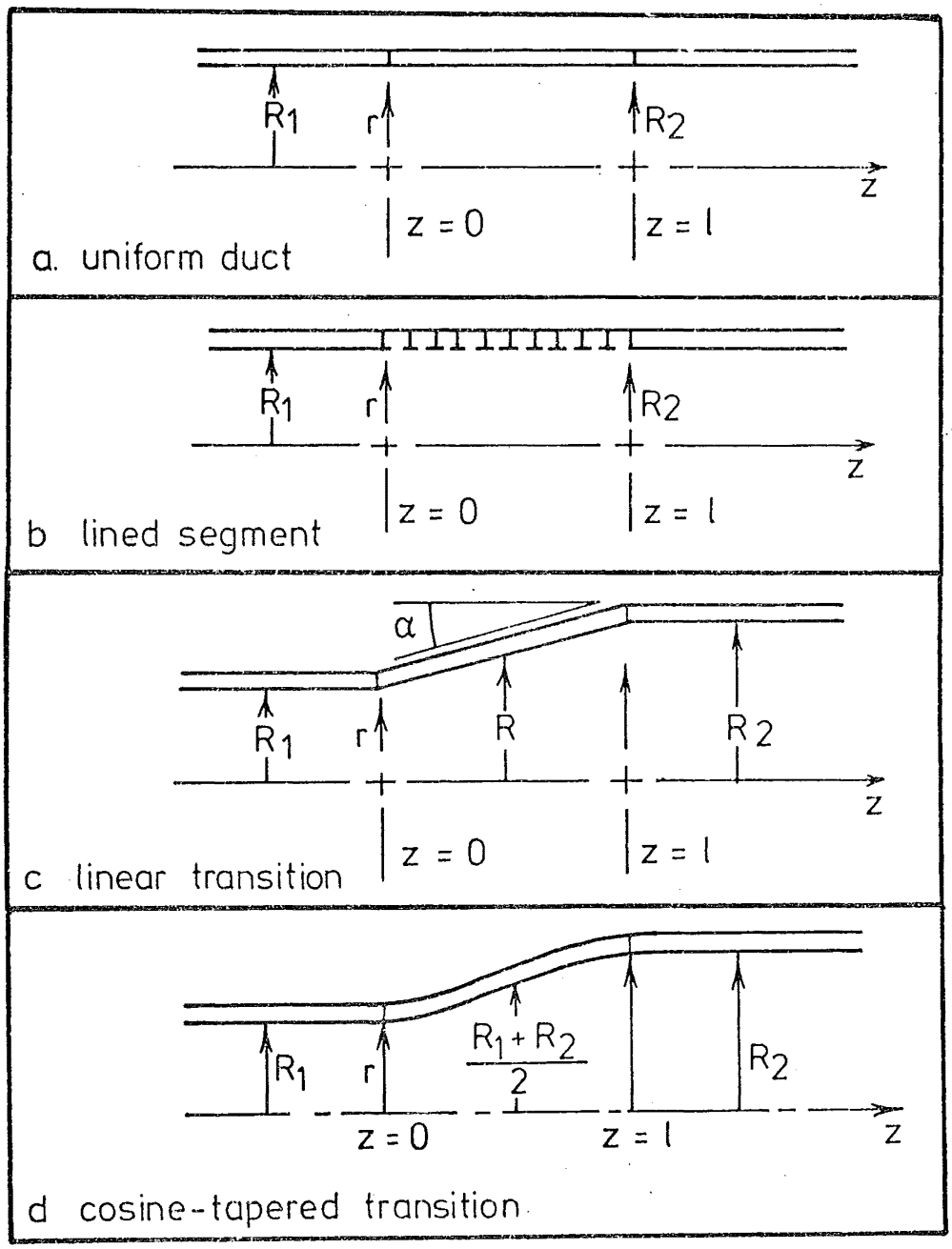

FIG. 2·5 DUCT GEOMETRIES

CHAPTER 3

SOLUTION METHODS FOR ACOUSTIC PROBLEMS

3.1 METHOD OF WEIGHTED RESIDUALS (MWR)

3.1.1 MWR: General Concept

The MWR is an approximate method of solution to a system of integro-differential equations, where an analytical solution has not been found or is in an inappropriate form. Since a thorough survey of the methods of weighted residuals was presented by Finlayson [76], only discussions relative to the methods used in the problem at hand are warranted.

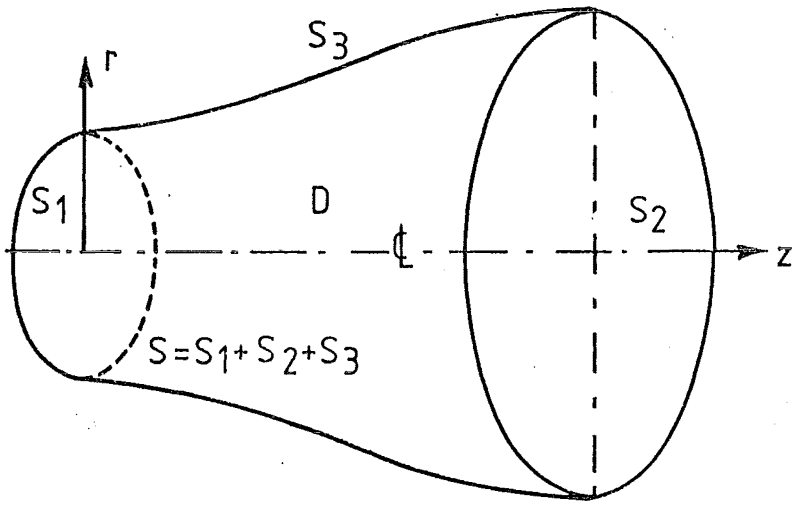

FIG. 3·1 DOMAIN D AND BOUNDARY S FOR AXISYMMETRIC DUCTS.

The governing equations (2.4.1) - (2.4.4) in the acoustic field and appropriate boundary conditions are a linear elliptic problem, which can be expressed in a general matrix form :

$$[A]\{u\} = \{f\} \qquad \text{in domain D} \tag{3.1.1}$$

$$[B]\{u\} = \{g\} \qquad \text{on boundary } S = S_1 + S_2 + S_3 \tag{3.1.2}$$

where $\{u\}$ is the column vector of variables u_i, $[A],[B]$ are matrix differential linear operations and $\{f\}$, $\{g\}$ are constant vectors. D is the region inside the duct section (Figure 3.1) bounded by surfaces S_1, S_2 and S_3, forming boundary S.

For the acoustic problem in the no-flow case there exists a variational functional while in the flow case there is none. As a consequence, in this study the MWR involving the variational principle is not considered.

For simplicity in describing the method in general one considers the field problem of one typical dependent variable u(r,z). Thus, each of the governing (domain + boundary) equations can be written generally

$$F(u) = G(u) \tag{3.1.3}$$

where F,G are functions of u. The solution of u(r,z) which satisfies the set of equations (3.1.3) is sought. In the method of weighted residuals u(r,z) is approximated by a trial solution of u_N of the form

$$u_N = \sum_{i=1}^{N} C_i \phi_i \tag{3.1.4}$$

where ϕ_i are linearly independent selected functions $\phi_i(r,z)$ existing over (D and S), and C_i are unknown parameters to be determined subsequently.

Because u_N is an approximate solution to equation (3.1.3), when equation (3.1.4) is substituted into equation (3.1.3), in general, one obtains a residual error R defined as

$$R = F(u_N) - G(u_N) \tag{3.1.5}$$

which is required to satisfy certain conditions in order to make this error a minimum or maintain it small in some specified sense.

More generally a weighted function of the residual W f(R) where W is the weight or weighting function, has to satisfy the smallness criterion. The function f(R) is chosen so that f(R) = 0 when R = 0, i.e. u_N equals the exact solution

The residuals formed from the domain equations (3.1.1) and boundary conditions (3.1.2) are referred to as the differential equation residuals and the boundary residuals respectively.

In all the commonly used residual methods the smallness criteria can be reduced to the general form

$$\int W\, f(R) \quad = 0 \tag{3.1.6}$$

where the integration is taken over the domain or the boundary as appropriate for the residual considered. The set of equations (3.1.6) when solved yields values for the unknown C_i.

The finite element method can also be regarded as a subclass of the general method of trial solutions of the type (3.1.4), in which the ϕ_i are defined piecewise continuous (via element by element) in the domain D when D has been discretized into subdomains or finite elements.

3.1.2 Galerkin Method in MWR

In the approximation methods of solutions the choice of trial functions and the choice of smallness criteria can lead to different methods of problem formulation such as : Galerkin Method, Subdomain Method, Collocation Method, Least-Square Method, Absolute Error Method, Method of Orthogonality, Method of Moments. These several criteria were unified by Crandall [77] as the Method of Weighted Residuals (MWR). Collatz [78] called them error distribution principles. As pointed out by Finlayson [76] the choice of criterion in MWR is not crucial since

many comparisons of different methods indicate that similar trends of convergence are achieved, especially for high-order approximations. For problems associated with variational principles the Galerkin method is commonly used because of its equivalence to the variational method. In the literature of MWR the Galerkin method gives highly accurate eigenvalues for a variety of problems [76,79].

In the Galerkin method [80], developed in 1915 as the first criterion of what is now known as MWR the weighting functions are just the approximating functions. Thus, equation (3.1.6) in this case becomes

$$\int_D \phi_i R \, dD = 0 \quad i = 1,2,...N \tag{3.1.7}$$

to yield N equations in C_i. The approximating functions are often members of a complete system of functions, although this property, required for mathematical purposes, is sometimes ignored in practice [81]. The Galerkin method then can be interpreted as making the residual orthogonal to members of the complete set. A fundamental property of a complete system of functions is that a piecewise continuous function can be orthogonal to each and every member only if the function is identically zero. Hence, in the Galerkin scheme the residual is forced to vanish only if it is orthogonal to each member of an infinite set of functions. In practice only a finite number of the members of a complete set are employed.

In the original Galerkin method [80], developed in the study of elastic equilibrium and stability of rods and plates Galerkin used C_i as constant coefficients. Now many similar techniques are often referred to as the Galerkin or Generalized Galerkin method:

a) ones in which $C_i = C_i(t)$ can be used for time dependent problems.

b) ones in which the trial solutions are of the general form $u_N = f(C_i,\phi_i)$ with weighting functions being $\partial f/\partial C_i$.

c) ones in which the weighting functions are of the form $\mathcal{L}(u_N)$, where $\mathcal{L}$ is a specified differential operator

Other modifications are possible. Duncan [82] makes the approximating functions satisfy derived or secondary boundary conditions which are determined by requiring that the domain equations be satisfied on the boundary. Kantorovich and Krylov [83] outline the method of reductions to ordinary differential equations, developed for 2D problems independently by Poritzky [84] in which partial differential equations are reduced to a system of ordinary equations by taking the domain and boundary integrals over all the independent coordinate variables except one. The approximate solution is then found by solving a set of ordinary differential equations involving this remaining independent variable. In general, MWR can be used to reduce the number of coordinate variables in any system of partial differential equations. The resulting simpler system may be a set of algebraic or ordinary differential equations or even a set of partial differential equations. But its solution remains only an approximate to the original problem.

3.1.3 Choice of Trial Solutions (or Basis Functions)

When the MWR is applied in practice the choice of trial functions is rather prejudicious but important since it provides the power of the method, in that known information can be incorporated into the trial solution. In lower-order approximations the choice may have significant influence on the results, but high approximations are less affected since numerical convergence becomes more dominant. The main influence is the rate of convergence rather than the eventual solution.

According to the conditions which the trial functions have to satisfy the MWR can be classified as :

a) Standard method in which boundary conditions are satisfied but domain equations are not.

b) Boundary method in which boundary conditions are not satisfied but domain equations are.

c) Mixed method in which neither boundary conditions nor domain equations are satisfied.

The mixed method poses special problems which have attracted particular attention. In Schuleshko's treatment of mixed methods [85] the differential equation residual is forced to be orthogonal to one set of weighting functions using (3.1.6) or (3.1.7) while the boundary residual is simultaneously forced to be orthogonal to another set of weighting functions using an appropriate surface integral. If N weighting functions are used this leads to 2N conditions with N unknowns C_i. For this procedure to work some of the conditions must be discarded, as noticed by Snyder, Spriggs and Stewart [86] in their discussion of the Galerkin method. On the other hand Bolotin [87] and Mikhlin [88] pointed out that for the Galerkin method the problem can be solved by adding the boundary residuals to the differential equation residuals in such a way that the differential equation residuals, when integrated by parts to expose boundary terms, cancel identical terms of the boundary residuals. The situation is analogous to the treatment of natural boundary conditions in the calculus of variations, and indeed only boundary conditions analogous to natural boundary conditions can be handled in this way [81]. The Galerkin procedure used in a mixed method is referred to as the Modified Galerkin Method.

In the following study of acoustic problems MWR in the form of the Modified Galerkin Method is applied to reduce the domain equations to a system of ordinary differential equations, which can be solved by an integration scheme. The Galerkin procedure is also used to formulate the problems by the finite element method. In the following study MWR denotes the method of weighted residuals in the form of the Modified Galerkin procedure.

3.1.4 MWR in Acoustic Problems

The importance of choosing appropriate basis functions for trial solutions has been stressed by Crandall [77]: "The variation between results obtained by different criteria to the same trial family ... is much less significant than the variations that can result from the choice of different trial families." Hence the first step to apply MWR to the study of acoustic problems in axisymmetric ducts is to specify the basis functions to be used in representing the approximate solutions.

The MWR has been successfully used to investigate the transmission of sound waves in nonuniform ducts, both in the no-flow case and the flow case, for two-dimensional channels [64,65]. In these geometries the appropriate basis functions to be used are trigonometric functions, which are eigenfunctions derived from the eigenproblems for uniform 2D ducts [Appendix C]. This leads to efficient computational schemes.

When MWR is extended to axisymmetric duct problems one is naturally inclined to use Bessel functions, the eigenfunctions in uniform circular ducts, to represent the solutions. It has been found that with Bessel function routines generally available this approach leads to less efficient computational schemes and a higher degree of effort involved in formulation. In an attempt to overcome this difficulty the axisymmetric acoustic problems have been formulated using as basis functions the same type of trigonometric functions as generated in the two-dimensional case. This has led to viable computational schemes both in the no-flow case and the flow case.

In MWR for u, a typical dependent variable in the governing equations (2.4.1) - (2.4.4), one can make approximations of the following type :

$$u \approx u_N = \sum_{m=1}^{N} u_m(z)\ \psi_m(r,z) \tag{3.1.8}$$

where $u_m(z)$ are coefficients depending on z and $\psi_m(r,z)$ are specified functions. The approximate solutions are substituted into the governing equations and the duct-wall boundary condition. The Galerkin orthogonalization process as a mixed method is applied to give a system of ordinary differential equations in the form :

$$[\mathcal{M}(r,z)]\frac{d}{dz}\{u_m(z)\} = [\mathcal{N}(r,z)]\{u_m(z)\} \tag{3.1.9}$$

where $[\mathcal{M}]$, $[\mathcal{N}]$ are $(n_v xN)$ x $(n_v xN)$ matrices in (r,z) and n_v is the number of dependent variables u involved in the formulation. For axisymmetric ducts this number is generally $n_v = 4$.

A numerical integration scheme such as the 4^{th} order Runge-Kutta method can be applied to integrate equation (3.1.9) from z = 0 to z = ℓ, having $\psi_n(r,z)$ in equation (3.1.8) generated at each integration step along the z axis. In this MWR formulation with trigonometric functions $[\mathcal{M}]$ and $[\mathcal{N}]$ can be analytically computed. Hence, in this way one can obtain :

$$\underset{(n_v Nx1)}{\{u_m(\ell)\}_{z=\ell}} = \underset{(n_v Nxn_v N)}{[TS]}\ \underset{(n_v Nx1)}{\{u_m(0)\}_{z=0}} \tag{3.1.10}$$

where [TS] is a transition matrix relating u_m at z = ℓ to u_m at z = 0 for m = 1,2...N.

Then, the coefficients $u_m(0)$ and $u_m(\ell)$ are made use of in order to relate propagation coefficients in semi-infinite duct sections by matching procedures at the ends of the nonuniformity as described in Section 2.1.2.

The formulations both for no-flow and flow cases are performed in detail and results are presented with appropriate discussions in the following chapters.

3.2 FINITE ELEMENT METHOD (FEM)

3.2.1 FEM : General Concept

The FEM is a method of weighted residuals in which the subdivision of the region or the domain under study into subdomains or finite elements or cells is the essential part of the procedure, with some functional representation of solution being adopted over each element so that the parameters of the representation become the unknowns of the problem. Thus, the FEM is a particular class of discretization procedure by which the original governing equations in a domain having infinite degrees of freedom are transformed into approximations with finite degrees of freedom. There are three categories of FEM defined on the basis of the element parameters : Nodal Method, Coefficient Method and Cell Method [89].

Due to the success of the nodal FEM in other fields of continuum mechanics it is chosen to study the acoustic problems reported here. For the general problem described by equations (3.1.1) and (3.1.2), in the nodal FEM, the element parameters are then values of u and/or their derivatives at nodes. The nodal FEM can be further subdivided according to the minimization procedure by which the governing equations in nodal values are formulated. There are several ways of formulation, of which two are commonly used in the literature of FEM [90] :

a) Variational FEM: An extremum principle involving a functional is used with finite element approximation to derive a set of equations in terms of nodal values.

b) Residual FEM: A process of MWR is incorporated in the finite element formulation by minimizing residual errors arising from approximations.

In the acoustic field a variational functional does not exist for the flow case, consequently the second approach is adopted with a Galerkin process to formulate the problems by FEM.

The basic approach by FEM to a field problem involves the following steps :

a) The type of element is chosen and the domain is subdivided accordingly. The element properties from the geometry and characteristic parameters are determined and stored for each element and each node. Elements and nodes are numbered explicitly and systematically.

b) The element matrices are calculated element by element and finally assembled into a system matrix connecting all nodal variables.

c) Appropriate boundary conditions are inserted into the system matrix.

d) The system matrix is partitioned to give a system of simultaneous equations, which can be solved for desired output quantities.

Because of the well-advanced development of FEM in other fields, notably in structural mechanics these steps are not presented in detail but rather can be referred to in standard texts [90,91]

3.2.2 Choice of Element and Discretization

The great majority of development of the FEM has taken place within the context of structural mechanics and solid mechanics. Concerning the relative advantage of various types of finite elements it is informative to note the comments of a specialist in this field, Zienkiewicz [90, page 104], who states that : "The question may well be asked as to whether any economic or other advantage is gained by increasing the complexity of an element. The answer here is not an easy one, although it can be stated as a general rule that as the order of an element increases so that the total number of unknowns in a problem can be reduced for a given accuracy of representation. Economic advantage requires, however, a reduction of total computations and data preparation effort and this does not follow automatically for a reduced number of total variables as, though equations solving times

may be reduced, the time required for element formulation increases. ....In general, the optimum element may have to be determined from case to case."

In the light of these comments and the required convergence criteria [89,90] to be satisfied in FEM formulations, the linear element (triangular or rectangular) is of the lowest order for sufficient representation of solutions in acoustic problems with conservation equations. However, in the view of complicated variations in the acoustic field. The quadratic rectangular eight-node finite element from the Serendipity family was chosen as the basis for this analysis.

In the governing acoustic equations (2.4.1) - (2.4.4) for axisymmetric duct geometry the harmonic angular dependence has already been assumed so that only two-dimensional discretization in (r,z) is required. Figure 3.2 shows a typical 3x4 finite element arrangement for a uniform duct section with a description of the numbering systems for nodes and elements. The nodes and elements are numbered columnwise starting from the duct wall ($r = R(z)$) towards the centre line ($r = 0$) and moving from one end ($z = 0$) to the other ($z = \ell$). The advantage of this system is to preserve the system matrix in block diagonal form when boundary conditions, by matching at the ends of a nonuniformity, are inserted into the system matrix. This will be seen in specific problem formulations.

3.2.3 Element Derivations

(i) Shape functions

One of the advantages offered by FEM is that the formulation of a problem in an irregular domain requires just about the same effort as for simpler domains because of convenient coordinate transformations. Figure 3.3 shows the orientation of an element in local coordinates (ξ,η) and global coordinates (r,z), which is used to map

a nonuniform configuration as shown in Figure 3.4. This is common practice when FEM is practically considered so that element derivations are conveniently based on local coordinates (ξ,η).

Consider the region of space inside a typical element shown in Figure 3.3(b), suppose within this region the acoustic variables u,v,w,p as well as the steady mean flow parameters $\bar{U}_o$, $\bar{W}_o$ $\bar{\rho}_o$,$\bar{p}_o$ of equations (2.4.1) - (2.4.4) at some position (r,z) are defined by relations of the following type :

$$u \approx \tilde{u} = [N_1,N_2,\ldots N_8] \begin{Bmatrix} u_1 \\ u_2 \\ \vdots \\ u_8 \end{Bmatrix} = [N]\{u\} \qquad (3.2.1)$$

where u_i $(i=1,2,\ldots 8)$ are the unknown values of u at the 8 nodes numbered on the boundary of the element. $\tilde{u}$ is an approximate solution of u, a typical dependent variable. N_i are shape functions in terms of $(r_i,z_i)_{(i=1,2,.8)}$ and functions of (r,z).

Now if a transformation from global coordinates (r,z) to local coordinates (ξ,η) is used one can write

$$\tilde{u} = [N]\{u\} \qquad (3.2.2)$$

N_i (i=1,2,..8) are functions of (ξ,η) and (ξ_i,η_i) such that at (ξ_i,η_i), $N_i = 1$ and $N_j = 0$ for $j \neq i$.

Suppose further the coordinate transformation is given by

$$\begin{aligned} r &= [N']\ \{r\} \\ z &= [N']\ \{z\} \end{aligned} \qquad (3.2.3)$$

where

$$[N'] = [N_1', N_2', .. N_8']$$

$$\{r\} = [r_1, r_2, .. r_8]^T$$

$$\{z\} = [z_1, z_2, .. z_8]^T$$

$$N_i' = N_i'(\xi,\eta) \quad \text{for} \quad i = 1,2,\ldots 8$$

If now [N] in equation (3.2.2) and [N'] in equation (3.2.3) are

taken so that $N_i' \equiv N_i$ for i = 1,2,3,...8, then this implies :

a) The points(viz. nodal points) defining the geometry of the element are the same as for the finite element variables u.

b) The shape functions (viz.[N]) defining the global coordinates and the dependent variables u within the element are the same.

Thus, the mapped elements are isoparametric [90].

The isoparametric family of elements, which has been used with great success in various problem areas [90] is adopted in this analysis.

For the quadratic rectangular 8-node element of the isoparametric family the interpolation polynomial is in the form

$$N_i = a_1 + a_2 \xi + a_3 \eta + a_4 \xi^2 + a_5 \xi\eta + a_6 \eta^2 + a_7 \xi^2\eta + a_8 \xi\eta^2 , \qquad (3.2.4)$$

which is an incomplete third-degree polynomial in (ξ,η). This expression can be cast in terms of nodal quantities by substituting the 8 nodal values of r_i, z_i and u_i for ξ,η at the 8 nodes in the undistorted element and inverting the resulting 8 x 8 matrix [89,90] to determine a_i (i = 1,2,..8). A more direct method [92, page 109] is to examine various mode shapes in an element and combine them appropriately [93] to yield the shape functions of the element in Figure 3.3 :

$$\left.\begin{aligned} N_i &= \frac{1}{4}(1+\xi\xi_i)(1+\eta\eta_i)(\xi\xi_i+\eta\eta_i-1) && \text{for } i = 1,3,5,7 \\ N_i &= \frac{1}{2}(1-\xi^2)(1+\eta\eta_i) && \text{for } i = 2,6 \\ N_i &= \frac{1}{2}(1+\xi\xi_i)(1-\eta^2) && \text{for } i = 4,8 \end{aligned}\right\} \qquad (3.2.5)$$

where for i = 1,2,..8 the consecutive values of ξ_i and η_i are :

ξ_i = -1,0,1,1,1,0,-1,-1

η_i = -1,-1,-1,0,1,1,1,0

For the quadratic 3-node line element, as shown in Figure 3.3, the shape functions degenerate to functions of one local coordinate η, being

$$\left.\begin{aligned} N_1 &= \frac{1}{2}\,\eta(\eta+1) \\ N_2 &= 1 - \eta^2 \\ N_3 &= \frac{1}{2}\,\eta(\eta-1) \end{aligned}\right\} \qquad (3.2.6)$$

The shape functions for midside and corner nodes are shown in Figure 3.5.

(ii) Derivatives.

In order to transform the governing equations (2.4.1) - (2.4.4) into the local coordinate system (ξ,η) the expressions for $\frac{\partial u}{\partial r}$ and $\frac{\partial u}{\partial z}$ are to be derived in (ξ,η), where u is defined by equation (3.2.1). For one element

$$\begin{aligned} u &= [N]\{u\} \quad \text{at } (r,z) \\ &= N_i u_i \,, \quad i = 1,2,\ldots 8 \end{aligned}$$

thus $$\frac{\partial u}{\partial r} = \frac{\partial N_i}{\partial r}\,u_i \,, \quad \frac{\partial u}{\partial z} = \frac{\partial N_i}{\partial z}\,u_i$$

and
$$\left.\begin{aligned} \frac{\partial N_i}{\partial \eta} &= \frac{\partial N_i}{\partial r}\cdot\frac{\partial r}{\partial \eta} + \frac{\partial N_i}{\partial z}\cdot\frac{\partial z}{\partial \eta} \\ \frac{\partial N_i}{\partial \xi} &= \frac{\partial N_i}{\partial r}\cdot\frac{\partial r}{\partial \xi} + \frac{\partial N_i}{\partial z}\cdot\frac{\partial z}{\partial \xi} \end{aligned}\right\} \qquad (3.2.7)$$

or
$$\left.\begin{aligned} \begin{Bmatrix} \frac{\partial N_i}{\partial \eta} \\ \frac{\partial N_i}{\partial \xi} \end{Bmatrix} &= \begin{bmatrix} \frac{\partial r}{\partial \eta} & \frac{\partial z}{\partial \eta} \\ \frac{\partial r}{\partial \xi} & \frac{\partial z}{\partial \xi} \end{bmatrix} \begin{Bmatrix} \frac{\partial N_i}{\partial r} \\ \frac{\partial N_i}{\partial z} \end{Bmatrix} \\ &= [J] \begin{Bmatrix} \frac{\partial N_i}{\partial r} \\ \frac{\partial N_i}{\partial z} \end{Bmatrix} \end{aligned}\right\} \qquad (3.2.8)$$

for i = 1,2,...8

where [J] is the Jacobian matrix

Hence

$$\begin{Bmatrix} \frac{\partial N_i}{\partial r} \\ \frac{\partial N_i}{\partial z} \end{Bmatrix} = [J]^{-1} \begin{Bmatrix} \frac{\partial N_i}{\partial \eta} \\ \frac{\partial N_i}{\partial \xi} \end{Bmatrix} \tag{3.2.9}$$

where $\frac{\partial r}{\partial \eta}$, $\frac{\partial r}{\partial \xi}$, $\frac{\partial z}{\partial \eta}$, $\frac{\partial z}{\partial \xi}$ and $\frac{\partial N_i}{\partial \eta}$, $\frac{\partial N_i}{\partial \xi}$ are calculated in terms of (ξ,η) by equation (3.2.3) and equation (3.2.5) respectively. For line elements with one local coordinate η

$$\left.\begin{aligned} &\frac{\partial u}{\partial r} = \frac{\partial N_i}{\partial r} \; u_i \;, \quad \frac{\partial u}{\partial z} = \frac{\partial N_i}{\partial z} \; u_i \\ \text{where} \quad &\frac{\partial N_i}{\partial r} = \frac{\partial N_i}{\partial \eta} \Big/ \frac{\partial r}{\partial \eta} \;, \quad \frac{\partial N_i}{\partial z} = \frac{\partial N_i}{\partial \eta} \Big/ \frac{\partial z}{\partial \eta} \end{aligned}\right\} \tag{3.2.10}$$

in this case $\frac{\partial N_i}{\partial \eta}$ are determined by equation (3.2.6)

(iii) Numerical integrations.

The FEM is a form of the method of weighted residuals in which basis functions are the piecewise continuous shape functions forming the components of [N]. Thus, in FEM formulations with a Galerkin procedure the integrals given by (3.1.6) together with relations (3.1.1) and (3.1.2) are to be evaluated in the form :

$$\int_D [G] \; dD \text{ in domain } D \tag{3.2.11}$$

and

$$\int_S [G'] \; dS \text{ on boundary } S \tag{3.2.12}$$

(Refer to Figure 3.1) where [G] and [G´] depend on [N] and/or its derivatives with respect to global coordinates. In the FEM the Gaussian quadrature integration is commonly used, by which the integrals are evaluated over each element and then assembled for the whole domain (or the whole boundary).

For axisymmetric duct problems the integrals (3.2.11) and (3.2.12) can be cast in a more specific form with the harmonic angular dependence implicitly assumed :

$$\int_D [G]\, dD = \int_A [G(r,z)]\, 2\pi r\, dr\, dz \tag{3.2.13}$$

and $$\int_S [G']\, dS = \int_C [G'(r,z)]\, 2\pi r\, ds \tag{3.2.14}$$

where s is the arc length along C in Figure 3.6.

To transform these into local coordinates (ξ,η) for use in numerical integration it is noted that, from the calculus , if , in Figure 3.6.

$$r = r(\xi,\eta)\ ,\ z = z(\xi,\eta) \qquad \text{for domain A}$$

and $$r = r(\eta)\ ,\ z = z(\eta) \qquad \text{for boundary C}$$

then $$dr\, dz = \det(J)\, d\xi\, d\eta \tag{3.2.15}$$

$$ds = \left[\left(\frac{\partial r}{\partial \eta}\right)^2 + \left(\frac{\partial z}{\partial \eta}\right)^2\right]^{\frac{1}{2}} d\eta \tag{3.2.16}$$

$$= J'(\eta)\, d\eta$$

where det(J) is the determinant of the Jacobian matrix as given by equation (3.2.7).

Therefore the integrals (3.2.13) and (3.2.14) can be taken over each element as

$$[I_e] = \int_{-1}^{+1}\int_{-1}^{+1} [G(\xi,\eta)]\, 2\pi r(\xi,\eta)\, \det(J)\, d\xi\, d\eta \text{ in A} \tag{3.2.17}$$

$$[I_e'] = \int_{-1}^{1} [G'(\eta)]\, 2\pi r(\eta)\, J'(\eta)\, d\eta \qquad \text{on C} \tag{3.2.18}$$

They are conveniently evaluated numerically by the use of Gauss quadratures in the form

$$I = \int_{-1}^{1}\int_{-1}^{1} f(\xi,\eta)\, d\xi\, d\eta = \sum_{i=n}^{n}\sum_{j=1}^{n} H_i\, H_j\, f(\xi_i,\eta_j) \tag{3.2.19}$$

and $$I' = \int_{-1}^{1} f'(\eta)\, d\eta = \sum_{j=1}^{n} H_j\, f'(\eta_j) \tag{3.2.20}$$

To determine the minimum order of Gauss quadrature needed it is noted that, for one dimension in η the integral (3.2.20) is evaluated

with n sampling points η_j and 2n unknowns (f_j' and η_j). Hence, a polynomial of degree (2n-1) could be constructed and exactly integrated to order of $0(\varepsilon)^{2n}$. So n is chosen so that the integrals (3.2.17) and (3.2.18) should be exactly evaluated to the highest term in the integrands in η (or/and ξ). It is equivalent to require

$$\int_{-1}^{1}\int_{-1}^{1} \det(J)\, d\eta\, d\xi \quad \text{or} \quad \int_{-1}^{1} J'(\eta)\, d\eta \quad \text{to be}$$

exactly integrated to that same order for any distorted form of the appropriate element [94, page 35].

Thus, examination of det(J) or $J'(\eta)$ yields the minimum number of Gauss points needed for each case. The det(J) given by equation (3.2.7) contains ξ^3 and η^3, hence a 2x2 Gauss rule is the lowest that can be accepted for the area integral (3.2.17); for the line integral $J'(\eta)$ contains η as the highest term, hence the minimum of n is 1.

In the study of axisymmetric duct problems the number of dependent variables (4 at each node for the flow case) at nodes limits the dimensionality of the system matrix,rendering the discretization grid of elements rather coarse. It is believed a high-order numerical integration scheme should be employed in order to achieve reasonable results. In practical implementations of the FEM following, a 4x4-point Gauss rule is used for area integrals and 4-point for line integrals.

In Figure 3.7 is shown a logic diagram in the form of a flow chart for a subroutine, in which the integrals are evaluated element by element. It is noted that in the sixth step of this logic diagram the stage to evaluate local shape functions and their local derivatives can be retained outside the loops and in the eighth step the multiplication constant 2π is neglected for convenience. However, in practical computations the computing time consumed by integrating and assembling is trivial in comparison to the solution time. For line integrals the procedure is similar.

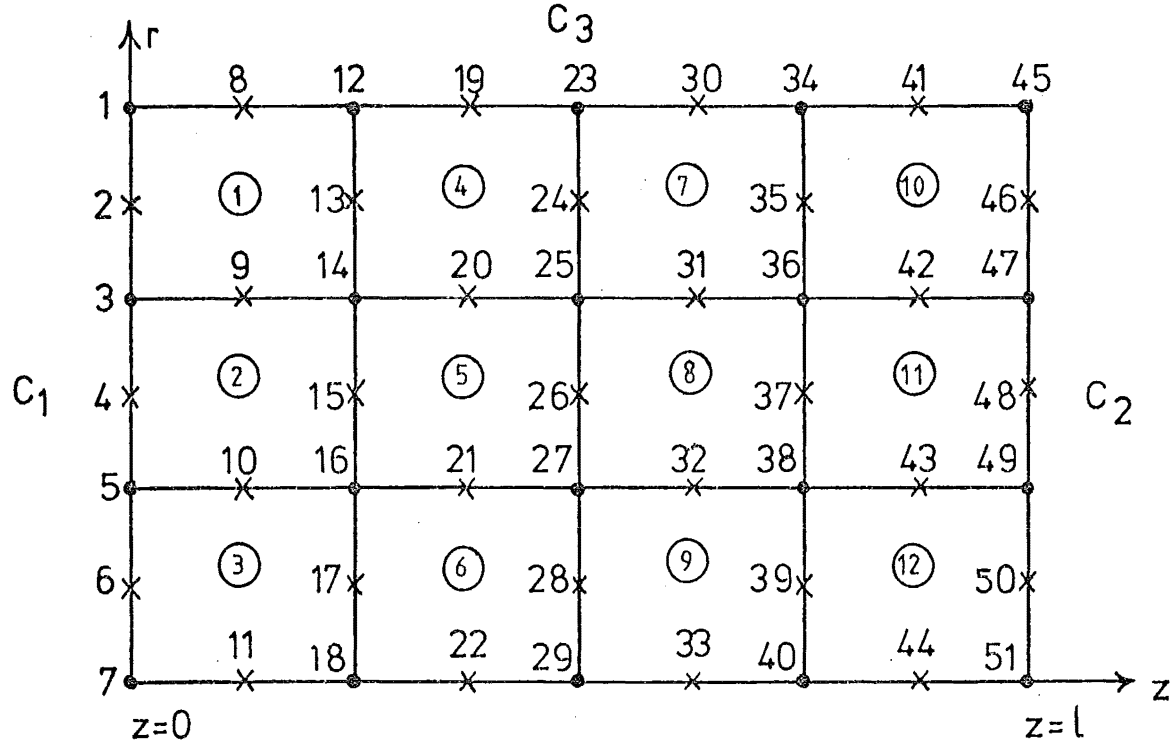

X midside node ● corner node

i = 1, 2, 3, ... 51: nodal number

(j), j = 1, 2, 3, ... 12: element number

FIG. 3·2 FEM (3 × 4) DISCRETIZATION FOR A UNIFORM DUCT SECTION

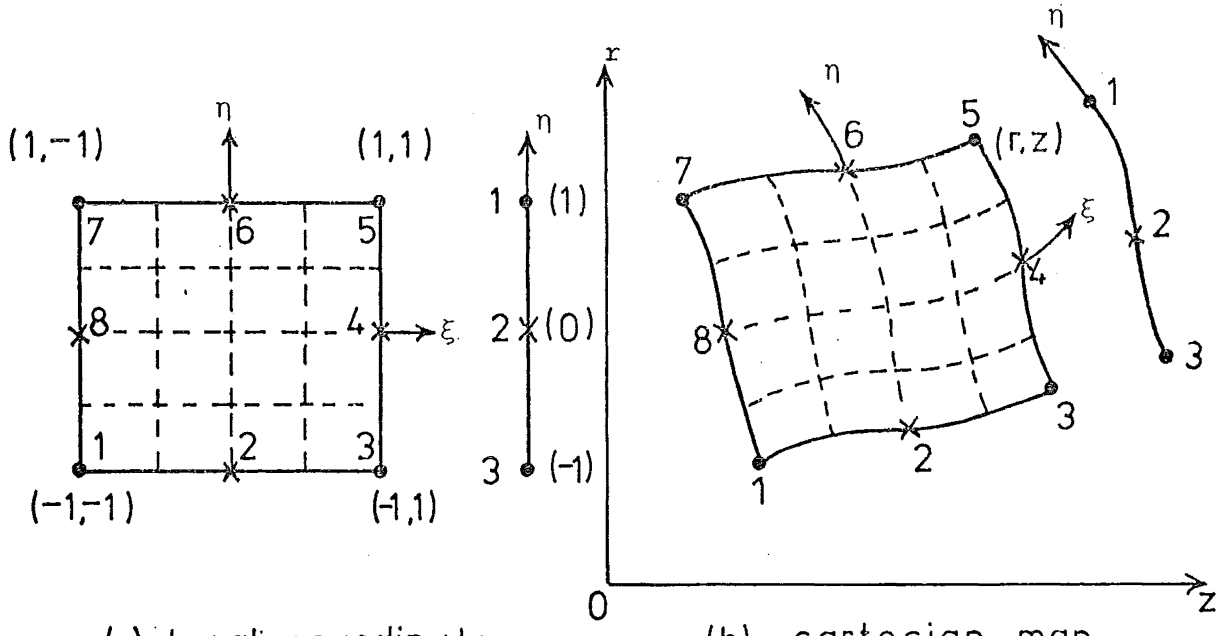

(a) local coordinates. (b) cartesian map.

FIG. 3·3 QUADRATIC SERENDIPITY ELEMENT

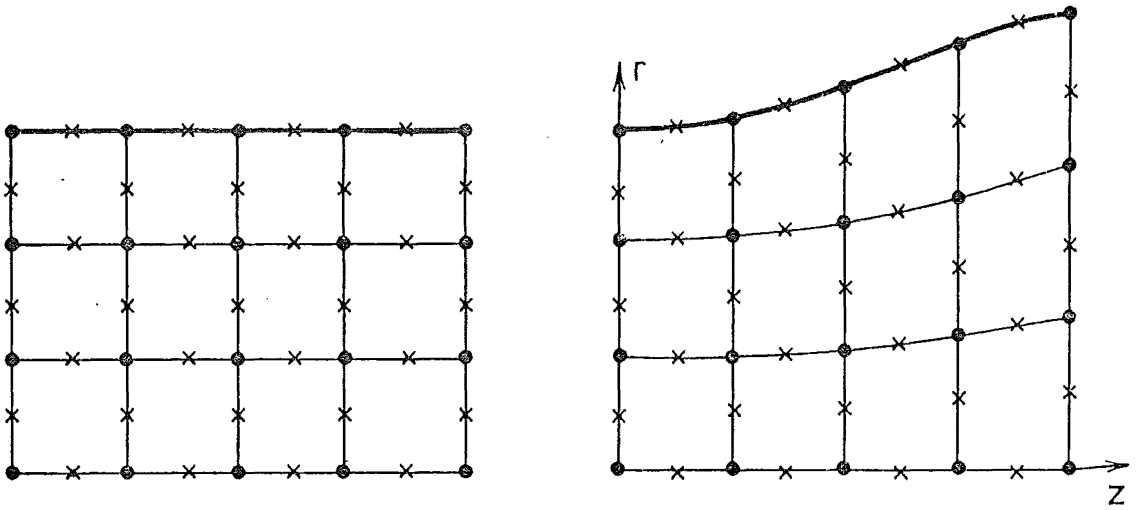

(a) local coordinates (b) Cartesian map

× midside node, • corner node

FIG. 3·4 ELEMENT MAPPING BY COORDINATE TRANSFORMATION

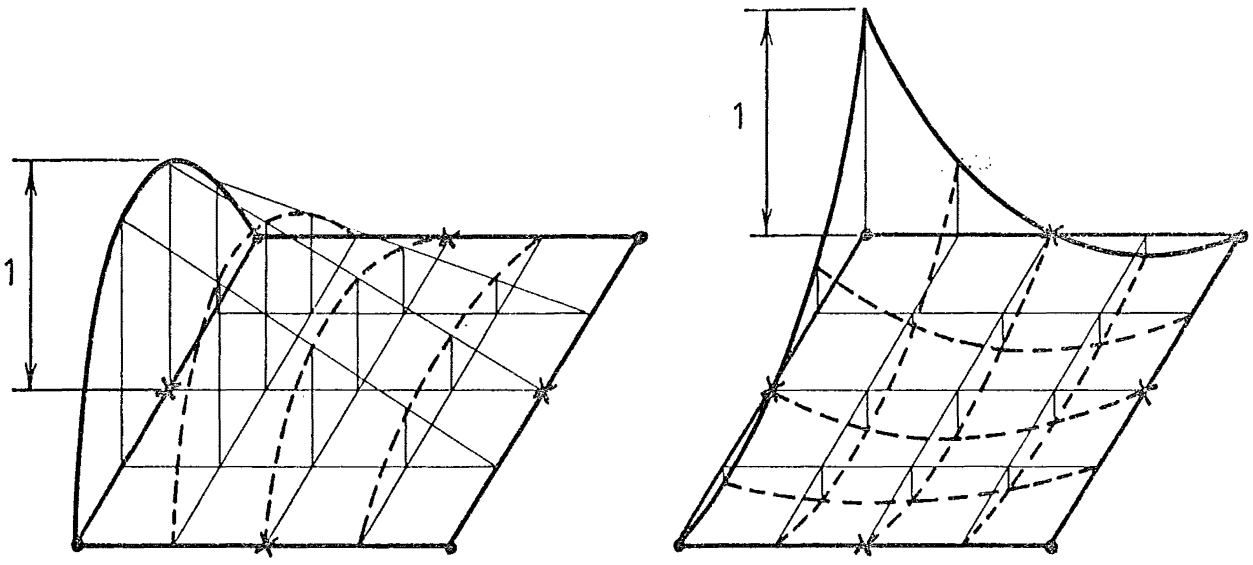

(a) rectangular element

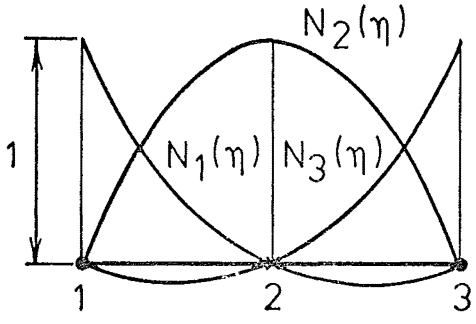

(b) line element

FIG. 3·5 SHAPE FUNCTIONS FOR SERENDIPITY ELEMENTS

3.2.4 System Matrix Assembly and Solution Technique

(i) Assembly.

For a discretized mesh of 3 x 4 elements shown in Figure 3.2 the system matrix, without boundary matching included, generated for this discretization by the numbering systems such as shown in this figure, may be developed as follows. Within each of the finite elements, interactions among nodal variables only occur between those dependent variables at the 8 nodes of that element. Thus, the integral $\int_A [G(r,z)]\, 2\pi r\, dr\, dz = 0$ in one element gives

$$[\, K^e \,]\, \{\delta^e\} = 0$$

where $\{\delta^e\} = [\delta_1^e , \delta_2^e , \delta_3^e \ .., \delta_8^e]^T$

and δ_i^e ($i = 1,2,...8$) are sets of nodal values at one node, i.e. for the flow case four variables (u,v,w,p) are involved and $\{\delta_i^e\} = [u_i, v_i, w_i, p_i]^T$. The order of δ_i^e is taken as numbered in the nodal numbering system when the element matrix $[K^e]$ is assembled into the system matrix. So, on assembly of the global matrix the values of dependent variables at one node are linked explicitly via $[K^e]$ with those at all the nodes of the elements by which that node is commonly shared. All other coefficients of those nodes with which there is no interaction via $[K^e]$ are zero. For the case of n_v dependent variables per node, the system matrix generated by rectangular 8-node finite elements in the 3 x 4 discretization of the domain shown in Figure 3.2 is in the form given in Figure 3.8(a) with description parameters defined as follows :

n_n : the total number of nodes

n_e : the total number of elements

n_{e_1} : the number of elements across the duct (on C_1)

n_{e_3} : the number of elements along the duct (on C_3)

n_r : the number of nodes on C_1

n_z : the number of nodes on C_3

n_{rm} : the number of mid-side nodes on C_1

n_{zm} : the number of mid-side nodes on C_3

n_v : the number of dependent variables per node

then $n_r = 2n_{e_1} + 1$

$n_{rm} = n_{e_1} + 1$

$n_z = 2n_{e_3} + 1$

$n_{zm} = n_{e_3} + 1$

n_w : the bandwidth of the system matrix

In general, for any number of elements discretized with numbering systems as in Figure 3.2 the global matrix, excluding contributions from matching of the ends of the nonuniformity, takes the pattern :

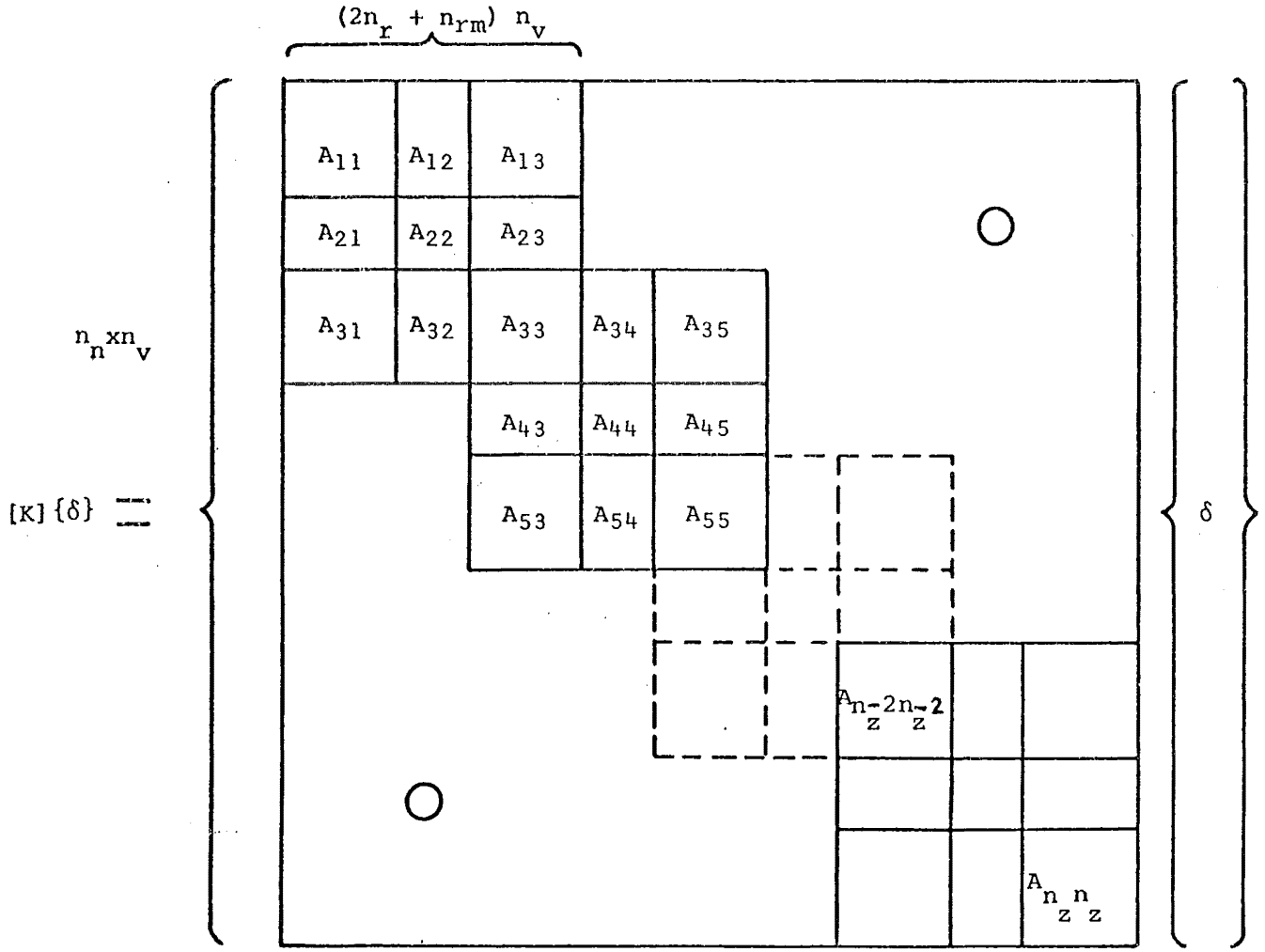

where $\{\delta\} = [\delta_1, \delta_2 \ldots \delta_{n_n}]^T$ and $\{\delta_i\} = [u_i, v_i, w_i, p_i]^T$, $i = 1,2,\ldots n_n$ with principal characteristics :

a) The global matrix [K] consists of overlapping diagonal blocks, such a block, called [A], is shown in Figure 3.9. There are n_{e_3} such blocks resulting from interactions between n_{e_3} columns of finite elements.

b) Two adjacent block matrices [A] share a common portion being a tridiagonal submatrix of size $(n_r n_v \times n_r n_v)$ such as A_{33}, A_{55}... A_{n_z-2, n_z-2}.

c) Such a block matrix [A] (Figure 3.9), contains five square block submatrices and four rectangular resulting from interactions between nodal variables in columns of nodes (Figure 3.2).

d) Each such a square or rectangular block submatrix as $[A_{11}]$, $[A_{12}]$, $[A_{22}]$..., in turn, contains overlapping square or rectangular diagonal blocks resulting from interactions between nodal variables in adjacent elements in one column. There are n_{e_1} such minor blocks resulting from interactions in one column of n_{e_1} elements.

A similar assembly procedure is applied for the duct-wall boundary condition over the line elements on C_3 and the boundary element matrix is also assembled into the global matrix [K] as for interior elements.

To illustrate how the diagonal pattern of the system matrix [K] evolves from isoparametric rectangular 8-node element discretization one can examine the interactions of nodal values in a simple 2x2 element mesh with a single dependent variable u at each node in Figure 3.10.

Note that non-zero coefficients in the system matrix [K] are due to the interactions of nodal values u_i at

a) nodes 1,2,6,9,10 with those at 1,2,3,6,7,9,10,11 in element (1)

b) nodes 4,5,8,12,13 with those at 3,4,5,7,8,11,12,13 in element (2)

c) shared nodes 3,7,11 with those at all the nodes in elements (1) and (2), resulting in non-zero coefficients at the centres of 9 square or rectangular blocks in [K] as shown.

d) In the system matrix the four square blocks of size 5x5 (n_r=5)

are resulting from interactions in the 1st. and 3rd. columns of nodes with themselves, the smaller square blocks of size 3x3 ($n_{rm} = 3$) from those in the 2nd. column of nodes with itself, the 4 rectangular blocks of sizes 5x3 or 3x5 from those in the 2nd. column of nodes with those in the 1st. or 3rd. columns.

(ii) Packing and Solution Technique

The global matrix [K] is a large sparse complex matrix containing $(n_n x n_v)^2$ coefficient points. For instance, for a 5x5 finite element mesh in flow-case problems the order is over 100,000 points. As a result, in practical programming implementations for our preliminary study the matrix [K] is packed and only the diagonal portion as shown in Figure 3.8 is stored in direct-access memory of a digital computer in the form of one-dimensional array, using mapping functions. The blocks $\square$ of size $(n_v x n_v)$ of [K] in Figure 3.9 are assumed to be fully occupied.

In the case for a 5x5 finite element mesh and $n_v = 4$ the size of such an array is of order of more than 65,535 complex elements. But the portion of [K] which is actually stored still contains a large number of zero coefficients occupying the core memory during the solution processing. Consequently, an algorithm has been developed [Appendix E] to solve the system of linear equations arising from the flow-case problem, using the L-U decomposition method [95] and optimizing the required storage by incorporating the solution procedure into the FEM assembling stage.

However, to establish the system of linear equations to be solved the matching at the ends of the nonuniformity is to be considered (see Section 2.1.2(ii)). A matching procedure will give rise to extra equations containing propagation coefficients in the uniform semi-infinite duct sections. These equations represent the interactions between the solutions at the interfaces and the end boundary conditions, thereby involving, on global assembly, only the nodal values of dependent variables on the appropriate boundary.

For the purpose of description, suppose here the least-square matching is considered just over the interface at z = 0. In Figure 3.2 only the nodes numbered 1,2,4,5,6,7, are concerned. Detailed formulation will be presented in specific problems. Thus, one can obtain a system of linear equations with a multiple load vector in the general form :

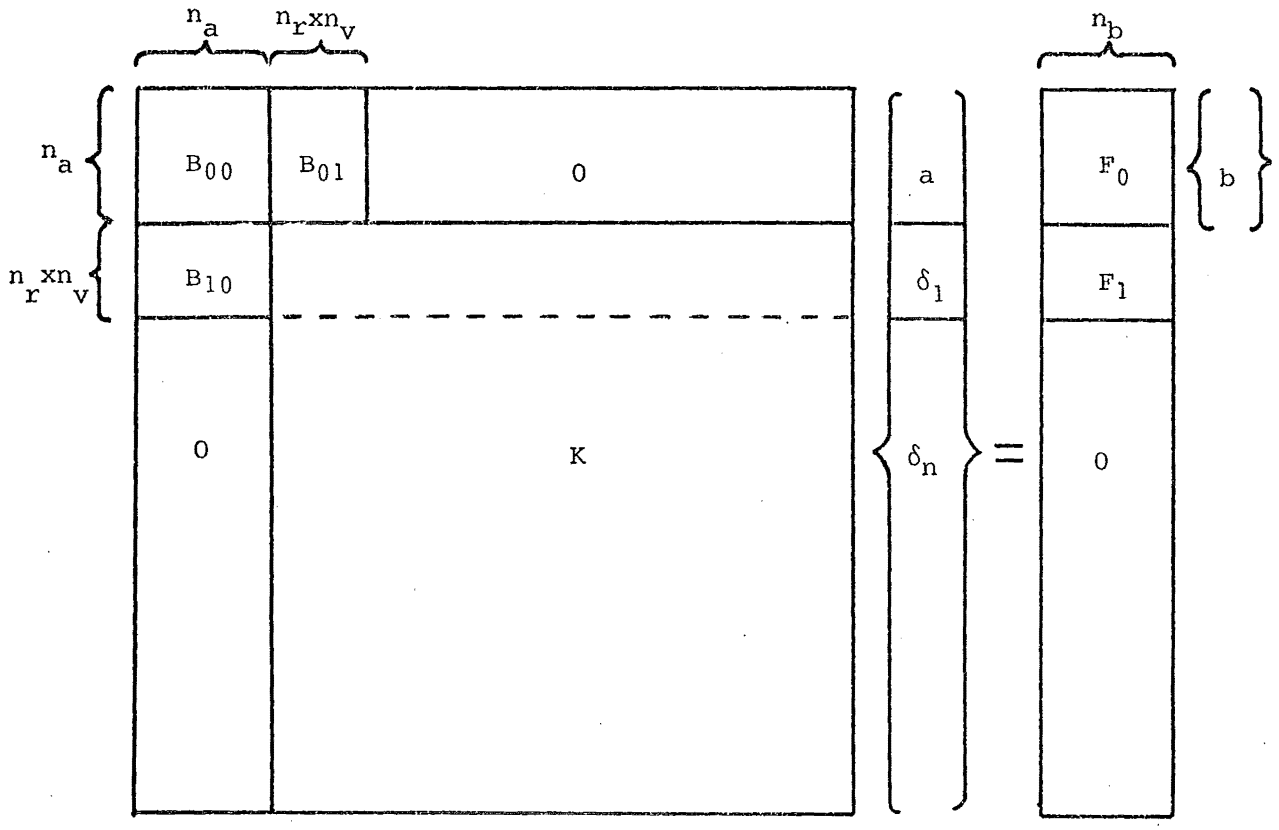

where

a) {a},{b} are propagation coefficients, (n_a coefficients a are to be determined in terms of n_b coefficients b.

b) Submatrices $[B_{00}],[B_{01}],[B_{10}],[F_0],[F_1]$ are full matrices derived from end matching with sizes as shown above.

c) $\{\delta\} = \lceil \delta_1 \,\vdots\, \delta_n \rfloor^T$, $\{\delta_1\}$ is a column vector containing nodal values of dependent variables at nodes on C_1 (Figure 3.2).

So, to preserve the system matrix, when matching submatrices added, in the diagonal pattern with the same band-width as for [K] n_a must be

such that :

$$n_r \times n_v + n_a \leq n_w$$

where n_w is the band-width of [K], which can be calculated. In practical programming this condition is usually satisfied. From Figure 3.9.

$$n_w = (n_r + n_{rm} + 3)\, x n_v$$

Hence, finally the system of simultaneous linear equations in a general form :

$$[C]\ \{X\} = \{F\}$$

where [C] is a complex matrix, is to be solved for each load vector of {F}. In such a large system derived from FEM formulations the Gaussian elimination is of advantage over iteration methods such as Gauss-Seidel Gauss-Jordan on the grounds of convergence. Furthermore, the multiple load vector renders the Gaussian elimination the most suitable direct method (of which the L-U decomposition method is one form) since all the load vectors are economically taken into account implicitly in the elimination process without repeating the same procedure for each load vector at a time.

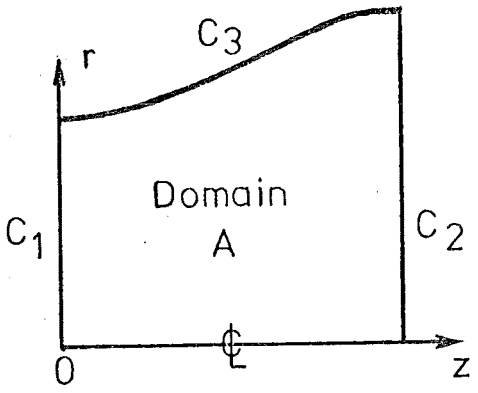

$$C = C_1 + C_2 + C_3$$

FIG. 3.6 REDUCED DOMAIN AND BOUNDARIES FOR AXISYMMETRIC DUCTS

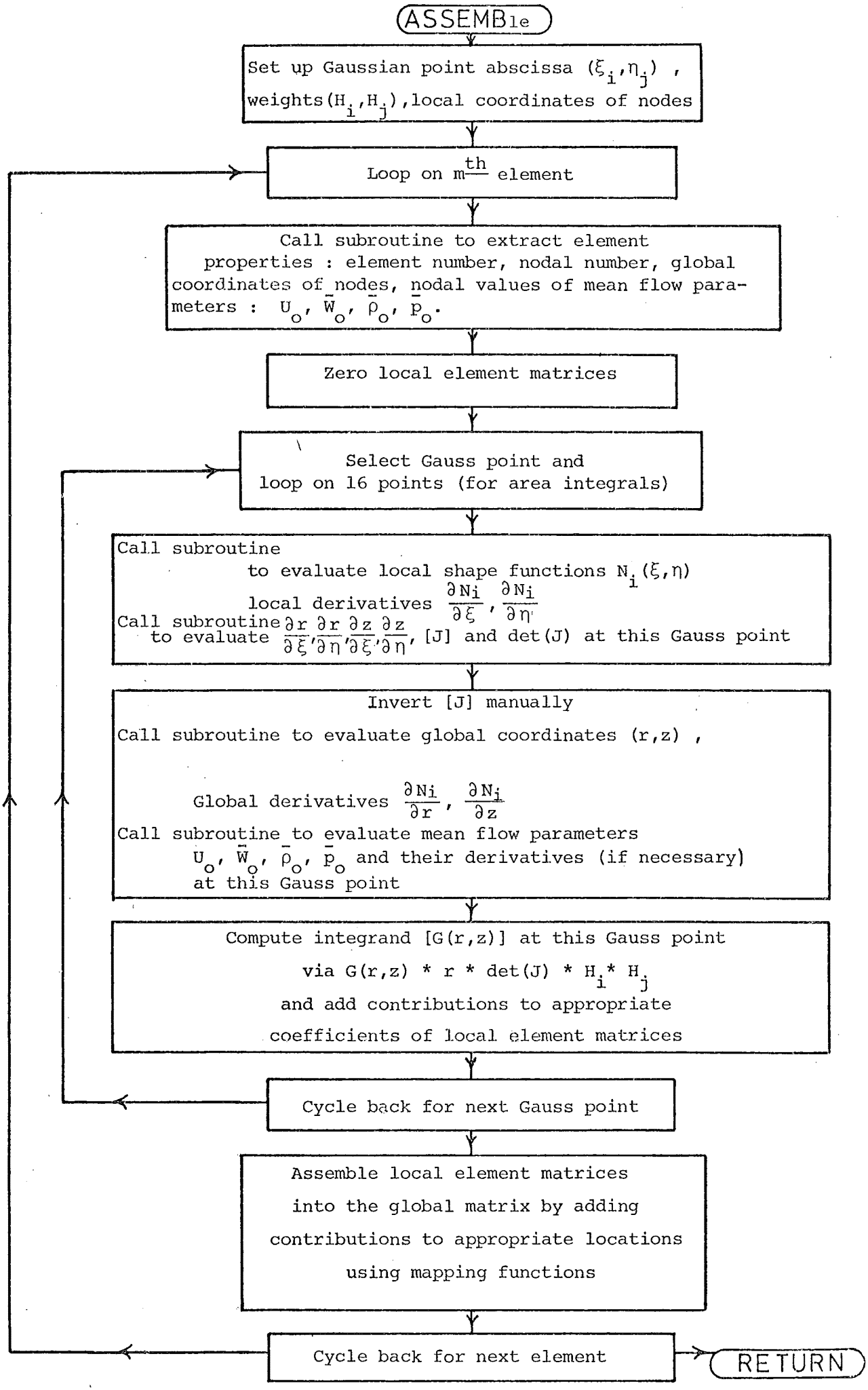

FIG. 3.7 LOGIC DIAGRAM FOR EVALUATION OF INTEGRALS IN FEM FORMULATION

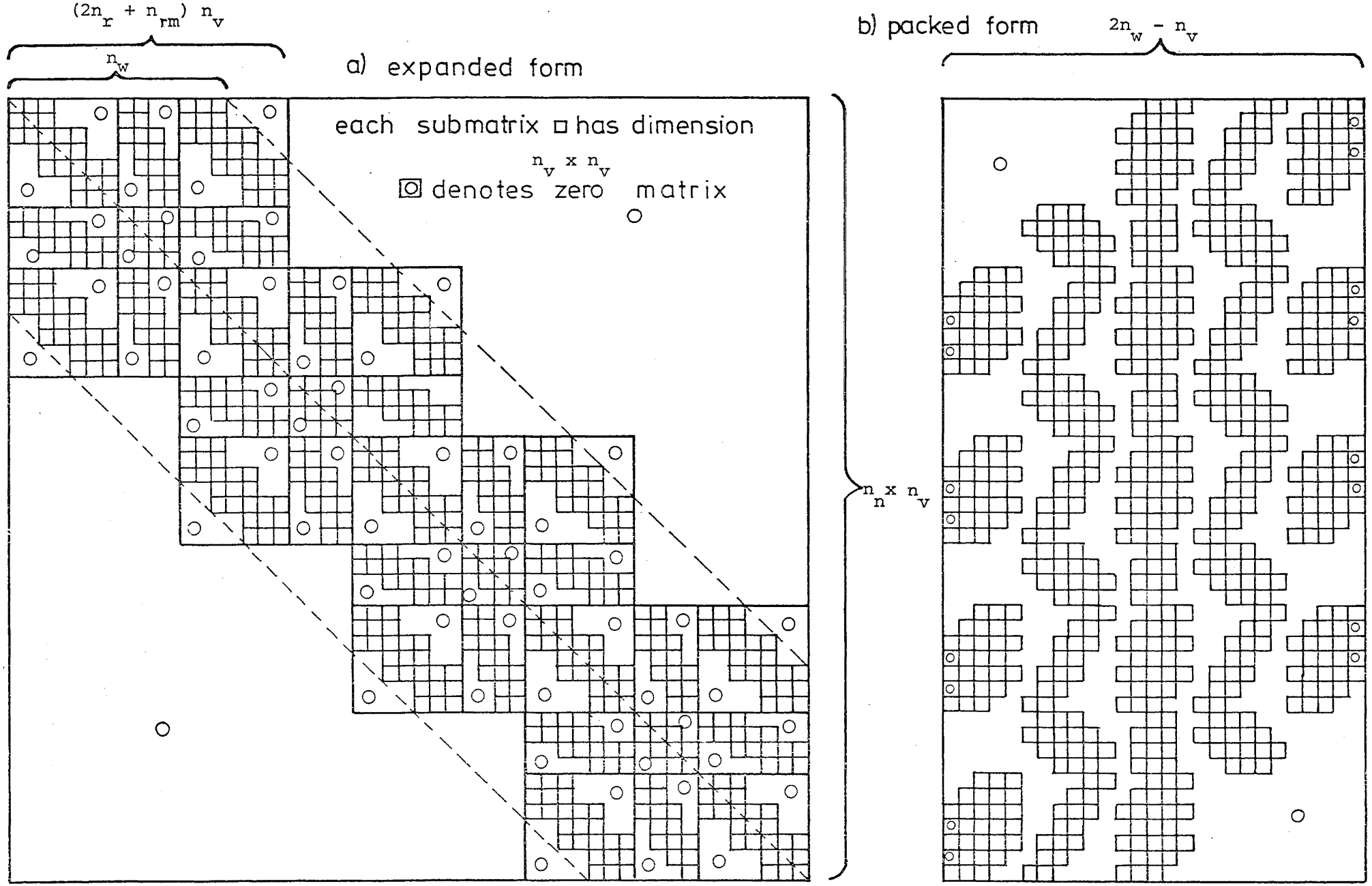

FIG. 3·8 GLOBAL MATRIX MAP FOR 3×4-ELEMENT DISCRETIZATION

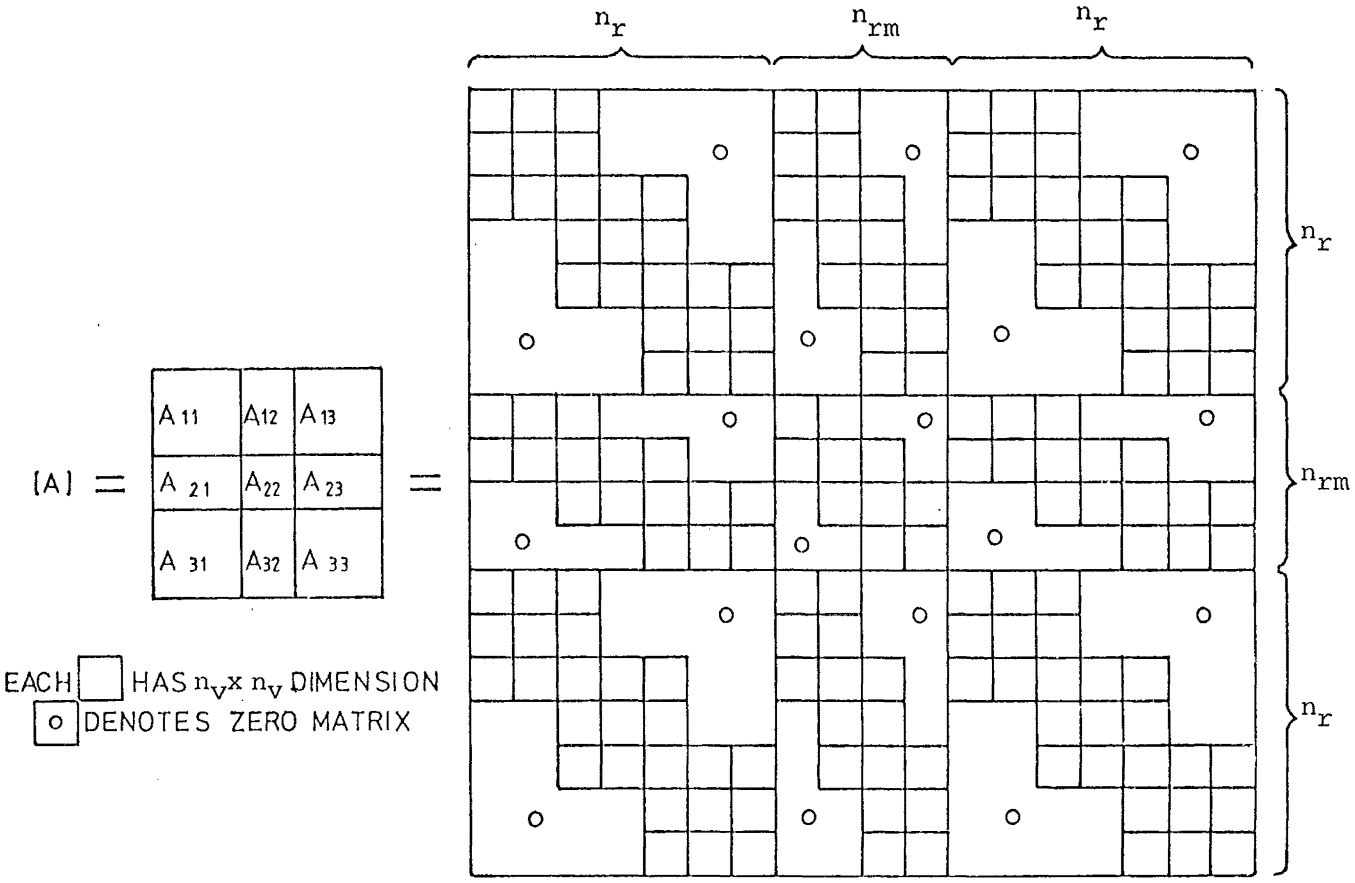

FIG. 3·9 STRUCTURE OF SUBMATRICES [A] IN THE GLOBAL MATRIX

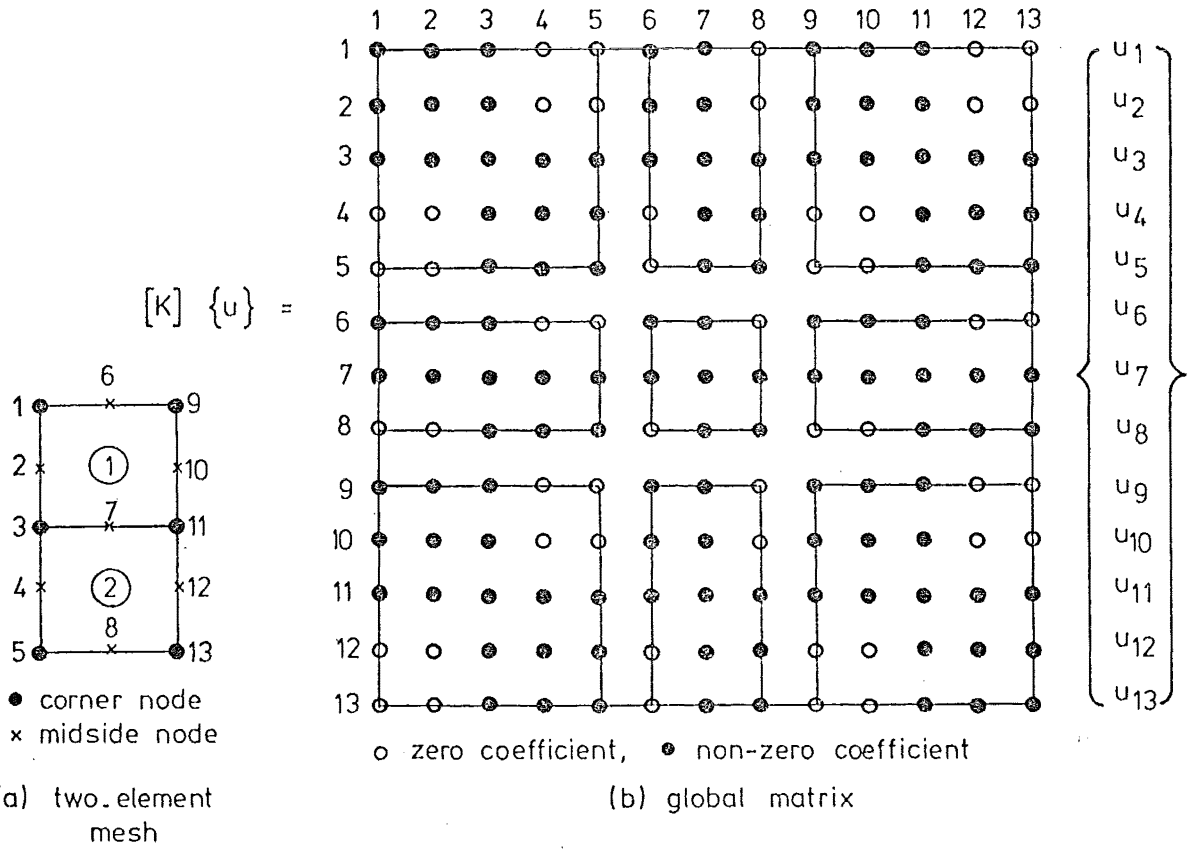

FIG. 3·10 GLOBAL MATRIX FOR 2-ELEMENT MESH WITH ONE NODAL VARIABLE

CHAPTER 4

SOUND TRANSMISSION IN UNIFORM FLOW DUCTS

The problem of sound transmission in uniform ducts with a uniform or sheared flow profile has been thoroughly investigated in the literature (see Chapter 1). The Runge-Kutta integration and Galerkin approximations have been the most successful approaches. To generate confidence in MWR and FEM in nonuniform duct problems, the sound transmission in the uniform flow case, which reduces to an eigenproblem, is solved by MWR and FEM. The convergence trend is established and results are compared on the basis of the Runge-Kutta values.

4.1 MATHEMATICAL MODEL AND GOVERNING EQUATIONS

For the semi-infinite circular duct of radius R shown in Figure 4.1 flow at velocity $\bar{W}_o$, uniform on the cross-section is assumed to exist. The wall is hard or soft with a known admittance. It is assumed the sound source is of discrete tone characteristic at frequency ω rad/s, If a harmonic dependence displaying standing waves in the radial and angular directions of the duct and progressive waves along the positive z axis takes the form of $e^{i\omega t} \cdot e^{-im_o\theta}$ one can write the governing equations in two ways :

(i) Convected wave equations

From Appendix C if the uniform mean flow field is also the reference state one can write

$$\frac{\partial^2 p}{\partial r^2} + \frac{1}{r}\frac{\partial p}{\partial r} + \left(k^2 - \frac{m_o^2}{r^2}\right) p - 2ik\, M_o \frac{\partial p}{\partial z} + \left(1 - M_o^2\right) \frac{\partial^2 p}{\partial z^2} = 0 \quad (4.1.1)$$

With the boundary condition for uniform flow :

$$ikA \left(p - 2i \frac{M_o}{k} \frac{\partial p}{\partial z} - \frac{M_o^2}{k^2} \frac{\partial p^2}{\partial z^2}\right) = - \frac{\partial p}{\partial r} \text{ at } r = R \quad (4.1.2)$$

where A is the specific admittance, $k = \frac{\omega}{c}$, $M_o = \bar{W}_o$ and c is the speed of sound in the mean flow medium.

(ii) Conservation equations

If the nondimensionalization in Section 2.2 is still applied to the uniform geometry the conservation equations can be written in nondimensional variables referred to a reference state. Thus, the general governing acoustic equations (2.4.1) - (2.4.5) become :

$$ik_r u + \bar{W}_o \frac{\partial u}{\partial z} + \frac{1}{\bar{\rho}_o} \frac{\partial p}{\partial r} = 0 \qquad (4.1.3)$$

$$ik_r v + \bar{W}_o \frac{\partial v}{\partial z} - \frac{im_o}{\bar{\rho}_o} \frac{p}{r} = 0 \qquad (4.1.4)$$

$$ik_r w + \bar{W}_o \frac{\partial w}{\partial z} + \frac{1}{\bar{\rho}_o} \frac{\partial p}{\partial z} = 0 \qquad (4.1.5)$$

$$ik_r p + \bar{W}_o \frac{\partial p}{\partial z} + \gamma \bar{p}_o \left[\frac{1}{r} \frac{\partial}{\partial r} (ru) - im_o \frac{v}{r} + \frac{\partial w}{\partial z} \right] = 0 \qquad (4.1.6)$$

and the boundary condition :

$$\underline{V} \cdot \underline{\nu} = u = Ap - \frac{i\bar{W}_o}{k_r} \frac{\partial}{\partial z} (Ap) \quad \text{at } r = R \qquad (4.1.7)$$

4.2 METHOD OF SOLUTION: MWR

4.2.1 Formulation with Convected Wave Equation

In the Modified Galerkin Method the solution is sought in the form of a finite series :

$$p(r,z) \approx p_N = \sum_{m=1}^{N} p_m(z) \, \psi_m(r) \qquad (4.2.1)$$

$\psi_m(r)$, m = 1,2...N are specified basis functions being member of a complete set of functions. The basis functions, as in a mixed method, do not necessarily satisfy either the differential equation or the boundary condition. By substituting the assumed solution (4.2.1) into equations (4.1.1) and (4.1.2) one, in general, obtains the residuals :

$$R_1 = \frac{\partial^2 p_N}{\partial r^2} + \frac{1}{r} \frac{\partial p_N}{\partial r} + \left(k^2 - \frac{m_o^2}{r^2} \right) p - 2ik M_o \frac{\partial p_N}{\partial z} + (1-M_o^2) \frac{\partial^2 p_N}{\partial z^2} \qquad (4.2.2)$$

$$R_2 = ikA\left[p_N - 2i\frac{M_o}{k}\frac{\partial p_N}{\partial z} - \frac{M_o^2}{k^2}\frac{\partial^2 p_N}{\partial z^2}\right] + \frac{\partial p_N}{\partial r} \text{ at } r = R \qquad (4.2.3)$$

As in the standard Galerkin minimization process these residuals are forced to be orthogonal to each member of the complete set formed by $\psi_m(r)$. For practical interest this set is truncated to N functions to give :

$$\int_0^R W_1 R_1 \psi_n(r) 2\pi r\, dr = 0 \qquad (4.2.4)$$

$$R_2 \psi_n(R) = 0 \qquad (4.2.5)$$

for n = 1,2,...N

The weighting factor $W_1 = r$ is used in equation (4.2.4) tc avcid singularity in analytical integrations. Utilizing the Leibnitz rule of differentiation to replace partial derivatives with respect to z by ordinary derivatives and integration by parts to expose boundary terms which, in turn, can be replaced by the boundary residual equation (4.2.5) one can reduce equation (4.2.4) in the form :

$$\sum_{m=1}^{N}\left[(1-M_o^2)\int_0^R r^2\psi_m(r)\psi_n(r)dr + \frac{i}{k}M_o^2 AR^2\psi_m(R)\psi_n(R)\right]\frac{d^2p_m}{dz^2}$$

$$-\sum_{m-1}^{N}\left[2ik\,M_o\int_0^R r^2\psi_m(r)\psi_n(r)dr + 2\,M_o\,AR^2\psi_m(R)\psi_n(R)\right]\frac{dp_m}{dz}$$

$$+\sum_{m=1}^{N}\left[\int_0^R \psi_m(r)\frac{\partial}{\partial r}\left(r^2\frac{\partial}{\partial r}\psi_n(r)\right)dr + \int_0^R \psi_m(r)\frac{\partial}{\partial r}\left(r\frac{\partial\psi_n(r)}{\partial r}\right)dr\right.$$

$$+ k^2\int_0^R r^2\psi_m(r)\psi_n(r)dr - m_o^2\int_0^R \psi_m(r)\psi_n(r)dr$$

$$\left. - (ik\,AR + 1)R\,\psi_m(R)\psi_n(R) - R^2\,\psi_m(R)\frac{\partial}{\partial r}\psi_n(R)\right]p_m = 0 \qquad (4.2.6)$$

for n = 1,2,...N

To demonstrate the method to calculate axial wave numbers an algebraic eigenvalue problem can be established by noting that the admittance A is constant in the uniform infinitely long duct. In that case the z dependence in the solution can be eliminated by taking :

$$p_m(z) = q_m \, e^{-ik_z z} \tag{4.2.7}$$

where q_m are constant , m = 1,2,...N

With equation (4.2.7) substituted into equation (4.2.6) one can write the resultant in matrix form with nondimensional terms, dividing the whole set by R, as follows :

$$\left\{ \underset{NxN}{[\ B\ ]}K^2 + \underset{NxN}{[\ C\ ]}K + \underset{NxN}{[\ D\ ]} \right\} \underset{Nx1}{\{q_m\}} = 0 \ , \ K = \frac{k_z}{k} \tag{4.2.8}$$

where

$$B_{nm} = -\frac{k^2}{R}(1-M_o^2)\int_0^R r^2\psi_m(r)\psi_n(r)dr - ikR\,M_o^2\,A\,\psi_m(R)\psi_n(R)$$

$$C_{nm} = -2\frac{k^2}{R}M_o\int_0^R r^2\psi_m(r)\psi_n(r)dr + 2ik\,RM_o\,A\,\psi_m(R)\psi_n(R)$$

$$D_{nm} = \frac{1}{R}\int_0^R \psi_m(R)\ \frac{\partial}{\partial r}\left(r^2\ \frac{\partial\psi_n(r)}{\partial r}\right)dr + \frac{1}{R}\int_0^R \psi_m(r)\ \frac{\partial}{\partial r}\left(r\psi_n(r)\right)dr$$

$$+ \frac{k^2}{R}\int_0^R r^2\psi_m(r)\psi_n(r)dr - \frac{m_o^2}{R}\int_0^R \psi_m(r)\ \psi_n(r)\ dr$$

$$- R\,\psi_m(R)\ \frac{\partial}{\partial r}\ \psi_n(R) - (ikAR+1)\ \psi_m(R)\ \psi_n(R) \tag{4.2.9}$$

Equation (4.2.8) is multiplied by $[B]^{-1}$ and restructured with the change of variables :

$$\{x_1\} = \{q_m\} \ , \ \{x_2\} = K\{q_m\}$$

The result gives the eigenvalue problem of the partitioned matrix :

$$\begin{bmatrix} 0 & I \\ \hline -\bar{D} & -\bar{C} \end{bmatrix} \begin{Bmatrix} x_1 \\ \hline x_2 \end{Bmatrix} = K \begin{Bmatrix} x_1 \\ \hline x_2 \end{Bmatrix} \qquad (4.2.10)$$

$2N \times 2N \quad 2N\times 1 \quad 2N\times 1$

where I is the identity matrix and

$$[\bar{C}] = [B]^{-1}[C]$$

$$[\bar{D}] = [B]^{-1}[D]$$

4.2.2 Formulation with Conservation Equations

In this formulation, the solutions of the equations (4.1.3) - (4.1.7) are sought in the form :

$$p(r,z) \approx p_N = \sum_{m=1}^{N} p_m(z)\psi_m(r) \qquad (4.2.11)$$

$$u(r,z) \approx u_N = \sum_{m=1}^{N} u_m(z)\phi_m(r) \qquad (4.2.12)$$

$$v(r,z) \approx v_N = \sum_{m=1}^{N} v_m(z)\psi_m(r) \qquad (4.2.13)$$

$$w(r,z) \approx w_N = \sum_{m=1}^{N} w_m(z)\psi_m(r) \qquad (4.2.14)$$

When equations (4.2.11) - (4.2.14) are substituted into equations (4.1.3) - (4.1.7) the following residuals are obtained :

$$R_1 = ik_r u_N + \bar{W}_o \frac{\partial u_N}{\partial z} + \frac{1}{\bar{\rho}_o} \frac{\partial p_N}{\partial r} \qquad (4.2.15)$$

$$R_2 = ik_r v_N + \bar{W}_o \frac{\partial v_N}{\partial z} - \frac{im_o}{\bar{\rho}_o} \frac{p_N}{r} \qquad (4.2.16)$$

$$R_3 = ik_r w_N + \bar{W}_o \frac{\partial w_N}{\partial z} + \frac{1}{\bar{\rho}_o} \frac{\partial p_N}{\partial z} \qquad (4.2.17)$$

$$R_4 = ik_r p_N + \bar{W}_o \frac{\partial p_N}{\partial z} + \gamma \bar{p}_o \left[\frac{1}{r} \frac{\partial (ru_N)}{\partial r} - im_o \frac{v_N}{r} + \frac{\partial w_N}{\partial z}\right] \qquad (4.2.18)$$

$$R_B = u_N - Ap + \frac{i\bar{W}_o}{k_r} \frac{\partial}{\partial z} (Ap_N) \qquad (4.2.19)$$

And the orthogonality of the residuals to $\psi_n(r)$ over the cross-section gives the residual equations :

$$\int_0^R W_1 \psi_n \, R_1 \, 2\pi r \, dr = 0 \tag{4.2.20}$$

$$\int_0^R W_2 \psi_n \, R_2 \, 2\pi r \, dr = 0 \tag{4.2.21}$$

$$\int_0^R W_3 \psi_n \, R_3 \, 2\pi r \, dr = 0 \tag{4.2.22}$$

$$\int_0^R W_4 \psi_n \, R_4 \, 2\pi r \, dr = 0 \tag{4.2.23}$$

$$R_B \psi_n(R) = 0 \quad \text{at } r = R \tag{4.2.24}$$

for $n = 1,2,\ldots N$.

where W_1, W_2, W_3, W_4 are weighting factors, which may be functions of r. In this formulation the weighting factors are taken as follows :

$$W_1 = 1, \; W_2 = 1, \; W_3 = 1, \; W_4 = r$$

The significance of this choice will be discussed in Section 4.2.5. Now the same steps are repeated as outlined for the formulation with the convected wave equation (Section 4.2.1) to obtain four sets of N equations in the matrix form as follows :

$$\underset{4N \times 4N}{\begin{bmatrix} DP^p & DP^w & 0 & 0 \\ DW^p & DW^w & 0 & 0 \\ 0 & 0 & DU^u & 0 \\ 0 & 0 & 0 & DV^v \end{bmatrix}} \underset{4Nx1}{\frac{d}{dz}\begin{Bmatrix} p_m \\ w_m \\ u_m \\ v_m \end{Bmatrix}} = \underset{4N \times 4N}{\begin{bmatrix} P^p & 0 & P^u & P^v \\ 0 & W^w & 0 & 0 \\ U^p & 0 & U^u & 0 \\ V^p & 0 & 0 & V^v \end{bmatrix}} \underset{4Nx1}{\begin{Bmatrix} p_m \\ w_m \\ u_m \\ v_m \end{Bmatrix}} \tag{4.2.25}$$

where

$$DP^p_{nm} = \bar{W}_o \, L_{nm} - \gamma \bar{p}_o \frac{i}{k_r} \frac{A}{\cos\alpha} \bar{W}_o \, R^2 \, \psi_m(R)\psi_n(R)$$

$$DP^w_{nm} = \gamma \bar{p}_o \, L_{nm}$$

$$P^p_{nm} = - ik_r \, L_{nm} - \gamma \bar{p}_o \frac{AR^2}{\cos\alpha} \, \psi_m(R)\psi_n(R)$$

$$P^{u}_{nm} = \gamma \bar{p}_o \left[M'_{nm} + \int_0^R r^2 \, \phi_m(r) \, \frac{\partial \psi_n(r)}{\partial r} \, dr \right]$$

$$P^{v}_{nm} = \gamma \bar{p}_o \, im_o \, M_{nm}$$

$$DW^{p}_{nm} = \frac{1}{\bar{\rho}_o} \, M_{nm}$$

$$DW^{w}_{nm} = \bar{W}_o \, M_{nm}$$

$$W^{w}_{nm} = - ik_r \, M_{nm}$$

$$DU^{u}_{nm} = \bar{W}_o \, M'_{nm}$$

$$U^{p}_{nm} = - \frac{1}{\bar{\rho}_o} R \, \psi_m(R)\psi_n(R) + \frac{1}{\bar{\rho}_o} \, N_{nm} + \frac{1}{\bar{\rho}_o} \int_0^R r\psi_m(r) \, \frac{\partial \psi_n(r)}{\partial r} \, dr$$

$$U^{u}_{nm} = - ik_r \, M'_{nm}$$

$$DV^{v}_{nm} = \bar{W}_o \, M_{nm}$$

$$V^{p}_{nm} = \frac{im_o}{\bar{\rho}_o} N_{nm}$$

$$V^{v}_{nm} = - ik_r \, M_{nm}$$

for (m=1,2,...N) and (n=1,2...N)

with definitions :

$$N_{nm} = \int_0^R \psi_m(r)\psi_n(r) \, dr$$

$$M_{nm} = \int_0^R r\psi_m(r)\psi_n(r) \, dr$$

$$L_{nm} = \int_0^R r^2\psi_m(r)\psi_n(r) \, dr$$

$$M'_{nm} = \int_0^R r\phi_m(r)\psi_n(r) \, dr$$

Now, in equation (4.2.25) if the solutions of p_m, w_m, u_m and v_m are assumed to have the harmonic dependence $e^{-ik_z z}$, the matrix equation (4.2.25) can be written in another form to yield an eigenvalue problem as follows :

$$\underset{4Nx4N}{[\mathcal{M}]} \quad \frac{k_z}{k_r} \underset{4Nx1}{\begin{Bmatrix} p_m \\ w_m \\ u_m \\ v_m \end{Bmatrix}} = \underset{4Nx4N}{[\mathcal{N}]} \underset{4Nx1}{\begin{Bmatrix} p_m \\ w_m \\ u_m \\ v_m \end{Bmatrix}}$$

or

$$\underset{4Nx4N}{[\mathcal{L}]} \underset{4Nx\,1}{\begin{Bmatrix} p_m \\ w_m \\ u_m \\ v_m \end{Bmatrix}} = K \underset{4Nx1}{\begin{Bmatrix} p_m \\ w_m \\ u_m \\ v_m \end{Bmatrix}} \tag{4.2.26}$$

where $[\mathcal{L}] = [\mathcal{M}]^{-1} [\mathcal{N}]$, $K = \frac{k_z}{k_r}$, k_z is the axial wave number and matrices $[\mathcal{M}]$ and $[\mathcal{N}]$ can be deduced from the components of equation (4.2.25).

4.2.3 Choice of Basis Functions

(i) Basis functions

The basis functions to be employed in the formulations yielding equations (4.2.10) and (4.2.26) are as yet unspecified. The most obvious choices are the Bessel functions $J_{m_o}(\kappa_n r)$ derived from a suitable uniform duct problem (Appendix C). In the formulations of equations (4.2.10) and (4.2.26) the use of these functions is not a severe problem because the coefficients of [B], [C] and [D] or $[\mathcal{M}]$ and $[\mathcal{N}]$ need be calculated only once for each case and the required integrations by numerical quadratures does not represent a major proportion of the computational time. However, the final goal of the research programme is to use MWR for nonuniform ducts. The solution scheme in this case requires a numerical integration axially and coefficient matrices must be computed a number of times depending on the number of integration steps (see Section 3.1.4). In this situation the generation of Bessel functions and the required integrals represents nearly the entire time requirement. If the Bessel functions are used as basis functions the MWR approach is not practical and economical

for axisymmetric ducts. In order to circumvent this problem, trigonometric functions have been experimented with in the form :

$$\psi_m(r) = \cos \kappa_m r \quad , \quad \phi_m(r) = \sin(\kappa_m r) \tag{4.2.27}$$

where κ_m are transverse eigenvalues for a uniform 2D duct of half height R (Appendix C). The use of basis functions of this type in the uniform duct case represented by the eigenvalue problem serves to establish the usefulness of the MWR approach in the nonuniform case. The routine use of the trigonometric functions in the uniform case may prove to be of only marginal benefit as the potential efficiency increment is minimal. In fact, for uniform ducts without flow the use of Bessel functions produces a trivial problem, as the Bessel functions are the exact solution. The same could be also true when flow is present if both positive and negative propagating modes are used. Furthermore the representation of solution in circular ducts by trigonometric functions represents a new experiment with the MWR as a mixed method. In 2D nonuniform ducts the basis functions employed in MWR are the eigenfunctions derived from a closely related problem, being the solutions in 2D uniform ducts. For axisymmetric nonuniform ducts the same type of basis functions is still used, however, the success of MWR in the 2D case does not guarantee convergence to solutions without further numerical experiments.

As the basis functions play an important role in MWR the eigenvalue problem serves as the first step to establish types of functions to be used subsequently in nonuniform duct problems.

In the eigenvalue problem for axisymmetric ducts the basis functions following are used in numerical experiments.

a) No-flow case :

$$\psi_m(r) = \cos(\kappa_m r)$$

where κ_m are roots of the eigen-equation

$$K_m R \tan K_m R = ikRA \qquad (4.2.28)$$

corresponding to symmetric modes in 2D ducts of half height R,

for A = 0 , $\qquad K_m R = (m-1)\pi$

or in the terms of anti-symmetric modes

$$\psi_m(r) = \sin(K_m R)$$

where $K_m R \text{ cotan } (K_m R) = -iAkR \qquad (4.2.29)$

for A = 0 , $\qquad K_m R = (m-1)\frac{\pi}{2}$

b) Flow case.

For the hardwall case the same eigenfunctions are obtained as in the no-flow case. But in the softwall case it is complicated by the fact that in the 2D flow duct, corresponding to N negative propagating nodes there are N positive ones of the same degree of significance. Thereby the dimensionality of the problem increases considerably with little improvement. In our preliminary study the no-flow basis functions given by (4.2.28) are still experimented with for the flow case.

c) Modified flow basis functions.

In reference [64] it was found that for two-dimensional ducts when flow is present and the wall admittance is not near zero, it is advantageous at low frequencies to use a modified set of basis functions with the values of $K_m R$ derived from the eigen-equation

$$KR \tan KR = ikRA \left[1 - \frac{M_o^2}{1-M_o^2} \left(\frac{KR}{kR}\right)^2 \right] \qquad (4.2.30)$$

This does not correspond to any physically meaningful problem but was arrived at by taking the high limit KR of the exact eigenvalue equation for the case when flow is present (Appendix C).

$$\left.\begin{aligned} KR \tan KR &= ikRA \left(1 - \frac{k_z}{k} M_o\right)^2 \\ \frac{k_z}{k} &= \frac{1}{1-M_o^2} \left\{ - M_o \pm \left[1 - (1-M_o^2)\left(\frac{KR}{kR}\right)^2 \right]^{\frac{1}{2}} \right\} \end{aligned}\right\} \qquad (4.2.31)$$

when kR is small the eigenvalues $\kappa_m R$ from equation (4.2.28) very rapidly approach the hardwall results for increasing m, even though $A \neq 0$. If equation (4.2.30) is used the proper high limit of $\kappa_m R$ is approached and this has implications in achieving rapid convergence. In 2-D ducts this approach has been proven useful for low kR ($kR \approx 1$) but does not offer any advantage at significantly higher frequencies. This type of basis functions is also adopted for numerical experiments in the present investigation.

(ii) Generating basis functions.

In application of MWR to nonuniform duct problems later the potential disadvantage of the solution method is the need to compute the eigenvalues of transcendental equations such as equations (4.2.28),(4.2.29),(4.2.30). These roots appear in the basis functions and hence in the coefficients of matrices in the form of equation (3.1.9). Thus, for a numerical integration scheme to solve for the transition matrix (3.1.10) the eigenvalues are to be generated at each station along the axial direction. If 5 to 10 basis functions are sufficient to obtain solutions converged for the purpose then 5 to 10 eigenvalues are required at each integration step.

The usual technique for obtaining the eigenvalues in 2D uniform ducts is a Newton-Raphson iteration based on suitable guesses. The iterative scheme is likely to be too costly computationally to be of practical value. Eversman [96,97] in his study of 2-D duct problems designed an integration scheme to compute the eigenvalues rapidly by changing transcendental equations into an initial value problem involving a non-linear ordinary differential equation [Appendix D]. This procedure is adopted in the study of axisymmetric ducts without any modification.

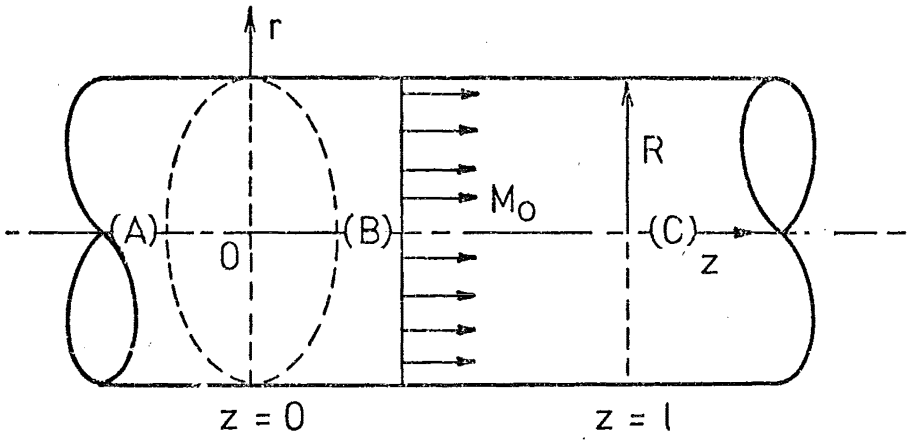

FIG. 4·1 UNIFORM DUCT WITH UNIFORM FLOW PROFILE

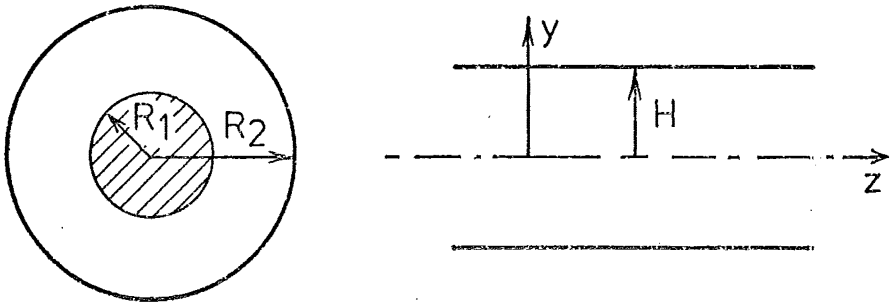

(a) annular (b) 2-D

FIG. 4·2 DUCT GEOMETRY FOR DERIVATION OF BASIS FUNCTIONS

4.2.4 Numerical Results and Discussions

The eigenproblem of equation (4.2.26) was solved by using a QR routine to obtain complex eigenvalues and eigenvectors of matrices of complex elements. A number of cases were treated and the results were compared with "exact" solutions. For a hardwalled duct the "exact" results are obtained from published tabular solutions [98] of the exact eigenvalue equation [Appendix C]. For comparison in a soft-walled duct with or without flow the "exact" solution was obtained by the Runge-Kutta integration scheme [Appendix D]. The comparisons show that the axial wave numbers in a uniform circular duct can be computed to within useful accuracy by MWR with trigonometric basis functions.

(i) No-flow case.

In our preliminary study the original formulation with convected wave equations by MWR of the eigenvalue problem was applied to a general axisymmetric duct, that is, an annular duct which can reduce to a circular duct of the radius equal to the outer radius of the annular geometry. The problem of circular ducts is considered more severe than the similar problem in annular geometry for the tendency of singularities due to the solutions representation at the duct axis ($r = 0$). Results obtained for hardwalled ducts showed that this is the case. An annular duct of a smaller inner radius yields a slower convergence of solutions. This trend is expected since physically the wave propagation in an annular geometry, as the annular ring becomes thinner, becomes closer to that of the rectangular duct with which the basis functions employed are associated. The study also showed that better results are obtained when, in deriving the trigonometric basis functions, one considers the annular domain as being analogous to a half of a 2-D channel. That is, in Figure 4.2, it is such that $H = R_2 - R_1$. So, when the inner boundary of the annular geometry shrinks to become the centre line of a reduced circular geometry it is

equivalent to a hardwalled centre line as in the 2D case. The agreement of results for hardwalled circular ducts generates confidence to establish the MWR with trigonometric functions further in eigenvalue problems for circular geometry.

a) $\cos(K_m r)$.

In hardwalled circular ducts with no flow the results of Table 4.1 with basis functions being cosine functions given by equation (4.2.28) shows that the convergence is definite, and useful results can be obtained in this low frequency case with as few as three basis functions. The same conclusion can be drawn from Table 4.2 for the soft-wall case. In both of these cases the cosine functions used as basis functions individually satisfy the duct-wall boundary condition but are not exact solutions to the problem (Bessel functions are the exact solutions).

For Tables 4.1 and 4.2 it is also noted that for $m_o = 0$ the cosine functions satisfy the hardwall natural boundary condition at the centre line, i.e. $\frac{dp}{dr}\Big|_{r=0} = 0$ and the forced condition $p(r=0) = 1$. For $m_o \neq 0$ one or both of these conditions are violated. This leads to explore other types of basis functions for possible improvement.

b) $\mathrm{Sin}(K_m r)$ and $1 - \cos(K_m r)$.

For anti-symmetric modes $m_o \neq 0$, the set of functions $\sin K_m r$ derived from equation (4.2.29) satisfies both of the boundary conditions : at duct centre line and at duct wall. The functions $(1 - \cos K_m r)$ can be forced to satisfy the duct-wall boundary condition (4.1.2), with $M_o = 0$:

$$\frac{dp}{dr} = - ikAp \quad \text{at } r = R$$

then $$\sin K_m R = - ikA\,(1 - \cos K_m R)$$

or $$\tan K_m R = ikA\,(1 - \sec K_m R) \qquad (4.2.32)$$

Hence, the set of functions $(1 - \cos K_m r)$ with K_m being derived from equation (4.2.32) also satisfies both of the boundary conditions for $m_o \neq 0$.

Experiments using those types of basis functions in the eigen-problem (4.2.26) showed that, as expected for $m_o = 0$ and the same problem dimensionality the convergence to the solution is much slower than that for the case of $\cos(K_m r)$ used as basis functions. For higher angular modes, i.e. $m_o \neq 0$, Tables 4.3 and 4.4 show $\cos K_m r$ is still useful in solution representation; in fact, the degrees of accuracy achieved by use of $\cos K_m r$ and $\sin K_m r$ are comparable whilst numerical results for $(1 - \cos K_m r)$ deteriorate for high angular modes. Note that for $m_o = 1, \left.\frac{dp}{dr}\right|_{r=0} \neq 0$ which is not satisfied by either $\cos K_m r$ or $(1 - \cos K_m r)$ functions. Consequently the conclusion can be drawn that the forced boundary condition at the duct centre line, for anti-symmetric angular modes, plays a trivial role in the solution convergence process, but for the symmetric mode it is significant to some extent.

(ii) Flow case.

a) No-flow basis function.

When flow is present the basis functions no longer individually satisfy the boundary condition. Table 4.5 shows the results for an unsymmetric mode, $m_o = 2$ and relatively high Mach number $M_o = -0.5$. With simple no-flow basis functions convergence is still occurring, although more basis functions to achieve a given accuracy as compared to the no-flow case. The $m_o = 2$ case is of particular interest because the high-order mode pair for each choice of the number of basis functions seems to approximate to a higher order mode pair. This does not happen for $m_o = 0$ or $m_o = 1$. It is of little consequence, as the higher modes are rapidly decaying and contribute little to the representation of the solution in the duct (except, perhaps, very close to the source).

b) Modified flow basis functions.

Reference to Table 4.6 shows that the modified flow basis functions given by equation (4.2.30) provide more rapid convergence

and improved accuracy, although the deterioration of high-order pairs is still present. This is consistent with the similar conclusion drawn in the 2D duct case of reference [64]. A number of calculations have been carried out at angular mode numbers as high as $m_o = 30$ with an indication of more difficult convergence at very high m_o. However, Tables 4.7 and 4.8 show that at moderately high m_o the modified flow basis functions are still useful at low frequencies and the accuracy of the results obtained apparently does not depend much upon the order of angular mode number m_o.

(ii) Other basis functions.

The functions $\sin \kappa_m r$ and $(1 - \cos \kappa_m r)$, similarly derived as for the no-flow case are used as basis functions for the flow case. But in this case both of these types do not satisfy the duct-wall boundary condition. The same conclusions can be made as for the no-flow case, hence the versatility of $\cos \kappa_m r$ functions is confirmed numerically.

4.2.5 Conservation Equations

(i) Weighting factor.

In the formulation with the convected wave equation the weighting factor $W_1 = r$ is used in equation (4.2.4) to circumvent singularities in analytical integration. But in fact its effect is to shift the residual weight towards the centre line, virtually forcing the residual to be zero at $r = 0$. Therefore one can expect a better accuracy to be achieved for the case $m_o \neq 0$ since $J_{m_o}(\bar{\kappa}_m r)\Big|_{r=0} = 1$ for $m_o = 0$ and $J_{m_o}(\bar{\kappa}_m r)\Big|_{r=0} = 0$ for $m_o \neq 0$. Numerical results in Table 4.7 show that this is the case, in spite of the slow convergence trend for higher angular modes. However, inspection of the equation (4.2.2) reveals that for $m_o = 0$ the weighting factor can be taken as $W_1 = 1$. Numerical experiments showed significant improvement can be achieved by this alteration.

In the formulation with conservation equations, just for the sake of avoiding singularities in analytical integration one could choose the weighting factors in equations (4.2.20) - (4.2.23) as follows :

$$W_1 = W_2 = W_3 = W_4 = 1.$$

But experiments showed a significantly slow convergence occurs in comparison to that of the convected wave equation case, even for $m_o = 0$. Further investigations are necessary since the conservation equation formulation (4.2.25) is just a reduced form of the case for the nonuniform duct with flow when the same concept of MWR is applied.

In fact, nearly identical eigenvalues are obtained as for the convected wave equation formulation if, for the conservation wave equations, the weighting factors are taken as $W_1 = W_2 = W_3 = 1$ and $W_4 = r$.

In an attempt to explain this coupling effect between the u-momentum and energy equations (4.1.3) and (4.1.6) one can make recourse to the process of combining momentum and energy equations to yield the single convected wave equation (4.1.1). The no-flow case is sufficient for arguments here because the terms involving the mach number M_o (or $\bar{W}_o$) do not contain r (or a function of r other than u_N, v_N, w_N, or p_N).

For the no-flow case the convected wave equation (4.1.1) becomes

$$\frac{1}{r}\frac{\partial}{\partial r}\left(r\frac{\partial p}{\partial r}\right) + \left(k^2 - \frac{m_o^2}{r^2}\right)p + \frac{\partial^2 p}{\partial z^2} = 0 \qquad (4.2.33)$$

and the conservation equations (4.1.3) - (4.1.6) can be written, with $k_r \equiv k$

momentum :

$$\begin{cases} iku + \dfrac{\partial p}{\partial r} = 0 & (4.2.34) \\ ikv - \dfrac{im_o}{r}p = 0 & (4.2.35) \\ ikw + \dfrac{\partial p}{\partial z} = 0 & (4.2.36) \end{cases}$$

$$\text{energy}: \quad ikp + \frac{1}{r}\frac{\partial}{\partial r}(ru) - im_o\frac{v}{r} + \frac{\partial w}{\partial z} = 0 \qquad (4.2.37)$$

With the relations for approximations (4.2.11) - (4.2.14), the Galerkin minimization applied on equation (4.2.33) with weighting factor r, yields, for n = 1,2,3...N

$$\int_0^R r\left[\frac{1}{r}\frac{\partial}{\partial r}\left(r\frac{\partial p_N}{\partial r}\right)+\left(k^2 - \frac{m_o^2}{r^2}\right)p_N + \frac{\partial^2 p_N}{\partial z^2}\right]\psi_n(r)\,2\pi r\,dr = 0 \qquad (4.2.38)$$

and on equation (4.2.37), with weighting factor W_4

$$\int_0^R W_4\left[ikp_N + \frac{1}{r}\frac{\partial}{\partial r}(ru_N) - im_o\frac{v_N}{r} + \frac{\partial w_N}{\partial z}\right]\psi_n(r)\;2\pi r\,dr = 0 \qquad (4.2.39)$$

or

$$\int_0^R W_4\; ikp_N\,\psi_n(r)\;2\pi r\;dr + \int_0^R W_4\,\frac{1}{r}\frac{\partial}{\partial r}(ru_N)\psi_n(r)\;2\pi r\,dr$$

$$+ \int_0^R W_4(-i)\;m_o\frac{v_N}{r}\psi_n(r)\;2\pi r\;dr + \int_0^R W_4\;\frac{\partial w}{\partial z}\;\psi_n(r)\;2\pi r\;dr = 0 \qquad (4.2.40)$$

Assuming the momentum equations are satisfied (just as substitution is carried out with differential equations) one can write, from equation (4.2.34) - (4.2.36)

$$ik\,u_N + \frac{\partial p_N}{\partial r} = 0$$

$$ik\,v_N - \frac{im_o}{r}p_N = 0$$

$$ik\,w_N + \frac{\partial p_N}{\partial z} = 0$$

and substitute these into equation (4.2.40) to eliminate u_N, v_N and w_N to give

$$\int_0^R W_4\;ikp_N\,\psi_n(r)\;2\pi r\;dr + \int_0^R W_4\,\frac{1}{r}\;\frac{\partial}{\partial r}\left(\frac{i}{k}\,r\,\frac{\partial p_N}{\partial r}\right)\psi_n(r)\;2\pi r\;dr$$

$$+ \int_0^R W_4\;\frac{(-i)}{k}\;\frac{m_o^2}{r^2}\,p_N\,\psi_n(r)\;2\pi r\;dr + \int_0^R W_4\,\frac{i}{k}\,\frac{\partial^2 p_N}{\partial z^2}\psi_n(r)\;2\pi r\;dr = 0$$

or

$$\int_0^R W_4\left[\frac{1}{r}\frac{\partial}{\partial r}\left(r\frac{\partial p_N}{\partial r}\right) + \left(k^2 - \frac{m_o^2}{r^2}\right)p_N + \frac{\partial^2 p_N}{\partial z^2}\right]\psi_n(r)\;2\pi r\;dr = 0 \qquad (4.2.41)$$

If $W_4 = r$ equation (4.2.41) is equivalent to equation (4.2.38), which is formulated by the convected wave equation.

Other combinations of the weighting factors were tried such as :

$$W_1 = \frac{1}{r}\ ,\ W_2 = 1,\ W_3 = \frac{1}{r}\ ,\ W_4 = 1$$

$$W_1 = \frac{1}{r}\ ,\ W_2 = 1,\ W_3 = 1\ ,\ W_4 = r$$

$$W_1 = 1\ ,\ W_2 = 1,\ W_3 = \frac{1}{r}\ ,\ W_4 = r$$

$$W_1 = \frac{1}{r}\ ,\ W_2 = 1,\ W_3 = 1\ ,\ W_4 = 1$$

- - - - - - - - - - - - - - - - - -

Numerical results showed in these cases, that the solution convergence is comparable to the case for the convected wave equation as long as one maintains $W_1 = 1$ and $W_4 = r$ in such combinations. This proves that a coupling exists between the u-momentum equation and the energy equation in the MWR formulation.

(ii) Hydrodynamic modes.

When flow is present the conservation equations with N basis functions yield in addition to the 2N acoustic modes : N positively running modes and N negatively running modes, a set of 2N solutions corresponding to hydrodynamic modes, which are convected with the flow. The hydrodynamic modes are rotational parts of small perturbation solutions. The existence of hydrodynamic modes has no clear precedent and the solution for the rotational parts is not well defined even for a uniform flow profile. However, theoretically, Möhring [99], when discussing the phenomenon for simple shear flow models, asserts that small perturbations of a compressible flow consist in general of hydrodynamic and acoustic disturbances. Both can be derived as solutions of the linearized equations and it is usually impossible to derive an equation which contains as solutions only the acoustic solutions. This is partially reflected in the fact that in cases where one linearized equation can be derived from the set of linearized equations, this equation is usually of higher order than the second.

Hence, for the problem at hand, when uniform flow is present the reduction of the conservation equations (of first order) to the convected wave equation (of second order) eliminates hydrodynamic solutions.

To derive some properties of hydrodynamic modes for the uniform flow profile one can write the conservation equations (4.1.3) - (4.1.6), with axial harmonic dependence assumed of the form $e^{-ik_z z}$, as follows :

$$ik_r \left(1 - \frac{k_z}{k_r} \bar{W}_o \right) u + \frac{1}{\bar{\rho}_o} \frac{dp}{dr} = 0 \qquad (4.2.42)$$

$$ik_r \left(1 - \frac{k_z}{k_r} \bar{W}_o \right) v - \frac{im_o}{\bar{\rho}_o} \frac{p}{r} = 0 \qquad (4.2.43)$$

$$ik_r \left(1 - \frac{k_z}{k_r} \bar{W}_o \right) w - \frac{ik_z}{\bar{\rho}_o} p = 0 \qquad (4.2.44)$$

$$ik_r \left(1 - \frac{k_z}{k_r} \bar{W}_o \right) p + \gamma \bar{p}_o \left[\frac{1}{r} \frac{d}{dr} (ru) - im_o \frac{v}{r} - ik_z w \right] = 0 \qquad (4.2.45)$$

From the exact solutions derived for the convected wave equation (Appendix C) one can assume

$$\left.\begin{aligned} p &= P\, J_{m_o}(Kr) \Rightarrow \frac{dp}{dr} = PK\, J'_{m_o}(Kr) \\ u &= U\, J'_{m_o}(Kr) \\ v &= \frac{V}{r} J_{m_o}(Kr) \\ w &= W\, J_{m_o}(Kr) \end{aligned}\right\} \qquad (4.2.46)$$

where P, U, V and W are constant for each node.

Substituting these into equations (4.2.42) - (4.2.45) one can obtain

$$ik_r \left(1 - \frac{k_z}{k_r} \bar{W}_o \right) U + \frac{1}{\bar{\rho}_o} K P = 0 \qquad (4.2.47)$$

$$ik_r \left(1 - \frac{k_z}{k_r} \bar{W}_o \right) V - \frac{im_o}{\bar{\rho}_o} P = 0 \qquad (4.2.48)$$

$$ik_r \left(1 - \frac{k_z}{k_r} \bar{W}_o \right) W - i \frac{k_z}{\bar{\rho}_o} P = 0 \qquad (4.2.49)$$

$$ik_r \left(1 - \frac{k_z}{k_r} \bar{W}_o \right) P J_{m_o}(\kappa r) + \gamma \bar{p}_o \left[U\kappa J''_{m_o}(\kappa r) + \frac{U}{r} J'_{m_o}(\kappa r) - \frac{im_o}{r^2} V J_{m_o}(\kappa r) \right.$$

$$\left. - ik_z W J_{m_o}(\kappa r) \right] = 0 \qquad (4.2.50)$$

In comparison of equations (4.2.47) and (4.2.48) V must be taken as $V = \frac{-im_o}{\kappa} U$. Substituting this into equation (4.2.50) and using the Bessel function relation $\lambda^2 J''_{m_o}(\lambda) + \lambda J'_{m_o}(\lambda) + (\lambda^2 - m_o^2) J_{m_o}(\lambda) = 0$ one can write the three remaining independent equations in the following matrix form

$$\underset{3x3}{[B]} \underset{3x1}{\begin{Bmatrix} U \\ P \\ W \end{Bmatrix}} = 0 \qquad (4.2.51)$$

where

$$[B] = \begin{bmatrix} ik_r \left(1 - \frac{k_z}{k_r} \bar{W}_o\right) & \frac{\kappa}{\bar{\rho}_o} & 0 \\ -\gamma \bar{p}_o \kappa & ik_r \left(1 - \frac{k_z}{k_r} \bar{W}_o\right) & -\gamma \bar{p}_o i k_z \\ 0 & -i \frac{k_z}{\bar{\rho}_o} & ik_r \left(1 - \frac{k_z}{k_r} \bar{W}_o\right) \end{bmatrix} \qquad (4.2.52)$$

The matrix equation (4.2.52) has a non-trivial solution when $\det(B) = 0$ or

$$\det(B) = ik_r \left(1 - \bar{W}_o \frac{k_z}{k_r}\right) \left\{ \left[ik_r \left(1 - \bar{W}_o \frac{k_z}{k}\right) \right]^2 + \gamma \bar{p}_o \kappa \left(\frac{\kappa}{\bar{\rho}_o} \right) \right\}$$

$$+ i \frac{k_z}{\bar{\rho}_o} \left[-i \gamma \bar{p}_o k_z \; ik_r \left(1 - \frac{k_z}{k_r} \bar{W}_o\right) \right] = 0$$

or

$$ik_r^3 \left(1 - \bar{W}_o \frac{k_z}{k_r}\right) \left\{ \frac{\gamma \bar{p}_o}{\bar{\rho}_o} \left[\left(\frac{k_z}{k_r}\right)^2 + \left(\frac{\kappa}{k_r}\right)^2 \right] - \left(1 - \bar{W}_o \frac{k_z}{k_r}\right)^2 \right\} = 0$$

or

$$ik^3 \bar{c}_o^3 \left(1 - M_o \frac{k_z}{k}\right) \left\{ \left(\frac{k_z}{k}\right)^2 + \left(\frac{\kappa}{k}\right)^2 - \left(1 - M_o \frac{k_z}{k}\right)^2 \right\} = 0$$

This gives two types of solutions :

$$\text{(a)} \quad \left(\frac{K}{k}\right)^2 = \left[\left(1 - M_o \frac{k_z}{k}\right) - \left(\frac{k_z}{k}\right)^2\right] \tag{4.2.53}$$

$$\text{(b)} \quad \text{and} \quad \left(1 - M_o \frac{k_z}{k}\right) = \left(1 - \bar{W}_o \frac{k_z}{k_r}\right) = 0 \tag{4.2.54}$$

with the duct-wall boundary condition being, from equation (4.1.7),

$$u = A \left(1 - \frac{k_z}{k_r} \bar{W}_o\right) P \qquad \text{at } r = R \tag{4.2.55}$$

or, by relations (4.2.42) and (4.2.46),

$$KR\, J'_{m_o}(KR) = - A\, ik_r R \left(1 - \bar{W}_o \frac{k_z}{k_r}\right)^2 J_{m_o}(KR) \tag{4.2.56}$$

Case (a): The relations (4.2.53) and (4.2.56) give rise to transverse and axial eigenvalues for acoustic modes, identically as derived in Appendix C. For acoustic modes $\left(1 - \bar{W}_o \frac{k_z}{k}\right) \neq 0$, the general momentum (2.2.19), for a uniform flow profile, becomes

$$\left(ik_r + \underline{\bar{V}}_o \cdot \text{grad}\right) \underline{V} + \frac{1}{\bar{\rho}_o} \text{grad } p = 0$$

or taking the curl of the left-hand side gives

$$\left(ik_r + \underline{\bar{V}}_o \cdot \text{grad}\right) \text{curl } \underline{V} + \frac{1}{\bar{\rho}_o} \text{curl (grad } p) = 0$$

For arbitrary p, curl (grad p) $\equiv$ 0 $\Rightarrow$ curl $\underline{V} \equiv$ 0. Hence, acoustic modes are irrotational.

Case (b): The solutions with axial eigenvalues given by equation (4.2.54) are hydrodynamic modes, which are convected with the flow. Further, for $\left(1 - \bar{W}_o \frac{k_z}{k_r}\right) = 0$, from the momentum equations (4.2.42) - (4.2.44) it must be that $p \equiv 0$, and from the boundary condition (4.2.55), u = 0 at r = R. Hence, hydrodynamic modes have no pressure disturbances and propagate convectively with the flow, as in a hardwalled duct for any wall admittance. It is also noted that, when $p \equiv 0$ the energy equation (4.1.6) degenerates to div $(\underline{V}) = 0$, $\underline{V} = (u,v,w)$ so that three dependent variables u,v,w, for hydrodynamic modes are connected by this relation (and u = 0 at r = R). This can be satisfied

by an infinite number of arbitrarily chosen solutions for which one can state in general that curl $\underline{V} \not\equiv 0$, i.e. the hydrodynamic modes, in general, are rotational.

4.2.6 Exact Solution and Further Observations

(i) Runge-Kutta eigenvalue integration scheme.

In order to assess the accuracy of MWR in the eigenproblem, for the hardwall case, i.e. A = 0 one can make comparisons with tabular values [98]. For the softwall case in general the coupled transcendental nonlinear algebraic equations (Appendix C)

$$\left.\begin{aligned} KR\, J'_{m_o}(KR) &= -\,AikR\left(1 - M_o \frac{k_z}{k}\right)^2 J_{m_o}(KR) \\ \frac{k_z}{k} &= \frac{1}{1-M_o^2}\left\{-M_o \pm \left[1 - (1 - M_o^2)\left(\frac{KR}{kR}\right)^2\right]^{\frac{1}{2}}\right\} \end{aligned}\right\} \qquad (4.2.57)$$

are to be solved for pairs of transverse and axial eigenvalues K and k_z. The usual approach is an iteration scheme with suitable guesses (e.g. the hardwall values).

In the preliminary study, the exact results are those obtained by the Runge-Kutta integration method applied on the governing differential equation, accounting for the boundary condition at the final integration stage by a suitable refining iteration scheme. This method was originally developed by Mungur and Plumbee [23] for sheared flow in annular ducts and subsequently extended by Eversman [27] to sheared flow in circular ducts. This is a powerful routine but not efficient when used for the simpler case of uniform flow profile. For the eigenproblem at hand the MWR can provide initial guesses to start the iteration scheme.

Eversman, in his study of 2-D geometry problems [96,97], succeeded in changing the coupled transcendental nonlinear eigen-equations to an initial value problem involving a nonlinear ordinary

differential equation, which can be solved by an integration scheme such as the fourth-order Runge-Kutta method. The procedure was applied to the eigenequations (4.2.57) for circular ducts with little modification (Appendix D). Numerical results proved that this approach leads to a powerful root finding routine capable of computing the transverse and axial wave numbers for circular ducts in general case, with the only required initial guesses being the hardwall values as starting points. These results are presented in the tables for comparisons with MWR values or FEM values.

(ii) Extra modes.

In the course of making comparisons of eigenvalues (for the flow case) computed by using the integration scheme with those obtained by MWR it was peculiar to find that two eigenvalues (one positively propagating the other negatively propagating) in the MWR routine do not turn up in the integration results. These extra eigenvalues only appear for wall admittances with a positive imaginary part. Having insight into the problem one could recognize that when the admittance has a positive imaginary part there are in fact two more starting values for the integration than can be accounted for by using hardwall values as initial conditions. These arise because for vanishingly small values of admittance A equations (4.2.57) admit two more solutions (one for the plus sign and, one for the minus sign) at infinity, which are complex numbers. The proof for their existence is given in Appendix D. This proof is rather loose because of approximations involved, but from which one can also conclude that, for these extra modes, when the admittance is passive (i.e. $Re(A) > 0$) the axial eigenvalue has the real and imaginary parts of the same sign, when active,(i.e. $Re(A) < 0$) they are of the opposite sign. This has been confirmed by numerical experiments. Tables 4.5 - 4.8 with these eigenvalues marked with asterisk show that the order of the extra modes decreases relatively to other acoustic modes as the

angular mode becomes higher.

An attempt to compute the eigenfunctions $J_{m_o}(Kr)$ for these extra modes showed that the acoustic pressure varies widely across the duct; it is small at the centre line and becomes very large at the duct wall. Its physical meaning has not appeared in the literature. Tester[100] called these extra modes "strange" modes and gave some approximate analytic examples of "strange" modes for two-dimensional case. Tester referred to the "strange" modes those defined as modes with kinematic phase velocities in the opposite direction to that of decay and concluded that these "strange" modes could thereby be interpreted as amplifying modes.

In fact, the direction of mode propagation is to be determined by the acoustic energy flow criteria [101]. The problem of acoustic flux and energy definitions for a softwalled duct with flow is still unsettled in the duct acoustics literature

Tester [102] considered the acoustic energy flow in lined duct containing uniform or "plug" flow as being made up of two components : in the uniform flow region and in the vanishingly thin shear layer. His application on the approximate analytic solutions of the "strange" modes shows that the axial energy flow within the shear layer is approximately twice that within the uniform flow region and is in the opposite direction, thus counteracting that energy flow and providing a net energy flow in the decay direction. Recently Eversman [103] has made a re-evaluation of the basis of derivation of the acoustic energy density and acoustic flux for a duct with uniform flow to provide forms which yield consistent results for softwalled ducts. His acoustic energy flow results for 2D case show that the extra modes for duct wall admittance with a positive imaginary part are indeed decaying modes.

TABLE 4.1

Comparison of MWR Values of k_z/k with Exact Values; Hardwalled Duct, $A = (0.0 + 0.0i)$; $kR = 1.0$, $M_o = 0$, $m_o = 1$

Mode	Galerkin-Number of Basis Functions N = 3	N = 5	N = 10	Exact-Tabular Values [98]
1^+	-1.5427i	-1.5452i	-1.5460i	-1.5459i
2^+	-5.2495i	-5.2382i	-5.2367i	-5.2368i
3^+	-8.3621i	-8.4756i	-8.4778i	-8.4775i
4^+		-11.6782i	-11.6631i	-11.6632i
5^+		-14.7092i	-14.8305i	-14.8299i
6^+			-17.9874i	-17.9877i
7^+			-21.1426i	-21.1407i
8^+			-24.2887i	-24.2908i
9^+			-27.4558i	-27.4388i
10^+			-30.4604i	-30.5856i

TABLE 4.2

Comparison of MWR Values of k_z/k with Runge-Kutta Values; Softwalled Duct $A = (1.00 + 1.00i)$; $kR = 1.0$, $M_o = 0$, $m_o = 0$

Mode	Galerkin-Number of Basis Functions N = 3	N = 5	N = 10	Exact-Runge-Kutta
1^+	1.879-0.845i	1.880-0.845i	1.880-0.845i	1.880-0.845i
2^+	0.280-3.403i	0.279-3.412i	0.278-3.414i	0.278-3.414i
3^+	0.143-6.864i	0.145-6.805i	0.145-6.797i	0.145-6.798i
4^+		0.099-10.008i	0.099-10.026i	0.099-10.025i
5^+		0.075-13.286i	0.075-13.208i	0.075-13.211i
6^+			0.061-16.383i	0.061-16.379i
7^+			0.051-19.533i	0.051-19.539i
8^+			0.044-22.706i	0.044-22.694i
9^+			0.039-25.825i	0.039-25.846i
10^+			0.034-29.078i	0.034-28.995i

TABLE 4.3

Comparison of MWR Values of k_z/k (with Different Types of Basis functions) with Runge-Kutta Values; Softwalled Duct, $A = (0.1+0.1i)$; $kR = 1.0$, $M_o = 0$, $m_o = 1$

Mode	MWR (10 BF)			Runge-Kutta
	$\cos \kappa_m r$	$\sin \kappa_m r$	$(1 - \cos \kappa_m r)$	
1^+	0.1009-1.4549i	0.1009-1.4549i	0.1008-1.4626i	0.1009-1.4548i
2^+	0.0199-5.2170i	0.0199-5.2171i	0.0201-5.2559i	0.0199-5.2171i
3^+	0.0120-8.4658i	0.0120-8.4654i	0.0123-8.5576i	0.0120-8.4659i
4^+	0.0086-11.6544i	0.0086-11.6552i	0.0091-11.8209i	0.0086-11.6558i
5^+	0.0068-14.8237i	0.0068-14.8222i	0.0073-15.0774i	0.0068-14.8269i
6^+	0.0056-17.9818i	0.0056-17.9846i	0.0065-18.3483i	0.0056-17.9913i
7^+	0.0047-21.1379i	0.0047-21.1323i	0.0056-21.6206i	0.0048-21.1551i
8^+	0.0041-24.2846i	0.0041-24.2957i	0.0056-24.9361i	0.0041-24.3227i
9^+	0.0036-27.4522i	0.0037-27.4184i	0.0050-28.2402i	0.0037-27.4980i
10^+	0.0032-30.4571i	0.0033-30.6592i	0.0061-31.7528i	0.0033-30.6847i

TABLE 4.4

Comparison of MWR Values of k_z/k (with Different Types of Basis functions) with Runge-Kutta Values; Softwalled Duct, $A = (1.0+1.0i)$; $kR = 1.0$, $M_o = 0$, $m_o = 3$

Mode	MWR (10 BF)			Runge-Kutta
	$\cos \kappa_m r$	$\sin \kappa_m r$	$(1 - \cos \kappa_m r)$	
1^+	0.7084-3.6257i	0.7084-3.6257i	0.7165-3.5994i	0.7083-3.6257i
2^+	0.1481-7.8046i	0.1481-7.8046i	0.1473-7.8015i	0.1481-7.8045i
3^+	0.0955-11.2062i	0.0955-11.2062i	0.0955-11.2097i	0.0955-11.2061i
4^+	0.0719-14.4797i	0.0719-14.4796i	0.0718-14.4767i	0.0719-14.4795i
5^+	0.0580-17.7026i	0.0580-17.7029i	0.0579-17.7054i	0.0580-17.7025i
6^+	0.0488-20.9008i	0.0488-20.8996i	0.0487-20.8978i	0.0488-20.8998i
7^+	0.0421-24.0816i	0.0421-24.0844i	0.0411-24.0859i	0.0421-24.0820i
8^+	0.0371-27.2663i	0.0371-27.2506i	0.0365-27.2524i	0.0371-27.2546i
9^+	0.0332-30.3248i	0.0332-30.4631i	0.0229-30.4440i	0.0332-30.4207i
10^+	—	—	0.0183-33.4793i	0.0299-33.5821i

TABLE 4.5

Comparison of MWR Values of k_z/k with Runge-Kutta Values; Softwalled Duct

$A = (0.72 + 0.42i)$; $kR = 1.0$, $M_o = -0.5$, $m_o = 2$

Mode	Galerkin-Number of Basis Functions N = 3	N = 5	N = 10	Exact-Runge-Kutta
1^+	0.520-5.404i	0.548-5.252i	0.580-5.136i	0.620-5.014i
1^-	0.379+1.315i	0.391+1.303i	0.400+1.296i	0.410+1.290i
2^+	-4.418-5.115i	-5.195-4.745i	-5.593-4.342i	-5.820-3.897i *
2^-	1.054+6.322i	1.141+6.278i	1.201+6.199i	1.259+6.085i
3^+		0.422-9.705i	0.422-9.395i	0.445-9.187i
3^-		1.012+10.133i	1.096+9.876i	1.146+9.668i
4^+	0.475-13.845i	0.490-13.530i	0.448-13.368i	0.453-13.062i
4^-	0.794+14.048i	0.904+13.732i	0.982+13.617i	1.022+13.315i *
5^+			0.487-17.167i	0.480-16.822i
5^-			0.906+17.314i	0.943+16.977i
6^+			0.524-21.031i	0.503-20.531i
6^-			0.846+21.125i	0.891+20.635i
7^+		0.627-24.504i	0.548-24.675i	0.522-24.213i
7^-		0.705+24.552i	0.812+24.740i	0.855+24.288i
8^+			0.586-28.666i	0.538-27.880i
8^-			0.762+28.706i	0.829+27.937i
9^+			0.592-32.055i	0.550-31.537i
9^-			0.755+32.087i	0.809+31.581i
10^+			0.674-50.429i	0.589-49.754i
10^-			0.660+50.435i	0.755+49.772i

* extra modes

TABLE 4.6

Comparison of MWR Values of k_z/k (with Modified Flow Basis Functions) with Runge-Kutta Values; Softwalled Duct

$A = (0.72 + 0.42i)$; $kR = 1.0$, $M_o = -0.5$, $m_o = 2$

Mode	Galerkin-Number of Basis Functions				Exact Runge-Kutta
	N = 3	N = 5	N = 7	N = 10	
1^+	0.712-4.996i	0.627-5.013i	0.622-5.014i	0.620-5.014i	0.620-5.014i
1^-	0.413+1.283i	0.410+1.290i	0.410+1.290i	0.410+1.290i	0.410+1.290i
2^+	-5.873-4.018i	-5.822-3.915i	-5.820-3.903i	-5.820-3.899i	-5.820-3.897i*
2^-	1.171+6.271i	1.254+6.096i	1.258+6.088i	1.259+6.086i	1.259+6.085i
3^+		0.441-9.183i	0.445-9.186i	0.446-9.187i	0.445-9.187i
3^-		1.144+9.664i	1.145+9.668i	1.145+9.670i	1.146+9.668i
4^+	0.006-11.547i	0.489-13.087i	0.458-13.063i	0.454-13.061i	0.453-13.062i
4^-	1.454+11.803i	1.030+13.433i	1.024+13.327i	1.022+13.315i	1.022+13.315i*
5^+			0.473-16.814i	0.482-16.822i	0.480-16.822i
5^-			0.942+16.965i	0.941+16.980i	0.943+16.977i
6^+		0.299-22.182i	0.519-20.581i	0.502-20.530i	0.503-20.531i
6^-		1.057+22.222i	0.902+20.734i	0.891+20.633i	0.891+20.635i
7^+				0.524-24.218i	0.522-24.213i
7^-				0.856+24.300i	0.855+24.288i
8^+				0.536-27.870i	0.538-27.880i
8^-				0.828+27.922i	0.829+27.937i
9^+			0.495-32.546i	0.558-31.606i	0.550-31.537i
9^-			0.847+32.557i	0.815+31.675i	0.809+31.581i
10^+				0.455-47.998i	0.583-46.116i
10^-				0.881+48.002i	0.762+46.137i

* extra modes

TABLE 4.7

Comparison of MWR Values of k_z/k (with Modified Flow Basis Functions) with Runge-Kutta Values; Softwalled Duct, $A = (0.72 + 0.42i)$; $kR = 1$, $M_o = -0.5$

Mode	$m_o = 0$		$m_o = 3$		$m_o = 4$	
	MWR (7 BF)	RUNGE-KUTTA	MWR (7 BF)	RUNGE-KUTTA	MWR (7 BF)	RUNGE-KUTTA
1^-	-0.871+0.176i	-0.868+0.176i	0.974+1.800i	0.975+1.800i	1.493+2.204i	1.493+2.204i
1^+	1.395-1.818i	1.405-1.832i	0.495-6.623i	0.493-6.624i	-6.417-3.899i*	-6.413-3.888i
2^-	1.037+3.134i	1.033+3.157i	1.230+7.415i	1.231+7.413i	1.176+8.741i	1.178+8.739i
2^+	0.595-5.535i	0.572-5.550i	-6.095-3.879i*	-6.093-3.871i	0.449-8.155i	0.449-8.155i
3^-	1.252+6.531i	1.261+6.523i	1.087+11.192i	1.087+11.188i	1.038+12.683i	1.039+12.678i
3^+	-5.580-3.971i*	-5.580-3.966i	0.444-10.828i	0.442-10.828i	0.450-12.398i	0.448-12.399i
4^-	1.133+9.906i	1.138+9.986i	0.982+14.926i*	0.982+14.922i	0.949+16.492i*	0.950+16.489i
4^+	0.430-9.474i	0.443-9.529i	0.467-14.719i	0.465-14.720i	0.478-16.322i	0.476-16.324i
5^-	1.026+13.555i*	1.019+13.606i	0.910+18.647i	0.917+18.627i	0.892+20.274i	0.896+20.237i
5^+	0.470-13.275i	0.453-13.360i	0.499-18.504i	0.491-18.498i	0.514-20.140i	0.500-20.133i

* extra modes

TABLE 4.8

Comparison of MWR Values of k_z/k (with Modified Flow Basis Functions) with Runge-Kutta Values; Softwalled Duct, $A = (0.72 + 0.42i)$; $kR = 1$, $M_o = -0.5$

Mode	$m_o = 8$		$m_o = 10$		$m_o = 12$	
	MWR (10 MBF)	RUNGE-KUTTA	MWR (10 MBF)	RUNGE-KUTTA	MWR (10 MBF)	RUNGE-KUTTA
1^-	3.164+3.280i*	3.160+3.280i	3.839+3.670i*	3.827+3.669i	4.450+4.016i*	4.424+4.010i
1^+	-7.699-4.226i*	-7.688-4.213i	-8.284-4.452i*	-8.261-4.430i	-8.835-4.689i*	8.793-4.652i
2^-	0.999+14.013i	1.000+14.012i	0.945+16.609i	0.947+16.608i	0.906+19.178i	0.908+19.177i
2^+	0.456-13.784i	0.455-13.784i	0.476-16.446i	0.475-16.446i	0.494-19.056i	0.493-19.056i
3^-	0.918+18.414i	0.919+18.412i	0.883+21.185i	0.884+21.185i	0.856+23.912i	0.858+23.912i
3^+	0.489-18.281i	0.488-18.282i	0.507-21.085i	0.505-21.086i	0.521-23.833i	0.520-23.835i
4^-	0.870+32.393i	0.871+22.481i	0.845+25.367i	0.846+25.370i	0.826+28.199i	0.827+28.205i
4^+	0.514-22.482i	0.513-22.396i	0.528-25.296i	0.527-25.301i	0.540-28.141i	0.540-28.149i
5^-	0.839+26.407i	0.839+26.404i	0.820+29.374i	0.822+29.375	0.805+32.281i	0.804+32.301i
5^+	0.532-26.341i	0.531-26.341i	0.544-29.320i	0.542-29.334i	0.553-32.237i	0.552-32.260i

*extra modes

4.3 METHOD OF SOLUTION: FEM

4.3.1 Formulation with Convected Wave Equation

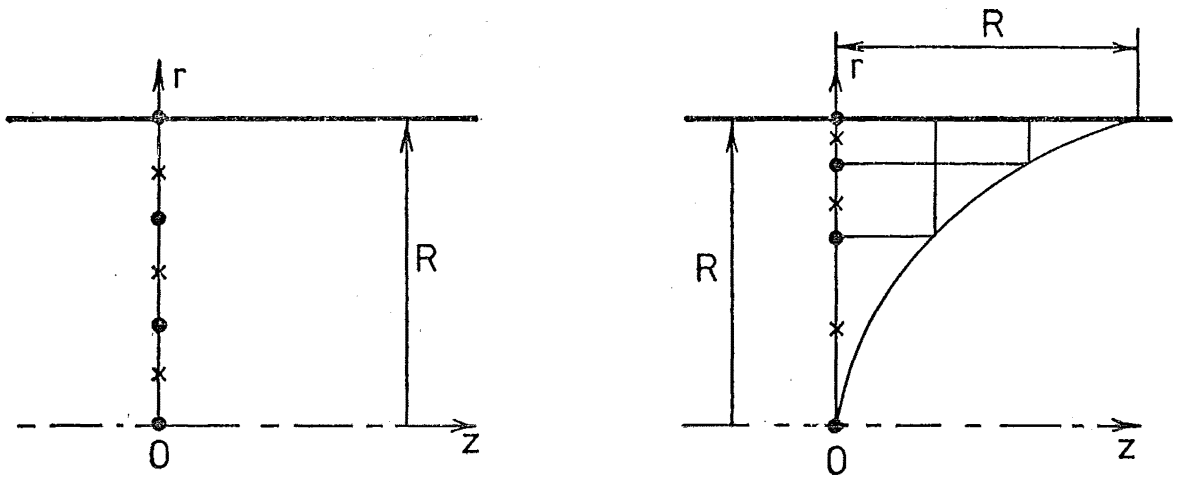

(a) uniform distribution (b) parabolic distribution

• end node, × middle node

FIG. 4·3 MESH OF 3 QUADRATIC LINE ELEMENTS ACROSS A DUCT

The governing equation (4.1.1) is repeated here

$$\frac{\partial p^2}{\partial r^2} + \frac{1}{r}\frac{\partial p}{\partial r} + \left(k^2 - \frac{m_o^2}{r^2}\right) p - 2kM_o i \frac{\partial p}{\partial z} + (1 - M_o^2)\frac{\partial^2 p}{\partial z^2} = 0 \qquad (4.3.1)$$

with the duct-wall boundary condition:

$$ikA\left(p - \frac{2iM_o}{k}\frac{\partial p}{\partial z} - \frac{M_o^2}{k^2}\frac{\partial^2 p}{\partial z^2}\right) = \frac{\partial p}{\partial r} \quad \text{at } r = R \qquad (4.3.2)$$

For a uniform duct the harmonic z dependence can be assumed of the form $e^{-ik_z z}$ so that equations (4.3.1) and (4.3.2) can be written

$$\frac{d^2 p}{dr^2} + \frac{1}{r}\frac{dp}{dr} + \left(k^2 - \frac{M_o^2}{r^2}\right) p - 2kM_o k_z p + (1 - M_o^2)(-k_z^2)\, p = 0 \qquad (4.3.3)$$

$$ikAp\left(1 - M_o \frac{k_z}{k}\right)^2 = -\frac{dp}{dr} \quad \text{at } r = R \qquad (4.3.4)$$

and the domain concerned reduces to a line segment with point boundaries at r = 0 and r = R as shown in Figure 4.3. In Figure 4.3 are also typical discretizations of quadratic line elements.

If the trial solution $\tilde{p} = [N]\{p\}$, where components of [N] are piecewise continuous functions constructed via elements, is substituted into equations (4.3.3) and (4.3.4) one can obtain the following residuals :

$$R_1 = \frac{d^2\tilde{p}}{dr^2} + \frac{1}{r}\frac{d\tilde{p}}{dr} + \left(k^2 - \frac{m_o^2}{r^2}\right)\tilde{p} - 2kM_o k_z \tilde{p} - (1 - M_o^2) k_z^2 \tilde{p} \qquad (4.3.5)$$

$$R_2 = ikA\,\tilde{p}\left(1 - M_o \frac{k_z}{k}\right) + \frac{d\tilde{p}}{dr} \quad \text{at } r = R \qquad (4.3.6)$$

The Galerkin process yields

$$\int_0^R N_i R_1\, 2\pi r\, dr = 0\,, \quad i = 1,2,\ldots n_n \qquad (4.3.7)$$

$$R_2 = 0 \quad \text{at } r = R \qquad (4.3.8)$$

where n_n is the number of nodes, N_i are components of [N].

Equations (4.3.5) and (4.3.7) are combined to give

$$\int_0^R \left[N_i \frac{d^2\tilde{p}}{dr^2} + \frac{N_i}{r}\frac{d\tilde{p}}{dr} + \left(k^2 - \frac{m_o^2}{r^2} - 2k\,M_o k_z - (1-M_o)k_z^2\right) N_i \tilde{p}\right] r\,dr = 0 \qquad (4.3.9)$$

for $i = 1,2,..n_n$

Consider the 1st. term, which can be integrated by parts to expose boundary terms

$$\int_0^R N_i \frac{d^2\tilde{p}}{dr^2}\, r\, dr = \left(rN_i \frac{dp}{dr}\right)_{r=R} - \int_0^R \frac{d\tilde{p}}{dr}\frac{d}{dr}(rN_i)\, dr$$

$$= R\left.\frac{d\tilde{p}}{dr}\right|_{r=R} - \int_0^R \frac{d\tilde{p}}{dr}(N_i + r\,N_{i_r})\, dr \qquad (4.3.10)$$

since, from the definition of shape functions in FEM, on the point boundary at $r = R$ $\quad N_i \equiv 1$

Now, if relation (4.3.10) is substituted back into equation (4.3.9) together with equation (4.3.8) one can arrange the resultant in a matrix equation :

$$K^2 \underset{n_n x n_n}{[\ B\ ]}\{p\} + K \underset{n_n x n_n}{[\ C\ ]}\{p\} + \underset{n_n x n_n}{[\ D\ ]}\underset{n_n x 1}{\{\ p\ \}} = 0 \qquad (4.3.11)$$

where $K = \frac{k_z}{k}$

and

$$B_{ij} = -(1 - M_o^2)\, k^2 \int_0^R N_i N_j\, r\, dr - (ikRA\, M_o^2)_{r=R}$$

$$C_{ij} = -2k^2 M_o \int_0^R N_i N_j\, r\, dr + (2ikRA\, M_o)_{r=R}$$

$$D_{ij} = \int_0^R \left(k^2 - \frac{m_o^2}{r^2}\right) N_i N_j\, r\, dr - \int_0^R N_{i_r} N_{j_r}\, r\, dr - (ikRA)_{r=R}$$

for $i = 1,2,\ldots n_n$, $j = 1,2,\ldots n_n$

Equation (4.3.11) is multiplied by $[B]^{-1}$ and restructured with the change of variables

$$\{x_1\} = \{p\}\ ,\quad \{x_2\} = K\{p\}$$

The result gives the eigenproblem of the partitioned matrix as in the MWR formulation

$$\underset{2n_n x\ 2n_n}{\begin{bmatrix} 0 & I \\ -\bar{D} & -\bar{C} \end{bmatrix}} \underset{2n_n x 1}{\begin{Bmatrix} x_1 \\ x_2 \end{Bmatrix}} = K \underset{2n_n x 1}{\begin{Bmatrix} x_1 \\ x_2 \end{Bmatrix}} \qquad (4.3.12)$$

where $[I]$ is the identity matrix and

$$[\bar{C}] = [B]^{-1}\,[C]$$

$$[\bar{D}] = [B]^{-1}\,[D]$$

4.3.2 Formulation with Conservation Equations

For a uniform duct, when a harmonic dependence $e^{-ik_z z}$ is assumed in the solution, the conservation equations (4.1.3) - (4.1.6) can be written, with $k \equiv k_r$

$$iku + \bar{W}_o\,(-ik_z)\,u + \frac{1}{\bar{\rho}_o}\frac{dp}{dr} = 0 \qquad (4.3.13)$$

$$ikv + \bar{W}_o\,(-ik_z)\,v - \frac{im_o}{r}\frac{p}{\bar{\rho}_o} = 0 \tag{4.3.14}$$

$$ikw + \bar{W}_o\,(-ik_z)\,w + \frac{1}{\bar{\rho}_o}\,(-ik_z)\,p = 0 \tag{4.3.15}$$

$$ikp + \bar{W}_o\,(-ik_z)\,p + \gamma\bar{p}_o\left[\frac{1}{r}\frac{d}{dr}(ru) - im_o\frac{v}{r} + (-ik_z)w\right] = 0 \tag{4.3.16}$$

and the duct-wall boundary condition (4.1.7) becomes

$$\underline{V}\cdot\underline{\nu} = u = A\left(1 - \frac{k_z}{k}\bar{W}_o\right)p \quad \text{at } r = R \tag{4.3.17}$$

As for the convected wave equation case the trial solutions $\tilde{u} = [N]\{u\}$, $\tilde{v} = [N]\{n\}$, $\tilde{w} = [N]\{w\}$, and $\tilde{p} = [N]\{p\}$ are substituted in equations (4.3.13) - (4.3.17) to give the residuals

$$R_1 = i(k - k_z\bar{W}_o)\,\tilde{u} + \frac{1}{\bar{\rho}_o}\frac{d\tilde{p}}{dr} \tag{4.3.18}$$

$$R_2 = i(k - k_z\bar{W}_o)\,\tilde{v} - i\frac{m_o}{r}\frac{\tilde{p}}{\bar{\rho}_o} \tag{4.3.19}$$

$$R_3 = i(k - k_z\bar{W}_o)\,\tilde{w} - \frac{ik_z}{\bar{\rho}_o}\tilde{p} \tag{4.3.20}$$

$$R_4 = i(k - k_z\bar{W}_o)\,\tilde{p} + \gamma\bar{p}_o\left[\frac{1}{r}\frac{d}{dr}(r\tilde{u}) - im_o\frac{\tilde{v}}{r} - ik_z\tilde{w}\right] \tag{4.3.21}$$

$$R_B = \tilde{u} - A\left(1 - \frac{k_z}{k}\bar{W}_o\right)\tilde{p} \quad \text{at } r = R \tag{4.3.22}$$

Again the Galerkin process applied on the residuals yields

$$\int_0^R N_i R_1\, 2\pi r\, dr = 0 \tag{4.3.23}$$

$$\int_0^R N_i R_2\, 2\pi r\, dr = 0 \tag{4.3.24}$$

$$\int_0^R N_i R_3\, 2\pi r\, dr = 0 \tag{4.3.25}$$

$$\int_0^R N_i R_4\, 2\pi r\, dr = 0 \tag{4.3.26}$$

and $$R_B = 0 \text{ at } r = R \tag{4.3.27}$$

Consider the term $\int_0^R N_i \frac{\gamma\bar{p}_o}{r}\frac{d}{dr}(r\tilde{u})\,2\pi r\,dr$ in equation (4.3.26)

which can be integrated by parts to expose boundary terms as follows :

$$\int_0^R N_i \frac{\gamma\bar{p}_o}{r} \frac{d}{dr} (r\tilde{u})\, 2\pi r\, dr = 2\pi\, \gamma\bar{p}_o \int_0^R N_i \frac{d}{dr} (r\tilde{u})\, dr$$

$$= 2\pi\, \gamma\bar{p}_o \left[(r\tilde{u}\, N_i)_{r=R} - \int_0^R r\tilde{u}\, N_{i_r}\, dr \right] \qquad (4.3.28)$$

With $N_i \equiv 1$ on the point boundary at r = R, equations (4.3.27) and (4.3.28) are combined so as to eliminate $\tilde{u}_{|r=R}$ to give

$$\int_0^R N_i \frac{\gamma\bar{p}_o}{r} \frac{d}{dr} (r\tilde{u})\, 2\pi r\, dr = \gamma\bar{p}_o \cdot 2\pi R\, A \left(1 - \frac{k_z}{k} \bar{W}_o\right) \tilde{p}(R)$$

$$- \gamma\bar{p}_o \int_0^R N_{i_r}\, \tilde{u}\, 2\pi r\, dr \qquad (4.3.29)$$

Now the trial solutions in terms of shape functions and nodal values can be used in equations (4.3.18) - (4.3.22) and (4.3.29), which, in turn, are substituted into equations (4.3.23) - (4.3.26) , The resulting equations can be arranged in the following matrix form :

$$\int_0^R \underset{4n_n \times 4n_n}{[\ N\ ]}\, 2\pi r\, dr \underset{4n_n \times 1}{\begin{Bmatrix} p \\ w \\ u \\ v \end{Bmatrix}} = K \int_0^R \underset{4n_n \times 4n_n}{[\ M\ ]}\, 2\pi r\, dr \underset{4n_n \times 1}{\begin{Bmatrix} p \\ w \\ u \\ v \end{Bmatrix}}$$

or
$$[\mathcal{N}]\ \{\delta\} = K\, [\mathcal{M}]\ \{\delta\} \qquad (4.3.30)$$

where $K = \frac{k_z}{k}$, $\{\delta\} = [\ p\ w\ u\ v\ ]^T$

$$[\mathcal{M}] = \int_0^R [\ M\ ]\, 2\pi r\, dr \ , \quad [\mathcal{N}] = \int_0^R [\ N\ ]\, 2\pi r\, dr$$

and

$$\underset{4n_n \times 4n_n}{[\ M\ ]} = \begin{bmatrix} \bar{W}_o N_i N_j + (i\gamma\bar{p}_o A\bar{W}_o)_{r=R} & \gamma\bar{p}_o\, N_i N_j & 0 & 0 \\ \frac{1}{\bar{\rho}_o} N_i N_j & \bar{W}_o\, N_i N_j & 0 & 0 \\ 0 & 0 & \bar{W}_o N_i N_j & 0 \\ 0 & 0 & 0 & \bar{W}_o N_i N_j \end{bmatrix} \qquad (4.3.31)$$

$$
[N]_{4n_n \times 4n_n} = \begin{bmatrix}
N_i N_j & 0 & \frac{\bar{\gamma p}_o}{k} i N_{i_r} N_j & -\bar{\gamma p}_o \frac{m_o}{kr} N_i N_j \\
-(i\bar{\gamma p}_o A)_{r=R} & & & \\
0 & N_i N_j & 0 & 0 \\
-\frac{i}{k\bar{\rho}_o} N_i N_{j_r} & 0 & N_i N_j & 0 \\
-\frac{m_o}{kr\bar{\rho}_o} N_i N_j & 0 & 0 & N_i N_j
\end{bmatrix} \qquad (4.3.32)
$$

for $(j = 1,2,\ldots n_n)$ and $(i = 1,2,\ldots n_n)$

Hence, the eigenproblem derived from equation (4.3.30) can be written in the standard form :

$$
[\mathcal{L}]_{4n_n \times 4n_n} \{\delta\}_{4n_n \times 1} = K \{\delta\}_{4n_n \times 1} \qquad (4.3.33)
$$

where $[\mathcal{L}]_{4n_n \times 4n_n} = [\mathcal{M}]^{-1}_{4n_n \times 4n_n} [\mathcal{N}]_{4n_n \times 4n_n}$

It is noted that in the case of formulation with the conservation equations one can force the boundary conditions

$$
\left.
\begin{aligned}
u &= A\left(1 - \frac{k_z}{k} \bar{W}_o\right) p \text{ at } r = R \\
\text{and} \quad u &= 0 \text{ at } r = 0 \text{ (for } m_o \neq 1)
\end{aligned}
\right\} \qquad (4.3.34)
$$

to be satisfied explicitly by deleting the rows of matrices $[\mathcal{N}]$ and $[\mathcal{M}]$ of equation (4.3.30) corresponding to the weighted u-momentum equations for nodes at r = R and r = 0 and replacing them by equations (4.3.34).

4.3.3 Numerical Results and Comparisons with MWR Values

(i) No-flow case.

The FEM, as expounded in Chapter 3, is a special formulation of the general method of weighted residuals, in which the basis functions are the piecewise continuous shape functions. Unlike the basis functions used in the MWR the shape functions do not satisfy any boundary conditions and entirely depend upon the choice of finite elements. Therefore one expects that the solution convergence by the FEM is much slower than

that by the MWR for the no-flow case. Table 4.9 shows a comparison of FEM eigenvalues with exact values, the results can be compared with the MWR values of Tables 4.1 and 4.2 for N = 10, i.e., on a comparable scale of dimensionality. In the FEM the number of pairs of positive and negative mode eigenvalues yielded is equal to the number of nodes (usually high) in the FEM discretization so that the high-order modes are not well resolved and the high-mode pair deterioration occurs earlier than in the case of MWR.

(ii) Flow case.

For the low frequency range ($kR \approx 1.0$), where the MWR possesses the advantage of modified flow basis functions the FEM convergence is relatively slower than that of the MWR. But at high frequencies the two methods give comparable values on a similar scale of dimensionality, especially with high admittances the FEM values seem to be more favourable.

Comparisons of eigenvalues given by the FEM formulated with the convected wave equation and the conservation equations, apart from the hydrodynamic modes as in the MWR, showed little discrepancies for the low-order pairs. For high-order modes there is an early deterioration with the convected wave equation; this may reflect the representation of second derivatives in terms of the same type of shape functions. As a general guide the number of pairs of reasonably reliable eigenvalues is not more than the number of elements in discretization. This may be deduced from the quadratic nature of the finite element shape functions, which can accommodate at most one stationary value of dependent variables inside each element. The flow-case values in the tables presented are obtained by the FEM with the conservation equations. Tables 4.10 and 4.11 show a typical trend of convergence to the Runge-Kutta values, which can be compared with the MWR values in Tables 4.5, 4.6, and 4.7.

Following the success in using different weighting factors in the MWR one can apply weighting factors 1 and r to the u-momentum and energy residual equations respectively in the FEM formulation. In fact, with piecewise continuous shape functions, it does not show the significance of coupling effect, which plays an important role in the MWR formulation as seen in Section 4.2 . Further, the factor r in the energy residual equation tends to shift the residual weight towards the duct centre line so that there results in an improvement for the case of angular mode $m_o \neq 0$ (since $J_{m_o}(\kappa r)\big|_{r=0} = 0$ for $m_o \neq 0$). Table 4.12 shows a higher degree of convergence with the weighting factor r for $m_o = 2$ in a hardwalled duct. Tables 4.13 and 4.14 present the results of the softwall case, which can be compared with those in Tables 4.10 and 4.11.

The concept of distributing residual weights suggests that better results can be obtained with more elements discretized near the duct wall than with a uniform mesh, since there the eigenfunctions (Bessel functions) have wide variations and become increasingly compressed towards the wall, especially for very high angular modes. Numerical experiments showed this is the case. For the results presented here the mesh employed has elements distributed parabolically, concentrating towards the duct-wall, as shown in Figure 4.3(b). This has proved to be satisfactory for a number of low angular modes.

(iii) Forced boundary condition.

In the FEM formulation the divergence term in the energy equation is integrated by parts to expose boundary terms, which are simplified by boundary residuals. The boundary condition treated in this way is the natural boundary condition. In a problem having a variational principle the above process for FEM corresponds exactly to the variational formulation. The FEM with the natural boundary condition is analogous to the case of MWR using basis functions which do not satisfy the duct-wall boundary condition. In FEM formulations,

due to the nature of the system of linear equations resulted to be solved, the boundary conditions can be forced to be satisfied explicitly as noted in Section 4.3.2. However, numerical results showed that the technique with natural boundary conditions gave consistently greater accuracy than with forced boundary conditions. Refer [104] for comparisons.

4.3.4 Condensation Technique

Extraction of eigenvalues and eigenvectors is a time consuming operation, which is usually more expensive than solution of simultaneous linear equations of the same dimensionality. A typical mesh of quadratic finite elements may have too many degrees of freedom for economical treatment while a few low-order eigenvalues may be required. In the context of structural mechanics (in which FEM acquires an extensive development) the "eigenvalue economizer" [92] is called on for economical treatment by eliminating many of the degrees of freedom in order to reduce the size of the eigenmatrix. The concept can be applied to the acoustic problem, in which the nodal values of eigenfunctions are expressed in terms of the no-flow values solved for with less effort.

Consider the eigenproblem (4.3.33) in the form

$$[\mathcal{K}(K)]\{\delta\} = 0 \tag{4.3.35}$$

where $[\mathcal{K}] = [\mathcal{L}] - K[I]$, $[I]$ is the identity matrix. Assuming the eigenvectors are of the form

$$\{\delta\} = \alpha_1\{\delta_{01}\} + \alpha_2\{\delta_{02}\} + \ldots \alpha_m\{\delta_{0m}\} \tag{4.3.36}$$

$$\left[\begin{array}{c:c:c:c} \delta_{01} & \delta_{02} & \cdots & \delta_{0m} \end{array}\right]\left\{\begin{array}{c} \alpha_1 \\ \alpha_2 \\ \vdots \\ \alpha_m \end{array}\right\} = \underset{n_n \times m}{[T]}\{\alpha\}\ ,\ m \leqslant n_n$$

where $[T]$ is the transformation matrix with $\delta_{01}, \delta_{02}\ldots$ being no-flow eigenvectors a reduced eigenproblem can be established by taking

$$\underset{m\times n_n}{[T]}^{T}\ \underset{n_n\times n_n}{[\mathcal{K}(K)]}\ \underset{n_n\times m}{[T]}\ \{\alpha\} = 0$$

or
$$\underset{m\times m}{[\mathcal{K}'(K)]}\{\alpha\} = 0 \qquad (4.3.37)$$

The eigenvalues of equation (4.3.37) will approximate those of equation (4.3.36). If $m < n_n$ one obtains low-order eigenvalues.

In construction of the transformation matrix $[T]$, containing m no-flow eigenvectors one can solve the no-flow eigenproblem (in Section 4.3.1) with an eigenmatrix of 1/4 size of $[\mathcal{K}(K)]$. This gives the eigenvector $\{p\}$, (part of δ_0). Inspection of equation (4.3.30) when $\bar{W}_o$ is set to be zero enables the condensation vectors for w, u, v to be constructed in the sense of FEM approximations in terms of :

$$\left[\int_0^R N_i N_j\ 2\pi r\ dr\right]\{w\} = \left[\int_0^R \frac{k_z}{k}\frac{1}{\bar{\rho}_o}\ N_i N_j\ 2\pi r\ dr\right]\{p\}$$

$$\left[\int_0^R N_i N_j\ 2\pi r\ dr\right]\{u\} = \left[\int_0^R \frac{i}{\bar{\rho}_o k}\ N_i N_{j_r}\ 2\pi r\ dr\right]\{p\}$$

$$\left[\int_0^R N_i N_j\ 2\pi r\ dr\right]\{v\} = \left[\int_0^R \frac{m_o}{kr}\frac{1}{\bar{\rho}_o}\ N_i N_j\ 2\pi r\ dr\right]\{p\}$$

These are available when equation (4.3.30) has been assembled.

As a result, with no-flow condensation the FEM becomes an almost exact numerical analogue of the MWR which uses a no-flow basis functions for the problem with flow. This implies that the number m of "master" degrees of freedom must be sufficient for representation of eigenvectors of the flow case, and the condensation technique results in a degradation in the accuracy of individual eigenvalues in comparison to the original ones. This trend is observed in numerical experiments [104].

4.4 CONCLUSIONS

The MWR using trigonometric basis functions has been developed for the eigenproblem in circular ducts with or without flow. The trend

of convergence has been established. The results compare favourably with exact solutions and especially give excellent agreements for the no-flow case.

Satisfactory eigenvalues were obtained for circular ducts, with hard and soft walls, with and without uniform mean flow, and for angular modes up to approximately $m_o = 20$. Experimentation with angular modes as high as $m_o = 30$ indicated that inaccuracies begin to creep in and very high angular mode results may not be practical without further basis function modification.

The eigenvalue scheme based on numerical integration of a nonlinear differential equation derived from the transcendental eigenequations has been extended from the two-dimensional case to circular lined ducts with uniform flow. This provides "exact" eigenvalues for comparisons. A proof has been given to reveal two extra modes which exist in uniform flow ducts only for admittances having a positive imaginary part. These modes have no counterparts in the hardwall case.

In view of extensions of the method to the transmission problem in nonuniform ducts with flow the effect of weighting factors on residual equations has been investigated providing useful experience for later use. Some appropriate properties of hydrodynamic modes have also been derived.

The FEM has been developed here for the eigenproblem not to compete with the MWR, but rather to generate confidence when applied to nonuniform duct problems. However, it has more flexibility for ducts with complicated cross-section. In the study of nonuniformities the MWR and FEM can be used to produce consistent uniform duct solutions for matching at the interfaces.

In considering the accuracy of the FEM it is found to be comparable to MWR approaches and favourably relative to exact eigenvalues for modes of sufficiently low order. Both the MWR and the FEM suffer the inherent degradation of accuracy for high-order modes. The situation becomes increasingly severe at high values of frequency, admittance, flow speed and for high angular modes.

TABLE 4.9

Comparison of FEM Values of k_z/k with Runge-Kutta Values; kR = 1.0, M_o = 0

	m_o = 0 A = (1.0 + 1.0i)		m_o = 1 A = (0. ,0.)	
Mode	FEM (5)	RUNGE-KUTTA	FEM (5)	RUNGE-KUTTA
1^+	1.880-0.845i	1.880-0.845i	-1.546i	-1.546i
2^+	0.279-3.415i	0.278-3.414i	-5.240i	-5.237i
3^+	0.151-6.867i	0.145-6.798i	-8.520i	-8.478i
4^+	0.102-10.346i	0.099-10.025i	-12.250i	-11.663i
5^+	0.079-13.591i	0.075-13.211i		-14.830i
6^+	0.094-17.929i	0.061-16.379i		-17.988i
7^+		0.051-19.539i	-21.678i	-21.141i
8^+		0.044-22.694i		-24.291i
9^+		0.039-25.846i	-27.160i	-27.439i
10^+		0.034-28.995i	-31.012i	-30.586i

TABLE 4.10

Comparison of FEM Values of k_z/k with Runge-Kutta Values; Softwalled Duct, A = (0.72 + 0.42i); kR = 1.0, M_o = -0.5, m_o = 0

Mode	FEM (2)	FEM (3)	FEM (5)	RUNGE-KUTTA
1^+	1.405-1.829i	1.404-1.829i	1.404-1.829i	1.405-1.832i
1^-	-0.868+0.176i	-0.868+0.176i	-0.868+0.176i	-0.868+0.176i
2^+	0.557-5.630i	0.570-5.558i	0.574-5.535i	0.572-5.550i
2^-	1.035+3.156i	1.031+3.153i	1.031+3.152i	1.033+3.157i
3^+	-5.566-3.975i	-5.577-3.967i	-5.579-3.966i	-5.580-3.966i
3^-	1.303+6.646i	1.275+6.645i	1.261+6.508i	1.261+6.523i
4^+	0.474-9.853i	0.417-9.774i	0.436-9.548i	0.443-9.529i
4^-	1.017+10.219i	1.173+10.261i	1.156+10.018i	1.138+9.986i
5^+	0.252-13.204i	0.541-13.051i	0.441-13.609i	0.453-13.360i
5^-	1.449+13.678i	0.884+13.200i	1.032+13.862i	1.019+13.606i
6^+		0.456-16.148i	0.645-15.898i	0.479-17.128i
6^-		0.987+16.331i	0.701+15.917i	0.942+17.280i
7^+			0.440-18.244i	0.502-20.874i
7^-			0.992+18.413i	0.891+20.977i
8^+			0.489-22.920i	0.520-24.616i
8^-			0.901+23.020	0.856+24.691i

TABLE 4.11

Comparison of FEM Values of k_z/k with Runge-Kutta Values; Softwalled Duct, $A = (0.72 + 0.42i)$; $kR = 1.0$, $M_o = -0.5$, $m_o = 2$

Mode	FEM (2)	FEM (3)	FEM (5)	RUNGE-KUTTA
1^+	0.615-5.040i	0.618-5.022i	0.619-5.015i	0.620-5.014i
1^-	0.410+1.291i	0.410+1.290i	0.410+1.290i	0.410+1.290i
2^+	-5.806-3.911i	-5.817-3.899i	-5.819-3.897i	-5.820-3.897i
2^-	1.270+6.128i	1.266+6.100i	1.261+6.088i	1.259+6.085i
3^+	0.471-9.168i	0.445-9.254i	0.442-9.215i	0.445-9.187i
3^-	1.080+9.594i	1.134+9.730i	1.152+9.701i	1.146+9.668i
4^+	0.232-13.320i	0.483-12.666i	0.463-13.107i	0.453-13.062i
4^-	1.452+13.810i	0.992+12.895i	1.002+13.349i	1.022+13.315i
5^+		0.465-16.483i	0.572-15.872i	0.480-16.822i
5^-		0.968+16.655i	0.810+15.961i	0.943+16.977i
6^+			0.468-18.568i	0.503-20.531i
6^-			0.952+18.711i	0.891+20.635i
7^+			0.493-23.000i	0.522-24.213i
7^-			0.896+23.096i	0.855+24.288i
8^+			0.436-28.065i	0.538-27.880i
8^-			0.956+28.166i	0.829+27.937i

TABLE 4.12

Comparison of FEM Values of k_z/k (with Different Weighting Factors) with Exact Values; Hardwalled Duct, A = (0.0 + 0.0i); kR = 5.0, M_o = -0.5, m_o = 2

Mode	Weighting Factor = 1			Exact Values	Weighting Factor = r		
	FEM (2)	FEM (3)	FEM (5)		FEM (2)	FEM (3)	FEM (5)
1^+	-1.798+0.000i	-1.798+0.000i	-1.798+0.000i	-1.798 + 0.000i	-1.798+0.000i	-1.798+0.000i	-1.798+0.000i
1^-	0.465+0.000i	0.465+0.000i	0.465+0.000i	0.465+0.000i	0.465+0.000i	0.465+0.000i	0.465+0.000i
2^+	-0.667-0.811i	-0.667-0.804i	-0.667-0.792i	-0.667-0.788i	-0.667-0.791i	-0.667-0.791i	-0.667-0.789i
3^+	-0.667-1.798i	-0.667-1.852i	-0.667-1.892i	-0.667-1.877i	-0.667-1.831i	-0.667-1.834i	-0.667-1.878i
4^+		-0.667-2.636i	-0.667-2.680	-0.667-2.734i		-0.667-2.681i	-0.667-2.645i
5^+			-0.667-3.138i	-0.667-3.532i			-0.667-3.136i
6^+		-0.667-3.548i	-0.667-3.986i	-0.667-4.166i	-0.667-4.000i	-0.667-3.581i	-0.667-4.006i
7^+	-0.667-4.474i		-0.667-4.900i	-0.667-5.063i	-0.667-4.802i	-0.667-5.021i	-0.667-4.910i
8^+	-0.667-5.777i		-0.667-6.161i	-0.667-5.813i			-0.667-6.164i

Note: Values for modes 2^-, 3^-, ...8^- are conjugates of values for positively running modes

TABLE 4.13

Comparison of FEM Values of k_z/K (with Weighting Factor r) with Runge-Kutta Values; Softwalled Duct, $A = (0.72 + 0.42i)$; $kR = 1.0$, $M_o = -0.5$, $m_o = 0$

Mode	FEM (2)	FEM (3)	FEM (5)	RUNGE-KUTTA
1^+	1.387-1.808i	1.396-1.820i	1.401-1.826i	1.405-1.832i
1^-	-0.868+0.176i	-0.868+0.176i	-0.868+0.176i	-0.868+0.176i
2^+	0.622-5.071i	0.606-5.254i	0.589-5.413i	0.572-5.550i
2^-	0.975+3.035i	1.002+3.096i	1.020+3.131i	1.033+3.157i
3^+	-5.571-3.969i	-5.579-3.967i	-5.580-3.966i	-5.580-3.966i
3^-	1.247+6.053i	1.215+6.189i	1.228+6.358i	1.261+6.523i
4^+	0.464-9.001i	0.473-8.894i	0.470-9.088i	0.443-9.529i
4^-	1.101+9.459i	1.098+9.349i	1.103+9.531i	1.138+9.986i
5^+	0.173-13.474i	0.455-12.142i	0.516-12.220i	0.453-13.360i
5^-	1.541+14.023i	1.054+12.424i	0.923+12.420i	1.019+13.606i
6^+		0.447-16.311i	0.518-14.539i	0.479-17.128i
6^-		0.996+16.500i	0.915+14.688i	0.942+17.280i
7^+			0.434-18.459i	0.502-20.874i
7^-			0.998+18.629i	0.891+20.977i
8^+		0.139-22.801i	0.492-23.151i	0.520-24.616i
8^-		0.139+23.090i	0.896+23.247i	0.856+24.691i

TABLE 4.14

Comparison of FEM Values of k_z/k (with Weighting Factor r) with Runge-Kutta Values; Softwalled Duct, $A = (0.72 + 0.42i)$; $kR = 1.0$, $M_o = -0.5$, $m_o = 2$

Mode	FEM (2)	FEM (3)	FEM (5)	RUNGE-KUTTA
1^+	0.619-5.016i	0.619-5.015i	0.620-5.014i	0.620-5.014i
1^-	0.410+1.290i	0.410+1.290i	0.410+1.290i	0.410+1.290i
2^+	-5.808-3.902i	-5.818-3.898i	-5.819-3.897i	-5.820-3.897i
2^-	1.261+6.088i	1.261+6.087i	1.260+6.086i	1.259+6.085i
3^+	0.462-9.146i	0.450-9.189i	0.444-9.196i	0.445-9.187i
3^-	1.103+9.593i	1.126+9.659	1.147+9.678i	1.146+9.668i
4^+			0.468-13.007i	0.453-13.062i
4^-			0.995+13.245i	1.022+13.315i
5^+			0.564-15.731i	0.480-16.822i
5^-			0.824-15.832i	0.943+16.977i
6^+			0.463-18.655i	0.503-20.531i
6^-			0.957+18.801i	0.891+20.635i
7^+	0.655-21.305i	0.157-22.807i	0.495-23.056i	0.522-24.213i
7^-	0.682+21.311i	1.358+23.087i	0.892+23.150i	0.855+24.288i
8^+		0.653-26.020i	0.436-28.137i	0.538-27.880i
8^-		0.687+26.024i	0.955+28.237i	0.829+27.937i

CHAPTER 5

SOUND TRANSMISSION IN DUCTS WITH NO FLOW

In the no-flow case, if the reference state is the ambient state in the duct, the governing equations (2.2.19) and (2.2.30) become :

$$ik\underline{V} = -\underline{\nabla} p \qquad \text{(momentum)} \tag{5.0.1}$$

$$ikp + \underline{\nabla}\cdot\underline{V} = 0 \qquad \text{(energy or continuity)} \tag{5.0.2}$$

or in the form of a Helmholtz wave equation

$$(\nabla^2 + k^2)p = 0 \tag{5.0.3}$$

where $$\nabla^2 \equiv \left(\frac{\partial}{\partial r^2} + \frac{1}{r}\frac{\partial}{\partial r} + \frac{\partial^2}{r^2\partial\theta^2} + \frac{\partial^2}{\partial z^2}\right)$$

and the duct-wall boundary condition (2.1.4) becomes

$$\underline{V}\cdot\underline{\nu} = Ap \tag{5.0.4}$$

or, from the momentum equation (5.0.1),

$$\underline{\nabla} p\cdot\underline{\nu} = -ikAp \quad \text{on} \quad C_3 \tag{5.0.5}$$

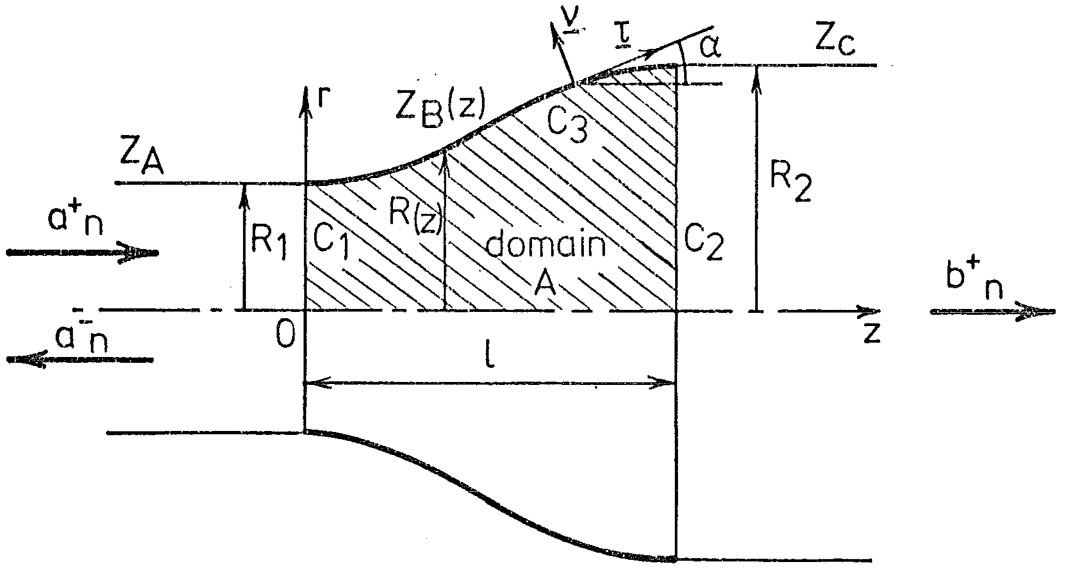

FIG 5·1 DUCT GEOMETRY AND CONFIGURATION.

5.1 MWR SOLUTION

5.1.1 Formulation

(i) General formulation:

Consider the duct section (B) shown in Figure 5.1, in which the wall is of admittance $A = A(z)$ at $r = R(z)$. In terms of cylindrical coordinates (r,θ,z) with an angular harmonic dependence explicitly assumed, the solution can be written in the form:

$$\begin{aligned} p &= p(r,z)\ e^{-im_o\theta} \\ \underline{V} &= (u,v,w)\ e^{-im_o\theta} \end{aligned} \tag{5.1.1}$$

where u,v,w are function of (r,z), m_o is the angular mode number. By substituting equations (5.1.1) into (5.0.1), (5.0.2) and (5.0.3) one obtains the conservation equations and boundary condition as following

$$iku(r,z) + \frac{\partial p(r,z)}{\partial r} = 0 \tag{5.1.2}$$

$$ikv(r,z) - \frac{im_o}{r}\, p(r,z) = 0 \tag{5.1.3}$$

$$ikw(r,z) + \frac{\partial p(r,z)}{\partial z} = 0 \tag{5.1.4}$$

$$ikp(r,z) + \frac{1}{r}\frac{\partial}{\partial r}\left(ru(r,z)\right) - \frac{im_o}{r}\, v(r,z) + \frac{\partial w}{\partial z}(r,z) = 0 \tag{5.1.5}$$

B.C.: $u\cos\alpha - w\sin\alpha = A(z)\ p(r,z)$ at $r = R(z)$ (5.1.6)

where $\tan\alpha = \dfrac{dR(z)}{dz}$: wall slope

Following the Modified Galerkin method one seeks the solutions to this problem in the form of a finite series of basis functions, as yet unspecified :

$$p(r,z) \approx p_N = \sum_{m=1}^{N} p_m\, \psi_m \tag{5.1.7}$$

$$u(r,z) \approx u_N = \sum_{m=1}^{N} u_m\, \phi_m \tag{5.1.8}$$

$$v(r,z) \approx v_N = \sum_{m=1}^{N} v_m\, \psi_m \tag{5.1.9}$$

$$w(r,z) \approx w_N = \sum_{M=1}^{N} w_m \psi_m \tag{5.1.10}$$

where p_m, u_m, v_m and w_m are functions of z, and ψ_m and ϕ_m are functions of (r,z). The introduction of a different basis function ϕ_m for the u component is consistent with the derivative with respect to r in the u-nomentum equation (5.1.2) in view of trigonometric functions being employed later.

If the trial solutions (5.1.7) - (5.1.10) are substituted into equations (5.1.2) - (5.1.6), in general, one obtains the residuals

$$R_1 = iku_N + \frac{\partial p_N}{\partial r} \tag{5.1.11}$$

$$R_2 = ikv_N - \frac{im_o}{r} p_N \tag{5.1.12}$$

$$R_3 = ikw_N + \frac{\partial p_N}{\partial z} \tag{5.1.13}$$

$$R_4 = ikp_N + \frac{1}{r}\frac{\partial}{\partial r}(ru_N) - \frac{im_o}{r} v_N + \frac{\partial w_N}{\partial z} \tag{5.1.14}$$

$$R_B = (u_N \cos\alpha - w_N \sin\alpha - Ap_N) \text{ at } r = R(z) \tag{5.1.15}$$

The residuals R_1, R_2, R_3, R_4 and R_B are forced to be orthogonal over appropriate domains to every member of the complete set formed by the basis functions themselves. To expose boundary terms the residuals are weighted at a station z along the duct axis as follows :

$$\int_0^R \frac{\partial}{\partial r}(r\,\psi_n)\, R_1 \quad 2\pi r\, dr = 0 \tag{5.1.16}$$

$$\int_0^R \psi_n\, R_2 \quad 2\pi r\, dr = 0 \tag{5.1.17}$$

$$\int_0^R \psi_n\, R_3 \quad 2\pi r\, dr = 0 \tag{5.1.18}$$

$$\int_0^R r\psi_n \, R_4 \quad 2\pi r \, dr = 0 \tag{5.1.19}$$

$$\psi_n(R) \, R_B = 0 \quad \text{at} \quad r = R(z) \tag{5.1.20}$$

for n = 1,2,3...N

When equations (5.1.11) - (5.1.14) are made use of, equations (5.1.16) - (5.1.20) become in a more detailed form :

$$\int_0^R r \, u_N \frac{\partial}{\partial r}(r\psi_n) \, dr = \frac{i}{k} \int_0^R r \frac{\partial p_N}{\partial r} \quad \frac{\partial}{\partial r}(r\psi_n) \, dr \tag{5.1.21}$$

$$\int_0^R r \, v_N \psi_n \, dr = \frac{m_o}{k} \int_0^R p_N \psi_n \, dr \tag{5.1.22}$$

$$ik \int_0^R r \, w_N \psi_n \, dr + \int_0^R r \frac{\partial p_N}{\partial z} \, \psi_n \, dr = 0 \tag{5.1.23}$$

$$ik \int_0^R r^2 \, p_N \psi_n \, dr + \int_0^R r \frac{\partial}{\partial r}(r u_N) \, \psi_n \, dr - im_o \int_0^R r \, v_N \psi_n \, dr$$

$$+ \int_0^R r^2 \frac{\partial w_N}{\partial z} \, \psi_n \, dr = 0 \tag{5.1.24}$$

$$(u_N \cos \alpha - w_N \sin \alpha) = A p_N \quad \text{at} \quad r = R(z) \tag{5.1.25}$$

for n = 1,2,3...N

Further operations are typified by considering the energy equation (5.1.24). Integration by parts is performed on the 2nd. term and elimination of u_N and v_N by the use of equations (5.1.21) and (5.1.22) gives :

$$k^2 \int_0^R \left(r^2 - \frac{m_o^2}{k^2}\right) p_N \psi_n \, dr - ik R^2 u_N(R) \psi_n(R)$$

$$- \int_0^R r \frac{\partial p_N}{\partial r} \frac{\partial}{\partial r}(r\psi_n) \, dr - ik \int_0^R r^2 \frac{\partial w_N}{\partial z} \psi_n \, dr = 0 \qquad (5.1.26)$$

By using the Leibnitz rule for differentiation of integrals containing a parameter, the partial derivatives of w_N and p_N with respect to z in (5.1.23) and (5.1.26) can be replaced by ordinary derivatives and the partial derivatives with respect to r can be eliminated by integration by parts to expose boundary terms, one obtains two sets of residual equations :

$$\frac{d}{dz} \int_0^R r p_N \psi_n \, dr = \int_0^R p_N \frac{\partial}{\partial z}(r\psi_n) \, dr + R p_N(R) \psi_n(R) \tan \alpha$$

$$- ik \int_0^R r w_N \psi_n \, dr \qquad (5.1.27)$$

$$\frac{d}{dz} \int_0^R r^2 w_N \psi_n \, dr = - ik \int_0^R \left(r^2 - \frac{m_o^2}{k^2}\right) p_N \psi_n \, dr + \frac{i}{k} \left[r \frac{\partial}{\partial r}(r\psi_n) p_N \right]_{r=R}$$

$$- \frac{i}{k} \int_0^R p_N \frac{\partial}{\partial r} \left[r \frac{\partial}{\partial r}(r\psi_n) \right] dr + \int_0^R r^2 w_N \frac{\partial \psi_n}{\partial z} \, dr$$

$$- R^2 \frac{\psi_n(R)}{\cos \alpha} (u_N \cos \alpha - w_N \sin \alpha) \qquad (5.1.28)$$

for n = 1,2,3...N

The boundary residual equation (5.1.25) can be substituted into the last term of (5.1.28) to eliminate u_N completely. The two sets of equations (5.1.27) and (5.1.28) can be then rewritten :

$$\frac{d}{dz}\int_0^R r\, p_N\psi_n\, dr = \int_0^R r\, p_N \frac{\partial\psi_n}{\partial z} - ik\int_0^R r\, w_N\psi_n\, dr$$

$$+ R\, p_N(R)\psi_n(R)\tan\alpha \qquad (5.1.29)$$

$$\frac{d}{dz}\int_0^R r^2\, w_N\psi_n\, dr = -ik\left[\int_0^R \left(r^2 - \frac{m_o^2}{k^2}\right) p_N\psi_n\, dr + \frac{1}{k^2}\int_0^R p_N \frac{\partial}{\partial}\left[r\frac{\partial}{\partial r}(r\psi_n)\right] dr\right]$$

$$+ \int_0^R r^2\, w_N \frac{\partial\psi_n}{\partial z}\, dr + \frac{iR}{k}\left[\frac{\partial}{\partial r}(r\psi_n) + ikR\frac{A}{\cos\alpha}\psi_n\right]_{r=R} p_N(R) \qquad (5.1.30)$$

for n = 1,2,3,...N

Using equations (5.1.7) and (5.1.10) one can write the residual equations (5.1.29) and (5.1.30) in a matrix form :

$$\begin{bmatrix} M_{nm} & 0 \\ 0 & N_{nm} \end{bmatrix} \begin{Bmatrix} \frac{dw_m}{dz} \\ \frac{dp_m}{dz} \end{Bmatrix} = \begin{bmatrix} W^w_{nm} & W^p_{nm} \\ P^w_{nm} & P^p_{nm} \end{bmatrix} \begin{Bmatrix} w_m \\ p_m \end{Bmatrix} \qquad (5.1.31)$$

where

$$M_{nm} = \int_0^R r^2\, \psi_n\psi_m\, dr \qquad (5.1.32)$$

$$N_{nm} = \int_0^R r\, \psi_n\psi_m\, dr \qquad (5.1.33)$$

$$W^w_{nm} = \int_0^R r^2 \frac{\partial\psi_n}{\partial z}\, \psi_m\, dr - \frac{d}{dz}\int_0^R r^2\, \psi_n\psi_m\, dr \qquad (5.1.34)$$

$$W^p_{nm} = -ik\left[\int_0^R \left(r^2 - \frac{m_o^2}{k^2}\right)\psi_n\psi_m\, dr + \frac{1}{k^2}\int_0^R \frac{\partial}{\partial r}\left[r\frac{\partial}{\partial r}(r\psi_n)\right]\psi_m\, dr\right]$$

$$+ \frac{iR}{k}\left[\frac{\partial}{\partial r}(r\psi_n) + ikR\frac{A}{\cos\alpha}\psi_n\right]_{r=R}\psi_m(R) \qquad (5.1.35)$$

$$P^{w}_{nm} = -ik \int_0^R r\, \psi_n \psi_m \, dr \tag{5.1.36}$$

$$P^{p}_{nm} = -\frac{d}{dz} \int_0^R r\, \psi_n \psi_m \, dr + \int_0^R r \frac{\partial \psi_n}{\partial z} \cdot \psi_m \, dr + R\, \psi_n(R) \cdot \psi_m(R) \tan\alpha \tag{5.1.37}$$

for $(m = 1,2,\ldots N)$ and $(n = 1,2,\ldots N)$

(ii) With basis functions specified

In the matrix equation (5.1.31), the basis functions are chosen as eigenfunctions in the 2D duct problem, that is

$$\psi_m(r,z) = \cos(K_m r) \quad , \; m = 1,2,\ldots N \tag{5.1.38}$$

The K_m are defined by the sequence of eigenvalues of the transcendental equation

$$K_m R \tan K_m R = iAkR \tag{5.1.39}$$

which is derived from the eigenproblem for propagation in a uniform 2D channel of half height R having the same admittance as the nonuniform duct has locally [Appendix C].

Then, the components of the equation (5.1.31) can be written more specifically as follows :

$$M_{nm} = \int_0^R r^2 \cos K_n r \cos K_m r \, dr \tag{5.1.40}$$

$$N_{nm} = \int_0^R r \cos K_n r \cos K_m r \, dr \tag{5.1.41}$$

$$W^{w}_{nm} = -\frac{dK_n}{dz} \int_0^R r^3 \sin K_n r \cos K_m r \, dr - \frac{d}{dz} M_{nm} \tag{5.1.42}$$

SEE ERRATA

$$W^{p}_{nm} = 3i \frac{\kappa_n R}{kR} \int_0^R r \sin \kappa_n r \cos \kappa_m r \, dr \tag{5.1.43}$$

$$+ \left(\frac{i}{k} \kappa_n^2 - ik\right) M_{nm}$$

$$+ (m_o^2 - 1) \frac{i}{k} \int_0^R \cos \kappa_n r \cos \kappa_m r \, dr$$

$$+ \left(\frac{1}{kR} - \frac{A}{\cos \alpha}\right) R^2 \cos \kappa_n R \cos \kappa_m R$$

$$- i \frac{\kappa_n R}{kR} \; R^2 \sin k_n R \cos \kappa_m R$$

$$P^{w}_{nm} = -ik \, N_{nm} \tag{5.1.44}$$

$$P^{p}_{nm} = - \frac{dN_{nm}}{dz} - \frac{d\kappa_n}{dz} \int_0^R r^2 \sin \kappa_n r \cos \kappa_m r \, dr$$

$$+ R \cos \kappa_n R \cos \kappa_m R \tan \alpha \tag{5.1.45}$$

for (m = 1,2...N) and (n = 1,2,...N)

Dividing the 1st. set of equations in (5.1.31) by R^2 and the 2nd. set by R, and changing variables by putting $\eta = \frac{r}{R}$, one can rewrite the resultant equations into a matrix form with nondimensional terms :

$$\begin{bmatrix} R\bar{M}_{nm} & 0 \\ 0 & R\bar{N}_{nm} \end{bmatrix} \begin{Bmatrix} \frac{dw_m}{dz} \\ \frac{dp_m}{dz} \end{Bmatrix} = \begin{bmatrix} \bar{W}^{w}_{nm} & \bar{W}^{p}_{nm} \\ \bar{P}^{w}_{nm} & \bar{P}^{p}_{nm} \end{bmatrix} \begin{Bmatrix} w_m \\ p_m \end{Bmatrix} \tag{5.1.46}$$

where

$$\bar{M}_{nm} = \int_0^1 \eta^2 \cos (\kappa_n R \, \eta) \cos (\kappa_m R \, \eta) \, d\eta \tag{5.1.47}$$

$$\bar{N}_{nm} = \int_0^1 \eta \cos (\kappa_n R \, \eta) \cos (\kappa_m R \, \eta) \, d\eta \tag{5.1.48}$$

$$\bar{W}^{w}_{nm} = R^2 \frac{d\kappa_m}{dz} \int_0^1 \eta^3 \cos (\kappa_m R \, \eta) \sin (\kappa_m R \, \eta) \, d\eta \tag{5.1.49}$$

$$\bar{W}^{p}_{nm} = 3i \frac{\kappa_n R}{kR} \int_0^1 \eta \sin(\kappa_n R\,\eta)\cos(\kappa_m R\,\eta)\, d\eta \qquad (5.1.50)$$

$$+ \left[\left(\frac{\kappa_n R}{kR}\right)^2 - 1\right] ikR\, \bar{M}_{nm}$$

$$+ (m_o^2 - 1) \frac{1}{kR} \int_0^1 \cos(\kappa_n R\,\eta)\cos(\kappa_m R)\eta\, d\eta$$

$$+ \left(\frac{1}{kR} - \frac{A}{\cos\alpha}\right) \cos(\kappa_n R)\cos(\kappa_m R)$$

$$- i \frac{\kappa_n R}{kR} \sin(\kappa_n R)\cos(\kappa_m R)$$

$$\bar{P}^{w}_{nm} = - ikR\, \bar{N}_{nm} \qquad (5.1.51)$$

$$\bar{P}^{p}_{nm} = R^2 \frac{d\kappa_m}{dz} \int_0^1 \eta^2 \sin(\kappa_m R\,\eta)\cos(\kappa_n R\,\eta)\, d\eta \qquad (5.1.52)$$

The matrix equation (5.1.46) can be rewritten in the form:

$$\frac{d}{dz} \begin{Bmatrix} w_m \\ \hline p_m \end{Bmatrix} = \left[\begin{array}{c|c} [R\bar{M}_{nm}]^{-1}[\bar{W}^{w}_{nm}] & [R\bar{M}_{nm}]^{-1}[\bar{W}^{p}_{nm}] \\ \hline [R\bar{N}_{nm}]^{-1}[\bar{P}^{w}_{nm}] & [R\bar{N}_{nm}]^{-1}[\bar{P}^{p}_{nm}] \end{array}\right] \begin{Bmatrix} w_m \\ \hline p_m \end{Bmatrix} \qquad (5.1.53)$$

The set of first order ordinary differential equations (5.1.53) governs the acoustic field in the nonuniform duct section in an approximate sense. By the use of an integration scheme such as a fourth-order Runge-Kutta it can be integrated from z = 0 to z = ℓ to yield a transition matrix relating w_m, p_m at z = 0 to w_m, p_m at z = ℓ:

$$\begin{Bmatrix} w_m(\ell) \\ p_m(\ell) \end{Bmatrix}_{z=\ell} = [TS] \begin{Bmatrix} w_m(0) \\ p_m(0) \end{Bmatrix}_{z=0} \qquad (5.1.54)$$

where [TS] is the transition matrix.

SEE ERRATA

5.1.2 Matching at the Ends of the Nonuniformity

With the matching procedures proposed in Section 2.1.2(ii) the acoustic field in the semi-infinite ducts must be solved for, which in fact is the eigenproblem encountered in Chapter 4. Here the matching at the ends of the nonuniformity is approached in two ways which are much dependent upon the method of solution to uniform duct problems.

(i) Exact solutions in uniform ducts.

For the semi-infinite duct (A) with $z < 0$, in general, one can write, for the m_o^{th} anglular mode:

$$\bar{w}(r,z) = \sum_{m=1} \left(\frac{\bar{k}_{zm}}{k} \right) \left[a_n^+ e^{-i\bar{k}_{zm} z} - a_n^- e^{+i\bar{k}_{zm} z} \right] J_{m_o}(\bar{K}_m r)$$

$$\bar{p}(r,z) = \sum_{m-1} \left[a_m^+ e^{-i\bar{k}_{zm} z} + a_m^- e^{+i\bar{k}_{zm} z} \right] J_{m_o}(\bar{K}_m r) \qquad (5.1.55)$$

SEE ERRATA

where a_m^+, a_m^- are the coefficients of the incident and reflected waves respectively. $\bar{k}_{zm}$, $\bar{K}_m$ are the eigenvalues for propagation given by the eigen equation

$$K_m R \, J'_{m_o}(\bar{K}_m R) = -i A k R \, J_{m_o}(\bar{K}_m R)$$

$$\frac{\bar{k}_{zm}}{k} = \pm \sqrt{1 - \left(\frac{\bar{K}_m R}{kR} \right)^2} \qquad (5.1.56)$$

where J_{m_o} is the Bessel function of the first kind of order m_o, and in equations (5.1.56) the plus sign is chosen if $\bar{k}_{zm}/k$ is real and if $\bar{k}_{zm}/k$ is complex the sign is chosen to make the imaginary part negative.

At the interface $z = 0$, in the nonuniformity, the approximation by equations (5.1.7) - (5.1.10) is used

$$w(r,z) = \sum_{m=1}^{N} w_m \cos K_m r$$

$$p(r,z) = \sum_{m=1}^{N} p_m \cos K_m r \qquad (5.1.57)$$

For matching at z = 0, the particle velocity and pressure are forced to be continuous, hence, from relations (5.1.55) and (5.1.57)

$$\bar{w}(r,z) = w(r,z)$$

$$\bar{p}(r,z) = p(r,z)$$

over the interface at z = 0

or
$$\begin{aligned} \sum_{m=1}^{N} \left(\frac{\bar{k}_{zm}}{k}\right)\left[a_m^+ - a_m^-\right] J_{m_o}(\bar{\kappa}_m r) &= \sum_{m=1}^{N} w_m \cos \kappa_m r \\ \sum_{m=1}^{N} \left[a_m^+ + a_m^-\right] J_{m_o}(\bar{\kappa}_m r) &= \sum_{m=1}^{N} p_m \cos \kappa_m r \end{aligned} \tag{5.1.58}$$

If the same number of uniform duct eigenfunctions as there are basis functions in the nonuniformity is used then the weighted residuals over equations (5.1.58) can be made use of to obtain a matrix relation between the a_m^+, a_m^- and the w_m, p_m at z = 0. This weighted residual procedure yields

$$\left[\begin{array}{c|c} \alpha_{nm} & \\ \hline & \alpha_{nm} \end{array}\right]\left\{\begin{array}{c} w_m(0) \\ \hline p_m(0) \end{array}\right\} = \left[\begin{array}{c|c} \left(\frac{\bar{k}_{zm}}{k}\right)\bar{\alpha}_{nm} & -\left(\frac{\bar{k}_{zm}}{k}\right)\bar{\alpha}_{nm} \\ \hline \bar{\alpha}_{nm} & \bar{\alpha}_{nm} \end{array}\right]\left\{\begin{array}{c} a_m^+ \\ \hline a_m^- \end{array}\right\} \tag{5.1.59}$$

or

$$\left\{\begin{array}{c} w_m(0) \\ \hline p_m(0) \end{array}\right\} = \left[\begin{array}{c|c} \left(\frac{\bar{k}_{zm}}{k}\right)[\bar{B}] & -\left(\frac{\bar{k}_{zm}}{k}\right)[\bar{B}] \\ \hline [\bar{B}] & [\bar{B}] \end{array}\right]\left\{\begin{array}{c} a_m^+ \\ \hline a_m^- \end{array}\right\} \tag{5.1.60}$$

where, at z = 0

$$\alpha_{nm} = \int_0^1 \eta \cos(\kappa_m R\,\eta)\cos(\kappa_n R\,\eta)\, d\eta$$

$$\bar{\alpha}_{nm} = \int_0^1 \eta\, J_{nm}(\bar{\kappa}_m R\,\eta)\cos(\kappa_n R\,\eta)\, d\eta$$

$$[\bar{B}] = [\alpha_{nm}]^{-1}\,[\bar{\alpha}_{nm}]$$

An exactly analogous relationship can be obtained at $z = \ell$:

$$\begin{Bmatrix} w_m(\ell) \\ \hline p_m(\ell) \end{Bmatrix} = \left[\begin{array}{c|c} \left(\frac{\hat{k}_{zm}}{k}\right)[\hat{B}] & -\left(\frac{\hat{k}_{zm}}{k}\right)[\hat{B}] \\ \hline [\hat{B}] & [\hat{B}] \end{array}\right] \left[\begin{array}{c|c} e^{+}_{mn} & \\ \hline & e^{-}_{mn} \end{array}\right] \begin{Bmatrix} b^{+}_{m} \\ \hline b^{-}_{m} \end{Bmatrix} \tag{5.1.61}$$

where, for $z > \ell$, b^{+}_{m} and b^{-}_{m} are coefficients of transmitted and reflected waves respectively, $\hat{k}_{zm}$ and $\hat{K}_{m}$ are eigenvalues for propagation in the uniform duct (C) and at $z = \ell$

$$\beta_{nm} = \int_0^1 \eta \cos(K_m R\,\eta)\cos(K_n R\,\eta)\, d\eta$$

$$\hat{\beta}_{nm} = \int_0^1 \eta\, J_{m_o}(\hat{K}_m R\,\eta)\cos(K_n R\,\eta)\, d\eta$$

$$[\hat{B}] = [\beta_{nm}]^{-1}\,[\hat{\beta}_{nm}]$$

$$e^{+}_{nm} = e^{-i\hat{k}_{zm}\ell} \cdot \delta_{nm}$$

$$e^{-}_{nm} = e^{i\hat{k}_{zm}\ell} \cdot \delta_{nm}$$

Hence from equation (5.160), (5.1.61) the relations between the wave amplitudes in the uniform ducts and the approximation coefficients for the pressure and particle velocity in the nonuniform section (B) in the form

$$\begin{Bmatrix} w_m(0) \\ p_m(0) \end{Bmatrix} = [A(0)] \begin{Bmatrix} a^{+} \\ a^{-} \end{Bmatrix} \tag{5.1.62}$$

$$\begin{Bmatrix} w_m(\ell) \\ p_m(\ell) \end{Bmatrix} = [A(\ell)] \begin{Bmatrix} b^{+} \\ b^{-} \end{Bmatrix} \tag{5.1.63}$$

By using equations (5.1.54), (5.1.62) and (5.1.63) the wave amplitudes for $z > 0$ can be related to those for $z < 0$, namely :

$$\begin{Bmatrix} b^+ \\ b^- \end{Bmatrix} = [A(\ell)]^{-1} [TS] [A(0)] \begin{Bmatrix} a^+ \\ a^- \end{Bmatrix} \tag{5.1.64}$$

or

$$\begin{Bmatrix} b^+ \\ b^- \end{Bmatrix} = [TF] \begin{Bmatrix} a^+ \\ a^- \end{Bmatrix}$$

where $[TF] = [A(\ell)]^{-1} [TS] [A(0)]$ is the transfer matrix.

(ii) MWR solutions in uniform ducts

To describe the wave propagation in the uniform ducts with the same degree of accuracy as the description in the nonuniform section one can return to the matrix equation (5.1.53) written in the form :

$$\underset{2Nx1}{\frac{d}{dz} \begin{Bmatrix} w_m \\ p_m \end{Bmatrix}} = \underset{2N\ 2N}{[\mathcal{L}(z)]} \underset{2Nx1}{\begin{Bmatrix} w_m \\ p_m \end{Bmatrix}} \tag{5.1.65}$$

and note that in a uniform infinite duct the coefficients of $[\mathcal{L}]$ are independent of z, hence, constant. In that case solutions to equation (5.1.65) can be assumed in the form :

$$\underset{2Nx1}{\begin{Bmatrix} w_m \\ p_m \end{Bmatrix}} = \underset{2Nx1}{\{a\}}\ e^{-ik_z z} \tag{5.1.66}$$

The determination of the axial values k_z and the corresponding eigenvectors representing the 2N modes of propagation follows from the algebraic eigenvalue problem

$$i \underset{2Nx2N}{[\mathcal{L}]} \underset{2Nx1}{\{a\}} = k_z \underset{2Nx1}{\{a\}} \tag{5.1.67}$$

(a) Modal matrix

The general QR algorithm is a convenient method of obtaining solutions of equation (5.1.67). The solution for the uniform sections (A) and (C) are written (there is one solution at each end)

$$\underset{2Nx1}{\begin{Bmatrix} w_m \\ p_m \end{Bmatrix}} = \underset{2Nx2N}{[M]} \; \underset{2Nx2N}{[e]} \; \underset{2Nx1}{\begin{Bmatrix} a^+ \\ a^- \end{Bmatrix}} \tag{5.1.68}$$

where $[M]$ is the partitioned modal matrix whose columns are the eigenvectors corresponding to the modes of propagation. The first N columns correspond to N positive propagating modes, the second N columns corresponding to negative propagating modes. The matrix $[e]$ is diagonal, partitioned in the same way as $[M]$, representing the general solution in the form of equation (5.1.66), with a typical element being $e_{nn} = e^{-ik_{zn}z}$, n = 1,2,3...N for positive z and n = N + 1, N + 2...2N for negative z.

From equations (5.1.7), (5.1.10) and (5.1.38) the assumed solution in a uniform section in terms of basis functions can be written as follows :

$$\underset{2x1}{\begin{Bmatrix} w_1(r,z) \\ - - - - \\ p_1(r,z) \end{Bmatrix}} = \underset{2x2N}{\left[\begin{array}{c|c} [\cos K_m r] & \\ \hline 1xN & [\cos K_m r] \\ & 1xN \end{array}\right]} \underset{2Nx1}{\begin{Bmatrix} w_m \\ - - \\ p_m \end{Bmatrix}}$$

$$= \underset{2x2N}{[C]} \underset{2xN1}{\begin{Bmatrix} w_m \\ p_m \end{Bmatrix}} \tag{5.1.69}$$

where the K_m, and hence the matrix $[C]$, are appropriate for the admittance in the uniform sections.

Equations (5.1.68) and (5.1.69) are combined to yield the solutions in the semi-infinite ducts (A) or (C) in terms of appropriate modal matrices :

$$\underset{2x1}{\begin{Bmatrix} w_1 \\ p_1 \end{Bmatrix}} = \underset{2x2N}{[C]} \; \underset{2Nx2N}{[M]} \; \underset{2Nx2N}{[e]} \; \underset{2Nx1}{\begin{Bmatrix} a^+ \\ a^- \end{Bmatrix}} \tag{5.1.70}$$

For convenience the diagonal matrix $[e]$ can be absorbed into the propagation coefficients, i.e. the coefficients are direct reflection or transmissions coefficients, which are referred to the appropriate end of the nonuniformity.

In order to attach a meaning to the amplitudes of acoustic modes a^+ and a^-, it is required to normalize the eigenvectors in $[M]$. To perform the normalization in a rational manner it is necessary to note that the assumed solution in the uniform ducts can be written in the modal form

$$\begin{Bmatrix} w_1 \\ p_1 \end{Bmatrix} = [C] \begin{bmatrix} M^w \\ - - \\ M^p \end{bmatrix} [e] \begin{Bmatrix} a^+ \\ a^- \end{Bmatrix}$$

In a given mode, say mode j, negative running or positive running, from the above equations the acoustic pressure is given by

$$\underset{1xN}{p_1(r,z)} = \underset{1xN}{[\cos \kappa_m r]} \underset{Nx1}{\begin{Bmatrix} M^p_j \end{Bmatrix}} e^{-ik_{zj} z} \cdot a_j$$

where $\begin{Bmatrix} M^p_j \end{Bmatrix}$ is the eigenvector in the modal matrix, representing the pressure contribution in the j^{th} mode. At the duct centre line (r = 0), the pressure is

$$p_1(r=0,z) = e^{-ik_{zj} z} \; a_j \sum_{i=1}^{N} M^p_{ij}$$

and at the duct wall (r = R)

$$p_1(r=R,z) = e^{-ik_{zj} z} \; a_j \sum_{i=1}^{N} M^p_{ij} \cos(\kappa_i R)$$

Thus, if $\sum_{i=1}^{N} M^p_{ij} = 1$, then a_j is the pressure at the duct centre line and if $\sum_{i=1}^{N} M^p_{ij} \cos(\kappa_i R) = 1$ then a_j is the pressure at the duct wall. In keeping with the most common convention in the duct acoustics the normalization is carved out in this manner.

To be consistent with the Bessel solution in uniform ducts (Appendix C) it is chosen so that, for $m_o = 0$, $J_{m_o}(\bar{\kappa}_m r) = 1$ at $r = 0$, a_j is the pressure of j^{th} mode at the duct centre line and for $m_o \neq 0$, $J_{m_o}(\bar{\kappa}_m r) = 0$ at $r = 0$, a_j is the pressure of j^{th} mode at the duct wall.

(b) Least-square matching

In Section 5.1.2(i) the weighted residual procedure has been used in the matching. In the following the least-square matching is formulated. In fact, if the same eigenfunctions are employed, the two approaches produce nearly identical results, and are exactly identical for the hardwall case because of real transverse eigenvalues.

For the matching at the ends of nonuniformity one can write, at $z = 0$ (refer to Figure 2.4)

$$\begin{Bmatrix} w_1 \\ p_1 \end{Bmatrix} = [C_{1'}][M_o] \begin{Bmatrix} a^+ \\ a^- \end{Bmatrix}_{z=0} \quad \text{on } S_1' \quad \text{(see Figure 2.4)}$$

and in the nonuniform field

$$\begin{Bmatrix} w \\ p \end{Bmatrix} = [C_1] \begin{Bmatrix} w_m(0) \\ p_m(0) \end{Bmatrix} \quad \text{on } S_1$$

The least-square procedure (Section 2.1.2(ii)) forces $\begin{Bmatrix} w_1 \\ p_1 \end{Bmatrix} = \begin{Bmatrix} w \\ p \end{Bmatrix}$ in the average over the interface or

$$[C_1] \begin{Bmatrix} w_m(0) \\ p_m(0) \end{Bmatrix} = [C_{1'}][M_o] \begin{Bmatrix} a^+ \\ b^- \end{Bmatrix}_{z=0} \quad \text{over } S_1 \text{ (or } S_1' \text{)}$$

by requiring, with $w_m(0)$, $p_m(0)$ as unknowns

$$\int_0^{R_1} [C_1^*]^T [C_1] 2\pi r \, dr \begin{Bmatrix} w_m(0) \\ p_m(0) \end{Bmatrix} = \int_0^{R_1} [C_1^*]^T [C_{1'}] 2\pi r \, dr \, [M_o] \begin{Bmatrix} a^+ \\ a^- \end{Bmatrix}_{z=0}$$

$$\text{or} \quad [C_{11}] \begin{Bmatrix} w_m(0) \\ p_m(0) \end{Bmatrix} = [C_{11'}][M_o] \begin{Bmatrix} a^+ \\ a^- \end{Bmatrix}_{z=0} \tag{5.1.71}$$

where

$$[C_{11}] = \int_0^{R_1} [C_1^*]^T [C_1]\, 2\pi r\, dr \;,\quad [C_{11'}] = \int_0^{R_1} [C_1^*]^T [C_{1'}]\, 2\pi r\, dr \qquad (5.1.72)$$

$$2Nx2N \qquad 2Nx2 \;\; 2x2N \qquad\qquad 2Nx2N \qquad 2Nx2 \;\; 2x2N$$

with the superscript T denoting transpose and the asterisk complex conjugate.

Similarly, at $z = \ell$, the least-square error minimization yields

$$\int_0^{R_2} [C_{2'}^*]^T [C_2]\, 2\pi r\, dr \begin{Bmatrix} w_m(\ell) \\ p_m(\ell) \end{Bmatrix} = \int_0^{R_2} [C_{2'}^*]^T [C_{2'}]\, 2\pi r\, dr\, [M_\ell] \begin{Bmatrix} b^+ \\ b^- \end{Bmatrix}_{z=\ell} \qquad (5.1.73)$$

over the interface $z = \ell$ with b^+, b^- being unknown propagation coefficients in the uniform duct (C). The analogous relation at the interface $z = \ell$ is

$$[C_{2'2}] \begin{Bmatrix} w_m(\ell) \\ p_m(\ell) \end{Bmatrix} = [C_{2'2'}]\, [M_\ell] \begin{Bmatrix} b^+ \\ b^- \end{Bmatrix}_{z=\ell} \qquad (5.1.74)$$

where $[C_{2'2}]$ and $[C_{2'2'}]$ are defined by equation (5.1.73) and determined similarly as in equation (5.1.72), and $[M_\ell]$ is the modal matrix in the semi-infinite duct section (C) obtained as in equation (5.1.68).

The equations (5.1.71) and (5.1.73) are combined with the relation (5.1.54) for the transition matrix to give the following relation:

$$\underset{2Nx1}{\begin{Bmatrix} b^+ \\ b- \end{Bmatrix}_{z=\ell}} = \underset{2Nx2N}{[\;TF\;]} \underset{2Nx1}{\begin{Bmatrix} a^+ \\ a^- \end{Bmatrix}_{z=\ell}} \qquad (5.1.75)$$

where $[TF]$ is the transfer matrix for the nonuniform section, given by,

$$[TF] = [M_\ell]^{-1}[C_{2'2'}]^{-1}[C_{2'2}]\, [TS]\, [C_{11}]^{-1}[C_{11'}]\, [M_o] \qquad (5.1.76)$$

It is noted that, if the wall admittance is continuous through the interfaces of ducts then $[C_{2'2'}] \equiv [C_{2'2}]$ and $[C_{11}] \equiv [C_{11'}]$. In

this case the relation (5.1.76) becomes

$$[TF] = [M_\ell]^{-1}[TS]\,[M_o] \tag{5.1.77}$$

5.1.3 Implementations and Results

(i) Integration

The basic numerical requirement for the MWR in the transmission problem is the integration of the first-order matrix differential equation (5.1.53) to generate the transition matrix which is subsequently used to compute the transfer matrix in equation (5.1.64) or (5.1.76). The integration process represents a major part of the solution time. In this study the fourth-order Runge-Kutta integration scheme is employed, which requires the calculation of the coefficient matrix of equation (5.1.53) twice at each station along the duct. Thus, the transcendental equation (5.1.39) : $\kappa_m R \tan \kappa_m R = iAkR$ is to be solved twice at each integration step for a number of basis functions required for a level of solution accuracy. The equation (5.1.39) can be conveniently solved by an eigenvalue integration scheme as for the uniform duct eigenproblem in Chapter 4. With the Runge-Kutta scheme used the minimal number of integration steps to achieve a reasonable degree of accuracy is at least 30 steps on the basis of unit duct length. In evaluating the coefficient matrix of equation (5.1.53) for the integration scheme one can reduce the computational time by introducing a weighting factor 1/r in the w-momentum residual equation (5.1.18), which then becomes

$$\int_0^R \frac{1}{r}\, R_3\, 2\pi r\, dr = 0$$

Thus, in equations (5.1.46) and (5.1.53) $\bar{N}_{nm}$ becomes

$$\bar{N}_{nm} = \int_0^1 \cos(\kappa_m R\,\eta)\,\cos(\kappa_n R\,\eta)\,d\eta \cdot \delta_{nm}$$

Due to the orthogonality of the basis functions, hence the matrix $[\bar{N}_{nm}]^{-1}$ can be deduced manually.

Numerical results do not reveal the significance of this alteration, showing the coupling effect between the w-momentum and energy equations is unimportant in the MWR formulation. The alteration was performed for the results presented here.

(ii) Basis functions

The cos $\kappa_m r$ basis functions given by equation (5.1.39) have been successfully used to date. However, as in the no-flow case eigenproblem (see Section 4.2.4(i)) it is noted that, for anti-symmetric propagation modes (i.e. $m_o \neq 0$) the cos $\kappa_m r$ functions do not satisfy the implied boundary conditions at the centre line (for a uniform duct $J_{m_o}(\bar{\kappa}r)\big|_{r=0} = 0$, $m_o \neq 0$). Consequently, the sin $\kappa_m r$ functions satisfying the boundary condition, generated by $\kappa_m R \cot \kappa_m R = -iAkR$ (see Section 4.2.4(i)) have been experimented with for the case $m_o \neq 0$. Numerical results, once again, do not show any significance of the forced boundary condition in the present MWR formulation. Apparently the differential equation residuals force this implied condition sufficiently.

(iii) Matching

In this MWR application, two methods have been used to formulate the end matching according to the solution to the eigenproblem in the semi-infinite ducts. With the exact eigenfunctions (Bessel functions) employed it is essentially the method of weighted residuals as proposed in Section 2.1.2(ii). In this case the integral of the form $\bar{\alpha}_{nm} = \int_0^1 \eta\, J_{m_o}(\bar{\kappa}_m R\,\eta)\cos(\kappa_n R\,\eta)\, d\eta$ in equation (5.1.59) is not analytically obtainable, consequently in implementation a 10-point Gaussian quadrature has been used to evaluate the integral. In the other matching method the least-square procedure is carried out with the uniform duct solutions given by the MWR itself, emphasizing compatibility in accuracy of the solution representation at the interfaces. It is noted

in practical computation that the eigenmatrix $[\mathcal{L}]$ of equation (5.1.67) is just a reduced form of the coefficient matrix in the differential equation (5.1.53) where all geometry variations along z axis vanish.

Both of the formulations have been implemented. Numerical experiments have shown that, for well cut-on modes at low frequencies ($kR_1 \lesssim 5.0$ say), the transmission and reflection coefficients obtained by the two matching techniques are nearly identical. The reduced geometry of a uniform duct provides a useful test case. At very high frequencies the Gaussian quadrature integration involving Bessel functions appears not to be able to cope with wide variations in the acoustic field. For highly cut-off modes the compability of accuracy level and dimensionality at the interfaces becomes significant because of the error amplification of the decay effect, which is dependent on the length scale. The second approach involving MWR solutions in the uniform ducts is applied for the results presented and discussed.

(iv) Preliminary results

Unlike the MWR in the 2D geometry, the MWR using trigonometric basis functions as described above does not give trivially exact results in the case of uniform circular ducts without flow. Therefore the uniform geometry may be treated as a test of accuracy and provides a baseline to assess the number of basis functions required and the effect of the length scale of the duct.

Numerical results for a uniform duct section with or without lining, joined by two semi-infinite ducts of the same admittance showed excellent agreements with the manually computed exact results. For a hardwalled or softwalled duct and at low frequencies ($kR_1 < 5.0$) a reasonable level of accuracy could be achieved with as few as three basis functions for many test cases. For high frequencies a higher number of basis functions should be used to attain the same degree of accuracy because of wide variations present in the acoustic field.

Except in the eigenproblem the number of basis functions employed in the transmission problem appears to have an upper limit, which depends on the duct length. In the eigenproblem the more basis functions are used the better results are expected, even though with a very high number of basis functions the rate of convergence may be slow because then the high-order basis functions tend to become less linearly independent. However, in the transmission problem for cut-off acoustic modes (or just about to be cut-off) at a certain reduced frequency the increase in the number of basis functions does not automatically result in a higher degree of solution convergence; in fact it may lead to a problem of numerical instability.

Since heavily cut-off modes cause large elements to appear in the transition matrix, a large number of basis functions, including cut-off modes, can lead to numerical instability in long ducts. The matter is less severe for a shorter duct since the decay effect of cut-off modes is dependent upon the length scale. For higher frequencies the acoustic modes become less cut-off (some may become cut-on), establishing a higher limit of basis functions to be used in the solution representation.

The results presented in the following are selected for some computationally challenging cases involving moderately high angular mode, high frequency, highly cut-off mode to show the potentiality of the method of utility.

(a) Convergence to the uniform hardwalled duct.

A uniform hardwalled duct is considered at angular mode $m_o = 4$, with $R_1 = R_2 = 1.0$ and $\ell = 0.5$. Tables 5.1 and 5.2 compare the results for $kR_1 = 5.0$ and $kR_1 = 10.0$ obtained by the MWR using 3 and 5 basis functions, with those analytically computed. Only diagonal terms of the matrices of reflection and transmission coefficients are shown.

Analytical results are obtained from the knowledge that in a uniform duct no reflection or spurious mode generation occurs, and the diagonal transmission terms can be deduced by noting that for right moving waves the pressure in mode n is given by

$$p_n = a_n e^{-ik^+_{zn} z} J_{m_o}(\kappa_n r)$$

The ratio of pressures at $z = \ell$ and $z = 0$ is

$$TRAN_{nn} = e^{-ik^+_{zn} \ell}$$

where k^+_{zn} (and κ_n), in general, can be solved for by an integration scheme (see Appendices C and D). The transmission coefficients referred to $z = 0$ are also compared in the tables to measure the effect of the accuracy of eigenvalues (solved for by the MWR in the end matching) against the duct length. These values should be one.

Table 5.1 for $kR_1 = 5.0$ with all incident modes being cut off shows good agreement for the first two modes in the case of 3 basis functions. Increasing to 5 basis functions improves the reflection and direct transmission coefficients for all modes except the first one, which appears to degrade slightly, showing the effect of additional cut-off modes. The transmission coefficients referred to $z = 0$ are more obviously affected. The case $kR_1 = 10.0$ with two cut-on modes, in Table 5.2, in general, shows a trend of convergence towards the exact solution with increasing number of basis functions, even though some traces of loss of accuracy still remain in reflection coefficients. Three basis functions seem not to be sufficient to represent the MWR solutions at this high frequency.

(b) Convergence to the uniform softwalled duct.

For the softwall case a duct of similar geometry is considered at the axisymmetric angular mode ($m_o = 0$) with a lining of specific admittance $A = (0.72 + 0.42i)$. Tables 5.3 and 5.4 for $kR_1 = 1.0$ and

$kR_1 = 5.0$ respectively show a definite and high-degree solution convergence even though for $kR_1 = 1.0$ all the incident modes are decaying. With only three basis functions the results are good enough for many practical purposes.

(c) Numerical instability.

For examples of numerical instability one may consider a uniform hardwalled duct: $R_1 = R_2 = 1.0$, $\ell = 0.5$ with angular modes $m_o = 6$ or 8. For $kR_1 = 5.0$ or $kR_1 = 10.0$ the numerical instability shows up with 5 basis functions, but 3 basis functions could yield acceptable values to the coefficients. Another case is a hardwalled duct: $R_1 = R_2 = 1.0$ with 5 basis functions used in the MWR. For angular mode $m_o = 3$ at frequencies $kR_1 = 5.0$ or $kR_1 = 10.0$, if the duct length is $\ell = 0.5$ the numerical instability does not occur, but it does for $\ell = 1.0$.

Note that high-order angular modes complicate the transmission problem in two ways. High-order modes have fewer propagating modes at a given frequency than lower ones. It is thus necessary for these modes to use predominantly cut-off modes to represent the solution unless the frequency is very high. But high frequencies tend to induce wide axial variations in the acoustic field by the nature of short wavelength transmission. On the other hand, for higher angular modes the effect of additional cut-off modes becomes more serious. To illustrate this point one can return to the results presented above. For the uniform hardwalled duct: $R_1 = R_2 = 1.0$, $\ell = 0.5$ with angular modes $m_o = 6$ or 8 one cut-on mode is excited at $kR_1 = 10.0$ so that, with 5 basis functions used, 4 cut-off modes are forced to be incident. This situation is compared with the same duct geometry of Tables 5.1 and 5.3 where all incident modes are cut-off (the softwall modes are more highly cut-off than the hardwall ones). For the latter case with

5 basis functions good results are observed while the former suffers the numerical instability.

Thus, for higher angular modes the barrier of numerical instability restricts the utility of the method to some further extent.

Geometry : Uniform , $R_1 = R_2 = 1.0$, $\ell = 0.5$

Characteristics : No-flow, Hardwalled Duct , $kR_1 = 5.0$
Angular Mode $m_o = 4$,
All Cut-off Modes

Incident Mode i	Reflection Coefficients in Mode i		
	MWR (3BF)	MWR (5BF)	EXACT
1	0.0000 + 0.0000i	0.0018 + 0.0000i	0.0000 + 0.0000i
2	0.0000 + 0.0000i	0.0000 + 0.0000i	0.0000 + 0.0000i
3	0.0000 + 0.0000i	0.0000 + 0.0000i	0.0000 + 0.0000i
4	-	0.0000 + 0.0000i	0.0000 + 0.0000i
Incident Mode i	Direct Transmission Coefficients at $z = \ell$ in Mode i		
	MWR (3BF)	MWR (5BF)	EXACT
1	0.4071 + 0.0000i	0.4092 + 0.0000i	0.4045 + 0.0000i
2	0.0180 + 0.0000i	0.0190 + 0.0000i	0.0200 + 0.0000i
3	0.0001 + 0.0000i	0.0027 + 0.0000i	0.0030 + 0.0000i
4	-	0.0003 + 0.0000i	0.0005 + 0.0000i
Incident Mode i	Transmission Coefficients referred to z = 0 in Mode i		
	MWR (3BF)	MWR (5BF)	EXACT
1	1.0000 + 0.0000i	1.0109 + 0.0000i	1.0000 + 0.0000i
2	1.0002 + 0.0000i	0.9483 + 0.0000i	1.0000 + 0.0000i
3	1.0720 + 0.0000i	0.9240 + 0.0000i	1.0000 + 0.0000i
4	-	0.691 + 0.0000i	1.0000 + 0.0000i

TABLE 5.1 Comparison of Reflection and Transmission Coefficients by MWR with Exact Values for Hardwall Case, $kR_1 = 5.0$, $m_o = 4$

Geometry : Uniform , $R_1 = R_2 = 1.0$, $\ell = 0.5$

Characteristics : No-flow, Hardwalled Duct , $kR_1 = 10.0$,
Angular Mode $m_o = 4$,
Two Cut-on Modes

Incident Mode i	Reflection Coefficients in Mode i		
	MWR (3BF)	MWR (5BF)	EXACT
1	0.0000 + 0.0000i	0.0001 + 0.0000i	0.0000 + 0.0000i
2	0.0000 + 0.0000i	-0.0001 + 0.0001i	0.0000 + 0.0000i
3	0.0000 + 0.0000i	0.0000 + 0.0000i	0.0000 + 0.0000i
4	-	0.0000 + 0.0000i	0.0000 + 0.0000i
Incident Mode i	Direct Transmission Coefficient z = ℓ in Mode i		
	MWR (3BF)	MWR (5BF)	EXACT
1	-0.4589 + 0.8884i	-0.4602 + 0.8878i	-0.4599 + 0.8880i
2	-0.1241 - 0.9923i	-0.2849 - 0.9587i	-0.2851 - 0.9585i
3	0.0000 + 0.0000i	0.0205 + 0.0000i	0.0203 + 0.0000i
4	-	0.0014 + 0.0000i	0.0020 + 0.0000i
Incident Mode i	Transmission Coefficients referred to z = 0 in Mode i		
	MWR (3BF)	MWR (5BF)	EXACT
1	0.9999 + 0.0003i	1.0000 + 0.0004i	1.0000 + 0.0000i
2	1.0000 + 0.0000i	1.0000 - 0.0001i	1.0000 + 0.0000i
3	1.0420 + 0.0000i	1.0151 + 0.0000i	1.0000 + 0.0000i
4	-	0.9750 + 0.0000i	1.0000 + 0.0000i

TABLE 5.2 Comparison of Reflection and Transmission Coefficients by MWR with Exact Values for Hardwall Case , kR_1=10.0, $m_o = 4$.

Geometry : Uniform , $R_1 = R_2 = 1.0$, $\ell = 0.5$

Characteristics : No-flow, Softwalled Duct: A = (0.72+0.42i), $kR_1 = 1.0$, Angular Mode $m_o = 0$

All Decaying Modes.

Incident Mode i	Reflection Coefficients in Mode i		
	MWR (3BF)	MWR (5BF)	EXACT
1	0.0000 + 0.0000i	0.0000 + 0.0000i	0.0000 + 0.0000i
2	0.0000 + 0.0000i	0.0000 + 0.0000i	0.0000 + 0.0000i
3	0.0000 + 0.0000i	0.0000 + 0.0000i	0.0000 + 0.0000i
4	-	0.0000 + 0.0000i	0.0000 + 0.0000i
Incident Mode i	Direct Transmission Coefficients at z = ℓ in Mode i		
	MWR (3BF)	MWR (5BF)	EXACT
1	0.5589 - 0.4773i	0.5589 - 0.4773i	0.5589 - 0.4773i
2	0.1665 - 0.0169i	0.1659 - 0.0167i	0.1657 - 0.0167i
3	0.0309 - 0.0016	0.0319 - 0.0017i	0.0320 - 0.0017i
4	-	0.0065 - 0.0002	0.0061 - 0.0023i
Incident Mode i	Transmission Coefficients referred to z = 0 in Mode i		
	MWR (3BF)	MWR (5BF)	EXACT
1	1.0000 + 0.0000i	1.0000 + 0.0000i	1.0000 + 0.0000i
2	1.0000 + 0.0000i	1.0000 + 0.0000i	1.0000 + 0.0000i
3	1.0000 + 0.0000i	1.0000 + 0.0000i	1.0000 + 0.0000i
4	-	1.0007 + 0.0000i	1.0000 + 0.0000i

TABLE 5.3 Comparison of Reflection and Transmission Coefficients by MWR and Exact Values for Softwall Case , $kR_1 = 1.0$, $m_o = 0$.

Geometry : Uniform $R_1 = R_2 = 1.0$, $\ell = 0.5$

Characteristics : No-flow, Softwalled Duct: $A = (0.72+0.42i)$, $kR_1 = 5.0$, Angular Mode $m_o = 0$

One Cut-on Mode

Incident Mode i	Reflection Coefficients in Mode i		
	MWR (3BF)	MWR (5BF)	EXACT
1	0.0000 + 0.0000i	0.0000 + 0.0000i	0.0000 + 0.0000i
2	0.0000 + 0.0000i	0.0000 + 0.0000i	0.0000 + 0.0000i
3	0.0000 + 0.0000i	0.0000 + 0.0000i	0.0000 + 0.0000i
4	-	0.0000 + 0.0000i	0.0000 + 0.0000i
Incident Mode i	Direct Transmission Coefficients at z = ℓ in Mode i		
	MWR (3BF)	MWR (5BF)	EXACT
1	-0.4284 - 0.7036i	-0.4259 - 0.7056i	-0.4253 - 0.7061i
2	-0.2683 - 0.2558i	-0.2683 - 0.2559i	-0.2684 - 0.2559i
3	0.0973 - 0.0395i	0.1009 - 0.0425i	0.1014 - 0.0429i
4	-	0.0134 - 0.0028i	0.0133 - 0.0028i
Incident Mode i	Transmission Coefficients referred to z = 0 in Mode i		
	MWR (3BF)	MWR (5BF)	EXACT
1	1.0000 + 0.0000i	1.0000 + 0.0000i	1.0000 + 0.0000i
2	1.0000 + 0.0000i	1.0000 + 0.0000i	1.0000 + 0.0000i
3	1.0000 + 0.0000i	1.0000 + 0.0000i	1.0000 + 0.0000i
4	-	1.0003 + 0.0001i	1.0000 + 0.0000i

TABLE 5.4 Comparison of Reflection and Transmission Coefficients by MWR and Exact Values for Softwall Case, $kR_1 = 5.0$, $m_o = 0$.

5.2 FEM SOLUTION

5.2.1 FEM with the Helmholtz Wave Equation

(i) Formulation.

If an angular harmonic dependence is taken in the form of $e^{-im_o\theta}$ then one can rewrite equation (5.0.3) and (5.0.5) as follows :

$$\nabla^2 p + \left(k^2 - \frac{m_o^2}{r^2}\right) p = 0 \qquad \text{in A}$$

and $$\underline{\nabla}\, p \cdot \underline{\nu} = -\, ik\, Ap \qquad \text{on } C_3$$

where ∇^2 is redefined as $\nabla^2 \equiv \left(\frac{\partial^2}{\partial r^2} + \frac{1}{r}\frac{\partial}{\partial r} + \frac{\partial^2}{\partial z^2}\right)$

Formally, if $\tilde{p} = [N]\,\{p\}$, (N_i are shape functions) is a trial solution in the FEM one can substitute it into the above governing equations to obtain the following residuals :

$$R_1 = \nabla^2\tilde{p} + \left(k^2 - \frac{m_o^2}{r^2}\right)\tilde{p} \tag{5.2.1}$$

$$R_B = \underline{\nabla}\, p \cdot \underline{\nu} + ik\, A\tilde{p} \quad \text{on } C_3 \tag{5.2.2}$$

the boundary conditions used in the end matching are

$$\left.\begin{aligned} \tilde{p} &= p_1 \quad \text{on } C_1 \\ \tilde{p} &= p_2 \quad \text{on } C_2 \end{aligned}\right\} \tag{5.2.3}$$

in the average over the interfaces.

The FEM formulation is then generated by using a method of weighted residuals to obtain an integrated form of the residual (5.2.1) over the domain of the nonuniform duct section (see Figure 5.1).

$$\int_A W_i \left(\nabla^2\tilde{p} + \left(k^2 - \frac{m_o^2}{r^2}\right)\tilde{p} \right) 2\pi r\, dr\, dz = 0 \;,\; i = 1,2,3\ldots n_n$$

where W_i are weighting functions (as yet unspecified).

By the use of the divergence theorem each of the above equations may be rewritten :

$$\int_A \left(\underline{\nabla} W_i \cdot \underline{\nabla} \tilde{p} - \left(k^2 - \frac{m_o^2}{r^2} \right) \tilde{p} W_i \right) 2\pi r \, dr \, dz$$

$$- \int_{C_1+C_2+C_3} W_i \underline{\nabla}\tilde{p} \cdot \underline{\nu} \, 2\pi r \, ds = 0, \quad i = 1,2,3...n_n \tag{5.2.4}$$

the boundary conditions (5.2.2) and (5.2.3) are employed in the weighted integration (5.2.4) to yield

$$\int_A \left(\underline{\nabla} W_i \cdot \underline{\nabla}\tilde{p} - \left(k^2 - \frac{m_o^2}{r^2} \right) W_i \tilde{p} \right) 2\pi r \, dr \, dz + \int_A W_i \frac{\partial p_1}{\partial z} 2\pi r \, dr$$

$$- \int_{C_2} W_i \frac{\partial p_2}{\partial z} 2\pi r \, dr + \int_{C_3} ik A\tilde{p} W_i \, 2\pi R \, ds = 0 \tag{5.2.5}$$

for $i = 1,2,3...n_n$

Now if the domain A is divided into n_e elements with n_n nodes the nodal value vector $\{p\}$ can be defined by

$$\{p\}^T = [p_i] \ , \ i = 1,2,3...n_n$$

where p_i is unknown nodal value of p at $i^{\underline{th}}$ node.

By standard FEM techniques an element shape matrix may be derived (see Section 3.2) so that in each element $\tilde{p}$ is defined by $\tilde{p} = [N(r,z)]^e \{p\}^e$ where $\{p\}^e$ is the nodal value vector for p in that particular element. With n_e such equations, one for each element, the shape matrix $[N(r,z)]$ for the whole domain can be implicitly defined so that

$$\tilde{p} = [N(r,z)] \{p\} = [N_i] \{p_i\} \tag{5.2.6}$$

for $i = 1,2,3...n_n$, where the components N_i are defined explicitly via the appropriate components of $[N(r,z)]^e$.

If now the shape functions N_i are taken as weighting functions, i.e. $W_i \equiv N_i$, $i = 1,2,3...n_n$ then this is effectively a Galerkin process of minimizing residuals. In addition, equation (5.2.6) is used to evaluate $\tilde{p}$ and $\underline{\nabla}\tilde{p}$ in equation (5.2.5) giving :

$$\left[\int_A (N_{iz}[N]_z + N_{ir}[N]_r - (k^2 - \frac{m_o^2}{r^2})N_i[N])2\pi r\, drdz\right]\{p\}$$

$$+ \int_{C_1} N_i \frac{\partial p_1}{\partial z} 2\pi r\, dr - \int_{C_2} N_i \frac{\partial p_2}{\partial z} 2\pi r\, dr$$

$$+ \left[\int_{C_3} ikA\, N_i\, [N]\, 2\pi R\, ds\right]\{p\} = 0 \ , \ i = 1,2,3...n_n \qquad (5.2.7)$$

where $$[N]_z = \frac{\partial}{\partial z}[N] = \left[\frac{\partial N_i}{\partial z}\right] = [N_{iz}]$$

and $$[N]_r = \frac{\partial}{\partial r}[N] = \left[\frac{\partial N_i}{\partial r}\right] = [N_{ir}] \ , \ i = 1,2,3...n_n$$

In equation (5.2.7) for the line integral over C_3 $N_i \equiv 0$ unless i corresponds to a node on C_3. This is looked after by FEM assembling techniques.

(ii) Matching at the ends of the nonuniformity.

If application of the matching procedure developed in Chapter 2 (see Section 2.1.2(ii)) it is noted that the end boundary conditions (5.2.3) require that

$$\tilde{p} = p_1 \text{ over } C_1 \ , \ \tilde{p} = p_2 \text{ over } C_2$$

in an average sense.

But in the uniform ducts (see Appendix C)

$$p_1 = \sum_{n=1}^{\infty} (a_n^+ J_{an}^+ + a_n^- J_{an}^-) \qquad (5.2.8)$$

$$p_2 = \sum_{n=1}^{\infty} (b_n^+ J_{bn}^+ + b_n^- J_{bn}^-) \qquad (5.2.9)$$

where a_n^+, a_n^-, b_n^-, b_n^+ are propagation constant appropriate to the geometry and consistent with the direction of propagation, and J_{an}, J_{bn} are appropriate eigenfunctions involving Bessel solutions (see Appendix C).

By assuming that in the semi-infinite duct for $z > \ell$ there is no reflection propagation, i.e. $b_n^- \equiv 0$ and with the approximation that the infinite series of equations (5.2.8) and (5.2.9) may be truncated after the first few terms one can obtain :

$$p_1 = \sum_{n=1}^{n_a} (a_n^+ \; J_{an}^+ + a_n^- \; J_{an}^-)$$

or $$p_1 = [J_a^+] \{a^+\} + [J_a^-] \{a^-\} \tag{5.2.10}$$

and $$p_2 = \sum_{n=1}^{n_b} (b_n^+ \; J_{bn}^+) = [J_b^+] \{b^+\} \tag{5.2.11}$$

where $\{a^+\} = [a_1^+ , a_2^+ \ldots , a_{n_a}^+]^T$,

$\{a^-\} = [a_1^- , a_2^- \ldots , a_{n_a}^-]^T$,

$\{b^+\} = [b_1^+ , b_2^+ \ldots , b_{n_b}^+]^T$,

and $[J_a^+] = [J_{a_1}^+ , J_{a_2}^+ \ldots , J_{an_a}^+]$,

$[J_a^-] = [J_{a_1}^- , J_{a_2}^- \ldots , J_{an_a}^-]$,

$[J_b^+] = [J_{b_1}^+ , J_{b_2}^+ \ldots , J_{bn_b}^+]$

For the end matching the boundary conditions (5.2.3) can be weighted over their respective boundaries as follows :

$$\int_{C_1} (p_1 - \tilde{p}) \; F_k \; 2\pi r \, dr = 0 \; , \quad k = 1,2,3 \ldots n_k \tag{5.2.12}$$

$$\int_{C_2} (p_2 - \tilde{p}) \; G_\ell \; 2\pi r \, dr = 0 \; , \quad \ell = 1,2,3 \ldots n_\ell \tag{5.2.13}$$

where F_k , G_ℓ are some functions to be specified later.

If now $n_k = n_a$, $n_\ell = n_b$ are taken then equations (5.2.7) (5.2.10) - (5.2.13) can be combined to give the following matrix equation :

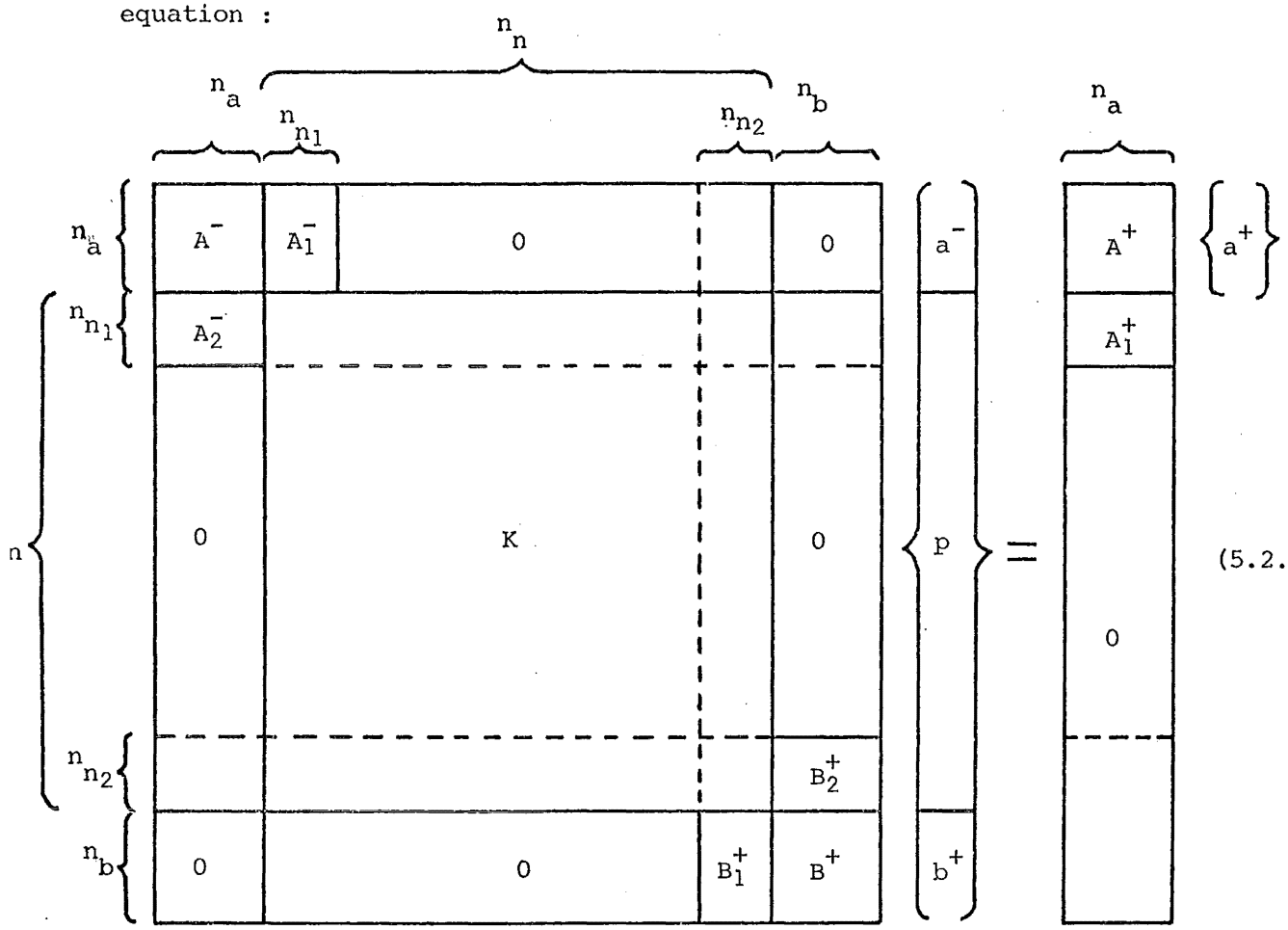

(5.2.14)

where

$$[K]_{(n_n x n_n)} = \int_A ([N]_z^T [N]_z + [N]_r^T [N]_r - (k^2 - \frac{m_o^2}{r^2}) [N]^T [N]) \, 2\pi r \, dr \, dz + \int_{C_3} ikA \, [N]^T [N] \, 2\pi R \, ds$$

$$[A_1^-]_{(n_a x n_a)} = - \int_{C_1} [F]^T [J_a^-] \, 2\pi r \, dr$$

$$[A_1^-]_{(n_a x n_{n_1})} = \int_{C_1} [F]^T [N] \, 2\pi r \, dr$$

$$[A_2^-]_{(n_{n_1} x n_a)} = \int_{C_1} [N]^T \frac{\partial}{\partial z} [J_a^-] \, 2\pi r \, dr$$

$$[A^+]_{(n_a x n_a)} = \int_{C_1} [F]^T [J_a^+] \, 2\pi r \, dr$$

$$[A_1^+]_{(n_{n_1} x n_a)} = -\int_{C_1} [N]^T \frac{\partial}{\partial z}[J_a^+] \quad 2\pi r\, dr$$

$$[B^+]_{(n_b x n_b)} = \int_{C_2} [J_b^+]^T [J_b^+] \quad 2\pi r\, dr$$

$$[B_1^+]_{(n_b x n_{n_2})} = -\int_{C_2} [G]^T [N] \quad 2\pi r\, dr$$

$$[B_2^+]_{(n_b x n_{n_2})} = -\int_{C_2} [N]^T \frac{\partial}{\partial z}[J_b^+] \quad 2\pi r\, dr$$

where

n_{n_1} : number of nodes on C_1

n_{n_2} : number of nodes on C_2

and

$$[N]_r = \frac{\partial}{\partial r}[N] = \left[\frac{\partial}{\partial r} N_i\right]$$

$$[N]_z = \frac{\partial}{\partial z}[N] = \left[\frac{\partial}{\partial z} N_i\right], \quad i = 1,2,3 \ldots n_n$$

Thus partitioned matrices may be assembled from element matrices by standard FEM techniques to give the system matrix in (5.2.14).

The matrix equation (5.2.14) can be solved by the Gaussian elimination routine to obtain $\{a^-\}$, $\{p\}$ and $\{b^+\}$ in terms of incident mode amplitudes $\{a^+\}$. In order to reduce the storage in computer implementation to some extent one can make the system matrix in equation (5.2.14) symmetric by choosing the weighting functions F_k and G_ℓ in equations (5.2.12) and (5.2.13) so that, in (5.2.14)

$$[A_1^-] = [A_2^-]^T$$

and

$$[B_1^+] = [B_2^+]^T ,$$

since $[A^-]$, $[B^+]$ are symmetric by the orthogonality of uniform duct eigenfunctions and $[K]$ is already symmetric.

Thus, [F] and [G] are now specified as follows

$$[F] = \frac{\partial}{\partial z}[J_a^-]$$
$$[G] = -\frac{\partial}{\partial z}[J_b^+] \qquad (5.2.15)$$

5.2.2 FEM with Conservation Equations

(i) Formulation.

The governing equation (5.0.1) - (5.0.2) and the boundary condition at the duct wall (5.0.4) can be expanded in cylindrical co-ordinates (r,θ,z) with the solution in the form of $e^{-im_o\theta}$ giving the conservation equations :

$$\begin{aligned} iku + \frac{\partial p}{\partial r} &= 0 \\ ikv - im_o \frac{p}{r} &= 0 \\ ikw + \frac{\partial p}{\partial z} &= 0 \\ ikp + \frac{1}{r}\frac{\partial (ru)}{\partial r} - im_o \frac{v}{r} + \frac{\partial w}{\partial z} &= 0 \end{aligned} \qquad (5.2.16)$$

with $\underline{V} = (u,v,w)$

and the boundary conditions being:

$$\underline{V}\cdot\underline{\nu} = u\cos\alpha - w\sin\alpha = Ap \quad \text{on} \quad C_3 \qquad (5.2.17)$$

$$\begin{aligned} p = p_1 &= \sum_{n=1}^{\infty} \left(a_n^+ J_{p_1 n}^+ + a_n^- J_{p_1 n}^- \right) \\ u = u_1 &= \sum_{n=1}^{\infty} \left(a_n^+ J_{u_1 n}^+ + a_n^- J_{u_1 n}^- \right) \\ v = v_1 &= \sum_{n=1}^{\infty} \left(a_n^+ J_{v_1 n}^+ + a_n^- J_{v_1 n}^- \right) \\ w = w_1 &= \sum_{n=1}^{\infty} \left(a_n^+ J_{w_1 n}^+ + a_n^- J_{w_1 n}^- \right) \quad \text{on } C_1 \end{aligned} \qquad (5.2.18)$$

and

$$
\begin{aligned}
p = p_2 &= \sum_{n=1}^{\infty} \left(b_n^+ \; J_{p_2 n}^+ + b_n^- \; J_{p_2 n}^- \right) \\
u = u_2 &= \sum_{n=1}^{\infty} \left(b_n^+ \; J_{u_2 n}^+ + b_n^- \; J_{u_2 n}^- \right) \\
v = v_2 &= \sum_{n=1}^{\infty} \left(b_n^+ \; J_{v_2 n}^+ + b_n^- \; J_{v_2 n}^- \right) \\
w = w_2 &= \sum_{n=1}^{\infty} \left(b_n^+ \; J_{w_2}^+ + b_n^- \; J_{w_2 n}^- \right) \qquad \text{on } C_2
\end{aligned}
\tag{5.2.19}
$$

where a_n^+, a_n^-, b_n^+, b_n^- are propagation coefficients and $J_{p_1 n}^+$, $J_{p_1 n}^-$ ... , $J_{p_2 n}^+$, $J_{p_2 n}^-$... are eigenfunctions for pressure and velocity components, appropriate to the uniform ducts (see Appendix C).

In the FEM formulation if $\tilde{p} = [N]\{p\}$, $\tilde{u} = [N]\{u\}$, $\tilde{v} = [N]\{v\}$, $\tilde{w} = [N]\{w\}$ are approximate solutions for p,u,v, and w one can substitute them in the conservation equations and obtain the following residuals :

$$
\begin{aligned}
R_1 &= ik\tilde{u} + \frac{\partial \tilde{p}}{\partial r} \\
R_2 &= ik\tilde{v} - i\, m_o \frac{\tilde{p}}{r} \\
R_3 &= ik\tilde{w} + \frac{\partial \tilde{p}}{\partial z} \\
R_4 &= ik\tilde{p} + \mathrm{div}(\underline{\tilde{V}})
\end{aligned}
\tag{5.2.20}
$$

where $\underline{\tilde{V}} = (\tilde{u}, \tilde{v}, \tilde{w})$

Applying weighting functions $W_i^{(u)}$, $W_i^{(v)}$, $W_i^{(w)}$, $W_i^{(p)}$ to the residuals (5.2.20) over the whole domain gives

$$
\begin{aligned}
\int_A W_i^{(u)} \; R_1 \; 2\pi r \, dr \, dz &= 0 \\
\int_A W_i^{(v)} \; R_2 \; 2\pi r \, dr \, dz &= 0 \\
\int_A W_i^{(w)} \; R_3 \; 2 \, r\pi dr \, dz &= 0 \\
\int_A W_i^{(p)} \; R_4 2 \, r\pi dr \, dz &= 0
\end{aligned}
\tag{5.2.21}
$$

for $i = 1,2,\ldots n_n$, n_n is the number of nodes.

Consider the energy residual equation

$$\int_A W_i^{(p)} \; R_4 \, 2\pi r \, dr \, dz = \int_A W_i^{(p)} \; (ik\tilde{p} + \text{div } \underline{\tilde{V}}) 2\pi r dr \, dz = 0 \qquad (5.2.22)$$

the divergence theorem can be applied to expose the boundary terms as follows :

$$\int_A W_i^{(p)} \; ik\tilde{p} \; 2\pi r \; dr \; dz - \int_A \underline{\nabla} \; W_i^{(p)} \cdot \underline{\tilde{V}} \; 2\pi r \; dr \; dz + \int_{C_1+C_2+C_3} W_i^{(p)} \; \underline{\tilde{V}} \cdot \underline{\nu} \; 2\pi r \; ds = 0$$

From the boundary conditions, equations (5.2.17) - (5.2.19),

$$\int_{C_3} W_i^{(p)} \; \underline{\tilde{V}} \cdot \underline{\nu} \; 2\pi r \; ds \; = \; \int_{C_3} W_i^{(p)} \; A \; \tilde{p} \; 2\pi r \; ds$$

$\tilde{w} \approx w_1$ on C_1 , $\tilde{w} \approx w_2$ on C_2 ,

one can rewrite

$$\int_A W_i^{(p)} \; ik\tilde{p} \; 2\pi r \, dr \, dz - \int_A \left(\frac{\partial W_i^{(p)}}{\partial r} \; \tilde{u} - \frac{im_o}{r} \; W_i^{(p)} \; \tilde{v} + \frac{\partial W_i^{(p)}}{\partial z} \; \tilde{w} \right) 2\pi r \, dr \, dz$$

$$+ \int_{C_2} W_i^{(p)} \; w_2 \; 2\pi r \, dr \; - \int_{C_1} W_i^{(p)} \; w_1 \; 2\pi r \; dr + \int_{C_3} W_i^{(p)} \; A\tilde{p} \; 2\pi R \; ds = 0 \qquad (5.2.23)$$

With the domain having n_e elements and n_n nodes an implicit shape matrix [N] can be defined for the whole domain via elements such that

$$\begin{aligned} \tilde{u} &= [N]\{u\} \; , \quad \tilde{v} = [N]\{v\} \\ \tilde{w} &= [N]\{w\} \; , \quad \tilde{p} = [N]\{p\} \end{aligned} \qquad (5.2.24)$$

where $[N] = [N(r,z)]$ may be assembled from element shape functions.

For the Galerkin minimization process one can take

$$W^{(p)}_i \equiv W^{(u)}_i \equiv W^{(u)}_i \equiv W^{(w)}_i = N_i \quad : \text{ shape functions} \tag{5.2.25}$$

where $i = 1,2,3...n_n$

so that equations (5.2.17) together with relations (5.2.23) - (5.2.25) can be combined to yield

$$\int_A N_i \left(ik[N]\{u\} + [N]_r\{p\} \right) \quad 2\pi r \, dr \, dz = 0 \tag{5.2.26}$$

$$\int_A N_i \left(ik[N]\{v\} - \frac{im_o}{r}[N]\{p\} \right) 2\pi r \, dr \, dz = 0 \tag{5.2.27}$$

$$\int_A N_i \left(ik[N]\{w\} + [N]_z\{p\} \right) \quad 2\pi r \, dr \, dz = 0 \tag{5.2.28}$$

$$\begin{aligned} &\int_A N_i \quad ik[N]\{p\} \; 2\pi r \, dr \, dz - \int_A \left(\frac{\partial}{\partial r} N_i [N]\{u\} - \frac{im_o}{r} N_i [N]\{v\} \right. \\ &+ \left. \frac{\partial}{\partial z} N_i [N]\{w\} \right) 2\pi r dr \, dz + \int_{C_2} N_i \, w_2 \, 2\pi r \, dr - \int_{C_1} N_i \, w_1 \, 2\pi r \, dr \\ &+ \int_{C_3} N_i \, A \, [N]\{p\} \, 2\pi R \, ds = 0 \end{aligned} \tag{5.2.29}$$

for $i = 1,2,3...n_n$

(ii) Matching at the ends of the nonuniformity.

For the end matching the solutions (5.2.18) and (5.2.19) in semi-infinite ducts can be truncated to a finite number of terms, with $b^-_n \equiv 0$, to be written as follows

$$\begin{aligned} p_1 &= \sum_{n=1}^{n_a} \left(a^+_n J^+_{p_1 n} + a^-_n J^-_{p_1 n} \right) = [J^+_{p_1}]\{a^+\} + [J^-_{p_1}]\{a^-\} \\ u_1 &= \sum_{n=1}^{n_a} \left(a^+_n J^+_{u_1 n} + a^-_n J^-_{u_1 n} \right) = [J^+_{u_1}]\{a^+\} + [J^-_{u_1}]\{a^-\} \\ v_1 &= \sum_{n=1}^{n_a} \left(a^+_n J^+_{v_1 n} + a^-_n J^-_{v_1 n} \right) = [J^+_{v_1}]\{a^+\} + [J^-_{v_1}]\{a^-\} \\ w_1 &= \sum_{n=1}^{n_a} \left(a^+_n J^+_{w_1 n} + a^-_n J^-_{w_1 n} \right) = [J^+_{w_1}]\{a^+\} + [J^-_{w_1}]\{a^-\} \end{aligned} \tag{5.2.30}$$

and

$$
\begin{aligned}
p_2 &= \sum_{n=1}^{n_b} b_n^+ J_{p_2 n}^+ &&= [J_{p_2}^+]\{b^+\} \\
u_2 &= \sum_{n=1}^{n_b} b_n^+ J_{u_2 n}^+ &&= [J_{u_2}^+]\{b^+\} \\
v_2 &= \sum_{n=1}^{n_b} b_n^+ J_{v_2 n}^+ &&= [J_{v_2}^+]\{b^+\} \\
w_2 &= \sum_{n=1}^{n_b} b_n^+ J_{w_2 n}^+ &&= [J_{w_2}^+]\{b^+\}
\end{aligned}
\tag{5.2.31}
$$

The least-square procedure for minimizing the squares of absolute errors

$$
E_1 = \int_{C_1} \left(|p_1 - \tilde{p}|^2 + |u_1 - \tilde{u}|^2 + |v_1 - \tilde{v}|^2 + |w_1 - \tilde{w}|^2 \right) 2\pi r \, dr \quad \text{at } z = 0 \tag{5.2.32}
$$

and

$$
E_2 = \int_{C_2} \left(|p_2 - \tilde{p}|^2 + |u_2 - \tilde{u}|^2 + |v_2 - \tilde{v}|^2 + |w_2 - \tilde{w}|^2 \right) 2\pi r \, dr \quad \text{at } z = 0 \tag{5.2.33}
$$

over the interfaces, gives extra equations in the form

$$
\frac{\partial E_1}{\partial a_i^-}(a_i^+, a_i^-) = 0 \quad , \quad \text{for } i = 1,2,\ldots n_a \tag{5.2.34}
$$

$$
\frac{\partial E_2}{\partial b_i^+}(b_i^+) = 0 \quad , \quad \text{for } i = 1,2,\ldots n_b \tag{5.2.35}
$$

Thus, in this least-square minimization a_i^+ ($i = 1,2\ldots n_a$) are considered as known variables and a_i^- , b_i^+ are to be determined in terms of a_i^+ so that these equations (5.2.34), (5.2.35) together with equations (5.2.26) - (5.2,29), given by the FEM formulation yield a well-posed system of simultaneous equations.

If relations (5.2.24), (5.2.30) and (5.2.31) are substituted into equations (5.2.32) and (5.2.33), which are subsequently employed in equations (5.2.34) and (5.2.35), taking the conjugates of the resulting equations one can obtain

$$\left(\frac{\partial E1}{\partial a_i^-}\right)^* = \int_{C_1} \left\{(p_1-\tilde{p})\, J^*_{p_1 i} + (u_1-\tilde{u})\, J^*_{u_1 i} + (v_1-\tilde{v})\, J^*_{v_1 i} + (w_1-\tilde{w})\, J^*_{w_1 i}\right\} 2\pi r\, dr$$

$$= \int_{C_1} \left(\left[J^*_{p_1 i}\ J^+_{p_1 j}\right]\{a^+_j\} + \left[J^*_{p_1 i}\ J^-_{p_1 j}\right]\{a^-_j\} - \left[J^*_{p_1 j}\ N_k\right]\{p_k\} \right) 2\pi r\, dr$$

$$+ \int_{C_1} \left(\left[J^*_{u_1 i}\ J^+_{u_1 j}\right]\{a^+_j\} + \left[J^*_{u_1 i}\ J^-_{u_1 j}\right]\{a^-_j\} - \left[J^*_{u_1 i}\ N_k\right]\{u_k\} \right) 2\pi r\, dr$$

$$+ \int_{C_1} \left(\left[J^*_{v_1 i}\ J^+_{v_1 j}\right]\{a^+_j\} + \left[J^*_{v_1 i}\ J^-_{v_1 j}\right]\{a^-_j\} - \left[J^*_{v_1 i}\ N_k\right]\{v_k\} \right) 2\pi r\, dr$$

$$+ \int_{C_1} \left(\left[J^*_{w_1 i}\ J^+_{w_1 j}\right]\{a^+_j\} + \left[J^*_{w_1 i}\ J^-_{w_1 j}\right]\{a^-_j\} - \left[J^*_{w_1 i}\ N_k\right]\{w_k\} \right) 2\pi r\, dr$$

$$= 0 \qquad (5.2.36)$$

where $i = 1,2,3,\ldots n_a$

$j = 1,2,3,\ldots n_a$

$k = 1,2,3,\ldots n_{n_1}$ (n_{n_1} is the number of nodes on C_1)

$$\left(\frac{\partial E2}{\partial b_i^+}\right)^* = \int_{C_2} \left\{(p_2-\tilde{p})\, J^*_{p_2 i} + (u_2-\tilde{u})\, J^*_{u_2 i} + (v_2-\tilde{v})\, J^*_{v_2 i} + (w_2-\tilde{w})\, J^*_{w_2 i}\right\} 2\pi r\, dr$$

$$= \int_{C_2} \left(\left[J^*_{p_2 i}\ J^+_{p_2 j}\right]\{b^+_j\} - \left[J^*_{p_2 i}\ N_k\right]\{p_k\} \right) 2\pi r\, dr$$

$$+ \int_{C_2} \left(\left[J^*_{u_2 i}\ J^+_{u_2 j}\right]\{b^+_j\} - \left[J^*_{u_2 i}\ N_k\right]\{u_k\} \right) 2\pi r\, dr$$

$$+ \int_{C_2} \left(\left[J^*_{v_2 i}\ J^+_{v_2 j}\right]\{b^+_j\} - \left[J^*_{v_2 i}\ N_k\right]\{v_k\} \right) 2\pi r\, dr$$

$$+ \int_{C_2} \left(\left[J^*_{w_2 i}\ J^+_{w_2 j}\right]\{b^+_j\} - \left[J^*_{w_2 i}\ N_k\right]\{w_k\} \right) 2\pi r\, dr$$

$$= 0 \qquad (5.2.37)$$

where $i = 1,2,3,\ldots n_b$

$j = 1,2,3,\ldots n_b$

$k = n_n - n_{n_2} + 1\ ,\ n_n - n_{n_2} + 2 \ldots n_n$ (n_{n_2} is the number of nodes on C_2)

and superscript * denotes complex conjugate.

Finally equations (5.2.26) - (5.2.29) are combined with equations (5.2.36) and (5.2.37) to give the system of simultaneous equations in the following matrix form :

$$
\begin{array}{c|c|c|c|c|c|c|c}
 & n_a & 4n_1 & 4n_n & & 4n_2 & n_b & \\
 & & & & & & & \\
n_a & A^- & A_1^- & 0 & & & 0 & a^- \\
4n_{n_1} & A_2^- & & & & & & \delta_1 \\
4n_n & 0 & & K & & & 0 & \delta_{in} \\
4n_{n_2} & & & & & & B_2^+ & \delta_2 \\
n_b & 0 & & 0 & & B_1^+ & B^+ & b^+
\end{array}
=
\begin{array}{c|c|c}
n_a & & \\
 & & \\
A^+ & a^+ & \\
A_1^+ & & \\
0 & & (5.2.38) \\
 & & \\
0 & &
\end{array}
$$

where

$$
[K]_{(4n_n \times 4n_n)} = \int_A \begin{bmatrix}
ik\, N_i N_j & -N_{iz} N_j & -N_{ir} N_j & \frac{im_o}{r} N_i N_j \\
-N_i N_{jz} & -ik\, N_i N_j & 0 & 0 \\
-N_i N_{jr} & 0 & -ik\, N_i N_j & 0 \\
+\frac{im_o}{r} N_i N_j & 0 & 0 & -ik\, N_i N_j
\end{bmatrix} 2\pi r\, dr
$$

with $i = 1,2,3 \ldots n_n$, $j = 1,2,3 \ldots n_n$

and $[\delta_1 \,;\, \delta_{in} \,;\, \delta_2]^T = [\delta_i]^T = [(p_i, w_i, u_i, v_i)]^T$ for $i = 1,2,3,..n_n$

The duct-wall boundary condition has not yet been included in [K], which is involved in the last term of the fourth equation of (5.2.29) being

$$\int_{C_3} A\,[N_i N_j]\{p\}\,2\pi R\,ds \quad \text{for } i = 1,2,3,..n_n \;,\; j = 1,2,3,...n_n$$

This can be assembled into the system matrix of equation (5.2.38) by noting that, in the above expression, $N_i \equiv N_j \equiv 0$ unless i or j corresponds to a node on C_3.

In derivation of the components of equation (5.2.38) the matching at z = 0 gives

$$[A^-]_{(n_a x n_a)} = \left[\int_{C_1}\left(J^{*-}_{p_1 i}\,J^{-}_{p_1 j} + J^{*-}_{w_1 i}\,J^{-}_{w_1 j} + J^{*-}_{u_1 i}\,J^{-}_{u_1 j} + J^{*-}_{v_1 i}\,J^{-}_{v_1 j}\right)2\pi r\,dr\right]$$

$$[A_1^-]_{(n_a x 4n_{n_1})} = -\int_{C_1}\left[J^{*-}_{p_1 i}\,N_k \;\middle|\; J^{*-}_{w_1 i}\,N_k \;\middle|\; J^{*-}_{u_1 i}\,N_k \;\middle|\; J^{*-}_{v_1 i}\,N_k\right]2\pi r\,dr$$

$$[A_2^-] = \left[-\int_{C_1} N_k\,J^{-}_{w_1 i}\;2\pi dr\right]$$

$$[A^+]_{(n_a x n_a)} = -\left[\int_{C_1}\left(J^{*-}_{p_1 i}\,J^{+}_{p_1 j} + J^{*-}_{w_1 i}\,J^{+}_{w_1 j} + J^{*-}_{u_1 i}\,J^{+}_{u_1 j} + J^{*-}_{v_1 i}\,J^{+}_{v_1 j}\right)2\pi r\,dr\right]$$

$$[A_1^+]_{(n_{n_1} x n_a)} = \left[\int_{C_1} N_k\,J^{+}_{w_1 i}\;2\pi r\,dr\right]$$

with $i = 1,2,3,...n_a$, $j = 1,2,3,...n_a$ and $k = 1,2,3,...n_{n_1}$

and the matching at $z = \ell$ gives

$$[B^+]_{(n_b x n_b)} = -\left[\int_{C_2}\left(J^{*+}_{p_2 i}\,J^{+}_{p_2 j} + J^{*+}_{w_2 i}\,J^{+}_{w_2 j} + J^{*+}_{u_2 i}\,J^{+}_{u_2 j} + J^{*+}_{v_2 i}\,J^{+}_{v_2 j}\right)2\pi r\,dr\right]$$

$$[B_1^+]_{(n_b x 4n_{n_2})} = +\int_{C_2}\left[J^{*+}_{p_2 i}\,N_k \;\middle|\; J^{*+}_{w_2 i}\,N_k \;\middle|\; J^{*+}_{u_2 i}\,N_k \;\middle|\; J^{*+}_{v_2 i}\,N_k\right]2\pi r\,dr$$

$$[B_2^+]_{(n_{n_2} x n_b)} = \left[\int_{C_2} N_k J^+_{w_2 j} \, 2\pi r dr \right]$$

with $i = 1,2,3,\ldots n_b$, $j = 1,2,3,\ldots n_b$ and $k = n_n - n_{n_2} + 1$, $n_n - n_{n_2} + 2, \ldots n_n$

Note that when assembled into the system matrix the submatrices, $[A_2^-]$, $[A_1^+]$ and $[B_2^+]$ just add contributions to coefficients at those locations corresponding to the energy equation in the FEM formulation.

5.2.3 Implementations and Results

(i) Matching.

In the no-flow case, if the uniform duct eigenproblem is solved for the purpose of end matching, one must manipulate the Helmholtz wave equation (see Section 4.3.1). In this case only the pressure nodal values are directly obtainable in terms of eigenvectors. But in the transmission problem formulated either with the Helmholtz (Section 5.2.1) or with the conservation equations (Section 5.2.2) the derivative of the acoustic pressure (in equation(5.2.7)) or the velocity field components (in equation(5.2.29)) in the uniform ducts, are required for the treatment of end boundary conditions. They are not available from the no-flow eigenproblem. However, one can construct them by returning to the FEM concept of approximations

e.g.

$$\frac{\partial p_1}{\partial z} \approx -ik_z [N] \{p_1\} ,$$

$$u_1 = \frac{i}{k} \frac{\partial p_1}{\partial r} \approx \frac{i}{k} [N]_r \{p_1\} \ldots$$

where components of [N] are shape functions and $\{p_1\}$ are pressure nodal values on the appropriate boundary.

In order not to complicate the problem at this stage of mathematical development the exact eigenfunctions (Bessel functions) are used in the matching implementation for both the formulations with the Helmholtz equation and the conservation equations. All integrals involving Bessel

functions are numerically evaluated via elements as for standard FEM integrations.

(ii) Conservation equations.

When the governing conservation equations are formulated with four dependent variables at each node the size of the system matrix increases considerably and is approximately sixteen times as large as in the case of the Helmholtz wave equation. In general, the system matrix in equation (5.2.38) is symmetric ([K] is symmetric itself) only if it is in the hardwall case (Bessel functions become purely real) and additionally the least-square absolute error minimization applies only to the w - velocity component at the interfaces. In that case, in equation (5.2.38), $[A^-]$ and $[B^+]$ become symmetric and $[A_2^-] = [A_1^-]^T$, $[B_2^+] = [B_1^+]^T$.

However, the approach with the conservation equations is not intended here to compete with the Helmholtz wave equation approach, or with the MWR for the case without flow. It serves merely as an indication of the way in which the FEM may be extended to the case with flow, for which the option of reducing the conservation equations to a single wave equation is no longer available when the flow is rotational. The implementation has also indicated that in the flow case, for which the system matrix will not become symmetric anyhow, the problem of high dimensionality may be severe, rendering the method apparently less practical than in the no-flow case.

(iii) Singularity and forced boundary conditions.

In the expression for [K] in equation (5.2.14) the singularity appears to occur as $r \to 0$ for anti-symmetric angular mode ($m_o \neq 0$). In fact, it does not affect the solution since numerical integration is used in evaluation of integrals. The apparent singularity causes large but finite values to be placed in the matrix [K] at the locations

corresponding to the nodal values of p along the centreline, resulting in very small values of p in the solution. This merely confirms numerically the anticipated result that $p \to 0$ as $r \to 0$ for $m_o \neq 0$. Alternatively the problem may be avoided by imposing the condition $p = 0$ on $r = 0$ as a forced boundary condition. Both methods were tried but the results for the reflection and transmission coefficients are virtually indistinguishable.

In both formulations which have been presented the duct-wall boundary condition is treated as the natural boundary condition in the variational calculus. In fact, it can be forced to be satisfied explicitly. The forced boundary condition concept is widely used in other FEM applications [74,89]. For the case of the conservation equations the condition : $u \cos \alpha - w \sin \alpha = Ap$ at $r = R$ can be simply forced by deleting one of four rows of the system matrix corresponding to each node on C_3 and replacing it by the expression above. In the Helmholtz wave equation formulation the boundary condition $\underline{\nabla} p \cdot \underline{\nu} = ikAp$ at $r = R$ cannot be simply forced explicitly because of the derivatives involved. A more general approach will be addressed in the flow case. For the results presented here the natural boundary condition is applied.

(iv) Preliminary results.

As with the MWR using trigonometric functions the FEM does not give trivial exact results for uniform ducts. The uniform geometry may be treated as a test of accuracy for the FEM and used to assess the effect of different element subdivisions and their compatibility with the number of transmitted and reflected modes imposed at each end of the duct. In the MWR the number of incident modes (equal to the number of reflected or transmitted mode) is usually taken to be equal to the number of basis functions used, which is limited by the numerical instability. This equality is essential in the case of matching with MWR uniform duct eigenfunctions. In the FEM the numbers of incident, reflected and

transmitted modes may be different and are only limited in the sense that the degrees of freedom in FEM discretization must be able to resolve these acoustic modes.

It is noted that the variation of the nodal variable (or variables) is quadratic along each element boundary (see Section 3.2.3). This must be taken into account in deciding how many incident, reflected and transmitted modes may reasonably be accommodated by a given element subdivision. As a rough guide one can assume that each element in the r or z direction can accommodate only one stationary value of the nodal value in that direction. With this criterion it may be expected that a 5 x 5 element subdivision gives acceptable results for at most four or five modes across the duct (i.e. a variation in the highest mode of the form $J_{m_o}(\kappa_n r)$, where κ_n are the transverse eigenvalues). Similarly a 8 x 8 element subdivision may resolve up to seven or eight nodes across the duct. The same criterion is applied along the duct, so that the 5 x 5 element subdivision is likely to be valid for values of k representing at most four half wavelength variations in the nodal variable along the duct (i.e. approximately $k\ell < 12.$), and the 8 x 8 element division may accommodate up to seven half wavelength variations (i.e. approximately $k\ell < 21.$). For high-order angular modes this accommodation capacity may be reduced to some extent for the same accuracy level.

For convenience the preliminary results are presented only for the hardwall c a s e with equal numbers of incident, reflected and transmitted modes. More computationally challenging cases involving soft-walled ducts will be considered later. The element mesh used in the computations is uniform along the z axis and has a parabolic distribution across the duct as in the eigenproblem (see Section 4.3). Since the transmission coefficients referred to $z = 0$ are calculated via exact eigenvalues in the uniform ducts they can be used to assess the accuracy

in the transmission problem (excluding the possible effect of eigenvalue approximations as in the MWR with the uniform duct eigenproblem also solved by the MWR). For all the results presented the Helmholtz wave equation was used in the FEM formulation.

Tables 5.5 and 5.6 show a typical trend of convergence in the FEM. The results can be compared with the MWR values and the exact results given in Tables 5.1 and 5.2. For the case of $kR_1 = 5.0$ of Tables 5.5 and 5.1 the accuracy levels achieved by FEM (5 x 5) and MWR (5BF) may be comparable. But for $kR_1 = 10.0$ the MWR (5BF) results appear to be more favourable in comparison with those of FEM (5 x 5), FEM (5 x 10) or FEM (8 x 8). This may reflect the effect of high frequency (shorter wavelength) upon the FEM resolution along the duct. In the MWR it is not so serious as long as the incident modes are not too highly cut-off. In Tables 5.5 and 5.6 it is found that there is a slight difference between the results for FEM (5 x 5) and FEM (5 x 10) while the results are significantly improved (compared with exact ones in Table 5.1 and 5.2) changing from FEM (5 x 10) to FEM (8 x 8). This fact reveals the significance of the transverse resolution, especially at this high angular mode ($m_o = 4$).

Tables 5.7 and 5.8 show the coefficients at various frequencies. Clearly the accuracy decreases when the frequency becomes higher especially for higher-order modes, even though at low frequencies there are more cut-off modes. Note that in Table 5.8 $m_o = 4$ for $kR_1 = 1$ or $kR_1 = 3$ some modes are highly cut-off. Thus in the FEM the adverse effect of high frequency seems to outweigh that of additional cut-off modes.

Comparisons of the results in Tables 5.7 and 5.9 also show an accuracy degradation with a longer duct. In Table 5.9 for the case of $kR_1 = 15$ (and $k\ell = 15.0$) there is a drastic deterioration, which appears to support the hypothesis above, based on the quadratic nature of

elements, that the 5 x 5 FEM subdivision is likely to give reasonable results for at most $k\ell < 12$.

In this study the conservation equation FEM results were obtained for a few cases. The enormous increase in the size of the system matrix renders it impractical for the no-flow case. It is of interest to note that the conservation equation FEM, although giving generally comparable resolution to that of the Helmholtz wave equation FEM for the same element subdivision, loses high modes at low frequencies but regains them as kR_1 increases. No rigorous explanation is offered for this behaviour but it is apparently related to the differing degree of resolution (there are no second derivatives in the conservation equations) with which the cut-off modes are represented in the two approaches.

In the conservation equation formulation, if the end matching is to minimize only the absolute error square of the acoustic pressure across the interfaces there is a slight improvement in the coefficients in comparison to those of the original formulation with the matching based on all four dependent variables. This may reflect the different degrees of driving the absolute errors to zero offered by the least-square method, which depend on the structure of the errors themselves.

Geometry : Uniform , $R_1 = R_2 = 1.0$, $\ell = 0.5$

Characteristics : No-flow, Hardwalled Duct, $kR_1 = 5.0$
Angular Mode $m_o = 4$,
All Cut-off Modes

Incident Mode i	Reflection Coefficients in Mode i		
	FEM(5 x 5)	FEM(5 x 10)	FEM(8 x 8)
1	-0.0008 + 0.0000i	-0.0008 + 0.0000i	-0.0002 + 0.0000i
2	-0.0007 + 0.0000i	-0.0005 + 0.0000i	0.0004 + 0.0000i
3	-0.0123 + 0.0000i	-0.0115 + 0.0000i	0.0005 + 0.0000i
Incident Mode i	Direct Transmission Coefficients at $z = \ell$ in Mode i		
	FEM(5 x 5)	FEM(5 x 10)	FEM(8 x 8)
1	0.4038 + 0.0000i	0.4038 + 0.0000i	0.4044 + 0.0000i
2	0.0199 + 0.0000i	0.0199 + 0.0000i	0.0200 + 0.0000i
3	0.0027 + 0.0000i	0.0027 + 0.0000i	0.0029 + 0.0000i
Incident Mode i	Transmission Coefficients referred to $z = 0$ in Mode i		
	FEM(5 x 5)	FEM(5 x 10)	FEM(8 x 8)
1	0.9983 + 0.0000i	0.9983 + 0.0000i	0.9996 + 0.0000i
2	0.9965 + 0.0000i	0.9963 + 0.0000i	0.9984 + 0.0000i
3	0.9031 + 0.0000i	0.9003 + 0.0000i	0.9926 + 0.0000i

TABLE 5.5 Convergence of Reflection and Transmission Coefficients Computed by FEM for a Uniform Hardwalled Duct, $kR_1 = 5.0$, $m_o = 4$.

Geometry : Uniform , $R_1 = R_2 = 1.0$, $\ell = 0.5$

Characteristics : No-flow, Hardwalled Duct , $kR_1 = 10.0$

Angular Mode $m_o = 4$,

Two Cut-on Modes

Incident Mode i	Reflection Coefficients in Mode i		
	FEM(5 x 5)	FEM(5 x 10)	FEM(8 x 8)
1	-0.0002 - 0.0001i	0.0000 + 0.0000i	-0.0000 + 0.0000i
2	0.0037 - 0.0011i	0.0037 - 0.0011i	0.0017 - 0.0001i
3	-0.0224 - 0.0000i	-0.0221 - 0.0000i	-0.0015 + 0.0000i
Incident Mode i	Direct Transmission Coefficients at z = ℓ in Mode i		
	FEM(5 x 5)	FEM(5 x 10) ,	FEM(8 x 8)
1	-0.4616 + 0.8871i	-0.4603 + 0.8877i	-0.4602 + 0.8878i
2	-0.2778 - 0.9606i	-0.2779 - 0.9606i	-0.2816 - 0.9595i
3	0.0174 + 0.0000i	0.0174 + 0.0000i	0.0200 - 0.0000i
Incident Mode i	Transmission Coefficients referred to z = 0 in Mode i		
	FEM(5 x 5)	FEM(5 x 10)	FEM(8 x 8)
1	1.0000 + 0.0019i	1.0000 + 0.0005i	1.0000 + 0.0003i
2	1.0000 + 0.0076i	1.0000 + 0.0075i	1.0000 + 0.0036i
3	0.8581 + 0.0000i	0.8586 + 0.0000i	0.9891 - 0.0000i

TABLE 5.6 Convergence of Reflection and Transmission Coefficients Computed by FEM for a Uniform Hardwalled Duct, $kR_1=10.0$, $m_o=4$

Geometry : Uniform , $R_1 = R_2 = 1.0$, $\ell = 0.5$

Characteristics : No-flow, Hardwalled Duct,

Angular Mode $m_o = 1$

FEM(5 x 5)

Incident Mode i	kR_1	Reflection Coefficient in Mode i	Direct Transmission Coefficients at $z = \ell$ in Mode i	Transmission Coefficients referred to $z = 0$ in Mode i
1	1.0	-0.000 + 0.000i	0.462 + 0.000i	1.000 + 0.000i
	5.0	-0.000 + 0.000i	-0 684 - 0.729i	1.000 + 0.000i
	8.0	-0.000 - 0.000i	-0.732 + 0.682i	1.000 + 0.001i
	10.0	-0.001 + 0.000i	0.198 + 0.980i	1.000 + 0.003i
	15.0	-0.004 - 0.002i	0.420 - 0.908i	1.000 + 0.022i
2	1.0	-0.000 + 0.000i	0.073 + 0.000i	0.998 + 0.000i
	5.0	-0.002 + 0.000i	0.395 - 0.000i	0.995 - 0.000i
	8.0	-0.000 - 0.000i	-0.987 - 0.161i	1.000 + 0.002i
	10.0	0.000 + 0.000i	-0.467 + 0.884i	1.000 + 0.004i
	15.0	-0.001 - 0.001i	0.762 - 0.648i	1.000 + 0.022i
3	1.0	-0.005 + 0.000i	0.014 + 0.000i	0.969 + 0.000i
	5.0	-0.005 - 0.000i	0.030 - 0.000i	0.969 - 0.000i
	8.0	-0.020 - 0.000i	0.212 - 0.000i	0.941 - 0.000i
	10.0	0.003 - 0.005i	-0.840 - 0.543i	0.999 + 0.004i
	15.0	0.000 - 0.002i	0.985 + 0.172i	0.998 + 0.056i

kR_1	Number of Cut-on Modes
1.0	0
5.0	1
8.0	2
10.0	3
15.0	4

TABLE 5.7 Reflection and Transmission Coefficients Computed by FEM(5 x 5) for a Uniform Hardwalled Duct, $\ell = 0.5$, $m_o = 1$

Geometry : Uniform , $R_1 = R_2 = 1.0$, $\ell = 0.5$

Characteristics : No-flow, Hardwalled Duct,

Angular Mode $m_o = 4$

FEM(5 x 5)

Incident Mode i	kR_1	Reflection Coefficient in Mode i	Direct Transmission Coefficients at $z = \ell$ in Mode i	Transmission Coefficients referred to $z = 0$ in Mode i
1	1.0	-0.000 + 0.000i	0.073 + 0.000i	1.000 + 0.000i
	3.0	-0.000 + 0.000i	0.111 - 0.000i	0.999 + 0.000i
	6.0	-0.001 + 0.000i	0.181 - 0.983i	1.000 + 0.001i
	10.0	-0.000 - 0.000i	-0.462 + 0.887i	1.000 + 0.002i
	15.0	-0.001 - 0.001i	0.757 - 0.654i	1.000 + 0.017i
2	1.0	-0.001 + 0.000i	0.010 + 0.000i	0.998 + 0.000i
	3.0	-0.001 + 0.000i	0.012 + 0.000i	0.997 + 0.000i
	6.0	-0.001 + 0.000i	0.029 + 0.000i	0.996 + 0.000i
	10.0	0.000 + 0.000i	-0.278 - 0.961i	1.000 + 0.008i
	15.0	-0.000 + 0.000i	0.919 + 0.394i	1.000 + 0.013i
3	1.0	-0.011 + 0.000i	0.002 + 0.000i	0.912 + 0.000i
	3.0	-0.011 + 0.000i	0.002 + 0.000i	0.909 + 0.000i
	6.0	-0.013 + 0.000i	0.003 + 0.000i	0.897 + 0.000i
	10.0	-0.022 + 0.000i	0.017 + 0.000i	0.858 + 0.000i
	15.0	0.015 + 0.017i	-0.752 + 0.659i	0.989 + 0.143i

kR_1	Number of Cut-on Modes
1.0	0
3.0	0
6.0	1
10.0	2
15.0	3

TABLE 5.8 Reflection and Transmission Coefficients Computed by FEM(5 x 5) for a Uniform Hardwalled Duct, $\ell = 0.5$, $m_o = 4$

Geometry : Uniform , $R_1 = R_2 = 1.0$, $\ell = 1.0$

Characteristics : No-flow, Hardwalled Duct,

Angular Mode $m_o = 1$

FEM(5 x 5)

Incident Mode i	kR_1	Reflection Coefficients in Mode i	Direct Transmission Coefficients at $z = \ell$ in Mode i	Transmission Coefficients referred to $z = 0$ in Mode i
1	1.0	-0.000 + 0.000i	0.213 + 0.000i	1.000 + 0.000i
	5.0	-0.001 + 0.000i	-0.066 + 0.998i	1.000 + 0.002i
	8.0	-0.005 - 0.001i	0.096 - 0.995i	1.000 + 0.028i
	10.0	-0.002 - 0.005i	-0.949 + 0.317i	0.997 + 0.082i
	15.0	-0.295 + 0.094i	-0.288 - 0.907i	0.860 + 0.407i
2	1.0	-0.001 + 0.000i	0.005 + 0.000i	0.999 + 0.000i
	5.0	-0.002 + 0.000i	0.156 + 0.000i	0.991 + 0.000i
	8.0	-0.000 - 0.000i	0.945 + 0.327i	1.000 + 0.015i
	10.0	-0.005 + 0.003i	-0.523 - 0.852i	0.998 + 0.055i
	15.0	-0.105 - 0.059i	0.495 - 0.856i	0.908 + 0.392i
3	1.0	-0.011 + 0.000i	0.002 + 0.000i	0.937 + 0.000i
	5.0	-0.009 + 0.000i	0.001 + 0.000i	0.922 + 0.000i
	8.0	-0.021 - 0.000i	0.045 + 0.000i	0.883 + 0.000i
	10.0	0.012 - 0.005i	0.389 + 0.921i	0.995 + 0.097i
	15.0	-0.021 + 0.020i	0.728 + 0.679i	0.865 + 0.493i

kR_1	Number of Cut-on Modes
1.0	0
5.0	1
8.0	2
10.0	3
15.0	4

TABLE 5.9 Reflection and Transmission Coefficients Computed by FEM(5 x 5) for a Uniform Hardwalled Duct, $\ell = 1.0$, $m_o = 1$

5.3 RESULTS AND COMPARISONS FOR NONUNIFORM DUCTS

Very few results have been published for the multimodal transmission of sound waves in nonuniform ducts. The two methods: MWR and FEM are being developed here in parallel in view of extension to the propagation problem in ducts with flow. One serves as a checkout for the other. Detailed comparisons for the no-flow case are necessary to generate confidence in the methods for a more general problem.

For the results presented in the following, the figures are point plots at a certain number of discrete frequencies, the MWR values are joined by straight segments. The MWR results were obtained with 50 axial Runge-Kutta integration steps on the basis of a unit duct length.

(i) Uniform geometry; discontinuous lining.

As examples of the comparisons between the MWR and FEM numerical values the case of a uniform lined duct section joined by two hardwalled semi-infinite ducts is considered. Tables 5.10, 5.11, 5.12, 5.13 present the 3 x 3 matrices of reflection and transmission coefficients obtained by the MWR with 5 basis functions and the FEM with 5 x 5 elements. Characteristic parameters were chosen to represent increasingly numerically challenging problems. Table 5.10 for the case of one incident cut-on mode shows an excellent agreement for the axisymmetric mode ($m_o = 0$) at low frequency $kR_1 = 1.0$. Table 5.11 reveals the effect of high frequency. Table 5.12 and 5.13 make comparisons for a shorter duct at a higher angular mode and high frequencies showing an expected trend of degradation, but the results are still useful. One should pay more attention to diagonal terms since their values play an important role in accuracy assessment of flux and power computations. Figures 5.2 - 5.7 plot reflection and transmission coefficients for a lined duct segment through a range of frequencies. Results for modes 1 and 2 are selected, which are the first modes to be cut-on if there are any propagating modes.

These figures show a very good agreement between the MWR (5BF) and FEM (5 x 5) values throughout the whole range of frequencies. The results for the second mode are still indistinguishable on the scale of graphs even through the sensitive frequency range between $kR_1 = 3.5$ and $kR_1 = 4.0$.

Geometry : Uniform, $R_1 = 1.0$, $R_2 = 1.0$, $\ell = 0.5$

Characteristics : $A = (0.72+0.42i)$, $kR_1 = 1.0$, $m_o = 0$

One Cut-on Mode

MWR(5BF)

Reflection Coefficients

	(1)	(2)	(3)
(1)	-0.290 + 0.053i	0.055 + 0.010i	-0.025 - 0.006i
(2)	-0.167 + 0.092i	0.008 - 0.023i	-0.005 + 0.012i
(3)	0.010 - 0.039i	-0.005 + 0.012i	0.003 - 0.007i

Transmission Coefficients

	(1)	(2)	(3)
(1)	0.569 - 0.425i	0.057 + 0.002i	-0.026 + 0.003i
(2)	0.003 + 0.095i	0.161 - 0.011i	-0.001 + 0.004i
(3)	-0.004 - 0.041i	-0.001 + 0.003i	0.031 - 0.001i

FEM(5 x 5)

Reflection Coefficients

	(1)	(2)	(3)
(1)	-0.290 + 0.054i	0.055 + 0.010i	-0.025 - 0.006i
(2)	-0.163 + 0.092i	0.008 - 0.023i	-0.006 + 0.012i
(3)	0.010 - 0.040i	-0.006 + 0.012i	-0.004 - 0.007i

Transmission Coefficients

	(1)	(2)	(3)
(1)	0.569 - 0.424i	0.057 - 0.002i	-0.026 + 0.002i
(2)	0.003 + 0.095i	0.160 - 0.011i	-0.001 + 0.004i
(3)	-0.004 - 0.042i	-0.001 + 0.003i	0.030 - 0.001i

TABLE 5.10 Comparison of Reflection and Transmission Matrices Computed by MWR and FEM for a Softwalled Duct, $kR_1 = 1.0$, $m_o = 0$.

Geometry : Uniform, $R_1 = 1.0$, $R_2 = 1.0$, $\ell = 0.5$; Characteristics : $A = (0.72 + 0.42i)$, $kR_1 = 10.0$, $m_o = 0$
Three Cut-on Modes

MWR(5BF)				FEM (5 x 5)			
Reflection Coefficients				Reflection Coefficients			
	(1)	(2)	(3)		(1)	(2)	(3)
(1)	-0.004 + 0.028i	0.003 - 0.014i	-0.009 + 0.012i	(1)	0.009 + 0.022i	-0.003 - 0.012i	-0.003 + 0.011i
(2)	0.023 - 0.089i	-0.018 + 0.041i	0.034 - 0.025i	(2)	-0.021 - 0.077i	0.001 + 0.037i	0.018 - 0.023i
(3)	-0.131 + 0.156i	0.077 - 0.047i	-0.075 - 0.027i	(3)	-0.041 + 0.169i	0.042 - 0.054i	-0.031 - 0.041i
Transmission Coefficients				Transmission Coefficients			
	(1)	(2)	(3)		(1)	(2)	(3)
(1)	0.160 + 0.721i	0.030 + 0.101i	0.016 - 0.068i	(1)	0.159 + 0.731i	0.029 + 0.098i	0.19 - 0.068i
(2)	0.194 + 0.683i	-0.120 + 0.713i	-0.077 + 0.179i	(2)	0.196 + 0.651i	-0.124 + 0.726i	-0.86 + 0.176i
(3)	0.312 - 1.001i	-0.196 + 0.394i	-0.643 + 0.196i	(3)	0.298 - 1.056i	-0.200 + 0.411i	-0.615 + 0.129i

TABLE 5.11 Comparison of Reflection and Transmission Matrices Computed by MWR and FEM for a Softwalled Duct, $kR_1=10.0$, $m_o = 0$.

Geometry : Uniform, $R_1 = 1$, $R_2 = 1.0$, $\ell = 0.2$; Two Cut-on Modes

Characteristics : $A = (0.1+0.1i)$, $kR_1 = 5.0$, $m_o = 2$

MWR(5BF)				FEM (5 x 5)			
Reflection Coefficients				Reflection Coefficients			
	(1)	(2)	(3)		(1)	(2)	(3)
(1)	-0.056 + 0.005i	-0.037 - 0.014i	-0.026 - 0.012i	(1)	-0.056 + 0.005i	-0.037 - 0.015i	-0.027 - 0.011i
(2)	0.008 - 0.021i	0.010 - 0.012i	0.008 - 0.009i	(2)	0.008 - 0.021i	0.004 - 0.012i	0.019 - 0.009i
(3)	0.003 - 0.007i	0.004 - 0.005i	0.003 - 0.004i	(3)	0.003 - 0.007i	0.010 - 0.005i	-0.011 - 0.004i
Transmission Coefficients				Transmission Coefficients			
	(1)	(2)	(3)		(1)	(2)	(3)
(1)	0.640 - 0.706i	-0.039 - 0.010i	-0.028 - 0.005i	(1)	0.640 - 0.706i	-0.039 - 0.010i	-0.029 - 0.005i
(2)	0.005 - 0.022i	0.418 - 0.011i	0.006 - 0.007i	(2)	0.006 - 0.022i	0.413 - 0.011i	0.014 - 0.007i
(3)	0.001 - 0.008i	0.003 - 0.004i	0.180 - 0.002i	(3)	0.001 - 0.008i	0.007 - 0.004i	0.174 - 0.002i

TABLE 5.12 Comparison of Reflection and Transmission Matrices Computed by MWR and FEM for a Softwalled Duct, $kR_1=5.0, m_o=2$.

Geometry : Uniform, $R_1 = 1.0$, $R_2 = 1.0$, $\ell = 0.2$; Characteristics : $A = (0.1+0.1i)$, $kR_1 = 15.0$, $m_o = 2$
Four Cut-on Modes

MWR(5BF)				FEM (5 x 5)			
Reflection Coefficients				Reflection Coefficients			
	(1)	(2)	(3)		(1)	(2)	(3)
(1)	-0.001 + 0.001i	0.000 + 0.003i	0.001 + 0.007i	(1)	-0.001 + 0.002i	0.000 + 0.003i	0.000 + 0.009i
(2)	0.000 + 0.002i	0.001 + 0.004i	0.001 + 0.007i	(2)	0.000 + 0.002i	0.000 + 0.004i	0.000 + 0.007i
(3)	0.001 + 0.005i	0.000 + 0.007i	-0.001 + 0.011i	(3)	0.000 + 0.007i	0.000 + 0.008i	-0.002 + 0.012i
Transmission Coefficients				Transmission Coefficients			
	(1)	(2)	(3)		(1)	(2)	(3)
(1)	-0.948 - 0.164i	0.027 + 0.041i	0.017 + 0.045i	(1)	-0.947 - 0.165i	0.026 + 0.042i	0.015 + 0.048i
(2)	0.018 + 0.029i	-0.882 - 0.412i	0.008 + 0.033i	(2)	0.019 + 0.028i	-0.882 - 0.415i	0.001 + 0.040i
(3)	0.013 + 0.036i	0.009 + 0.037i	-0.621 - 0.745i	(3)	0.012 + 0.037i	0.001 + 0.045i	-0.603 - 0.759i

TABLE 5.13 Comparison of Reflection and Transmission Matrices Computed by MWR and FEM for a Softwalled Duct, $kR_1=15.0$, $m_o=2$.

Geometry : Linearly Tapered, $R_1 = 1.0$, $R_2 = 1.268$, $\ell = 1.0$

Characteristics : No-flow, Hardwalled duct

Angular Mode $m_o = 0$

kR_1	MWR(3BF)	MWR(5BF)	MWR(7BF)	FEM(5x5)
		Reflection Coefficients		
0.5	-0.227 + 0.122i	-0.215 + 0.117i	-0.210 + 0.114i	-0.195 + 0.109i
1.0	-0.125 + 0.190i	-0.117 + 0.181i	-0.113 + 0.177i	-0.103 + 0.168i
1.5	-0.015 + 0.180i	-0.011 + 0.170i	-0.009 + 0.166i	-0.004 + 0.155i
2.0	0.052 + 0.111i	0.052 + 0.103i	0.052 + 0.100i	0.052 + 0.091i
2.5	0.052 + 0.033i	0.050 + 0.028i	0.049 + 0.026i	0.047 + 0.021i
3.0	-0.002 - 0.018i	-0.004 - 0.020i	-0.006 - 0.021i	-0.009 - 0.023i
3.5	-0.033 + 0.031i	-0.031 + 0.032i	-0.030 + 0.032i	-0.027 + 0.034i
4.0	-0.021 + 0.049i	-0.017 + 0.047i	-0.016 + 0.046i	-0.011 + 0.044i
4.5	0.000 + 0.052i	0.002 + 0.047i	0.003 + 0.045i	0.005 + 0.041i
		Transmission Coefficients		
0.5	0.647 - 0.347i	0.657 - 0.355i	0.663 - 0.358i	0.675 - 0.367i
1.0	0.407 - 0.618i	0.411 - 0.630i	0.413 - 0.636i	0.418 - 0.650i
1.5	0.061 - 0.745i	0.057 - 0.757i	0.056 - 0.763i	0.051 - 0.778i
2.0	-0.312 - 0.687i	-0.321 - 0.695i	-0.325 - 0.699i	-0.337 - 0.708i
2.5	-0.612 - 0.448i	-0.625 - 0.450i	-0.630 - 0.450i	-0.645 - 0.452i
3.0	-0.756 - 0.077i	-0.768 - 0.071i	-0.773 - 0.068i	-0.786 - 0.059i
3.5	-0.682 + 0.277i	-0.687 + 0.286i	-0.689 + 0.290i	-0.694 + 0.301i
4.0	-0.469 + 0.565i	-0.470 + 0.574i	-0.470 + 0.579i	-0.470 + 0.590i
4.5	-0.142 + 0.723i	-0.138 + 0.732i	-0.136 + 0.736i	-0.131 + 0.746i

TABLE 5.14 Convergence of MWR Values for Mode 1 with Unit Incident Mode 1

Geometry : Linearly Tapered, $R_1 = 1.0$, $R_2 = 1.268$, $\ell = 1.0$

Characteristics : No-flow, Hardwalled Duct

Angular Mode $m_o = 0$

kR_1	MWR(3BF)	MWR(5BF)	MWR(7BF)	FEM(5x5)
		Reflection Coefficients		
0.5	0.003 + 0.018i	0.003 + 0.020i	0.004 + 0.020i	0.004 + 0.022i
1.0	0.012 + 0.035i	0.013 + 0.038i	0.014 + 0.039i	0.015 + 0.043i
1.5	0.026 + 0.050i	0.029 + 0.054i	0.030 + 0.056i	0.033 + 0.061i
2.0	0.047 + 0.064i	0.052 + 0.057i	0.054 + 0.073i	0.060 + 0.079i
2.5	0.084 + 0.081i	0.092 + 0.087i	0.097 + 0.090i	0.107 + 0.094i
3.0	0.210 + 0.077i	0.226 + 0.081i	0.234 + 0.082i	0.259 + 0.084i
3.5	0.156 - 0.030i	0.165 - 0.033i	0.169 - 0.035i	0.181 - 0.041i
4.0	0.140 - 0.116i	0.156 - 0.127i	0.163 - 0.133i	0.176 - 0.149i
4.5	0.095 - 0.148i	0.104 - 0.163i	0.106 - 0.170i	0.111 - 0.187i
		Transmission Coefficients		
0.5	0.007 + 0.019i	0.008 + 0.021i	0.008 + 0.022i	0.009 + 0.024i
1.0	0.028 + 0.032i	0.031 + 0.035i	0.032 + 0.037i	0.036 + 0.040i
1.5	0.062 + 0.034i	0.069 + 0.037i	0.072 + 0.038i	0.079 + 0.041i
2.0	0.110 + 0.018i	0.121 + 0.018i	0.126 + 0.018i	0.139 + 0.017i
2.5	0.186 - 0.029i	0.201 - 0.036i	0.210 - 0.039i	0.230 - 0.047i
3.0	0.546 - 0.247i	0.567 - 0.275i	0.583 - 0.290i	0.633 - 0.332i
3.5	-0.352 - 0.533i	-0.398 - 0.567i	-0.418 - 0.580i	-0.471 - 0.616i
4.0	-0.565 - 0.808i	-0.612 - 0.075i	-0.634 - 0.072i	-0.686 - 0.063i
4.5	-0.452 + 0.237i	-0.482 + 0.268i	-0.493 + 0.282i	-0.525 + 0.316i

TABLE 5.15 Convergence of MWR Values for Mode 2 with Unit Incident Mode 1

(ii) Nonuniform geometry, hard walls.

To investigate the effect of geometric nonuniformity alone one may consider the hardwall case for a linearly tapered duct. Figures 5.8 - 5.19 show comparisons of the MWR(5BF) and FEM(5 x 5) results for a 15° tapered angle. The duct lengths are varied, $\ell = 0.5$ giving about 29% increase in original cross-sectional area and $\ell = 1.0$ about 61%. The latter case is considered very challenging to computational methods. A frequency range of $0.5 \leqslant kR_1 \leqslant 4.5$ has been considered for axially symmetric propagation.

In these figures there appears to be a reasonable agreement for diagonal terms in the reflection and transmission matrices, i.e. the coefficients of modes which are excited by the incident mode of the same order, except in Figures 5.8 and 5.14 where the reflection coefficients of mode 1 with mode 1 incident are relatively small in the frequency range considered. The results for mode 2 with mode 1 incident show a degradation which creates a gap between the results obtained by the two methods. There are sensitive indications in the region where the incident mode 2 becomes cut-on (between $kR_1 = 3.5$ and $kR_1 = 4.0$). However, it is noticed there is a correlation between the results of the two methods.

Note that for the results above the same numbers of basis functions and finite elements have been used as for the case of uniform geometry in Section 5.3.1. But Tables 5.10 and 5.11 and Figures 5.2 - 5.7 have shown a better agreement even though in general a softwall case with admittance discontinuity seems to be more severe computationally than a hardwall case. This proves that the speed of convergence is dependent upon the nonuniform duct configuration, for which, of the two methods, one must have a higher convergence rate than the other.

To have better judgement for the two methods one can compare the

results of successive runs with more and more basis functions and elements. For the same geometry (ℓ = 1.0) and characteristic parameters as above, the FEM with 5 x 5, 5 x 10, 8 x 8 elements yield little changes in the values of coefficients whilst for the MWR with increasing numbers of basis functions a convergence trend is observed to be occurring towards the FEM values. Tables 5.14 and 5.15 show this definite converging trend for the whole frequency range of interest. The implication is that the solution accuracy achieved by the MWR for a nonuniform duct geometry is lower than that for a compatible uniform duct of reduced geometry at the same level of approximations (i.e. with the same number of basis functions used).

5.4 POWER TRANSMISSION

While the reflection and transmission coefficients may provide a means of assessing the acoustic performance of a nonuniform acoustically treated element, there are drawbacks in interpreting the results. Consideration of the acoustic power transmission is more fundamental and physically more significant.

5.4.1 Formulae and Implementation

The acoustic power at a given duct cross-section, propagating axially, is the integral of the acoustic intensity over the cross-sectional area

$$W = \int_A I \, dA \tag{5.4.1}$$

where the acoustic intensity, I, is given by

$$I = \frac{1}{4} (pw^* + p^* w), \text{ where } * \text{ denotes complex conjugate}$$

$$\text{Thus , } \quad W = \frac{\pi}{2} \int_0^R (pw^* + p^* w) \, r \, dr \tag{5.4.2}$$

In the following calculations it is assumed that the number of incident modes introduced to the nonuniform duct is that number of modes which would propagate in a hardwalled duct of the same geometry, and the propagating incident modes carry equal acoustic energy (theoretically cut-off modes have zero amplitudes on the inlet side).

(i) MWR.

To develop computational formulae for the MWR with end-matching using MWR eigenfunctions in the uniform ducts one has recourse to the eigensolution in the form of the modal matrix (Section 5.1.2(ii)).

At $z = 0$

$$\begin{Bmatrix} w \\ p \end{Bmatrix} = [C]\,[M] \begin{Bmatrix} a^+ \\ a^- \end{Bmatrix}$$

$$= \underset{2\times 2N}{\begin{bmatrix} \cos \kappa_m r & \\ & \cos \kappa_m r \end{bmatrix}} \underset{2N\times 2N}{\begin{bmatrix} M_w^+ & M_w^- \\ M_p^+ & M_p^- \end{bmatrix}} \underset{2N\times 1}{\begin{Bmatrix} a^+ \\ a^- \end{Bmatrix}} \qquad (5.4.3)$$

with appropriate basis functions for the axial station or more explicitly

$$w = \underset{1\times N}{[\cos \kappa_m r]}\,\underset{N\times N}{[M_w^+]}\,\underset{N\times 1}{\{a^+\}} + \underset{1\times N}{[\cos \kappa_m r]}\,\underset{N\times N}{[M_w^-]}\,\underset{N\times 1}{\{a^-\}}$$

$$p = \underset{1\times N}{[\cos \kappa_m r]}\,\underset{N\times N}{[M_p^+]}\,\underset{N\times 1}{\{a^+\}} + \underset{1\times N}{[\cos \kappa_m r]}\,\underset{N\times N}{[M_p^-]}\,\underset{N\times 1}{\{a^-\}}$$

Substituting these expressions into equation (5.4.2) one can obtain

$$W = \underset{1\times 2N}{\begin{Bmatrix} a^+ \\ a^- \end{Bmatrix}^T} \underset{2N\times 2N}{\begin{bmatrix} P_a^{++} & P_a^{+-} \\ P_a^{-+} & P_a^{--} \end{bmatrix}} \underset{2N\times 1}{\begin{Bmatrix} a^+ \\ a^- \end{Bmatrix}^*} \qquad (5.4.4)$$

$$= \begin{Bmatrix} a^+ \\ a^- \end{Bmatrix}^T [P_a] \begin{Bmatrix} a^+ \\ a^- \end{Bmatrix}^*$$

where a typical component of $[P_a]$ is given by

$$[P_a^{+-}] = \frac{\pi R_1^2}{2} \left([M_p^+]^T [E] [M_w^-]^* + [M_w^+]^T [E] [M_p^-]^* \right) \qquad (5.4.5)$$

with $\underset{N\times N}{[E]} = \int_0^1 \underset{N\times 1}{\{\cos \kappa_n R_1 \eta\}} \underset{1\times N}{[\cos \kappa_m^* R_1 \eta]}\, \eta\, d\eta$

For other components of $[P_a]$ the two superscripts are replaced consistently.

For a hardwalled duct, in the expression (5.4.4) the contributions of $[P_a^{+-}]$ and $[P_a^{-+}]$ will cancel each other. Thus, in general, if the interactions between negative and positive acoustic modes are ignored one can express the incident power W_i and the reflected power W_r as follows :

$$W_i = \{a^+\}^T [P_a^{++}] \{a^+\}^*, \quad W_r = \{a^-\} [P_a^{--}] \{a^-\}^* \tag{5.4.6}$$

Assume each incident mode carries a unit of energy. The amplitude of incident mode i can be deduced :

$$1. = a_i^+ P_{aii}^{++} a_i^{+*}$$

Hence

$$|a_i^+| = 1 / \sqrt{P_{aii}^{++}} \tag{5.4.7}$$

With $\{a^-\} = [\text{REFL}] \{a^+\}$ from the transmission solution the reflected power W_r can be calculated via incident amplitudes

$$W_r = \{a^+\}^T [\text{REFL}]^T [P_a^{--}] [\text{REFL}]^* \{a^+\}^* \tag{5.4.8}$$

Similarly at $z = \ell$ one can obtain a relation analogous to equation (5.4.4)

$$W = \begin{Bmatrix} b^+ \\ - \\ b^- \end{Bmatrix}^T \left[\begin{array}{c|c} P_b^{++} & P_b^{+-} \\ - - & - - \\ P_b^{-+} & P_b^{--} \end{array}\right] \begin{Bmatrix} b^+ \\ - \\ b^- \end{Bmatrix}^*$$

where components P_b^{++} , P_b^{+-} ... are defined as in equation (5.4.5).

But here $\{b^-\} \equiv 0$, so the transmitted power can be expressed as

$$W_t = \{b^+\}^T [P_b^{++}] \{b^+\}^*$$

or, with $\{b^+\} = [\text{TRAN}] \{a^+\}$

$$W_t = \{a^+\}^T [\text{TRAN}]^T [P_b^{++}] [\text{TRAN}]^* \{a^+\}^* \tag{5.4.9}$$

(ii) FEM

In the FEM matching formulation exact eigenfunctions have been used, so the power calculations here are based on the Bessel functions.

The acoustic pressure and the axial particle velocity component are expressed as follows, at z = 0 :

$$p = \sum_{n=1}^{N} \left(a_n^+ J_{m_o}(K_n^+ r) + a_n^- J_{m_o}(K_n^- r) \right)$$

$$w = \sum_{n=1}^{N} \left(\alpha_n^+ a_n^+ J_{m_o}(K_n^+ r) + \alpha_n^- a_n^- J_{m_o}(K_n^- r) \right)$$

where N is the number of incident modes considered, and $\alpha_n^+ = k_{zn}^+/k$, $\alpha_n^- = k_{zn}^-/k$ (see Appendix C).

In vector-matrix forms

$$p = [J^+]\{a^+\} + [J^-]\{a^-\}$$

$$w = [J^+]\lceil\alpha^+\rfloor\{a^+\} + [J^-]\lceil\alpha^-\rfloor\{a^-\}$$

where

$$[J^+] = \left[J_{m_o}(K_1^+ r),\ J_{m_o}(K_2^+ r), \ldots J_{m_o}(K_N^+ r) \right]$$

$$[J^-] = \left[J_{m_o}(K_1^- r),\ J_{m_o}(K_2^- r), \ldots J_{m_o}(K_N^- r) \right]$$

$$\alpha_{nn}^+ = k_{zn}^+/k \ , \ \alpha_{nn}^- = k_{zn}^-/k \ , \ n = 1,2,3 \ldots N$$

Substituting these expressions into equation (5.4.2) yields

$$W = \begin{Bmatrix} a^+ \\ - \\ a^- \end{Bmatrix}^T \begin{bmatrix} P_a^{++} & \vdots & P_a^{+-} \\ \cdots & \cdots & \cdots \\ P_a^{-+} & \vdots & P_a^{--} \end{bmatrix} \begin{Bmatrix} a^+ \\ - \\ a^- \end{Bmatrix}^*$$

where the component $[P_a^{+-}]$ is given by

$$[P_a^{+-}] = \frac{\pi}{2} R_1^2 \left([J^+ J^{-*}]\lceil\alpha^-\rfloor^* + \lceil\alpha^-\rfloor [J^- J^{+*}] \right)$$

and typically, with $\eta = \frac{r}{R_1}$

$$[J^+ J^{-*}] = \int_0^1 \left\{ J_{m_o}(K_n^+ R_1 \eta) \right\} \left[J_{m_o}^*(K_m^- R_1 \eta) \right] \eta \, d\eta \qquad (5.4.10)$$

NxN Nx1 1xN

At z = ℓ similar derivations can be obtained.

Thus,the incident amplitudes, the incident, reflection and transmission powers can be similarly deduced as for the MWR, except that for the hardwall case the expression (5.4.10) for $[P_a^{++}]$, $[P_a^{--}]$

can be evaluated using the orthogonality of the Bessel functions.

5.4.2 Results and Comparisons

For assessment of acoustic performance some parameters are defined.

Transmission efficiency : $\eta_t = \left|\frac{W_t}{W_i}\right|$

Reflection efficiency : $\eta_r = \left|\frac{W_r}{W_i}\right|$

Absorption efficiency : $\eta_a = 1 - (\eta_t + \eta_r)$

For the hardwalled duct $\eta_t + \eta_r = 1.$, $\eta_a = 0.$

Now with the efficiencies available at this stage one can re-examine the solution convergence offered by the MWR and the FEM. A hardwalled duct of cosine-converging-diverging geometry is considered. The throat radius $R_t = 0.93$ represents about 14% reduction in uniform duct cross-sectional area. Tables 5.16 and 5.17 make comparisons and show convergence trends of the coefficients and the efficiencies given by the MWR and the FEM with increasing dimensionality. The FEM values have little changes, in fact FEM(5 x 5) can give very good results for the efficiencies (judged by $\eta_t + \eta_r = 1.$) In several hardwall cases the FEM(5 x 5) yields good results up to 3 decimal points for η_t and η_r, which should total 1.000.

Tables 5.18 and 5.19 show the MWR(6BF) and FEM(8 x 8) results for a uniform softwalled duct section. The antisymmetric mode $m_o = 1$ at high frequency $kR_1 = 10.0$ has been considered. A correlation is still observed in efficiency values.

Figures 5.20 and 5.21 give practical applications of the computational methods to a softwalled cosine-converging nonuniform duct. The

transmission and absorption efficiencies are point-plotted for a range of frequencies of interest. In Figure 5.20 for $m_o = 1$ there are two distinct discontinuities near $kR_1 = 5.3$ and $kR_1 = 8.5$ which result from the first introduction of mode 2 and mode 3 incident to the inlet duct. In Figure 5.21 for $m_o = 4$ the incident mode 2 starts to cut on at about $kR_1 = 9.3$, and the agreement deteriorates at high frequencies. Apparently more basis functions and finite elements should be employed when mode 3 cuts on.

It was noted that for $m_o = 4$, 5 basis functions have been used in the MWR. Increasing to 6 basis functions would cause numerical instability (as discussed in Section 5.1.3(iv)) at some low frequencies ($kR_1 < 10$ say). This signifies limitations of the MWR at high angular mode and low frequency.

Geometry : Cosine-Converging-Diverging, R_1=1.0, R_t = 0.93, R_2 = 1.0, ℓ = 0.75

Characteristics : No-flow, Hardwalled Duct, kR_1 = 5.0 ,

Angular Mode m_o = 0 , 2 Cut-on Modes

MWR(6BF)		MWR(8BF)		MWR(9BF)	
(1)	(2)	(1)	(2)	(1)	(2)
(1) -0.050 - 0.091i	-0.009 + 0.046i	(1)-0.050 - 0.091i	-0.009 + 0.046i	(1)-0.054 - 0.093i	-0.009 + 0.048i
(2) -0.103 + 0.514i	0.167 - 0.130i	(2)-0.098 + 0.498i	0.164 - 0.128i	(2)-0.079 + 0.419i	0.150 - 0.118i
Reflection Efficiency: 0.014		Reflection Efficiency: 0.014		Reflection Efficiency: 0.013	
FEM(5 x 5)		FEM(5 x 10)		FEM(8 x 8)	
(1)	(2)	(1)	(2)	(1)	(2)
(1) -0.051 - 0.088i	-0.009 + 0.047i	(1)-0.051 - 0.089i	-0.009 + 0.047i	(1)-0.051 - 0.089i	-0.009 + 0.047i
(2) -0.084 + 0.447i	0.155 - 0.123i	(2)-0.084 + 0.448i	0.155 - 0.123i	(2)-0.083 + 0.447i	0.155 - 0.122i
Reflection Efficiency: 0.013		Reflection Efficiency: 0.013		Reflection Efficiency: 0.013	

TABLE 5.16 Comparison of Reflection Matrices and Efficiencies Computed by MWR and FEM for a Hardwalled Duct, kR_1=5.0, m_o=0.

Geometry : Cosine-Converging-Diverging, R_1=1.0, R_t = 0.93, R_2 = 1.0, ℓ = 0.75

Characteristics: No-flow, Hardwalled Duct, kR_1 = 5.0 ,

Angular Mode m_o = 0 , 2 Cut-on Modes

MWR(6BF)		MWR(8BF)		MWR(9BF)	
(1)	(2)	(1)	(2)	(1)	(2)
(1) -0.804 + 0.559i	-0.010 + 0.019i	(1)-0.804 + 0.560i	-0.010 + 0.019i	(1) -0.805 + 0.562i	-0.010 + 0.018i
(2) -0.113 + 0.219i	-0.631 - 0.726i	(2)-0.108 + 0.208i	-0.633 - 0.726i	(2) -0.087 + 0.164i	-0.635 - 0.732i
Transmission Efficiency: 0.978		Transmission Efficiency: 0.980		Transmission Efficiency: 0.990	
FEM(5 x 5)		FEM(5 x 10)		FEM(8 x 8)	
(1)	(2)	(1)	(2)	(1)	(2)
(1) -0.804 + 0.564i	-0.010 + 0.018i	(1)-0.803 + 0.565i	-0.010 + 0.018i	(1) -0.803 + 0.565i	-0.010 + 0.018i
(2) -0.092 + 0.175i	-0.634 - 0.730i	(2)-0.092 + 0.175i	-0.634 - 0.730i	(2) -0.092 + 0.174i	-0.635 - 0.729i
Transmission Efficiency: 0.987		Transmission Efficiency: 0.987		Transmission Efficiency: 0.987	

TABLE 5.17 Comparison of Transmission Matrices and Efficiencies Computed by MWR and FEM for a Hardwalled Duct, kR_1=5.0, m_o = 0.

Geometry : Uniform, $R_1 = 1.0$, $R_2 = 1.0$, $\ell = 0.5$

Characteristics : No-flow, Lined Segment, $A_1 = 0.$, $A = (0.72+0.42i)$, $A_2 = 0.$, $kR_1 = 10.0$, Angular Mode $m_o = 1$, 3 Cut-on Modes

MWR(6BF)				FEM(8 x 8)			
Reflection Coefficients				Reflection Coefficients			
	(1)	(2)	(3)		(1)	(2)	(3)
(1)	-0.01 + 0.04i	-0.01 + 0.06i	-0.04 + 0.06i	(1)	0.01 + 0.04i	0.00 + 0.06i	-0.03 + 0.07i
(2)	-0.01 + 0.05i	-0.02 + 0.05i	-0.03 + 0.05i	(2)	0.00 + 0.05i	-0.01 + 0.06i	-0.02 + 0.06i
(3)	-0.06 + 0.08i	-0.05 + 0.08i	-0.02 + 0.14i	(3)	-0.04 + 0.10i	-0.03 + 0.09i	0.01 + 0.15i
Reflection Efficiency: 0.05				Reflection Efficiency: 0.05			
Transmission Coefficients				Transmission Coefficients			
	(1)	(2)	(3)		(1)	(2)	(3)
(1)	0.08 + 0.65i	0.01 - 0.33i	0.18 - 0.12i	(1)	0.07 + 0.66i	0.00 - 0.32i	0.19 - 0.13i
(2)	0.01 - 0.28i	-0.35 + 0.64i	0.22 - 0.03i	(2)	0.00 - 0.28i	-0.35 + 0.64i	0.23 - 0.04i
(3)	0.26 - 0.16i	0.36 - 0.05i	-0.56 - 0.19i	(3)	0.25 - 0.17i	0.36 - 0.06i	-0.53 - 0.20i
Transmission Efficiency: 0.12				Transmission Efficiency: 0.13			

TABLE 5.18 Comparison of Reflection and Transmission Matrices, and Efficiencies Computed by MWR and FEM for a Softwalled Duct, $kR_1 = 10.0$, $m_o = 1$.

Geometry : Cosine-Converging-Diverging, $R_1 = 1.0$, $R_t = 0.93$, $R_2 = 1.0$, $\ell = 0.75$

Characteristics : No-flow, Hardwalled Duct, $kR_1 = 10.0$,

Angular Mode $m_o = 1$, 3 Cut-on Modes

MWR(8BF)			FEM(8 x 8)		
Reflection Coefficients			Reflection Coefficients		
(1)	(2)	(3)	(1)	(2)	(3)
(1) -0.01 + 0.01i	-0.02 + 0.02i	-0.07 + 0.01i	(1) -0.01 + 0.01i	-0.02 + 0.01i	-0.06 + 0.01i
(2) -0.02 + 0.01i	-0.03 + 0.02i	-0.08 - 0.02i	(2) -0.02 + 0.01i	-0.03 + 0.01i	-0.08 - 0.02i
(3) -0.09 + 0.02i	-0.14 - 0.04i	-0.05 - 0.28i	(3) -0.08 + 0.02i	-0.13 - 0.03i	-0.05 - 0.27i
Reflection Efficiency: 0.06			Reflection Efficiency: 0.05		
Transmission Coefficients			Transmission Coefficients		
(1)	(2)	(3)	(1)	(2)	(3)
(1) 0.47 - 0.85i	0.01 + 0.09i	-0.15 + 0.10i	(1) 0.46 - 0.86i	0.01 + 0.08i	-0.15 + 0.10i
(2) 0.01 + 0.08i	0.96 + 0.05i	-0.19 + 0.00i	(2) 0.01 + 0.07i	0.96 + 0.04i	-0.19 + 0.01i
(3) -0.21 + 0.14i	-0.31 + 0.01i	-0.84 + 0.29i	(3) -0.20 + 0.14i	-0.29 + 0.01i	-0.85 + 0.29i
Transmission Efficiency: 0.95			Transmission Efficiency: 0.95		

TABLE 5.19 Comparison of Reflection and Transmission Matrices, and Efficiencies Computed by MWR and FEM for a Hardwalled Duct, $kR_1 = 10.0$, $m_o = 1$.

5.5 DISCUSSION AND CONCLUSIONS

5.5.1 Computational Efficiency

The measure of efficiency for computational schemes based on the computing time for a given test case may not be regarded as sound since the accuracy level offered by each method is dependent upon a particular combination of characteristic parameters and duct configuration. For example, the FEM solution time seems to be independent of whether a non-uniform geometry reduces to a uniform one or a softwalled duct becomes a hardwalled one. For the MWR an appreciable amount of computing time can be saved for the hardwall case since the basis functions are readily obtainable, and for a uniform duct segment (with constant admittance along the wall) with discontinuous lining at the end of the nonuniformity the coefficient matrix in the Runge-Kutta integration scheme needs to be evaluated only once. Limitations of the methods must be also taken into account, for instance, high dimensionality for the conservation equation FEM, numerical instability for the MWR with highly cut-off modes.

For the no-flow case, used to the best advantages in extremely computationally severe cases the FEM appears to be more favourable in terms of computational efficiency and convergence speed. However, this conclusion does not extrapolate to the case when flow is present.

Perhaps the best advantage offered by the FEM arises when the acoustic field is to be constructed from the nodal values. These nodal values would normally be available as a result of the solution routine and only simple computations involving the shape functions would be required to obtain the solution field. In the MWR in the present form only reflection and transmission coefficients are available. Construction of the acoustic field from the basis functions would require either another integration of the governing equations or storage of the transition matrix at selected integration steps.

Another advantage of the FEM is the flexibility of application. While the FEM here is tailored to fit the problem in the present investigation its general approach is systematic and applicable to a much wider class of problems, especially with irregular boundaries, with minimal modifications. The MWR is devised specifically for this particular problem. A considerable modification would be required to treat a different one. For example, in extension from the case of circular to annular geometry programming implementations for the FEM would require very little modifications, meanwhile for the MWR many routines are to be changed.

5.2.2 Conclusions

The MWR and the FEM provide two totally different methods of solution to the field equations for acoustic transmission in nonuniform ducts. The fact that they yield nearly equivalent results when applied to the same problem serves as a valuable verification of both methods. This will be of more importance in the case when flow is present and there are virtually no standard results against which to make comparisons.

Several test cases have been presented with numerical results, showing the potential of the two methods for the flow case. In all test cases of a duct of uniform geometry the two methods showed exceptional agreement for numerical approximations.

A reasonable correlation was even observed for computationally extremely challenging circumstances. The case of a uniform lined duct segment joined by two hardwalled semi-infinite ducts showed the validity of the matching methods at the interfaces, which needs to be established before any extension to the flow case.

For nonuniform ducts some severe cases have been considered, e.g. with up to 61% increase in original cross-sectional area for a hardwalled

duct. Transmission efficiency computations have been performed for some general combinations of characteristic parameters, for example, lined duct with angular mode up to $m_o = 4$ at moderately high frequencies. The correlation and convergence trends generate confidence in the computational schemes. It was noticed that in nonuniform duct geometry the MWR convergence rate seems slower than that of the FEM in comparison to the case of uniform geometry.

Apart from the complexity in formulations and implementations, the MWR has the disadvantage of numerical instability due to the impact of highly cut-off modes. This is an inherent difficulty for any numerical method to solve the wave propagation problem. The situation is more severe to the MWR in the sense that it restricts the degrees of freedom in approximations, i.e. the number of basis functions used, particularly for lined ducts at high angular modes and low frequencies. Nevertheless, the transmission of cut-off modes may not be of practical interest.

The numerical instability in the MWR corresponds to a deterioration in the FEM if the same number of incident modes are introduced. However, in the FEM the numbers of incident, reflected and transmitted may be different and independent of the level of solution convergence. The FEM's flexibility in this sense together with its advantageous computational efficiency appears to make it more attractive for the flow case. This may be elusive since then the FEM will encounter the severity of high dimensionality, which has been exemplified by the no-flow problem formulated with the conservation equations.

In the next stage the two methods will explore the transmission problem in ducts with flow.

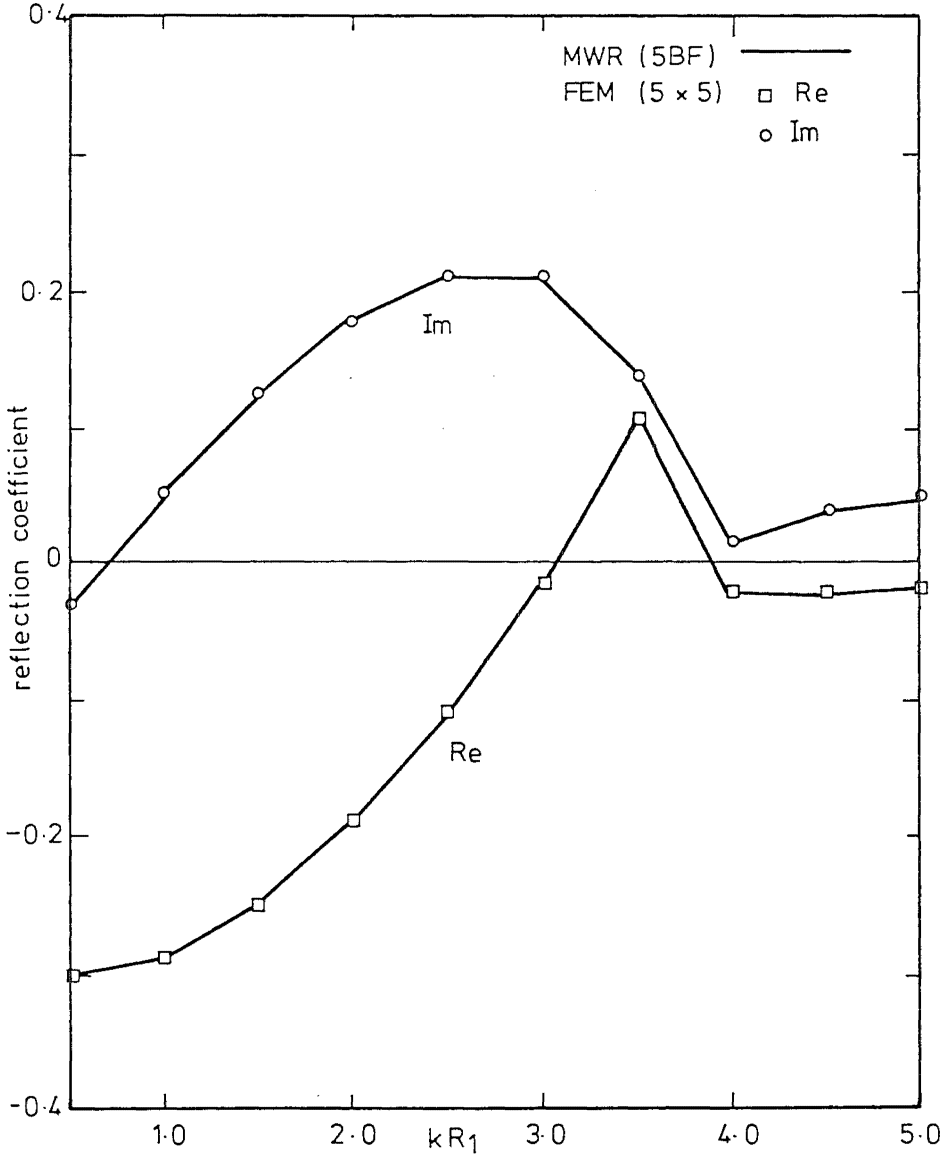

FIG. 5·2 REFLECTION COEFFICIENTS FOR MODE 1 WITH UNIT INCIDENT MODE 1

Geometry: uniform, $R_1 = 1{\cdot}0$, $R_2 = 1{\cdot}0$, $l = 0{\cdot}5$
Characteristics: no flow, $A = (0{\cdot}72 + 0{\cdot}42i)$, $A_1 = 0$, $A_2 = 0$, $m_o = 0$

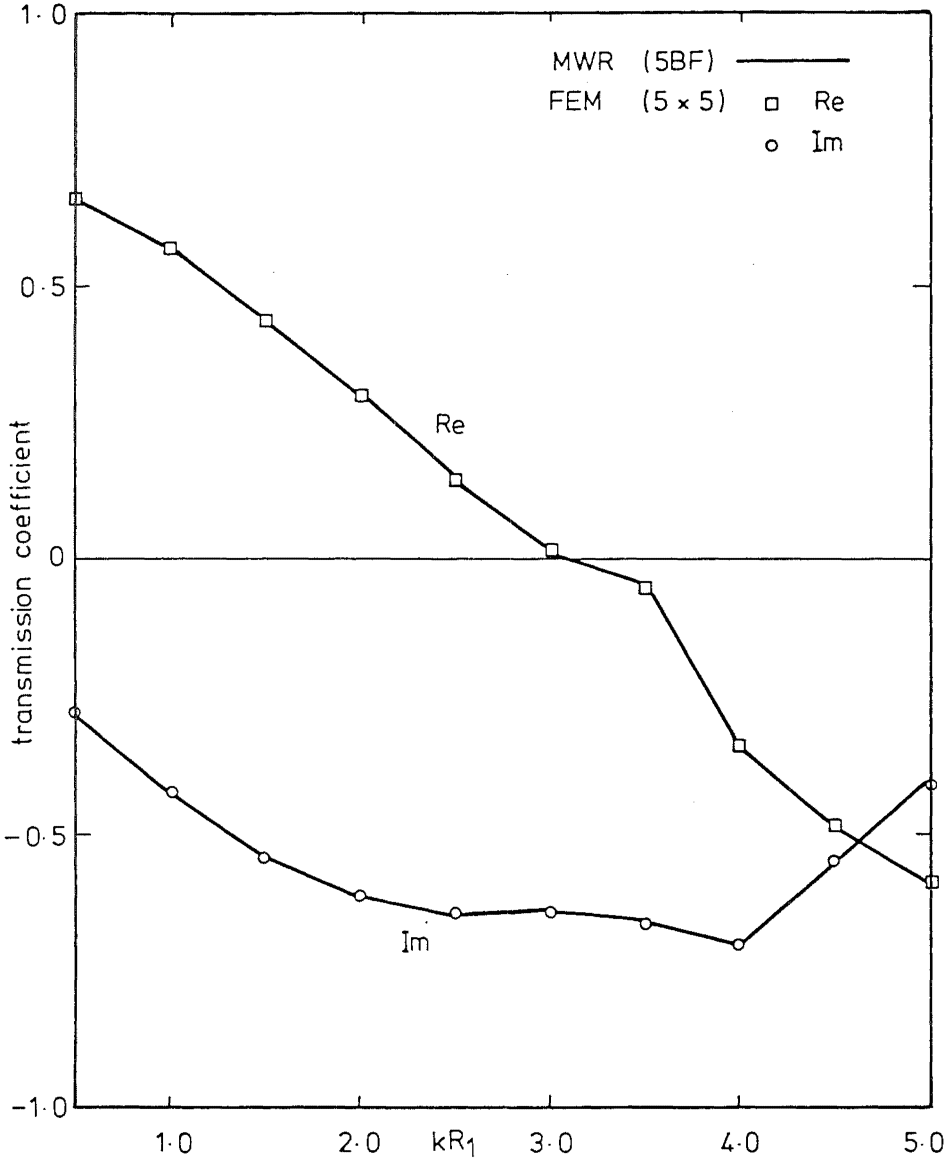

FIG. 5·3 TRANSMISSION COEFFICIENTS FOR MODE 1 WITH UNIT INCIDENT MODE 1

Geometry: uniform, $R_1 = 1{\cdot}0$, $R_2 = 1{\cdot}0$, $l = 0{\cdot}5$
Characteristics: no flow, $A = (0{\cdot}72 + 0{\cdot}42i)$, $A_1 = 0$, $A_2 = 0$, $m_o = 0$

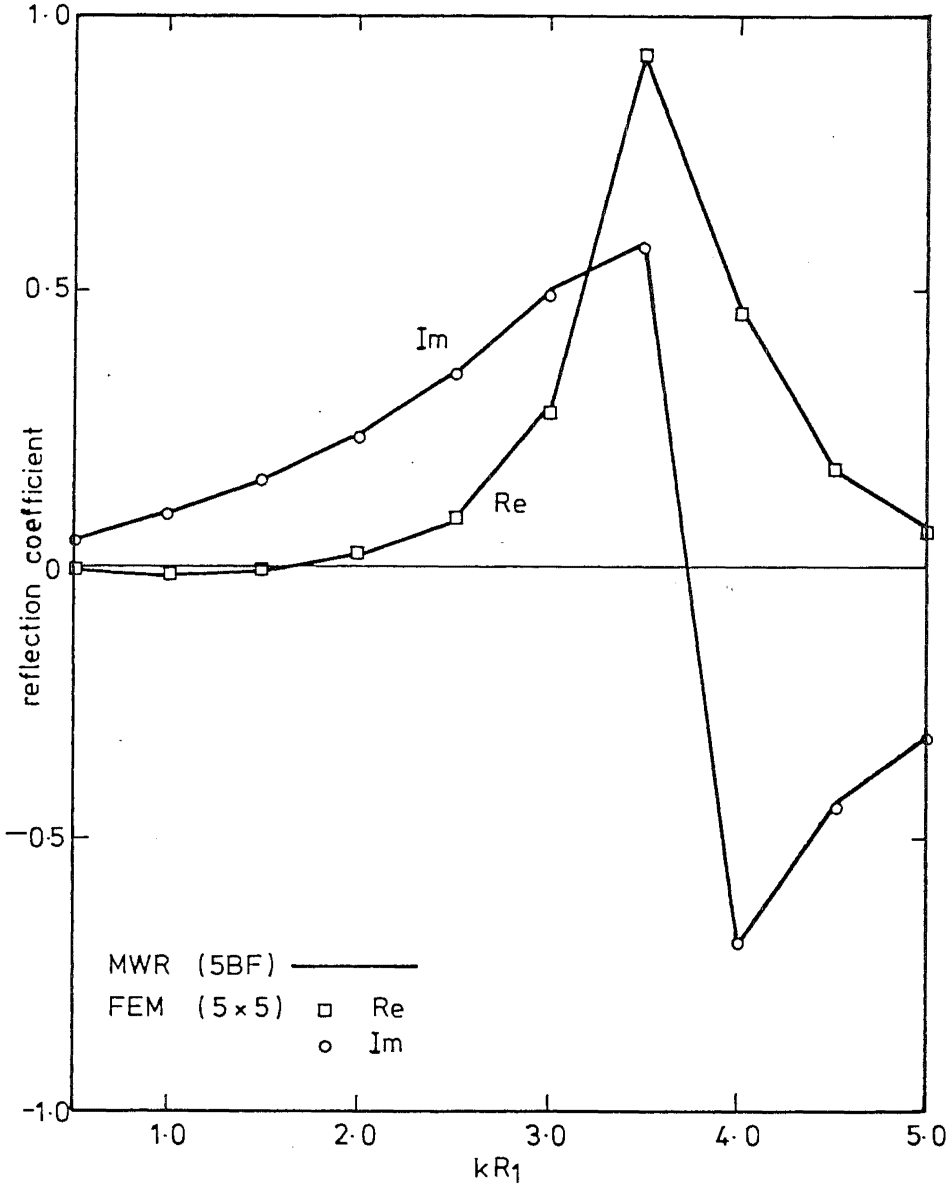

FIG. 5·4 REFLECTION COEFFICIENTS FOR MODE 2 WITH UNIT INCIDENT MODE 1.

Geometry: uniform, $R_1 = 1{\cdot}0$, $R_2 = 1{\cdot}0$, $l = 0{\cdot}5$

Characteristics: no flow, $A = (0{\cdot}72 + 0{\cdot}42i)$, $A_1 = 0$, $A_2 = 0$, $m_o = 0$

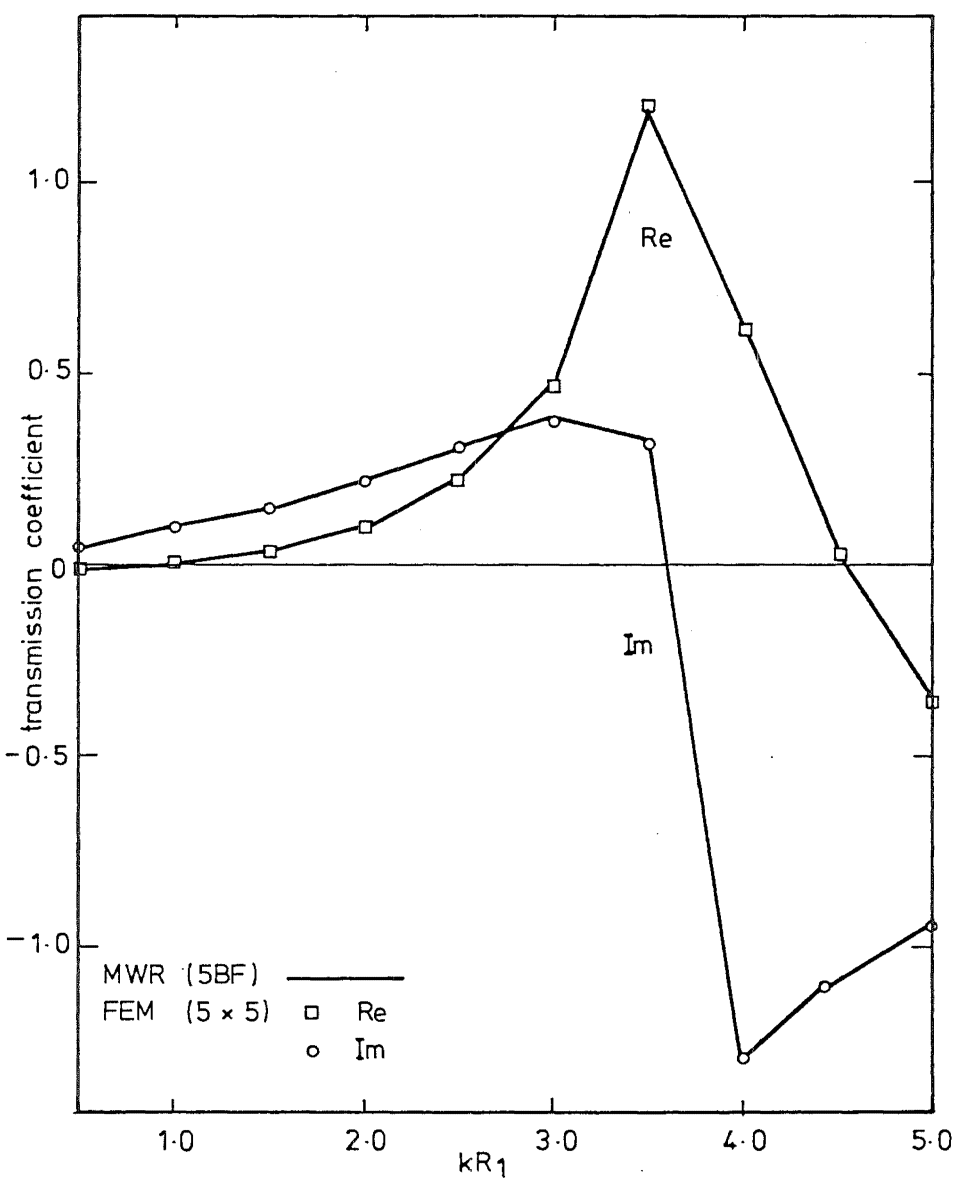

FIG. 5·5 TRANSMISSION COEFFICIENTS FOR MODE 2 WITH UNIT INCIDENT MODE 1.

Geometry: uniform, $R_1 = 1{\cdot}0$, $R_2 = 1{\cdot}0$, $l = 0{\cdot}5$

Characteristics: no flow, $A = (0{\cdot}72 + 0{\cdot}42i)$, $A_1 = 0$, $A_2 = 0$, $m_o = 0$

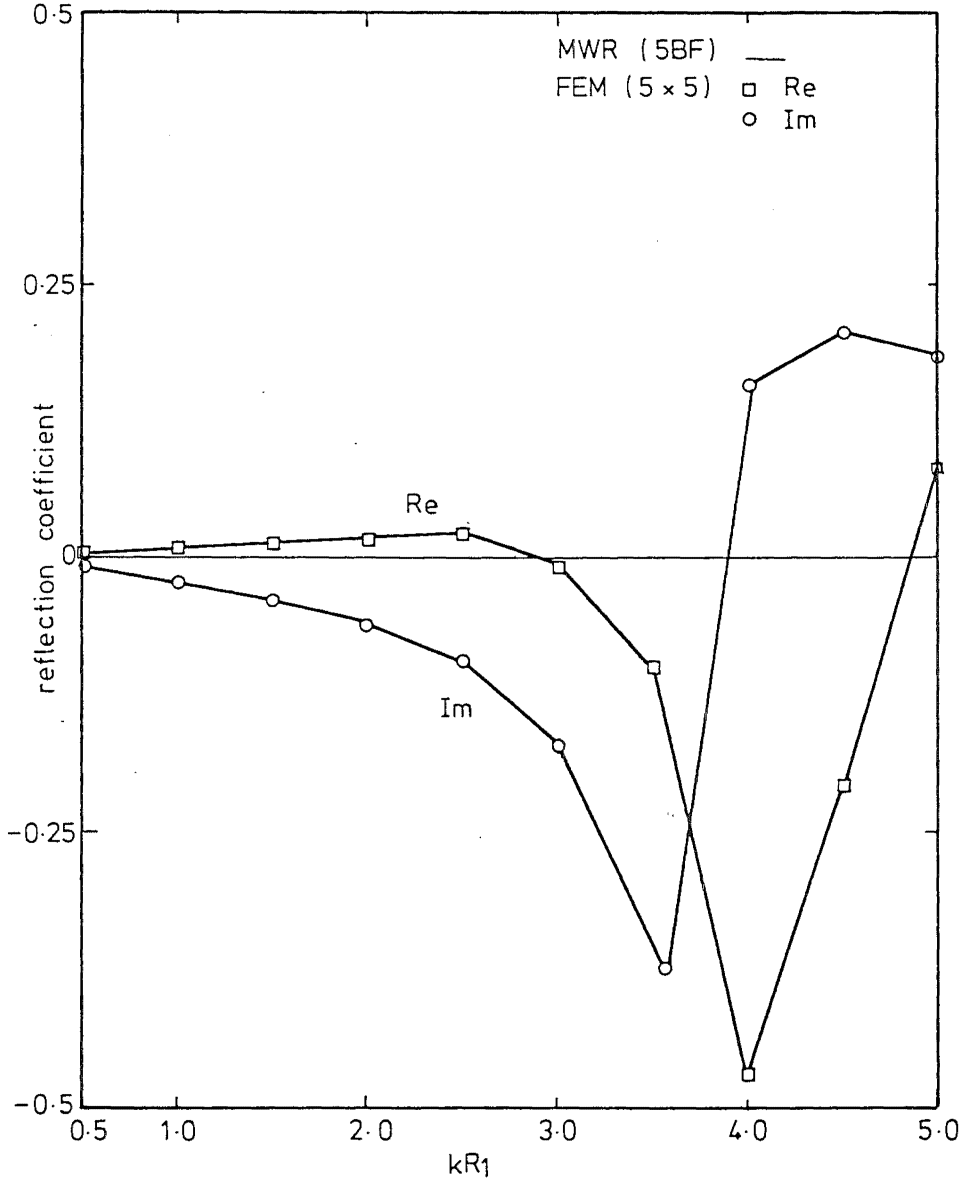

FIG. 5·6 REFLECTION COEFFFICIENTS FOR MODE 2 WITH UNIT INCIDENT MODE 2.

Geometry: uniform $R_1 = 1{\cdot}0$, $R_2 = 1{\cdot}0$, $l = 0{\cdot}5$
Characteristics: no flow, $A = (0{\cdot}72 + 0{\cdot}42i)$, $A_1 = 0$, $A_2 = 0$, $m_o = 0$

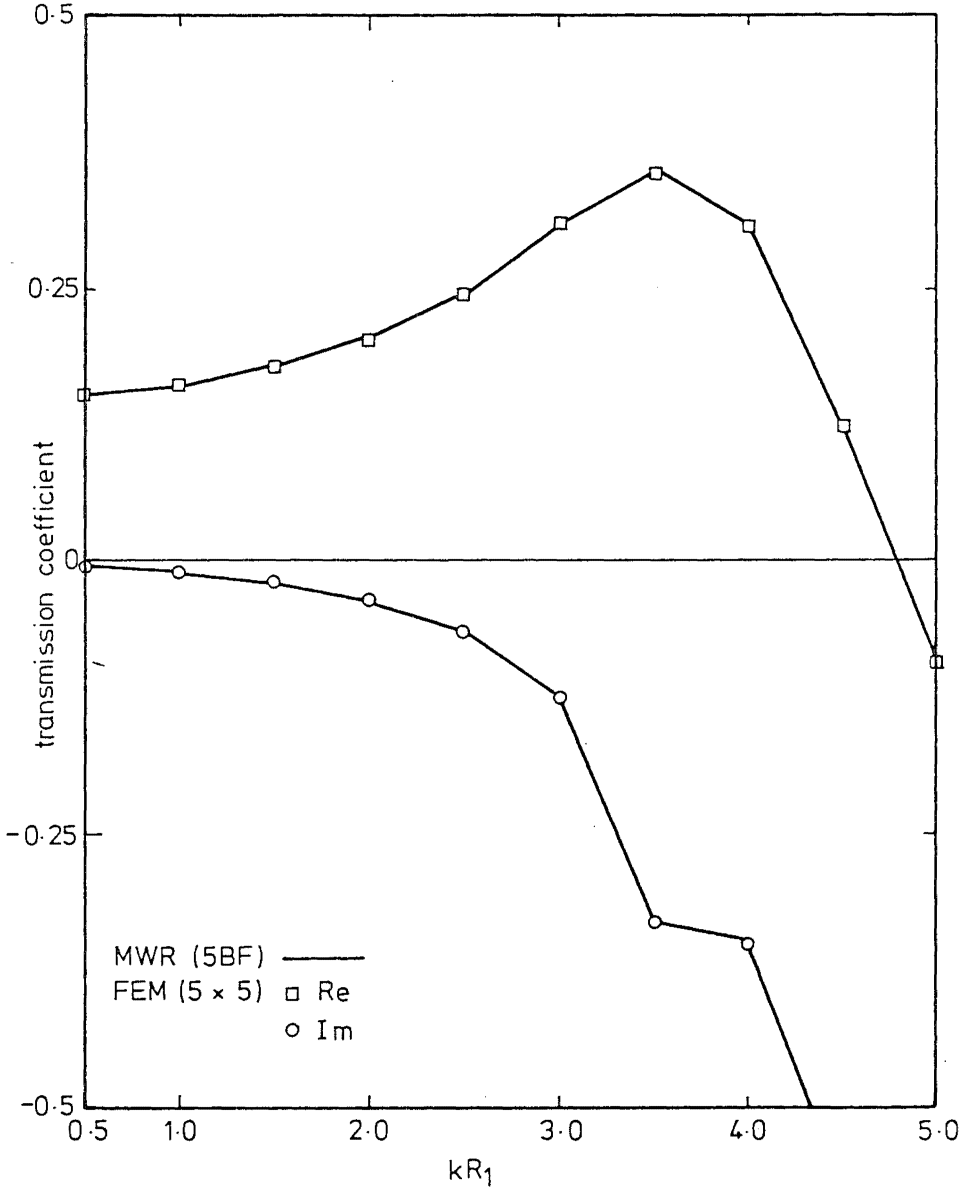

FIG. 5·7 TRANSMISSION COEFFICIENTS FOR MODE 2 WITH UNIT INCIDENT MODE 2.

Geometry: uniform $R_1 = 1{\cdot}0$, $R_2 = 1{\cdot}0$, $l = 0{\cdot}5$
Characteristics: no flow, $A = (0{\cdot}72 + 0{\cdot}42i)$, $A_1 = 0$, $A_2 = 0$, $m_o = 0$

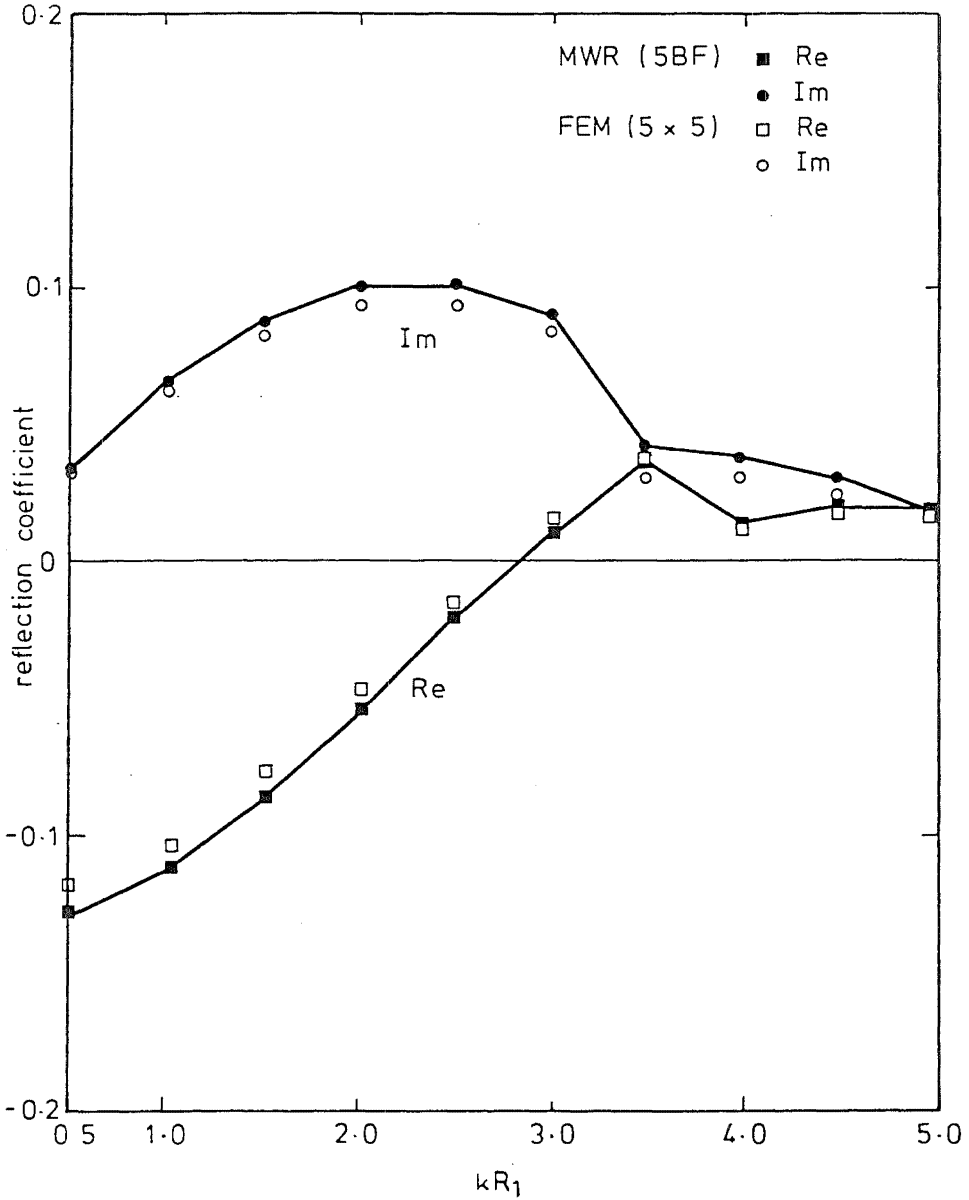

FIG. 5·8 REFLECTION COEFFICIENTS FOR MODE 1 WITH UNIT INCIDENT MODE 1

Geometry: linearly tapered, $R_1 = 1{\cdot}0$, $R_2 = 1{\cdot}134$, $l = 0{\cdot}5$

Characteristics: no flow, hardwalled duct, $m_0 = 0$

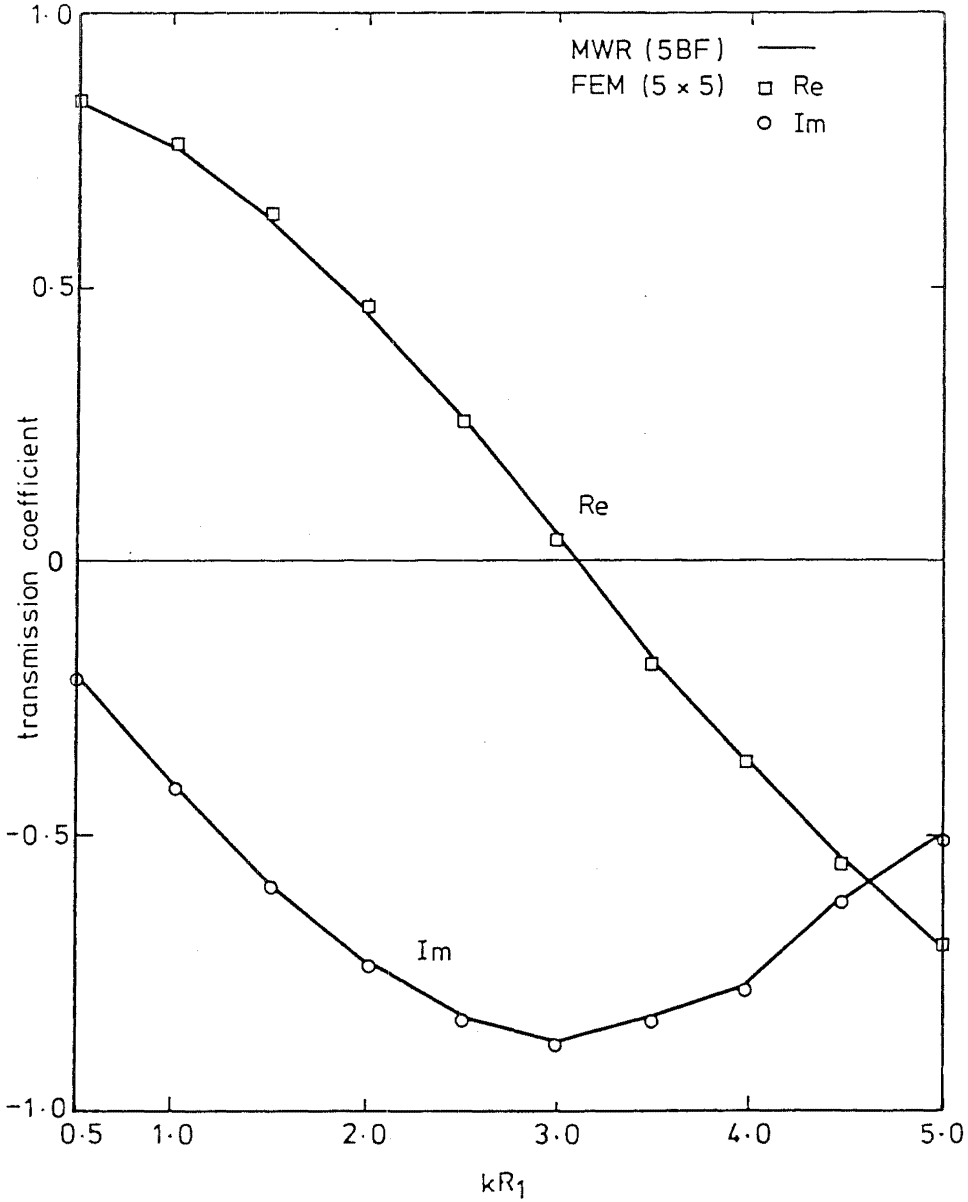

FIG. 5·9 TRANSMISSION COEFFICIENTS FOR MODE 1 WITH UNIT INCIDENT MODE 1

Geometry: linearly tapered, $R_1 = 1{\cdot}0$, $R_2 = 1{\cdot}134$, $l = 0{\cdot}5$

Characteristics: no flow, hardwalled duct, $m_0 = 0$

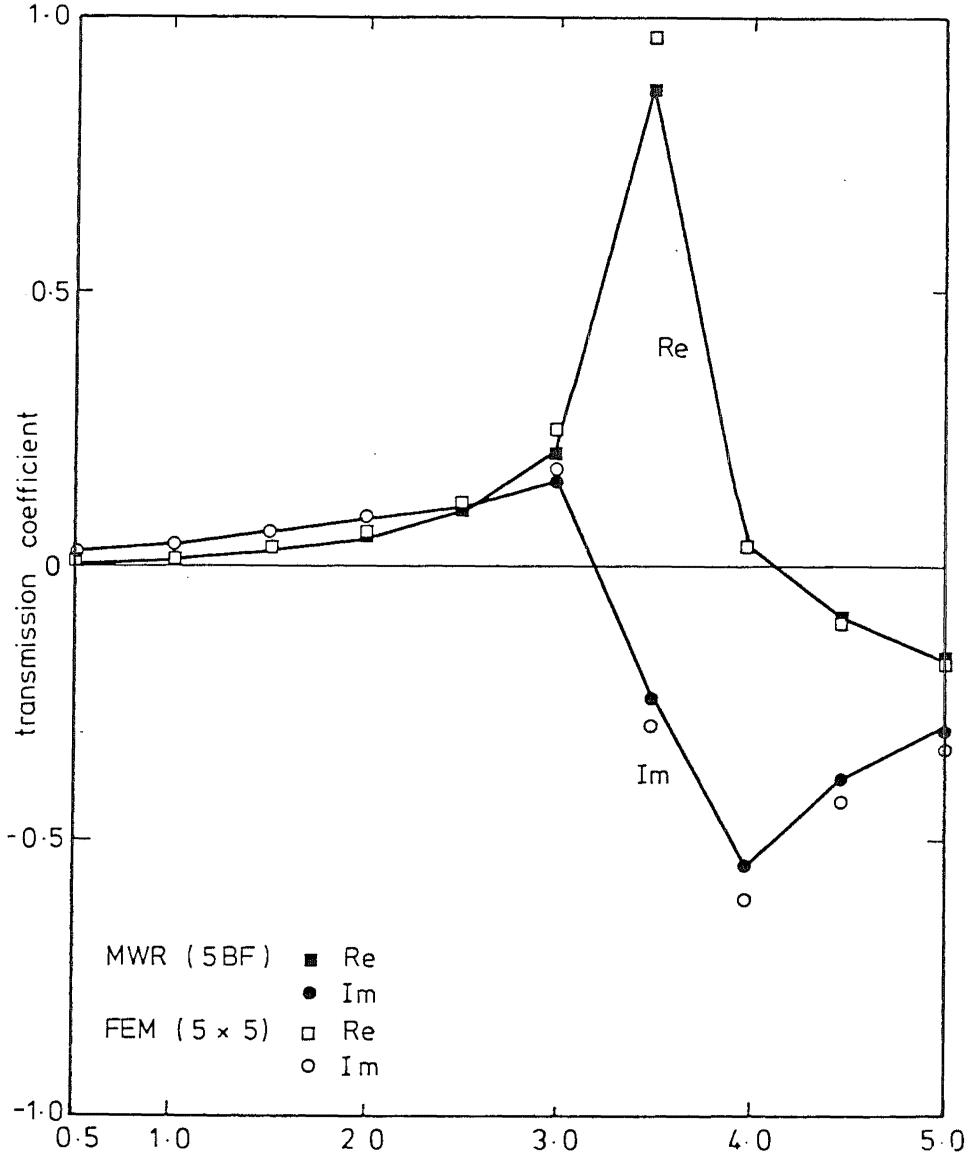

FIG. 5·10 REFLECTION COEFFICIENTS FOR MODE 2 WITH UNIT INCIDENT MODE 1

Geometry: linearly tapered, $R_1 = 1{\cdot}0$, $R_2 = 1{\cdot}134$, $l = 0{\cdot}5$

Characteristics: no flow, hardwalled duct, $m_0 = 0$

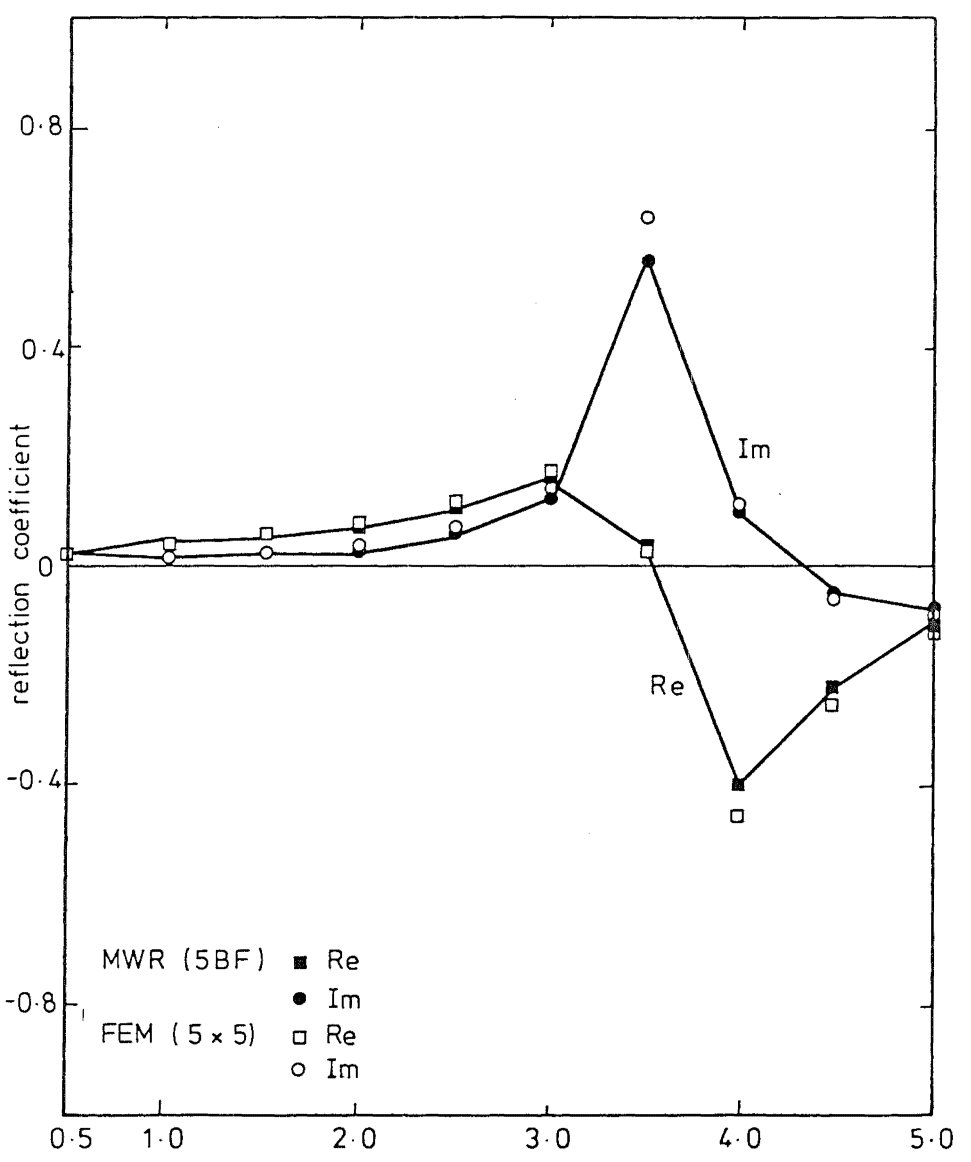

FIG 5·11 TRANSMISSION COEFFICIENTS FOR MODE 2 WITH UNIT INCIDENT MODE 1

Geometry: linearly tapered, $R_1 = 1{\cdot}0$, $R_2 = 1{\cdot}134$, $l = 0{\cdot}5$

Characteristics: no flow, hardwalled duct, $m_0 = 0$

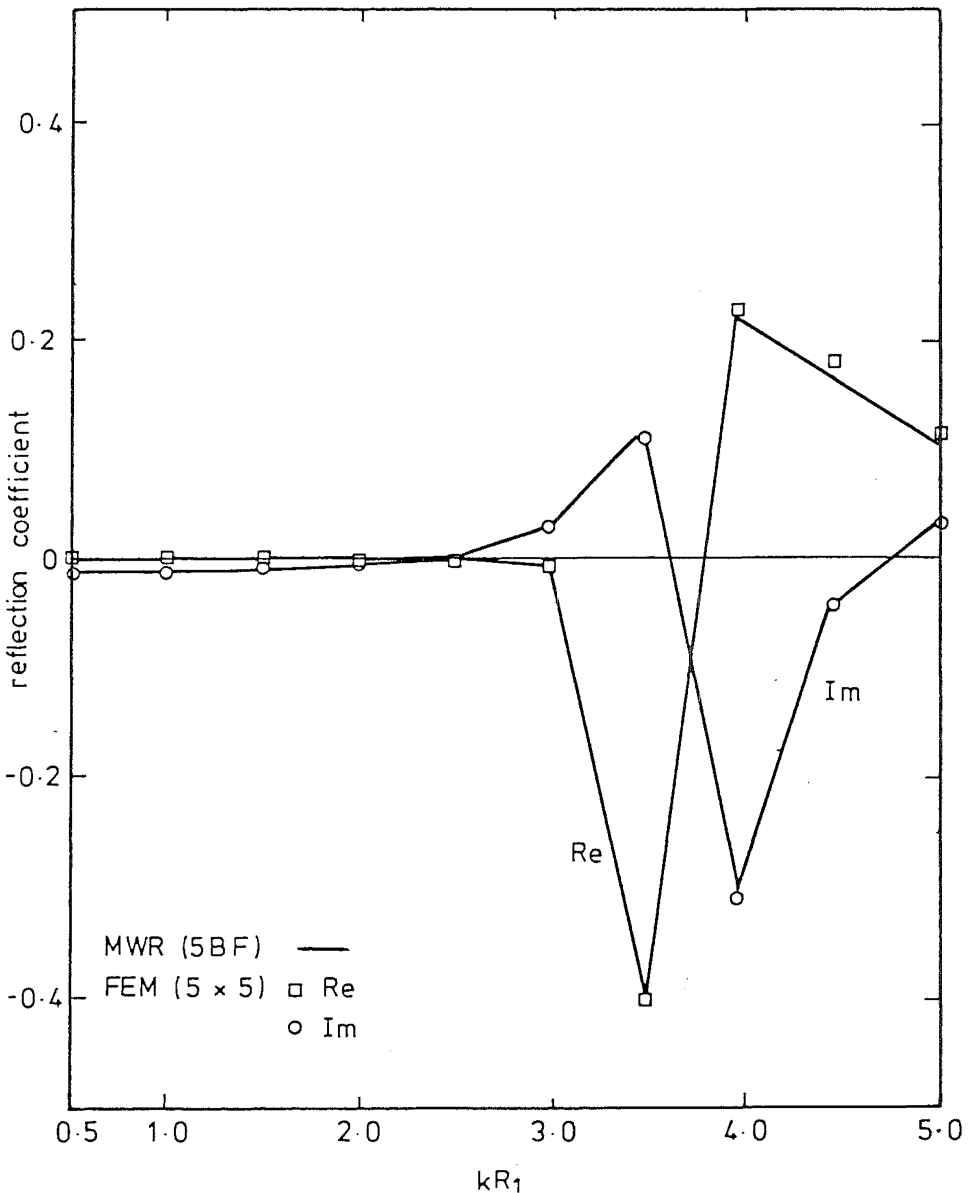

FIG. 5·12 REFLECTION COEFFICIENTS FOR MODE 2 WITH UNIT INCIDENT MODE 2

Geometry: linearly tapered, $R_1 = 1{\cdot}0$, $R_2 = 1{\cdot}134$, $l = 0{\cdot}5$

Characteristics: no flow, hardwalled duct, $m_0 = 0$

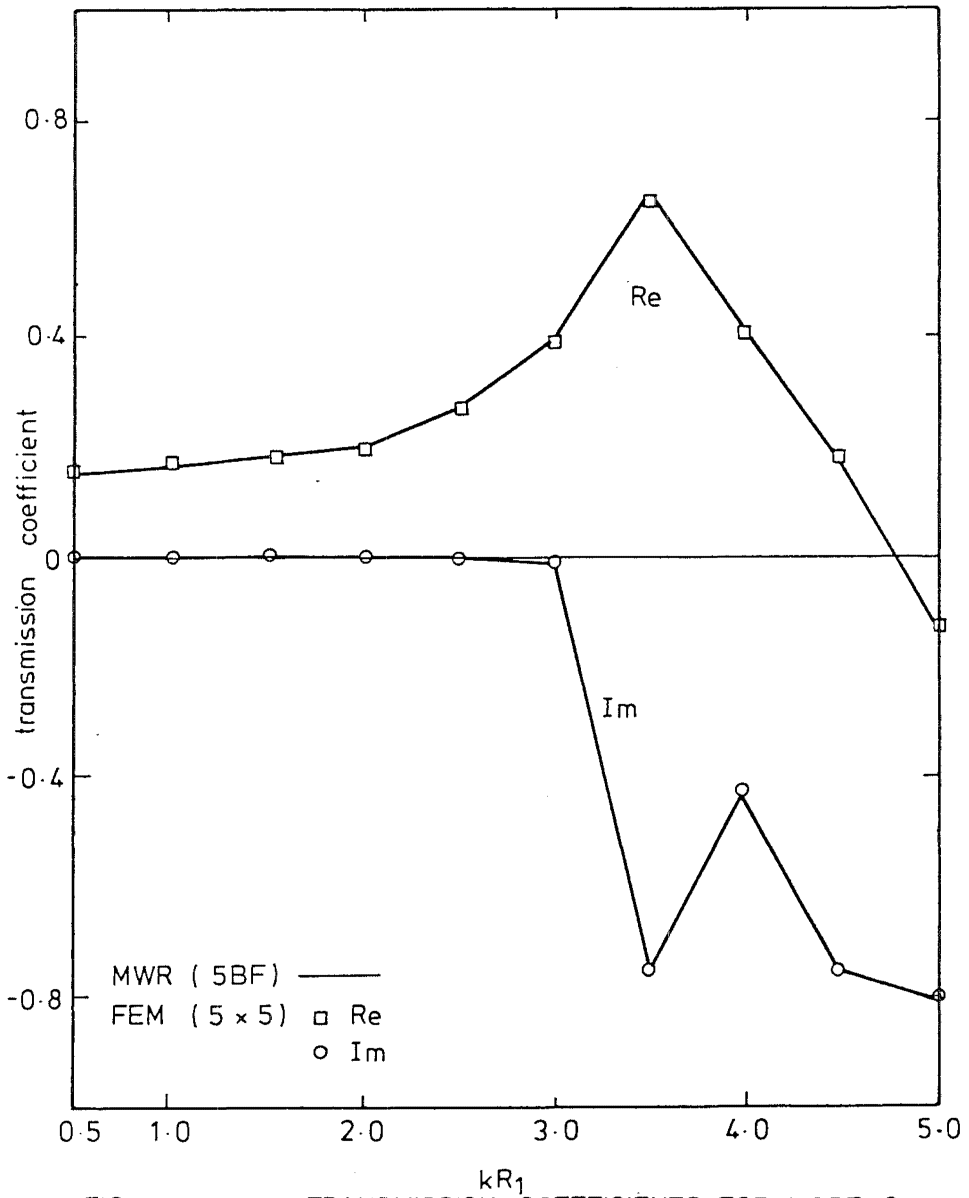

FIG. 5·13 TRANSMISSION COEFFICIENTS FOR MODE 2 WITH UNIT INCIDENT MODE 2

Geometry: linearly tapered, $R_1 = 1{\cdot}0$, $R_2 = 1{\cdot}134$, $l = 0{\cdot}5$

Characteristics: no flow, hardwalled duct, $m_0 = 0$

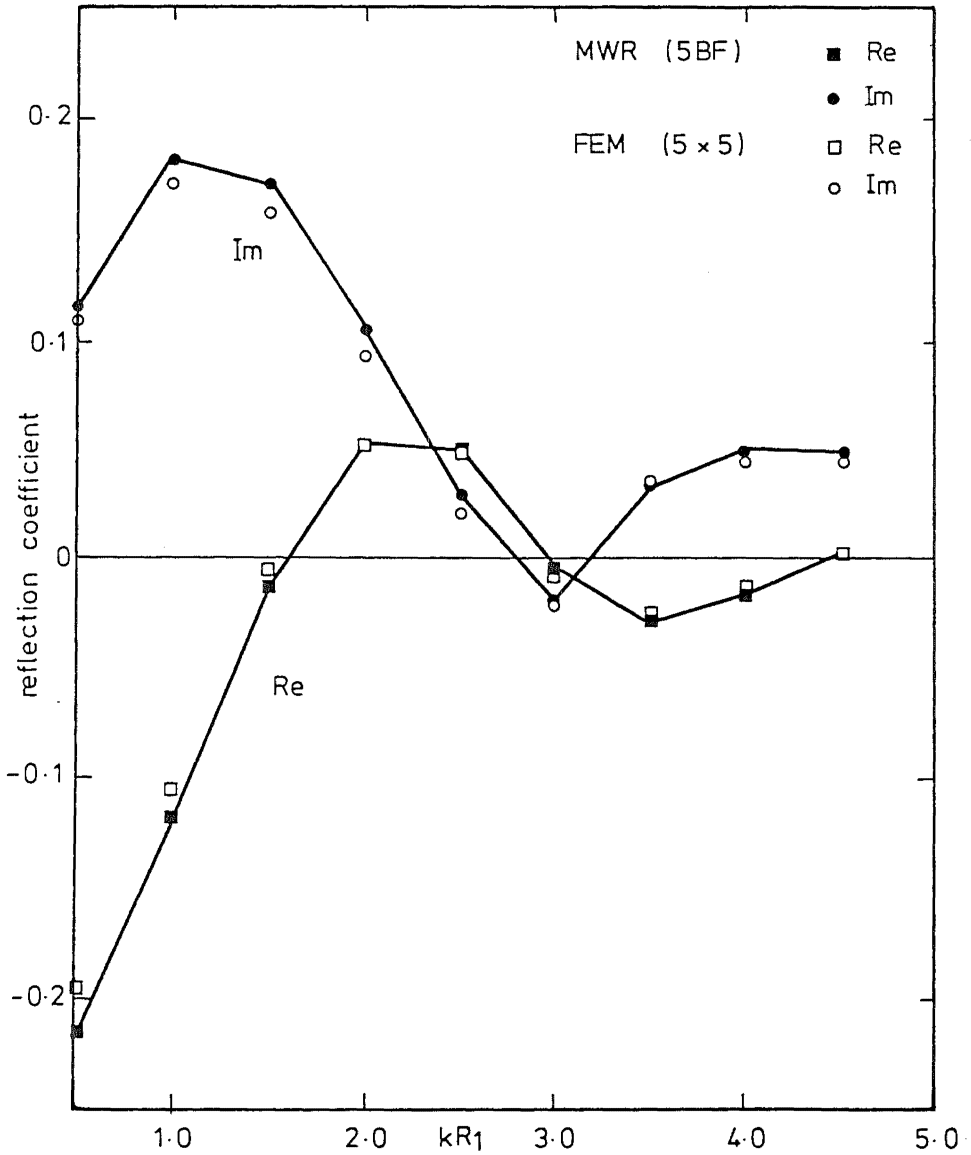

FIG 5·14 REFLECTION COEFFICIENTS FOR MODE 1 WITH UNIT INCIDENT MODE 1

Geometry: linearly tapered, $R_1 = 1{\cdot}0$, $R_2 = 1{\cdot}268$, $l = 1{\cdot}0$

Characteristics: no flow, hardwalled duct, $m_o = 0$

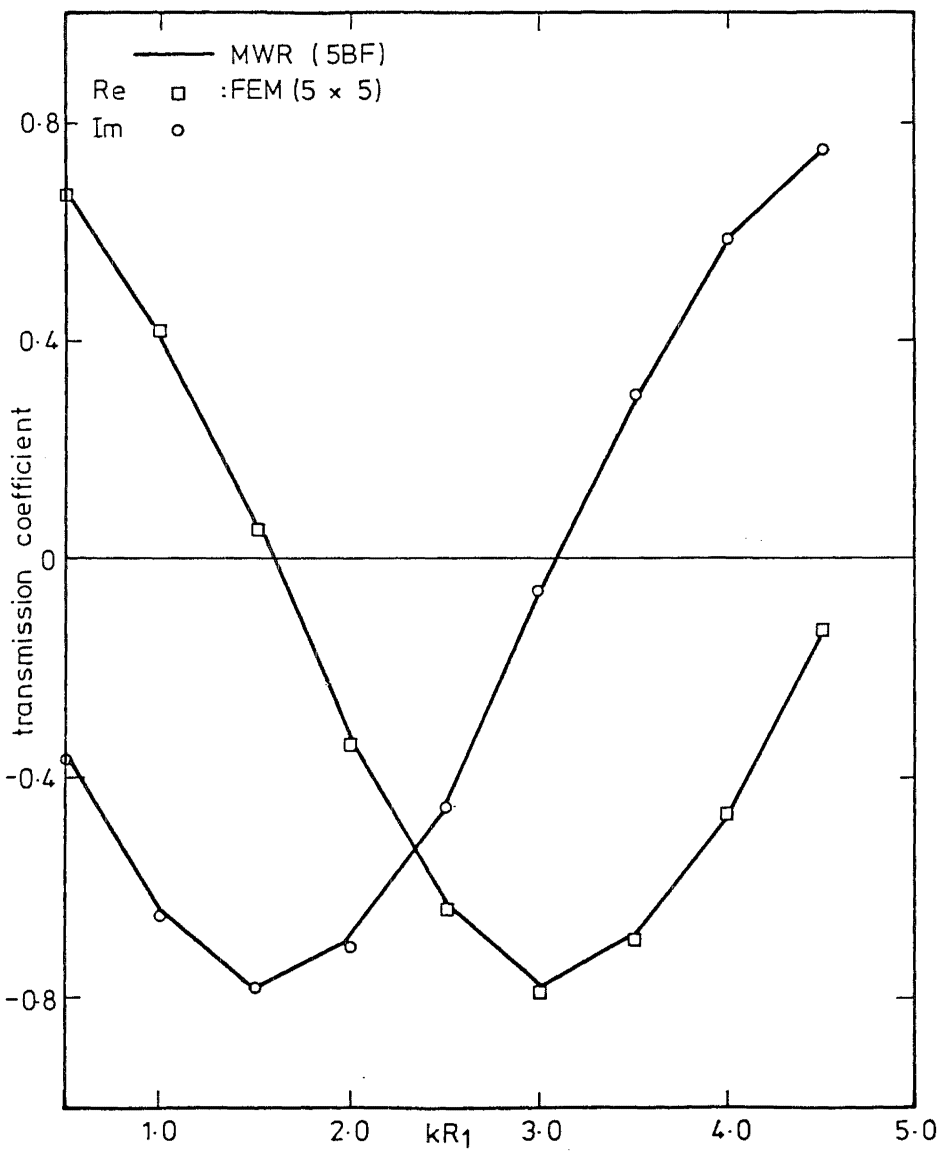

FIG. 5·15 TRANSMISSION COEFFICIENTS FOR MODE 1 WITH UNIT INCIDENT MODE 1

Geometry: linearly tapered, $R_1 = 1{\cdot}0$, $R_2 = 1{\cdot}268$, $l = 1{\cdot}0$

Characteristics: no flow, hardwalled duct, $m_o = 0$

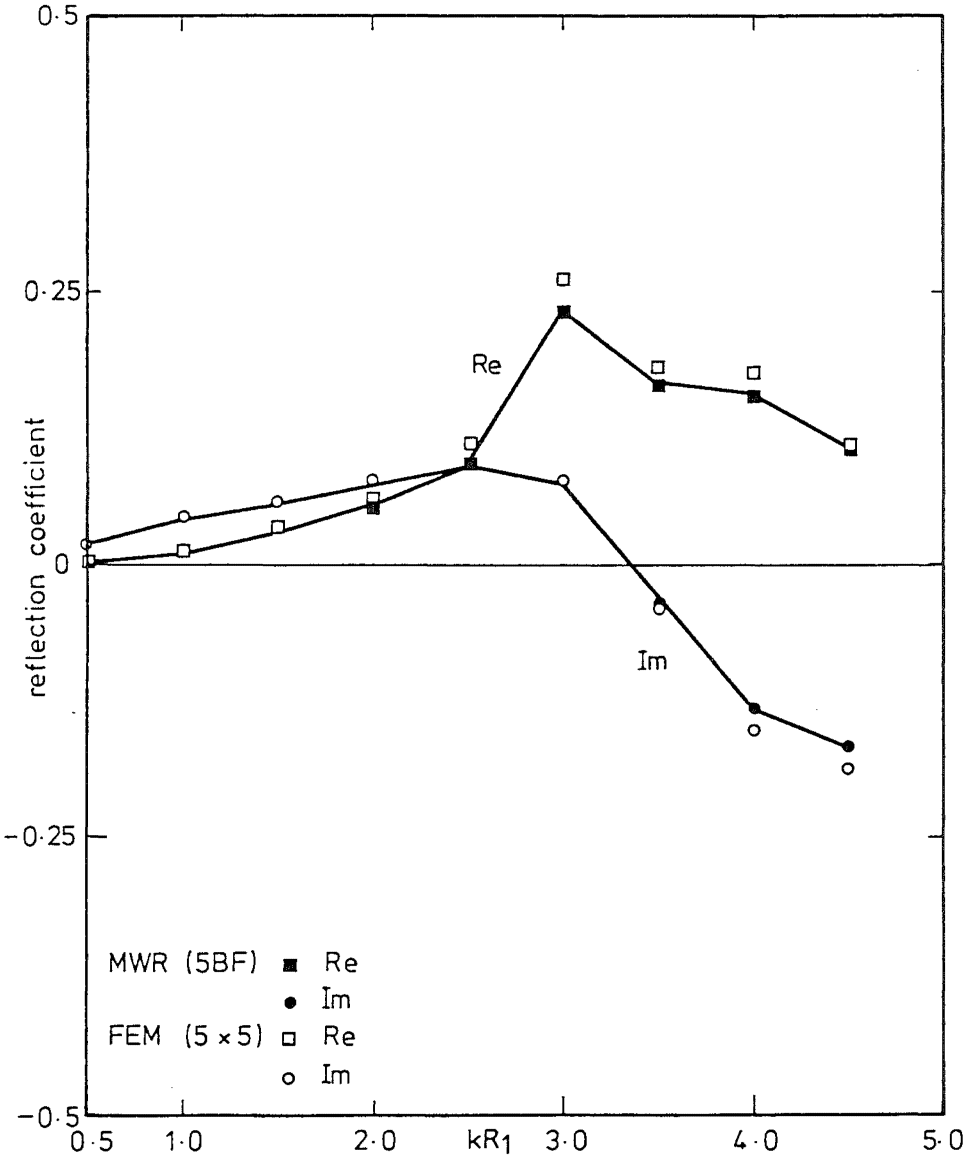

FIG. 5·16 REFLECTION COEFFICIENTS FOR MODE 2 WITH UNIT INCIDENT MODE 1.

Geometry: linearly tapered, $R_1 = 1{\cdot}0$, $R_2 = 1{\cdot}268$, $l = 1{\cdot}0$

Characteristics: no flow, hardwalled duct, $m_0 = 0$

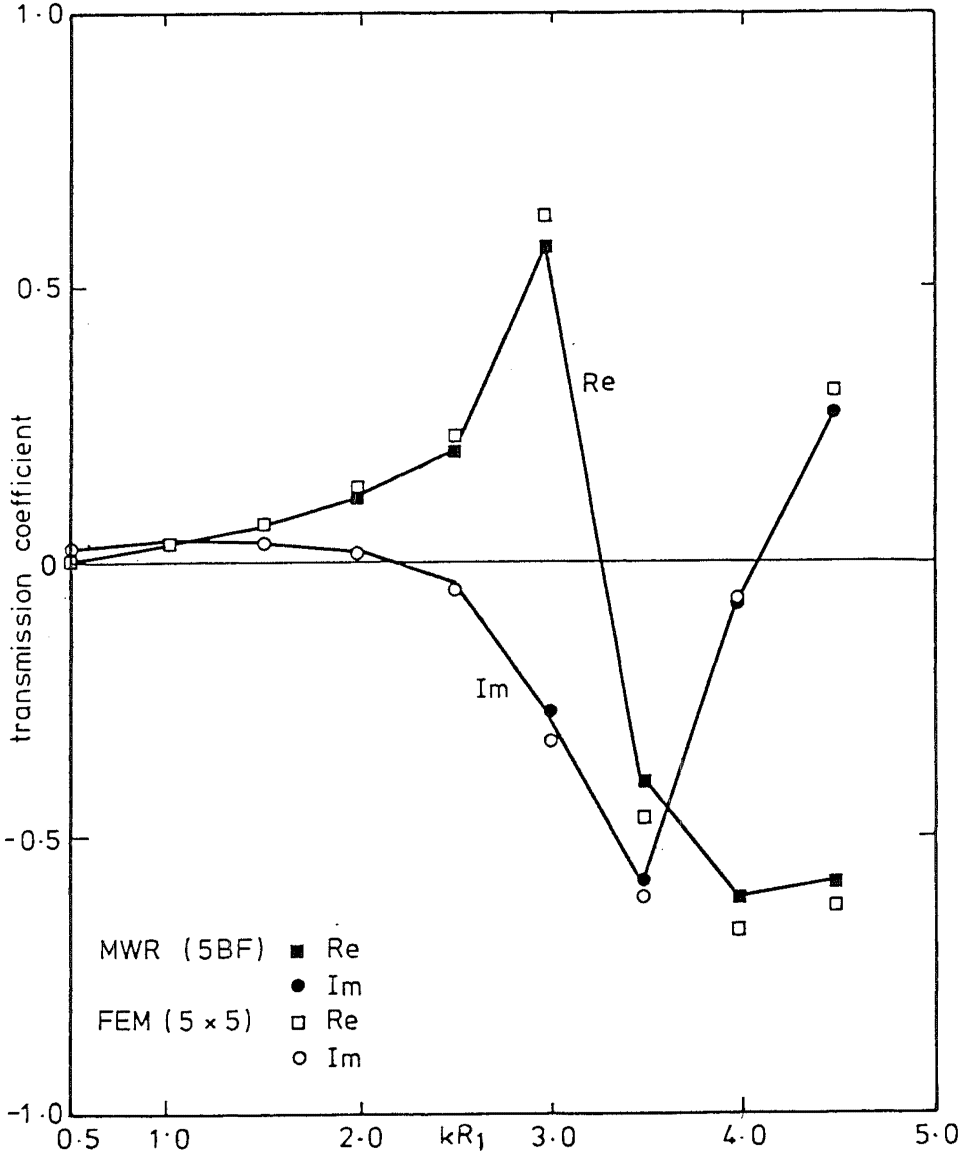

FIG. 5·17 TRANSMISSION COEFFICIENTS FOR MODE 2 WITH UNIT INCIDENT MODE 1

Geometry: linearly tapered, $R_1 = 1{\cdot}0$, $R_2 = 1{\cdot}268$, $l = 0{\cdot}5$

Characteristics: no flow, hardwalled duct, $m_0 = 0$

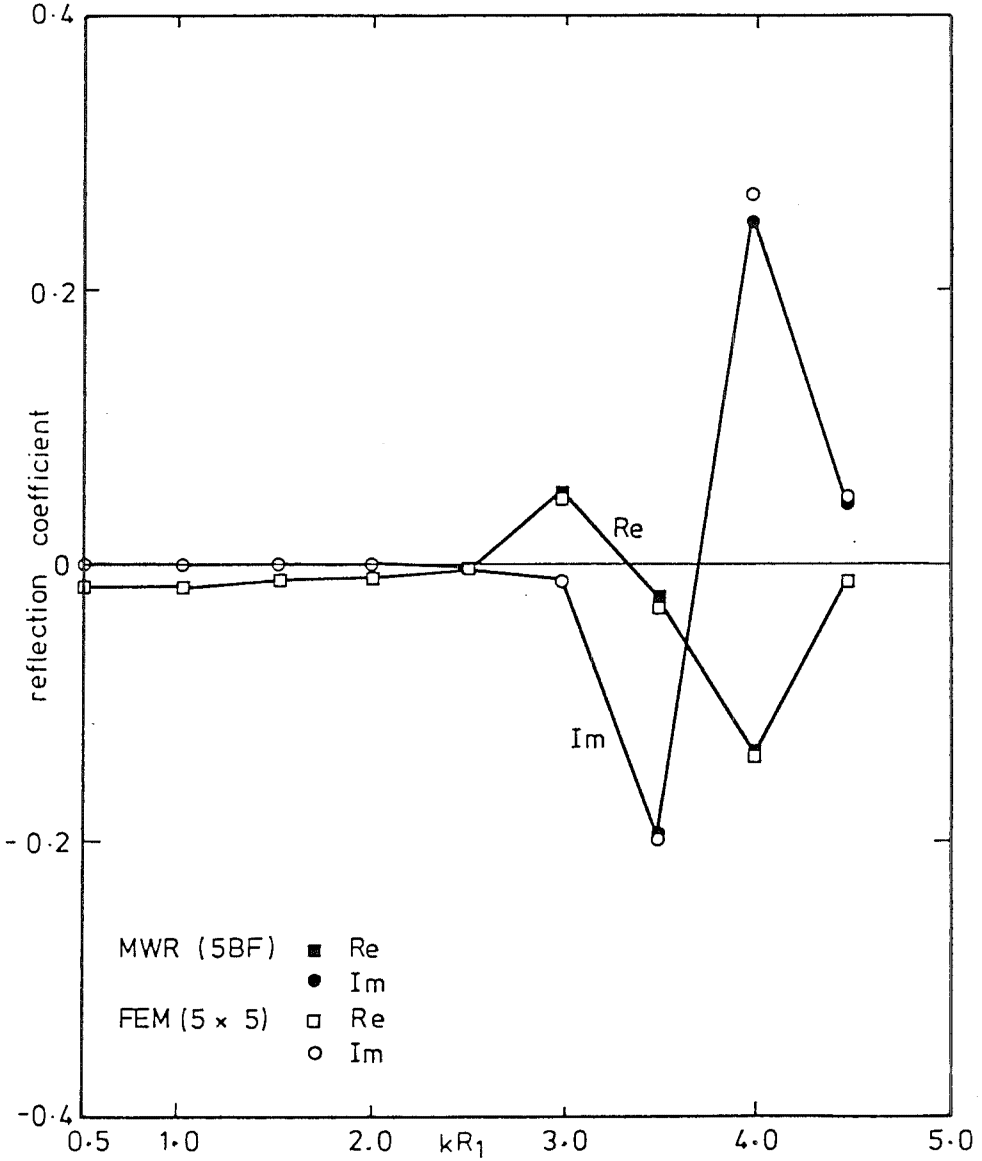

FIG. 5·18 REFLECTION COEFFICIENTS FOR MODE 2 WITH UNIT INCIDENT MODE 2

Geometry: linearly tapered, $R_1 = 1{\cdot}0$, $R_2 = 1{\cdot}268$, $l = 0{\cdot}5$

Characteristics: no flow, hardwalled duct, $m_0 = 0$

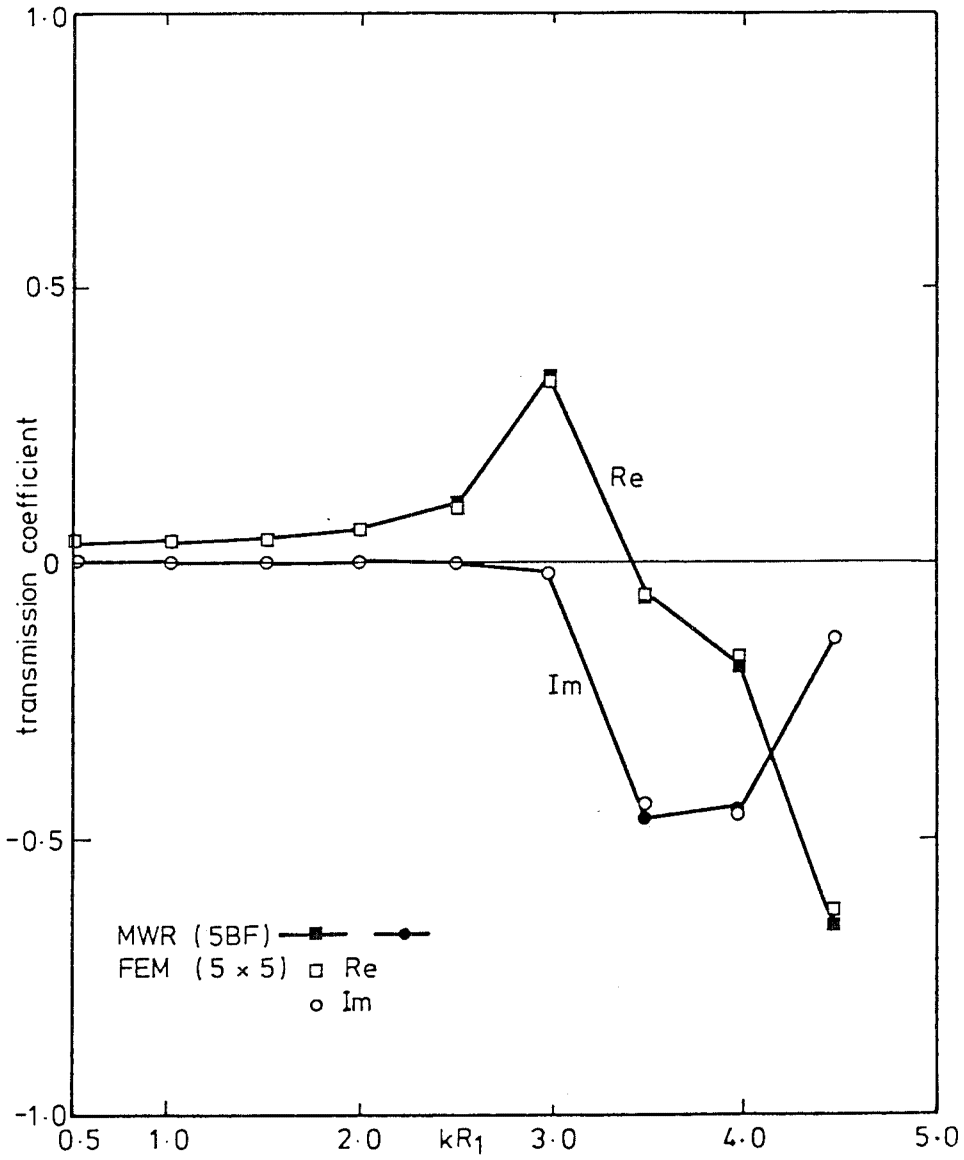

FIG. 5·19 TRANSMISSION COEFFICIENTS FOR MODE 2 WITH UNIT INCIDENT MODE 2.

Geometry: linearly tapered, $R_1 = 1{\cdot}0$, $R_2 = 1{\cdot}268$, $l = 0{\cdot}5$

Characteristics: no flow, hardwalled duct, $m_0 = 0$

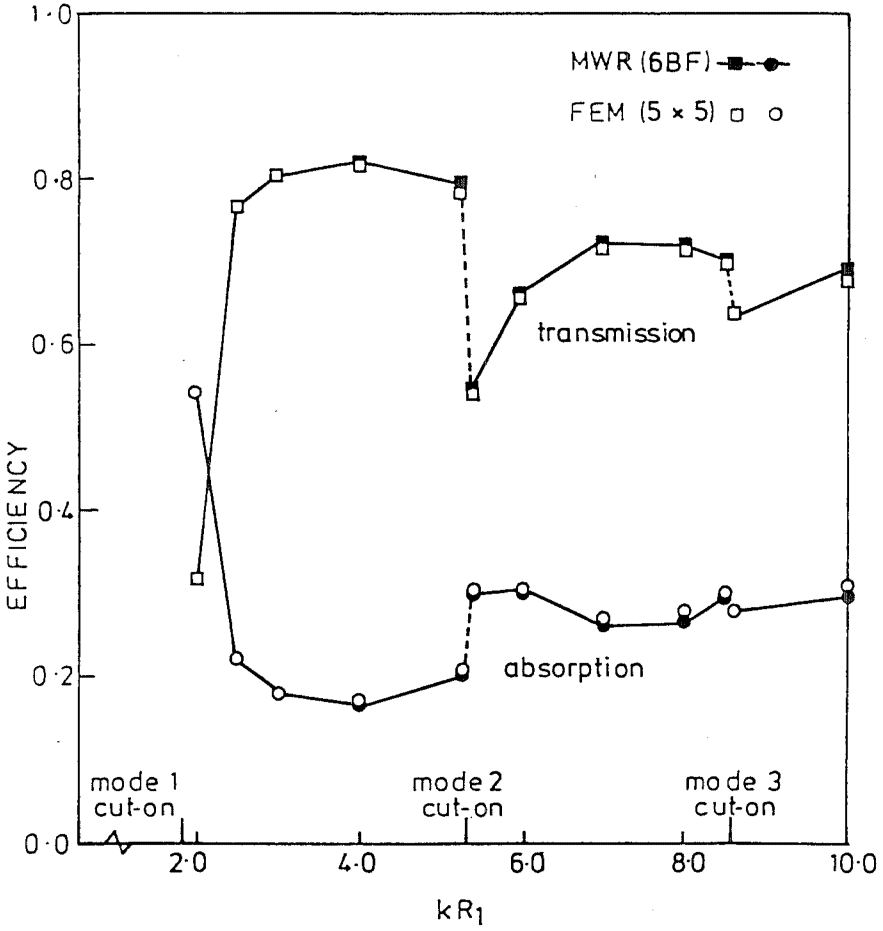

FIG. 5·20 COMPARISONS OF TRANSMISSION AND ABSORPTION EFFICIENCIES COMPUTED BY MWR AND FEM

GEOMETRY: COSINE - CONVERGING, R_1=1·0, R_2=0·925, l = 0·5
CHARACTERISTICS: NO FLOW, A=(0·1+0·1i), A_1=0, A_2=0,
ANGULAR MODE m_o=1

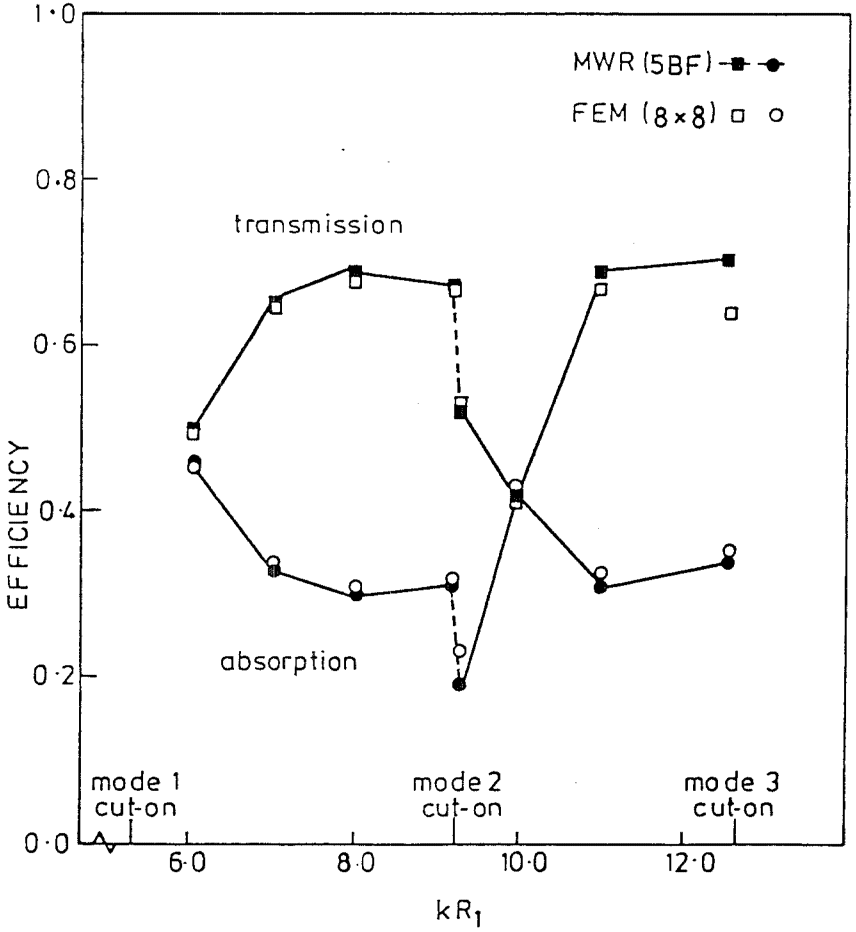

FIG. 5·21 COMPARISONS OF TRANSMISSION AND ABSORPTION EFFICIENCIES COMPUTED BY MWR AND FEM

GEOMETRY: COSINE - CONVERGING, R_1=1·0, R_2=0·925, l=0·5
CHARACTERISTICS: NO FLOW, A=(0·1+0·1i), A_1=0, A_2=0,
ANGULAR MODE m_o= 4

CHAPTER 6

MWR FOR SOUND TRANSMISSION IN DUCTS WITH FLOW

For formulation of the acoustic transmission problem for duct with flow the governing acoustic equations, the boundary condition at the duct walls and the mean flow field approximations are summarized here from Chapter 2 with no modification.

The governing acoustic equations :

$$\left(ik_r + \frac{\partial \bar{U}_o}{\partial r}\right) u + \frac{\partial \bar{U}_o}{\partial z} w + \bar{U}_o \frac{\partial u}{\partial r} + \bar{W}_o \frac{\partial u}{\partial z} + \frac{1}{\bar{\rho}_o} \frac{\partial p}{\partial r} = 0 \tag{6.0.1}$$

$$\left(ik_r + \frac{\bar{U}_o}{r}\right) v + \bar{U}_o \frac{\partial v}{\partial r} + \bar{W}_o \frac{\partial v}{\partial z} - \frac{im_o}{\bar{\rho}_o} \frac{p}{r} = 0 \tag{6.0.2}$$

$$\left(ik_r + \frac{\partial \bar{W}_o}{\partial z}\right) w + \bar{U}_o \frac{\partial w}{\partial r} + \bar{W}_o \frac{\partial w}{\partial z} + \frac{1}{\bar{\rho}_o} \frac{\partial p}{\partial z} - \frac{\partial \bar{p}_o/\partial z}{\gamma \bar{p}_o \bar{\rho}_o} p = 0 \tag{6.0.3}$$

$$ik_r p + \bar{U}_o \frac{\partial p}{\partial r} + \bar{W}_o \frac{\partial p}{\partial z} + \gamma \bar{p}_o \left[\frac{1}{r} \frac{\partial}{\partial r} (ru) - im_o \frac{v}{r} + \frac{\partial w}{\partial z}\right]$$

$$+ \frac{\partial \bar{p}_o}{\partial z} w + \gamma \left[\frac{1}{r} \frac{\partial}{\partial r} (r\bar{U}_o) + \frac{\partial \bar{W}_o}{\partial z}\right] p = 0 \tag{6.0.4}$$

The duct-wall boundary condition, $r = R(z)$:

$$\underline{V} \cdot \underline{\nu} = Ap - \frac{i\bar{V}_{o\tau}}{k_r} \frac{\partial}{\partial \tau} (Ap) \tag{6.0.5}$$

or $$u \cos\alpha - w \sin\alpha = Ap - \frac{i\bar{W}_o}{k_r} \left[\frac{\partial (Ap)}{\partial z} + A \frac{dR}{dz} \cdot \frac{\partial p}{\partial r}\right] \tag{6.0.6}$$

The mean flow field parameters :

$$\bar{M}_o = \bar{M}_o(z) \tag{6.0.7}$$

$$\frac{d\bar{M}_o}{dz} = -\frac{\bar{M}_o}{1-\bar{M}_o^2} \left[1 + \frac{\gamma-1}{2} \bar{M}_o^2\right] \frac{1}{\pi R^2} \frac{d(\pi R^2)}{dz}$$

$$= - \frac{\bar{M}_o}{1-\bar{M}_o^2} \left[1 + \frac{\gamma-1}{2} \bar{M}_o^2\right] \frac{2}{R} \tan\alpha \qquad (6.0.8)$$

$$\bar{\rho}_o = \bar{\rho}_o\,(z) = \frac{\left[1 + \frac{\gamma-1}{2} M_r^2\right]^{\frac{1}{\gamma-1}}}{\left[1 + \frac{\gamma-1}{2} \bar{M}_o^2\right]^{\frac{1}{\gamma-1}}} \qquad (6.0.9)$$

$$\bar{p}_o = \bar{p}_o\,(z) = \frac{1}{\gamma} \frac{\left[1 + \frac{\gamma-1}{2} M_r^2\right]^{\frac{\gamma}{\gamma-1}}}{\left[1 + \frac{\gamma-1}{2} \bar{M}_o^2\right]^{\frac{\gamma}{\gamma-1}}} \qquad (6.0.10)$$

$$\bar{c}_o = \bar{c}_o\,(z) = \frac{\left[1 + \frac{\gamma-1}{2} M_r^2\right]^{\frac{1}{2}}}{\left[1 + \frac{\gamma-1}{2} \bar{M}_o^2\right]^{\frac{1}{2}}} \qquad (6.0.11)$$

$$\bar{W}_o = \bar{W}_o\,(z) = \bar{M}_o \bar{c}_o \qquad (6.0.12)$$

$$U_o = U_o\,(r,z) = \bar{W}_o \frac{r}{R} \frac{dR}{dz} = \bar{W}_o \frac{r}{R} \tan\alpha \qquad (6.0.13)$$

and

$$\frac{\partial U_o}{\partial r} = \frac{\bar{W}_o}{R} \tan\alpha$$

$$\frac{\partial U_o}{\partial z} = r \left(\frac{d\bar{W}_o}{dz} \frac{\tan\alpha}{R} - \frac{\bar{W}_o}{R^2} \tan^2\alpha + \frac{\bar{W}_o}{R} \frac{d\tan\alpha}{dz} \right) \qquad (6.0.14)$$

6.1 MWR FORMULATIONS

In Chapter 5 MWR was employed to study acoustic propagation in nonuniform ducts with no flow. This method is used with minor changes in the study of nonuniform ducts with flow.

6.1.1 General Formulation

The solutions of the field equations (6.0.1) - (6.0.4) and appropriate boundary conditions, are sought in the form of finite series

$$p(r,z) \approx p_N = \sum_{m=1}^{N} p_m(z)\ \psi_m(r,z) \tag{6.1.1}$$

$$u(r,z) \approx u_N = \sum_{m=1}^{N} u_m(z)\ \phi_m(r,z) \tag{6.1.2}$$

$$v(r,z) \approx v_N = \sum_{m=1}^{N} v_m(z)\ \theta_m(r,z) \tag{6.1.3}$$

$$w(r,z) \approx w_N = \sum_{m=1}^{N} w_m(z)\ \chi_m(r,z) \tag{6.1.4}$$

The success of MWR is dependent upon an appropriate choice of basis functions. In the no flow-case of Chapter 5 the basis functions were chosen to be trigonometric functions which are the transverse eigenfunctions in a uniform 2D channel with properties existing locally in the nonuniform duct. This philosophy is carried over to the duct with a steady mean flow. In view of using trigonometric functions as trial solutions, and to simplify the general formulation to some extent one can choose :

$$\theta_m(r,z) \equiv \psi_m(r,z)$$
$$\chi_m(r,z) \equiv \psi_m(r,z) \tag{6.1.5}$$

for $m = 1,2....N$

If the trial solutions (6.1.1) - (6.1.4) together with relations (6.1.5) are substituted into the governing equations (6.0.1) - (6.0.4) and the duct-wall boundary condition (6.0.6), in general, one obtains the following residuals :

$$R_1 = \left(ik_r + \frac{\partial U_o}{\partial r}\right)u_N + \frac{\partial U_o}{\partial z} w_N + U_o \frac{\partial u_N}{\partial r} + \bar{W}_o \frac{\partial u_N}{\partial z} + \frac{1}{\bar{\rho}_o} \frac{\partial p_N}{\partial r} \tag{6.1.6}$$

$$R_2 = \left(ik_r + \frac{U_o}{r}\right)v_N + U_o \frac{\partial v_N}{\partial r} + \bar{W}_o \frac{\partial v_N}{\partial z} - \frac{im_o}{\bar{\rho}_o} \frac{p_N}{r} \tag{6.1.7}$$

$$R_3 = \left(ik_r + \frac{\partial \bar{W}_o}{\partial z}\right)w_N + U_o \frac{\partial w_N}{\partial r} + \bar{W}_o \frac{\partial w_N}{\partial z} + \frac{1}{\bar{\rho}_o} \frac{\partial p_N}{\partial z} - \frac{\frac{\partial \bar{p}_o}{\partial z}}{\gamma \bar{p}_o \bar{\rho}_o} p_N \tag{6.1.8}$$

$$R_4 = ik_r p_N + U_o \frac{\partial p_N}{\partial r} + \bar{W}_o \frac{\partial p_N}{\partial z} + \gamma \bar{p}_o \left[\frac{1}{r} \frac{\partial (r u_N)}{\partial r} - im_o \frac{v_N}{r} + \frac{\partial w_N}{\partial z}\right]$$

$$+ \frac{\partial \bar{p}_o}{\partial z} w_N + \gamma \left[\frac{1}{r} \frac{\partial (r U_o)}{\partial r} + \frac{\partial \bar{W}_o}{\partial z}\right] p_N \tag{6.1.9}$$

$$R_B = (u_N \cos\alpha - w_N \sin\alpha) - Ap + \frac{i\bar{W}_o}{k_r} \left[\frac{\partial}{\partial z}(Ap_N) + \tan\alpha \; A \frac{\partial p_N}{\partial r}\right]$$

$$\text{at} \quad r = R(z) \tag{6.1.10}$$

In the Modified Galerkin Method the residuals are weighted at each station z along the duct axis as follows :

$$\int_0^R \psi_n R_1 \quad 2\pi r \, dr = 0 \tag{6.1.11}$$

$$\int_0^R \psi_n R_2 \quad 2\pi r \, dr = 0 \tag{6.1.12}$$

$$\int_0^R \psi_n R_3 \quad 2\pi r \, dr = 0 \tag{6.1.13}$$

$$\int_0^R r\psi_n R_4 \quad 2\pi r \, dr = 0 \tag{6.1.14}$$

$$R_B\psi_n(R) = 0 \qquad \text{at } r = R(z) \tag{6.1.15}$$

for $n = 1,2,3....N$

It is noted that a weighting factor r has been introduced in equation (6.1.14). This philosophy is carried over from the experience in solving the uniform duct eigenproblem with the governing conservation equations. In fact, the derivations of equations (6.1.11) - (6.1.15) would become an eigenproblem when all geometry variations along z axis vanish and a harmonic dependence $e^{-ik_z z}$ is assumed.

When the residuals (6.1.6) - (6.1.9) are substituted into the integrals (6.1.11) - (6.1.14) using the relations (6.0.9) - (6.0.14) the steady mean flow parameters one can write four sets of N equations :

$$\left(ik_r + \bar{W}_o \frac{\tan\alpha}{R}\right)\int_0^R r u_N \psi_n \, dr + \left(\frac{d\bar{W}_o}{dz}\frac{\tan\alpha}{R} - \bar{W}_o \frac{\tan^2\alpha}{R^2} + \frac{\bar{W}_o}{R} d\frac{\tan\alpha}{dz}\right)$$

$$\int_0^R r^2 w_N \psi_n \, dr + \bar{W}_o \frac{\tan\alpha}{R}\int_0^R r^2 \frac{\partial u_N}{\partial r} \psi_n \, dr + \bar{W}_o \int_0^R r \frac{\partial u_N}{\partial z} \psi_n \, dr +$$

$$\frac{1}{\bar{\rho}_o}\int_0^R r \frac{\partial p_N}{\partial r} \psi_n \, dr = 0 \tag{6.1.16}$$

$$\left(ik_r + \bar{W}_o \frac{\tan\alpha}{R}\right)\int_0^R r v_N \psi_n \, dr + \bar{W}_o \frac{\tan\alpha}{R}\int_0^R r^2 \frac{\partial v_N}{\partial r} \psi_n \, dr$$

$$+ \bar{W}_o \int_0^R r \frac{\partial v_N}{\partial z} \psi_n \, dr - \frac{im_o}{\bar{\rho}_o}\int_0^R p_N \psi_n \, dr = 0 \tag{6.1.17}$$

$$\left(ik_r + \frac{d\bar{W}_o}{dz}\right)\int_0^R rw_N\psi_n\,dr + \bar{W}_o\,\frac{\tan\alpha}{R}\int_0^R r^2\,\frac{\partial w_N}{\partial r}\,\psi_n\,dr + \bar{W}_o\int_0^R r\,\frac{\partial w_N}{\partial z}\,\psi_n\,dr$$

$$+ \frac{1}{\bar{\rho}_o}\int r\,\frac{\partial p_N}{\partial z}\,\psi_n\,dr - \frac{1}{\gamma\bar{\rho}_o\bar{p}_o}\,\frac{d\bar{p}_o}{dz}\int_0^R rp_N\psi_n\,dr = 0 \qquad (6.1.18)$$

$$\left[ik_r + \gamma\left(2\bar{W}_o\,\frac{\tan\alpha}{R} + \frac{d\bar{W}_o}{dz}\right)\right]\int_0^R r^2p_N\psi_n\,dr +$$

$$\bar{W}_o\,\frac{\tan\alpha}{R}\int_0^R r^3\,\frac{\partial p_N}{\partial r}\,\psi_n\,dr + \bar{W}_o\int_0^R r^2\,\frac{\partial p_N}{\partial z}\,\psi_n\,dr$$

$$+ \gamma\bar{p}_o\int_0^R r\,\frac{\partial\,(ru_N)}{\partial r}\,\psi_n\,dr - \gamma\bar{p}_o\,im_o\int_0^R rv_N\psi_n\,dr$$

$$+ \gamma\bar{p}_o\int_0^R r^2\,\frac{\partial w_N}{\partial z}\,\psi_n\,dr + \frac{d\bar{p}_o}{dz}\int_0^R r^2w_N\psi_n\,dr = 0 \qquad (6.1.19)$$

where $p_N = \sum_{m=1}^{N} p_m\psi_m$, $u_N = \sum_{m=1}^{N} u_m\phi_m$, $v_N = \sum_{m=1}^{N} v_m\psi_m$, $w_N = \sum_{m=1}^{N} w_m\psi_m$

and $n = 1,2,3\ldots N$

As for the no-flow case, by using the Leibnitz rule for differentiation of integrals containing a parameter the partial derivatives with respect to z can be replaced by ordinary derivatives. The derivatives with respect to r can be eliminated by integration by parts. When performed on the $4^{\underline{th}}$ and $6^{\underline{th}}$ terms of equation (6.1.19) which originates from the div($\underline{V}$) in the governing equations this process will expose boundary terms which, in turn, are simplified by the use of the boundary residual (6.1.15). Hence, one can rewrite the four sets of equations (6.1.16) - (6.1.19) in the following form :

$$\left(ik_r + \bar{W}_o \frac{\tan\alpha}{R}\right)\int_0^R ru_N\psi_n\,dr + \left(\frac{d\bar{W}_o}{dz}\frac{\tan\alpha}{R} - \bar{W}_o\frac{\tan^2\alpha}{R^2} + \frac{\bar{W}_o}{R}\frac{d\tan\alpha}{dz}\right)\int_0^R r^2 w_N\psi_n\,dr$$

$$- \frac{\bar{W}_o\tan\alpha}{R}\int_0^R u_N\frac{\partial}{\partial r}(r^2\psi_n)\,dr + \bar{W}_o\frac{d}{dz}\int_0^R ru_N\psi_n\,dr - \bar{W}_o\int_0^R ru_N\frac{\partial\psi_n}{\partial z}\,dr$$

$$+ \frac{1}{\bar{\rho}_o}R\,p_N(R,z)\psi_n(R,z) - \frac{1}{\bar{\rho}_o}\int_0^R p_N\frac{\partial}{\partial r}(r\psi_n)\,dr = 0 \qquad (6.1.20)$$

$$\left(ik_r + \bar{W}_o\frac{\tan\alpha}{R}\right)\int_0^R rv_N\psi_n\,dr - \bar{W}_o\frac{\tan\alpha}{R}\int_0^R v_N\frac{\partial}{\partial r}(r^2\psi_n)\,dr + \bar{W}_o\frac{d}{dz}\int_0^R rv_N\psi_n\,dr$$

$$- \bar{W}_o\int_0^R rv_N\frac{\partial\psi_n}{\partial z}\,dr - \frac{im_o}{\bar{\rho}_o}\int_0^R p_N\psi_n\,dr = 0 \qquad (6.1.21)$$

$$\left(ik_r + \frac{d\bar{W}_o}{dz}\right)\int_0^R rw_N\psi_n\,dr - \frac{\bar{W}_o\tan\alpha}{R}\int_0^R w_N\frac{\partial}{\partial r}(r^2\psi_n)\,dr + \bar{W}_o\frac{d}{dz}\int_0^R rw_N\psi_n\,dr$$

$$- \bar{W}_o\int_0^R rw_N\frac{\partial\psi_n}{\partial z}\,dr + \frac{1}{\bar{\rho}_o}\frac{d}{dz}\int_0^R rp_N\psi_n\,dr - \frac{1}{\bar{\rho}_o}\int_0^R rp_N\frac{\partial\psi_n}{\partial z}\,dr$$

$$- \frac{1}{\bar{\rho}_o}Rp_N(R,z)\psi_n(R,z)\tan\alpha - \frac{1}{\gamma\bar{p}_o\bar{\rho}_o}\frac{d\bar{p}_o}{dz}\int_0^R rp_N\psi_n\,dr = 0 \qquad (6.1.22)$$

$$\left[ik_r + \gamma\left(2\bar{W}_o\frac{\tan\alpha}{R} + \frac{d\bar{W}_o}{dz}\right)\right]\int_0^R r^2p_N\psi_n\,dr - \bar{W}_o\frac{\tan\alpha}{R}\int_0^R p_N\frac{\partial}{\partial r}(r^3\psi_n)\,dr$$

$$+ \bar{W}_o\frac{d}{dz}\int_0^R r^2p_N\psi_n\,dr - \bar{W}_o\int_0^R r^2p_N\frac{\partial\psi_n}{\partial z}\,dr - \gamma\bar{p}_o\int_0^R ru_N\frac{\partial}{\partial r}(r\psi_n)\,dr$$

$$- \gamma\bar{p}_o\,im_o\int_0^R rv_N\psi_n\,dr + \gamma\bar{p}_o\frac{d}{dz}\int_0^R r^2w_N\psi_n\,dr - \gamma\bar{p}_o\int_0^R r^2w_N\frac{\partial\psi_n}{\partial z}\,dr$$

$$+ \frac{d\bar{p}_o}{dz} \int_0^R r^2 w_N \psi_n \, dr + \gamma \bar{p}_o R^2 \psi_n(R,z) \left[\frac{A}{\cos\alpha} \, p_N(R,z) - \frac{i\bar{W}_o}{k_r \cos\alpha} \right.$$

$$\left. \left(\frac{\partial}{\partial z} (A p_N) + \tan\alpha \, \frac{\partial p_N}{\partial r} \right)_{r=R} \right] = 0 \qquad (6.1.23)$$

with $n = 1,2,3...N$

The MWR is completed when the finite series representing for p_N, u_N, v_N, w_N, given by equations (6.1.1) - (6.1.5) are inserted into equations (6.1.21) - (6.1.23):

$$\left[\bar{W}_o \int_0^R r\phi_m \psi_n \, dr \right] \left\{ \frac{du_m}{dz} \right\} = \left[- \bar{W}_o \frac{d}{dz} \int_0^R r\phi_m \psi_n \, dr + \bar{W}_o \int_0^R r\phi_m \frac{\partial \psi_n}{\partial z} \, dr \right.$$

$$+ \bar{W}_o \frac{\tan\alpha}{R} \int_0^R \phi_m \frac{\partial}{\partial r} (r^2 \psi_n) \, dr$$

$$\left. - \left(ik_r + \bar{W}_o \frac{\tan\alpha}{R} \right) \int_0^R r\phi_m \psi_n \, dr \right] \left\{ u_m \right\}$$

$$+ \left[\left(- \frac{d\bar{W}_o}{dz} \frac{\tan\alpha}{R} + \bar{W}_o \frac{\tan^2\alpha}{R^2} - \frac{\bar{W}_o}{R} \frac{d \tan\alpha}{dz} \right) \int_0^R r^2 \psi_m \psi_n \, dr \right] \left\{ w_m \right\}$$

$$+ \left[- \frac{1}{\rho_o} R \, \psi_m(R,z) \psi_n(R,z) + \frac{1}{\bar{\rho}_o} \int_0^R \psi_m \frac{\partial}{\partial r} (r\psi_n) \, dr \right] \left\{ p_m \right\} \qquad (6.1.24)$$

$$\left[\bar{W}_o \int_0^R r\psi_m \psi_n \, dr \right] \left\{ \frac{dv_m}{dz} \right\} = \left[- \bar{W}_o \frac{d}{dz} \int_0^R r\psi_m \psi_n \, dr - \left(ik_r + \bar{W}_o \frac{\tan\alpha}{R} \right) \int_0^R r\psi_m \psi_n \, dr \right.$$

$$\left. + \bar{W}_o \frac{\tan\alpha}{R} \int_0^R \psi_m \frac{\partial}{\partial r} (r^2 \psi_n) \, dr + \bar{W}_o \int_0^R r\psi_m \frac{\partial \psi_n}{\partial z} \, dr \right] \left\{ v_m \right\}$$

$$+ \left[\frac{im_o}{\bar{\rho}_o} \int_0^R \psi_m \psi_n \, dr \right] \{p_m\} \qquad (6.1.25)$$

$$\left[\bar{W}_o \int_0^R r\psi_m \psi_n \, dr \right] \left\{ \frac{dw_m}{dz} \right\} + \left[\frac{1}{\bar{\rho}_o} \int_0^R r\psi_m \psi_n \, dr \right] \left\{ \frac{dp_m}{dz} \right\} = \left[- \bar{W}_o \frac{d}{dz} \int_0^R r\psi_m \psi_n \, dr \right.$$

$$- \left(ik_r + \frac{d\bar{W}_o}{dz} \right) \int_0^R r\psi_m \psi_n \, dr + \bar{W}_o \frac{\tan\alpha}{R} \int_0^R \psi_m \frac{\partial}{\partial r} (r^2 \psi_n) \, dr + \bar{W}_o \int_0^R r\psi_m \frac{\partial \psi_n}{\partial z} \, dr \Bigg] \{w_m\}$$

$$+ \left[- \frac{1}{\bar{\rho}_o} \frac{d}{dz} \int_0^R r\psi_m \psi_n \, dr + \frac{1}{\bar{\rho}_o} \int_0^R r\psi_m \frac{\partial \psi_n}{\partial z} \, dr \right.$$

$$\left. + \frac{1}{\bar{\rho}_o} R \, \psi_m(R,z) \, \psi_n(R,z) \tan\alpha + \frac{1}{\gamma \bar{p}_o \bar{\rho}_o} \frac{d\bar{p}_o}{dz} \int_0^R r \, \psi_m \psi_n \, dr \right] \{p_m\} \qquad (6.1.26)$$

$$\left[\gamma \bar{p}_o \int_0^R r^2 \psi_m \psi_n \, dr \right] \left\{ \frac{dw_m}{dz} \right\} + \left[\bar{W}_o \int_0^R r^2 \psi_m \psi_n \, dr - \gamma \bar{p}_o \frac{i}{k_r} \bar{W}_o \frac{A}{\cos\alpha} R^2 \psi_m(R,z) \psi_n(R,z) \right] \left\{ \frac{dp_m}{dz} \right\}$$

$$= \left[\gamma \bar{p}_o \int_0^R r\phi_m \frac{\partial}{\partial r} (r\psi_n) \, dr \right] \{u_m\} + \left[\gamma \bar{p}_o im_o \int_0^R r\psi_m \psi_n \, dr \right] \{v_m\}$$

$$+ \left[- \gamma \bar{p}_o \frac{d}{dz} \int_0^R r^2 \psi_m \psi_n \, dr + \gamma \bar{p}_o \int_0^R r^2 \psi_m \frac{\partial \psi_n}{\partial z} \, dr - \frac{d\bar{p}_o}{dz} \int_0^R r^2 \psi_m \psi_n \, dr \right] \{w_m\}$$

$$+ \left[\left(-ik_r - 2\gamma \bar{W}_o \frac{\tan\alpha}{R} - \gamma \frac{d\bar{W}_o}{dz} \right) \int_0^R r^2 \psi_m \psi_n \, dr + \bar{W}_o \frac{\tan\alpha}{R} \int_0^R \psi_m \frac{\partial}{\partial r} (r^3 \psi_n) \, dr \right.$$

$$- \bar{W}_o \frac{d}{dz} \int_0^R r^2 \psi_m \psi_n \, dr + \bar{W}_o \int_0^R r^2 \psi_m \frac{\partial}{\partial z} \psi_n \, dr$$

$$- \gamma \bar{p}_o R^2 \psi_n(R,z) \left\{ \frac{A}{\cos\alpha} \psi_m(R,z) - \frac{i\bar{W}_o}{k_r \cos\alpha} \left[\frac{dA}{dz} \psi_m(R,z) + A \frac{\partial \psi_m(R,z)}{\partial z} \right. \right.$$

$$\left. \left. \left. + \tan\alpha \, A \frac{\partial \psi_m(R,z)}{\partial r} \right) \right\} \right] \{p_m\} \qquad (6.1.27)$$

for (m = 1,2...N) and (n = 1,2...N)

In the right-hand side of equations (6.1.24) - (6.1.27) the Leibnitz rule of differentiation can be applied to ordinary derivatives with respect to z to simplify terms further, so that one can write these four sets of equations with definitions :

$$N_{nm} = \int_0^R \psi_m \psi_n \, dr \;,\; M_{nm} = \int_0^R r\psi_m \psi_n \, dr \;,\; L_{nm} = \int_0^R r^2 \psi_m \psi_n \, dr$$

$$M'_{nm} = \int_0^R r\phi_m \psi_n \, dr,\; L'_{nm} = \int_0^R r^2 \phi_m \psi_n \, dr \qquad (6.1.28)$$

in the matrix form following

$$\begin{bmatrix} DP^p & DP^w & 0 & 0 \\ DW^p & DW^w & 0 & 0 \\ 0 & 0 & DU^u & 0 \\ 0 & 0 & 0 & DV^v \end{bmatrix} \frac{d}{dz} \begin{Bmatrix} p_m \\ w_m \\ u_m \\ v_m \end{Bmatrix} = \begin{bmatrix} P^p & P^w & P^u & P^v \\ W^p & W^w & 0 & 0 \\ U^p & U^w & U^u & 0 \\ V^p & 0 & 0 & V^v \end{bmatrix} \begin{Bmatrix} p_m \\ w_m \\ u_m \\ v_m \end{Bmatrix} \qquad (6.1.29)$$

where

$$DP^p_{nm} = \bar{W}_o \, L_{nm} - \gamma \bar{p}_o \frac{i}{k_r} \frac{A}{\cos\alpha} \bar{W}_o \, R^2 \, \psi_m(R,z) \, \psi_n(R,z)$$

$$DP^w_{nm} = \gamma \bar{p}_o \, L_{nm}$$

$$P^p_{nm} = \left[-ik_r - (2\gamma - 3)\bar{W}_o \frac{\tan\alpha}{R} - \gamma \frac{d\bar{W}_o}{dz} \right] L_{nm} + \bar{W}_o \frac{\tan\alpha}{R} \int_0^R r^3 \psi_m \frac{\partial}{\partial r} \psi_n \, dr$$

$$- \bar{W}_o \int_0^R r^2 \frac{\partial \psi_m}{\partial z} \psi_n \, dr - R^2 \psi_m(R,z) \, \psi_n(R,z) \left(\bar{W}_o \tan\alpha + \gamma \bar{p}_o \frac{A}{\cos\alpha} \right)$$

$$+ \gamma \bar{p}_o R^2 \frac{i}{k_r} \frac{A}{\cos\alpha} \bar{W}_o \, \psi_n(R,z) \left(\frac{1}{A} \frac{dA}{dz} \psi_m(R,z) + \frac{\partial \psi_m(R,z)}{\partial z} + \tan\alpha \frac{\partial \psi_m(R,z)}{\partial r} \right)$$

$$P^w_{nm} = - \gamma \bar{p}_o \int_0^R r^2 \frac{\partial \psi_m}{\partial z} \psi_n \, dr - \gamma \bar{p}_o \, R^2 \psi_m(R,z) \psi_n(R,z) \tan\alpha - \frac{d\bar{p}_o}{dz} L_{nm}$$

$$P^u_{nm} = \gamma\bar{p}_o M'_{nm} + \gamma\bar{p}_o \int_0^R r^2\phi_m \frac{\partial\psi_n}{\partial r}\, dr$$

$$P^v_{nm} = \gamma\bar{p}_o\, im_o\, M_{nm}$$

$$DW^p_{nm} = \frac{1}{\bar{\rho}_o} M_{nm}$$

$$DW^w_{nm} = \bar{W}_o M_{nm}$$

$$W^p_{nm} = -\frac{1}{\bar{\rho}_o} \int_0^R r \frac{\partial\psi_m}{\partial z} \psi_n\, dr + \frac{1}{\gamma\bar{p}_o\bar{\rho}_o} \frac{d\bar{p}_o}{dz} M_{nm}$$

$$W^w_{nm} = -\bar{W}_o \int_0^R r \frac{\partial\psi_m}{\partial z} \psi_n\, dr - \bar{W}_o R\, \psi_m(R,z)\psi_n(R,z)\tan\alpha$$

$$+ \left(2\bar{W}_o \frac{\tan\alpha}{R} - ik_r - \frac{d\bar{W}_o}{dz}\right) M_{nm} + \bar{W}_o \frac{\tan\alpha}{R} \int_0^R r^2\psi_m \frac{\partial\psi_n}{\partial r}\, dr$$

$$DU^u_{nm} = \bar{W}_o M'_{nm}$$

$$U^p_{nm} = -\frac{1}{\bar{\rho}_o} R\, \psi_m(R,z)\psi_n(R,z) + \frac{1}{\bar{\rho}_o} N_{nm} + \frac{1}{\bar{\rho}_o} \int_0^R r\, \psi_m \frac{\partial\psi_n}{\partial r}\, dr$$

$$U^w_{nm} = \left(-\frac{d\bar{W}_o}{dz} \frac{\tan\alpha}{R} + \bar{W}_o \frac{\tan^2\alpha}{R^2} - \frac{\bar{W}_o}{R} \frac{d\tan\alpha}{dz}\right) L_{nm}$$

$$U^u_{nm} = -\bar{W}_o \int_0^R r \frac{\partial\psi_m}{\partial z} \psi_n\, dr - \bar{W}_o R\, \phi_m(R,z)\psi_n(R,z)\tan\alpha$$

$$+ \bar{W}_o \frac{\tan\alpha}{R} \int_0^R r^2\phi_m \frac{\partial\psi_n}{\partial r}\, dr$$

$$- \left(ik_r - \frac{\bar{W}_o \tan\alpha}{R}\right) M'_{nm}$$

$$DV^v_{nm} = \bar{W}_o M_{nm}$$

$$V^{p}_{nm} = \frac{im_o}{\bar{\rho}_o} N_{nm}$$

$$V^{v}_{nm} = - \bar{W}_o \int_0^R r \frac{\partial \psi_m}{\partial z} \psi_n \, dr - \bar{W}_o R \, \psi_m(R,z)\psi_n(R,z) \tan\alpha$$

$$- \left(ik_r - \bar{W}_o \frac{\tan\alpha}{R} \right) M_{nm} + \bar{W}_o \frac{\tan\alpha}{R} \int_0^R r^2 \psi_m \frac{\partial \psi_n}{\partial r} \, dr$$

6.1.2 With Basis Functions Specified

When the trigonometric functions are employed so that

$$\psi_m = \cos \kappa_m r \quad , \quad \phi_m = \sin \kappa_m r$$

the matrix equation (6.1.29) can be rewritten in nondimensional terms by changing variables according to the definition $\eta = \frac{r}{R}$ and dividing the first N p_m - equations by R^2 and the rest by R, as follows :

$$\begin{bmatrix} \overline{\overline{DP}}^{p} & \overline{\overline{DP}}^{w} & 0 & 0 \\ \overline{\overline{DW}}^{p} & \overline{\overline{DW}}^{w} & 0 & 0 \\ 0 & 0 & \overline{\overline{DU}}^{u} & 0 \\ 0 & 0 & 0 & \overline{\overline{DV}}^{v} \end{bmatrix} \frac{d}{dz} \begin{Bmatrix} p_m \\ w_m \\ u_m \\ v_m \end{Bmatrix} = \begin{bmatrix} \bar{\bar{P}}^{p} & \bar{\bar{P}}^{w} & \bar{\bar{P}}^{u} & \bar{\bar{P}}^{u} \\ \bar{\bar{W}}^{p} & \bar{\bar{W}}^{w} & 0 & 0 \\ \bar{\bar{U}}^{p} & \bar{\bar{U}}^{w} & \bar{\bar{U}}^{u} & 0 \\ \bar{\bar{V}}^{p} & 0 & 0 & \bar{\bar{V}}^{v} \end{bmatrix} \begin{Bmatrix} p_m \\ w_m \\ u_m \\ v_m \end{Bmatrix} \quad (6.1.30)$$

where

$$\overline{\overline{DP}}^{p}_{nm} = R \bar{W}_o \bar{L}_{nm} - \gamma \bar{p}_o \frac{i}{k_r R} \frac{A}{\cos\alpha} \bar{W}_o R \cos(\kappa_m R)\cos(\kappa_n R)$$

$$\overline{\overline{DP}}^{w}_{nm} = R \gamma \bar{p}_o \bar{L}_{nm}$$

$$\bar{\bar{P}}^{p}_{nm} = \left[ik_r R - (2\gamma-3)\bar{W}_o \tan\alpha - \gamma R \frac{D\bar{W}_o}{dz} \right] \bar{L}_{nm}$$

$$- \bar{W}_o \tan\alpha \, \kappa_n R \, \bar{K}'_{mn} + \bar{W}_o R^2 \frac{d\kappa_m}{dz} \bar{K}_{nm}$$

$$- \left(\bar{W}_o \tan\alpha + \gamma \bar{p}_o \frac{A}{\cos\alpha} \right) \cos\kappa_m R \cos\kappa_n R$$

$$+ \gamma\bar{p}_o \frac{i}{k_r R} \frac{A}{\cos\alpha} \bar{W}_o \cos\kappa_n R \left[\frac{1}{A} R \frac{dA}{dz} \cos\kappa_m R - R \frac{d(\kappa_m R)}{dz} \sin\kappa_m R\right]$$

$$\bar{P}^w_{nm} = \gamma\bar{p}_o R^2 \frac{d\kappa_m}{dz} \bar{K}'_{nm} - \gamma\bar{p}_o \cos\kappa_m R \cos\kappa_n R \tan\alpha - R\frac{d\bar{p}_o}{dz} \bar{L}_{nm}$$

$$\bar{P}^u_{nm} = \gamma\bar{p}_o \bar{M}'_{nm} - \gamma\bar{p}_o \kappa_n R \bar{L}''_{nm}$$

$$\bar{P}^v_{nm} = \gamma\bar{p}_o im_o \bar{M}_{nm}$$

$$D\bar{W}^p_{nm} = \frac{1}{\bar{\rho}_o} R \bar{M}_{nm}$$

$$D\bar{W}^w_{nm} = R \bar{W}_o \bar{M}_{nm}$$

$$\bar{W}^p_{nm} = \frac{1}{\bar{\rho}_o} R^2 \frac{d\kappa_m}{dz} \bar{L}'_{nm} + \frac{1}{\gamma\bar{p}_o\bar{\rho}_o} R \frac{d\bar{p}_o}{dz} \bar{M}_{nm}$$

$$\bar{W}^w_{nm} = \bar{W}_o R^2 \frac{d\kappa_m}{dz} \bar{L}'_{nm} - \bar{W}_o \cos(\kappa_m R) \cos(\kappa_n R) \tan\alpha$$

$$+ \left(2\bar{W}_o \tan\alpha - ik_r R - R \frac{d\bar{W}_o}{dz}\right) \bar{M}_{nm} - \bar{W}_o \tan\alpha \kappa_n R \bar{L}'_{mn}$$

$$D\bar{U}^u_{nm} = \bar{W}_o R \bar{M}'_{nm}$$

$$\bar{U}^p_{nm} = -\frac{1}{\bar{\rho}_o} \cos\kappa_m R \cos\kappa_n R + \frac{1}{\bar{\rho}_o} \bar{N}_{nm} - \frac{\kappa_n R}{\bar{\rho}_o} \bar{M}'_{mn}$$

$$\bar{U}^w_{nm} = \left(-R\frac{d\bar{W}_o}{dz} \tan\alpha + \bar{W}_o \tan^2\alpha - \bar{W}_o R \frac{d\tan\alpha}{dz}\right) \bar{L}_{nm}$$

$$\bar{U}^u_{nm} = -\bar{W}_o R^2 \frac{d\kappa_m}{dz} \bar{L}_{nm} - \bar{W}_o \tan\alpha \sin(\kappa_m R) \cos(\kappa_n R)$$

$$- \bar{W}_o \tan\alpha \kappa_n R \bar{L}''_{nm} - (ik_r R - \bar{W}_o \tan\alpha) \bar{M}'_{nm}$$

$$D\bar{V}^v = \bar{W}_o R \bar{M}_{nm}$$

$$\bar{V}^{p}_{nm} = \frac{im_o}{\bar{\rho}_o} \bar{N}_{nm}$$

$$\bar{V}^{v}_{nm} = \bar{W}_o R^2 \frac{d\kappa_m}{dz} \bar{L}'_{nm} - \bar{W}_o \cos \kappa_m R \cos \kappa_n R \tan \alpha$$

$$- (ik_r R - \bar{W}_o \tan \alpha) \bar{M}_{nm} - \bar{W}_o \tan \alpha \, \kappa_n R \, \bar{L}'_{mn}$$

with definitions :

$$\bar{N}_{nm} = \int_0^1 \cos (\kappa_m R\eta) \cos (\kappa_n R\eta) \, d\eta$$

$$\bar{M}_{nm} = \int_0^1 \eta \cos (\kappa_m R\eta) \cos (\kappa_n R\eta) \, d\eta$$

$$\bar{L}_{nm} = \int_0^1 \eta^2 \cos (\kappa_m R\eta) \cos (\kappa_n R\eta) \, d\eta$$

$$\bar{K}_{nm} = \int_0^1 \eta^3 \cos (\kappa_m R\eta) \cos (\kappa_n R\eta) \, d\eta \qquad (6.1.31)$$

$$\bar{M}'_{nm} = \int_0^1 \eta \sin (\kappa_m R\eta) \cos (\kappa_n R\eta) \, d\eta$$

$$\bar{L}'_{nm} = \int_0^1 \eta^2 \sin (\kappa_m R\eta) \cos (\kappa_n R\eta) \, d\eta$$

$$\bar{K}'_{nm} = \int_0^1 \eta^3 \sin (\kappa_m R\eta) \cos (\kappa_n R\eta) \, d\eta$$

$$\bar{L}''_{nm} = \int_0^1 \eta^2 \sin (\kappa_m R\eta) \sin (\kappa_n R\eta) \, d\eta$$

The set of coupled linear ordinary differential equations (6.1.30) for the axial variation of the coefficients in the assumed solution can be represented in the form :

$$\underset{4Nx4N}{[\mathcal{M}(z)]}\ \frac{d}{dz}\ \underset{4Nx1}{\begin{Bmatrix} p_m \\ w_m \\ u_m \\ v_m \end{Bmatrix}} = \underset{4Nx4N}{[\mathcal{N}(z)]}\ \underset{4Nx1}{\begin{Bmatrix} p_m \\ w_m \\ u_m \\ v_m \end{Bmatrix}} \tag{6.1.32}$$

or

$$\frac{d}{dz}\ \underset{4Nx1}{\begin{Bmatrix} p_m \\ w_m \\ u_m \\ v_m \end{Bmatrix}} = \underset{4Nx4N}{[\mathcal{L}(z)]}\ \underset{4Nx1}{\begin{Bmatrix} p_m \\ w_m \\ u_m \\ v_m \end{Bmatrix}} \tag{6.1.33}$$

where $[\mathcal{L}(z)] = [\mathcal{M}(z)]^{-1}[\mathcal{N}(z)]$

This can be integrated to yield a transition matrix relating the values of p_m, w_m, u_m, v_m at $z = \ell$ to those at $z = 0$

$$\begin{Bmatrix} p_m \\ w_m \\ u_m \\ v_m \end{Bmatrix}_{z=\ell} = [\ TS\ ] \begin{Bmatrix} p_m \\ w_m \\ u_m \\ v_m \end{Bmatrix}_{z=0} \tag{6.1.34}$$

where [TS] is the transition matrix.

6.2 MATCHING OF THE NONUNIFORM SECTION TO UNIFORM SECTIONS

For matching at the ends of the nonuniformity, as for the no-flow case the eigenproblems in semi-infinite ducts are to be solved. In the light of the conclusions on the method of solution in Section 5.1 the eigen-problem for the flow case is solved by the MWR with conservation equations as in Section 4.2.5. This approach is advantageous in two ways :

(a) It describes the wave propagation in the uniform ducts with the same degree of accuracy as the description in the non-uniform duct section. This is proved highly successful in the no-flow case.

(b) It maintains the same number of dependent variables, i.e. the unknown assumed coefficients in matching procedure, in both the uniform ducts and the nonuniformity.

6.2.1 Least-Square Matching by MWR Eigenfunctions

The application of the least-square matching procedure is similar to the no-flow case except for the hydrodynamic modes arising in the modal matrices in the flow case. To establish the eigenproblem by MWR it is convenient to return to the matrix equation (6.1.33)

$$\frac{d}{dz}\{\delta\} = [\mathcal{L}(z)]\{\delta\} \tag{6.2.1}$$

where $\{\delta\} = [p_m \mid w_m \mid u_m \mid v_m]^T$, $m = 1,2,3...N$,
and $[\mathcal{L}(z)]$ is independent of z for uniform semi-infinite ducts. Therefore solutions to equation (6.2.1) can be assumed in the form

$$\{\delta\} = \{q\}e^{-ik_z z} \tag{6.2.2}$$

to give an algebraic eigenproblem

$$\underset{4Nx4N}{i\,[\mathcal{L}]}\ \underset{4Nx1}{\{q\}} = \underset{}{k_z}\ \underset{4Nx1}{\{q\}} \tag{6.2.3}$$

which is recognized as the eigenproblem in Section 4.2.2 This eigenproblem can be solved by the general QR algorithm to yield axial eigenvalues k_z and corresponding eigenvectors. Thus, the solution for the uniform duct sections (A) and (C) can be written in the form

$$\underset{4Nx1}{\{\delta\}} = \underset{4Nx4N}{[M]}\ \underset{4Nx4N}{[e]}\ \underset{4Nx1}{\begin{Bmatrix} q^+ \\ q^- \\ q^H \end{Bmatrix}} \tag{6.2.4}$$

where [M] is the partitioned modal matrix, as in the no-flow case, containing the eigenvectors corresponding to the modes of propagation. For the flow case, in [M] the first N columns are eigenvectors corresponding to positively propagating modes, the second N columns to negatively propagating modes, and the last 2N columns are hydrodynamic modes characterized by propagation velocity equal to the uniform flow velocity

and zero pressure contribution. The matrix [e] is diagonal and partitioned in the same way, with the typical element being

$$e_{nn} = e^{-ik_{z_n} z}.$$

q^+, q^-, q^H are column vectors of modal amplitudes in the positive running, negative running and hydrodynamic modes, respectively.

To attach a meaning to the amplitudes of the acoustic modes, q^+ and q^-, the normalization is performed on the acoustic eigenvectors of the modal matrix [M] as for the no-flow case, i.e. in such a way that q_i is the acoustic pressure of mode i at the duct centre line for the axisymmetric angular mode ($m_o = 0$), and the acoustic pressure at the duct wall for higher-order angular modes ($m_o \neq 0$). The construction of hydrodynamic modes will be detailed in the following Section 6.2.2.

Once the modal matrices $[M_o]$, $[M_\ell]$ at z = 0 and z = ℓ respectively, are available, the least-square matching as for the no-flow case (see Section 5.1.2(ii)) yields the transfer matrix [TF] relating the modal amplitudes at z = ℓ to those at z = 0 :

$$\underset{4Nx1}{\begin{Bmatrix} q^+ \\ q^- \\ q^H \end{Bmatrix}_{z=\ell}} = \underset{4Nx4N}{[TF]} \underset{4Nx1}{\begin{Bmatrix} q^+ \\ q^- \\ q^H \end{Bmatrix}_{z=0}} \qquad (6.2.5)$$

The matrix [TF] is derived from

$$[TF] = [M_\ell]^{-1}[C_2{}'_2{}']^{-1}[C_2{}'_2][TS][C_{11}]^{-1}[C_{11}'][M_o] \qquad (6.2.6)$$

where [TS] is the transition matrix given by relation (6.1.34). The matrices $[C_2{}'_2{}']$, $[C_2{}'_2]$, $[C_{11}]$ and $[C_{11}']$ are constructed similarly to those in the no-flow case from equations (5.1.72) - (5.1.73) with appropriate basis functions, and typically given by

$$[C_{11}'] = \int_0^{R_1} [C_1^*]^T [C_1'] \, 2\pi r \, dr \qquad (6.2.7)$$

$$4Nx4N \qquad 4Nx4 \quad 4x4N$$

where the superscript T denotes transpose, the asterisk denotes complex conjugate , and the subscripts 1,1',2 and 2' are referred to the interfaces S_1, S_1', S_2 and S_2' respectively in Figure 2.4 . A typical matrix [C] in the integrand (6.2.7) is defined by

$$[C] = \begin{bmatrix} [\cos \kappa_m r] & & & \\ 1xN & [\cos \kappa_m r] & & \\ & 1xN & [\sin \kappa_m r] & \\ & & 1xN & [\cos \kappa_m r] \\ & & & 1xN \end{bmatrix} \qquad (6.2.8)$$

$$4x4 \qquad\qquad 4x4N$$

This originates from the representation of the MWR solutions at appropriate z stations, in the form

$$\begin{Bmatrix} p \\ w \\ u \\ v \end{Bmatrix} \approx \begin{Bmatrix} p_N \\ w_N \\ u_N \\ v_N \end{Bmatrix} = [C] \{\delta\} \qquad (6.2.9)$$

$$4x1 \qquad 4x1 \qquad 4x4N \quad 4Nx1$$

As for the no-flow case, if the wall admittance is continuous through the interfaces of duct sections then, in equation (6.2.5), $[C_2'_2'] \equiv [C_2'_2]$ and $[C_{11}] \equiv [C_{11}']$. In this case the relation (6.2.6) becomes

$$[TF] = [M_\ell]^{-1} [TS] [M_o] \qquad (6.2.10)$$

$$4Nx4N \quad 4Nx4N \quad 4Nx4N \quad 4Nx4N$$

6.2.2 Representation of Hydrodynamic Modes

In construction of the modal matrix [M] a problem arises in the computation of the eigenvectors corresponding to the hydrodynamic modes.

The hydrodynamic eigenvalues are 2N equal values k_{z_n} of equation (6.2.3), identifiable by $k_z = k/M_o = k_r/\bar{W}_o$ (where k is local wave number). In all computations to date the QR algorithm resolves these eigenvalues satisfactorily, but the corresponding vectors are inaccurate, which is predictable by careful examination of the computational scheme used (because of multiple eigenvalues). This problem can be circumvented by recourse to the expanded form of equation (6.2.3), which shows that when $k_z = k_r/\bar{W}_o$ a solution must be of the form : $\{p_m\} = 0$,

$$\left[-ik_z R\,\bar{L}_{nm}\right]\{w_m\} = \left[\bar{M}'_{nm} - \kappa_n R\,\bar{L}''_{nm}\right]\{u_m\} + \left[im_o \bar{M}_{nm}\right]\{v_m\} \qquad (6.2.11)$$

Thus, 2N independent eigenvectors can be constructed by the above relationships by appropriate choices of elements in $\{u_m\}$ and $\{v_m\}$.

Consider the modal matrix following :

$$[M]_{4N\times 4N}\{\delta\} = 4N \left\{ \begin{bmatrix} \cdot & \cdot & 0 & 0 \\ \cdot & \cdot & W_1 & W_2 \\ \cdot & \cdot & I & 0 \\ \cdot & \cdot & 0 & I \end{bmatrix} \begin{Bmatrix} p_m \\ w_m \\ u_m \\ v_m \end{Bmatrix} \right. \qquad (6.2.12)$$

(N, N, 2N)

where $[I]$ is the identity matrix. For hydrodynamic modes there are no pressure contributions so that the eigenvector components corresponding to p_m can be set to be zero. It is noted that in the relation (6.2.6) or (6.2.10) one of the modal matrices must be inverted. For the purpose of avoiding problems in the matrix inversion the 2N hydrodynamic eigenvectors are constructed in such a way that the diagonal terms of the modal matrix $[M]$ do not vanish, and can be conveniently chosen as shown in (6.2.12). In that case $[W_1]$ and $[W_2]$ can be derived from relation (6.2.11) as follows :

$$[W_1]_{N\times N} = \left[-ik_z R\,\bar{L}_{nm}\right]^{-1}\left[\bar{M}'_{nm} - \kappa_n R\,\bar{L}''_{nm}\right]$$
$$[W_2]_{N\times N} = \left[-ik_z R\,\bar{L}_{nm}\right]^{-1}\cdot\left[im_o\,\bar{M}_{nm}\right] \qquad (6.2.13)$$

for $m = 1,2,\ldots N$ and $n = 1,2,\ldots N$

Note that the hydrodynamic mode eigenfunctions established in this way are expressed in terms of the basis functions used for acoustic modes. For the hardwall case, it is just the standard Galerkin Method since the hydrodynamic boundary condition is satisfied : $u^H = 0$ at $r = R$. In the case of a lined duct the situation is the reverse in that the hydrodynamic eigenfunctions are approximated by soft-wall basis functions. But, as discussed in Section 4.2.5(ii), the hydrodynamic modes in uniform flow propagate convectively with the flow as in a hardwalled duct for any wall admittance.

6.3 IMPLEMENTATION

6.3.1 Numerical Integration

In the nonuniform duct study the set of first order linear ordinary differential equations (6.1.33) is integrated numerically by the fourth-order Runga-Kutta method, computing the coefficient matrix $[\mathcal{L}(z)]$ twice at each step of integration. Thus, the computation time spent for evaluation of the coefficient matrix represents a major portion of the solution time in the MWR as noted in the no-flow case.

With the trigonometric basis functions employed in the formulations $[\mathcal{L}(z)]$ can be evaluated analytically from the components of equations (6.1.30) and (6.1.32), generating the basis functions and solving for the mean flow parameters along the axis.

(i) Mean flow field. The solutions for the mean flow parameters $\bar{W}_o$, $\bar{\rho}_o$, $\bar{p}_o$, $\bar{c}_o$ and/or their derivatives (with respect to z only) are based on the solution for the flow Mach number $\bar{M}_o(z)$ at each step, for which, from equation (6.0.8)

$$\frac{d\bar{M}_o}{dz} = - \frac{\bar{M}_o}{1-\bar{M}_o^2} \left[1 + \frac{\gamma-1}{2} \bar{M}_o^2 \right] \frac{2}{R} \tan \alpha$$

This nonlinear differential equation can also be solved numerically by the fourth-order Runge-Kutta integration scheme so that from the relations (6.0.9) - (6.0.12) the parameters $\bar{W}_o$, $\bar{\rho}_o$, $\bar{p}_o$, $\bar{c}_o$ are calculated as the input quantities in evaluating the coefficient matrix $[\mathcal{L}(z)]$.

The required derivatives can be deduced as follows :

$$\frac{d\bar{p}_o}{dz} = \frac{d\bar{p}_o}{d\bar{M}_o} \frac{d\bar{M}_o}{dz} \quad , \quad \frac{d\bar{W}_o}{dz} = \frac{d\bar{W}_o}{d\bar{M}_o} \frac{d\bar{M}_o}{dz}$$

$$\frac{d\bar{c}_o}{dz} = \frac{d\bar{c}_o}{d\bar{M}_o} \frac{d\bar{M}_o}{dz} \quad , \quad \frac{d\bar{\rho}_o}{dz} = \frac{d\bar{\rho}_o}{d\bar{M}_o} \frac{d\bar{M}_o}{dz}$$

where, from equations (6.0.9) - (6.0.12)

$$\frac{d\bar{p}_o}{d\bar{M}_o} = -\bar{M}_o \left[1 + \frac{\gamma-1}{2} M_r^2\right]^{\frac{\gamma}{\gamma-1}} \left[1 - \frac{\gamma-1}{2} \bar{M}_o^2\right]^{\frac{1-2\gamma}{\gamma-1}}$$

$$\frac{d\bar{W}_o}{d\bar{M}_o} = \frac{\left[1 + \frac{\gamma-1}{2} M_r^2\right]^{\frac{1}{2}}}{\left[1 + \frac{\gamma-1}{2} \bar{M}_o^2\right]^{\frac{3}{2}}}$$

$$\frac{d\bar{c}_o}{d\bar{M}_o} = -\frac{\gamma-1}{2} \bar{M}_o \frac{\left[1 + \frac{\gamma-1}{2} M_r^2\right]^{\frac{1}{2}}}{\left[1 + \frac{\gamma-1}{2} \bar{M}_o^2\right]^{\frac{3}{2}}}$$

$$\frac{d\bar{\rho}_o}{d\bar{M}_o} = -\bar{M}_o \frac{\left[1 + \frac{\gamma-1}{2} M_r^2\right]^{\frac{1}{\gamma-1}}}{\left[1 + \frac{\gamma-1}{2} \bar{M}_o^2\right]^{\frac{\gamma}{\gamma-1}}}$$

(ii) Basis functions. In the light of the conclusions drawn from the eigenproblem in Chapter 4, the basis functions used for the flow case are the modified flow basis functions (see Section 4.2.4) for the low frequency range ($k_r R \approx 1$), and the no-flow basis functions should be employed for high frequencies. In the generating equations the basis functions are derived on the basis of local characteristic parameters. In the transmission problem they are manipulated in terms of reference state parameters in the present nondimensionalization as follows :

(a) No-flow basis functions : $\cos(\kappa_m r)$ with κ_m given by

$$\kappa_m R \tan \kappa_m R = i\, k_\ell R\, A_\ell \tag{6.3.1}$$

where k_ℓ, A_ℓ are local values of wave number and specific admittance respectively. But

$$\begin{aligned} k_\ell &= \frac{\omega}{\bar{c}_o^*} = \frac{\omega}{c_r}\,\frac{c_r}{\bar{c}_o^*} = k_r/\bar{c}_o \\ A_\ell &= \frac{\bar{\rho}_o^*\bar{c}_o^*}{Z} = \frac{\rho_r c_r}{Z}\cdot\frac{\bar{\rho}_o^*\bar{c}_o^*}{\rho_r c_r} \\ &= A\;\bar{\rho}_o\bar{c}_o \end{aligned} \tag{6.3.2}$$

where A is the specific admittance in the reference state. Hence, equation (6.3.1) becomes

$$\kappa_m R \tan \kappa_m R = ik_r R\, A\, \bar{\rho}_o \tag{6.3.3}$$

To compute the nondimensional term $R\,\dfrac{d(\kappa_m R)}{dz}$ in the coefficient matrices $[\mathcal{M}(z)]$ and $[\mathcal{N}(z)]$ of equation (6.1.32) one can differentiate equation (6.3.3) as follows :

$$R\,\frac{d(\kappa_m R)}{dz}\left[\tan \kappa_m R + \kappa_m R\,(1+\tan^2 \kappa_m R)\right]$$

$$= ik_r R\;A\bar{\rho}_o\left(\frac{dR}{dz} + \frac{1}{A}R\frac{dA}{dz} + \frac{1}{\bar{\rho}_o}R\frac{d\bar{\rho}_o}{dz}\right)$$

(b) Modified flow basis function : $\cos \kappa_m r$ with κ_m given by

$$\kappa_m R \tan \kappa_m R = ik_\ell R\, A_\ell\left[1 - \frac{\bar{M}_o^2}{1-\bar{M}_o^2}\left(\frac{\kappa_m R}{k_\ell R}\right)^2\right] \tag{6.3.4}$$

From relations (6.3.2) one can rewrite equation (6.3.4) in the form

$$\kappa_m R \tan \kappa_m R = ik_r R\, A\bar{\rho}_o\left[1 - \frac{\bar{M}_o^2}{1-\bar{M}_o^2}\,\bar{c}_o^2\left(\frac{\kappa_m R}{k_r R}\right)^2\right] \tag{6.3.5}$$

Differentiation with respect to z of equation (6.3.5) yields

$$R\frac{d\kappa_m R}{dz}\left[\tan\kappa_m R + \kappa_m R\,(1+\tan^2\kappa_m R) + 2\,i\,A\,\frac{\bar{M}_o^2}{1-\bar{M}_o^2}\,\bar{\rho}_o\bar{c}_o^2\,\frac{\kappa_m R}{k_r R}\right]$$

$$= ik_r R A\bar{\rho}_o\left\{\frac{dR}{dz} + \frac{1}{\bar{\rho}_o}\cdot R\frac{d\bar{\rho}_o}{dz} + \frac{1}{A}\cdot R\frac{dA}{dz} - \frac{\bar{M}_o^2}{1-\bar{M}_o^2}\cdot\bar{c}_o^2\left(\frac{\kappa_m R}{k_r R}\right)^2\right.$$

$$\left.\left(\frac{2}{\bar{M}_o(1-\bar{M}_o^2)}R\frac{d\bar{M}_o}{dz} + \frac{1}{\bar{\rho}_o}R\frac{d\bar{\rho}_o}{dz} + \frac{2}{\bar{c}_o}R\frac{d\bar{c}_o}{dz} + \frac{1}{A}R\frac{dA}{dz} - \frac{dR}{dz}\right)\right\}$$

In evaluation of the coefficient matrix $[\mathcal{L}(z)] = [\mathcal{M}(z)]^{-1}[\mathcal{N}(z)]$ it is noted that, for A = 0, i.e. for the hardwall case the transcendental equation (6.3.3) or (6.3.5), which generates the basis functions has the first root equal to zero, rendering the matrix $[\mathcal{M}(z)]$ singular. In order not to complicate the programme structure in computer implementation for the hardwall case one may conveniently use a very small value of A instead of A = 0.

6.3.2 Hydrodynamic Modes in the Transmission Problem

For the sound propagation problem in a nonuniform duct with flow the MWR yields the solution in the form

$$\begin{Bmatrix} q^+ \\ q^- \\ q^H \end{Bmatrix}_{z=\ell} = [\,TF\,] \begin{Bmatrix} q^+ \\ q^- \\ q^H \end{Bmatrix}_{z=0} \tag{6.3.6}$$

where [TF] is the transfer matrix given by equation (6.2.6) or (6.2.10)

The primary interest of the research programme is focused on the acoustic propagation, although the expression (6.2.6) or (6.2.10) for [TF] shows that, unless [TF] is of special form (e.g. for uniform ducts with a uniform flow profile), there is a coupling between acoustic and hydrodynamic modes. Since the existence of hydrodynamic modes has no clear precedent, and furthermore, the present study is directed towards the acoustic propagation problem, it can be assumed that the flow entering the nonuniform duct section carries no hydrodynamic disturbances. This

means that the hydrodynamic modes will play a different role depending upon whether the flow is in the positive or negative direction, and it is necessary to distinguish between the two cases

(i) Flow in the positive z direction. In this case $\{q^H\} = 0$ for $z < 0$. For the acoustic modes it is possible to write equation (6.3.6) in the partitioned form

$$\left\{\begin{matrix} q^+ \\ q^- \end{matrix}\right\}_{z=\ell} = \left[\begin{matrix} S^{++} & S^{+-} \\ S^{-+} & S^{--} \end{matrix}\right] \left\{\begin{matrix} q^+ \\ q^- \end{matrix}\right\}_{z=0} \tag{6.3.7}$$

Thus, it is straightforward to define the transmission and reflection matrices as for the no-flow case.

$$\{q^+\}_{z=\ell} = [\text{TRAN}]\ \{q^+\}_{z=0}$$

$$\{q^-\}_{z=0} = [\text{REFL}]\ \{q^+\}_{z=0}$$

where

$$\begin{aligned} [\text{REFL}] &= -[S^{--}]^{-1}\ [S^{-+}] \\ [\text{TRAN}] &= [S^{++}] + [S^{+-}]\ [\text{REFL}] \end{aligned} \tag{6.3.8}$$

(ii) Flow in the negative z direction. Assuming that $\{q^H\}_{z=\ell} = 0$ one can write the appropriate partitioned form of equation (6.3.6)

$$\left\{\begin{matrix} q^+ \\ q^- \\ 0 \end{matrix}\right\}_{z=\ell} = \left[\begin{matrix} S^{++} & S^{+-} & S^{+H} \\ S^{-+} & S^{--} & S^{-H} \\ S^{H+} & S^{H-} & S^{HH} \end{matrix}\right] \left\{\begin{matrix} q^+ \\ q^- \\ q^H \end{matrix}\right\}_{z=0}$$

This leads to

$$\left\{\begin{matrix} q^+ \\ q^- \end{matrix}\right\}_{z=\ell} = \left(\left[\begin{matrix} S^{++} & S^{+-} \\ S^{-+} & S^{--} \end{matrix}\right] - \left[\begin{matrix} S^{+H} \\ S^{-H} \end{matrix}\right] \left[S^{HH}\right]^{-1} \left[\begin{matrix} S^{H+} & S^{H-} \end{matrix}\right] \right) \left\{\begin{matrix} q^+ \\ q^- \end{matrix}\right\}_{z=0}$$

$$= \begin{bmatrix} \tilde{S}^{++} & \tilde{S}^{+-} \\ \tilde{S}^{+-} & \tilde{S}^{--} \end{bmatrix} \begin{Bmatrix} q^{+} \\ q^{-} \end{Bmatrix}_{z=0} \qquad (6.3.9)$$

The reflection and transmission matrices are defined as in equation (6.3.8) with $[\tilde{S}]$ replacing $[S]$

6.3.3 Acoustic Field

In the MWR the acoustic field inside the nonuniform duct section is not immediately obtainable from the solution to the transmission problem. To compute the acoustic variables p, w, u, v at any station z one can make recourse to the solution representation in the MWR of the form

$$\begin{Bmatrix} p \\ w \\ u \\ v \end{Bmatrix}_{z} = [C]_{z} \{\delta\}_{z} \qquad \text{for } 0 < z < \ell$$

where $[C]_z$ is defined by equation (6.2.8) with basis functions appropriate to the station z. Note that in the Runge-Kutta integration process applied on equation (6.2.1) one can store the intermediate transition matrix $[TS]_z$ so that

$$\{\delta\}_{z} = [TS]_{z} \{\delta\}_{z=0+\varepsilon}$$

At z = 0 the relation (6.2.4) and the matching through the interface yield, (see Section 5.1.2(ii))

$$\{\delta\}_{z=0+\varepsilon} = [C_{11}]^{-1} [C_{11}'] [M_o] \begin{Bmatrix} q^{+} \\ q^{-} \\ q^{H} \end{Bmatrix}_{z=0-\varepsilon}$$

Hence $$\{\delta\}_{z} = [TS] [C_{11}]^{-1} [C_{11}'] [M_o] \begin{Bmatrix} q^{+} \\ q^{-} \\ q^{H} \end{Bmatrix}_{z=0-\varepsilon}$$

From the transmission solution, if $\{q^{-}\}_{z=0-\varepsilon} = [REFL] \{q^{+}\}_{z=0-\varepsilon}$ and $\{q^{H}\}_{z=0-\varepsilon} [HR_1] \{q^{+}\}_{z=0-\varepsilon}$ are available then, from the above relations,

one can express p, w, u, v at z in terms of incident mode amplitudes as follows :

$$\begin{Bmatrix} p \\ w \\ u \\ v \end{Bmatrix} = [C]_z \; [TS]_z \; [C_{11}]^{-1} \; [C_{11}'] \; [M_o] \begin{bmatrix} [I] \\ [REFL] \\ [HR_1] \end{bmatrix} \{q^+\}_{z=0-\varepsilon}$$

where $[I]$ is the identity matrix, $[HR_1]$ is defined as above and can be deduced from the transmission solution, and $[C_{11}]$, $[C_{11}']$ are defined typically by relation (6.2.7).

At $z = 0$ or $z = \ell$ the acoustic solution is more readily available if one notes that :

at $z = 0$, on the interface S_1' (refer to Figure 2.4)

$$\begin{Bmatrix} p \\ w \\ u \\ v \end{Bmatrix}_{z=0-\varepsilon} = [C]_{z=0-\varepsilon} \; [M_o] \begin{Bmatrix} q^+ \\ q^- \\ qH \end{Bmatrix}_{z=0-\varepsilon}$$

$$= [C]_{z=0-\varepsilon} \; [M_o] \begin{bmatrix} [I] \\ [REFL] \\ [HR_1] \end{bmatrix} \{q^+\}_{z=0-\varepsilon}$$

at $z = \ell$, on the interface S_2' in Figure 2.4

$$\begin{Bmatrix} p \\ w \\ u \\ v \end{Bmatrix}_{z=\ell+\varepsilon} = [C]_{z=\ell+\varepsilon} \; [M_\ell] \begin{Bmatrix} q^+ \\ q^- \\ qH \end{Bmatrix}_{z=\ell+\varepsilon}$$

$$= [C]_{z=\ell+\varepsilon} \; [M_\ell] \begin{bmatrix} [TRAN] \\ [0] \\ [HR_2] \end{bmatrix} \{q^+\}_{z=0-\varepsilon}$$

where $[HR_2]$ is defined by $\{q^H\}_{z=\ell+\varepsilon} = [HR_2]\{q^+\}_{z=0-\varepsilon}$ and can be deduced from the transmission solution.

6.4 POWER TRANSMISSION

In order to assess the acoustic performance of duct nonuniformities and duct linings it is often convenient to compare incident acoustic power and transmitted acoustic power. This is a straightforward procedure in ducts with no flow. When a mean flow is present the problem is more complicated, and it is by no means clear how acoustic energy density and energy flux are to be defined in the general case when the flow is nonuniform.

Recently, Eversman [103] has reviewed the two commonly used definitions of acoustic energy flux in the literature, which are classified by Candel [105] as Type I (typified by the Morfey [106] relationships) and Type II (typified by the Ryshov and Shefter [107] relationships). The two types of definitions are often used interchangeably as a basis for simple calculations of insertion loss or transmission loss in hardwalled ducts. When the duct has acoustically absorptive walls neither of the two flux expressions gives correct results, and then additional source terms must be taken into account [103].

In the following study formulae are developed for the hardwall case. The acoustic power at a given duct cross-section, propagating axially, is defined as the integral over the cross-sectional area

$$W = \int_A I \, dA \tag{6.4.1}$$

where the acoustic intensity, I is given by

$$I = \frac{\rho_r c_r^3}{4}\left[(1 + M_o^2)(pw^* + p^*w) + 2M_o\left(\rho_o c_o ww^* + \frac{1}{\rho_o c_o} pp^*\right)\right] \tag{6.4.2}$$

where * denotes complex conjugate.

This is consistent with the Morfey definition and is written in terms of the present nondimensional variables.

In either of the two uniform ducts (incident or transmitting side) the solutions for $p(r,z)$ and $w(r,z)$ are readily obtainable from the eigenproblem in the form of modal matrices $[M]$ (see Section 6.2.1).

Thus, in general

$$\underset{4x1}{\begin{Bmatrix} p \\ w \\ u \\ v \end{Bmatrix}} = \underset{4x4N}{[C]} \; \underset{4Nx4N}{[M]} \; \underset{4Nx1}{\begin{Bmatrix} q^+ \\ q^- \\ q^H \end{Bmatrix}}$$

$$= \begin{bmatrix} C_p & & & \\ & C_w & & \\ & & C_u & \\ & & & C_v \end{bmatrix} \begin{bmatrix} M_p \\ M_w \\ M_u \\ M_v \end{bmatrix} \begin{Bmatrix} q^+ \\ q^- \\ q^H \end{Bmatrix} \tag{6.4.3}$$

Hence, from equation (6.4.3)

$$p = [C_p][M_p^+ \; M_p^- \; M_p^H] \begin{Bmatrix} q^+ \\ q^- \\ q^H \end{Bmatrix} \tag{6.4.4}$$

$$w = \underset{1xN}{[C_w]}\underset{Nx4N}{[M_w^+ \; M_w^- \; M_w^H]} \underset{4Nx1}{\begin{Bmatrix} q^+ \\ q^- \\ q^H \end{Bmatrix}}$$

The relations (6.4.4) and (6.4.2) are substituted into equation (6.4.1) to yield, at $z = 0$

$$W = \frac{\rho_r c_r^3}{4} \begin{Bmatrix} q^+ \\ q^- \\ q^H \end{Bmatrix} \begin{bmatrix} P_a^{++} & P_a^{+-} & P_a^{+H} \\ P_a^{-+} & P_a^{--} & P_a^{-H} \\ P_a^{H+} & P_a^{H-} & P_a^{HH} \end{bmatrix} \begin{Bmatrix} q^+ \\ q^- \\ q^H \end{Bmatrix}^* \tag{6.4.5}$$

where the components of the power matrix $[P_a]$ are typically given by

$$[P_a^{+-}] = (1 + M_o^2)\left([M_p^{+}]^T [E] [M_w^{-}]^* + [M_w^{+}]^T [E] [M_p^{-}]^*\right)$$

$$+ 2M_o\left(\rho_o c_o [M_w^{+}]^T [E] [M_w^{-}]^* + \frac{1}{\rho_o c_o} [M_p^{+}]^T [E] [M_p^{-}]^*\right)$$

with

$$\underset{NxN}{[E]} = \int_0^1 \underset{Nx1}{\left\{\cos \kappa_n R_1 \eta\right\}} \underset{1xN}{\left[\cos \kappa_m^* R_1 \eta\right]} 2\pi R_1^2 \eta \, d\eta$$

For other components of $[P_a]$ the two superscripts are replaced consistently.

If the hydrodynamic modes are excluded in power transmission computations (furthermore, for hardwalled ducts the contributions of $[P_a^{+-}]$ and $[P_a^{-+}]$ are cancelled) the incident power W_i and the reflected power W_r can be expressed as follows :

$$W_i = \{q^+\}^T [P_a^{++}] \{q^+\}^* \quad , \quad W_r = \{q^+\}^T [P_a^{--}] \{q^-\}^* \qquad (6.4.6)$$

If each incident mode is assumed to carry a unit of energy the amplitude of incident mode i can be deduced :

$$1 = \frac{\rho_r c_r^3}{4} q_i^+ P_{a\,ii}^{++} q_i^{+*}$$

or

$$\left|q_i^+\right| = 2 / c_r \sqrt{\rho_r c_r P_{a\,ii}^{++}} \qquad (6.4.7)$$

As in the no-flow case (Chapter 5) the reflected power W_r and the transmitted power W_t can be calculated as follows :

$$W_r = \{q^+\}^T [REFL]^T [P_a^{--}] \; [REFL]^* \{q^+\}^* \qquad (6.4.8)$$

$$W_t = \{q^+\}^T [TRAN]^T [P_b^{++}] \; [TRAN]^* \{q^+\}^* \qquad (6.4.9)$$

where $[P_b]$ is the power matrix at $z = \ell$, and [REFL] and [TRAN] are coefficient matrices from the transmission problem.

6.5 UNIFORM DUCT RESULTS AND DISCUSSIONS

The uniform duct geometry in which the general computational scheme reduces to certain special cases may serve as a test of accuracy. Many general conclusions in the no-flow case such as the inherent effects of heavily cut-off modes, high frequency, high angular mode, high-valued lining admittance, long duct are still applicable for the flow case. The following results give gross indications of the consistency of the present formulation.

(i) Convergence to the hardwall case

The computation of the modal coefficients in a uniform hardwalled duct provides a means to determine the accuracy of the uniform flow terms in the equations of formulation. To this end a hardwalled duct with $R_1 = R_2 = 1.0$, $\ell = 0.5$ is considered at Mach number 0.5 and frequency $k_r R_1 = 5.0$. Table 6.1 presents the diagonal terms of coefficient matrices for the symmetric angular mode, to be compared with exact values (see Section 5.1.3(iv)). Convergence towards exact solutions is observed with increasing the number of basis functions (BF). In fact, the agreement is very good with as few as three basis functions.

(ii) Convergence to the softwall case

Transmission in a uniform softwalled duct is also considered and provides a convenient check case. The softwall case is more challenging to the MWR since the basis functions used do not satisfy the duct-wall boundary condition as for the hardwall case. Tables 6.2 and 6.3 show the results for a straight softwalled duct with specific lining admittance $A = 0.72 - 0.42i$ at $k_r R_1 = 8.0$, $m_o = 2$, Mach number -0.5 with $\ell = 0.2$ and $\ell = 0.5$ respectively. The convergence trend is still observed but much slower than for the hardwall case above. When the duct becomes longer the accuracy of the results decreases because the exponential behaviour of decaying modes is dependent upon the length scale. This combination of parameters is considered computationally challenging to numerical methods.

For this frequency the MWR used the no-flow basis functions. At lower frequencies the effect of cut-off modes may become severe. For $k_r R_1 \approx 1$, modified flow basis functions (Section 4.2.4(i)) should give a higher rate of convergence.

(iii) Hydrodynamic mode coefficients

In the flow model used hydrodynamic modes play a trivial role in acoustic computations. Results presented here serve merely as a check-out of consistency for the mathematical method.

In the analysis of the transfer matrix [TF] in equation (6.3.6) it is noted that if only hydrodynamic modes are introduced at the inlet one can write, from equation (6.3.6)

$$\{q^H\}_{z=\ell} = [S^{HH}] \{q^H\}_{z=0}$$

In a uniform duct with a uniform flow profile the transfer matrix $[S^{HH}]$ is diagonal and exactly given by

$$S^{HH}_{nn} = e^{-ik^H_{zn}\ell}$$

where $\frac{k^H_{zn}}{k_r} = \frac{1}{\bar{W}_o}$ (See Section 4.2.5(ii))

In Tables 6.1, 6.2 and 6.3 the hydrodynamic mode coefficients referred to z = 0 are diagonal terms of $[S^{HH}]$ (computed by the MWR) multiplied by the factor $e^{+ik^H_{zn}\ell}$. At the flow speed, Mach number $|M_o| = 0.5$, a very good agreement is obtained. At lower speed the agreement degrades as the wavelength becomes shorter (from $\frac{k^H_z}{k} = \frac{1}{\bar{W}_o}$). However, the accuracy of hydrodynamic mode coefficients then seems not to affect seriously that of acoustic solution representation.

Results for nonuniform ducts with flow will be presented in Chapter 8 and comparisons will be made against those of the FEM.

Geometry : Uniform , $R_1 = R_2 = 1.0$, $\ell = 0.5$,

Characteristics : Hardwalled Duct with Flow , $M_1 = 0.5$

$k_r R_1 = 5.0$, Angular Mode $m_o = 0$,

Two Cut-on Modes

Incident Mode i	Reflection Coefficients in Mode i		
	MWR(3BF)	MWR(5BF)	EXACT
1	.0000 + .0000 i	.0000 + .0000 i	.0000 + .0000 i
2	.0000 + .0000 i	.0000 + .0000 i	.0000 + .0000 i
3	.0000 + .0000 i	.0000 + .0000 i	.0000 + .0000 i
Incident Mode i	Direct Transmission Coefficients at z = ℓ in Mode i		
	MWR(3BF)	MWR(5BF)	EXACT
1	-.0957 - .9954 i	-.0957 - .9954 i	-.0957 - .9954 i
2	.6736 - .7390 i	.6765 - .7364 i	.6773 - .7357 i
3	-.0090 + .0935 i	-.0095 + .0989 i	-.0096 + .0997 i
Incident Mode i	Transmission Coefficients referred to z = 0 in Mode i		
	MWR(3BF)	MWR(5BF)	EXACT
1	1.0000 + .0000 i	1.0000 + .0000 i	1.0000 + .0000 i
2	1.0000 + .0000 i	1.0000 + .0000 i	1.0000 + .0000 i
3	.9998 + .0000 i	1.0000 + .0000 i	1.0000 + .0000 i
Incident Mode i	Hydrodynamic Mode Coefficients referred to z = 0 in Mode i		
	MWR(3BF)	MWR(5BF)	EXACT
1	.9999 - .0003i	.9995 + .0005 i	1.0000 + .0000 i
2	.9999 - .0003i	.9995 + .0005 i	1.0000 + .0000 i
3	.9999 - .0003i	.9995 + .0005 i	1.0000 + .0000 i

TABLE 6.1 Comparison of Reflection, Transmission and Hydrodynamic Mode Coefficients by MWR with Exact Values for a Uniform Hardwalled Duct with Flow.

Geometry : Uniform , $R_1 = R_2 = 1.0$, $\ell = 0.2$

Characteristics : Softwalled Duct with Flow , $A = (0.72 - 0.42i)$, $M_1 = -0.5$, $k_r R_1 = 8.0$, Angular Mode $m_o = 2$, All Decaying Modes

Incident Mode i	Reflection Coefficients in Mode i		
	MWR(5BF)	MWR(7BF)	EXACT
1	.000 + .000 i	.000 + .000 i	.000 + .000 i
2	.000 + .000 i	.000 + .000 i	.000 + .000 i
3	.000 + .000 i	.000 + .000 i	.000 + .000 i
Incident Mode i	Direct Transmission Coefficients at z = ℓ in Mode i		
	MWR(5BF)	MWR(7BF)	EXACT
1	-.927 - .287 i	-.929 - .283 i	-.935 - .272 i
2	-.359 - .748 i	.388 - .748 i	-.429 - .744 i
3	.109 - .223 i	.106 - .226 i	.102 - .237 i
Incident Mode i	Transmission Coefficients referred to z = 0 in Mode i		
	MWR(5BF)	MWR(7BF)	EXACT
1	1.000 - .000 i	1.000 + .000 i	1.000 + .000 i
2	1.000 + .000 i	1.000 + .000 i	1.000 + .000 i
3	1.000 + .000 i	1.000 + .000 i	1.000 + .000 i
Incident Mode i	Hydrodynamic Mode Coefficients referred to z = 0 in Mode i		
	MWR(5BF)	MWR(7BF)	EXACT
1	1.000 - .000 i	1.000 - .000 i	1.000 + .000 i
2	1.000 - .000 i	1.000 - .000 i	1.000 + .000 i
3	1.000 - .000 i	1.000 - .000 i	1.000 + .000 i

Table 6.2 Comparison of Reflection, Transmission and Hydrodynamic Mode Coefficients by MWR with Exact Values for a Uniform Softwalled Duct with Flow, $\ell = 0.2$.

Geometry : Uniform , $R_1 = R_2 = 1.0$, $\ell = 0.5$

Characteristics : Softwalled Duct with Flow , $A = (0.72 - 0.42i)$, $M_1 = -0.5$, $k_r R_1 = 8.0$, Angular Mode $m_o = 2$, All Decaying Modes

Incident Mode i	Reflection Coefficients in Mode i		
	MWR(5BF)	MWR(7BF)	EXACT
1	.000 + .000 i	.000 + .000 i	.000 + .000 i
2	.000 + .000 i	.000 + .000 i	.000 + .000 i
3	.000 + .000 i	.000 + .000 i	.000 + .000 i
Incident Mode i	Direct Transmission Coefficients at z = ℓ in Mode i		
	MWR(5BF)	MWR(7BF)	EXACT
1	.632 - .678 i	.626 - .688 i	.608 - .710 i
2	.206 + .593 i	.260 + .598 i	.341 + .592 i
3	-.029 - .010 i	-.030 - .010 i	-.033 - .008 i
Incident Mode i	Transmission Coefficients referred to z = 0 in Mode i		
	MWR(5BF)	MWR(7BF)	EXACT
1	1.000 + .000 i	1.000 + .000 i	1.000 + .000 i
2	1.000 + .000 i	1.000 + .000 i	1.000 + .000 i
3	1.000 + .000 i	.999 + .002 i	1.000 + .000 i
Incident Mode i	Hydrodynamic Mode Coefficients referred to z = 0 in Mode i		
	MWR(5BF)	MWR(7BF)	EXACT
1	1.000 - .001 i	1.000 - .001 i	1.000 + .000 i
2	1.000 - .001 i	1.000 - .001 i	1.000 + .000 i
3	1.000 - .001 i	1.000 - .001 i	1.000 + .000 i

Table 6.3 Comparison of Reflection, Transmission and Hydrodynamic Mode Coefficients by MWR with Exact Values for a Uniform Softwalled Duct with Flow, $\ell = 0.5$.

CHAPTER 7

FEM FOR SOUND TRANSMISSION IN DUCTS WITH FLOW

The FEM formulation of the acoustic problem in ducts with flow is similar to that for the no-flow case with conservation equations. In the flow case the mean flow field is assumed to be available and nodal values are stored for each node and each element.

The governing acoustic equations in the nonuniform field are :

$$\left(ik_r + \frac{\partial U_o}{\partial r}\right) u + \frac{\partial U_o}{\partial z} w + U_o \frac{\partial u}{\partial r} + \bar{W}_o \frac{\partial u}{\partial z} + \frac{1}{\bar{\rho}_o} \frac{\partial p}{\partial r} = 0 \tag{7.0.1}$$

$$\left(ik_r + \frac{U_o}{r}\right) v + U_o \frac{\partial v}{\partial r} + \bar{W}_o \frac{\partial v}{\partial z} - \frac{im_o}{\bar{\rho}_o} \frac{p}{r} = 0 \tag{7.0.2}$$

$$\left(ik_r + \frac{\partial \bar{W}_o}{\partial z}\right) w + U_o \frac{\partial w}{\partial r} + \bar{W}_o \frac{\partial w}{\partial z} + \frac{1}{\bar{\rho}_o} \frac{\partial p}{\partial z} - \frac{1}{\gamma \bar{p}_o \bar{\rho}_o} \frac{\partial \bar{p}_o}{\partial z} p = 0 \tag{7.0.3}$$

$$ik_r p + U_o \frac{\partial p}{\partial r} + \bar{W}_o \frac{\partial p}{\partial z} + \gamma \bar{p}_o \left[\frac{1}{r} \frac{\partial (ru)}{\partial r} - im_o \frac{v}{r} + \frac{\partial w}{\partial z}\right]$$
$$+ \frac{\partial \bar{p}_o}{\partial z} w + \gamma \left[\frac{1}{r} \frac{\partial (rU_o)}{\partial r} + \frac{\partial \bar{W}_o}{\partial z}\right] p = 0 \tag{7.0.4}$$

The boundary condition at the duct wall, r = R(z) is

$$\underline{V} \cdot \underline{\nu} = Ap - \frac{i\bar{V}_{o\tau}}{k_r} \frac{\partial}{\partial \tau} (Ap) \tag{7.0.5}$$

or $$u \cos \alpha - w \sin \alpha = Ap - \frac{i\bar{W}_o}{k_r} \left[\frac{\partial (Ap)}{\partial z} + A \tan \alpha \frac{\partial p}{\partial r}\right] \text{ at } r = R(z) \tag{7.0.6}$$

7.1 FEM FORMULATION

As in a standard FEM procedure one assumes that $\tilde{p} = [N]\{p\}$, $\tilde{u} = [N]\{u\}$, $\tilde{v} = [N]\{v\}$ and $\tilde{w} = [N]\{w\}$ are approximate solutions for dependent variables, where components of $[N]$ are shape functions defined implicitly via elements, $\{p\}$, $\{u\}$, $\{v\}$ and $\{w\}$ are nodal values appropriate to variables. The concept was expounded in Chapter 3 and applied previously in Chapters 4 and 5.

If the trial solutions above are substituted into equations (7.0.1) - (7.0.4), in general, one obtains the residuals :

$$R_1 = \left(ik + \frac{\partial U_o}{\partial r}\right) \tilde{u} + \frac{\partial U_o}{\partial z} \tilde{w} + U_o \frac{\partial \tilde{u}}{\partial r} + \bar{W}_o \frac{\partial \tilde{u}}{\partial z} + \frac{1}{\bar{\rho}_o} \frac{\partial \tilde{p}}{\partial r} \tag{7.1.1}$$

$$R_2 = \left(ik_r + \frac{U_o}{r}\right) \tilde{v} + U_o \frac{\partial \tilde{v}}{\partial r} + \bar{W}_o \frac{\partial \tilde{v}}{\partial z} - \frac{im_o}{\bar{\rho}_o} \frac{\tilde{p}}{r} \tag{7.1.2}$$

$$R_3 = \left(ik_r + \frac{\partial \bar{W}_o}{\partial z}\right) \tilde{w} + U_o \frac{\partial \tilde{w}}{\partial r} + \bar{W}_o \frac{\partial \tilde{w}}{\partial z} + \frac{1}{\bar{\rho}_o} \frac{\partial \tilde{p}}{\partial z} - \frac{1}{\gamma \bar{\rho}_o \bar{p}_o} \frac{\partial \bar{p}_o}{\partial z} \tilde{p} \tag{7.1.3}$$

$$R_4 = \left(ik_r + \frac{\gamma}{r} \frac{\partial (rU_o)}{\partial r} + \gamma \frac{\partial \bar{W}_o}{\partial z}\right) \tilde{p} + \bar{U}_o \frac{\partial \tilde{p}}{\partial r} + \bar{W}_o \frac{\partial \tilde{p}}{\partial z} - \gamma \bar{p}_o \, im_o \frac{\tilde{v}}{r}$$

$$+ \frac{\partial \bar{p}_o}{\partial z} \tilde{w} + \gamma \bar{p}_o \left[\frac{1}{r} \frac{\partial (r\tilde{u})}{\partial r} + \frac{\partial \tilde{w}}{\partial z}\right] \tag{7.1.4}$$

With weighting functions W_i , $i = 1,2,3...n_n$ (n_n is the number of nodes in the discretized mesh) the residuals are weighted over the whole appropriate domain as follows :

$$\int_A W_i \, R_1 \, 2\pi \, r \, dr \, dz = 0 \tag{7.1.5}$$

$$\int_A W_i \, R_2 \, 2\pi \, r \, dr \, dz = 0 \tag{7.1.6}$$

$$\int_A W_i \, R_3 \, 2\pi \, r \, dr \, dz = 0 \tag{7.1.7}$$

$$\int_A W_i \, R_4 \, 2\pi \, r \, dr \, dz = 0 \tag{7.1.8}$$

for $i = 1,2...n_n$

Consider the last term in equation (7.1.8)

$$\int_A W_i \gamma \bar{p}_o \left(\frac{1}{r} \frac{\partial (r\tilde{u})}{\partial r} + \frac{\partial \tilde{w}}{\partial z}\right) 2\pi \, r \, dr \, dz.$$

Using the divergence theorem one can expose the boundary terms as follows :

$$\int_A W_i \gamma \bar{p}_o \left[\frac{1}{r} \frac{\partial (r\tilde{u})}{\partial r} + \frac{\partial \tilde{w}}{\partial z} \right] 2\pi \, r \, dr \, dz = \int_A W_i \gamma \bar{p}_o \frac{\tilde{u}}{r} 2\pi \, r \, dr \, dz$$

$$+ \int_A W_i \gamma \bar{p}_o \left(\frac{\partial \tilde{u}}{\partial r} + \frac{\partial \tilde{w}}{\partial z} \right) 2\pi \, r \, dr \, dz$$

$$= \int_A W_i \gamma \bar{p}_o \frac{\tilde{u}}{r} \, 2\pi \, r \, dr \, dz + \int_C W_i \gamma \bar{p}_o r \, (\tilde{u},\tilde{w}) \cdot \underline{\nu} \, 2\pi \, ds$$

$$- \int_A \frac{\partial}{\partial r} \left(W_i \gamma \bar{p}_o r \right) \tilde{u} \, 2\pi \, dr \, dz$$

$$- \int_A \frac{\partial}{\partial z} \left(W_i \gamma \bar{p}_o r \right) \tilde{w} \, 2\pi \, dr \, dz$$

$$= \int_{C_3} \gamma \bar{p}_o W_i \, \underline{\tilde{V}} \cdot \underline{\nu} \, 2\pi \, R \, ds + \int_{C_2} \gamma \bar{p}_o W_i \, w_2 \, 2\pi \, r \, dr$$

$$- \int_{C_1} \gamma \bar{p}_o W_i \, w_1 \, 2\pi \, r \, dr - \int_A \frac{\partial}{\partial r} \left(\gamma \bar{p}_o W_i \right) \tilde{u} \, 2\pi \, r \, dr \, dz$$

$$- \int_A \frac{\partial}{\partial z} \left(\gamma \bar{p}_o W_i \right) \tilde{w} \, 2\pi \, r \, dr \, dz \qquad (7.1.9)$$

where $\underline{\tilde{V}} = (\tilde{u},\tilde{w})$ and $\underline{\nu}$ is unit normal in (r,z) plane. The end boundary conditions $\tilde{w} = w_1$ on C_1, and $\tilde{w} = w_2$ on C_2 have been applied, where w_1 and w_2 are appropriate solutions in the uniform ducts.

For the Galerkin process the weighting functions are shape functions, i.e. $W_i \equiv N_i$. Thus, with the relation (7.1.9) the residual equations (7.1.5) - (7.1.8) can be rewritten as four sets of n_n linear equations, omitting the multiplicative factor 2π for convenience.

$$0 = \int_A [N]^T R_1 \, r \, dr \, dz = \left[\iint_A \left(ik_r + \frac{\partial U_o}{\partial r} \right) [N]^T[N] \, r \, dr \, dz + \int_A U_o [N]^T [N]_r \, r \, dr \, dz \right.$$
$$\left. + \int_A \bar{W}_o [N]^T [N]_z \, r \, dr \, dz \right] \{u\}$$
$$+ \left[\int_A \frac{\partial U_o}{\partial z} [N]^T[N] \, r \, dr \, dz \right] \{w\}$$
$$+ \left[\int_A \frac{1}{\bar{\rho}_o} [N]^T [N]_r \, r \, dr \, dz \right] \{p\} \qquad (7.1.10)$$

$$0 = \int_A [N]^T R_2 \, r \, dr \, dz = \left[\iint_A \left(ik_r + \frac{U_o}{r} \right) [N]^T[N] \, r \, dr \, dz + \int_A U_o [N]^T [N]_r \, r \, dr \, dz \right.$$
$$\left. + \int_A \bar{W}_o [N]^T [N]_z \, r \, dr \, dz \right] \{v\}$$
$$+ \left[- \int_A \frac{im_o}{\bar{\rho}_o r} [N]^T[N] \, r \, dr \, dz \right] \{p\} \qquad (7.1.11)$$

$$0 = \int_A [N]^T R_3 \, r \, dr \, dz = \left[\iint_A \left(ik_r + \frac{\partial \bar{W}_o}{\partial z} \right) [N]^T[N] \, r \, dr \, dz + \int_A U_o [N]^T [N]_r \, r \, dr \, dz \right.$$
$$\left. + \int_A \bar{W}_o [N]^T [N]_z \, r \, dr \, dz \right] \{w\}$$

$$+\left[\int_A \frac{1}{\bar{\rho}_o}[N]^T[N]_z\, r\, dr\, dz - \int_A \frac{1}{\gamma \bar{p}_o \bar{\rho}_o}\frac{\partial \bar{p}_o}{\partial z}[N]^T[N]\, r\, dr\, dz\right]\{p\} \qquad (7.1.12)$$

$$0 = \int_A [N]^T R_4\, r\, dr\, dz = \left[\int_A \left(ik_r + \frac{\gamma}{r}\frac{\partial(rU_o)}{\partial r} + \gamma\frac{\partial \bar{W}_o}{\partial z}\right)[N]^T[N]\, r\, dr\, dz\right.$$

$$\left. + \int_A U_o[N]^T[N]_r\, r\, dr\, dz + \int_A \bar{W}_o[N]^T[N]_z\, r\, dr\, dz\right]\{p\}$$

$$+\left[-\int_A \frac{\partial}{\partial r}\left(\gamma \bar{p}_o[N]^T\right)[N]\, r\, dr\, dz\right]\{u\}$$

$$+\left[-\int_A \gamma \bar{p}_o \frac{im_o}{r}[N]^T[N]\, r\, dr\, dz\right]\{v\}$$

$$+\left[\int_A \frac{\partial \bar{p}_o}{\partial z}[N]^T[N]\, r\, dr\, dz - \int_A \frac{\partial}{\partial z}\left(\gamma \bar{p}_o[N]^T\right)[N]\, r\, dr\, dz\right]\{w\}$$

$$+\int_{C_3} \gamma \bar{p}_o[N]\, \tilde{\underline{v}}\cdot\underline{\nu}\, R\, ds + \int_{C_2} \gamma \bar{p}_o[N]^T w_2\, r\, dr$$

$$-\int_{C_1} \gamma \bar{p}_o[N]^T w_1\, r\, dr \qquad (7.1.13)$$

where $$[N]_r = \frac{\partial}{\partial r}[N] = [N_{ir}] = \left[\frac{\partial N_i}{\partial r}\right], \quad i = 1,2,\ldots n_n$$

$$[N]_z = \frac{\partial}{\partial z}[N] = [N_{iz}] = \left[\frac{\partial N_i}{\partial z}\right], \quad i = 1,2,\ldots n_n$$

and n_n is the number of nodes in the discretization.

(i) Interior elements. For each 8-node finite element equations (7.1.10) - (7.1.13) give 8 x 4 linear equations representing interactions of four dependent variables u, v, w and p at 8 nodes, in the form of a 32 x 32 element matrix. If these element matrices are assembled by standard FEM techniques over the whole domain A excluding the boundaries C_1, C_2 and C_3 one obtains a system matrix [K] of order $4n_n \times 4n_n$, where n_n is the total number of nodes in the domain. [K] can be derived pointwise from equations (7.1.10) - (7.1.13) in the following way :

$$[K]\ \{\delta\} = \left[\int_A [K']\ r\,dr\,dz\right] \{\delta\} \qquad (7.1.14)$$

where $\{\delta\} = [w_i\ u_i\ v_i\ p_i]^T$, $i = 1,2,3\ldots n_n$

and [K'] is consistent with the structure of $\{\delta\}$ and given by :

$$[K'] = \begin{bmatrix} \left(ik_r + \frac{\partial \bar{W}_o}{\partial z}\right) N_i N_j + U_o N_i N_{jr} + \bar{W}_o N_i N_{jz} & 0 & 0 & \frac{1}{\bar{\rho}_o} N_i N_{jz} - \frac{1}{\gamma \bar{p}_o \bar{\rho}_o} \frac{\partial \bar{p}_o}{\partial z} N_i N_j \\ \frac{\partial U_o}{\partial z} N_i N_j & \left(ik_r + \frac{\partial U_o}{\partial r}\right) N_i N_j + U_o N_i N_{jr} + \bar{W}_o N_i N_{jr} & 0 & \frac{1}{\bar{\rho}_o} N_i N_{jr} \\ 0 & 0 & \left(ik_r + \frac{U_o}{r}\right) N_i N_j + U_o N_i N_{jr} + \bar{W}_o N_i N_{jz} & -\frac{im_o}{\bar{\rho}_o r} N_i N_j \\ \frac{\partial \bar{p}_o}{\partial z} N_i N_j - \gamma \frac{\partial \bar{p}_o}{\partial z} N_i N_j - \gamma \bar{p}_o N_{iz} N_j & -\gamma \bar{p}_o N_{ir} N_j & -\gamma \bar{p}_o \frac{im_o}{r} N_i N_j & \left(ik_r + \frac{\gamma}{r}\frac{\partial (rU_o)}{\partial r} + \gamma \frac{\partial \bar{W}_o}{\partial z}\right) N_i N_j + U_o N_i N_{jr} + \bar{W}_o N_i N_{jz} \end{bmatrix} \qquad (7.1.15)$$

for $(i = 1,2,\ldots n_n)$ and $(j = 1,2,3,\ldots n_n)$.

(ii) Boundary conditions. At this stage the boundary conditions have not yet been included. The last three terms in equation (7.1.13) represent the boundary conditions for the problem under study. The term

$$\int_{C_3} \gamma \bar{p}_o [N]^T \tilde{\underline{v}} \cdot \underline{\nu} \, R \, ds$$

is recognized as involving the duct-wall boundary condition given by equations (7.0.5) - (7.0.6). Hence

$$\int_{C_3} \gamma \bar{p}_o [N]^T \tilde{\underline{v}} \cdot \underline{\nu} \, R \, ds = \left[\int_{C_3} \gamma \bar{p}_o \, N_i \left(AN_j - \frac{i\bar{V}_{o\tau}}{k_r} \frac{\partial}{\partial \tau} (AN_j) \right) R \, ds \right] \{p\} \quad (7.1.16)$$

for $i = 1,2,3,\ldots n_n$, $j = 1,2,3,\ldots n_n$

can be integrated over line finite elements on boundary C_3, and superimposed onto the system matrix $[K]$ at appropriate locations, i.e. in equation (7.1.16) $N_i \equiv 0$ unless i corresponds to a node on C_3. It is noted that for the hardwall case, i.e. $A = 0$, the integral vanishes and the duct-wall boundary condition is implicitly taken care of by interior finite elements. The boundary condition treated in this way is the natural boundary condition, which has been extensively addressed in the general context of the MWR and previously in the context of the eigenproblem and transmission problem with the FEM.

A second treatment is to force the boundary condition to be satisfied by making use of the explicit form of the FEM system matrix But, in general, the condition, from equation (7.0.6)

$$u \cos\alpha - w \sin\alpha = Ap - \frac{i\bar{W}_o}{k_r} \left[\frac{\partial (Ap)}{\partial z} + A \tan\alpha \frac{\partial p}{\partial r} \right]$$

cannot be forced explicitly as in the no-flow case or the eigenproblem because of the derivative terms. However, here one can recourse to the

concept of the MWR and establish the boundary residual

$$R_B = \tilde{u} \cos\alpha - \tilde{w} \sin\alpha - A\tilde{p} + \frac{i\bar{W}_o}{k_r}\left[\frac{\partial(A\tilde{p})}{\partial z} + A \tan\alpha \frac{\partial \tilde{p}}{\partial r}\right]$$

This can be weighted by implicitly defined global shape functions N_i over the whole duct-wall boundary to obtain

$$\int_{C_3} N_i \, R_B \, 2\pi R \, ds = 0 \quad , \quad i = 1,2,3,\ldots n_n$$

where $N_i \equiv 0$ unless i corresponds to a node on C_3. Then, one forces the duct-wall boundary condition by deleting the rows of the original Galerkin system matrix [K] in equation (7.1.14), corresponding to nodes on the boundary C_3, and assembling the above expression in their place. The discrepancy resulting from the natural and forced boundary conditions will be discussed later.

The last two terms in equation (7.1.13) are involved in matching procedures at the ends of the nonuniformity, which are detailed in the following section.

7.2 MATCHING OF THE NONUNIFORM SECTION TO UNIFORM SECTIONS

Two methods of matching at the ends of the nonuniformity are considered for the flow case : least-square matching and point matching (or collocation). The point matching method is approached when the transmission problem involving hydrodynamic modes in a uniform geometry is not solved satisfactorily by the "pure" least-square matching. It will be discussed further.

7.2.1 Least-Square Matching

The least-square procedure is carried out as for the no-flow case formulated with conservation equations (see Section 5.2.2) except that, for the flow case, there exist hydrodynamic modes in the

semi-infinite duct solutions. If the solutions to the acoustic propagation problem are sought in the form of matrices of transmission and reflection coefficients as in the MWR (see Section 6.3.2) two cases, depending upon the direction of the mean flow, are distinguished :

(i) Flow in the positive z direction.

Assuming the contributions of the hydrodynamic modes in the uniform ducts to be of the form

$$\left.\begin{aligned} p^H &\equiv 0 \\ w^H &= \sum_{n=1}^{\infty} a_n^H J_{wn}^H \approx \sum_{n=1}^{n_H} a_n^H J_{wn}^H = [J_w^H]\ \{a^H\} \\ u^H &= \sum_{n=1}^{\infty} a_n^H J_{un}^H \approx \sum_{n=1}^{n_H} a_n^H J_{un}^H = [J_u^H]\ \{a^H\} \\ v^H &= \sum_{n=1}^{\infty} a_n^H J_{vn}^H \approx \sum_{n=1}^{n_H} a_n^H J_{vn}^H = [J_v^H]\ \{a^H\} \end{aligned}\right\} \qquad (7.2.1)$$

where a_n^H are hydrodynamic mode coefficients and J_u^H , J_w^H , J_v^H are functions to be specified, one can establish the system matrix in the following way :

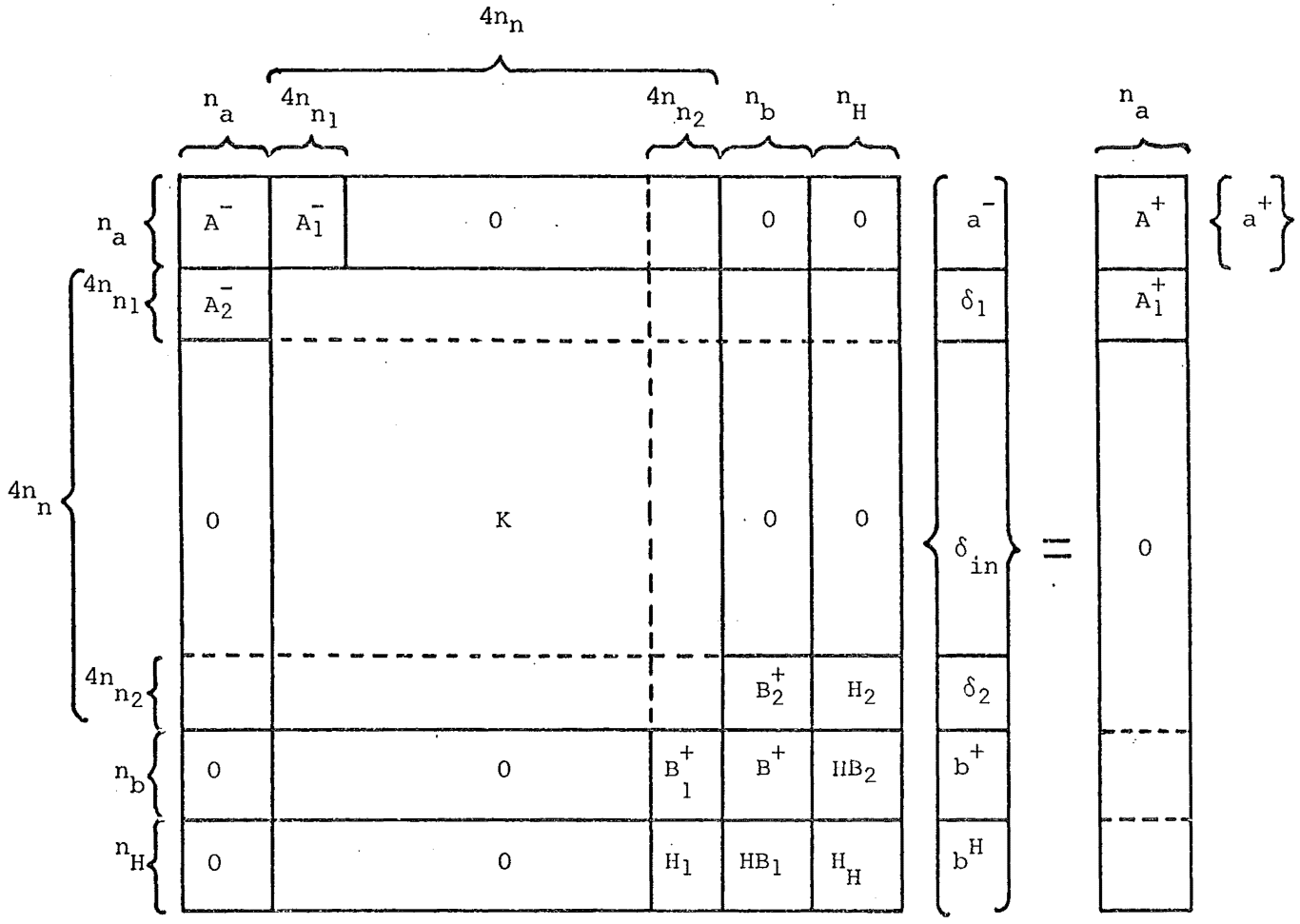

where $[K]$ and $\{\delta\} = \left[\delta_1 \,\vdots\, \delta_{in} \,\vdots\, \delta_2\right]^T$ are given by relation (7.1.14), $[b^H]$ are coefficients of the hydrodynamic modes at the outlet, and $[A^-]$, $[A_1^-]$, $[A^+]$, $[B^+]$ and $[B_1^+]$ are derived similarly as for the no-flow problem but here with the flow-case eigenfunctions (see Section 5.2.2(ii)). The matching at $z = \ell$ yields

$$[H_H]_{(n_H x n_H)} = \left[\int_{C_2} \left({}^{*H}J_{w_2 i}\, J^H_{w_2 j} + {}^{*H}J_{u_2 i}\, J^H_{u_2 j} + {}^{*H}J_{v_2 i}\, J^H_{v_2 j} \right) 2\pi\, r\, dr\right]$$

$$[HB_1]_{(n_H x n_b)} = \left[\int_{C_2} \left({}^{*H}J_{w_2 i}\, J^+_{w_2 m} + {}^{*H}J_{u_2 i}\, J^+_{u_2 m} + {}^{*H}J_{v_2 i}\, J^+_{v_2 m} \right) 2\pi\, r\, dr\right]$$

$$[H_1]_{(n_H x 4n_{n_2})} = -\int_{C_2} \left[0 \,\vdots\, {}^{*H}J_{w_2 i}\, N_k \,\vdots\, {}^{*H}J_{u_2 i} N_k \,\vdots\, {}^{*H}J_{v_2 i}\, N_k\right] 2\pi\, r\, dr$$

$$[HB_2]_{(n_b x n_H)} = \left[\int_{C_2} \left({}^{*+}J_{w_2 m}\, J^H_{w_2 i} + {}^{*+}J_{u_2 m}\, J^H_{u_2 i} + {}^{*+}J_{v_2 m}\, J^H_{v_2 i} \right) 2\pi\, r\, dr\right]$$

$$[H_2]_{(n_{n_2} x n_H)} = \left[\int_{C_2} N_k\, J^H_{w_2 i}\, \gamma \bar{p}_o\, r\, dr\right]$$

$$[B_2^+]_{(n_{n_2} x n_b)} = \left[\int_{C_2} N_k\, J^H_{w_2 i}\, \gamma \bar{p}_o\, r\, dr\right]$$

with $i = 1,2,3,\ldots n_H$ (n_H : number of hydrodynamic modes),

$j = 1,2,3,\ldots n_H$, $k = n_n - n_{n_2} + 1\,,\ n_n - n_{n_2} + 2\,,\ \ldots n_n$,

$m = 1,2,3\ldots n_b$

In addition, the matching at $z = 0$ gives

$$[A_2^-]_{(n_{n_1} x n_a)} = \left[-\int_{C_1} N_k\, J^-_{w_1 i}\, \gamma \bar{p}_o\, r\, dr\right]$$

$$[A_1^+]_{(n_{n_1} x n_a)} = \left[\int_{C_1} N_k \, J^+_{w_1 i} \, \gamma \bar{p}_o \, r \, dr \right]$$

SEE ERRATA

with $i = 1,2,3,\ldots n_a$, $k = 1,2,3,\ldots n_{n_1}$

Note that J_{w2} , J_{u2}, J_{v2} ... are eigenfunctions consistent with superscripts and subscripts and $[A_2^-]$, $[A_1^+]$, $[B_2^+]$ and $[H_2]$ just add contributions to appropriate coefficients in the system matrix, corresponding to the energy equation in the FEM formulation.

(ii) Flow in the negative direction.

The system matrix given by the FEM formulation with the least-square matching takes the form

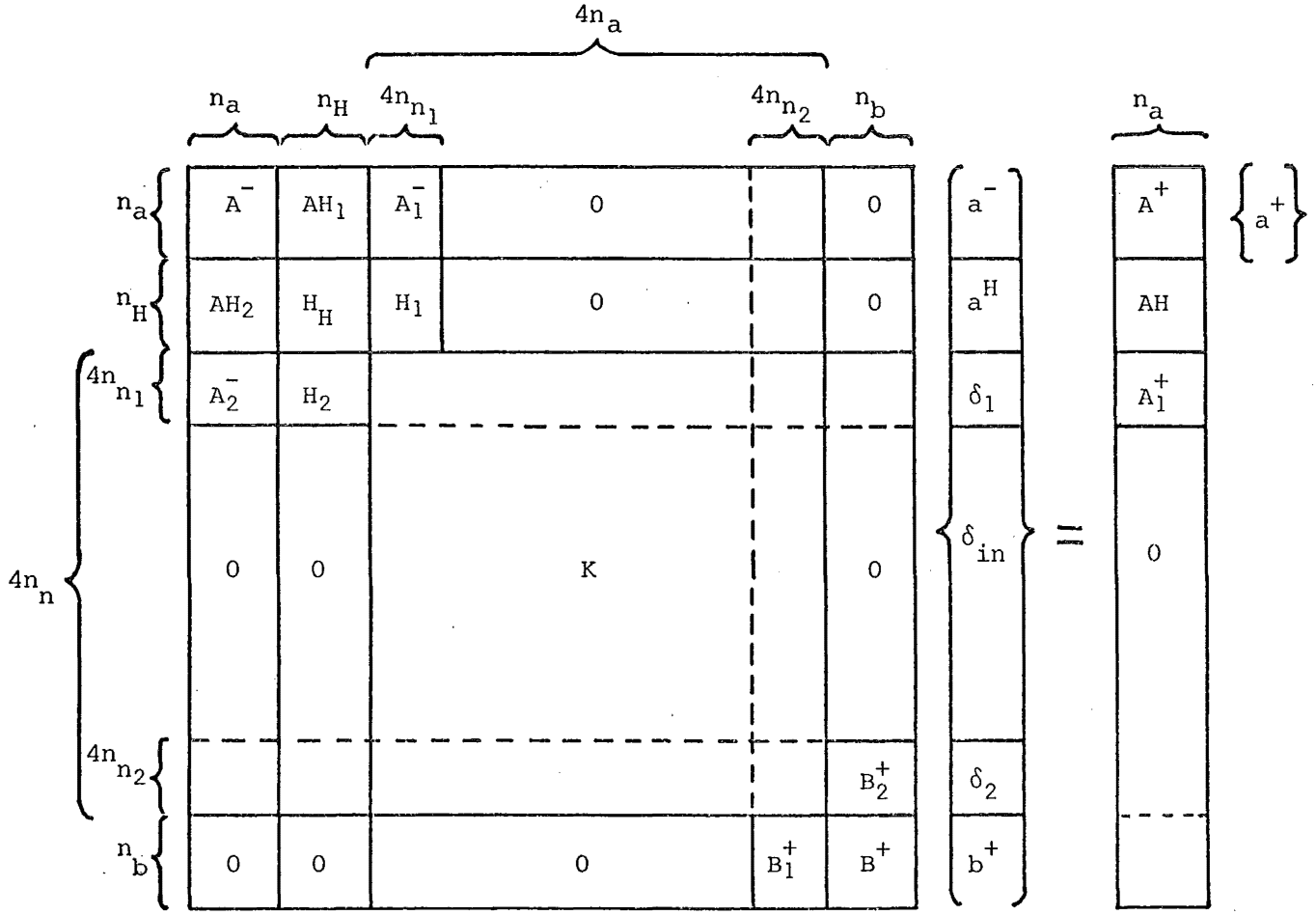

where $[K]$, $[\delta_1 \,\vdots\, \delta_{in} \,\vdots\, \delta_2]^T$, $[A^-]$, $[A_1^-]$, $[A_2^-]$, $[A^+]$, $[A_1^+]$, $[B^+]$, $[B_1^+]$, $[B_2^+]$ are defined similarly as for the case of flow in the positive z direction, being components of equation (7.1.18), $\{a^H\}$ contains coefficients of the hydrodynamic modes at the inlet. In addition,

$$[AH_1]_{(n_a x n_H)} = \left[\int_{C_1} \left({}^{*-}J_{w_1 m} \, J^H_{w_1 j} + {}^{*-}J_{u_1 m} \, J^H_{u_1 j} + {}^{*-}J_{v_1 m} \, J^H_{v_1 j} \right) 2\pi \, r \, dr \right]$$

$$[AH_2]_{(n_H x n_a)} = \left[\int_{C_1} \left({}^{*H}J_{w_1 i} \, J^-_{w_1 m} + {}^{*H}J_{u_1 i} \, J^-_{u_1 m} + {}^{*H}J_{v_1 i} \, J^-_{v_1 m} \right) 2\pi \, r \, dr \right]$$

$$[H_H]_{(n_H x n_H)} = \left[\int_{C_1} \left({}^{*H}J_{w_1 i} \, J^H_{w_1 j} + {}^{*H}J_{u_1 i} \, J^H_{u_1 j} + {}^{*H}J_{v_1 i} \, J^-_{v_1 j} \right) 2\pi \, r \, dr \right]$$

$$[H_1]_{(n_H x 4n_{n_1})} = - \int_{C_1} \left[0 \,\vdots\, {}^{*H}J_{w_1 i} \, N_k \,\vdots\, {}^{*H}J_{u_1 i} \, N_k \,\vdots\, {}^{*H}J_{v_1 i} \, N_k \right] 2\pi \, r \, dr$$

$$[H_2]_{(n_{n_1} x n_H)} = \left[- \int_{C_1} N_k \, J^H_{w_1 j} \, \gamma \bar{p}_o \, r \, dr \right]$$

$$[AH]_{(n_H x n_a)} = \left[- \int_{C_1} \left({}^{*H}J_{w_1 i} \, J^+_{w_1 m} + {}^{*H}J_{u_1 i} \, J^+_{u_1 m} + {}^{*H}J_{v_1 i} \, J^+_{v_1 m} \right) 2\pi \, r \, dr \right]$$

with $i = 1,2,3,\ldots n_H$ (n_H: number of the hydrodynamic modes), $j = 1,2,3,\ldots n_H$, $k = 1,2,3\ldots n_{n_1}$, $m = 1,2,3,\ldots n_a$.

7.2.2 Point Matching

In this computational scheme the point matching method is applied only at one end of the nonuniformity, at the other end the least-square method is still used. For convenience the point matching is performed at $z = \ell$. In this case the system matrix can be written in the form :

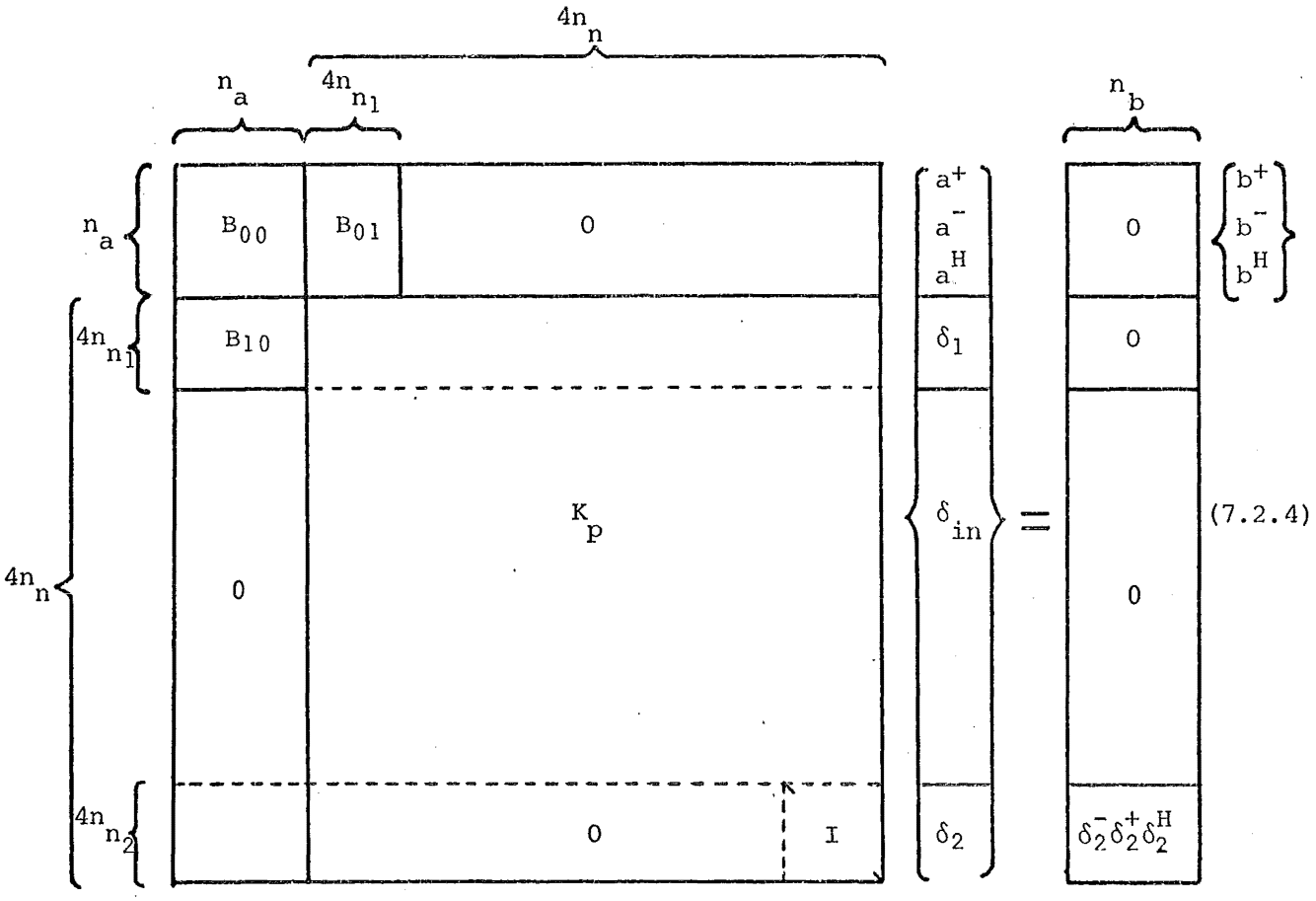

In the matrix equation (7.2.4) the submatrices $[B_{00}]$, $[B_{10}]$, $[B_{01}]$ arise from the least-square matching at the interface z = 0, by which the square of absolute error of the solutions at z = 0 (see Section 2.1.2(ii)) is minimized with respect to all propagation coefficients: a^+, a^-, a^H. Thereby one can write more specifically

$$[B_{00}]_{(n_a \times n_a)} = \begin{array}{c} \\ n_{a+} \\ \\ n_{a-} \\ \\ n_{aH} \end{array} \begin{array}{c} \begin{array}{ccc} n_{a+} & n_{a-} & n_{aH} \end{array} \\ \left[\begin{array}{ccc} B^{++} & B^{+-} & B^{+H} \\ B^{-+} & B^{--} & B^{-H} \\ B^{H+} & B^{H-} & B^{HH} \end{array}\right] \end{array} \qquad (7.2.5)$$

where one can take $n_{a+} = n_{a-} = n_{aH}$ for convenience.

A typical expression for the coefficients of submatrices such as

$[B^{++}]$, $[B^{+-}]$, $[B^{+H}]$, ... is

$$B_{ij}^{+-} = \int_{C_1} \left(J^{*+}_{p_1 i} J^{-}_{p_1 j} + J^{*+}_{w_1 i} J^{-}_{w_1 j} + J^{*+}_{u_1 i} J^{-}_{u_1 j} + J^{*+}_{v_1 i} J^{-}_{v_1 j} \right) 2\pi \, r \, dr \, ,$$

for other components of $[B_{00}]$ the two superscrips are replaced appropriately.

$$[B_{01}]_{(n_a \times 4n_{n_1})} = - \int_{C_1} \left[\begin{array}{c|c|c|c} J^{*+}_{p_1 i N_k} & J^{*+}_{w_1 i N_k} & J^{*+}_{u_1 i N_k} & J^{*+}_{v_1 i N_k} \\ \hline J^{*-}_{p_1 i N_k} & J^{*-}_{w_1 i N_k} & J^{*-}_{u_1 i N_k} & J^{*-}_{v_1 i N_k} \\ \hline 0 & J^{*H}_{w_1 i N_k} & J^{*H}_{u_1 i N_k} & J^{*H}_{v_1 i N_k} \end{array}\right] 2\pi \, r \, dr$$

and

$$[B_{10}]_{(n_{n_1} \times n_a)} = - \int_{C_1} \left[\begin{array}{c|c|c} N_k J^{+}_{w_1 j} & N_k J^{-}_{w_1 j} & N_k J^{H}_{w_1 j} \end{array}\right] \gamma \bar{p}_o \, r \, dr$$

with $i = 1,2,3...n_{a+}$, $j = 1,2,3...n_{a+}$, $k = 1,2,3...n_{n_1}$ and $n_a = n_{a+} + n_{a-} + n_{aH}$. $[B_{10}]$ just add contributions to the system matrix coefficients at those locations corresponding to the energy equations, i.e. the appropriate p equations.

At the interface $z = \ell$, the point matching is to prescribe the solutions in the nonuniform duct section to be those in the semi-infinite duct (for $z > \ell$) at specified locations, which, in this situation, are the nodes on C_2 (see Section 2.1.2(ii)). In that sense of collocation the process is similar to forcing a boundary condition. Thus, in the matrix equation (7.2.4) $[K_p]$ is a modified form of $[K]$ given by equation (7.1.14), in which the rows of coefficients corresponding to the unknown nodal values on the interface at $z = \ell$ are superseded by the eigen - solutions :

$$[I]\{\delta_2\} = [\delta_2^+ \quad \delta_2^- \quad \delta_2^H] \begin{Bmatrix} b^+ \\ b^- \\ b^H \end{Bmatrix} \tag{7.2.6}$$

where $[I]$ is the identity matrix, the eigenvectors δ_2^+, δ_2^-, δ_2^H contain nodal values of the eigenfunctions corresponding to positively running, negatively running and hydrodynamic modes respectively, and can be computed from the eigenproblem in a uniform duct.

For the least-square matching the matrix equation (7.2.2) or (7.2.3), when solved by the Gaussian elimination scheme, yields directly the reflection and transmission matrices, i.e., $\{a^-\}$ and $\{b^+\}$ being expressed in terms of $\{a^+\}$, meanwhile, for the point matching, the matrix equation (7.2.4) then gives rise to the solution of the form

$$\begin{Bmatrix} a^+ \\ a^- \\ a^H \end{Bmatrix}_{z=0} = [P] \begin{Bmatrix} b^+ \\ b^- \\ b^H \end{Bmatrix}_{z=\ell} \tag{7.2.7}$$

Hence

$$\begin{Bmatrix} b^+ \\ b^- \\ b^H \end{Bmatrix}_{z=\ell} = [TF] \begin{Bmatrix} a^+ \\ a^- \\ a^H \end{Bmatrix}_{z=0}$$

where $[TF] = [P]^{-1}$.

This case can be manipulated in the same way as in the MWR (see Section 6.3.2) to give the matrices of reflection and transmission coefficients, depending on the flow direction.

7.3 IMPLEMENTATION

The final stage in a FEM procedure is to solve a system of simultaneous equations; in order to establish the system matrix standard FEM techniques are concerned. These aspects together with optimum storage strategy and solution method have been covered in Chapter 3. In this

section consideration is given to practical implementation in completing the FEM formulation.

7.3.1 Mean Flow Field

The problem of the steady flow model is to be solved before entering the acoustic problem, and is so done conveniently in the discretizing process. Thus, one can store appropriate data for all nodes or all elements in two-dimensional arrays with the first index being the order in the discretized numbering system.

The flow Mach number $\bar{M}_o(z)$ and the parameters $\bar{W}_o$, U_o, $\bar{\rho}_o$, $\bar{p}_o$ in equation (7.1.15) can be solved for in the same way as in the MWR (see Section 6.3.1(i)). The number of steps in the Runge-Kutta integration scheme is divided evenly among the axial elements. This is consistent with the problem of high Mach number when more elements are compressed towards the throat in a converging flow duct.

In the FEM numerical integration process, once $\bar{M}_o$ has been known the quantities $\bar{W}_o$, U_o, $\bar{\rho}_o$, $\bar{p}_o$ and/or their derivatives can be calculated analytically as in the MWR. However, for consistency with FEM approximations, at any integration point in the domain, one can express typically

$$U_o = [N]\ \{U_o\}\ ,\quad \frac{\partial U_o}{\partial r} = [N]_r\ \{U_o\}\ ,\quad \frac{\partial U_o}{\partial z} = [N]_z\ \{U_o\}$$

where $\{\bar{U}_o\}$ are the nodal values of U_o extracted from the data arrays above, and components of $[N]$ are the shape functions readily available in the FEM formulation. This is performed in the study.

7.3.2 Eigenproblem in Matching

Unlike in the MWR, the matching procedure in the FEM has very little modification when the eigenproblem in the uniform ducts is solved analytically or by the same method as for the transmission problem. In either way numerical integrations are still used. In the course of development both analytical and numerical approaches have been carried out.

The exact solutions (Bessel functions) to the eigenproblem have been derived in Appendix C. The eigenvalues have been solved for by a numerical integration scheme in Appendix D. In matching with exact eigenfunctions, for unlined ducts, i.e. A = 0, one can make use of the orthogonality of Bessel functions for integrations.

With the compatibility of accuracy level in solution description at the interfaces, which has been stressed in the MWR, here the eigenproblem can be conveniently solved numerically by the FEM with the conservation equations (see Section 4.3.2). The discretized mesh is identical to that on the boundary C_1 or C_2. In this situation the general QR algorithm gives the modal matrix of the form

$$\{\delta\} = [\delta^+ \quad \delta^- \quad \delta^H] \begin{Bmatrix} a^+ \\ a^- \\ a^H \end{Bmatrix} \tag{7.3.1}$$

where $\{\delta\}$ are the nodal values of dependent variables on the appropriate boundary (C_1 or C_2). The eigenvectors $\{\delta^+\}$, $\{\delta^-\}$, and $\{\delta^H\}$ contain the nodal values of eigenfunctions. The form (7.3.1) of the modal matrix is particularly useful in the point matching since it fits the required form of equation (7.2.6).

The normalization of acoustic modes is performed in the same way as in the MWR, i.e. for the axisymmetric angular mode, propagation coefficients are appropriate acoustic pressures at the duct centre line, and for antisymmetric angular modes they are the pressure at the duct wall. The problem of hydrodynamic modes also arises because of multiple eigenvalues and will be treated in the following Section 7.3.3.

7.3.3 Representation of Hydrodynamic Modes

The solutions for hydrodynamic modes in the uniform ducts used in the FEM matching formulation must be represented explicitly. If one recalls having solved the eigenproblem in

Chapter 4 (see Sections 4.2.5 and 4.3.5) the hydrodynamic modes for a uniform flow profile have to satisfy the following conditions:

$$\left.\begin{aligned} & p^H \equiv 0 \\ & \text{div } (\underline{v}^H) = 0 \quad , \quad \underline{v}^H = (u^H, v^H, w^H) \\ & u^H = 0 \quad \text{at} \quad r = R \end{aligned}\right\} \tag{7.3.2}$$

and $$\frac{k_z^H}{k_r} = \frac{1}{\bar{W}_o}$$

Consequently, the solutions in the form of equations (7.2.1) are not defined unless an additional relation satisfied by $\underline{v}^H$ is arbitrarily assumed. The simplest way is to make the situation closely analogous to that in the 2D geometry, in which v^H vanishes and u^H and w^H are in terms of trigonometric functions. Thus, from relations (7.3.2) one can assume equations (7.2.1) in detailed forms

$$\left.\begin{aligned} & p^H \equiv 0 \\ & v^H \equiv 0 \\ & u^H = \sum_{n=1}^{\infty} a_n^H \sin\left[(2n-1)\frac{\pi}{2}\frac{r}{R}\right] \end{aligned}\right\} \tag{7.3.3}$$

from $\text{div } (\underline{v}^H) = 0$

or $$\left(\frac{1}{r}\frac{\partial}{\partial r}(ru^H) + \frac{\partial w^H}{\partial z} + \frac{1}{r}\frac{\partial v^H}{\partial \theta}\right) = 0$$

$$\left(\frac{\partial u^H}{\partial r} + \frac{u^H}{r} - ik_z^H w^H\right) = 0 \quad \text{with} \quad v^H = 0$$

hence

$$w^H = \sum_{n=1}^{\infty} a_n^H \left\{-\frac{1}{r}\sin\left[(2n-1)\frac{\pi}{2}\frac{r}{R}\right] - (2n-1)\frac{\pi}{2R}\cos\left[(2n-1)\frac{\pi}{2}\frac{r}{R}\right]\right\}\frac{i\bar{w}_o}{k_r} \tag{7.3.4}$$

It is also noted that the condition $\text{div } (u^H, 0, w^H)$ restricts the construction of u^H in two ways:

(a) Hydrodynamic solutions have no plane mode (i.e. the first mode u^H = constant).

(b) The limit of $\frac{u^H}{r}$ must be finite as $r \to 0$.

Otherwise, the expression above for w^H would become singular when $r \to 0$. The choice of $u_n^H = a_n^H \sin\left[(2n-1)\frac{\pi}{2}\frac{r}{R}\right]$, for n = 1,2,3...is satisfactory.

7.3.4 Acoustic Field

In the FEM with the least-square matching the solutions to the acoustic field in the nonuniform duct section are readily obtainable with nodal values of dependent variables in terms of incident mode amplitudes. They are part of the solutions to the system of simultaneous equations in the FEM.

However, with the point matching the Gaussian elimination method gives the solution of the matrix equation (7.2.4) of the form

$$\left[\begin{array}{c|c} I & \begin{matrix} a^+ \\ a^- \\ a^H \\ - - - \\ \delta \end{matrix} \end{array}\right] = \left[\begin{array}{c|c} & \begin{matrix} b^+ \\ b^- \\ b^H \end{matrix} \\ \begin{matrix} [P] \\ - - - \\ [Q] \end{matrix} & \end{array}\right] \tag{7.3.5}$$

where [I] is the identity matrix and [P], [Q] contain solution column vectors. Note that the solution (7.3.5) implies equation (7.2.7).

Thus, from equation (7.3.5) one obtains

$$\{\delta\} = [Q] \left\{\begin{matrix} b^+ \\ b^- \\ b^H \end{matrix}\right\}_{z=\ell} \tag{7.3.6}$$

When equation (7.2.7) has accounted for terminating conditions and flow direction as in the MWR (Section 6.3.2) to give coefficient matrices such as $\{b^+\} = [TRAN]\{a^+\}$, $\{b^H\} = [HR_2]\{a^+\}$, as in Section 6.3.3 one can write

$$\left\{\begin{matrix} b^+ \\ b^- \\ b^H \end{matrix}\right\}_{z=\ell} = \left[\begin{matrix} [TRAN] \\ [\,0\,] \\ [HR_2] \end{matrix}\right] \{a^+\}_{z=0} \tag{7.3.7}$$

Equations (7.3.6) and (7.3.7) can be combined to yield

$$\{\delta\} = [Q] \begin{bmatrix} [TRAN] \\ [\ 0\ ] \\ [HR_2] \end{bmatrix} \{a^+\}_{z=0} \tag{7.3.8}$$

expressing explicitly the nodal values $\{\delta\}$ in terms of incident mode amplitudes.

7.4 POWER TRANSMISSION

Here the integral (6.4.1) for acoustic power at the interfaces is evaluated via line elements on the boundaries as a typical line integration in the FEM (See Section 3.2.3). The nodal values of p and w are available from the eigenproblem in matching at the interfaces in the form of the modal matrix (7.3.1). For convenience the power matrix is sought in the form of (6.4.5).

From the modal matrix (7.3.1) one can extract nodal values for p and w so that inside each element on the boundary one can write

$$p = \begin{bmatrix} [N_i]_1 & [N_i]_2 \ldots [N_i]_m \end{bmatrix} \begin{bmatrix} \{p_i\}_1 & & \\ & \{p_i\}_2 & \\ & & \ddots \\ & & & \{p_i\}_m \end{bmatrix} \begin{Bmatrix} a^+ \\ a^- \\ a^H \end{Bmatrix} \tag{7.4.1}$$

$$w = \begin{bmatrix} [N_i]_1 & [N_i]_2 \ldots [N_i]_m \end{bmatrix} \begin{bmatrix} \{w_i\}_1 & & \\ & \{w_i\}_2 & \\ & & \ddots \\ & & & \{w_i\}_m \end{bmatrix} \begin{Bmatrix} a^+ \\ a^- \\ a^H \end{Bmatrix} \tag{7.4.2}$$

where N_i are shape functions, $\{p_i\}$, $\{w_i\}$ are nodal values of p and w respectively in that element corresponding to propagation modes, m is the total number of modes introduced (positively, negatively running and hydrodynamic). For quadratic line elements i = 1,2,3. $[N_i]_1$, $[N_i]_2 \ldots [N_i]_m$ are identical.

Substituting relations (7.4.1) and (7.4.2) into equation (6.4.2) and manipulating vectors and matrices one can obtain the integrand of (6.4.1) in the form

$$I = \frac{\rho_r c_r^3}{4} \begin{Bmatrix} a^+ \\ a^- \\ a^H \end{Bmatrix}^T \left[(1+M_o^2)([pw^*] + [p^*w]) + 2M_o\rho_o c_o [ww^*] + \frac{2M_o}{\rho_o c_o}[pp^*] \right] \begin{Bmatrix} a^+ \\ a^- \\ a^H \end{Bmatrix}^* \quad (7.4.3)$$

where the matrices $[pw^*]$, $[p^*w]$, $[ww^*]$ and $[pp^*]$ are defined typically as follows:

$$[pw^*]_{k\ell} = \{p_i\}_k^T [N_i N_j] \{w_j^*\}_\ell \quad (7.4.4)$$

with $k = 1,2,3,\ldots m$, $\ell = 1,2,3,\ldots m$, $i = 1,2,3$, $j = 1,2,3$.
For other matrices the nodal values and their conjugates are superseded accordingly.

Thus, equation (7.4.3) can be arranged in the form :

$$I = \frac{\rho_r c_r^3}{4} \begin{Bmatrix} \underline{a}^+ \\ \underline{a}^- \\ \underline{a}^H \end{Bmatrix}^T \begin{bmatrix} \underline{P}^{++} & \underline{P}^{+-} & \underline{P}^{+H} \\ \underline{P}^{-+} & \underline{P}^{--} & \underline{P}^{-H} \\ \underline{P}^{H+} & \underline{P}^{H-} & \underline{P}^{HH} \end{bmatrix} \begin{Bmatrix} \underline{a}^+ \\ \underline{a}^- \\ \underline{a}^H \end{Bmatrix}^* \quad (7.4.5)$$

which is evaluated over all elements in the FEM numerical integration to yield the power matrix in the form of (6.4.5).

In implementation the nodal vectors $\{p_i\}$, $\{w_i\}$ are extracted systematically from modal matrices via the numbering systems.

Hereafter the analysis follows the same path as in the MWR.

7.5 PRELIMINARY RESULTS AND DISCUSSIONS

Limited results for uniform ducts with flow presented in this section are obtained in the course of FEM development, and the evaluation of the approach used. Further applications to general duct configurations will be seen in Chapter 8.

7.5.1 Hydrodynamic Mode and Matching Procedure

In the end matching it is noted that the complete set of eigenproblem solutions has been used, comprising positive, negative and hydrodynamic modes. Omitting the contribution of hydrodynamic modes in the matching would not reveal significant change in coefficient results, even for the nonuniform duct case. However, computation of hydrodynamic mode coefficients in a uniform duct may serve as an alternative checkout of consistency of the FEM to some extent.

The least-square matching and the point matching have been formulated. In general, with the uniform duct as a test case, the two approaches produces comparable results for acoustic transmission coefficients. The results in Table 7.1 illustrate this point, in which uniform hardwalled duct, $R_1 = R_2 = 1.0$, $\ell = 0.5$ is considered at Mach number 0.5, frequency $k_r R_1 = 5$, angular mode $m_o = 0$. (Compare with exact transmission coefficients in Table 6.1). In this positive flow case hydrodynamic disturbance is assumed not to exist in the inlet at $z = 0$, therefore the exact hydrodynamic coefficients at $z = \ell$ should be zero. Table 7.1 also shows that the point matching seems to be more favourable for reflection and hydrodynamic mode coefficients.

The point matching approach is advantageous over the least-square one in two ways :

(a) As being seen in the formulations, for the least-square matching there are appreciable modifications in programming implementation when the flow direction is to change from positive to negative or vice versa, according to the assumed existence of hydrodynamic disturbance. In the point matching the transfer matrix is obtained before the flow direction is taken into account (see Sections 7.2.2 and 7.2.4) as in the MWR, hence it is simpler.

(b) As in the MWR (Section 6.5(iii)) it is of interest to consider the test case when only hydrodynamic modes are introduced with the flow into a uniform duct. The point matching yields the hydrodynamic mode coefficients at an accuracy level comparable with that of acoustic modes, while the least-square matching gives incorrect results which tend to vanish. It is believed that the least-square procedure effectively eliminates the hydrodynamic solutions.

7.5.2 Forced Boundary Condition and Eigenproblem in Matching

Table 7.1 also compares the results in the case of the duct-wall boundary condition being natural and forced, with the point matching using exact eigenfunctions. In uniform hardwalled ducts the boundary condition is forced by setting the transverse velocity component $u = 0$ at $r = R$ and $r = 0$ (for $m_o \neq 1$). Note that the coefficients of the first two cut-on modes are nearly equivalent while there is a slight difference for the third mode, which is cut off.

Comparison of the coefficients appears inconclusive on the effect of the forced boundary condition. In uniform ducts one can make comparisons of the acoustic field solutions offered by the FEM with the exact solutions. Figure 7.1 plots the pressure variation of acoustic modes along the duct (with the same parameters as for Table 7.1). In Figure 7.2 are the pressure profiles at certain stations z. Note that the first mode (plane mode) is not affected by the treatment of the boundary condition. Clearly the natural values are closer to the exact solution while forcing the boundary condition tends to cause fluctuations about the exact solution, and it is more severe in the neighbourhood of the duct centreline. This partly accounts for the success of the Galerkin approach in the MWR, in which the duct-wall boundary condition

is taken care of "naturally".

The last part of the results in Table 7.1 shows an improvement when the eigenproblem in end matching is solved by the FEM as well. It is more obvious to the reflection and hydrodynamic mode coefficients. Thus, the importance of the accuracy compatibility in solution description at the interfaces is confirmed numerically here for the FEM.

7.5.3 Convergence to the Uniform Duct Case

For the results presented in the following, the point matching with FEM eigenfunctions is applied.

(i) Hardwall case

The hardwall case has been demonstrated in Table 7.1 with the FEM using a discretized mesh of 5 elements across and 4 elements along. A high degree of convergence has been achieved for cut-on modes. In fact,the FEM (3x4) with 3 elements across the duct can give reasonable results for many practical purposes.

(ii) Softwall case

A uniform softwalled duct is considered at Mach number -0.5, frequency $k_r R_1 = 8.0$, angular mode $m_o = 2$. Tables 7.2 and 7.3 show the results for $\ell = 0.2$ and $\ell = 0.5$ respectively, with increasing dimensionality in the FEM. The exact results are given in Table 6.2. The trend of convergence, and the adverse effect of increasing the duct length are also observed for the flow case.

(iii) Hydrodynamic mode

With the same parameters as in Table 7.3 the solution nodal values along the centreline are plotted in Fig.7.3 for the hydrodynamic w - velocity component of modes 1 and 2. The hydrodynamic disturbances are introduced with the flow at $z = \ell$. Normalization is performed such that the hydrodynamic mode coefficient is the w - velocity component at $r = 0$.

Note that hydrodynamic modes have the same axial variation because of identical axial eigenvalues $\left(\frac{k^H_{z_n}}{k_r} = \frac{1}{\bar{W}_o} \right)$. A good agreement is still observed in spite of wide variations present in the field at this high frequency. The accuracy decreases for mode 2 as expected, showing the effect of transverse resolution on the axial phase variation.

(iv) Comparison with MWR

The values of parameters in Tables 7.1, 7.2, and 7.3 are deliberately chosen so that their results can be compared with those of Tables 6.1, 6.2 and 6.3 obtained by the MWR. At the levels of approximation, comparisons of the direct transmission coefficients given by the MWR and the FEM are still inconclusive on advantages of one method over the other. However, the MWR appears to give results more favourable for the reflection and hydrodynamic mode coefficients. This suggests that, for uniform ducts, the integration in the MWR has a better resolution along the duct than the FEM representation, based on piecewise continuous shape functions. Further, even though the degrees of accuracy of the direct transmission coefficients are comparable, the MWR transmission coefficients referred to $z = 0$ are clearly more accurate. But the experiment shows that for the softwall case the eigenvalues given by FEM (4) are nearly equivalent to those given by MWR (7BF). This fact may signify the more important role of solution compatibility at the interfaces in the MWR than in the FEM (see also the conclusions in Section 6.5(ii)).

	Reflection Coefficients in Mode i	Transmission Coefficients at z = ℓ in Mode i	Hydrodynamic Mode Coefficients at z = ℓ in Mode i
Incident Mode i	FEM (5x4): LSQ, Exact EIGEN, Natural BC		
1	-.0090 + .0030i	-.0977 -1.0000i	.0000 + .0000i
2	-.0004 - .0003i	.6781 - .7359i	.0001 + .0028i
3	-.0169 + .0005i	-.0110 + .1000i	-.0142 - .0041i
Incident Mode i	FEM (5x4): PM, Exact EIGEN, Natural BC		
1	.0000 + .0000i	-.0982 - .9986i	.0000 + .0000i
2	.0001 + .0012i	.6766 - .7347i	.0021 + .0013i
3	-.0050 + .0044i	-.0075 + .0846i	.0013 - .0046i
Incident Mode i	FEM (5x4): PM, Exact EIGEN, Forced BC		
1	.0000 + .0000i	-.0982 - .9986i	.0000 + .0000i
2	.0001 + .0014i	.6765 - .7350i	-.0018 + .0018i
3	-.0016 + .0019i	-.0115 + .0924i	.0015 - .0008i
Incident Mode i	FEM (5x4): PM, FEM EIGEN, Natural BC		
1	.0000 + .0000i	-.0982 - .9986i	.0000 + .0000i
2	.0000 + .0000i	.6774 - .7359i	.0000 + .0000i
3	-.0000 - .0001i	-.0098 + .0862i	.0001 - .0002i

LSQ = Least-Square Matching, EIGEN = Eigenfunctions

PM = Point Matching

TABLE 7.1 Comparison of Reflection, Transmission and Hydrodynamic Mode Coefficients Computed by FEM with Different Treatments of BC and Matching Procedures at $z = \ell$ for a Uniform Hardwalled Duct, $R_1 = R_2 = 1.0$, $\ell = 0.5$, $M_1 = 0.5$, $k_r R_1 = 5.0$, $m_o = 0$.

Geometry : Uniform, $R_1 = R_2 = 1.0$, $\ell = 0.2$

Characteristics: Softwalled Duct with Flow, A = (0.72-0.42i)

$M_1 = -0.5$, $k_r R_1 = 8.0$, Angular Mode $m_o = 2$

All Decaying Modes

Incident Mode i	Reflection Coefficients in Mode i		
	FEM(4x2)	FEM(5x2)	FEM(4x4)
1	-.0015 - .0015i	-.0015 - .0024i	-.0007 - .0014i
2	-.0172 - .0048i	-.0012 - .0028i	-.0002 - .0046i
3	-.0409 - .0212i	-.0169 - .0113i	-.0111 - .0024i
Incident Mode i	Direct Transmission Coefficients at z = ℓ in Mode i		
	FEM(4x2)	FEM(5x2)	FEM(4x4)
1	.9918 - .3040i	.9915 - .3041i	.9507 - .2817i
2	-.4553 - .7689i	-.4472 - .7740i	-.4320 - .7634i
3	.0756 - .1979i	.0996 - .2141i	.1120 - .2309i
Incident Mode i	Transmission Coefficients referred to z = 0 in Mode i		
	FEM(4x2)	FEM(5x2)	FEM(4x4)
1	1.0656 + .0146i	1.0654 + .0149i	1.0186 - .0045i
2	1.0429 - .0155i	1.0420 - .0025i	1.0238 - .0050i
3	.8287 - .0351i	.9201 + .0258i	1.0036 - .0447i
Incident Mode i	Hydrodynamic Mode Coefficients referred to z = 0 in Mode i		
	FEM(4x2)	FEM(5x2)	FEM(4x4)
1	1.0698 - .0305i	1.0698 - .0305i	1.0161 - .0063i
2	1.0761 - .0312i	1.0715 - .0299i	1.0190 - .0068i
3	1.1216 - .0370i	1.0904 - .0354i	1.0425 - .0146i

TABLE 7.2 Reflection, Transmission and Hydrodynamic Mode Coefficients Computed by FEM for a Uniform Softwalled Duct with Flow, $\ell = 0.2$.

Geometry : Uniform, $R_1 = R_2 = 1.0$, $\ell = 0.5$

Characteristics: Softwalled Duct with Flow, A = (0.72-0.42i)

$M_1 = -0.5$, $k_r R_1 = 8.0$, Angular Mode $m_o = 2$

All Decaying Modes

Incident Mode i	Reflection Coefficients in Mode i		
	FEM(4x4)	FEM(4x6)	Exact
1	-.002 - .002i	.003 - .003i	.000 + .000i
2	.010 + .001i	.014 + .002i	.000 + .000i
3	-.013 - .023i	-.023 - .032i	.000 + .000i
Incident Mode i	Direct Transmission Coefficients at z = ℓ in Mode i		
	FEM(4x4)	FEM(4x6)	Exact
1	.649 - .794i	.626 - .747i	.608 - .710i
2	.323 + .579i	.316 + .592i	.341 + .592i
3	-.173 + .012i	-.054 + .024i	-.033 - .008i
Incident Mode i	Transmission Coefficients referred to z = 0 in Mode i		
	FEM(4x4)	FEM(4x6)	Exact
1	1.097 - .026i	1.043 - .012i	1.000 + .000i
2	.975 + .005i	.987 + .023i	1.000 + .000i
3	5.023 - 1.548i	1.435 - 1.090i	1.000 + .000i
Incident Mode i	Hydrodynamic Mode Coefficients referred to z = 0 in Mode i		
	FEM(4x4)	FEM(4x6)	Exact
1	1.131 - .040i	1.053 - .011i	1.000 + .000i
2	1.1136 - .035i	1.055 - .011i	1.000 + .000i
3	1.212 + .031i	1.073 - .005i	1.000 + .000i

TABLE 7.3 Reflection, Transmission and Hydrodynamic Coefficients Computed by FEM for a Uniform Softwalled Duct with Flow, $\ell = 0.5$.

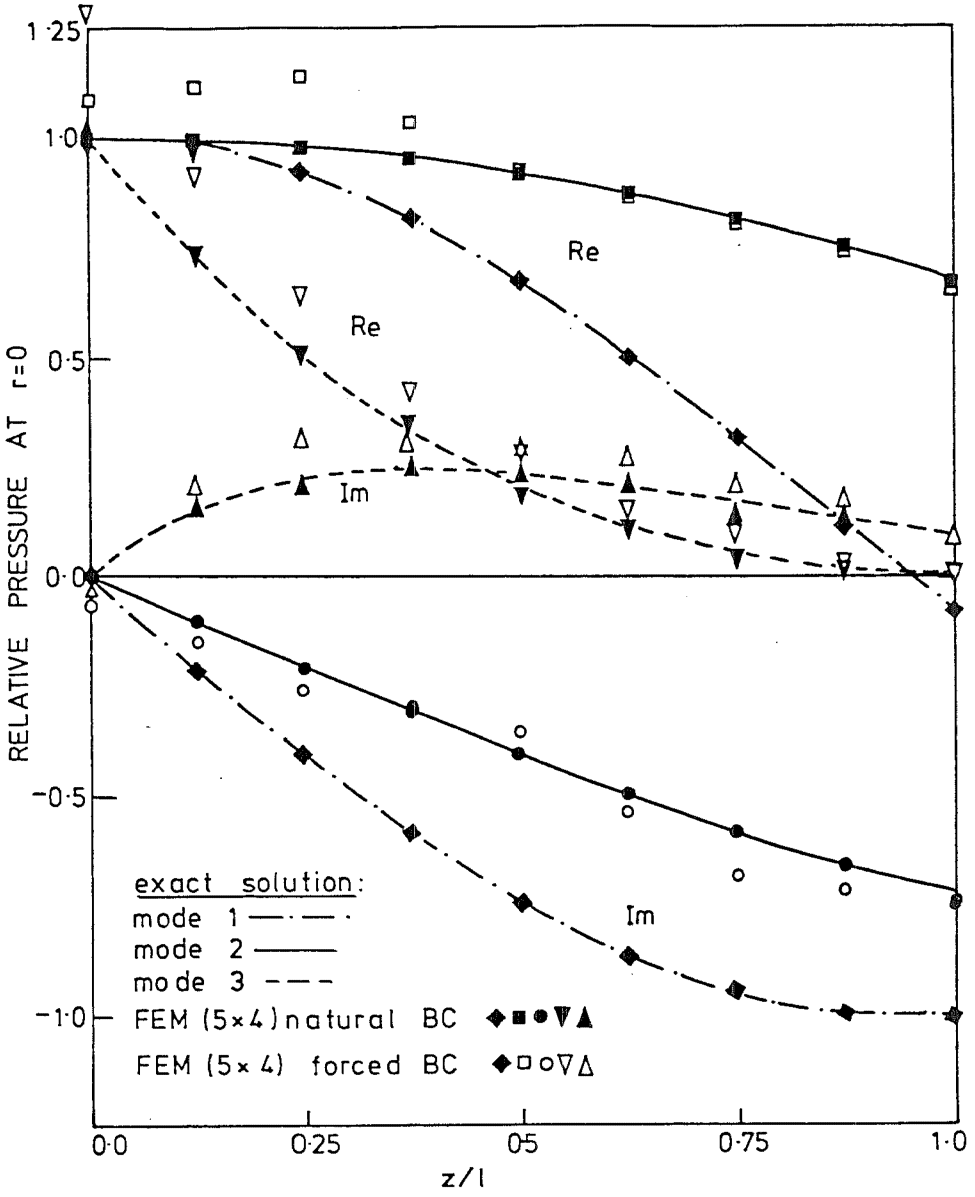

FIG.7·1 AXIAL PRESSURE VARIATIONS IN HARDWALLED DUCT;

$R_1 = R_2 = 1{\cdot}0$, $l = 0{\cdot}5$, $M = 0{\cdot}5$, $k_r R_1 = 5{\cdot}0$, $m_o = 0$

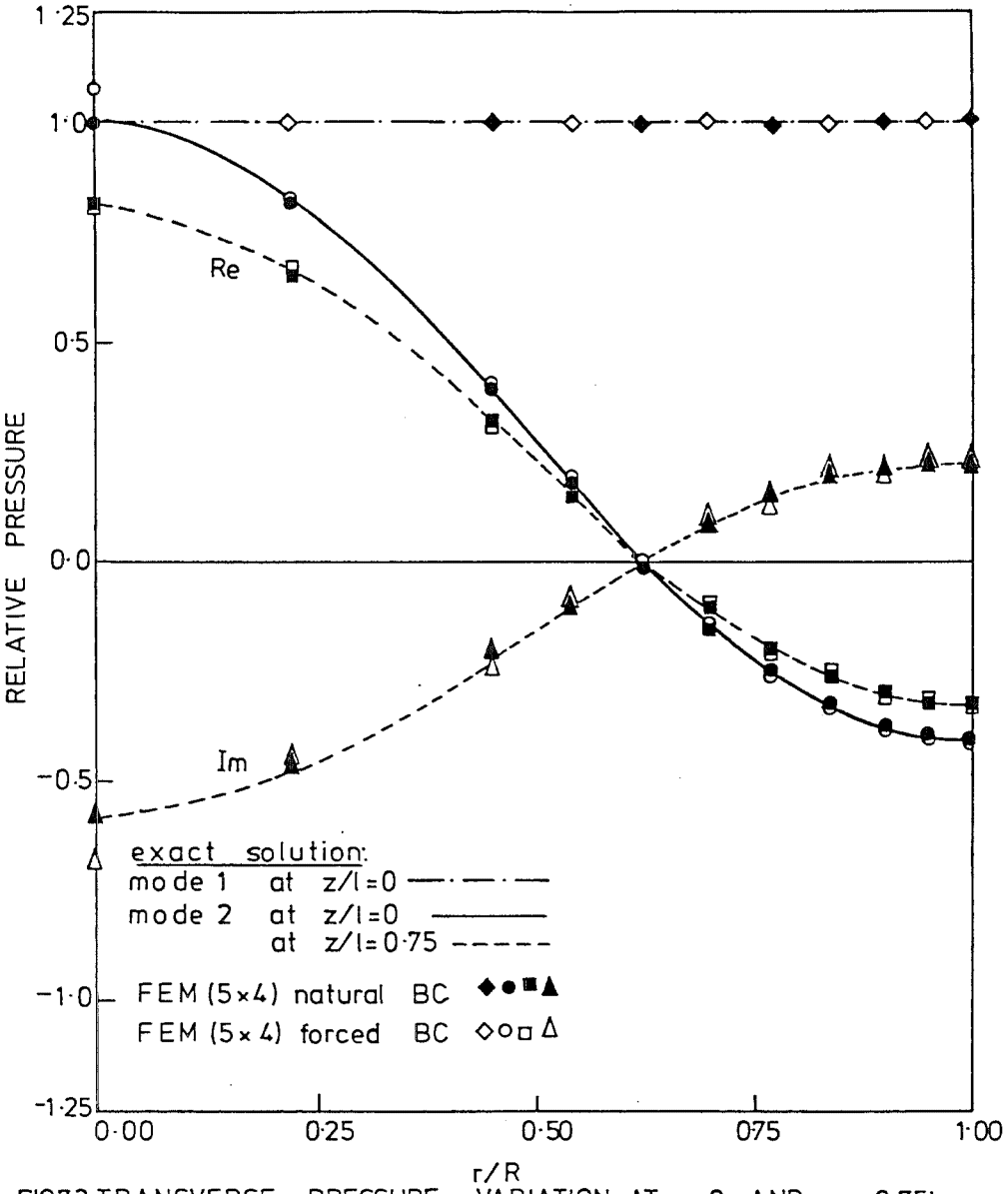

FIG7·2 TRANSVERSE PRESSURE VARIATION AT z=0 AND z=0·75l IN UNIFORM HARDWALLED DUCT;

$R_1 = R_2 = 1{\cdot}0$, $l = 0{\cdot}5$, $M = 0{\cdot}5$, $k_r R_1 = 5{\cdot}0$, $m_o = 0$, IN MODES 1 AND 2 INCIDENT

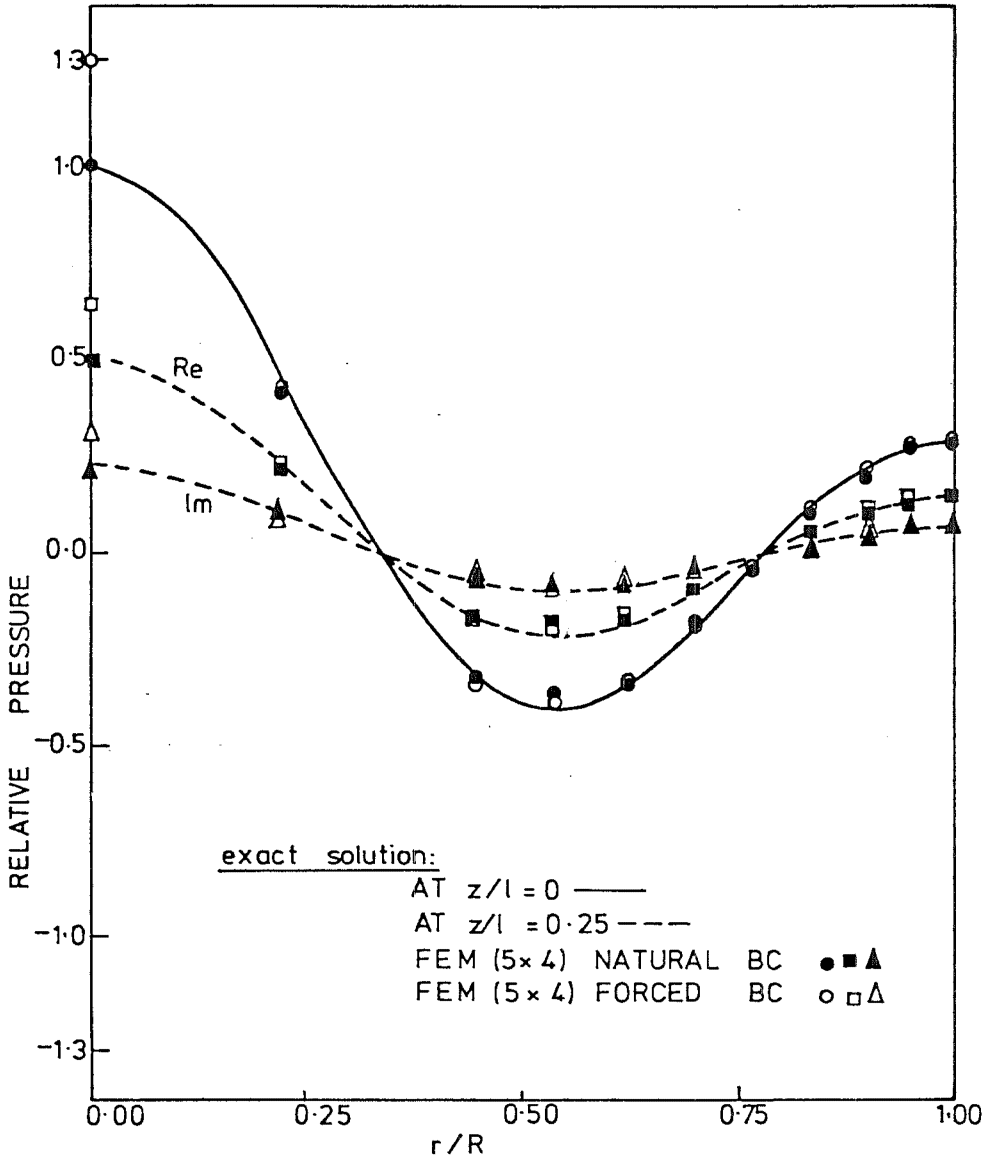

FIG 7·3 TRANSVERSE PRESSURE VARIATION AT z=0 AND z=0·25l IN UNIFORM HARDWALLED DUCT; $R_1=R_2=1{\cdot}0$, $l=0{\cdot}5$, $M=0{\cdot}5$, $k_rR_1=5{\cdot}0$, $m_o=0$ IN MODE 3 INCIDENT

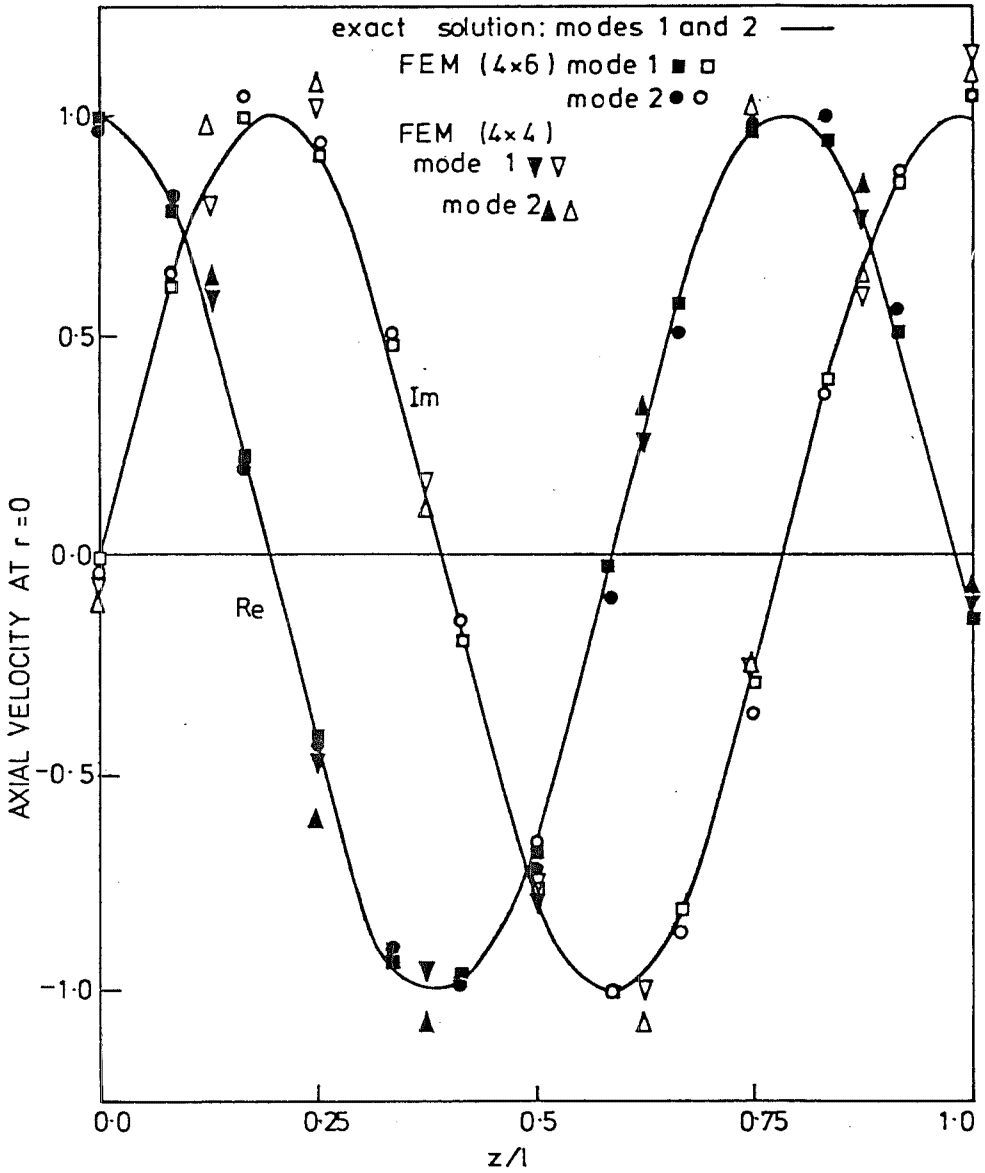

FIG 7·4 AXIAL VELOCITY VARIATION OF HYDRODYNAMIC MODES IN UNIFORM SOFTWALLED DUCT; $R_1=R_2=1{\cdot}0$, $l=0{\cdot}5$, $A=(0{\cdot}72-0{\cdot}42i)$, $M_1=-0{\cdot}5$, $k_rR_1=8{\cdot}0$, $m_o=2$

CHAPTER 8

MWR AND FEM RESULTS FOR NONUNIFORM DUCTS WITH FLOW

8.1 DISCUSSION AND PRELIMINARY COMPARISON

8.1.1 Acoustic Problems in Ducts with Flow

In Chapter 5 the MWR and the FEM have been developed as solution techniques for studies of acoustic transmission in nonuniform ducts with no flow. Both of the methods provide relatively simple and accurate computational schemes for many cases. Formulations for the flow case have been performed in Chapters 6 and 7. Results for uniform ducts have shown the convergence and the consistency of the computational schemes when reduced to a simple geometry.

When mean flow is present the modelling of the transmission problem is complicated in several ways. A primary difficulty arises because the field equations represent acoustic perturbations on a compressible mean flow. The mean flow field must be specified and is presumably available in a particular problem from other computational routines. In the present analysis, in order to concentrate on the acoustic problem, a simplified flow field based on a modified one-dimensional model is employed.

A second difficulty arises because of the form of the field equations. In the no-flow case they can be condensed to two first-order equations (Section 5.1.1) or the second-order Helmoltz wave equation (Section 5.2.1). When flow is present a condensation of this type is only available if the entire problem, mean flow and acoustic perturbations, is assumed to be irrotational, and the field equations remain in conservation form. The approximate mean flow model employed here is rotational and flow fields based on a sheared flow model can be introduced, if desired.

A third difficulty posed by the consideration of duct mean flow is the presence of hydrodynamic modes in which fluid disturbances are swept along at local flow velocity. In ducts with uniform flow the hydrodynamic modes are rotational and the acoustic perturbations are irrotational (Section 4.2.5(ii)). A principal feature of the model for multimodal propagation employed is the rigorous matching of the solution to radiation conditions at the ends of duct nonuniformities. This matching must include the hydrodynamic modes if the representation inside the nonuniformity is to be compatible with the representation in the radiated solutions. The compatibility is essential as seen in the MWR formulation.

The primary goal in the research programme is to develop numerical techniques for the solution of the field equations for propagation in nonuniform ducts carrying high speed flow. Towards this end the MWR and the FEM have been chosen, partly to produce alternative techniques to substantiate accuracy, and partly because of the individual strengths of the two methods. Confidence in numerical routines has been gained in the previous chapters. Certain improvements, especially for the FEM formulation, have been made, and continue to be made, as experimentation has been very much a feature of the research work.

In this chapter the MWR and FEM results for nonuniform ducts are presented and compared in several cases where both methods can be used to good advantage. The FEM is implemented with natural boundary condition. Computations of reflection and transmission efficiencies are based on the assumption that the amplitudes of cut-on modes incident on the source side are such that each of the modes carries unit power when the modal interactions are ignored. The efficiencies are defined in the same way as for the no-flow case (see Section 5.4.2). It is noted that there are no standard results in the literature, against which to make comparisons.

8.1.2 Preliminary Comparison

Comparisons in this section are mainly based on 3 x 3 matrices of modal coefficients. As a first example a uniform duct section of wall admittance A = (0.1 - 0.1i), joined by two semi-infinite hardwalled ducts is considered at Mach number -0.1, frequency $k_r R_1 = 1.0$, angular mode $m_o = 0$. The duct length is short, $\ell = 0.2$. The FEM results were obtained with a 5 (transverse) x 2 (axial) element mesh. The point matching was performed with FEM eigenfunctions in the uniform ducts. The MWR used 5 modified flow basis functions (Section 4.2.4(i)). In Table 8.1 it was found that the agreement between the MWR and FEM reflection and transmission coefficients is exceptionally good, while for the hydrodynamic mode coefficients (see Sections 6.5(iii) and 7.5.1 for derivations) the FEM accuracy level is much lower than the MWR one. Increasing Mach number to -0.5, frequency to $k_r R_1 = 5.0$ (the MWR used no-flow basis functions) degrades the accuracy of all the results in Table 8.2 in general as expected; however, correlations are still observed here. These test cases extend the validity of the matching methods at the ends of the nonuniformity, which was established for the no-flow case.

The linearly tapered hardwalled duct, in which the taper angle parameter may serve as a measure of degree of nonuniformity, is considered at frequency $k_r R_1 = 5.0$, angular modes $m_o = 0$, with results in Tables 8.3, 8.4 and 8.5. The duct length is $\ell = 0.5$ while the outlet duct radius is varied, $R_2 = 1.1, 1.134, 1.268$ giving about 21%, 29%, 61% increase in the original cross-sectional area respectively. Note that for the case $R_2 = 1.268$, $M_1 = -0.5$ the FEM matching employed the least-square method using exact eigenfunctions in the uniform ducts. The MWR (5BF) and FEM (5 x 4) accuracies are comparable for the above cases. The correlation is more obvious for the diagonal terms of the coefficient matrices. These test cases show that, in general, the agreement of the

results degrades when the taper angle increases, but not to an extent which reflects the degree of nonuniformity. The case of $R_2 = 1.268$ giving 61% increase in the original cross-sectional area is considered extreme for practical purposes. The computational methods are still useful.

Another case presented by Table 8.6 is general and computationally challenging to some extent, in which a cosine-converging-diverging duct section of wall admittance $A = 0.2 - 0.2i$ is joined by two uniform hardwalled ducts. A Mach number $M_1 = -0.3$ at $z = 0$, $R_1 = 1.0$ leads to a Mach number of $M_t = -0.383$ at the throat of radius $R_t = 0.9$. Note that in this situation the MWR's basis functions do not satisfy the duct-wall boundary condition. Thus, it is expected that the convergence for softwalled ducts is slower for the hardwall case. Numerical results in Table 8.6 show this is the case, in comparison to those in Tables 8.3 - 8.5. Acoustic flux and power computations available at this stage enable comparisons of reflection and transmission efficiencies. The accuracy of reflection coefficients decreases, partly because of the complication of the problem, partly because of their small values. However, the diagonal transmission coefficients and the efficiencies are still in reasonable agreement.

8.2 NONUNIFORM DUCTS WITH FLOW AT LOW MACH NUMBER

Experience and confidence in the MWR and FEM routines have been accumulated at this stage. In the following, a number of test configurations involving axisymmetric nonuniform, acoustically treated ducts, for which the MWR and the FEM can be used to compute transmission properties in the form of modal reflection and transmission coefficients and efficiencies, will be considered. In addition, valuable insight into the behaviour of the computational schemes, particularly in the

FEM, is obtained by assessing the pressure field in the duct, both in the axial and transverse directions. Comparisons of the pressure field are restricted to the transverse variations at the nonuniformity interfaces because the solutions at $z = 0$ and $z = \ell$ are more readily available in the MWR (see Section 6.3.3).

In the FEM formulation piecewise continuous shape functions are not forced to have continuous slopes at corner nodes. Thus, the nodal slope continuity in the pressure field may serve as a gross indication of accuracy when quadratic interpolation is taken along each element boundary.

For the results presented, the FEM point matching is applied with FEM eigenfunctions in the uniform semi-infinite ducts while the MWR uses the no-flow basis functions previously discussed. The format of multimodal comparisons is such that a multimodal acoustic disturbance is introduced at the source side of the nonuniform duct section. The incident modes are normalized to have unit amplitude (which is the pressure at $r = 0$ for $m_o = 0$ and the pressure at $r = R$ for $m_o \neq 0$). For computations of power and efficiency each of the incident cut-on modes carries unit power.

(i) Hardwall case

As a first detailed comparison consider a cosine-converging-diverging duct configuration, $\ell = 0.75$. A Mach number -0.30 at $z = 0$, $R_1 = 1.0$ leads to a Mach number -0.35 at the throat of radius $R_t = 0.93$ at $z = \ell/2$. The contraction ratio R_t/R_1 gives about 13.5% reduction in cross-sectional area. Tables 8.7 and 8.8 compare the results for the axisymmetric mode, $m_o = 0$ at frequency $k_r R_1 = 5.0$ with increasing dimensionality. The agreement between the MWR and FEM results is reasonable even though the convergence trend is not as obvious as in the no-flow case. Figures 8.1, 8.2 and 8.3 plot the FEM nodal values of the pressure along the duct centreline while Figures 8.4, 8.5 and 8.6

compare the transverse pressure variations at the ends of the nonuniform duct section. A good correlation is observed for the transverse variations except that the pressure of the cut-off mode 3 is so small at $z = \ell$. Figures 8.1 - 8.3 show that the FEM (3 x 8) mesh gives smoother curves, connecting nodal values on the centreline, than the FEM (3 x 5). In fact, more obviously for incident mode 1 in Figure 8.1, the FEM (3 x 5) values tend to fluctuate about the FEM (3 x 8) curves, approximating the solution in an average sense.

Another test case involving a cosine-converging duct configuration, $R_1 = 1.0$, $R_2 = 0.925$, $\ell = 0.5$, area contraction ratio $(R_2/R_1)^2 = 0.855$ is considered at $k_r R_1 = 5.0$, $m_o = 0$, $M_1 = -0.30$. A higher degree of agreement is achieved in Tables 8.9, 8.10 and Figures 8.7 - 8.12, reaffirming the effect of length scale, as noted in the no-flow case.

In both the no-flow and flow cases the long duct poses an inherent difficulty in transmission problems. In the MWR a large number of basis functions, including many extreme cut-off modes, can cause numerical instability in long ducts (see Section 5.1.3(iv)) while the introduction of cut-off modes in the FEM results in a degradation of accuracy in modal coefficients. It is accounted for by the exponential behaviour to cause small values of coefficients associated with cut-off modes. The situation may be more aggravated for the flow case. Figures 8.3, 8.9 show the axial behaviour of cut-off modes. As typically seen in Figures 8.1, 8.2, 8.7 and 8.8, cut-on modes have rapid change in slope and wide variations along the duct, apparently characteristic of waveforms. The MWR's axial integration seems to cope with cut-on modes satisfactorily. For the FEM, because the capacity to accommodate nodal variables is limited to quadratic variations along each element boundary (see Section 5.2.3(iv)), consequently at the same level of accuracy, a longer duct requires more axial elements for sufficient resolutions. The situation becomes more severe at high

frequency, and near the throat at high flow speed because of wavelength - shortening effects.

The same geometry and parameters are employed in another test case, except that the inlet Mach number increases to $M_1 = -0.45$ at $z = 0$ corresponding to $M_2 = -0.56$ at $z = \ell$. Tables 8.11, 8.12 and Figures 8.13 - 8.18 show the results for this case. While the MWR and FEM coefficients in the tables are comparable, the figures show that the degradation of accuracy due to Mach number effect for mode 1 is more incipient than for other modes, at least of the cut-on modes.

It is noted that for the cosine-converging geometry both the MWR and FEM yield a physically unrealistic value of transmission efficiencies which is greater than unity. It is more obvious for the case of $M_1 = -0.45$. This does not occur in the cosine-converging-diverging hardwalled duct of Table 8.8, nor in the softwall case of Table 8.6. Thus, the model flow field, which is rotational, is hypothesized to produce acoustic disturbance, of which the intensity may increase with higher flow speed.

(ii) Antisymmetric modes

The first antisymmetric angular mode $m_o = 1$ is considered at frequency $k_r R_1 = 6.0$ in a cosine-converging duct configuration $R_1 = 1.0$, $R_2 = 0.925$, $\ell = 0.5$ with Mach number $M_1 = -0.30$ at $z = 0$ and $M_2 = -0.36$ at $z = \ell$. This case is computationally challenging to the MWR in the sense that a forced boundary condition is violated. If one recalls that in the MWR approximation the transverse velocity component is set to be $u \approx u_N = \sum_{m=1}^{N} u_m \sin \kappa_m r$ (see Section 6.1.2) then at $r = 0$ apparently u_N is forced to vanish no matter what the u_m are. But the uniform circular duct eigenfunctions are the Bessel functions $J_{m_o}(\kappa_n r)$, (see Appendix C) from which $u = \sum_{n=1}^{\infty} u_n J'_{m_o}(\kappa_n r)$ and $J'_{m_o}(\kappa_n r) \neq 0$ when $m_o = 1$ and $r \to 0$.

Tables 8.13, 8.14 still show a good agreement between the MWR and FEM results. The slope continuity in Figures 8.19 - 8.21 shows that five elements along the axial direction in the FEM (3 x 5) mesh are sufficient for axial resolutions. While the correlation in transverse pressure variations in Figures 8.22 - 8.24 is reasonable elsewhere, a degradation of accuracy is observed in the neighbourhood of the duct centreline. The MWR's violation of the forced boundary condition partly accounts for this deterioration. In fact, it is also found that increasing from 5BF to 6BF in the MWR generally narrows the gap between the results at r = 0, and makes the MWR values smaller near r = 0. This is expected since in the uniform ducts $J_{m_o}(\kappa_n r)\Big|_{r=0} = 0$ for $m_o \neq 0$.

For the same geometry and other parameters Tables 8.15, 8.16 and Figures 8.25 - 8.30 present the results at angular mode $m_o = 2$, frequency $k_r R_1 = 8.0$. At this angular mode the MWR's violation disappears and there should be an improvement. Figures 8.28 - 8.30 show this is the case. If angular mode is kept at $m_o = 1$ and inlet Mach number is increased up to $M_1 = -0.45$ experiments showed that the MWR (5BF) or MWR (6BF) gives acceptable results while the FEM (4 x 6) modal coefficients are incorrect (judged by efficiencies). It is believed more elements are required for transverse resolutions in this case.

The concept of distributing residual weights, which was successful in high angular mode eigenproblems (see Section 4.3.3(ii)) has not been tried yet for the flow case.

(iii) Transverse discretization

A number of results have been obtained by the FEM with parabolic distribution of elements across the duct (see Figure 4.3(b) and Section 4.3.3(ii)) including the eigenproblem (Chapter 4) and the no-flow case (Chapter 5). The nonuniform distribution of elements is to account for

rapid variations of high-order Bessel functions near the duct wall. The parabolic distribution is derived from the subdivision of the non-uniform duct section into 3_D elements of equal annular cross-sectional area. In the reduced 2_D domain of the axisymmetric duct section the line elements across the duct (Figure 4.3(b)) become parabolically distributed. Physically, the parabolic distribution of elements allows the acoustic plane mode to transmit equal power through each annular cross-section of the 3_D elements, and in the flow case the flow rate through each annulus is equal. In the transmission problems with or without flow, up to $m_o = 4$, the advantage of the parabolic distribution is not clear for modal reflection and transmission coefficients. This point can be illustrated by comparing the results in Tables 8.15, 8.16 and Figures 8.25 - 8.27. But Figures 8.28 - 8.30 show that the FEM with uniform mesh of elements produces better comparisons with the MWR, particularly near the duct centreline ($r = 0$), where one expects the pressure to be relatively small for $m_o = 2$. This is accounted for, partly by a rapid change in slope near $r = 0$, partly by the propensity of the solution representation at $r = 0$ to cause a singularity. Thus, a uniform distribution appears to be favourable for low-order angular modes ($m_o \leq 4$ say).

Table 8.17 and Figures 8.31 - 8.36 compare the results for the same duct with flow at angular mode $m_o = 4$, frequency $k_r R_1 = 11.0$. It is not possible to increase the number of basis functions in the MWR as 6 basis functions give incorrect results for this case, revealing the difficulty associated with severely decaying cut-off modes at this high angular mode. The discontinuity of axial pressure variations at corner nodes in Figures 8.31 - 8.33 shows insufficient resolution and the deficiency in slope of piecewise continuous shape functions at this high frequency. However, good correlation is still observed for transverse pressure variations in Figures 8.34 - 8.36, with the FEM employing a uniform mesh.

(iv) Softwall case

A cosine-converging duct section of wall admittance $A = (0.72 - 0.42i)$ is joined by two hardwalled semi-infinite ducts. The geometry is $R_1 = 1.0$, $R_2 = 0.925$, $\ell = 0.5$. The acoustic wave propagation is considered in this configuration, at angular mode $m_o = 0$, frequency $k_r R_1 = 5.0$, inlet Mach number $M_1 = -0.3$. Tables 8.18, 8.17 show a deterioration between the MWR and FEM coefficients in comparison to the hardwall case in Tables 8.9, 8.10, but a good agreement in transmission efficiencies is still observed. The slope continuity in Figures 8.37 - 8.39 show that the axial resolutions are not seriously affected by the wall admittance and change in the transverse element discretization. Transmission and reflection coefficients are apparently more sensitive than pressure variations and transmission efficiencies.

Figures 8.40 - 8.42 compare the transverse pressure variations at the ends of the nonuniform duct. The variation in mode 1 is most sensitive, particularly near the centreline ($r = 0$) and the duct wall ($r = R$). Increasing from 5 basis functions to 6 basis functions in the MWR reveals a convergence towards the FEM values, especially near the centreline. In comparison with the hardwall results in Figures 8.10 - 8.12 this fact shows that the MWR's convergence is slower for the softwall case than for the hardwall. This trend is expected since the MWR basis functions do not satisfy the duct-wall boundary condition in the softwall case.

8.3 NONUNIFORM DUCTS WITH FLOW AT HIGH MACH NUMBER

8.3.1 Limitations of Computational Methods

The most challenging acoustic problems arise when high Mach number mean flow is introduced in nonuniform ducts. In high Mach number flows the wavelength-shortening effect near the throat is accelerated because small duct cross-sectional area changes cause

large changes in Mach number, high flow gradients, and rapid change in wavelength. In addition, the difficulty is compounded by large pressure amplitudes as the nonlinear regime is approached. It is also believed that axial and transverse variations at high Mach numbers become much more strongly inter-related than in low Mach number cases due to complicated reflection and transmission phenomena. Because of high flow gradients near the throat the modified one-dimensional flow model employed may become inappropriate. The acoustic wave propagation in nonuniform ducts carrying very high Mach number flow poses an elusive problem to any computational method.

For the low Mach number case the MWR and the FEM have been shown to have comparable accuracy in several test cases. However,the adequacy of FEM's mesh size and MWR's number of basis functions is still a matter of trial-and-error experiments. For high Mach number the situation is unpredictable. The effect of cut-off modes may become more pronounced in the MWR while the FEM encounters the severity of high dimensionality because of increased requirements on resolution near the throat.

With this complexity, the following test cases are chosen to represent typical problems which are computationally practical, taking into account limitations of the methods. A uniform mesh is used for the FEM scheme.

8.3.2 Numerical Results

The same cosine-converging geometry as for several low Mach number test cases, $R_1 = 1.0$, $R_2 = 0.925$, $\ell = 0.5$, is considered at frequency $k_1R_1 = 4.0$, angular mode $m_c = 0$. A Mach number $M_1 = -0.55$ is introduced at $z = 0$, corresponding to Mach number $M_2 = -0.73$ at $z = \ell$. This case is well into the region where the effects of high speed flow become strongly established.

The MWR was successively run with 5, 6, 7 basis functions while the FEM (4 x 6) and FEM (4 x 7) meshes were used. The FEM grids were also modified so as to compress several elements into the region near the throat (see Figure 8.43). In general, comparisons of Tables 8.20 - 8.22 show reasonable correlation between the MWR and FEM results even though they are not as good as the low Mach number cases. Inspection of the pressure variations along the duct axis in Figures 8.44 - 8.46 reveals that the incident mode 1 is most sensitive to high Mach number effects on the basis of slope continuity of nodal values at FEM corner nodes. The compressed FEM meshes do not yield any obvious improvements.

Figures 8.47 - 8.49 make comparisons of the transverse pressure variations at the ends of the nonuniform duct. Good correlations are observed for modes 2 and 3. Compressing more elements towards the throat gives little difference in the FEM results. However, for mode 1 there is a discrepancy between the FEM and MWR values, which deteriorates particularly near the duct centreline ($r = 0$). In Figure 8.47 it was also found that the gap between the MWR (5BF) and MWR (7BF) values is smaller than that between either the MWR (5BF) or MWR (7BF), and MWR (6BF) values. For modes 2 and 3 the MWR (5BF) and MWR (7BF) give nearly identical results for transverse pressures. Thus, one can conclude that the MWR convergence is not monotonic. This reflects on the convergence trend of the coefficient and efficiency values in Table 8.20.

The second case increases the Mach number at $z = 0$ to $M_1 = -0.58$ corresponding to a Mach number $M_2 = -0.80$ at $z = \ell$. At this high speed the regime of nonlinear acoustic behaviour is well established near the throat. Results for this case are given in Tables 8.23 - 8.25 and Figures 8.50 - 8.55 in the same format as above. Similar conclusions can be made here. The problem of axial and transverse resolutions at high Mach number is clearly seen in mode 1 because of wavelength -

shortening effects near the throat. The inconsistent behaviour of the MWR (6BF) is more obvious in Figure 8.53. It is noted that the FEM (4 x 7) compressed mesh does not give any improvement for mode 1, in fact a deterioration was observed, which can be judged by a sudden change in the coefficient and efficiency values of Tables 8.24 - 8.25.

8.3.3 Subsonic Choking

The most interesting feature of high Mach number test cases is their implications in terms of the phenomenon of subsonic acoustic choking. Numerical simulation of the subsonic choking is a goal in the study of duct acoustics. An indication of choking should be revealed in the calculation of the transmission efficiency, which is the ratio of transmitted power to incident power. If there is any trace of subsonic choking due to high speed flow the transmission efficiency must be significantly below unity for a range of frequency, and decrease further as the flow speed increases.

At this point it is not possible to determine whether the MWR or the FEM is more accurate at high Mach numbers. The FEM encounters obvious resolution problems; the situation becomes more serious for higher frequencies. The MWR suffers inconsistent convergence in addition to the effect of extreme cut-off modes.

While the reliability of the MWR and FEM at very high subsonic Mach numbers together with the economy and dimensionality of these routines does not warrant generation of acoustic power spectra for a large range of frequency, any traces of subsonic choking would serve as a guide for further explorations. Towards this end computations of efficiencies have been performed. Re-examination of the transmission efficiency values for the test cases with hardwalled ducts carrying low or high speed flow has revealed no trace of subsonic choking as the transmission efficiencies obtained are very close to unity.

For the cosine-converging geometry both the MWR and FEM occasionally yield a physically unrealistic value of transmission efficiencies which is greater than unity. This behaviour is not encountered in the cosine-converging-diverging geometry previously discussed nor in cases involving acoustically treated walls. For this reason it is assumed that the model flow field, which is not fully physically justifiable and which is rotational, leads to the observed phenomenon. This makes it difficult to fully isolate the choking phenomenon, if present, until a more realistic flow model is available.

The following test case is designed to look for the subsonic acoustic choking. A cosine-converging-diverging configuration of hardwalled duct is considered, $R_1 = R_2 = 1.0$, $R_t = 0.925$, $\ell = 0.75$. The inlet flow Mach number is selectively varied, $M_1 = -0.58, -0.59, -0.60$ corresponding to Mach number at the throat $M_t = -0.80, -0.83, -0.865$. Acoustic disturbances propagate through the nonuniform duct at angular mode $m_o = 0$. It is necessary to point out here that for this converging-diverging geometry the ratio $(R_1 - R_t)/(\ell/2)$ may serve as a measure of the duct nonuniformity. Too short a duct makes this ratio very large, which may be too severe for the computational methods.

Table 8.26 presents the transmission efficiencies computed by MWR with different numbers of basis functions at frequencies $k_r R_1 = 4.0$ and 5.0. No rigorous explanation is offered for the behaviour of the results because of the nature of the acoustic problem at high speed flow. But the conclusion may be drawn that no obvious evidence of subsonic acoustic choking is observed for this particular test case.

8.4 DISCUSSIONS AND CONCLUSIONS

8.4.1 Computational Efficiency

General discussions on the computational efficiency and advantages of the MWR and FEM have been covered for the no-flow case

(see Section 5.5.1) many of them are still applicable for the flow case. This section is more concerned about the economy and dimensionality in practical computations.

A feature of the MWR and FEM approaches reported here is the restriction to in-core computer implementations. The FEM is purposely limited to mesh sizes compatible with core limitations so that useful results can be generated with relatively modest computational requirement. The array limit of the Burroughs B6718 computer in use is 65,535 elements (approximately a size of 256 x 256), placing the maximum size on the FEM system matrix. With the system matrix in packed form (see Section 3.2.4(ii) and Figure 3.8) and restricted to in-core storage, the finest FEM grids that can be employed in the flow problem are FEM (5 x 4) and FEM (4 x 7). A relaxation of the restriction to in-core computation will be required for extensive analysis in the high Mach number case and when complex flow modelling is employed.

In order to reduce the problem of high dimensionality an attempt has been made to develop an algorithm for solving a system of linear equations by the L-U decomposition method (see Appendix E). This approach optimizes the required storage by incorporating the L-U solution procedure into the FEM assembly stage, and uses secondary storages outside the core. However, to compensate for a reduction in storage requirement an appreciable number of mapping routines are to be used in storing and retrieving matrix coefficients via one-dimensional arrays. This increases considerably the solution time, rendering the L-U decomposition method impractical in comparison to the MWR. The dilemma occurs partly because of the complication of the system matrix arising from quadratic Serendipity element discretization (compare with Abrahamson's algorithm for linear rectangular element discretization in [74]).

The MWR has lower dimensionality than the FEM, but consumes more computing time, most of which is spent on the Runge-Kutta integration scheme. The solution time varies widely and depends on a particular combination of parameters (see Discussions in Section 5.5.1(ii)). For a duct of very small wall admittance, with 25 steps of axial integration, increasing from MWR (5BF) to MWR (6BF) nearly doubles the solution time. The MWR (7BF) consumes about 2.5 times as much as that for the MWR (5BF). In this case the solution times of the MWR (6BF) and the FEM (4 x 7) are comparable. However, primary attention should be paid to the capability of the methods to solve the problem satisfactorily and the economy factor should be secondary.

8.4.2 Conclusions

A cautious and systematic approach has been taken to the application of the MWR and the FEM to the problems of acoustic transmission in nonuniform ducts with flow. The two methods have been developed in parallel in order to verify successes based on the computations of modal coefficients, transmission and reflection efficiencies, and the acoustic field in the duct. The computer implementationshave been specifically limited to in-core solution methods and results have been obtained on the relative performance and limitations of the two methods.

Several test cases in selected geometries have been presented to show that the MWR and FEM yield results of comparable accuracy for moderate Mach numbers (conservatively $|M_a| \leq 0.56$ everywhere in the duct) except in computationally challenging cases, for instance, at high angular mode ($m_o > 4$). The slope continuity at element nodes provides an additional assessment of the FEM accuracy. Plotting the transverse pressure variations at the ends of the nonuniform duct enabled reconsideration of the transverse element discretization in the FEM for moderate angular modes, and revealed the effect of boundary

condition violation on the MWR convergence for angular mode $m_o = 1$. It is interesting to note that the first cut-on mode is most sensitive to wall admittance, Mach number, and length scale. If there is any divergence between the MWR and FEM results or an appearance of slope discontinuity in the FEM nodal values the first mode is most likely to show the deterioration.

For high Mach number the FEM encounters resolution problems which are connected with the development of the acoustic field near the throat, which cannot be adequately represented by the chosen shape functions within the mesh size constraints imposed by the in-core solution scheme. The MWR exhibits an inconsistent convergence particularly in the neighbourhood of the centreline, which tends towards singular behaviour.

The attempt to simulate the subsonic acoustic choking has failed to come to firm conclusions.

Geometry : Uniform, $R_1 = R_2 = 1.0$, $\ell = 0.2$

Characteristics : Softwalled Duct with Flow, $M_1 = -0.1$, $k_r R_1 = 1.0$, $A_1 = 0$, $A_2 = 0$, $A = (0.1-0.1i)$, Angular Mode $m_o = 0$, FEM: Point Matching with FEM Eigenfunctions

MWR(5BF)				FEM(5 x 2)			
Reflection Coefficients	(1)	(2)	(3)	Reflection Coefficients	(1)	(2)	(3)
(1)	-0.015 + 0.023i	0.002 - 0.007i	-0.000 + 0.005i	(1)	-0.015 + 0.023i	0.002 - 0.007i	-0.000 + 0.005i
(2)	0.008 + 0.013i	-0.003 - 0.003i	0.002 + 0.001i	(2)	0.008 + 0.013i	-0.003 - 0.003i	0.003 + 0.001i
(3)	-0.002 - 0.010i	0.001 + 0.003i	-0.002 - 0.001i	(3)	-0.002 + 0.001i	0.001 + 0.001i	-0.001 - 0.000i
Transmission Coefficients	(1)	(2)	(3)	Transmission Coefficients	(1)	(2)	(3)
(1)	0.957 - 0.192i	0.002 - 0.009i	-0.000 + 0.006i	(1)	0.957 - 0.192i	0.002 - 0.009i	0.000 + 0.006i
(2)	0.014 + 0.005i	0.472 - 0.010i	0.002 - 0.000i	(2)	0.015 + 0.005i	0.473 - 0.010i	0.000 - 0.000i
(3)	-0.011 + 0.001i	0.003 - 0.001i	0.246 - 0.004i	(3)	-0.010 - 0.003i	0.003 + 0.000i	0.252 - 0.005i
Hydrodynamic Mode Coefficients	(1)	(2)	(3)	Hydrodynamic Mode Coefficients	(1)	(2)	(3)
(1)	1.000 - 0.000i	0.000 + 0.000i	0.000 + 0.000i	(1)	1.029 + 0.011i	0.009 + 0.002i	0.014 - 0.001i
(2)	0.000 + 0.000i	1.000 + 0.000i	0.000 + 0.000i	(2)	0.014 + 0.006i	1.070 + 0.020i	0.079 + 0.001i
(3)	-0.000 + 0.000i	0.000 + 0.000i	1.000 + 0.000i	(3)	0.001 + 0.004i	-0.005 + 0.027i	1.009 + 0.068i

Table 8.1 Reflection, Transmission and Hydrodynamic Mode Coefficient Matrices for a Uniform Softwalled Duct with Flow, $M_1 = -0.1$.

Geometry : Uniform, $R_1 = R_2 = 1.0$, $\ell = 0.2$

Characteristics : Softwalled Duct with Flow, $M_1 = -0.5$, $k_r R_1 = 5.0$, $A_1 = 0$, $A_2 = 0$. $A = (0.1-0.1i)$

Angular Mode $m_o = 0$, FEM: Point Matching with FEM Eigenfunctions

MWR(5BF)				FEM(5 x 2)			
Reflection Coefficients	(1)	(2)	(3)	Reflection Coefficients	(1)	(2)	(3)
(1)	0.01 + 0.02i	-0.00 - 0.01i	0.00 + 0.00i	(1)	0.01 + 0.02i	-0.00 - 0.01i	0.00 + 0.00i
(2)	-0.04 - 0.09i	0.01 + 0.04i	0.00 - 0.02i	(2)	-0.03 - 0.09i	0.01 + 0.04i	0.00 - 0.02i
(3)	-0.19 - 0.12i	0.07 + 0.06i	-0.03 - 0.03i	(3)	-0.15 - 0.12i	0.05 + 0.05i	-0.02 - 0.02i
Transmission Coefficients	(1)	(2)	(3)	Transmission Coefficients	(1)	(2)	(3)
(1)	-0.33 - 0.88i	-0.03 - 0.02i	0.01 + 0.01i	(1)	-0.35 - 0.90i	-0.03 - 0.02i	0.01 + 0.01i
(2)	-0.22 - 0.11i	-0.02 - 0.94i	-0.02 - 0.02i	(2)	-0.24 - 0.14i	-0.03 - 0.95i	-0.02 - 0.02i
(3)	-0.11 + 0.19i	-0.06 - 0.06i	0.28 - 0.23i	(3)	-0.12 + 0.16i	-0.06 - 0.05i	0.29 - 0.23i
Hydrodynamic Mode Coefficients	(1)	(2)	(3)	Hydrodynamic Mode Coefficients	(1)	(2)	(3)
(1)	1.01 - 0.01i	0.00 + 0.00i	0.00 + 0.00i	(1)	1.03 + 0.01i	-0.00 + 0.00i	-0.00 - 0.00i
(2)	0.00 - 0.00i	1.00 + 0.00i	0.00 + 0.00i	(2)	-0.00 + 0.00i	1.03 + 0.02i	-0.00 + 0.03i
(3)	-0.01 + 0.00i	0.00 + 0.00i	1.00 + 0.00i	(3)	0.00 + 0.01i	-0.01 + 0.05i	0.99 + 0.18i

Table 8.2 Reflection, Transmission and Hydrodynamic Mode Coefficient Matrices for a Uniform Softwalled Duct with Flow, $M_1 = -0.5$.

Geometry : Linearly Tapered, $R_1 = 1.0$, $R_2 = 1.1$, $\ell = 0.5$

Characteristics : Hardwalled Duct with Flow, $k_r R_1 = 5.0$, $M_1 = -0.10$, $M_2 = -0.082$,
Angular Mode $m_o = 0$, FEM: Point Matching with FEM Eigenfunctions

MWR(5BF)				FEM(5 x 4)			
Reflection Coefficients				Reflection Coefficients			
	(1)	(2)	(3)		(1)	(2)	(3)
(1)	0.01 + 0.01i	-0.01 - 0.01i	-0.00 + 0.01i	(1)	0.01 + 0.01i	-0.01 - 0.01i	-0.00 + 0.01i
(2)	-0.06 - 0.09i	0.02 + 0.07i	0.02 - 0.01i	(2)	0.07 - 0.11i	0.02 + 0.08i	0.03 - 0.00i
(3)	-0.08 - 0.09i	0.02 + 0.06i	-0.00 - 0.00i	(3)	-0.07 - 0.07i	0.01 + 0.05i	-0.01 - 0.00i
Transmission Coefficients				Transmission Coefficients			
	(1)	(2)	(3)		(1)	(2)	(3)
(1)	-0.81 - 0.33i	0.02 + 0.02i	-0.00 - 0.01i	(1)	-0.83 - 0.33i	0.03 + 0.02i	-0.00 - 0.01i
(2)	-0.19 - 0.21i	-0.33 - 0.79i	0.01 + 0.04i	(2)	-0.23 - 0.24i	-0.32 - 0.79i	0.01 + 0.03i
(3)	-0.13 + 0.06i	0.08 - 0.01i	0.10 - 0.02i	(3)	-0.12 + 0.05i	0.07 - 0.01i	0.11 - 0.02i

Table 8.3 Reflection and Transmission Coefficient Matrices for a Linearly Tapered Hardwalled Duct with Flow, $R_2/R_1 = 1.1$.

Geometry : Linearly Tapered, $R_1 = 1.0$, $R_2 = 1.134$, $\ell = 0.5$

Characteristics : Hardwalled Duct with Flow, $k_r R_1 = 5.0$, $M_1 = -0.50$, $M_2 = -0.36$,
Angular Mode $m_o = 0$, FEM: Point Matching with FEM Eigenfunctions

MWR(5BF)				FEM(5 x 4)			
Reflection Coefficients				Reflection Coefficients			
	(1)	(2)	(3)		(1)	(2)	(3)
(1)	-0.00 + 0.00i	-0.00 + 0.00i	-0.00 + 0.01i	(1)	0.00 + 0.00i	-0.00 - 0.00i	-0.00 + 0.00i
(2)	-0.03 - 0.02i	0.03 + 0.00i	0.01 - 0.00i	(2)	-0.04 - 0.03i	0.03 + 0.00i	0.01 - 0.01i
(3)	-0.14 - 0.19i	0.07 + 0.17i	-0.03 - 0.04i	(3)	-0.07 - 0.18i	0.03 + 0.17i	-0.01 - 0.03i
Transmission Coefficients				Transmission Coefficients			
	(1)	(2)	(3)		(1)	(2)	(3)
(1)	-0.23 + 0.64i	0.02 - 0.05i	-0.01 + 0.01i	(1)	-0.23 + 0.66i	0.02 - 0.06i	-0.01 + 0.01i
(2)	-0.37 + 0.26i	-0.61 + 0.38i	0.07 - 0.01i	(2)	-0.40 + 0.29i	-0.61 + 0.37i	0.06 - 0.00i
(3)	0.09 + 0.16i	-0.03 - 0.18i	0.03 - 0.07i	(3)	0.06 + 0.16i	-0.02 - 0.18i	0.03 - 0.06i

Table 8.4 Reflection and Transmission Coefficient Matrices for a Linearly Tapered Hardwalled Duct with Flow, $R_2/R_1 = 1.134$.

Geometry : Linearly Tapered, $R_1 = 1.0$, $R_2 = 1.268$, $\ell = 0.5$

Characteristics : Hardwalled Duct with Flow, $k_r R_1 = 5.0$, $M_1 = -0.50$, $M_2 = -0.28$

Angular Mode $m_o = 0$, FEM: Least-square matching with Exact Eigenfunctions

MWR(5BF)				FEM(5 x 4)			
Reflection Coefficients				Reflection Coefficients			
	(1)	(2)	(3)		(1)	(2)	(3)
(1)	-0.01 + 0.00i	-0.01 + 0.01i	-0.00 + 0.01i	(1)	-0.00 + 0.01i	-0.00 + 0.00i	-0.00 + 0.01i
(2)	-0.02 - 0.06i	0.04 - 0.03i	0.01 - 0.00i	(2)	-0.03 - 0.06i	0.05 - 0.04i	0.00 - 0.01i
(3)	-0.20 - 0.27i	0.14 + 0.27i	-0.07 - 0.09i	(3)	-0.07 - 0.26i	0.06 + 0.27i	-0.04 - 0.05i
Transmission Coefficients				Transmission Coefficients			
	(1)	(2)	(3)		(1)	(2)	(3)
(1)	-0.29 + 0.41i	0.03 - 0.08i	-0.02 + 0.01i	(1)	-0.26 + 0.42i	0.02 - 0.10i	-0.02 + 0.02i
(2)	-0.67 + 0.18i	-0.44 + 0.27i	0.08 - 0.01i	(2)	-0.69 + 0.19i	-0.42 + 0.26i	0.07 - 0.01i
(3)	0.08 + 0.24i	-0.02 - 0.38i	0.04 - 0.03i	(3)	0.04 + 0.23i	-0.03 - 0.37i	0.03 - 0.06i

Table 8.5 Reflection and Transmission Coefficient Matrices for a Linearly Tapered Hardwalled Duct with Flow, $R_2/R_1 = 1.268$

Geometry : Cosine-Converging-Diverging, $R_1 = 1.0$, $R_t = 0.9$, $R_2 = 1.0$, $\ell = 0.5$

Characteristics : Softwalled Duct with Flow, $M_1 = -0.3$, $M_t = -0.38$, $M_2 = -0.3$, $k_r R_1 = 5.0$, $A_1 = 0$, $A_2 = 0$, $A = 0.2-0.2i$

Angular Mode $m_o = 0$, FEM: Point Matching with FEM Eigenfunctions.

MWR(5BF)				FEM(5 x 4)			
Reflection Coefficients				Reflection Coefficients			
	(1)	(2)	(3)		(1)	(2)	(3)
(1)	0.06 - 0.05i	-0.05 + 0.01i	0.01 + 0.01i	(1)	0.05 - 0.03i	-0.05 + 0.01i	0.01 + 0.02i
(2)	-0.11 - 0.05i	0.18 + 0.04i	0.02 - 0.07i	(2)	-0.23 - 0.10i	0.19 + 0.08i	0.02 - 0.07i
(3)	-0.43 + 0.15i	0.14 - 0.01i	0.01 - 0.01i	(3)	-0.42 + 0.07i	0.14 - 0.00	0.00 - 0.02i
Reflection Efficiency : 0.030				Reflection Efficiency : 0.027			
Transmission Coefficients				Transmission Coefficients			
	(1)	(2)	(3)		(1)	(2)	(3)
(1)	-0.71 + 0.34i	-0.08 + 0.08i	0.02 + 0.00i	(1)	-0.69 + 0.32i	-0.09 + 0.08i	0.03 - 0.00i
(2)	-0.51 + 0.62i	-0.68 - 0.32i	-0.13 - 0.05i	(2)	-0.67 + 0.78i	-0.62 - 0.31i	-0.11 - 0.05i
(3)	0.23 + 0.32i	0.02 - 0.18i	0.01 - 0.09i	(3)	0.13 + 0.34i	0.05 - 0.18i	0.02 - 0.08i
Transmission Efficiency : 0.960				Transmission Efficiency : 0.959			

Table 8.6 Reflection and Transmission Coefficient Matrices and Efficiency for a Cosine-Converging-Diverging Softwalled Duct with Flow, $R_t/R_1 = 0.9$.

Geometry : Cosine-Converging-Diverging, $R_1 = 1.0$, $R_t = 0.93$, $R_2 = 1.0$, $\ell = 0.75$

Characteristics : Hardwalled Duct with Flow, $k_r R_1 = 5.0$, $M_1 = -0.30$, $M_t = -0.35$, $M_2 = -0.30$

Angular Mode $m_o = 0$, 2 Cut-on Modes.

MWR(5BF)		MWR(6BF)		MWR(7BF)	
(1)	(2)	(1)	(2)	(1)	(2)
(1) -0.041 - 0.026i	0.010 + 0.031i	(1) -0.042 - 0.030i	0.010 + 0.032i	(1) -0.041 - 0.027i	0.010 + 0.031i
(2) 0.018 + 0.107i	0.042 - 0.096i	(2) 0.023 + 0.136i	0.048 - 0.111i	(2) 0.018 + 0.109i	0.043 - 0.098i
Reflection Efficiency : 0.013		Reflection Efficiency : 0.013		Reflection Efficiency : 0.013	
FEM(3 x 5)		FEM(3 x 8)		FEM(4 x 6)	
(1)	(2)	(1)	(2)	(1)	(2)
(1) -0.039 - 0.029i	0.009 + 0.030i	(1) -0.041 - 0.028i	0.009 + 0.030i	(1) -0.040 - 0.028i	0.009 + 0.030i
(2) 0.018 + 0.134i	0.044 - 0.105i	(2) 0.021 + 0.136i	0.045 - 0.108i	(2) 0.020 + 0.130i	0.044 - 0.103i
Reflection Efficiency : 0.013		Reflection Efficiency : 0.013		Reflection Efficiency : 0.013	

Table 8.7 Reflection Coefficient Matrices and Reflection Efficiency for a Cosine-Converging-Diverging Hardwalled Duct with Flow, $R_t/R_1 = 0.93$.

Geometry : Cosine-Converging-Diverging, $R_1 = 1.0$, $R_t = 0.93$, $R_2 = 1.0$, $\ell = 0.75$

Characteristics : Hardwalled Duct with Flow, $k_r R_1 = 5.0$, $M_1 = -0.30$, $M_t = -0.35$, $M_2 = -0.30$

Angular Mode $m_o = 0$, 2 Cut-on Modes

MWR(5BF)		MWR(6BF)		MWR(7BF)	
(1)	(2)	(1)	(2)	(1)	(2)
(1) 0.756 + 0.639i	0.025 + 0.002i	(1) 0.755 + 0.636i	0.028 + 0.002i	(1) 0.758 + 0.637i	0.025 + 0.002i
(2) 0.156 + 0.000i	-0.496 + 0.840i	(2) 0.257 - 0.004i	-0.498 + 0.828i	(2) 0.164 - 0.001i	-0.496 + 0.839i
Transmission Efficiency : 1.000		Transmission Efficiency : 0.977		Transmission Efficiency : 0.996	
FEM(3 x 5)		FEM(3 x 8)		FEM(4 x 6)	
(1)	(2)	(1)	(2)	(1)	(2)
(1) 0.764 + 0.627i	0.025 + 0.002i	(1) 0.765 + 0.629i	0.024 + 0.002i	(1) 0.766 + 0.627i	0.025 + 0.002i
(2) 0.207 - 0.004i	-0.502 + 0.838i	(2) 0.192 - 0.012i	-0.495 + 0.840i	(2) 0.198 - 0.011i	-0.499 + 0.840i
Transmission Efficiency : 0.994		Transmission Efficiency: 0.991		Transmission Efficiency : 0.993	

Table 8.8 Transmission Coefficient Matrices and Transmission Efficiency for a Cosine-Converging-Diverging Hardwalled Duct with Flow, $R_t/R_1 = 0.93$.

Geometry : Cosine-Converging , $R_1 = 1.0$, $R_2 = 0.925$, $\ell = 0.5$

Characteristics : Hardwalled Duct with flow , $M_1 = -0.3$, $M_2 = -0.36$, $k_r R_1 = 5.0$

Angular Mode $m_o = 0$

MWR(5BF)		MWR(6BF)		MWR(7BF)	
(1)	(2)	(1)	(2)	(1)	(2)
(1) -0.021 - 0.008i	0.009 + 0.011i	(1)-0.022 - 0.008i	0.009 + 0.011i	(1)-0.021 - 0.008i	0.009 + 0.011i
(2) 0.028 + 0.034i	-0.008 - 0.048i	(2) 0.038 + 0.049i	-0.011 - 0.057i	(2) 0.030 + 0.036i	-0.008 - 0.049i
Reflection Efficiency : 0.002		Reflection Efficiency : 0.003		Reflection Efficiency : 0.003	
FEM(3 x 5)		FEM(4 x 6)		FEM(4 x 6) Compressed towards throat	
(1)	(2)	(1)	(2)	(1)	(2)
(1) -0.020 - 0.008i	0.009 + 0.011i	(1)-0.020 - 0.009i	0.009 + 0.011i	(1)-0.020 - 0.009i	0.009 + 0.011i
(2) 0.036 + 0.052i	-0.008 - 0.056i	(2) 0.031 + 0.043i	-0.009 - 0.053i	(2) 0.024 + 0.046i	-0.008 - 0.053i
Reflection Efficiency : 0.003		Reflection Efficiency : 0.003		Reflection Efficiency : 0.002	

TABLE 8.9 Reflection Coefficient Matrices and Reflection Efficiency for a Cosine-Converging Hardwalled Duct with Flow $M_1 = -0.3$, $M_2 = -0.36$, $m_o = 0$.

Geometry : Cosine-Converging , $R_1 = 1.0$, $R_2 = 0.925$, $\ell = 0.5$

Characteristics : Hardwalled Duct with Flow, $M_1 = -0.3$, $M_2 = -0.36$, $k_r R_1 = 5.0$

Angular Mode $m_o = 0$, 2 Cut-on Modes

MWR(5BF)		MWR(6BF)		MWR(7BF)	
(1)	(2)	(1)	(2)	(1)	(2)
(1) -0.968 + 0.658i	-0.050 + 0.004i	(1)-0.950 + 0.650i	-0.057 + 0.004i	(1)-0.963 + 0.657	0.052 + 0.003i
(2) 0.358 - 0.084i	-1.076 - 0.394i	(2) 0.474 - 0.066i	-1.107 - 0.418i	(2) 0.371 - 0.085	1.080 - 0.397i
Transmission Efficiency : 1.004		Transmission Efficiency : 0.997		Transmission Efficiency : 1.002	
FEM(3 x 5)		FEM(4 x 6)		FEM(4 x 6) Compressed towards throat	
(1)	(2)	(1)	(2)	(1)	(2)
(1) -0.967 + 0.656i	-0.054 + 0.002i	(1)-0.961 + 0.656i	-0.054 + 0.001i	(1)-0.955 + 0.632i	0.054 + 0.001i
(2) 0.424 - 0.114i	-1.100 - 0.405i	(2) 0.413 - 0.100i	-1.096 - 0.404i	(2) 0.406 - 0.100i	1.092 - 0.413i
Transmission Efficiency : 1.022		Transmission Efficiency : 1.013		Transmission Efficiency : 0.998	

Table 8.10 Transmission Coefficient Matrices and Transmission Efficiency for a Cosine-Converging Hardwalled Duct with Flow , $M_1 = -0.3$, $M_2 = -0.36$, $m_o = 0$.

Geometry : Cosine-Converging, $R_1 = 1.0$, $R_2 = 0.925$, $\ell = 0.5$

Characteristics : Hardwalled Duct with Flow, $M_1 = -0.45$, $M_2 = -0.56$, $k_r R_1 = 5.0$

Angular Mode $m_o = 0$, 2 Cut-on Modes.

MWR(5BF)			MWR(7BF)		
(1)	(2)	(3)	(1)	(2)	(3)
(1) -0.009 + 0.002i	0.008 + 0.004i	0.003 - 0.004i	(1) -0.010 + 0.000i	0.008 + 0.004i	0.003 - 0.004i
(2) -0.034 + 0.001i	-0.015 - 0.023i	-0.003 + 0.001i	(2) -0.035 + 0.001i	-0.014 - 0.023i	-0.004 + 0.002i
(3) 0.061 + 0.147i	-0.006 - 0.100i	0.010 + 0.009i	(3) 0.061 + 0.136i	-0.008 - 0.096i	0.010 + 0.007i
Reflection Efficiency : 0.003			Reflection Efficiency : 0.003		
FEM(3 x 5)			FEM(4 x 6)		
(1)	(2)	(3)	(1)	(2)	(3)
(1) -0.011 + 0.001i	0.008 + 0.004i	0.002 - 0.003i	(1) -0.010 + 0.000i	0.008 + 0.004i	0.002 - 0.004i
(2) -0.051 + 0.018i	-0.010 - 0.027i	-0.006 + 0.005i	(2) -0.041 + 0.005i	-0.013 - 0.023i	-0.004 + 0.003i
(3) 0.047 + 0.123i	-0.000 - 0.097i	0.007 - 0.003i	(3) 0.061 + 0.116i	-0.010 - 0.089i	0.012 + 0.003i
Reflection Efficiency : 0.003			Reflection Efficiency : 0.003		

Table 8.11 Reflection Coefficient Matrices and Reflection Efficiency for a Cosine-Converging Hardwalled Duct with Flow, $M_1 = -0.45$, $M_2 = -0.56$, $m_o = 0$.

Geometry : Cosine-Converging, $R_1 = 1.0$, $R_2 = 0.925$, $\ell = 0.5$

Characteristics : Hardwalled Duct with Flow, $M_1 = -0.45$, $M_2 = -0.56$, $k_r R_1 = 5.0$

Angular Mode $m_o = 0$, 2 Cut-on Modes.

MWR(5BF)			MWR(7BF)		
(1)	(2)	(3)	(1)	(2)	(3)
(1) 0.492 + 1.221i	-0.015 + 0.072i	0.010 - 0.006i	(1) 0.494 + 1.213i	-0.016 + 0.075i	0.010 - 0.006i
(2) -0.080 - 0.506i	-0.602 + 1.092i	-0.104 + 0.024i	(2) -0.079 - 0.522i	-0.606 + 1.097i	-0.102 + 0.023i
(3) -0.198 + 0.033i	0.098 + 0.058i	-0.014 - 0.087i	(3) -0.186 + 0.036i	0.096 + 0.055i	-0.016 - 0.086i
Transmission Efficiency : 1.008			Transmission Efficiency : 1.006		
FEM(3 x 5)			FEM(4 x 6)		
(1)	(2)	(3)	(1)	(2)	(3)
(1) 0.497 + 1.206i	-0.020 + 0.079i	0.009 - 0.006i	(1) 0.500 + 1.151i	-0.020 + 0.079i	0.011 - 0.007i
(2) -0.095 - 0.620i	-0.631 + 1.121i	-0.085 + 0.014i	(2) -0.094 - 0.602i	-0.617 + 1.085i	-0.100 + 0.020i
(3) -0.196 + 0.055i	0.105 + 0.046i	-0.017 - 0.064i	(3) -0.160 + 0.033i	0.087 + 0.046i	-0.019 - 0.078i
Transmission Efficiency : 1.023			Transmission Efficiency : 1.015		

Table 8.12 Transmission Coefficient Matrices and Transmission Efficiency for a Cosine-Converging Hardwalled Duct, $M_1 = -0.45$, $M_2 = -0.56$, $m_o = 0$.

Geometry : Cosine-Converging $R_1 = 1.0$, $R_2 = 0.925$, $\ell = 0.5$

Characteristics : Hardwalled Duct with Flow, $M_1 = -0.30$, $M_2 = -0.36$, $k_r R_1 = 6.0$

Angular Mode $m_o = 1$, 2 Cut-on Modes

MWR(5BF)			MWR(6BF)		
(1)	(2)	(3)	(1)	(2)	(3)
(1) -0.026 + 0.003i	-0.038 - 0.037i	0.013 - 0.014i	(1) -0.026 + 0.002i	-0.038 - 0.037i	0.013 - 0.013i
(2) -0.036 - 0.029i	-0.001 - 0.089i	0.001 + 0.019i	(2) -0.035 - 0.029i	-0.001 - 0.088i	0.006 + 0.019i
(3) 0.011 + 0.022i	-0.009 + 0.041i	0.003 - 0.001i	(3) 0.011 + 0.022i	-0.009 + 0.042i	0.003 - 0.001i
Reflection Efficiency : 0.023			Reflection Efficiency : 0.023		
FEM(3 x 5)			FEM(4 x 6)		
(1)	(2)	(3)	(1)	(2)	(3)
(1) -0.025 + 0.001i	-0.036 - 0.037i	0.014 - 0.012i	(1) -0.025 + 0.001i	-0.037 - 0.037i	0.013 - 0.013i
(2) -0.037 - 0.028i	0.000 - 0.085i	0.001 + 0.031i	(2) -0.032 - 0.027i	0.000 - 0.083i	0.002 + 0.023i
(3) 0.010 + 0.020i	-0.014 + 0.038i	0.002 - 0.007i	(3) 0.009 + 0.021i	-0.011 + 0.037i	0.001 - 0.004i
Reflection Efficiency : 0.022			Reflection Efficiency : 0.021		

Table 8.13 Reflection Coefficient Matrices and Reflection Efficiency for a Cosine-Converging Hardwalled Duct with Flow, $M_1 = -0.30$, $M_2 = -0.36$, $m_o = 1$.

Geometry : Cosine-Converging $R_1 = 1.0$, $R_2 = 0.925$, $\ell = 0.5$

Characteristics : Hardwalled Duct with Flow, $M_1 = -0.30$, $M_2 = -0.36$, $k_r R_1 = 6.0$

Angular Mode $m_o = 1$, 2 Cut-on Modes.

MWR(5BF)				MWR(6BF)			
	(1)	(2)	(3)		(1)	(2)	(3)
(1)	-0.423 + 1.067i	0.203 - 0.085i	0.031 - 0.000i	(1)	-0.421 + 1.067i	0.205 - 0.084i	0.031 - 0.001i
(2)	-0.225 + 0.098i	-1.097 - 0.447i	0.082 + 0.075i	(2)	-0.220 + 0.099i	-1.097 - 0.442i	0.081 + 0.075i
(3)	-0.020 - 0.016i	0.002 - 0.038i	0.013 - 0.034i	(3)	-0.020 - 0.015i	0.002 - 0.039i	0.013 - 0.033i
Transmission Efficiency : 0.994				Transmission Efficiency : 0.992			
FEM(3 x 5)				FEM(4 x 6)			
	(1)	(2)	(3)		(1)	(2)	(3)
(1)	-0.422 + 1.071i	0.212 - 0.080i	0.034 - 0.002i	(1)	-0.419 + 1.069i	0.212 - 0.080i	0.034 - 0.001i
(2)	-0.212 + 0.099i	-1.103 - 0.435i	0.051 + 0.084i	(2)	-0.210 + 0.108i	-1.102 - 0.437i	0.078 + 0.078i
(3)	-0.024 + 0.003i	0.004 - 0.039i	0.051 - 0.005i	(3)	-0.018 - 0.013i	0.007 - 0.034i	0.021 - 0.017i
Transmission Efficiency : 0.991				Transmission Efficiency : 0.986			

Table 8.14 Transmission Coefficient Matrices and Transmission Efficiency for a Cosine-Converging Hardwalled Duct with Flow, $M_1 = -0.30$, $M_2 = -0.36$, $m_o = 1$.

Geometry : Cosine-Converging, $R_1 = 1.0$, $R_2 = 0.925$, $\ell = 0.5$

Characteristics : Hardwalled Duct with Flow, $M_1 = -0.30$, $M_2 = -0.36$, $k_r R_1 = 8.0$

Angular Mode $m_o = 2$, 2 Cut-on Modes

MWR(5BF)				MWR(6BF)			
	(1)	(2)	(3)		(1)	(2)	(3)
(1)	-0.004 + 0.009i	-0.033 + 0.003i	0.008 - 0.022i	(1)	-0.004 + 0.009i	-0.033 + 0.002i	0.008 - 0.022i
(2)	-0.019 + 0.004i	-0.035 - 0.034i	0.016 + 0.004i	(2)	-0.018 + 0.003i	-0.033 - 0.034i	0.016 + 0.005i
(3)	0.025 + 0.016i	0.015 + 0.057i	-0.001 - 0.005i	(3)	0.026 + 0.018i	0.016 + 0.059i	-0.001 - 0.004i
Reflection Efficiency : 0.006				Reflection Efficiency : 0.006			
FEM(4 x 6) Uniform Mesh				FEM(4 x 6) Compressed towards wall			
	(1)	(2)	(3)		(1)	(2)	(3)
(1)	-0.005 + 0.007i	-0.032 + 0.001i	0.009 - 0.022i	(1)	-0.006 + 0.007i	-0.033 + 0.001i	0.009 - 0.021i
(2)	-0.015 + 0.004i	-0.033 - 0.032i	0.018 + 0.004i	(2)	-0.017 + 0.003i	-0.033 - 0.034i	0.018 + 0.007i
(3)	0.024 + 0.014i	0.015 + 0.053i	-0.002 - 0.007i	(3)	0.022 + 0.013i	0.013 + 0.051i	-0.004 - 0.007i
Reflection Efficiency : 0.006				Reflection Efficiency : 0.005			

Table 8.15 Reflection Coefficient Matrices and Reflection Efficiency for a Cosine-Converging Hardwalled Duct with Flow, $M_1 = -0.30$, $M_2 = -0.35$, $m_o = 2$.

Geometry : Cosine-Converging, $R_1 = 1.0$, $R_2 = 0.925$, $\ell = 0.5$

Characteristics : Hardwalled Duct with Flow, $M_1 = -0.30$, $M_2 = -0.36$, $k_r R_1 = 8.0$

Angular Mode $m_o = 2$, 2 Cut-on Modes

MWR(5BF)			MWR(6BF)		
(1)	(2)	(3)	(1)	(2)	(3)
(1) 0.932 + 0.660i	-0.026 - 0.289i	0.016 - 0.030i	(1) 0.934 + 0.658i	-0.023 - 0.288i	0.017 - 0.030i
(2) 0.050 + 0.256i	-0.719 - 0.920i	0.106 - 0.023i	(2) 0.056 + 0.246i	-0.710 - 0.918i	0.108 - 0.024i
(3) -0.028 + 0.007i	-0.035 - 0.034i	0.001 - 0.038i	(3) -0.030 + 0.007i	-0.035 - 0.036i	0.002 - 0.038i
Transmission Efficiency : 1.023			Transmission Efficiency : 1.008		
FEM(4 x 6) Uniform Mesh			FEM(4 x 6) Compressed towards wall		
(1)	(2)	(3)	(1)	(2)	(3)
(1) 0.943 + 0.640i	-0.013 - 0.299i	0.018 - 0.031i	(1) 0.944 + 0.640i	-0.012 - 0.298i	0.017 - 0.031i
(2) 0.064 + 0.242i	-0.714 - 0.916i	0.115 - 0.022i	(2) 0.066 + 0.244i	-0.723 - 0.909i	0.114 - 0.023i
(3) -0.043 + 0.001i	-0.030 - 0.037i	0.001 - 0.017i	(3) -0.025 + 0.012i	-0.034 - 0.033i	0.012 - 0.015i
Transmission Efficiency : 1.005			Transmission Efficiency : 1.012		

Table 8.16 Transmission Coefficient Matrices and Transmission Efficiency for a Cosine-Converging Hardwalled Duct with Flow, $M_1 = -0.30$, $M_2 = -0.36$, $m_o = 2$.

Geometry : Cosine-Converging, $R_1 = 1.0$, $R_2 = 0.925$, $\ell = 0.5$

Characteristics : Hardwalled Duct with Flow, $M_1 = -0.30$, $M_2 = -0.36$, $k_r R_1 = 11.0$, Angular Mode $m_o = 4$, 2 Cut-on Modes

Transmission Coefficient			Reflection Coefficient)		
MWR(5BF)			MWR(5BF)		
(1)	(2)	(3)	(1)	(2)	(3)
(1) 0.381 - 1.061i	-0.398 + 0.064i	-0.025 - 0.011i	(1) -0.002 - 0.005i	-0.007 + 0.008i	-0.004 - 0.027i
(2) 0.291 - 0.092i	0.845 + 0.784i	0.020 - 0.117i	(2) 0.003 + 0.005i	-0.025 - 0.002i	0.015 - 0.004i
(3) -0.001 + 0.036i	-0.063 + 0.013i	-0.015 - 0.030i	(3) 0.039 + 0.003i	0.055 + 0.067i	-0.008 - 0.005i
Transmission Efficiency : 1.032			Reflection Efficiency : 0.001		
FEM(4 x 6) Uniform Mesh			FEM(4 x 6) Uniform Mesh		
(1)	(2)	(3)	(1)	(2)	(3)
(1) 0.360 - 1.111i	-0.424 + 0.034i	-0.028 - 0.012i	(1) -0.004 - 0.004i	-0.006 + 0.003i	-0.001 - 0.024i
(2) 0.279 - 0.143i	0.815 + 0.738i	0.011 - 0.120i	(2) -0.011 + 0.004i	-0.023 + 0.010i	0.021 - 0.002i
(3) 0.030 + 0.025i	-0.057 - 0.015i	-0.021 - 0.026i	(3) -0.032 + 0.003i	0.056 + 0.060i	-0.007 - 0.010i
Transmission Efficiency : 1.007			Reflection Efficiency : 0.002		

Table 8.17 Reflection and Transmission Coefficient Matrices and Efficiencies for a Cosine-Converging Hardwalled Duct with Flow, $M_1 = -0.30$, $M_2 = -0.36$, $m_o = 4$.

Geometry : Cosine-Converging, $R_1 = 1.0$, $R_2 = 0.925$, $\ell = 0.5$

Characteristics : Softwalled Duct with Flow, $M_1 = -0.30$, $M_2 = -0.36$, $k_r R_1 = 5.0$, $A_1 = 0$, $A_2 = 0$
$A = (0.72-0.42i)$, Angular Mode $m_o = 0$, 2 Cut-on Modes.

MWR(5BF)			MWR(6BF)		
(1)	(2)	(3)	(1)	(2)	(3)
(1) 0.044 + 0.034i	-0.024 - 0.025i	-0.002 + 0.022i	(1) 0.042 + 0.040i	-0.022 - 0.028i	-0.004 + 0.022i
(2) -0.266 - 0.299i	0.071 + 0.184i	0.052 - 0.087i	(2) -0.269 - 0.318i	0.074 + 0.196i	0.049 - 0.096i
(3) -0.444 - 0.211i	0.146 + 0.109i	-0.030 - 0.064i	(3) -0.402 - 0.176i	0.133 + 0.093i	-0.022 - 0.062i
Reflection Efficiency : 0.01			Reflection Efficiency : 0.01		
FEM(4 x 6) Compressed towards wall			FEM(4 x 6) Uniform Mesh		
(1)	(2)	(3)	(1)	(2)	(3)
(1) 0.066 + 0.040i	-0.031 - 0.036i	-0.003 + 0.024i	(1) 0.062 + 0.037i	-0.031 - 0.035i	-0.003 + 0.027i
(2) -0.374 - 0.391i	0.081 + 0.248i	0.050 - 0.095i	(2) -0.358 - 0.373i	0.078 + 0.241i	0.055 - 0.103i
(3) -0.482 - 0.274i	0.149 + 0.129i	-0.031 - 0.069i	(3) -0.468 - 0.206i	0.148 + 0.108i	-0.035 - 0.062i
Reflection Efficiency : 0.02			Reflection Efficiency : 0.02		

Table 8.18 Reflection Coefficient Matrices and Reflection Efficiency for a Cosine-Converging Softwalled Duct with Flow, $M_1 = -0.30$, $M_2 = -0.36$, $m_o = 0$.

Geometry : Cosine-Converging, $R_1 = 1.0$, $R_2 = 0.925$, $\ell = 0.5$

Characteristics : Softwalled Duct with Flow, $M_1 = -0.30$, $M_2 = -0.36$, $k_r R_1 = 5.0$

$A_1 = 0$, $A_2 = 0$, $A = (0.72-0.42i)$

Angular Mode $m_o = 0$, 2 Cut-on Modes

MWR(5BF)				MWR(6BF)			
	(1)	(2)	(3)		(1)	(2)	(3)
(1)	-0.781 + 0.260i	-0.169 + 0.071i	0.015 + 0.002i	(1)	-0.793 + 0.298i	-0.161 + 0.062i	0.015 + 0.003i
(2)	-0.878 + 0.827i	-0.536 - 0.419i	-0.110 - 0.092i	(2)	-1.018 + 0.879i	-0.478 - 0.403i	-0.115 - 0.094i
(3)	0.155 + 0.230i	0.039 - 0.098i	0.005 - 0.068i	(3)	0.101 + 0.184i	0.040 - 0.064i	0.012 - 0.071i
Transmission Efficiency : 0.92				Transmission Efficiency : 0.91			
FEM(4 x 6) Compressed towards wall				FEM(4 x 6) Uniform Mesh			
	(1)	(2)	(3)		(1)	(2)	(3)
(1)	-0.785 + 0.281i	-0.158 + 0.062i	0.014 - 0.002i	(1)	-0.786 + 0.282i	-0.160 + 0.062i	0.016 + 0.002i
(2)	-1.087 + 0.863i	-0.508 - 0.399i	-0.113 - 0.067i	(2)	-1.071 + 0.831i	-0.514 - 0.389i	-0.123 - 0.074i
(3)	0.063 + 0.303i	0.078 - 0.068i	0.021 - 0.064i	(3)	0.042 + 0.281i	0.078 - 0.059i	0.024 - 0.066i
Transmission Efficiency : 0.93				Transmission Efficiency : 0.93			

Table 8.19 Transmission Coefficient Matrices and Transmission Efficiency for a Cosine-Converging Softwalled Duct with Flow, $M_1 = -0.30$, $M_2 = -0.36$, $m_o = 0$.

Geometry : Cosine-Converging, $R_1 = 1.0$, $R_2 = 0.925$, $\ell = 0.5$

Characteristics : $M_1 = -0.55$, $M_2 = -0.73$, $k_r R_1 = 4.0$

Angular Mode $m_o = 0$, 2 Cut-on Modes

Each Entry	Reflection Efficiency	Transmission Efficiency
MWR (5BF)	0.006	1.015
MWR (6BF)	0.008	0.998
MWR (7BF)	0.006	1.012

Reflection Coefficient

	(1)	(2)	(3)
(1)	-0.005 - 0.002i -0.011 - 0.003i -0.007 - 0.002i	0.006 + 0.006i 0.008 + 0.007i 0.007 + 0.006i	0.003 - 0.003i 0.002 - 0.002i 0.003 - 0.002i
(2)	-0.108 - 0.013i -0.157 - 0.011i -0.114 - 0.013i	0.003 - 0.022i 0.010 - 0.015i 0.004 - 0.021i	0.014 - 0.002i 0.006 - 0.001i 0.013 - 0.002i
(3)	-0.007 + 0.160i 0.005 + 0.114i -0.003 + 0.149i	0.032 - 0.086i 0.023 - 0.074i 0.030 - 0.084i	0.008 + 0.016i 0.028 - 0.023i 0.009 + 0.014i

Transmission Coefficient

	(1)	(2)	(3)
(1)	1.409 + 0.948i 1.378 + 0.596i 1.405 + 0.933i	0.028 + 0.122i 0.027 + 0.143i 0.026 + 0.127i	0.003 - 0.009i 0.002 - 0.014i 0.002 - 0.010i
(2)	-0.521 - 0.689i -0.522 - 0.970i -0.533 - 0.712i	-0.268 + 1.486i -0.329 + 1.564i -0.272 + 1.495i	-0.127 + 0.102i -0.108 + 0.089i -0.124 + 0.099i
(3)	-0.174 + 0.282i -0.123 + 0.213i -0.159 + 0.280i	0.165 - 0.001i 0.138 - 0.006i 0.159 - 0.003i	-0.021 - 0.043i -0.027 - 0.042i -0.023 - 0.043i

Table 8.20 Transmission and Reflection Coefficient Matrices and Efficiencies for a Hardwalled Duct with Flow, $M_1 = -0.55$, $M_2 = -0.73$, $m_o = 0$.

Geometry : Cosine-Converging, $R_1 = 1.0$, $R_2 = 0.925$, $\ell = 0.5$

Characteristics : Hardwalled Duct with Flow, $M_1 = -0.55$, $M_2 = -0.73$, $k_r R_1 = 4.0$

Angular Mode $m_o = 0$, 2 Cut-on Modes

FEM(4 x 6) Uniform Mesh

	(1)	(2)	(3)
(1)	-0.008 - 0.001i	0.007 + 0.006i	0.003 - 0.002i
(2)	-0.133 - 0.012i	0.007 - 0.019i	0.010 - 0.001i
(3)	0.005 + 0.126i	0.024 - 0.079i	0.011 + 0.012i

Reflection Efficiency : 0.007

FEM(4 x 6) Compressed towards throat

	(1)	(2)	(3)
(1)	-0.007 - 0.002i	0.007 + 0.006i	0.002 - 0.003i
(2)	-0.140 - 0.012i	0.010 - 0.017i	0.010 - 0.000i
(3)	0.007 + 0.129i	0.024 - 0.079i	0.011 + 0.012i

Reflection Efficiency : 0.006

FEM(4 x 7) Uniform Mesh

	(1)	(2)	(3)
(1)	-0.009 - 0.001i	0.007 + 0.006i	0.003 - 0.002i
(2)	-0.133 - 0.012i	0.006 - 0.019i	0.010 - 0.001i
(3)	0.001 + 0.129i	0.025 - 0.079i	0.011 + 0.012i

Reflection Efficiency : 0.007

FEM(4 x 7) Compressed towards throat

	(1)	(2)	(3)
(1)	-0.009 - 0.003i	0.007 + 0.006i	0.002 - 0.002i
(2)	-0.137 - 0.006i	0.010 - 0.019i	0.011 - 0.000i
(3)	0.005 + 0.130i	0.024 - 0.079i	0.011 + 0.012i

Reflection Efficiency : 0.006

Table 8.21 Reflection Coefficient Matrices and Efficiency for a Cosine-Converging Hardwalled Duct with Flow, $M_1 = -0.55$, $M_2 = -0.73$, $m_o = 0$.

Geometry : Cosine-Converging, $R_1 = 1.0$, $R_2 = 0.925$, $\ell = 0.5$

Characteristics : Hardwalled Duct with Flow, $M_1 = -0.55$, $M_2 = -0.73$, $k_r R_1 = 4.0$

Angular Mode $m_o = 0$, 2 Cut-on Modes

FEM(4 x 6) Uniform Mesh			FEM(4 x 6) Compressed towards throat		
(1)	(2)	(3)	(1)	(2)	(3)
(1) 1.422 + 0.913i	0.021 + 0.144i	0.003 - 0.013i	(1) 1.408 + 0.868i	0.021 + 0.141i	0.003 - 0.012i
(2) -0.579 - 0.776i	-0.288 + 1.537i	-0.123 + 0.095i	(2) -0.566 - 0.802i	-0.282 + 1.505i	-0.120 + 0.093i
(3) -0.127 + 0.214i	0.138 - 0.009i	-0.025 - 0.029i	(3) -0.142 + 0.233i	0.141 - 0.013i	-0.026 + 0.002i
Transmission Efficiency : 1.041			Transmission Efficiency : 0.992		
FEM(4 x 7) Uniform Mesh			FEM(4 x 7) Compressed towards throat		
(1)	(2)	(3)	(1)	(2)	(3)
(1) 1.412 + 0.908i	0.021 + 0.142i	0.003 - 0.012i	(1) 1.385 + 0.865i	0.021 + 0.140i	0.002 - 0.012i
(2) -0.572 - 0.775i	-0.287 + 1.530i	-0.122 + 0.095i	(2) -0.573 - 0.777i	-0.283 + 1.495i	-0.119 + 0.093i
(3) -0.119 + 0.230i	0.138 - 0.010i	-0.025 - 0.032i	(3) -0.119 + 0.236i	0.138 - 0.013i	-0.025 - 0.015i
Transmission Efficiency : 1.025			Transmission Efficiency : 0.978		

Table 8.22 Transmission Coefficient Matrices and Efficiency for a Cosine-Converging Hardwalled Duct with Flow, $M_1 = -0.55$, $M_2 = -0.73$, $m_o = 0$.

Geometry : Cosine-Converging, $R_1 = 1.0$, $R_2 = 0.925$, $\ell = 0.5$,

Characteristics : $M_1 = -0.58$, $M_2 = -0.80$, $k_r R_1 = 4.0$

Angular Mode $m_o = 0$, 2 Cut-on Modes

Each Entry	Reflection Efficiency	Transmission Efficiency
MWR (5BF)	0.007	1.017
MWR (6BF)	0.009	0.990
MWR (7BF)	0.007	1.012

Reflection Coefficient

	(1)	(2)	(3)
(1)	-0.005 - 0.004i -0.007 + 0.001i -0.005 - 0.003i	0.005 + 0.004i 0.007 + 0.004i 0.005 + 0.004i	0.003 - 0.003i 0.002 - 0.003i 0.003 - 0.003i
(2)	-0.117 + 0.064i -0.162 + 0.086i -0.124 + 0.061i	0.007 - 0.014i 0.007 - 0.011i -0.005 - 0.015i	0.013 + 0.001i 0.007 + 0.001i 0.012 - 0.001i
(3)	0.018 + 0.164i 0.024 + 0.118i 0.020 + 0.154i	0.024 - 0.099i 0.014 - 0.084i 0.021 - 0.096i	0.010 + 0.020i 0.015 + 0.013i 0.011 + 0.018i

Transmission Coefficient

	(1)	(2)	(3)
(1)	1.890 - 0.896i 1.802 - 0.898i 1.868 - 0.905i	0.167 + 0.064i 0.192 + 0.083i 0.172 + 0.070i	-0.007 - 0.008i -0.011 - 0.011i -0.008 - 0.009i
(2)	-1.158 + 0.267i -1.500 + 0.059i -1.195 + 0.264i	1.464 + 1.113i 1.506 + 1.255i 1.472 + 1.137i	0.005 + 0.203i 0.008 + 0.181i 0.005 + 0.200i
(3)	0.143 + 0.581i 0.118 + 0.449i 0.136 + 0.557i	0.213 - 0.197i 0.178 - 0.177i 0.206 - 0.192i	-0.049 - 0.060i -0.061 - 0.050i -0.051 - 0.057i

Table 8.23 Transmission and Reflection Coefficient Matrices and Efficiencies for a Hardwalled Duct with Flow, $M_1 = -0.58$, $M_2 = -0.80$, $m_o = 0$.

Geometry : Cosine-Converging, $R_1 = 1.0$, $R_2 = 0.925$, $\ell = 0.5$

Characteristics : Hardwalled Duct with Flow, $M_1 = -0.58$, $M_2 = -0.80$, $k_r R_1 = 4.0$

Angular Mode $m_o = 0$, 2 Cut-on Modes

FEM(4 x 6) Uniform Mesh			FEM(4 x 6) Compressed towards throat		
(1)	(2)	(3)	(1)	(2)	(3)
(1) -0.006 - 0.004i	0.006 + 0.004i	0.002 - 0.003i	(1) -0.004 - 0.004i	0.006 + 0.004i	0.002 - 0.003i
(2) -0.140 + 0.073i	0.001 - 0.012i	0.010 + 0.001i	(2) -0.145 + 0.071i	0.004 - 0.010i	0.010 + 0.001i
(3) 0.020 + 0.128i	0.017 - 0.088i	0.013 + 0.016i	(3) 0.024 + 0.132i	0.016 - 0.089i	0.014 + 0.016i
Reflection Efficiency : 0.008			Reflection Efficiency : 0.008		
FEM(4 x 7) Uniform Mesh			FEM(4 x 7) Compressed towards throat		
(1)	(2)	(3)	(1)	(2)	(3)
(1) -0.006 - 0.003i	0.006 + 0.004i	0.002 - 0.003i	(1) -0.006 - 0.005i	0.007 + 0.003i	-0.002 - 0.003i
(2) -0.138 + 0.073i	-0.000 - 0.012i	0.010 + 0.001i	(2) -0.216 + 0.273i	-0.004 - 0.032i	0.023 + 0.007i
(3) 0.019 + 0.136i	0.018 - 0.089i	0.014 + 0.016i	(3) 0.042 + 0.092i	-0.009 - 0.069i	0.014 + 0.008i
Reflection Efficiency : 0.008			Reflection Efficiency : 0.028		

Table 8.24 Reflection Coefficient Matrices and Efficiency for a Cosine-Converging Hardwalled Duct with Flow, $M_1 = -0.58$, $M_2 = -0.80$, $m_o = 0$.

Geometry : Cosine-Converging, $R_1 = 1.0$, $R_2 = 0.925$, $\ell = 0.5$

Characteristics : Hardwalled Duct with Flow, $M_1 = -0.58$, $M_2 = -0.80$, $k_r R_1 = 4.0$

Angular Mode $m_o = 0$, 2 Cut-on Modes

FEM(4 x 6) Uniform Mesh

	(1)	(2)	(3)
(1)	1.915 - 0.966i	0.192 + 0.095i	-0.010 - 0.010i
(2)	-1.320 + 0.277i	1.541 + 1.210i	0.003 + 0.201i
(3)	0.114 + 0.438i	0.175 - 0.183i	-0.061 - 0.035i

Transmission Efficiency : 1.099

FEM(4 x 6) Compressed towards throat

	(1)	(2)	(3)
(1)	1.882 - 0.958i	0.184 + 0.092i	-0.009 - 0.010i
(2)	-1.285 + 0.207i	1.500 + 1.175i	0.003 + 0.194i
(3)	0.077 + 0.462i	0.183 - 0.181i	-0.074 + 0.007i

Transmission Efficiency : 1.051

FEM(4 x 7) Uniform Mesh

	(1)	(2)	(3)
(1)	1.882 - 0.952i	0.189 + 0.092i	-0.009 - 0.010i
(2)	-1.309 + 0.267i	1.522 + 1.195i	0.002 + 0.199i
(3)	0.142 + 0.459i	0.173 - 0.183i	-0.059 - 0.038i

Transmission Efficiency : 1.065

FEM(4 x 7) Compressed towards throat

	(1)	(2)	(3)
(1)	1.868 - 0.962i	0.181 + 0.093i	-0.011 - 0.011i
(2)	-1.792 - 0.017i	1.547 + 1.149i	0.017 + 0.228i
(3)	0.154 + 0.600i	0.192 - 0.387i	-0.029 + 0.026i

Transmission Efficiency : 0.969

TABLE 8.25 Transmission Coefficient Matrices and Efficiency for a Cosine-Converging Duct with Flow, $M_1 = -0.58$, $M_2 = -0.80$, $m_o = 0$.

M_1	M_t	$k_r R_1$	MWR(5BF)	MWR(6BF)	MWR(7BF)
-0.58	-0.80	4.0	0.997		0.938
		5.0		0.924	0.962
-0.59	-0.83	4.0	0.993	0.910	0.988
		5.0	0.971		1.029
-0.60	-0.865	4.0		0.869	0.998
		5.0	0.846		0.953

Table 8.26 Transmission Efficiency Computed by MWR for Cosine-Converging-Diverging Hardwalled Duct at High Mach Numbers, $R_1 = R_2 = 1.0$, $R_t = 0.925$, $\ell = 0.75$, Angular Mode $m_o = 0$.

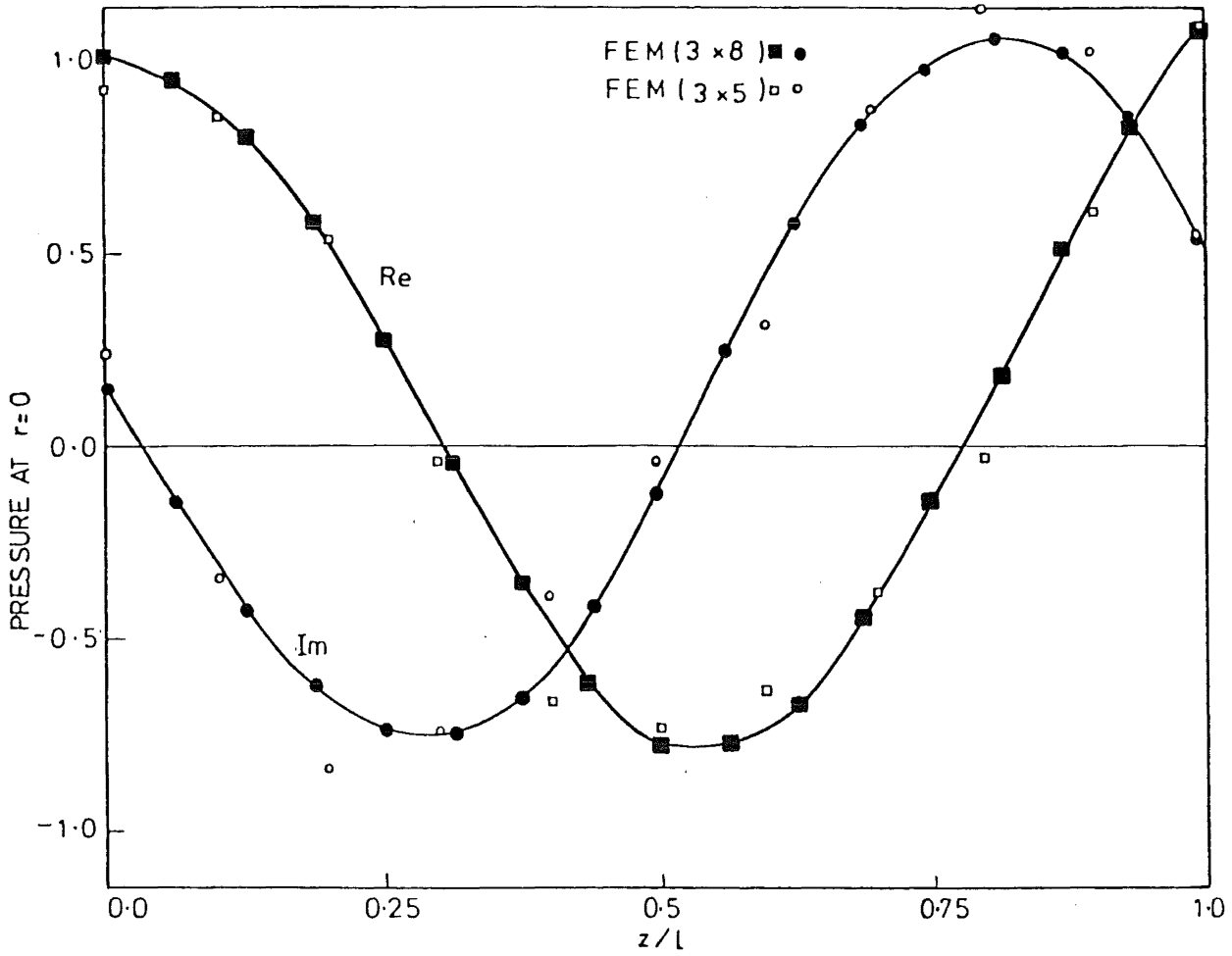

FIG. 8·1 AXIAL PRESSURE VARIATION IN CONVERGING-DIVERGING HARDWALLED DUCT, $R_1 = 1{\cdot}0$, $R_2 = 1{\cdot}0$, $R_t = 0{\cdot}93$, $l = 0{\cdot}75$, $M_1 = -0{\cdot}30$, $M_t = -0{\cdot}35$, $M_2 = -0{\cdot}30$, $k_r R_1 = 5{\cdot}0$, $m_o = 0$, IN MODE 1

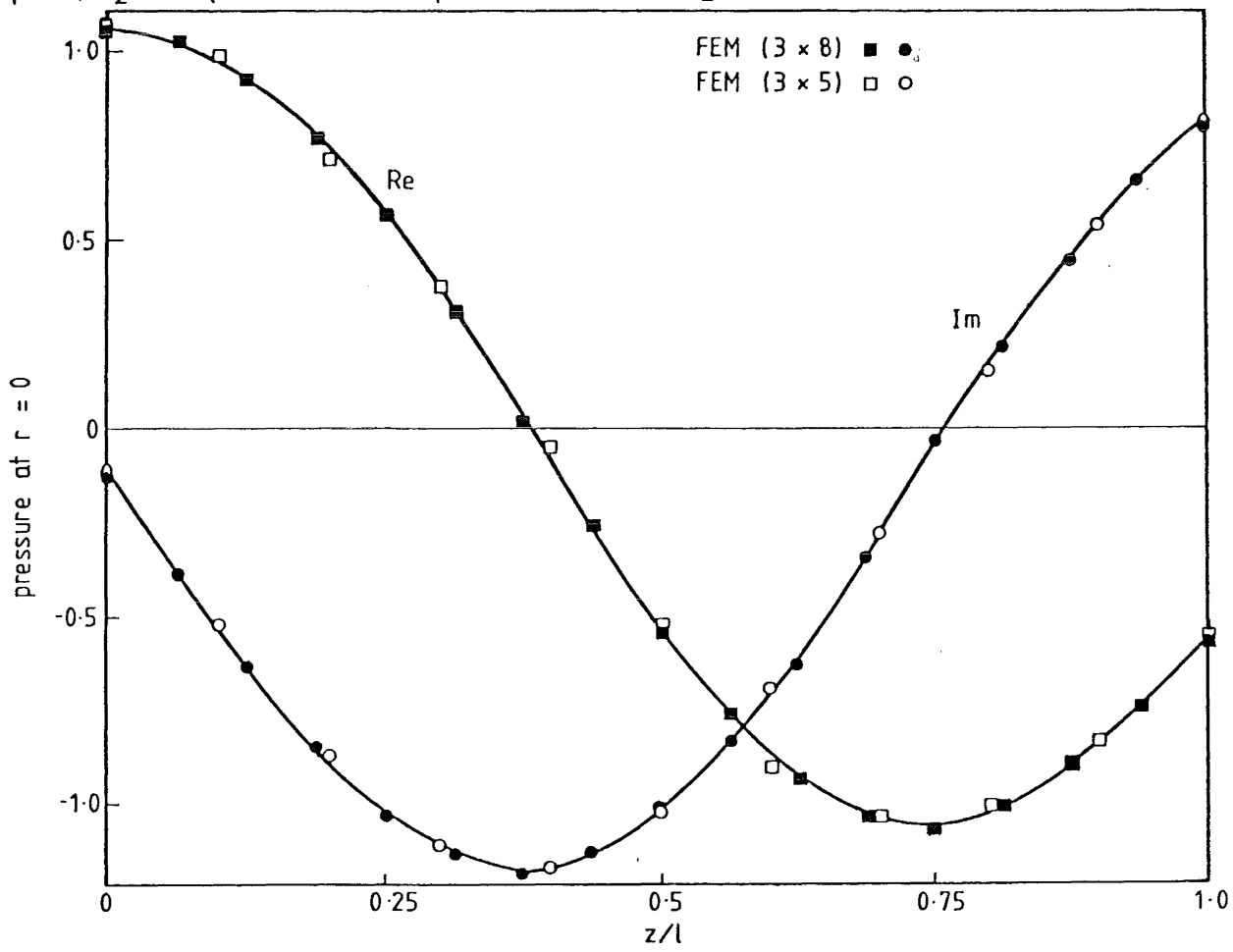

FIG. 8·2 PRESSURE VARIATION IN CONVERGING-DIVERGING HARDWALLED DUCT, $R_1 = 1{\cdot}0$, $R_t = 0{\cdot}93$, $R_2 = 1{\cdot}0$, $l = 0{\cdot}75$, $M_1 = -0{\cdot}30$, $M_t = -0{\cdot}35$, $M_2 = -0{\cdot}30$, $k_r R_1 = 5{\cdot}0$, $m_o = 0$, IN MODE 2

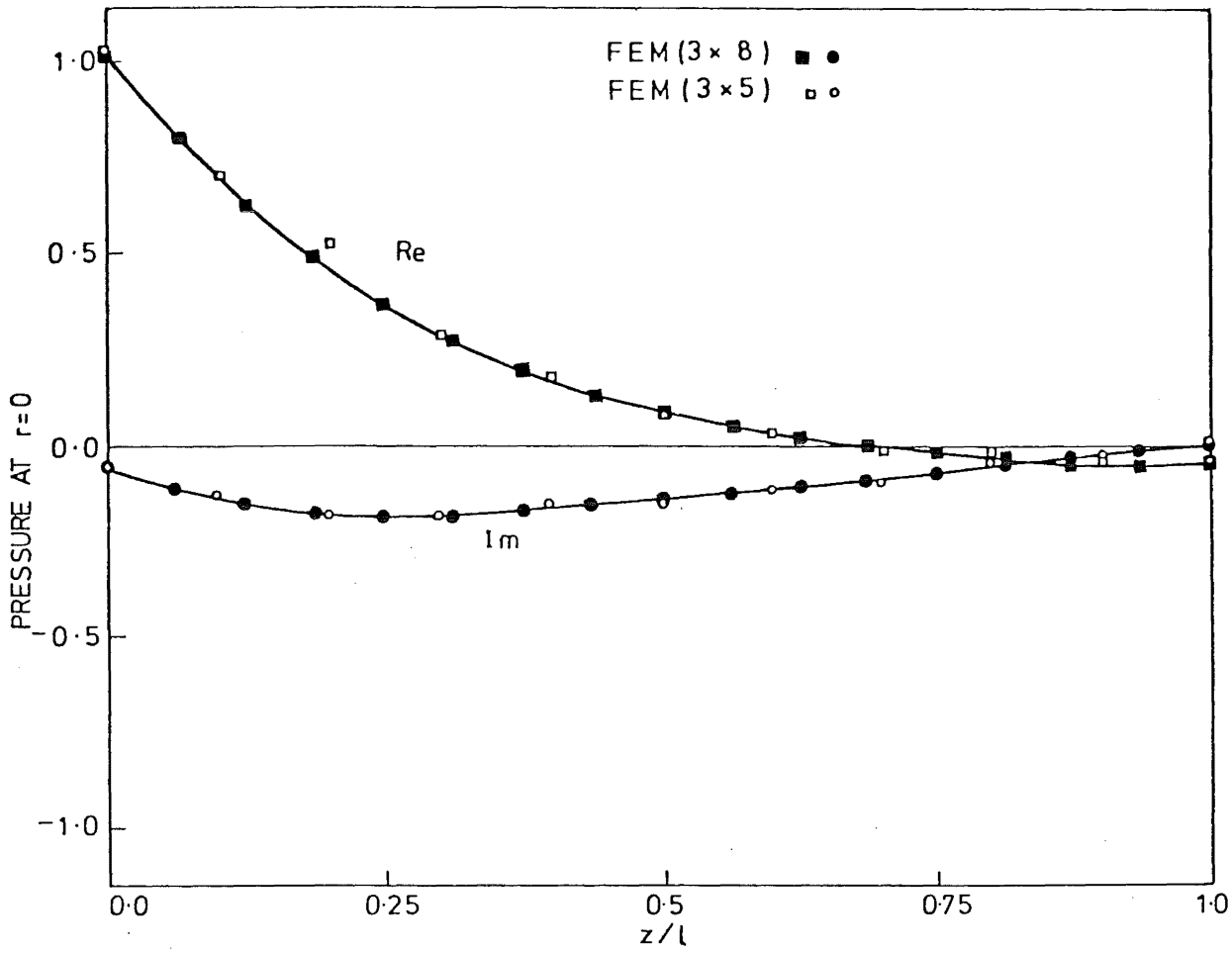

FIG.8·3 AXIAL PRESSURE VARIATION IN CONVERGING-DIVERGING HARDWALLED DUCT;
$R_1 = 1{\cdot}0, R_t = 0{\cdot}93, R_2 = 1{\cdot}0, l = 0{\cdot}75, M_1 = -0{\cdot}30, M_t = -0{\cdot}35, M_2 = -0{\cdot}30, k_r R_1 = 5{\cdot}0, m_o = 0,$ IN MODE 3

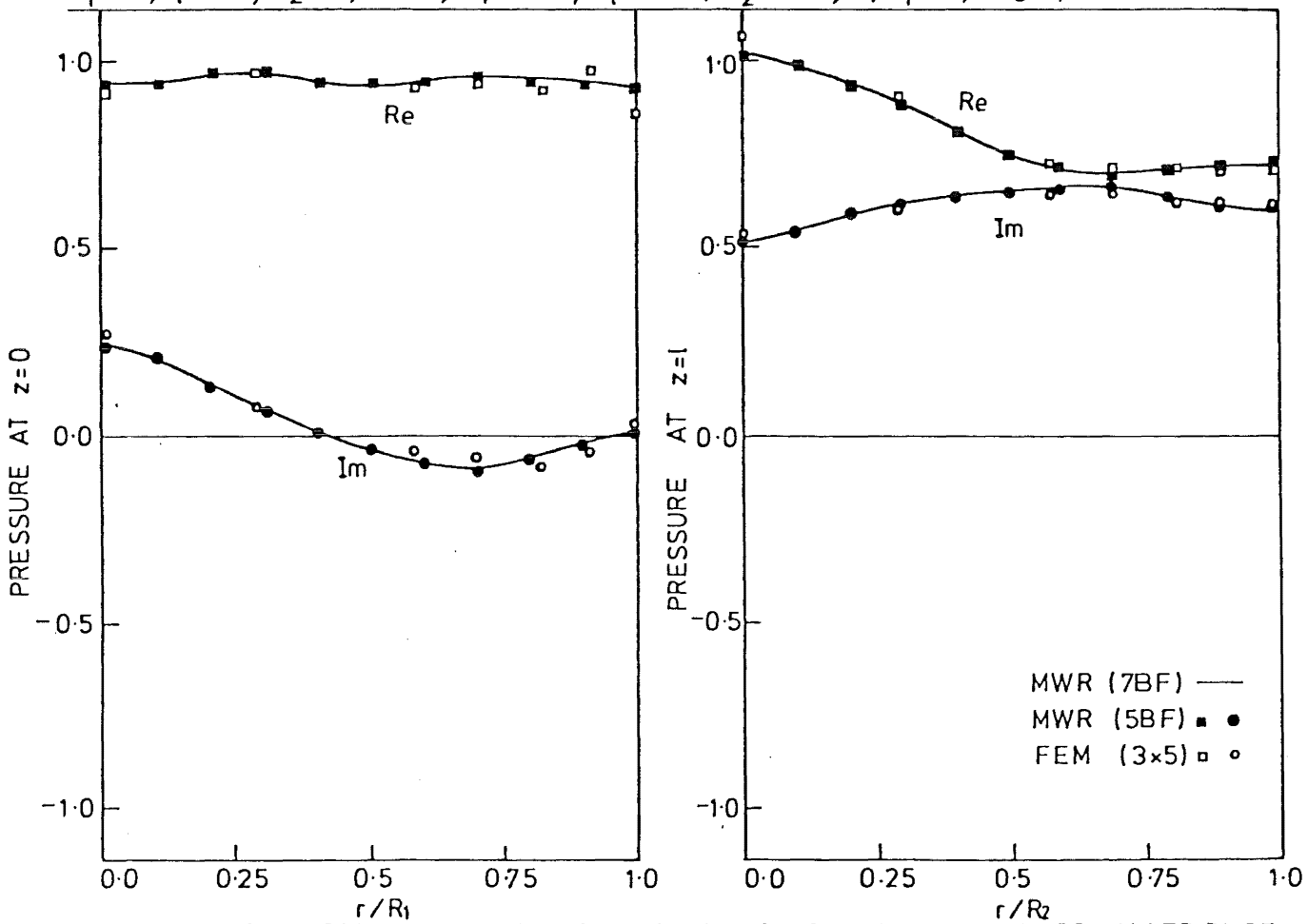

FIG.8·4 TRANSVERSE PRESSURE VARIATIONS IN CONVERGING-DIVERGING HARDWALLED DUCT;
$R_1 = 1{\cdot}0,\ R_t = 0{\cdot}93,\ R_2 = 1{\cdot}0,\ l = 0{\cdot}75,\ M_1 = -0{\cdot}30,\ M_t = -0{\cdot}35,\ M_2 = -0{\cdot}30,\ k_r R_1 = 5{\cdot}0,\ m_o = 0,$ IN MODE 1

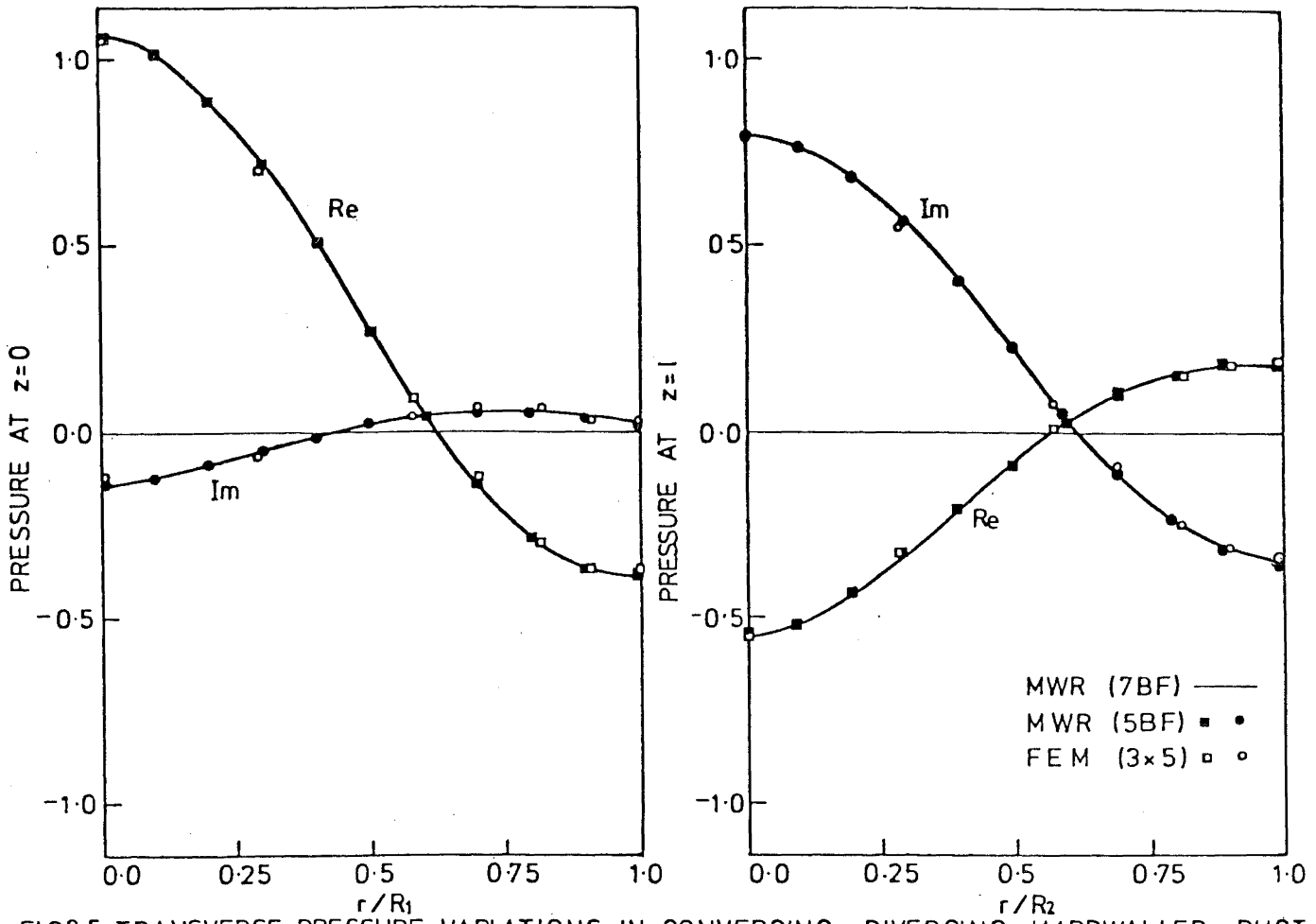

FIG.8·5 TRANSVERSE PRESSURE VARIATIONS IN CONVERGING – DIVERGING HARDWALLED DUCT, $R_1=1{\cdot}0$, $R_t=0{\cdot}93$, $R_2=1{\cdot}0$, $l=0{\cdot}75$, $M_1=-0{\cdot}30$, $M_t=-0{\cdot}35$, $M_2=-0{\cdot}30$, $k_rR_1=5{\cdot}0$, $m_o=0$, IN MODE 2

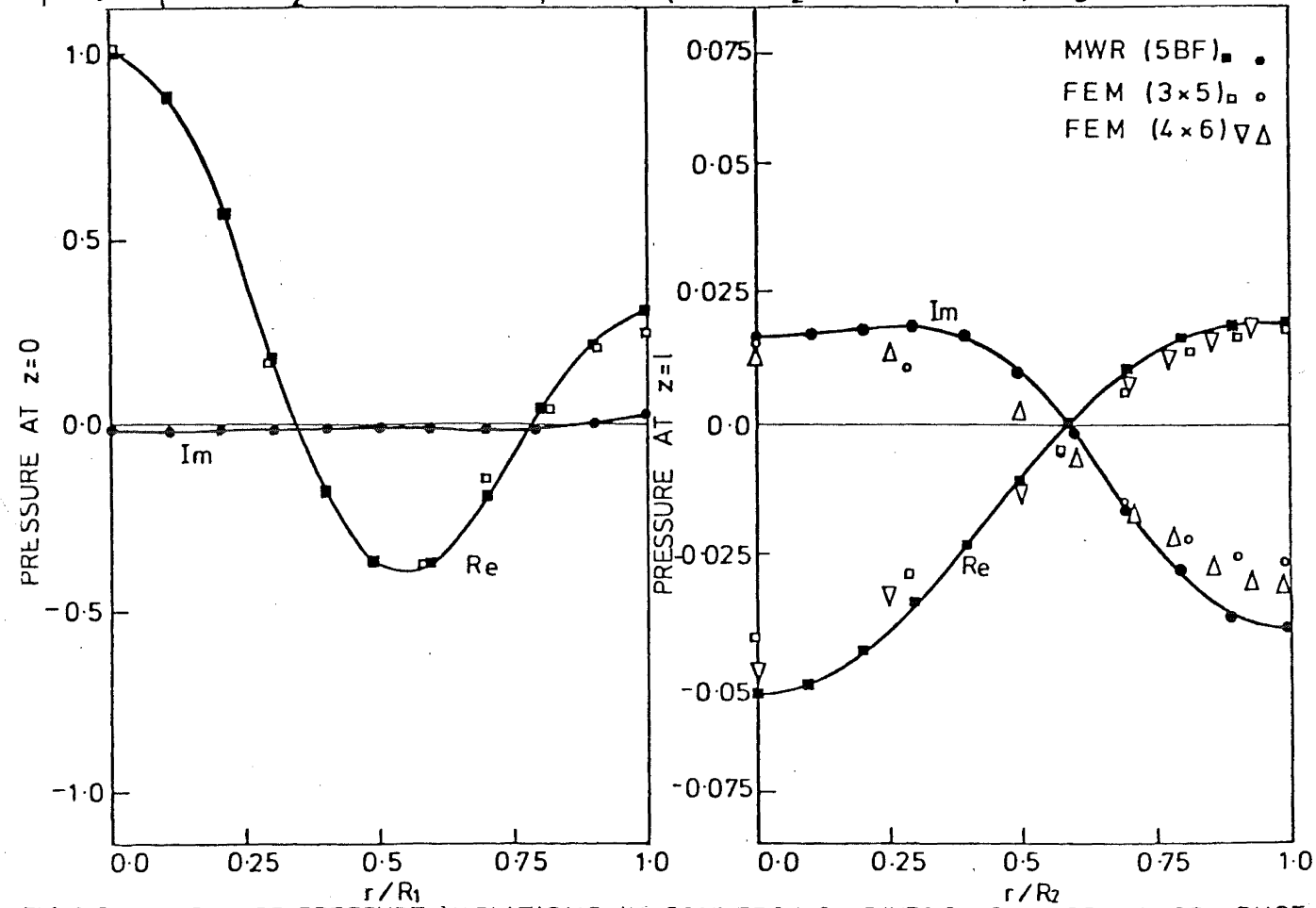

FIG.8·6 TRANSVERSE PRESSURE VARIATIONS IN CONVERGING – DIVERGING HARDWALLED DUCT, $R_1=1{\cdot}0$, $R_t=0{\cdot}93$, $R_2=1{\cdot}0$, $l=0{\cdot}75$, $M_1=-0{\cdot}30$, $M_t=-0{\cdot}35$, $M_2=-0{\cdot}3$, $k_rR_1=5{\cdot}0$, $m_o=0$, IN MODE 3

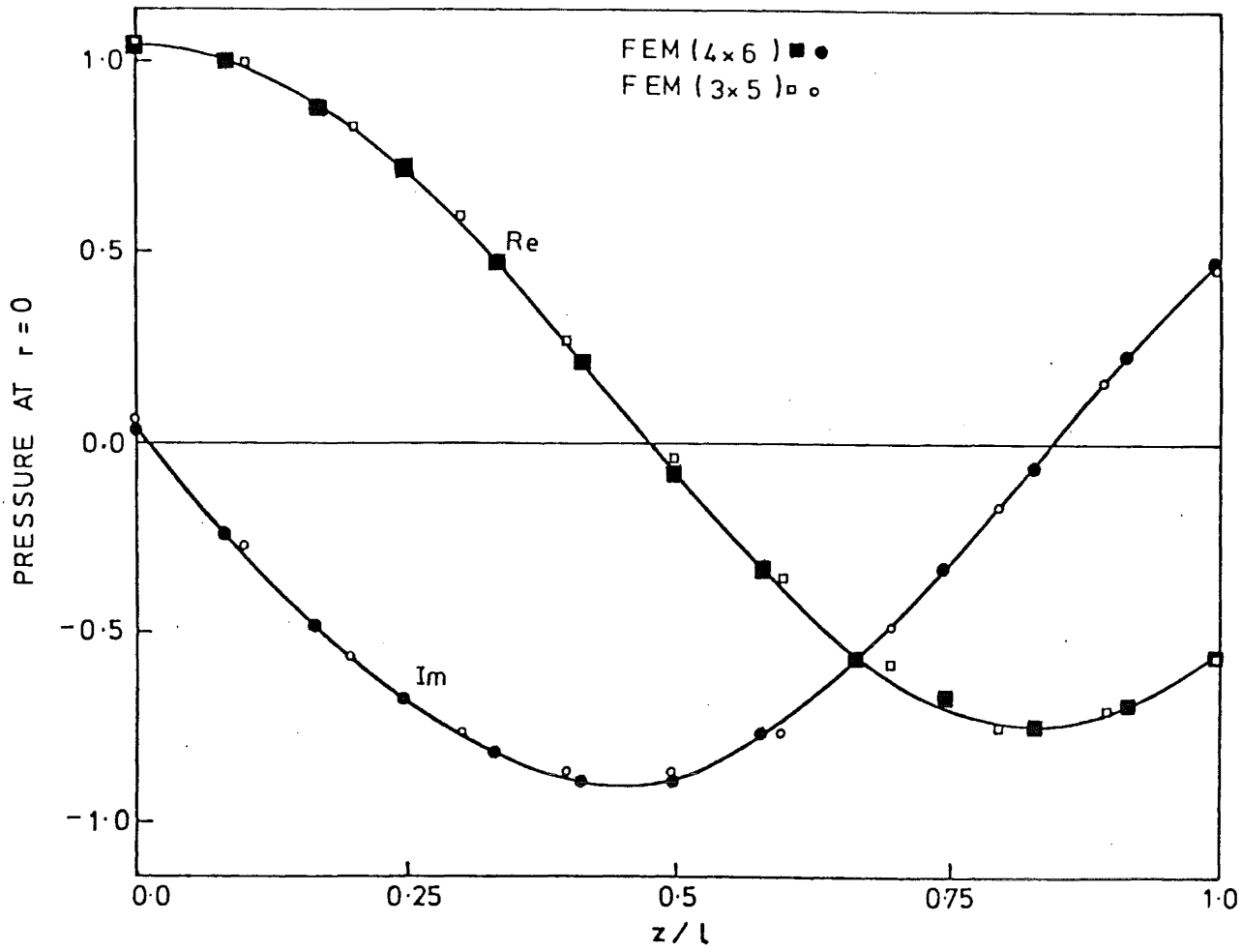

FIG.8·7 AXIAL PRESSURE VARIATION IN COSINE-CONVERGING HARDWALLED DUCT, $R_1=1{\cdot}0$, $R_2=0{\cdot}925$, $l=0{\cdot}5$, $M_1=-0{\cdot}30$, $M_2=-0{\cdot}36$, $k_rR_1=5{\cdot}0$, $m_o=0$, IN MODE 1.

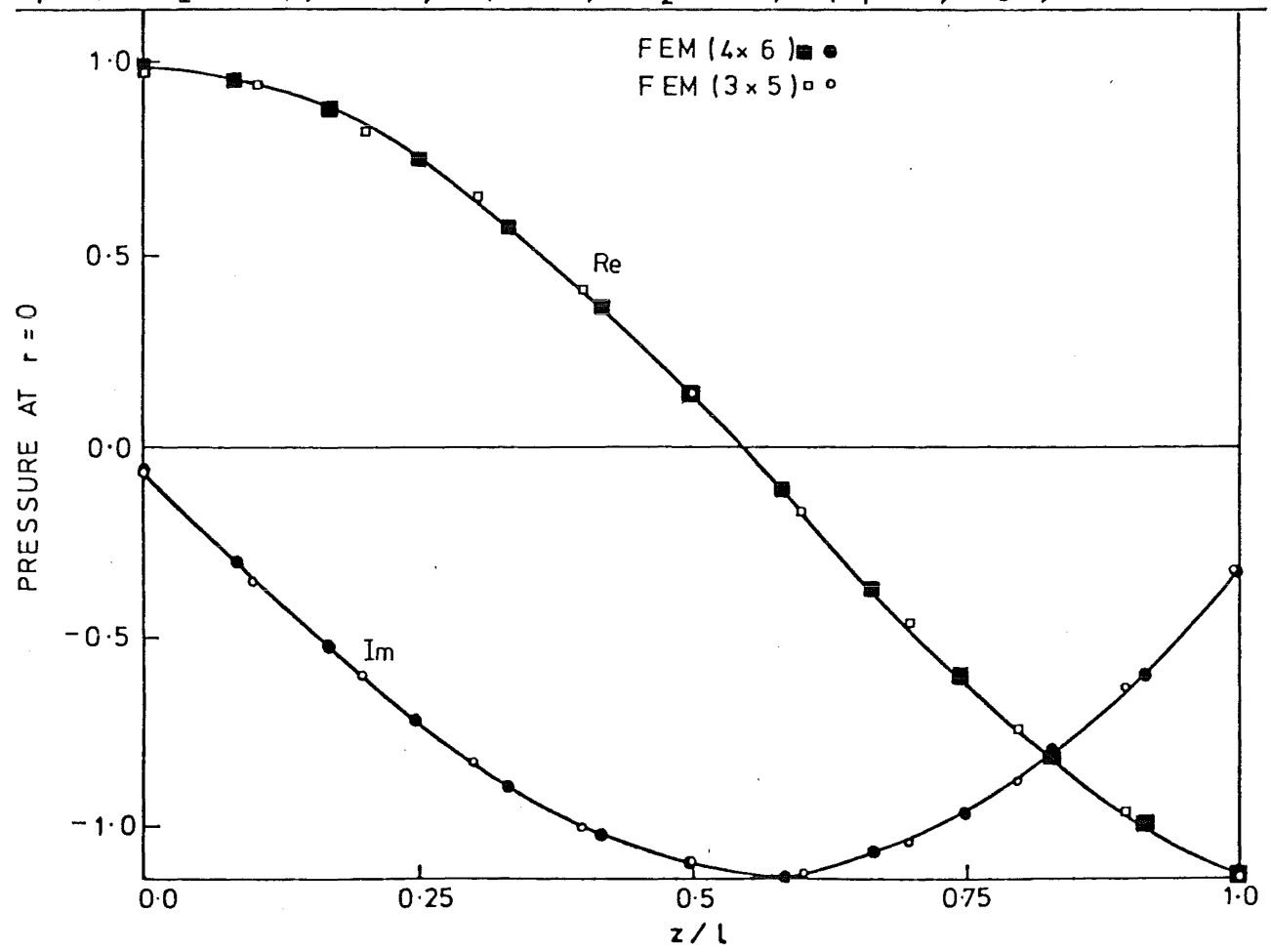

FIG.8·8 AXIAL PRESSURE VARIATION IN COSINE-CONVERGING HARDWALLED DUCT, $R_1=1{\cdot}0$, $R_2=0{\cdot}925$, $l=0{\cdot}5$, $M_1=-0{\cdot}30$, $M_2=-0{\cdot}36$, $k_rR_1=5{\cdot}0$, $m_o=0$, IN MODE 2

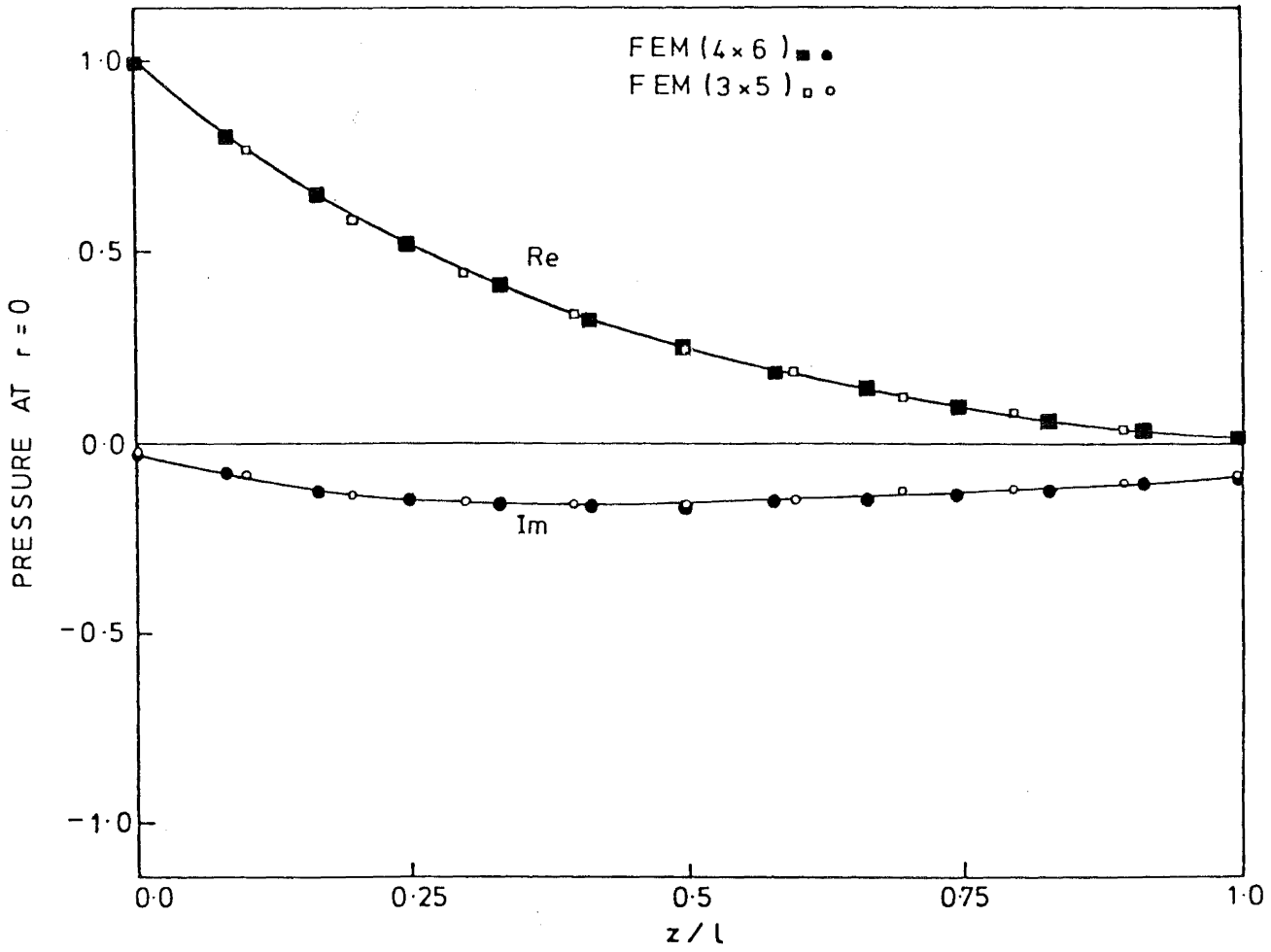

FIG.8·9 AXIAL PRESSURE VARIATION IN COSINE-CONVERGING HARDWALLED DUCT, R_1=1·0, R_2=0·925, l=0·5, M_1=-0·30, M_2=-0·36, $k_r R_1$=5·0, m_o=0, IN MODE 3

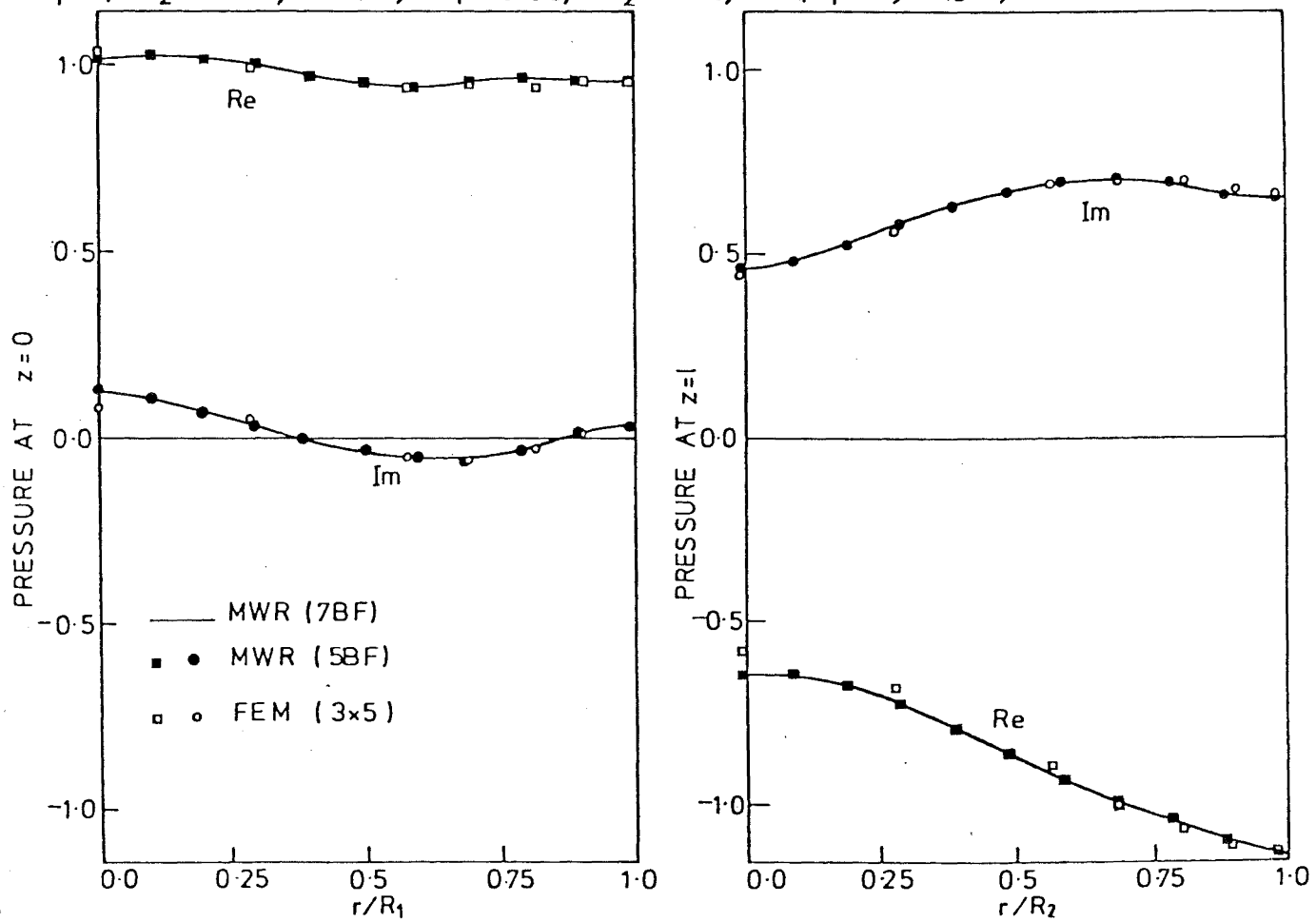

FIG.8·10 TRANSVERSE PRESSURE VARIATIONS IN COSINE-CONVERGING HARDWALLED DUCT, R_1=1·0, R_2=0·925, l=0·5, M_1=-0·30, M_2=-0·36, $k_r R_1$=5·0, m_o=0, IN MODE 1

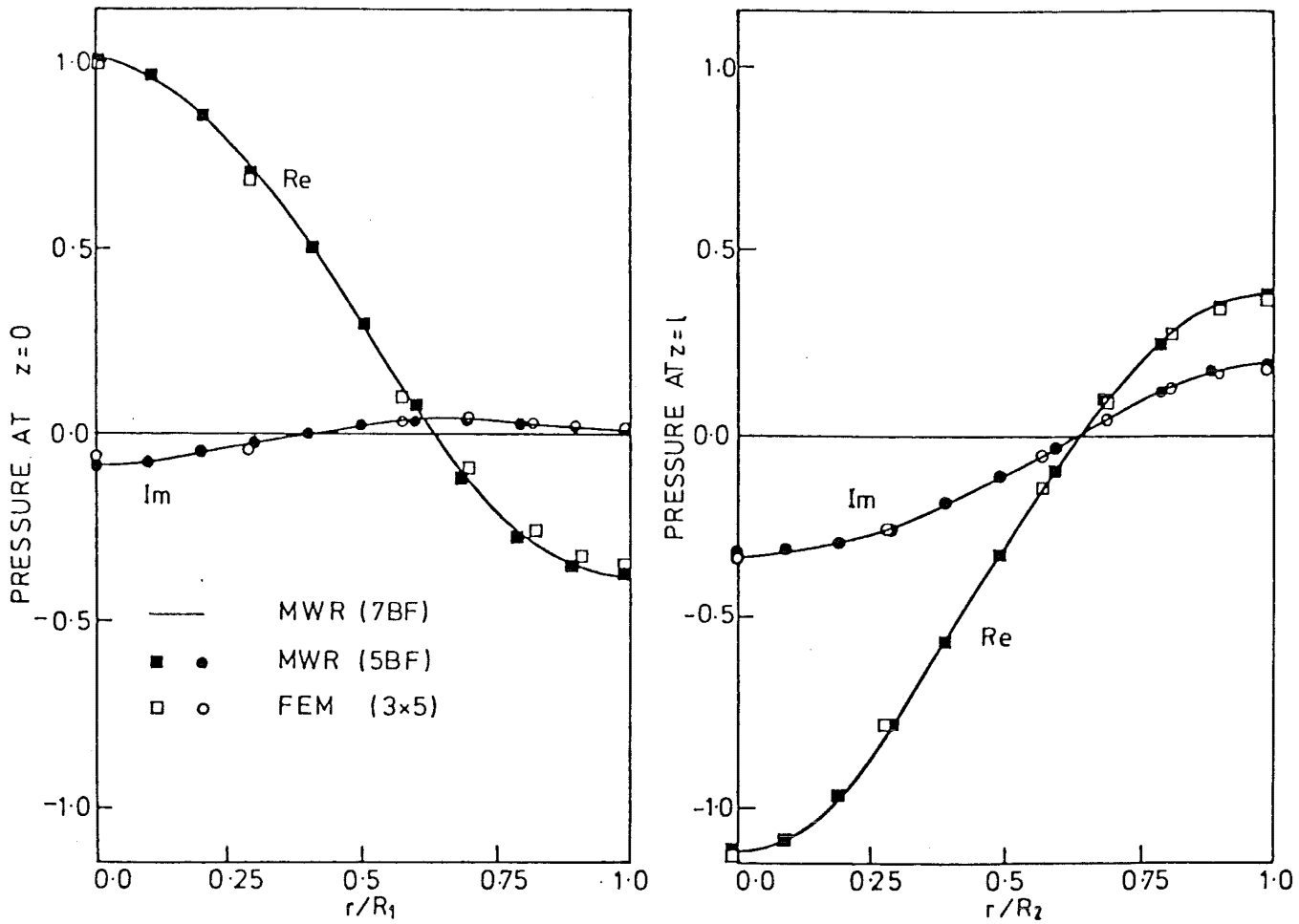

FIG.8·11 TRANSVERSE PRESSURE VARIATIONS IN COSINE-CONVERGING HARDWALLED DUCT, $R_1=1{\cdot}0$, $R_2=0{\cdot}925$, $l=0{\cdot}5$, $M_1=-0{\cdot}30$, $M_2=-0{\cdot}36$, $k_r R_1=5{\cdot}0$, $m_o=0$, IN MODE 2

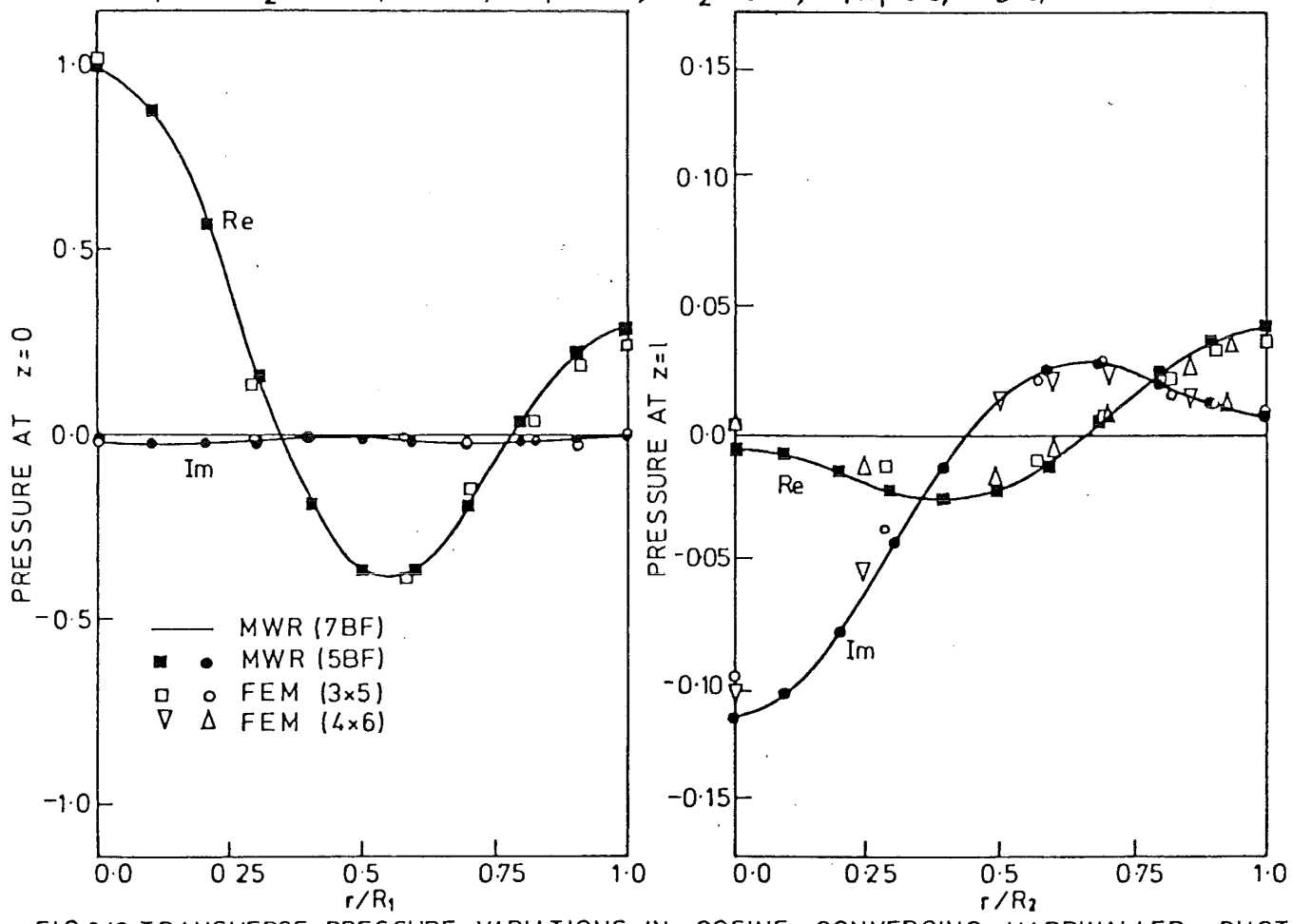

FIG.8·12 TRANSVERSE PRESSURE VARIATIONS IN COSINE-CONVERGING HARDWALLED DUCT. $R_1=0$, $R_2=0{\cdot}925$, $l=0{\cdot}5$, $M_1=-0{\cdot}30$, $M_2=-0{\cdot}36$, $k_r R_1=5{\cdot}0$, $m_o=0$, IN MODE 3

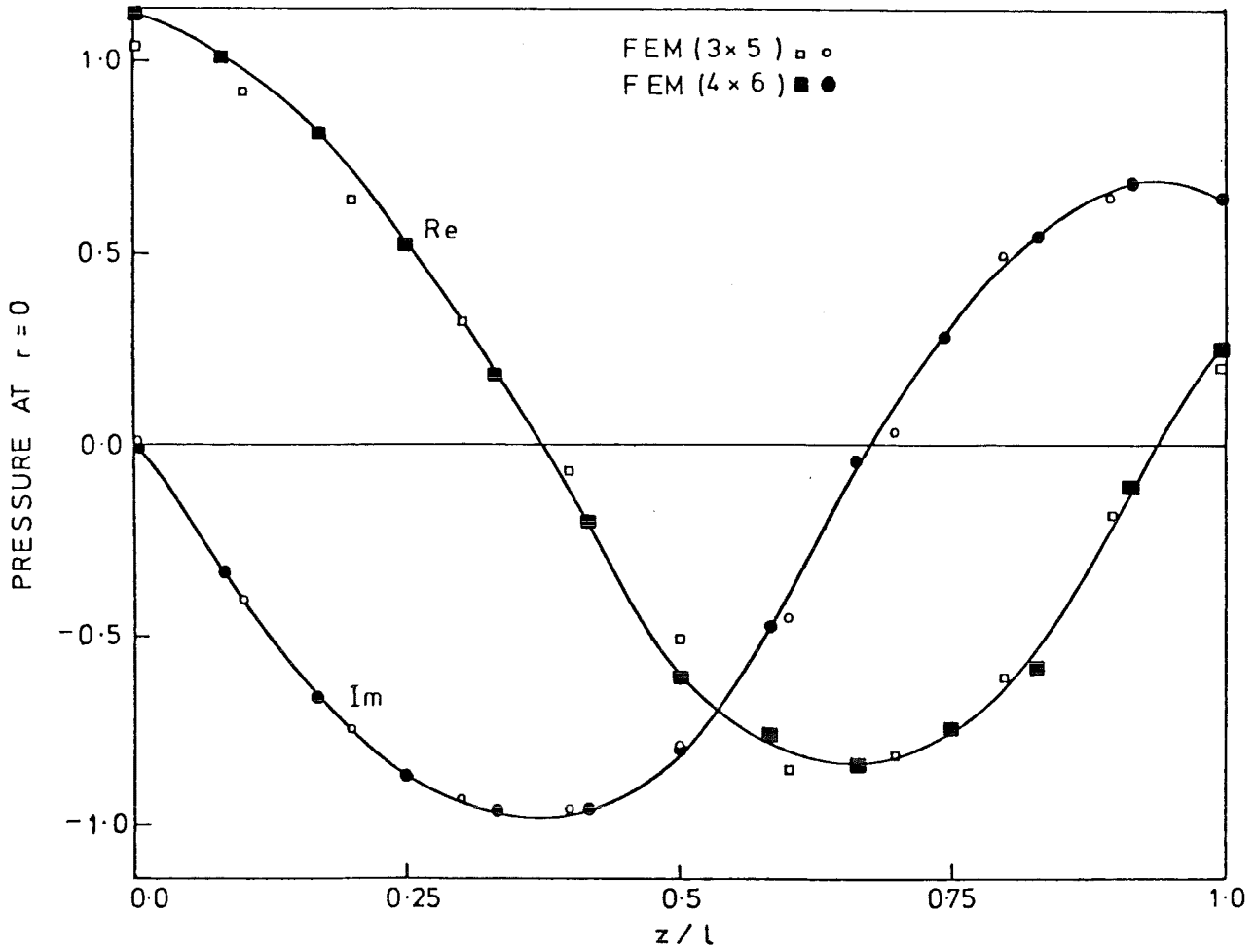

FIG. 8·13 AXIAL PRESSURE VARIATION IN COSINE-CONVERGING HARDWALLED DUCT; $R_1 = 1{\cdot}0$, $R_2 = 0{\cdot}925$, $l = 0{\cdot}5$, $M_1 = -0{\cdot}45$, $M_2 = -0{\cdot}56$, $k_r R_1 = 5{\cdot}0$, $m_o = 0$, IN MODE 1

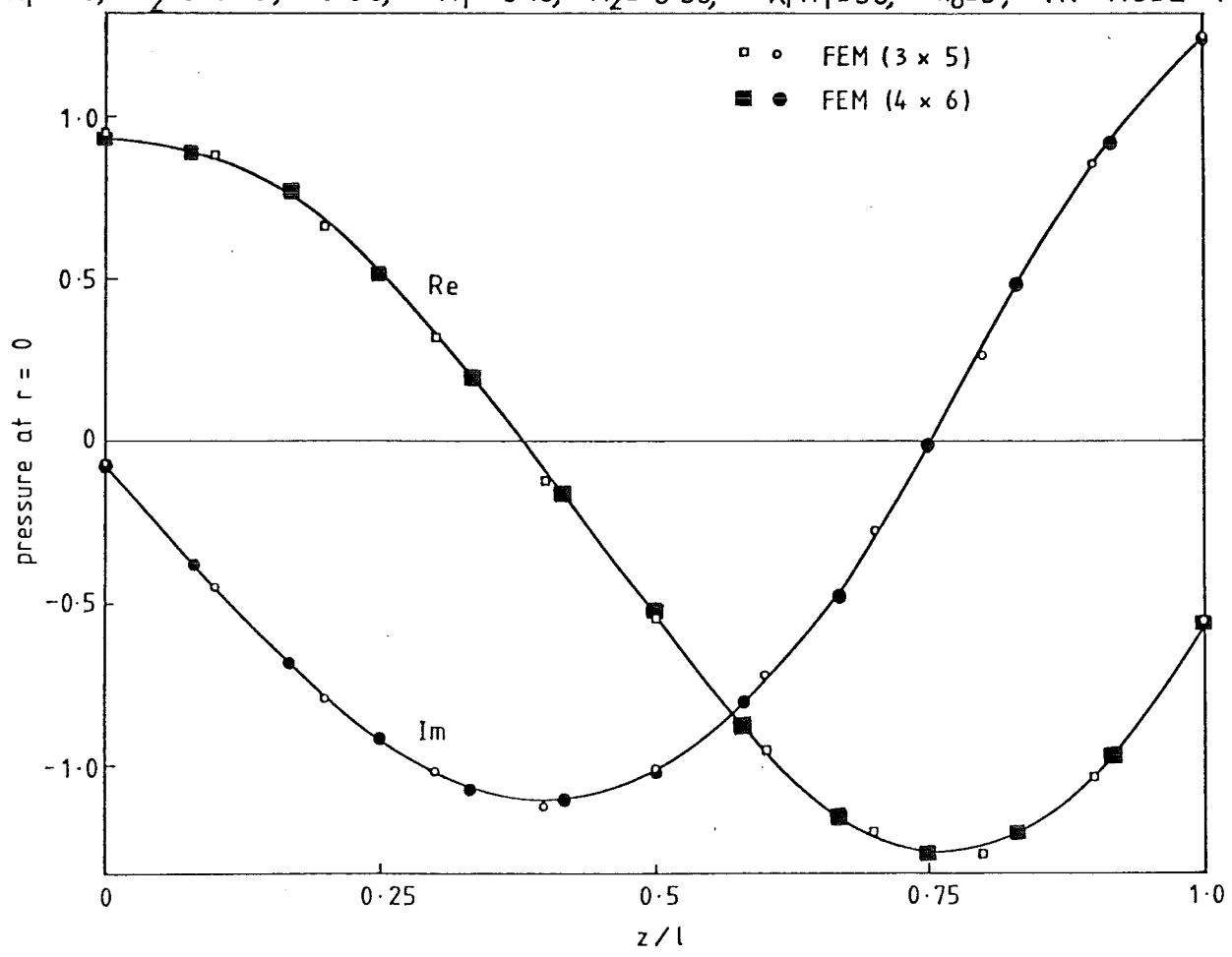

FIG. 8·14 AXIAL PRESSURE VARIATION IN COSINE-CONVERGING HARDWALLED DUCT; $R_1 = 1{\cdot}0$, $R_2 = 0{\cdot}925$, $l = 0{\cdot}5$, $M_1 = -0{\cdot}45$, $M_2 = -0{\cdot}56$, $k_r R_1 = 5{\cdot}0$, $m_o = 0$, IN MODE 2

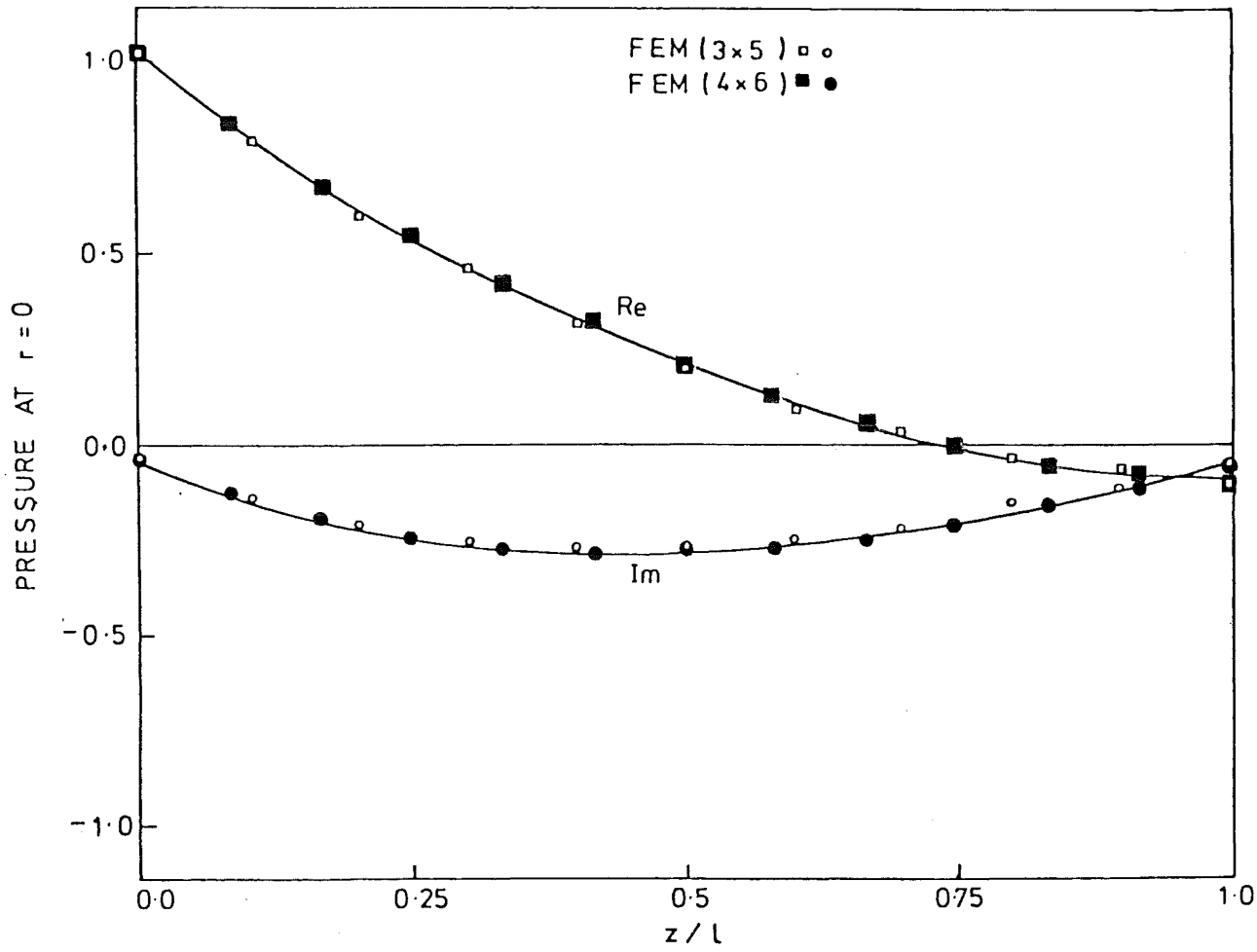

FIG. 8·15 AXIAL PRESSURE VARIATION IN COSINE-CONVERGING HARDWALLED DUCT; $R_1=1{\cdot}0$, $R_2=0{\cdot}925$, $l=0{\cdot}5$, $M_1=-0{\cdot}45$, $M_2=-0{\cdot}56$, $k_r R_1=5{\cdot}0$, $m_o=0$, MODE 3

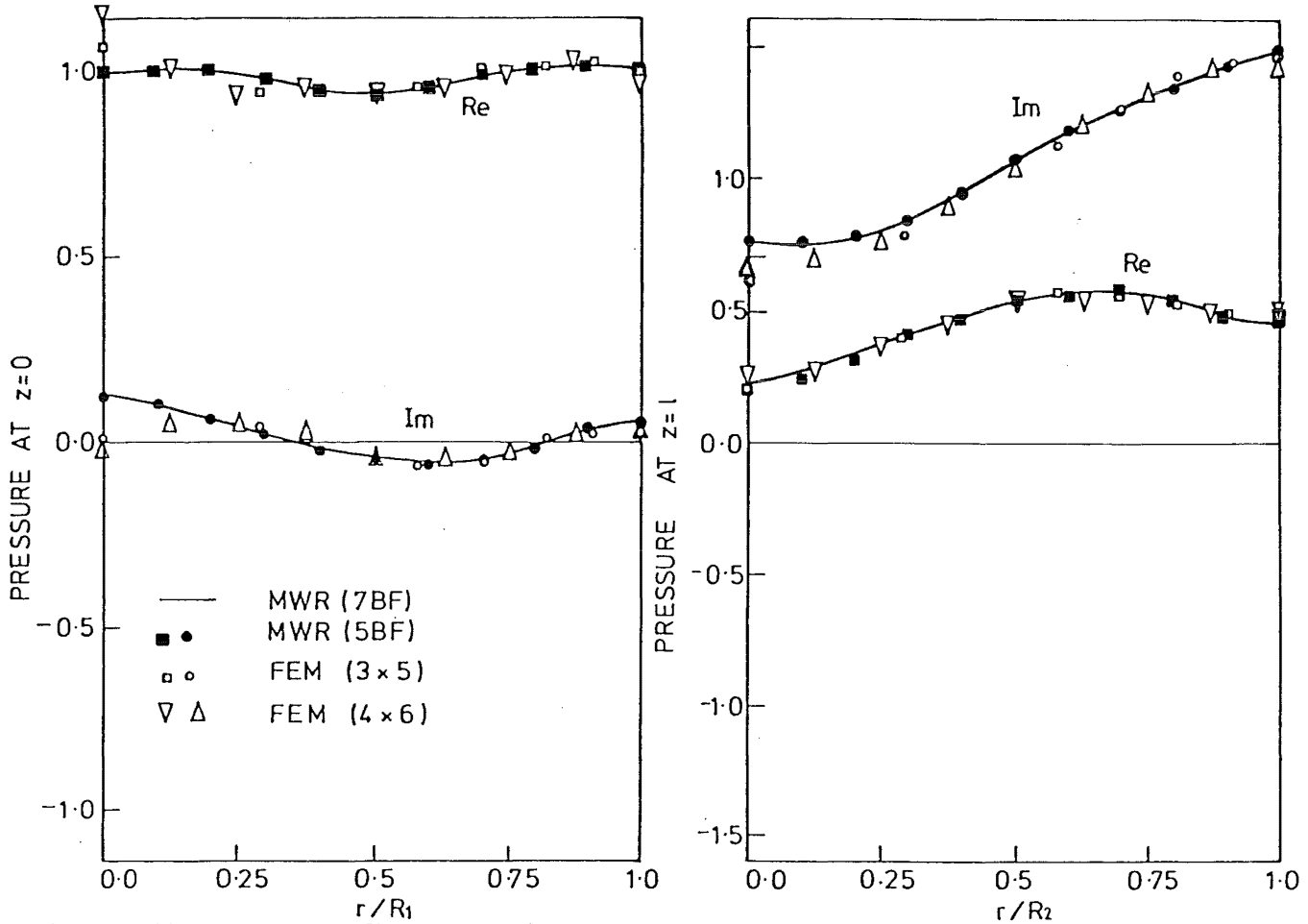

FIG 8·16 TRANSVERSE PRESSURE VARIATIONS IN COSINE-CONVERGING HARDWALLED DUCT; $R_1=1{\cdot}0$, $R_2=0{\cdot}925$, $l=0{\cdot}5$, $M_1=-0{\cdot}45$, $M_2=-0{\cdot}56$, $k_r R_1=5{\cdot}0$, $m_o=0$, IN MODE 1

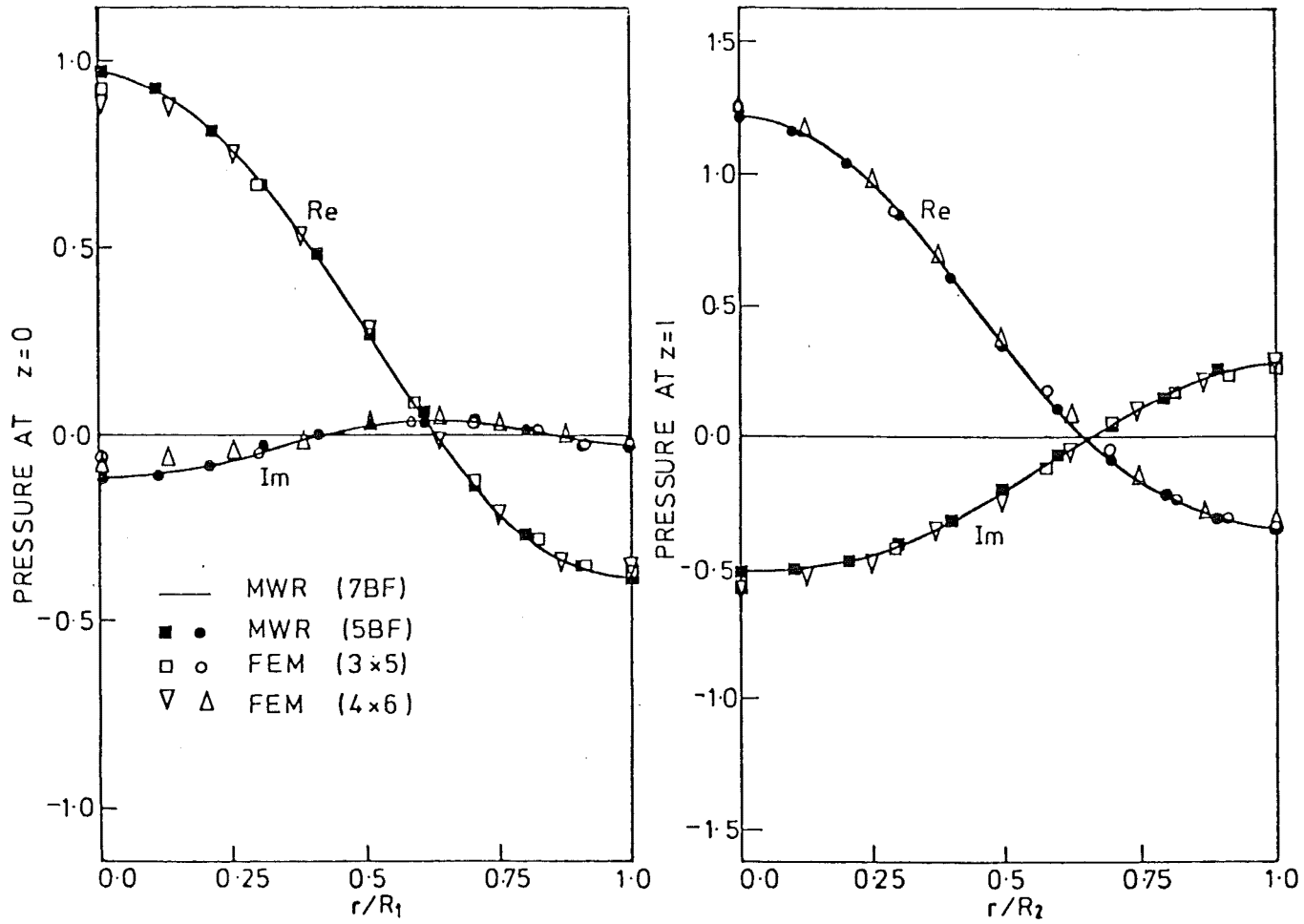

FIG.8.17 TRANSVERSE PRESSURE VARIATIONS IN COSINE-CONVERGING HARDWALLED DUCT; $R_1=1.0$, $R_2=0.925$, $l=0.5$, $M_1=-0.45$, $M_2=-0.56$, $k_rR_1=5.0$, $m_o=0$, IN MODE 2

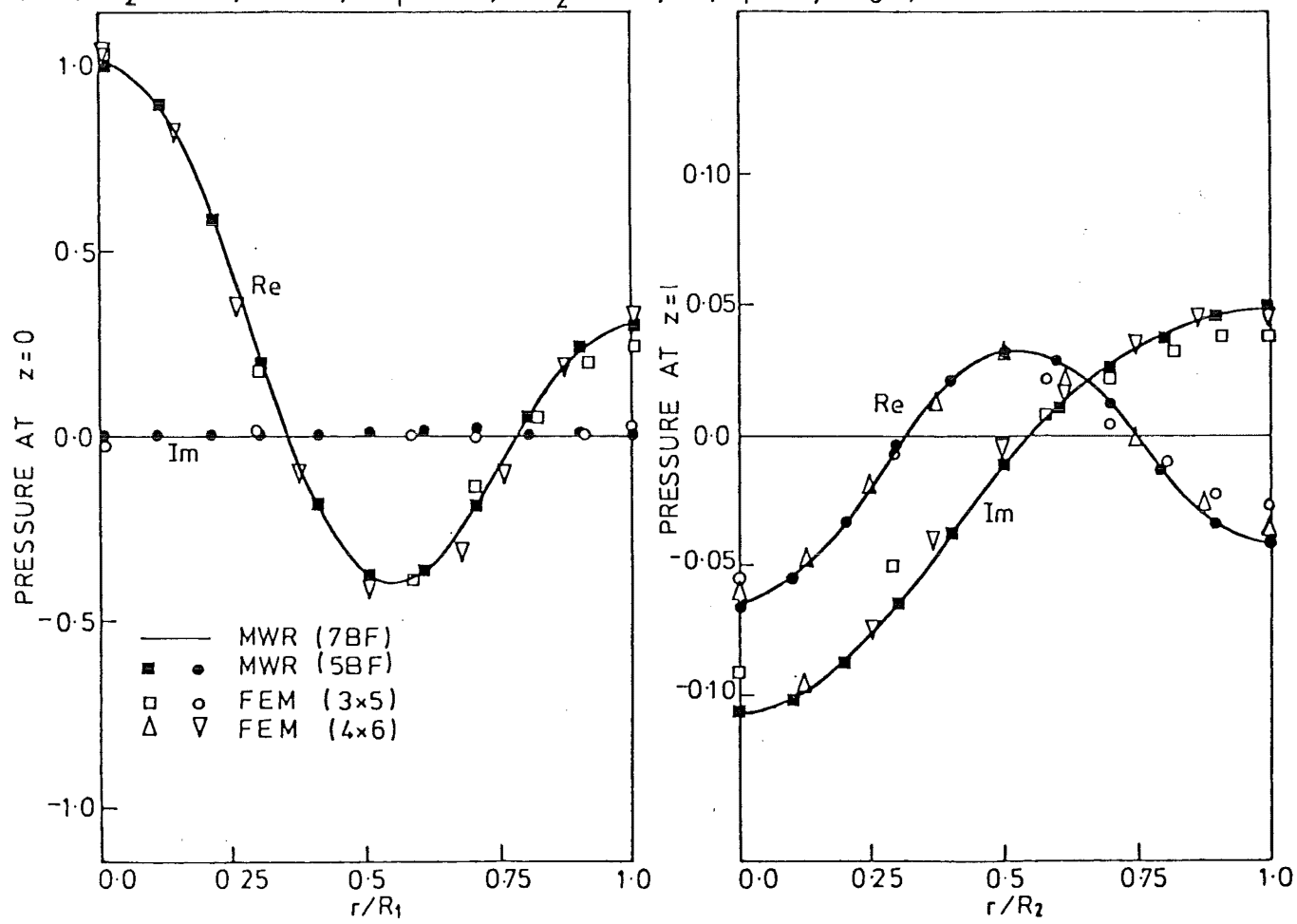

FIG.8.18 TRANSVERSE PRESSURE VARIATIONS IN COSINE-CONVERGING HARDWALLED DUCT; $R_1=1.0$, $R_2=0.925$, $l=0.5$, $M_1=-0.45$, $M_2=-0.56$, $k_rR_1=5.0$, $m_o=0$, IN MODE 3

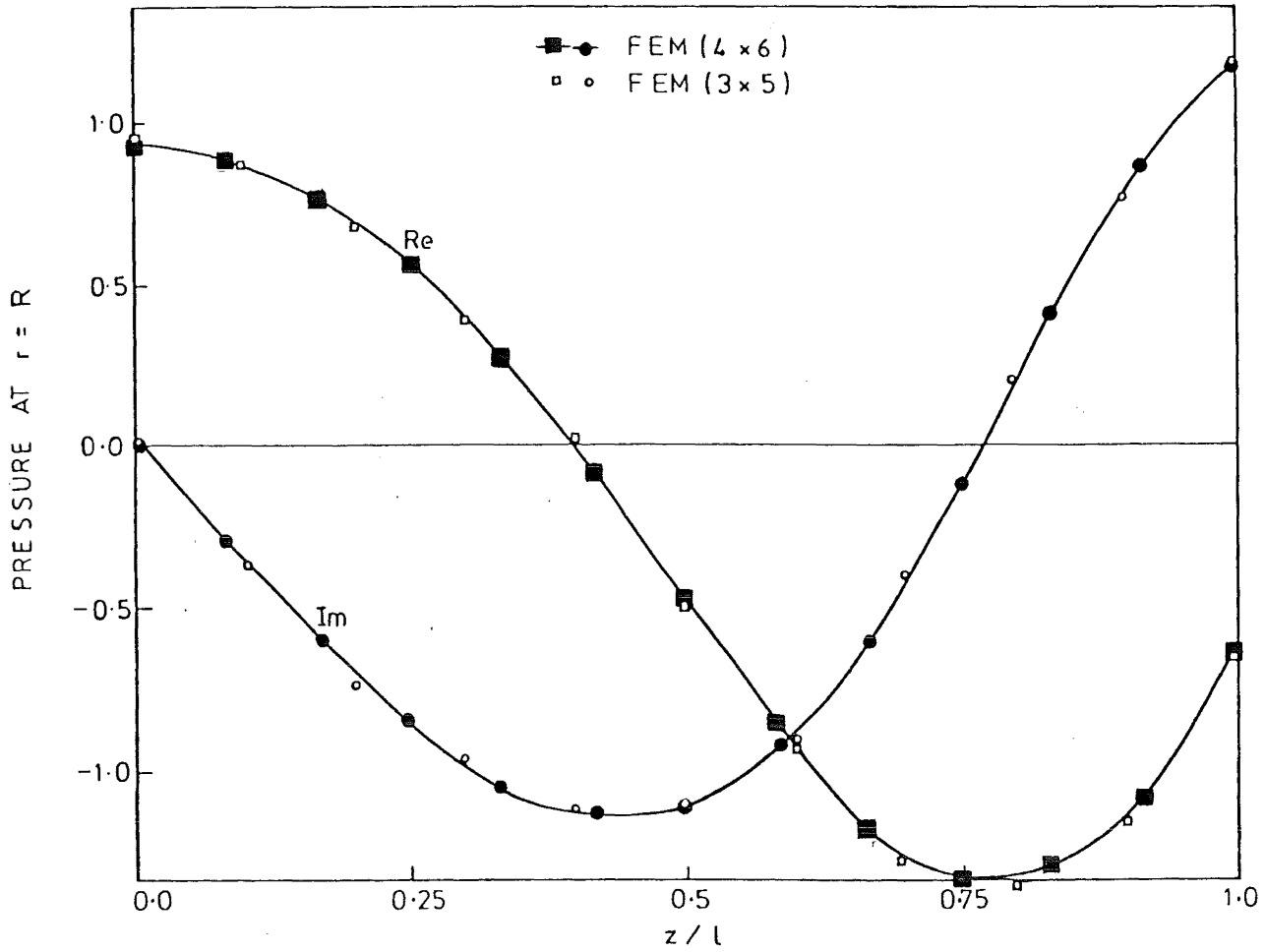

FIG.8·19 AXIAL PRESSURE VARIATION IN COSINE-CONVERGING HARDWALLED DUCT, $R_1=1{\cdot}0$, $R_2=0{\cdot}925$, $l=0{\cdot}5$, $M_1=-0{\cdot}30$, $M_2=-0{\cdot}36$, $k_rR_1=6{\cdot}0$, $m_o=1$, IN MODE 1

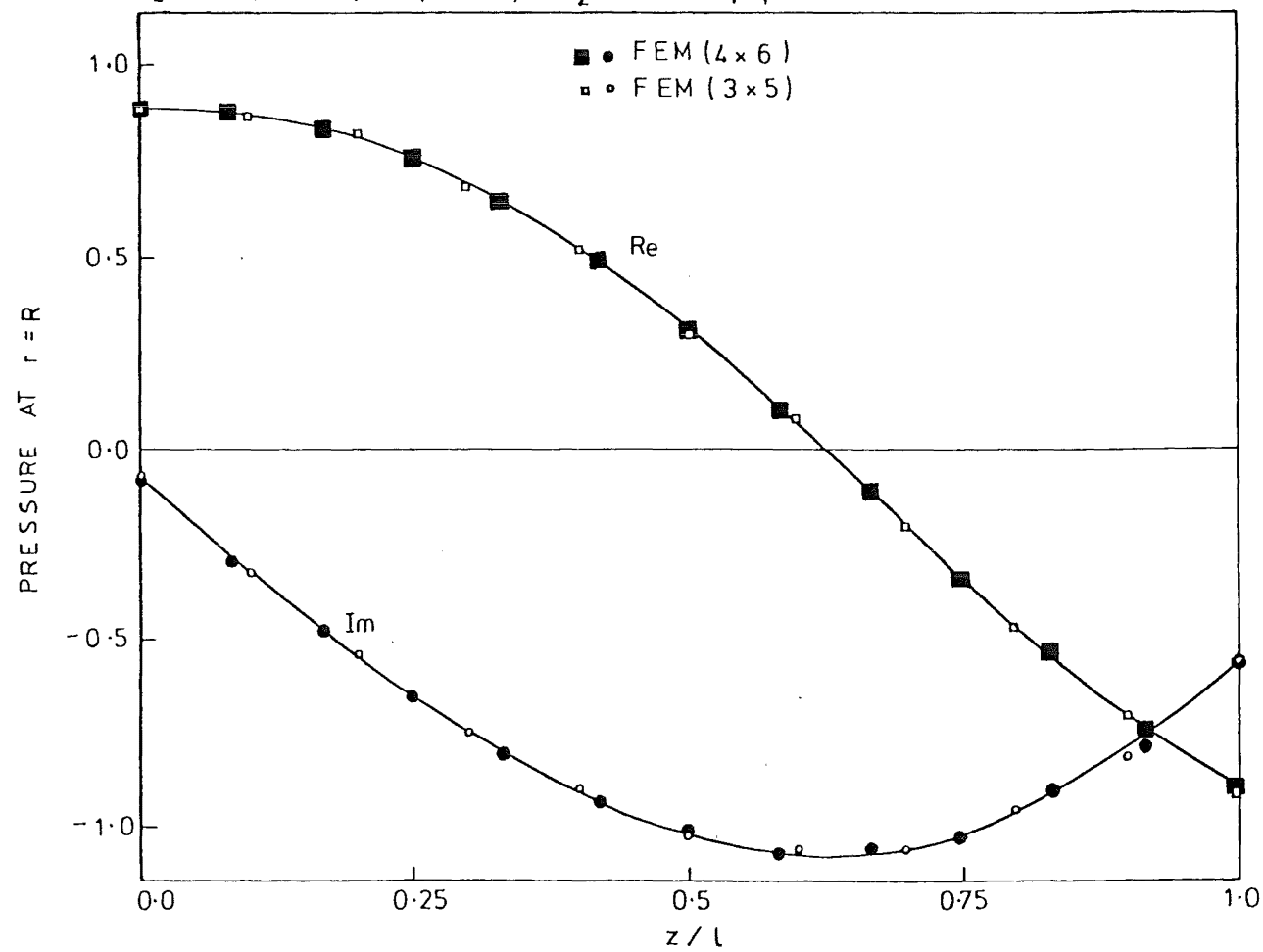

FIG.8·20 AXIAL PRESSURE VARIATION IN COSINE-CONVERGING HARDWALLED DUCT, $R_1=1{\cdot}0$, $R_2=0{\cdot}925$, $l=0{\cdot}5$, $M_1=-0{\cdot}30$, $M_2=-0{\cdot}36$, $k_rR_1=6{\cdot}0$, $m_o=1$, IN MODE 2

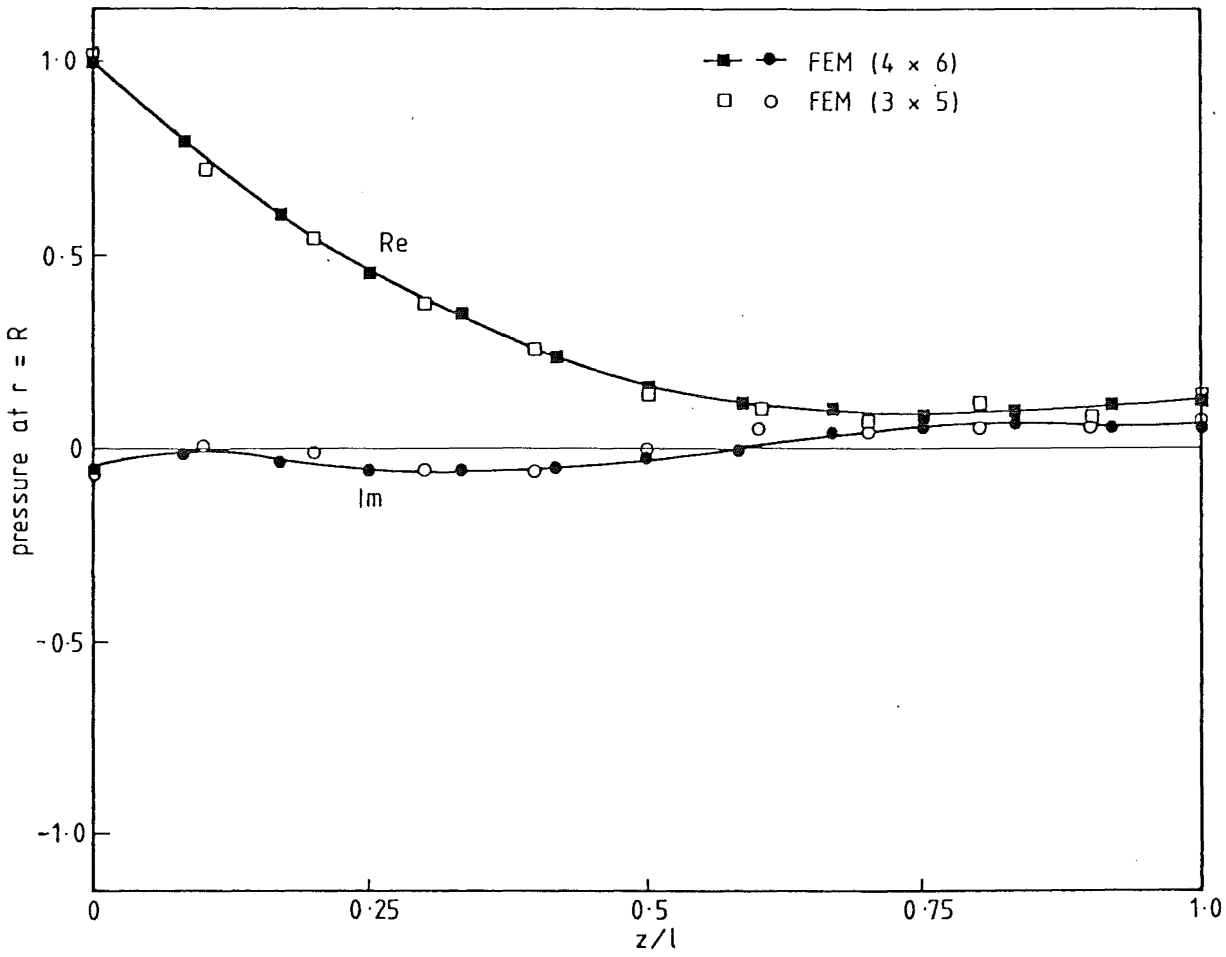

FIG. 8·21 AXIAL PRESSURE VARIATION IN COSINE-CONVERGING HARDWALLED DUCT; $R_1 = 1{\cdot}0$, $R_2 = 0{\cdot}925$, $l = 0{\cdot}5$, $M_1 = -0{\cdot}30$, $M_2 = -0{\cdot}36$, $k_r R_1 = 6{\cdot}0$, $m_0 = 1$, IN MODE 3

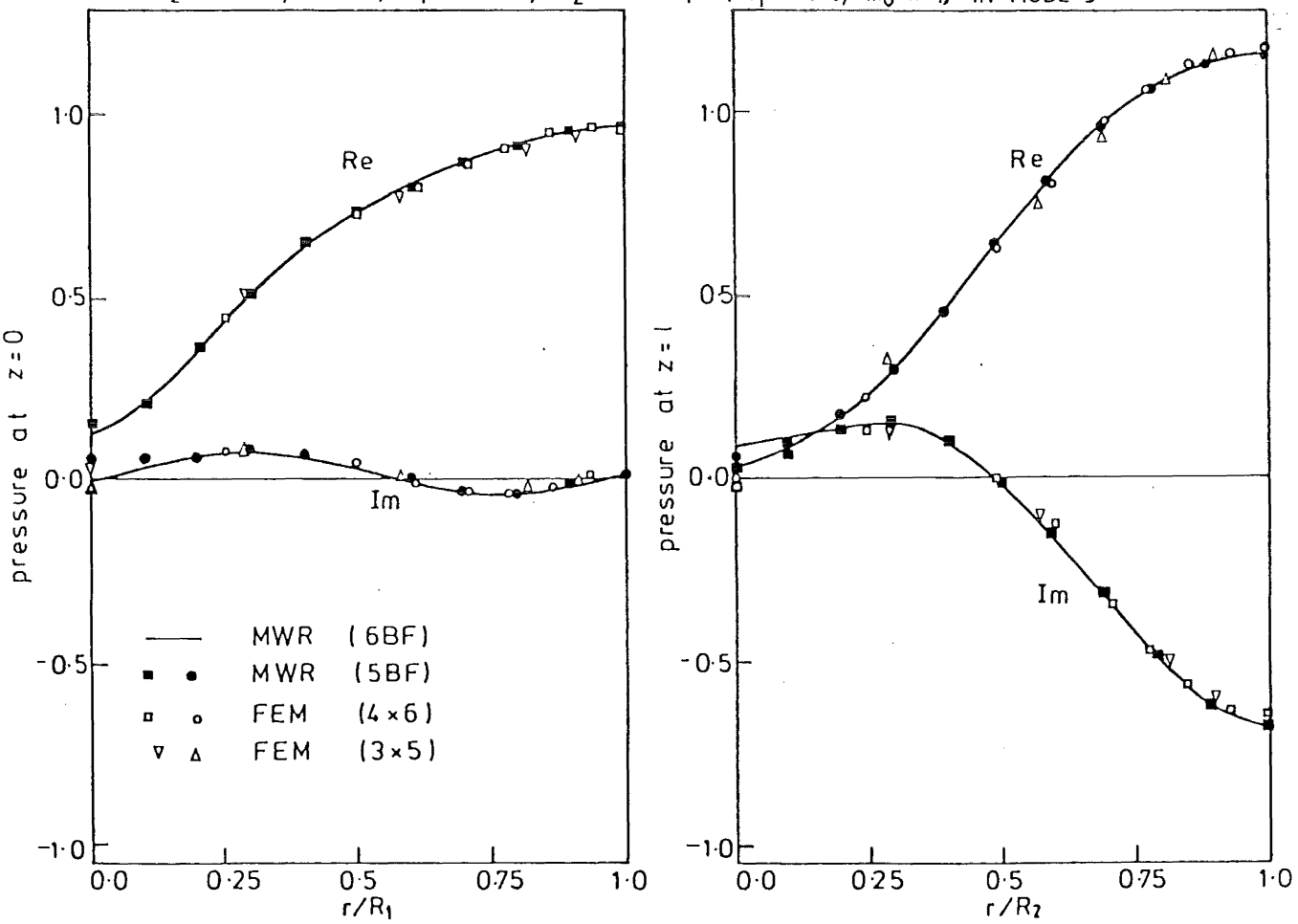

FIG. 8·22 TRANSVERSE PRESSURE VARIATIONS IN COSINE-CONVERGING HARDWALLED DUCT $R_1 = 1{\cdot}0$, $R_2 = 0{\cdot}925$, $l = 0{\cdot}5$, $M_1 = -0{\cdot}30$, $M_2 = -0{\cdot}36$, $k_r R_1 = 6{\cdot}0$, $m_0 = 1$, IN MODE 1

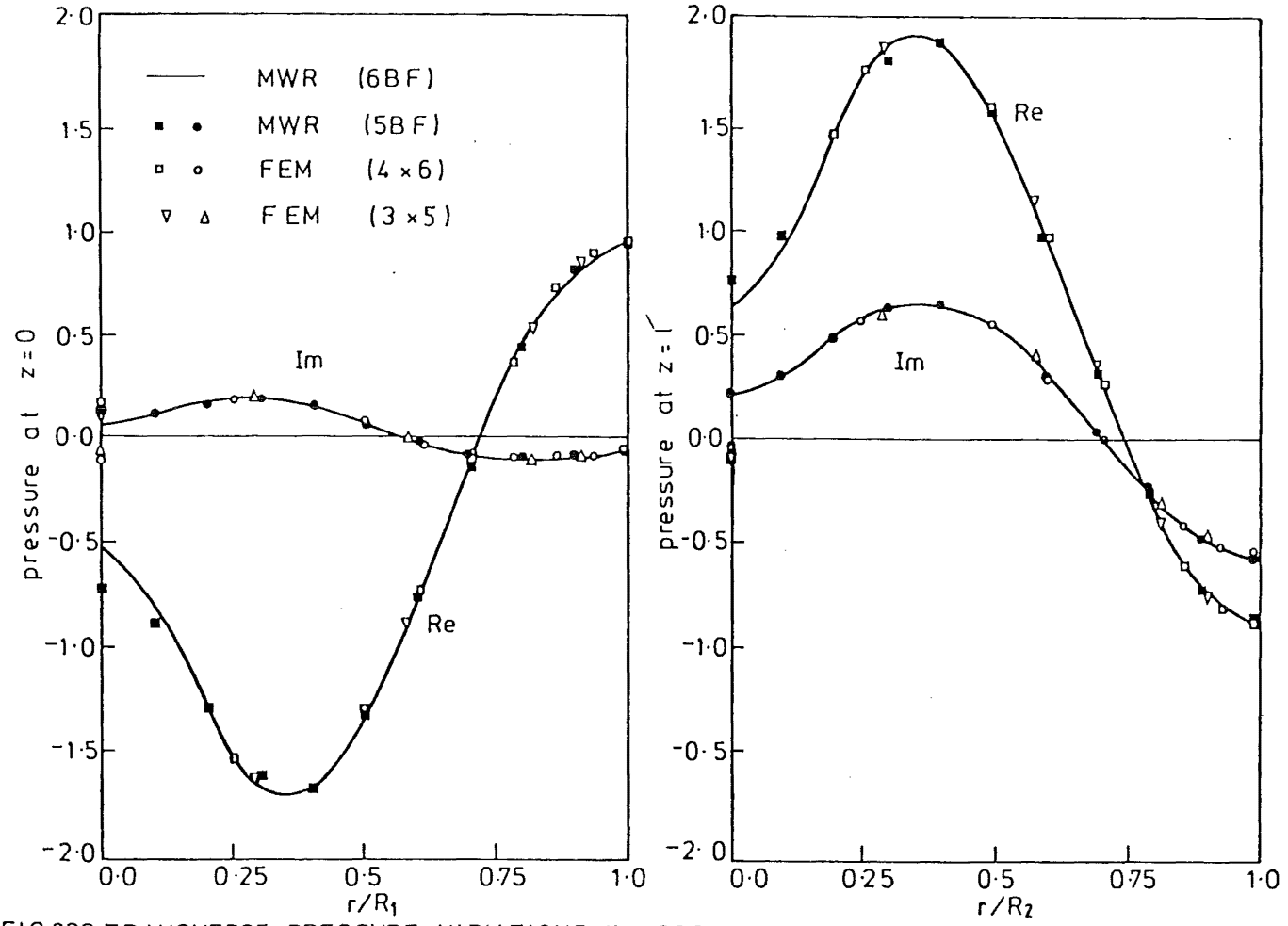

FIG.823 TRANSVERSE PRESSURE VARIATIONS IN COSINE-CONVERGING HARDWALLED DUCT; $R_1=1{\cdot}0$, $R_2=0{\cdot}925$, $l=0{\cdot}5$, $M_1=-0{\cdot}30$, $M_2=-0{\cdot}36$, $k_rR_1=6{\cdot}0$, $m_o=1$, IN MODE 2.

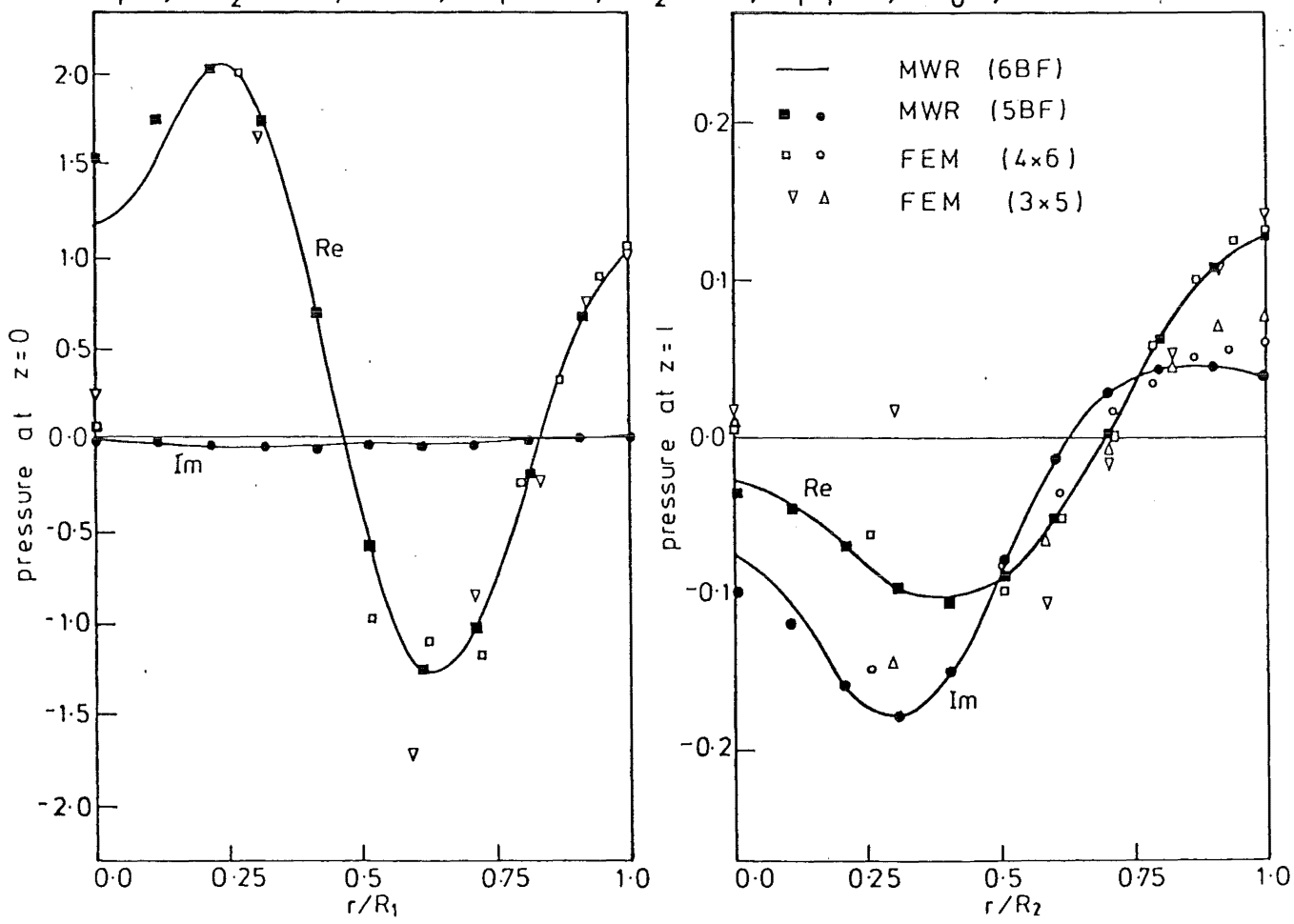

FIG.824 TRANSVERSE PRESSURE VARIATIONS IN COSINE-CONVERGING HARDWALLED DUCT; $R_1=1{\cdot}0$, $R_2=0{\cdot}925$, $l=0{\cdot}5$, $M_1=-0{\cdot}30$, $M_2=-0{\cdot}36$, $k_rR_1=6{\cdot}0$, $m_o=1$, IN MODE 3.

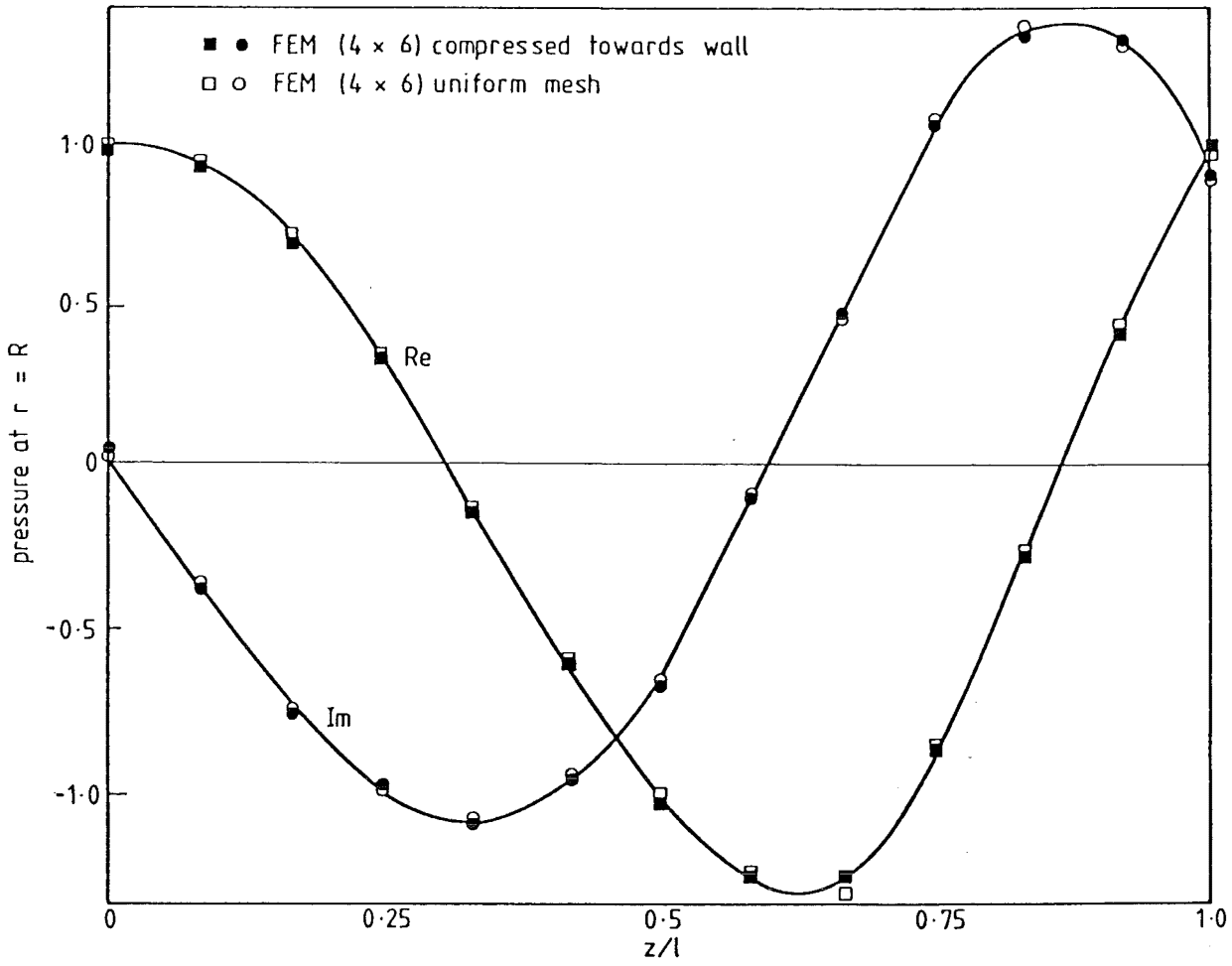

FIG. 8·25 AXIAL PRESSURE VARIATION IN COSINE-CONVERGING HARDWALLED DUCT, $R_1 = 1{\cdot}0$; $R_2 = 0{\cdot}925$, $l = 0{\cdot}5$, $M_1 = -0{\cdot}30$, $M_2 = -0{\cdot}36$, $k_r R_1 = 8{\cdot}0$, $m_o = 2$, IN MODE 1

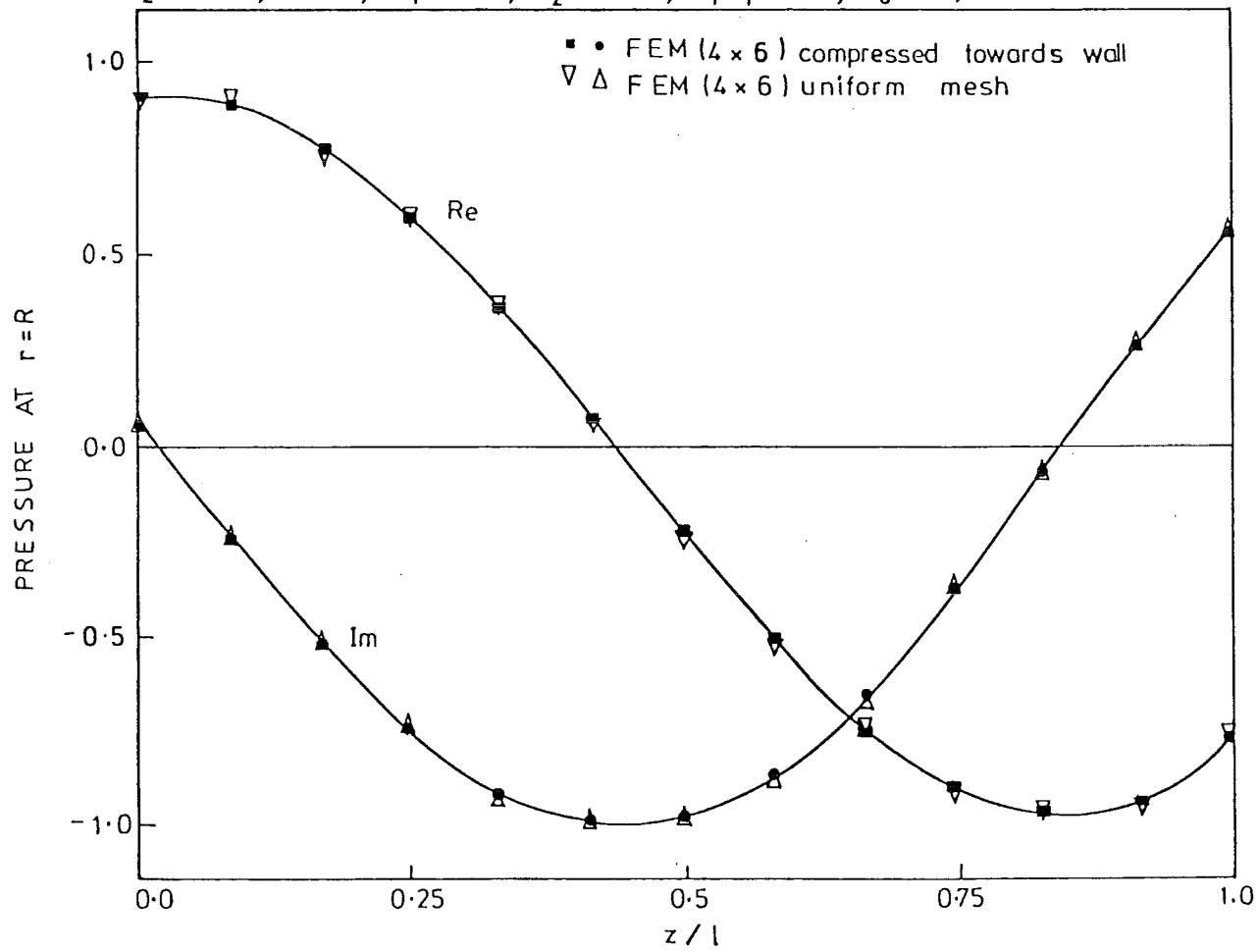

FIG. 826 AXIAL PRESSURE VARIATION IN COSINE-CONVERGING HARDWALLED DUCT; $R_1 = 1{\cdot}0$, $R_2 = 0{\cdot}925$, $l = 0{\cdot}5$, $M_1 = -0{\cdot}30$, $M_2 = -0{\cdot}36$, $k_r R_1 = 8{\cdot}0$, $m_o = 2$, IN MODE 2

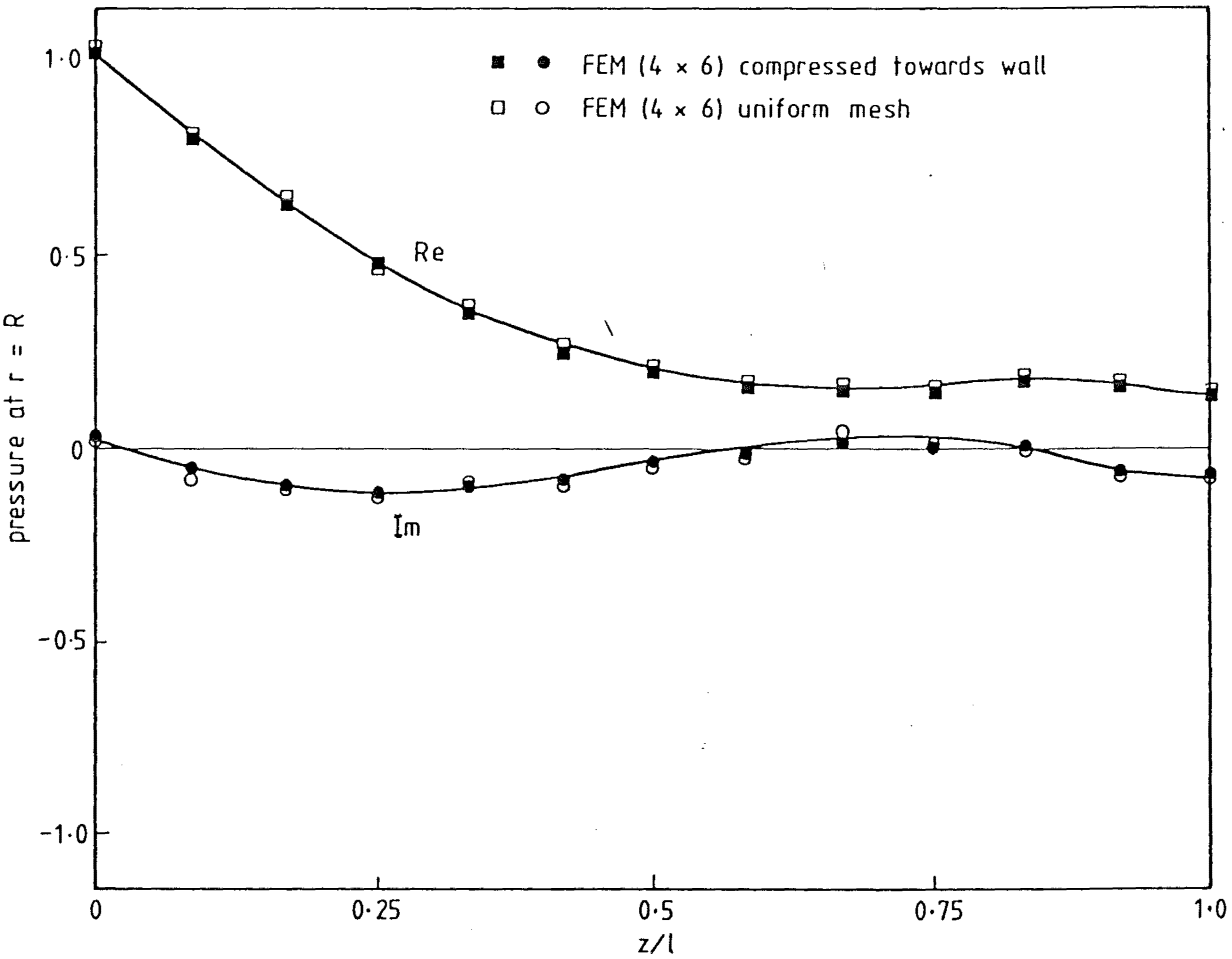

FIG. 8·27 AXIAL PRESSURE VARIATION IN COSINE-CONVERGING HARDWALLED DUCT, $R_1 = 1{\cdot}0$; $R_2 = 0{\cdot}925$, $l = 0{\cdot}5$, $M_1 = -0{\cdot}30$, $M_2 = -0{\cdot}36$, $k_r R_1 = 8{\cdot}0$, $m_o = 2$, IN MODE 3

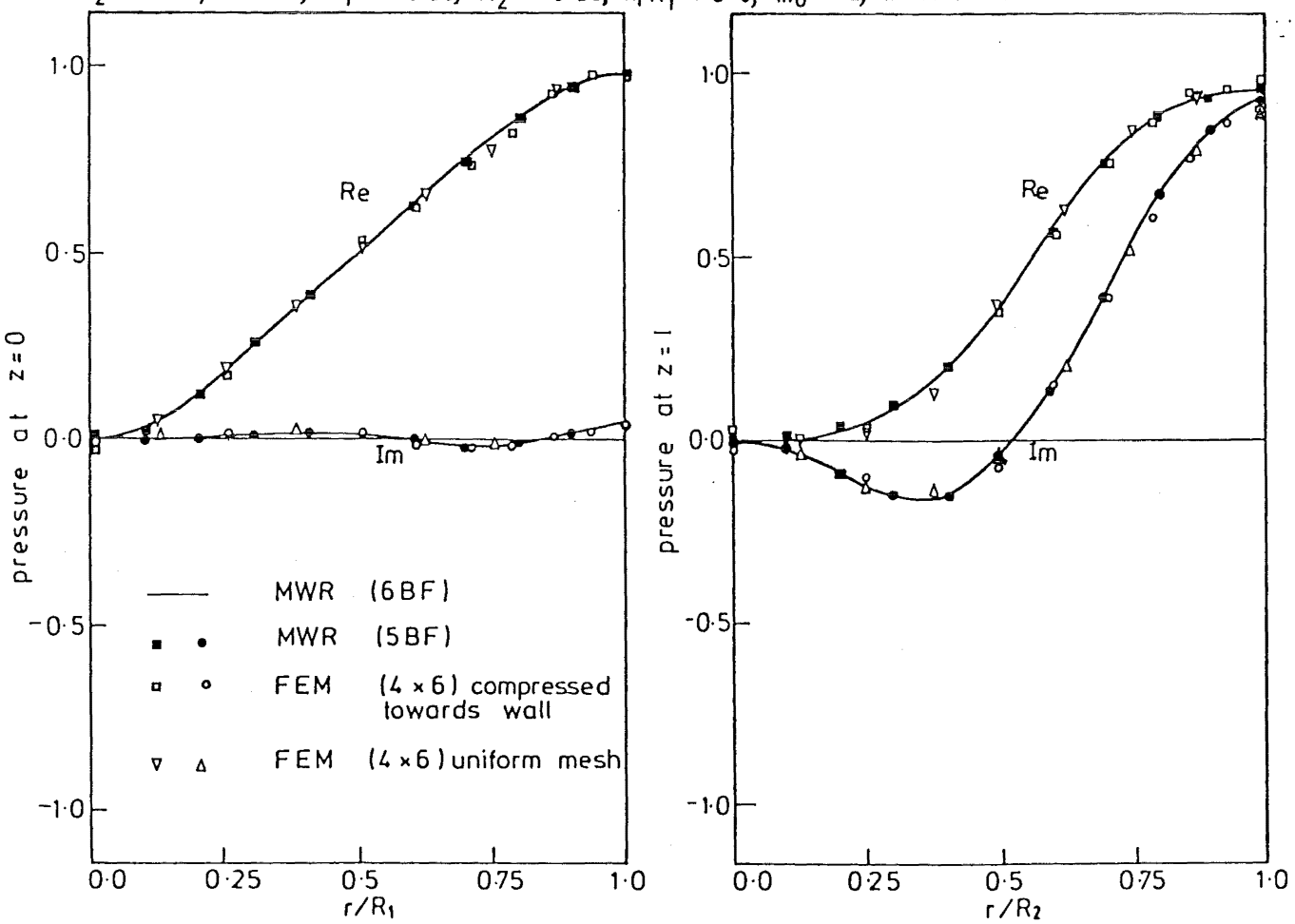

FIG. 8·28 TRANSVERSE PRESSURE VARIATIONS IN COSINE-CONVERGING HARDWALLED DUCT, $R_1 = 1{\cdot}0$, $R_2 = 0{\cdot}925$, $l = 0{\cdot}5$, $M_1 = -0{\cdot}30$, $M_2 = -0{\cdot}36$, $k_r R_1 = 8{\cdot}0$, $m_o = 2$, IN MODE 1

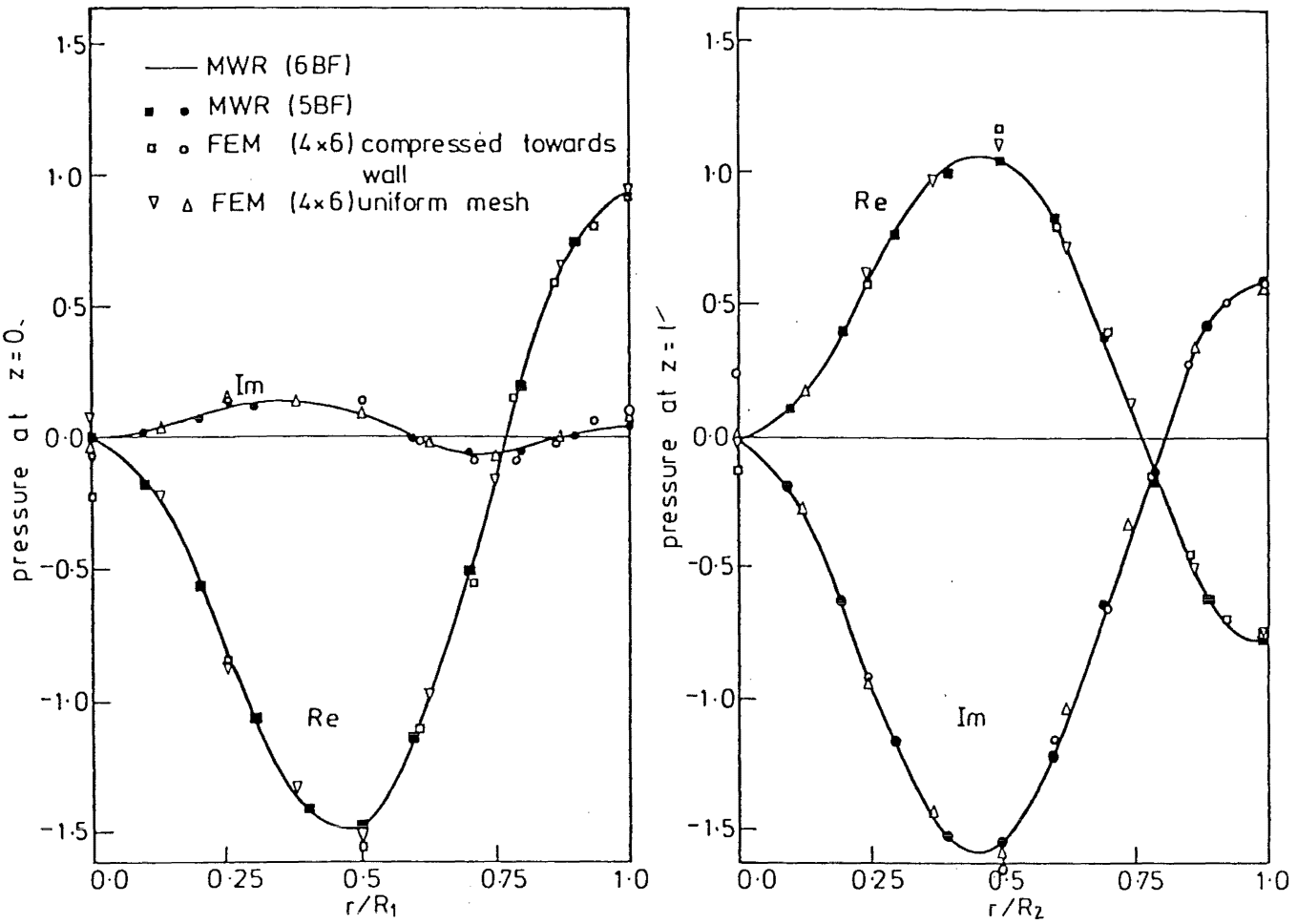

FIG.8·29 TRANSVERSE PRESSURE VARIATIONS IN COSINE-CONVERGING HARDWALLED DUCT, $R_1=1{\cdot}0$, $R_2=0{\cdot}925$, $l=0{\cdot}5$, $M_1=-0{\cdot}30$, $M_2=-0{\cdot}36$, $k_rR_1=8{\cdot}0$, $m_o=2$, IN MODE 2

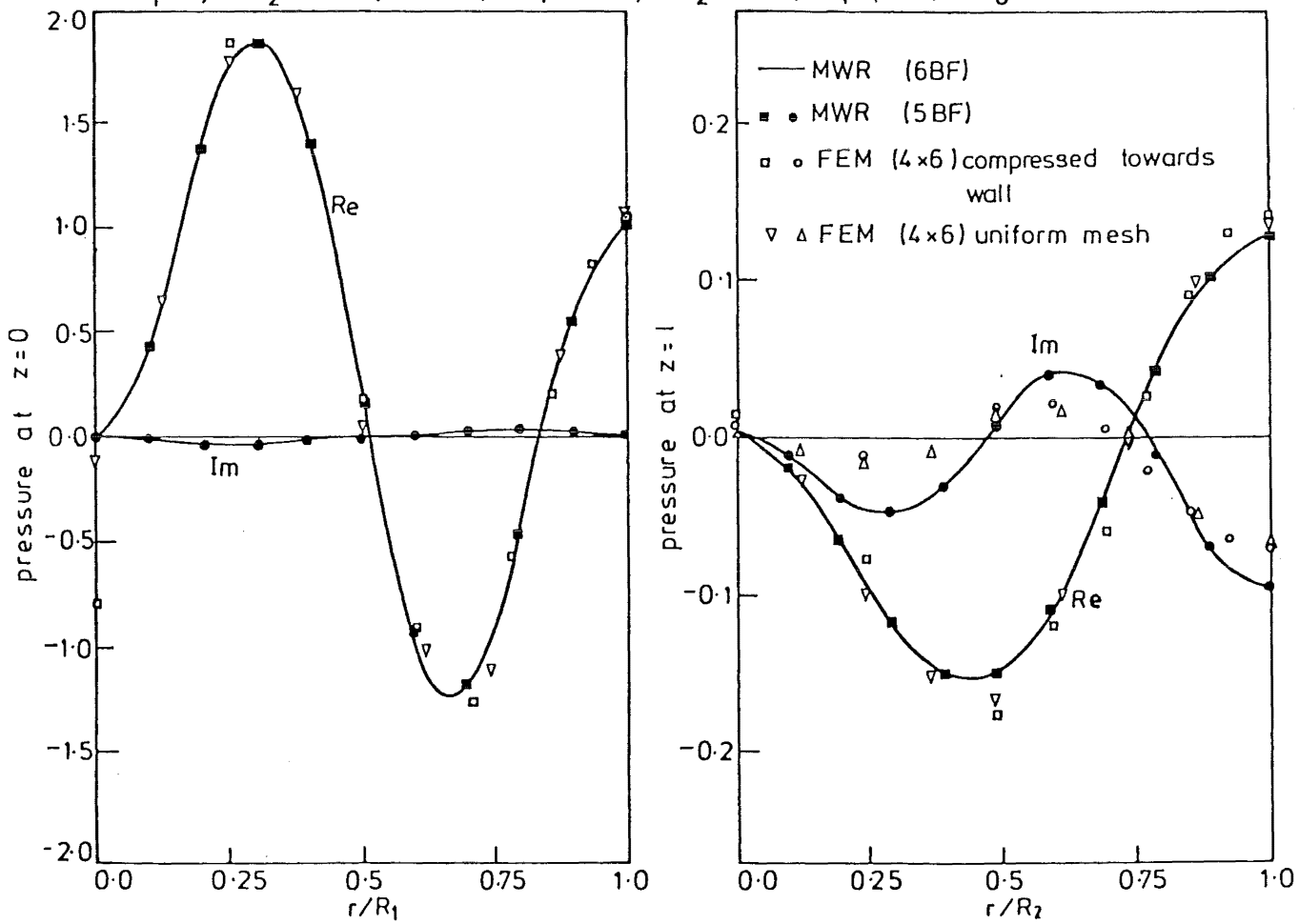

FIG.8·30 TRANSVERSE PRESSURE VARIATIONS IN COSINE-CONVERGING HARDWALLED DUCT, $R_1=1{\cdot}0$, $R_2=0{\cdot}925$, $l=0{\cdot}5$, $M_1=-0{\cdot}30$, $M_2=-0{\cdot}36$, $k_rR_1=8{\cdot}0$, $m_o=2$, IN MODE 3

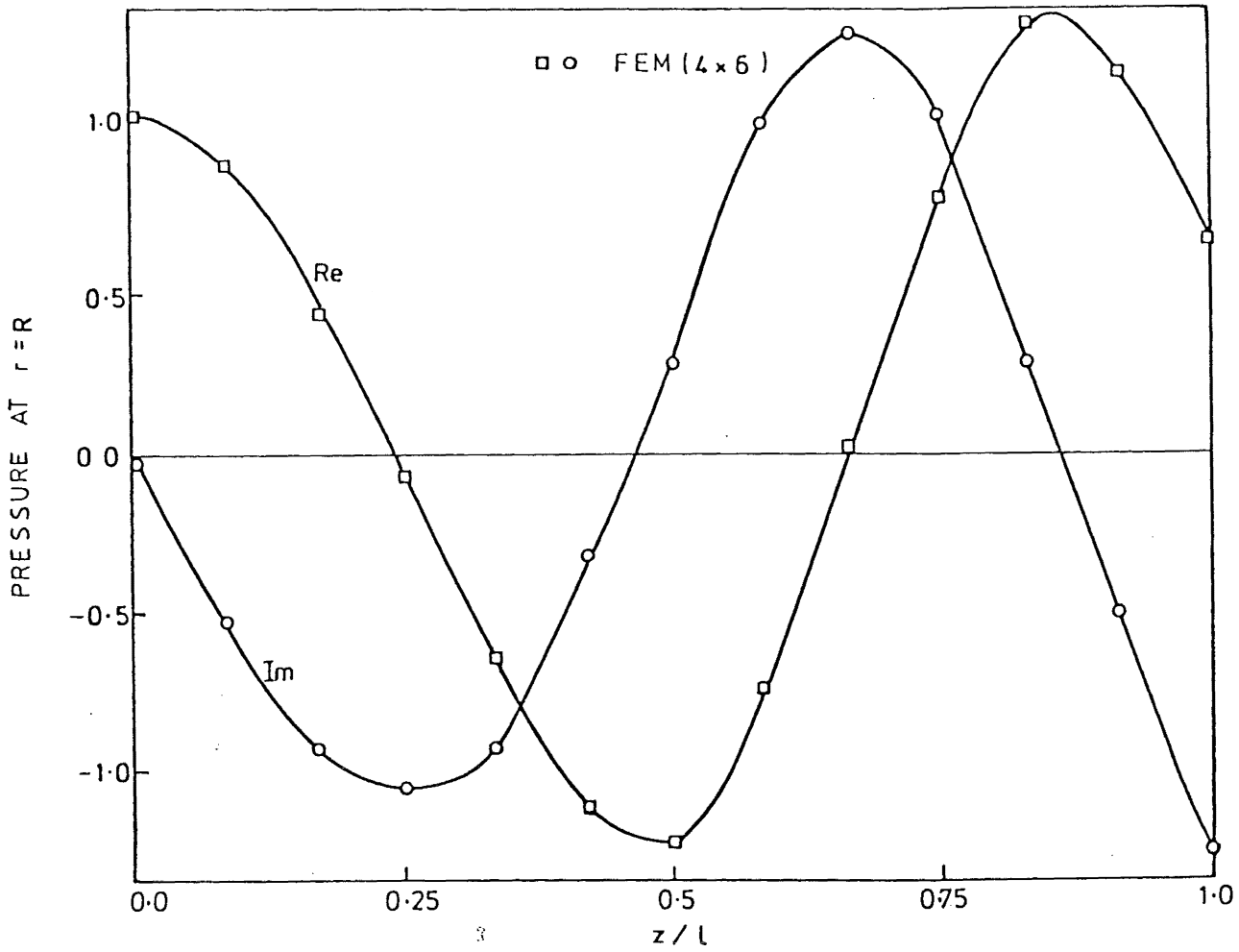

FIG.8·31 AXIAL PRESSURE VARIATION IN COSINE-CONVERGING HARDWALLED DUCT; $R_1=1{\cdot}0$, $R_2=0{\cdot}925$, $l=0{\cdot}5$, $M_1=-0{\cdot}30$, $M_2=-0{\cdot}36$, $k_rR_1=11{\cdot}0$, $m_o=4$, IN MODE 1

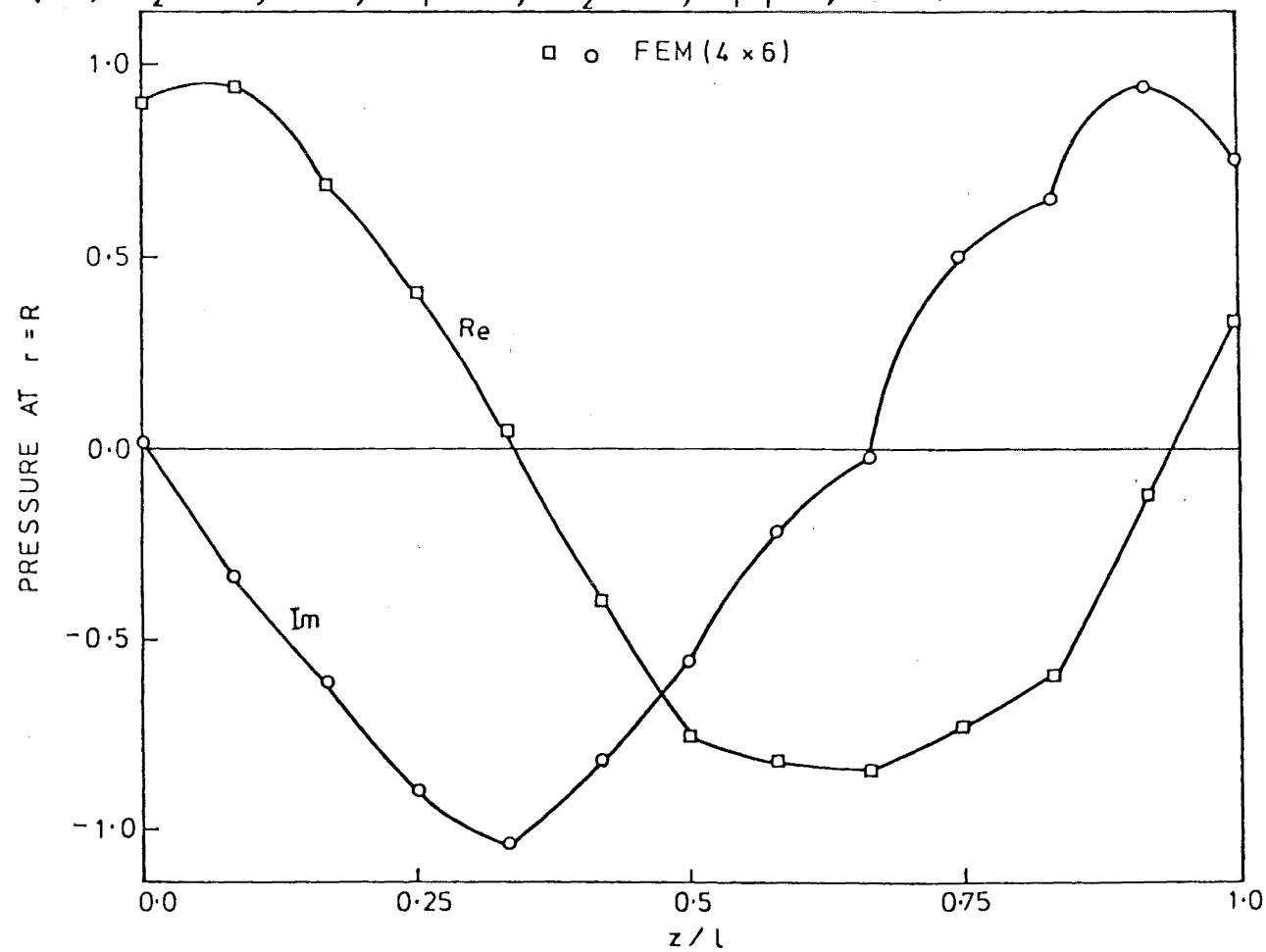

FIG. 8·32 AXIAL PRESSURE VARIATION IN COSINE-CONVERGING HARDWALLED DUCT; $R_1=1{\cdot}0$, $R_2=0{\cdot}925$, $l=0{\cdot}5$, $M_1=-0{\cdot}30$, $M_2=-0{\cdot}36$, $k_rR_1=11{\cdot}0$, $m_o=4$, IN MODE 2

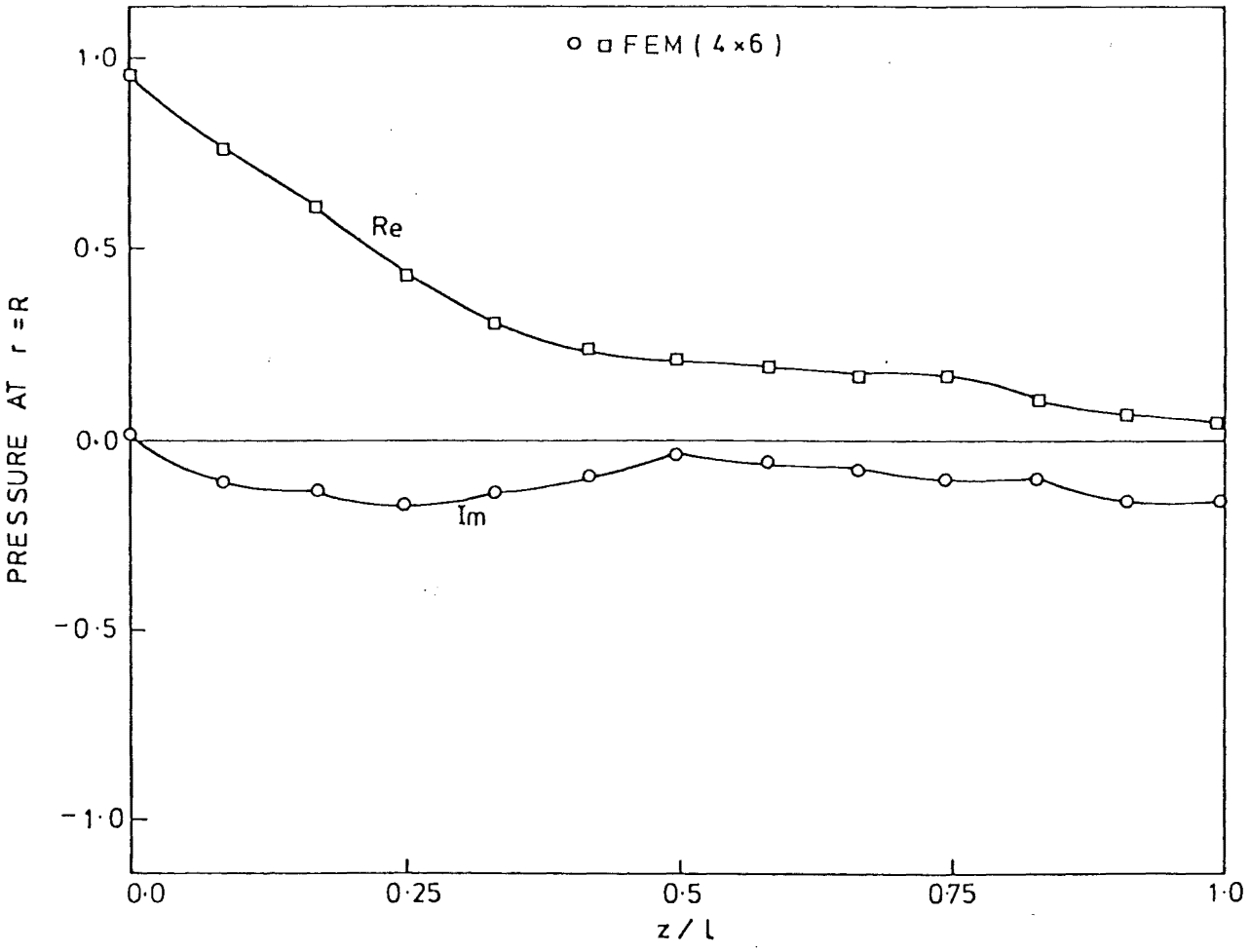

FIG.8·33 AXIAL PRESSURE VARIATION IN COSINE-CONVERGING HARDWALLED DUCT; R_1=1·0, R_2=0·925, l=0·5, M_1=-0·30, M_2=-0·36, k_rR_1=11·0, m_o=4, IN MODE 3

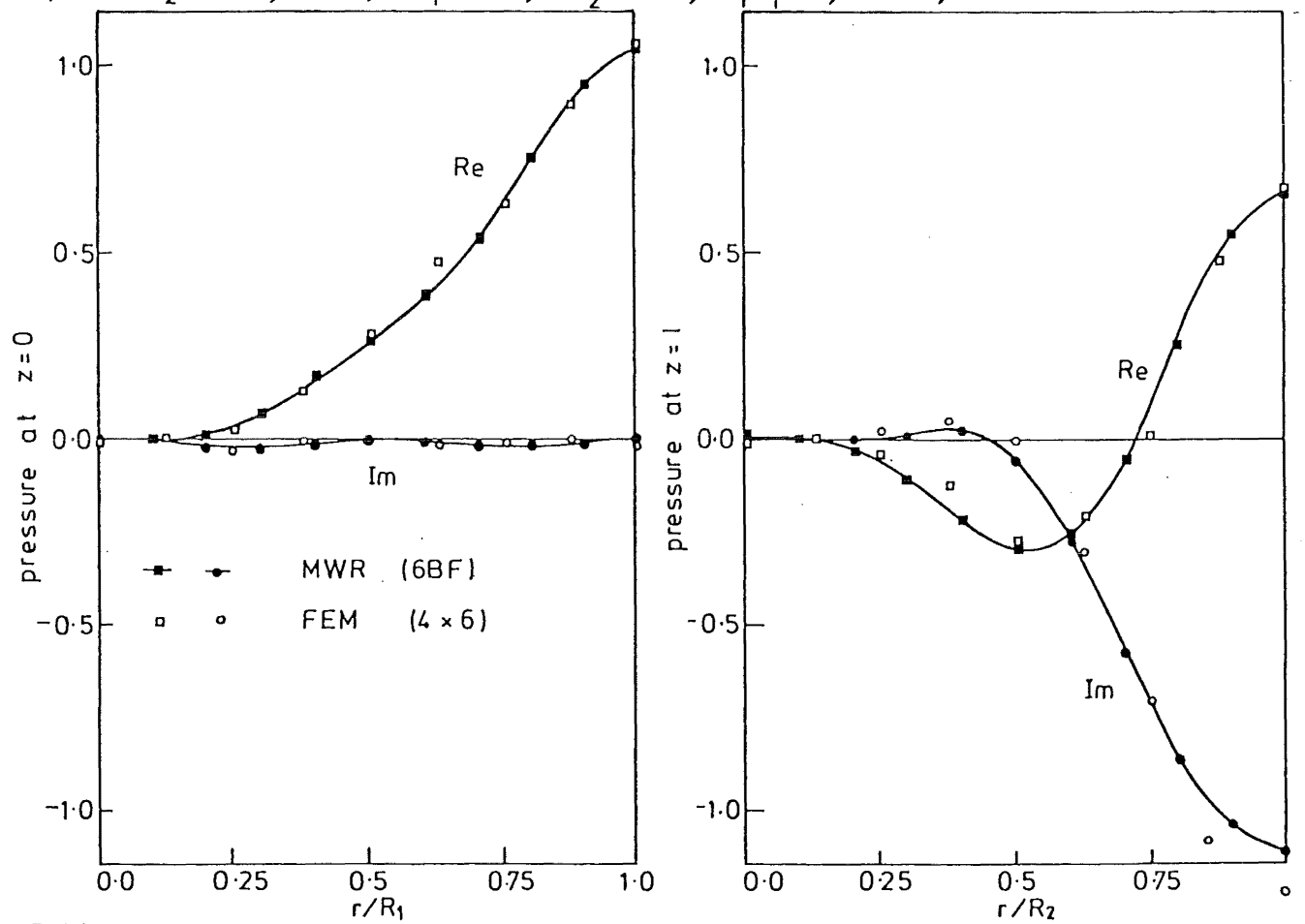

FIG.8·34 TRANSVERSE PRESSURE VARIATIONS IN COSINE-CONVERGING HARDWALLED DUCT; R_1=1·0, R_2=0·925, l=0·5, M_1=-030, M_2=-0·36, k_rR_1=11·0, m_o=4, IN MODE 1

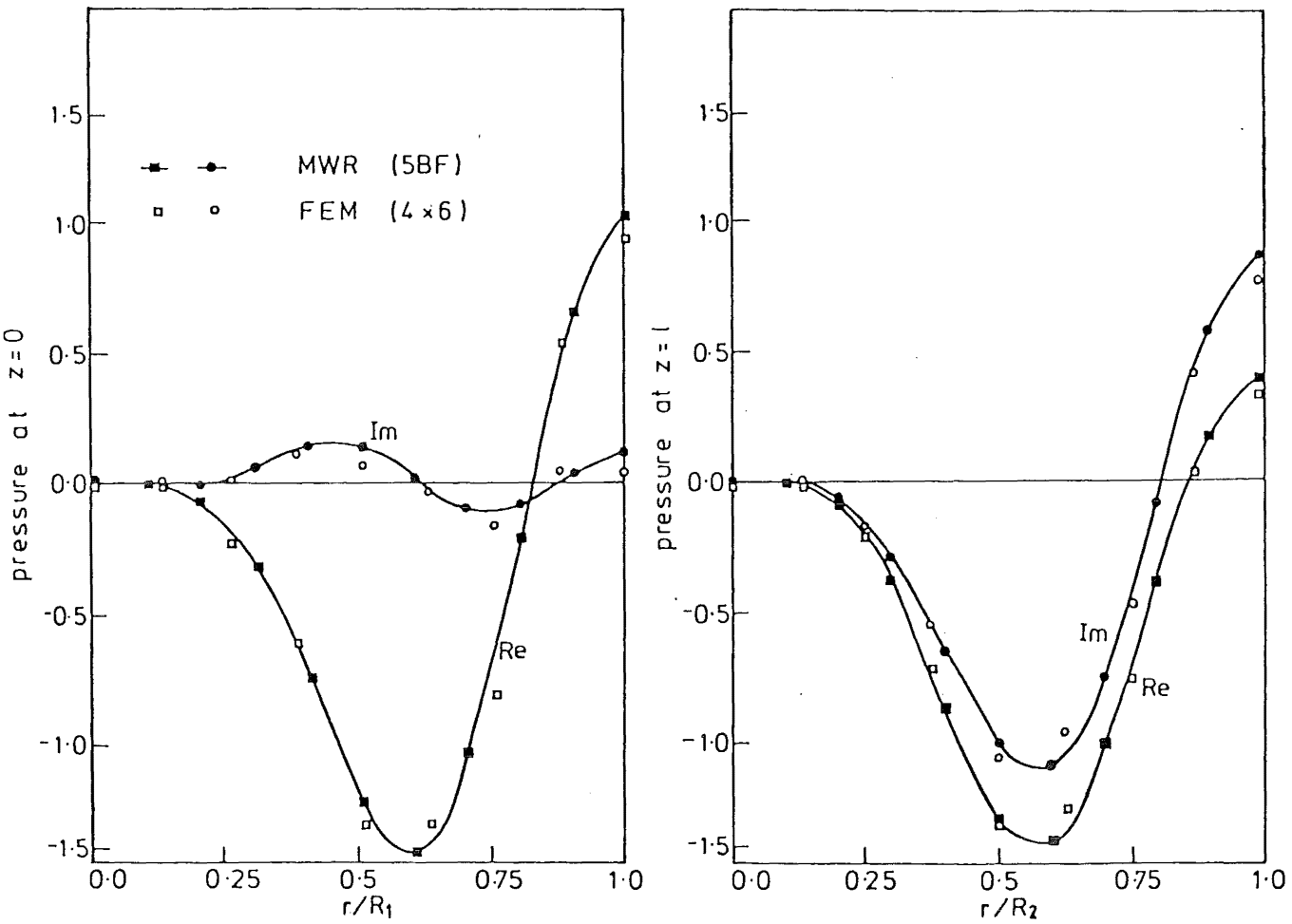

FIG.8.35 TRANSVERSE PRESSURE VARIATIONS IN COSINE-CONVERGING HARDWALLED DUCT; $R_1=1{\cdot}0$, $R_2=0{\cdot}925$, $l=0{\cdot}5$, $M_1=-0{\cdot}30$, $M_2=-0{\cdot}36$, $k_rR_1=11{\cdot}0$, $m_o=4$, IN MODE 2

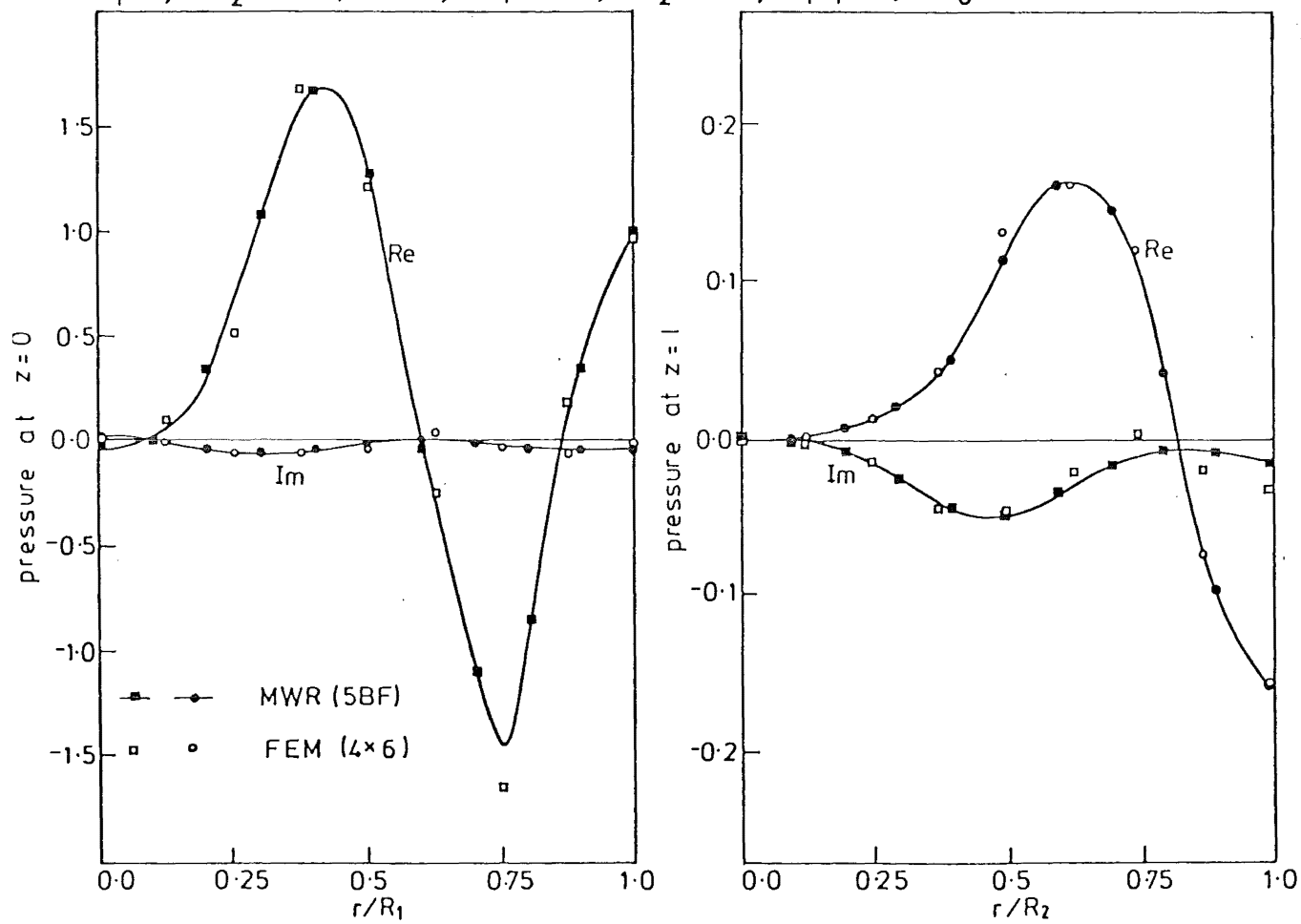

FIG.8.36 TRANSVERSE PRESSURE VARIATIONS IN COSINE-CONVERGING HARDWALLED DUCT; $R_1=1{\cdot}0$, $R_2=0{\cdot}925$, $l=0{\cdot}5$, $M_1=-0{\cdot}30$, $M_2=-0{\cdot}36$, $k_rR_1=11{\cdot}0$, $m_o=4$, IN MODE 3

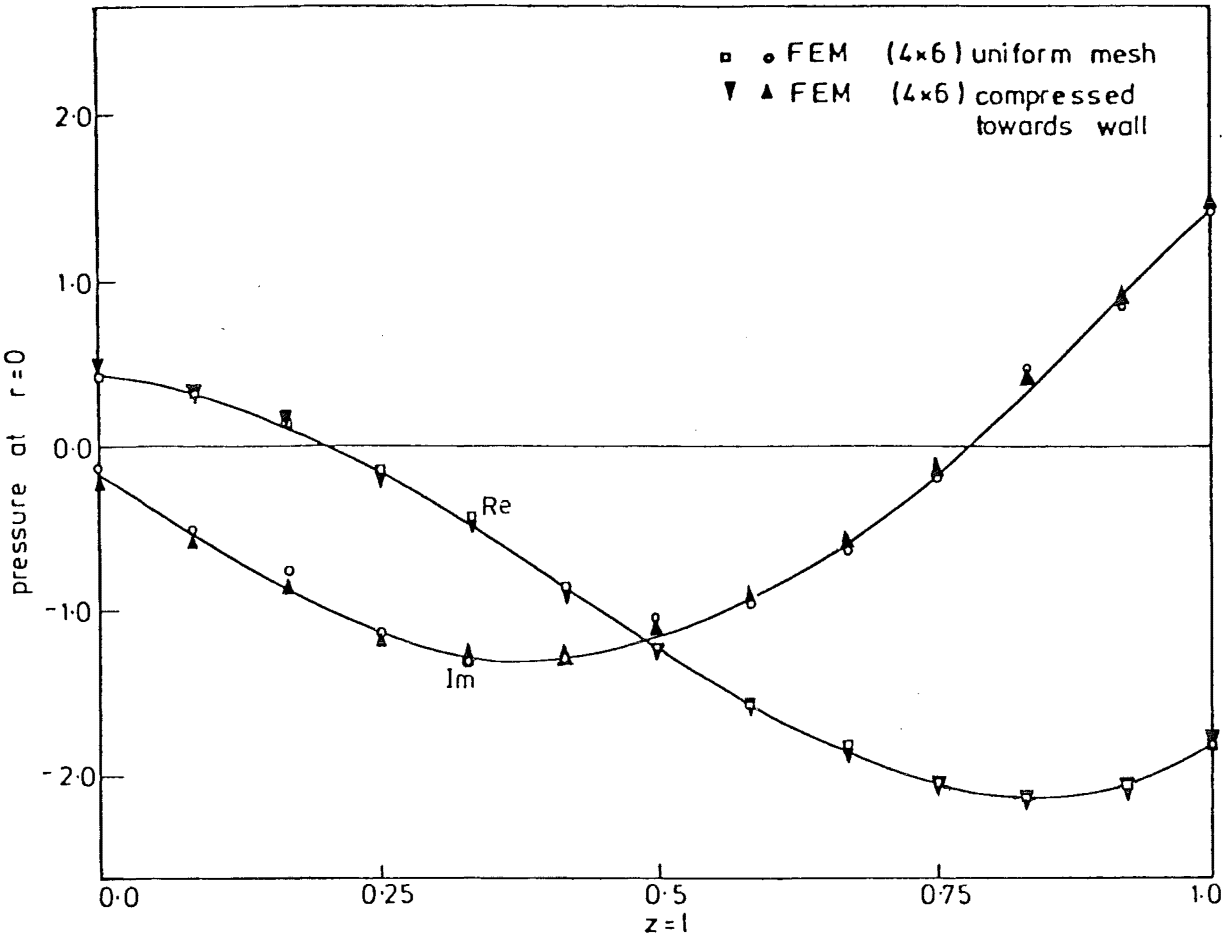

FIG. 8·37 AXIAL PRESSURE VARIATION IN COSINE-CONVERGING SOFTWALLED DUCT; $R_1=1{\cdot}0$, $R_2=0{\cdot}925$, $l=0{\cdot}5$, $M_1=-0{\cdot}30$, $M_2=-0{\cdot}36$, $k_rR_1=5{\cdot}0$, $A_1=0$, $A_2=0$, $A=(0{\cdot}72-0{\cdot}42i)$, $m_o=0$, IN MODE 1

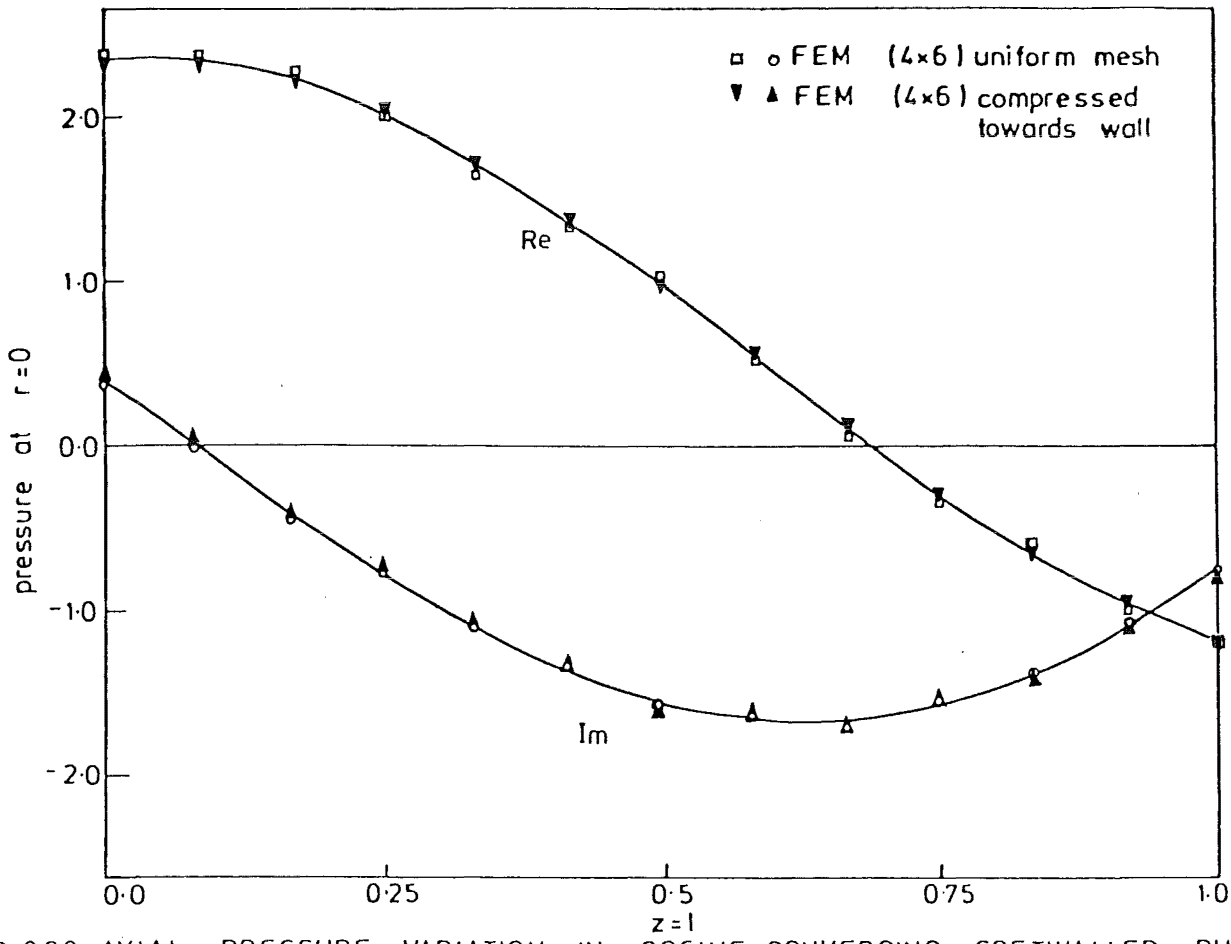

FIG. 8·38 AXIAL PRESSURE VARIATION IN COSINE-CONVERGING SOFTWALLED DUCT; $R_1=1{\cdot}0$, $R_2=0{\cdot}925$, $l=0{\cdot}5$, $M_1=-0{\cdot}30$, $M_2=-0{\cdot}36$, $k_rR_1=5{\cdot}0$, $A_1=0$, $A_2=0$, $A=(0{\cdot}72-0{\cdot}42i)$, $m_o=0$, IN MODE 2

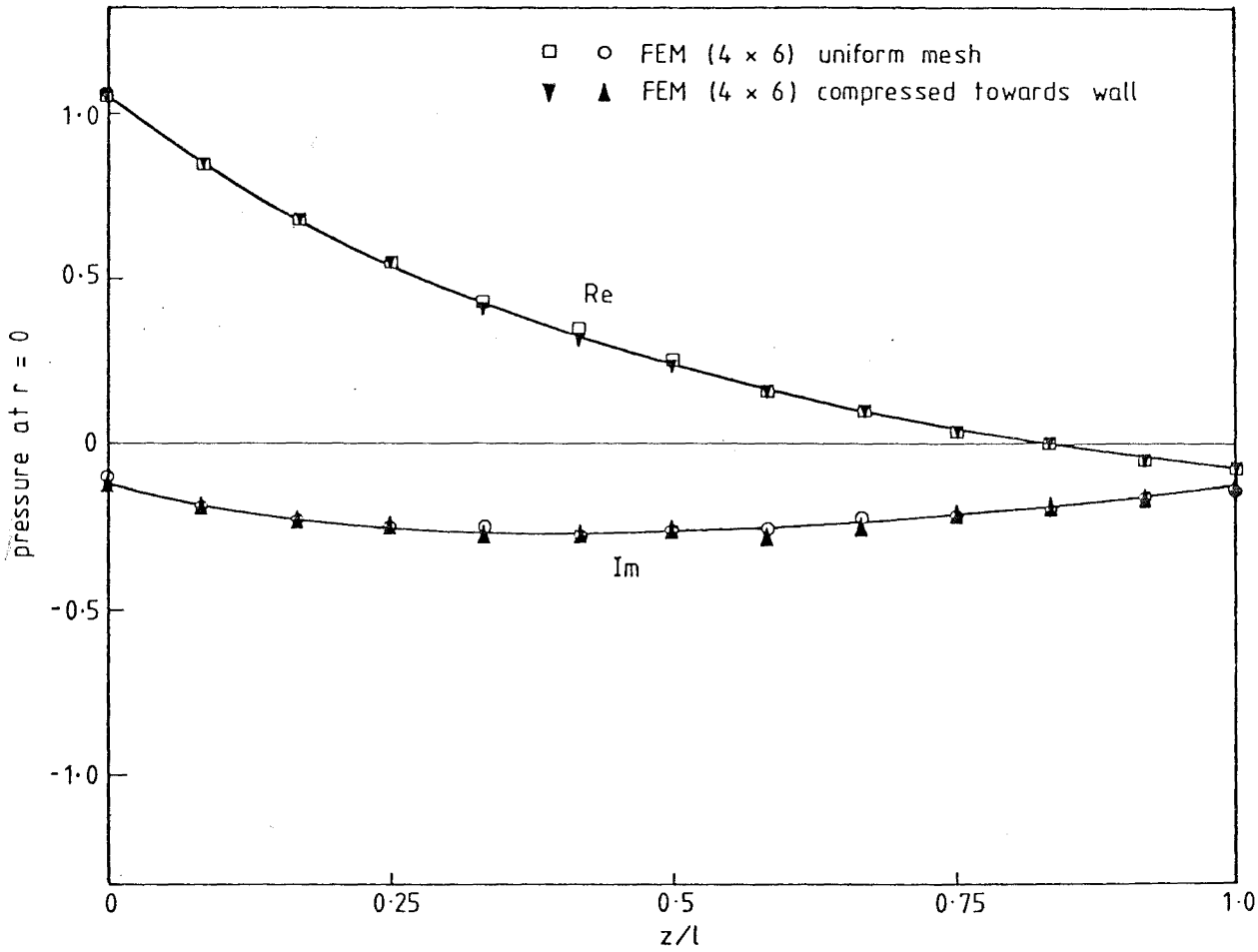

FIG. 8·39 AXIAL PRESSURE VARIATION IN COSINE-CONVERGING SOFTWALLED DUCT; $R_1 = 1{\cdot}0$, $R_2 = 0{\cdot}925$, $l = 0{\cdot}5$, $M_1 = -0{\cdot}30$, $M_2 = -0{\cdot}36$, $k_r R_1 = 5{\cdot}0$, $A_1 = 0$, $A_2 = 0$, $A = (0{\cdot}72 - 0{\cdot}42i)$, $m_0 = 0$, IN MODE 3

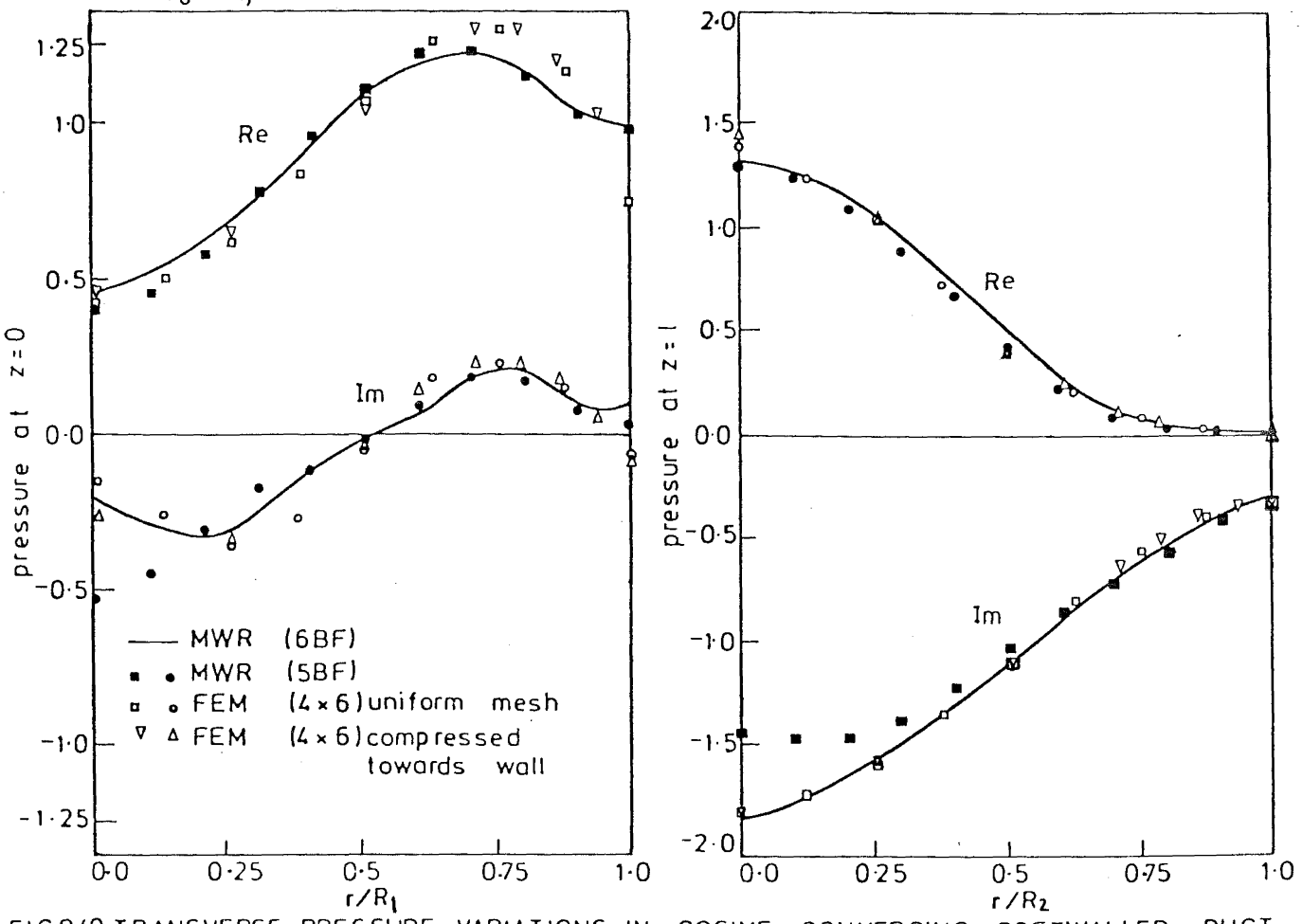

FIG. 8·40 TRANSVERSE PRESSURE VARIATIONS IN COSINE-CONVERGING SOFTWALLED DUCT, $R_1 = 1{\cdot}0$, $R_2 = 0{\cdot}925$, $l = 0{\cdot}5$, $M_1 = -0{\cdot}30$, $M_2 = -0{\cdot}36$, $k_r R_1 = 5{\cdot}0$, $A_1 = 0$, $A_2 = 0$, $A = (0{\cdot}72 - 0{\cdot}42i)$, $m_0 = 0$, IN MODE 1

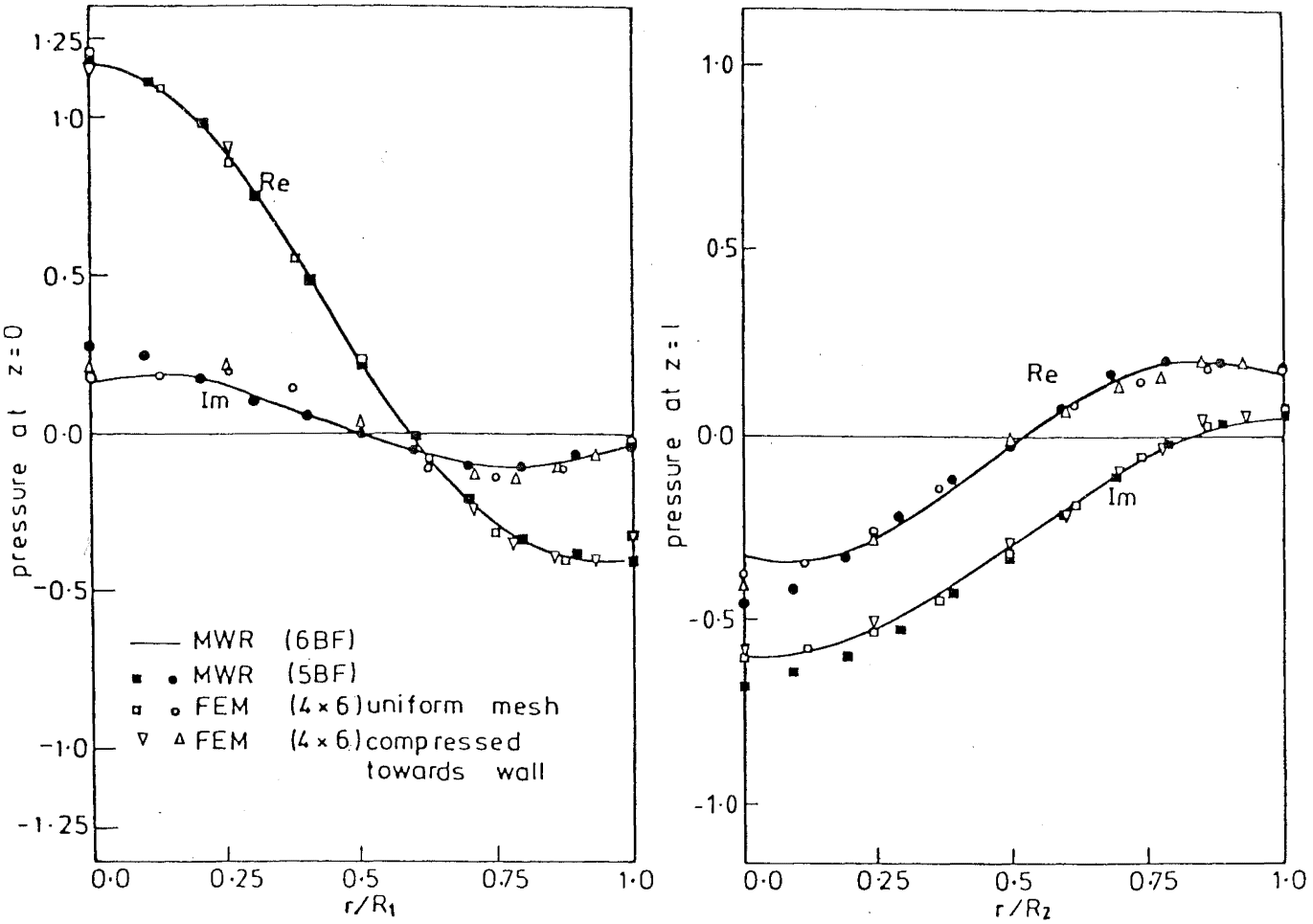

FIG.8·41 TRANSVERSE PRESSURE VARIATIONS IN COSINE-CONVERGING SOFTWALLED DUCT, $R_1=1{\cdot}0$, $R_2=0{\cdot}925$, $l=0{\cdot}5$, $M_1=-0{\cdot}30$, $M_2=-0{\cdot}36$, $k_rR_1=5{\cdot}0$, $A_1=0$, $A_2=0$, $A=(0{\cdot}72-0{\cdot}42i)$, $m_o=0$, IN MODE 2

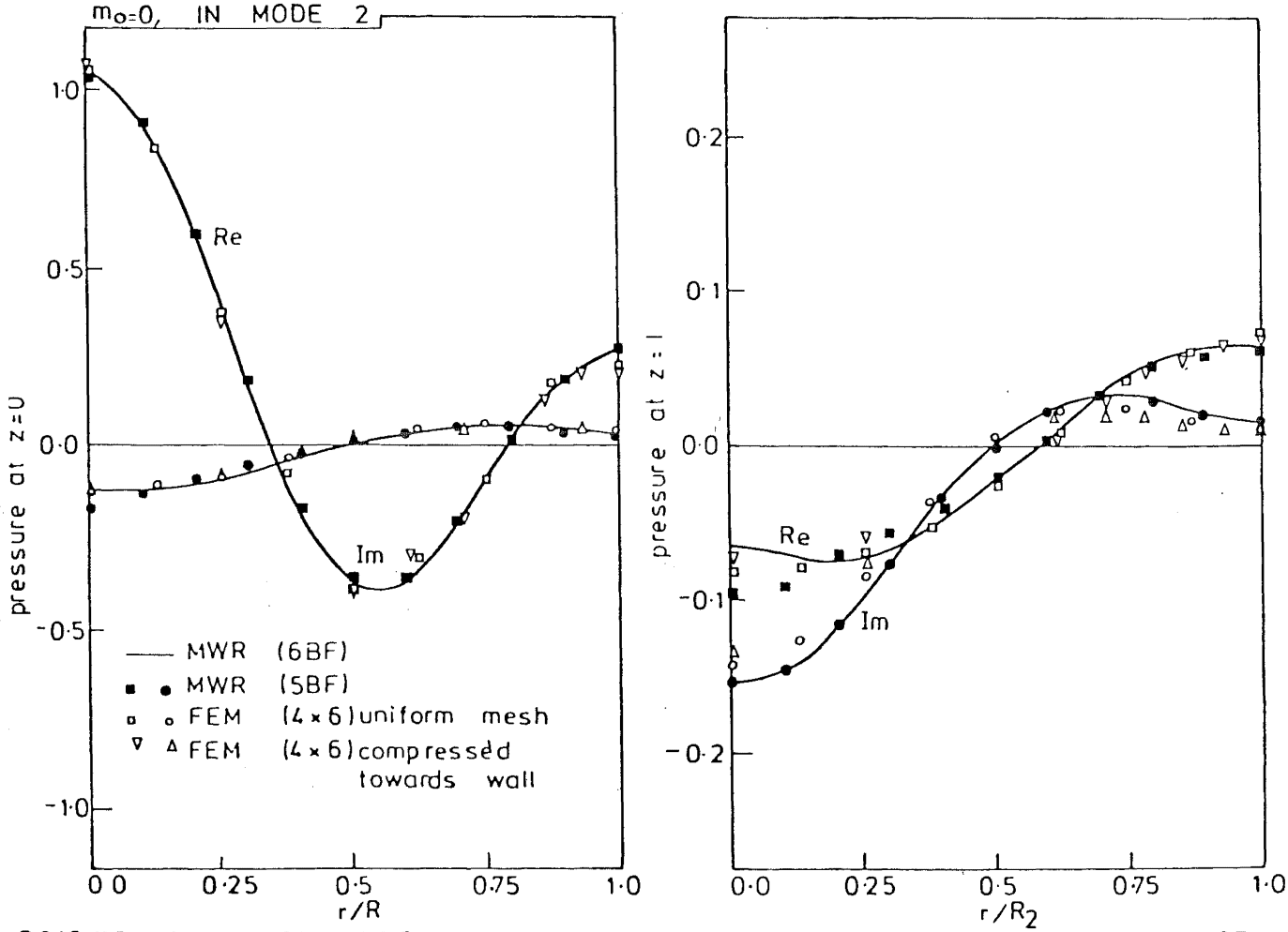

FIG.8·42 TRANSVERSE PRESSURE VARIATIONS IN COSINE-CONVERGING SOFTWALLED DUCT, $R_1=1.0$, $R_2=0{\cdot}925$, $l=0.5$, $M_1=-0{\cdot}30$, $M_2=-0{\cdot}36$, $k_rR_1=5{\cdot}0$, $A_1=0$, $A_2=0$, $A=(0{\cdot}72-0{\cdot}42i)$, $m_o=0$, IN MODE 3

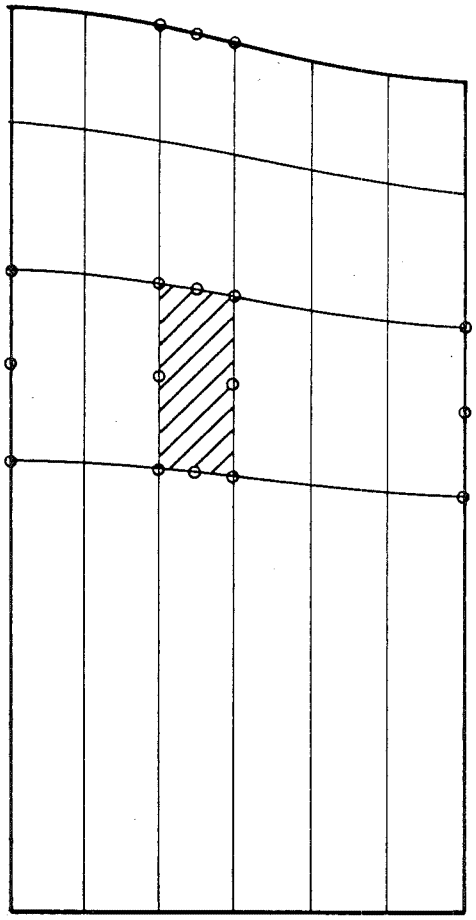

(a) FEM (4 × 6)

Compressed towards wall
(parabolic distribution)

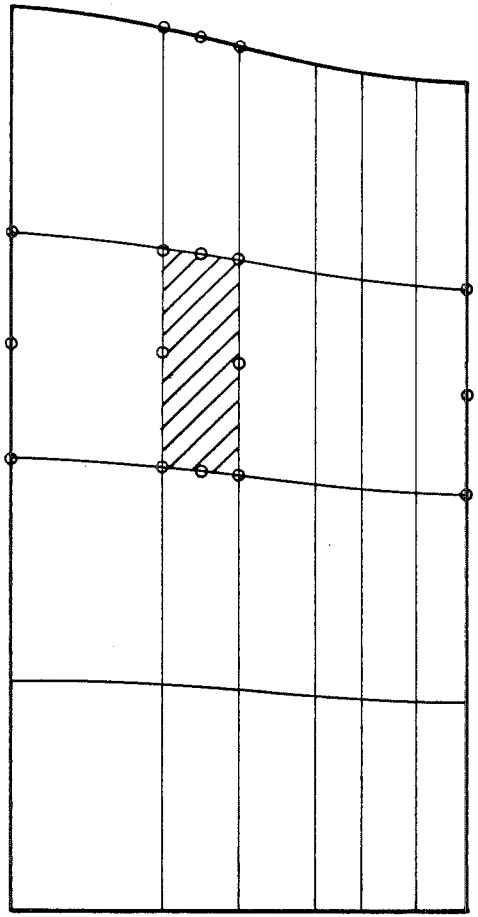

(b) FEM (4 × 6)

Compressed towards throat

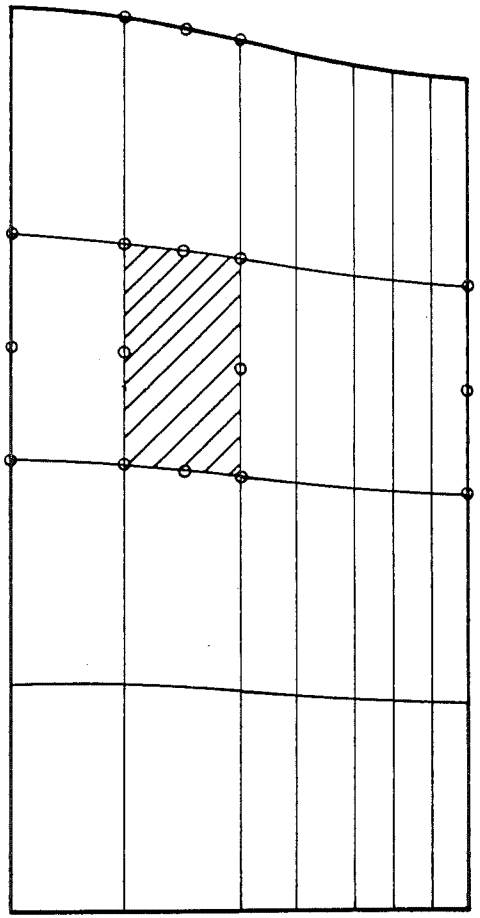

(c) FEM (4 × 7)

Compressed towards throat

FIG 8·43 ELEMENT MESHES FOR A COSINE-CONVERGING DUCT, $R_1 = 1{\cdot}0$, $R_2 = 0{\cdot}925$, $l = 0{\cdot}5$.

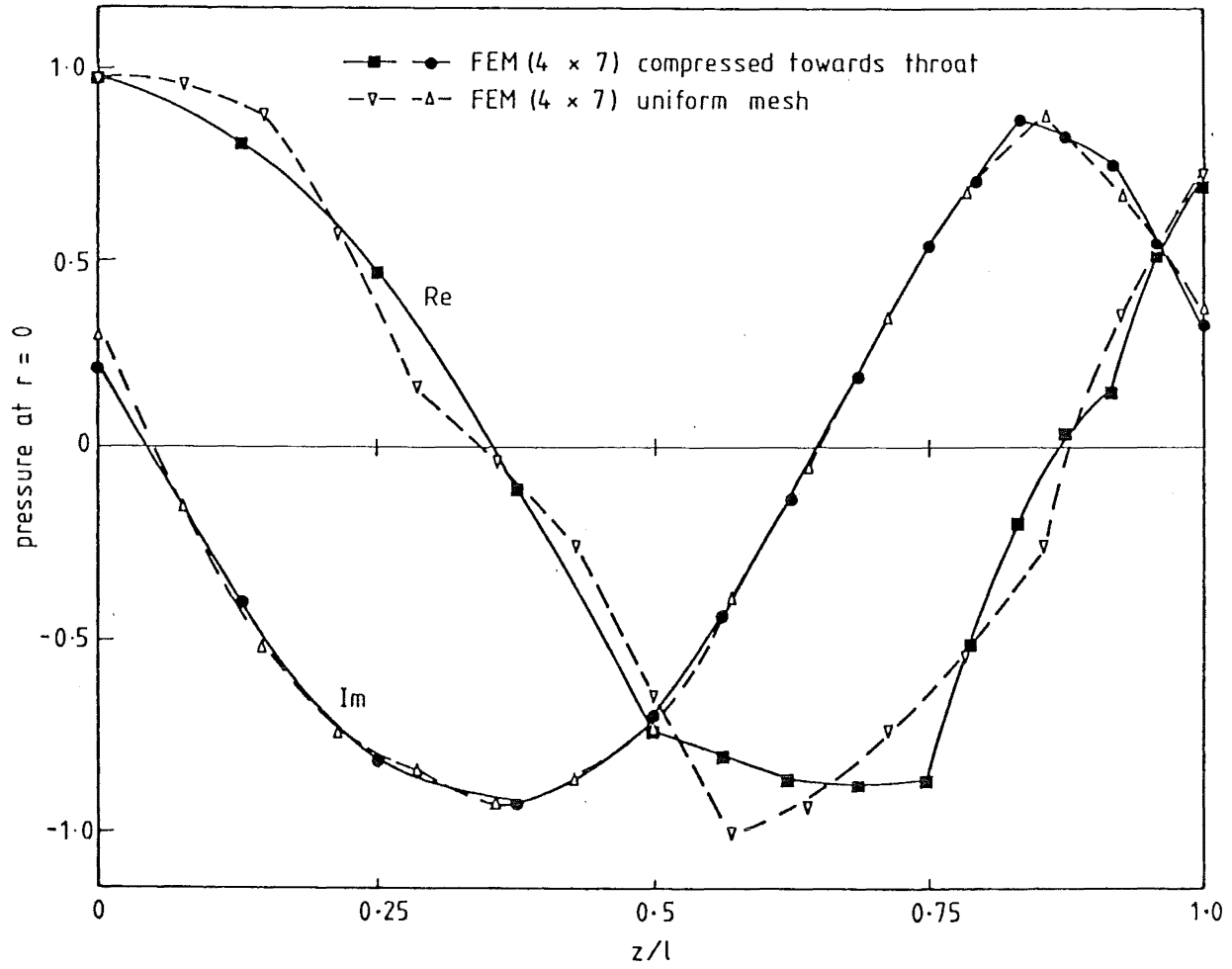

FIG. 8·44 AXIAL PRESSURE VARIATION IN COSINE-CONVERGING HARDWALLED DUCT, $R_1 = 1{\cdot}0$, $R_2 = 0{\cdot}925$, $l = 0{\cdot}5$, $M_1 = -0{\cdot}55$, $M_2 = -0{\cdot}73$, $k_r R_1 = 4{\cdot}0$, $m_o = 0$, IN MODE 1

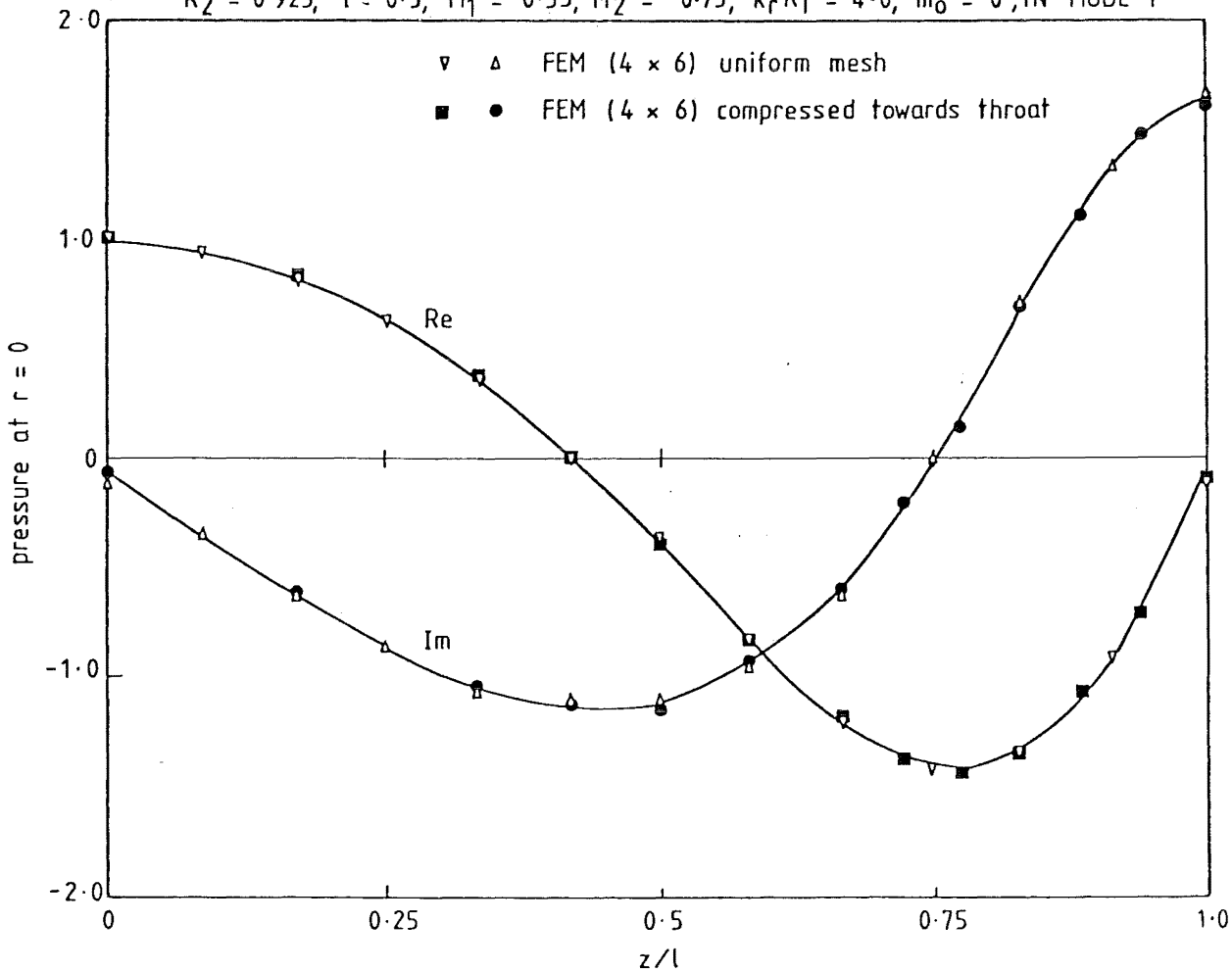

FIG. 8·45 AXIAL PRESSURE VARIATION IN COSINE-CONVERGING HARDWALLED DUCT, $R_1 = 1{\cdot}0$, $R_2 = 0{\cdot}925$, $l = 0{\cdot}5$, $M_1 = -0{\cdot}55$, $M_2 = -0{\cdot}73$, $k_r R_1 = 4{\cdot}0$, $m_o = 0$, IN MODE 2

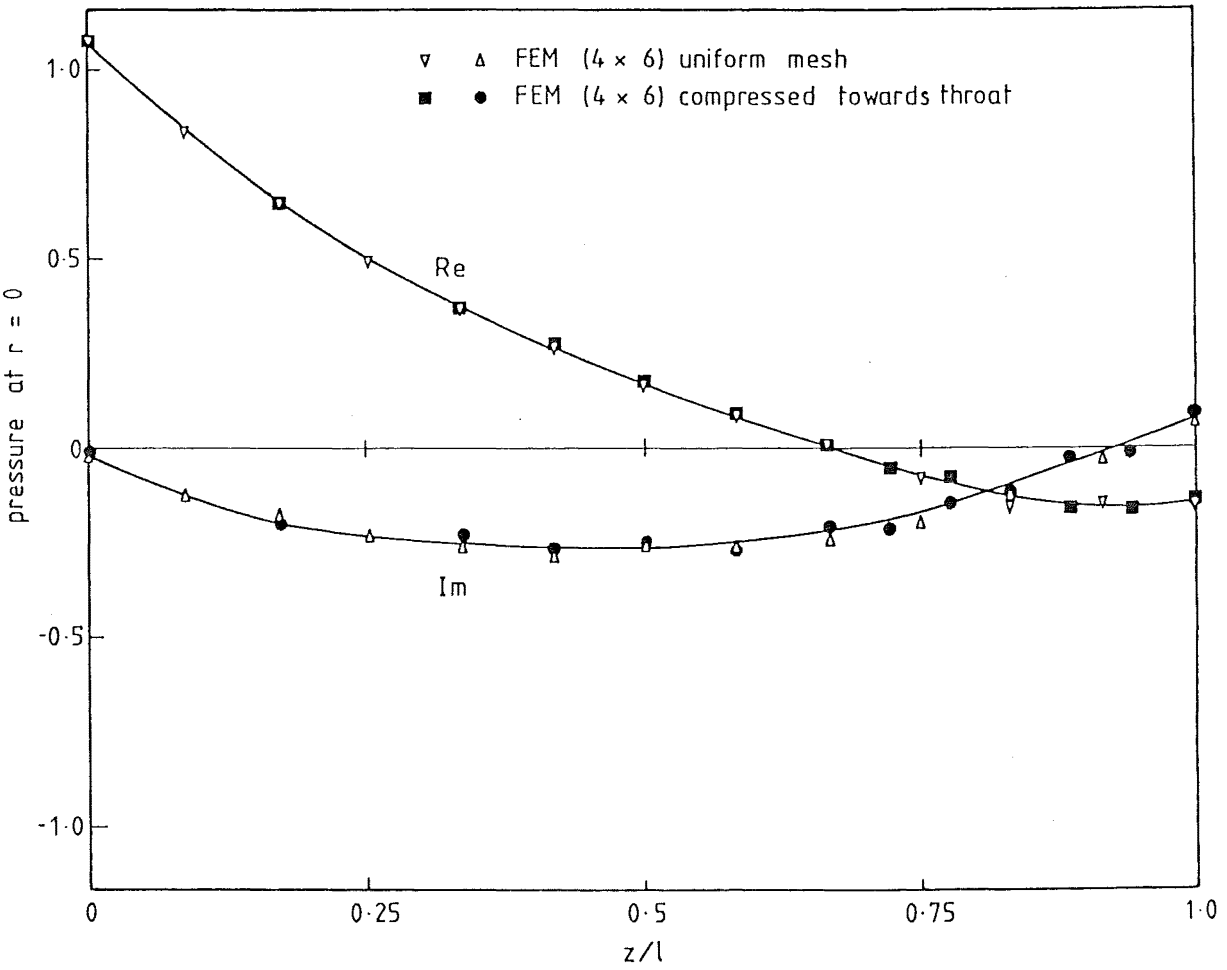

FIG 8·46 AXIAL PRESSURE VARIATION IN COSINE-CONVERGING HARDWALLED DUCT, $R_1 = 1{\cdot}0$, $R_2 = 0{\cdot}925$, $l = 0{\cdot}5$, $M_1 = -0{\cdot}55$, $M_2 = -0{\cdot}73$, $k_r R_1 = 4{\cdot}0$, $m_o = 0$ IN MODE 3

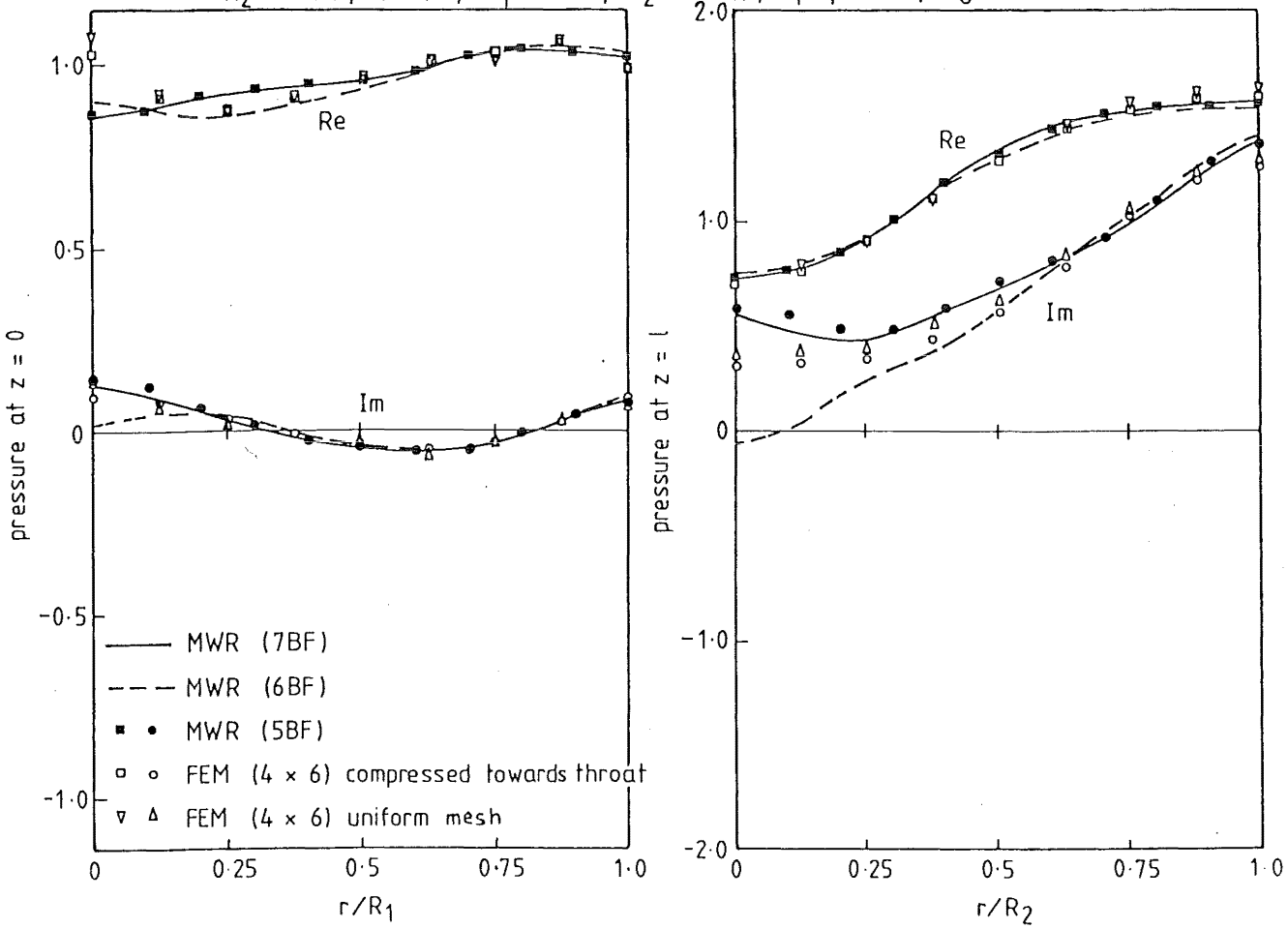

FIG·8·47 TRANSVERSE PRESSURE VARIATIONS IN COSINE-CONVERGING HARDWALLED DUCT, $R_1 = 1{\cdot}0$, $R_2 = 0{\cdot}925$, $l = 0{\cdot}5$, $M_1 = -0{\cdot}55$, $M_2 = -0{\cdot}73$, $k_r R_1 = 4{\cdot}0$, $m_o = 0$, IN MODE 1

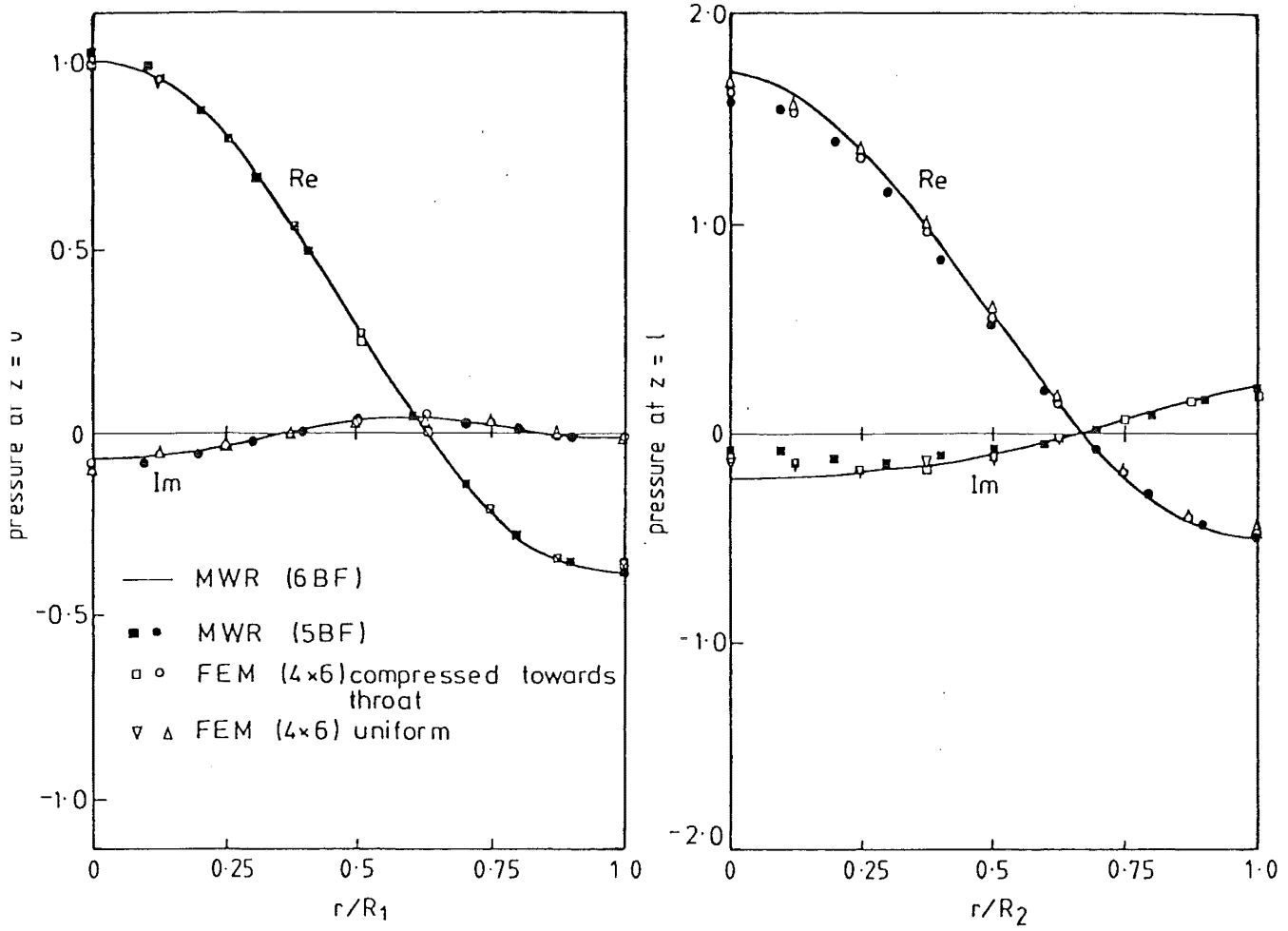

FIG. 8·48 TRANSVERSE PRESSURE VARIATIONS IN COSINE-CONVERGING HARDWALLED DUCT; $R_1 = 1{\cdot}0$, $R_2 = 0{\cdot}925$, $l = 0{\cdot}5$, $M_1 = -0{\cdot}55$, $M_2 = -0{\cdot}73$, $k_r R_1 = 4{\cdot}0$, $m_0 = 0$, IN MODE 2

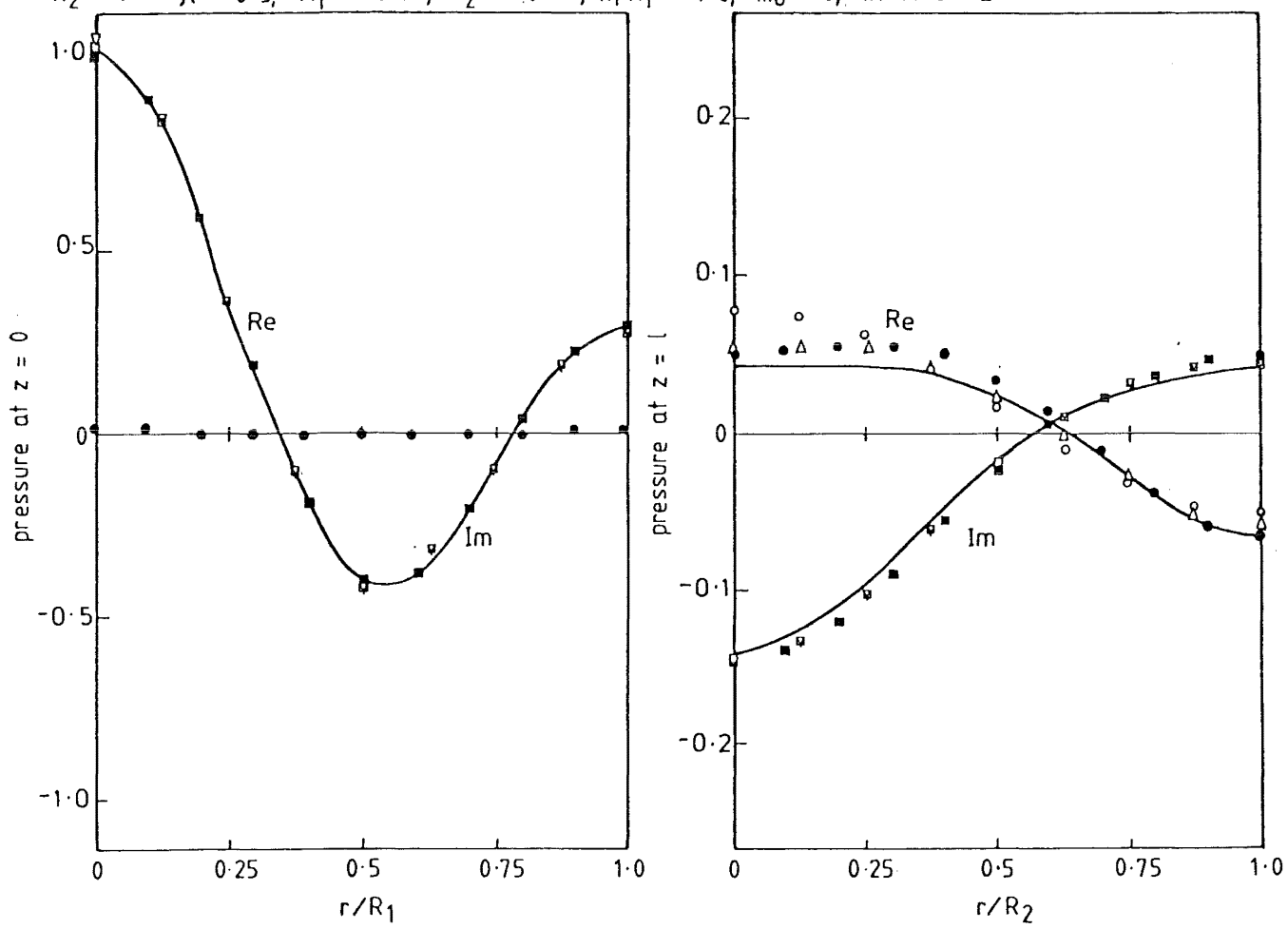

FIG. 8·49 TRANSVERSE PRESSURE VARIATIONS IN COSINE-CONVERGING HARDWALLED DUCT; $R_1 = 1{\cdot}0$, $R_2 = 0{\cdot}925$, $l = 0{\cdot}5$, $M_1 = -0{\cdot}55$, $M_2 = -0{\cdot}73$, $k_r R_1 = 4{\cdot}0$, $m_0 = 0$, IN MODE 3

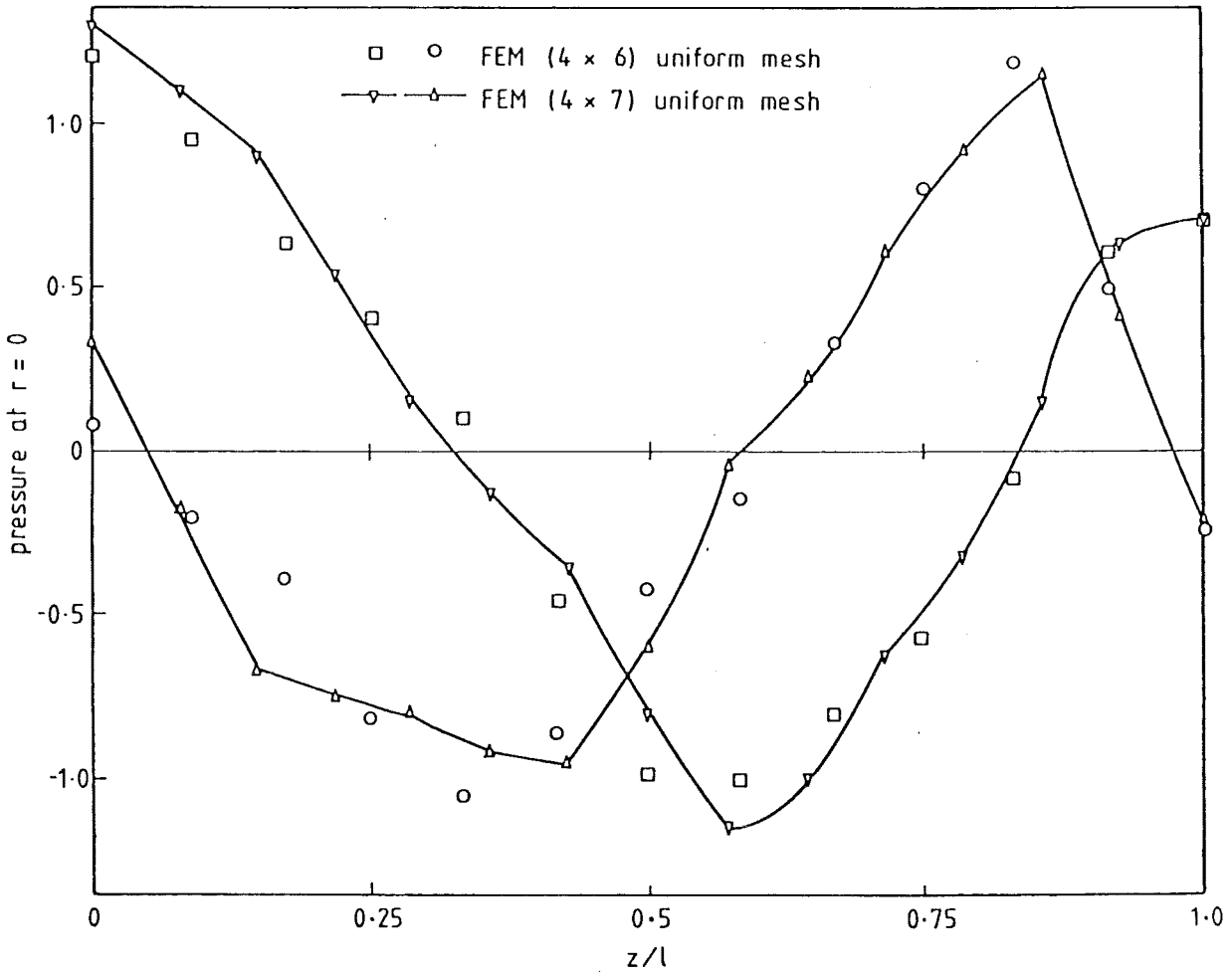

FIG. 8·50 AXIAL PRESSURE VARIATION IN COSINE-CONVERGING HARDWALLED DUCT; $R_1 = 1{\cdot}0$, $R_2 = 0{\cdot}925$, $l = 0{\cdot}5$, $M_1 = -0{\cdot}58$, $M_2 = -0{\cdot}80$, $k_r R_1 = 4{\cdot}0$, $m_o = 0$, IN MODE 1

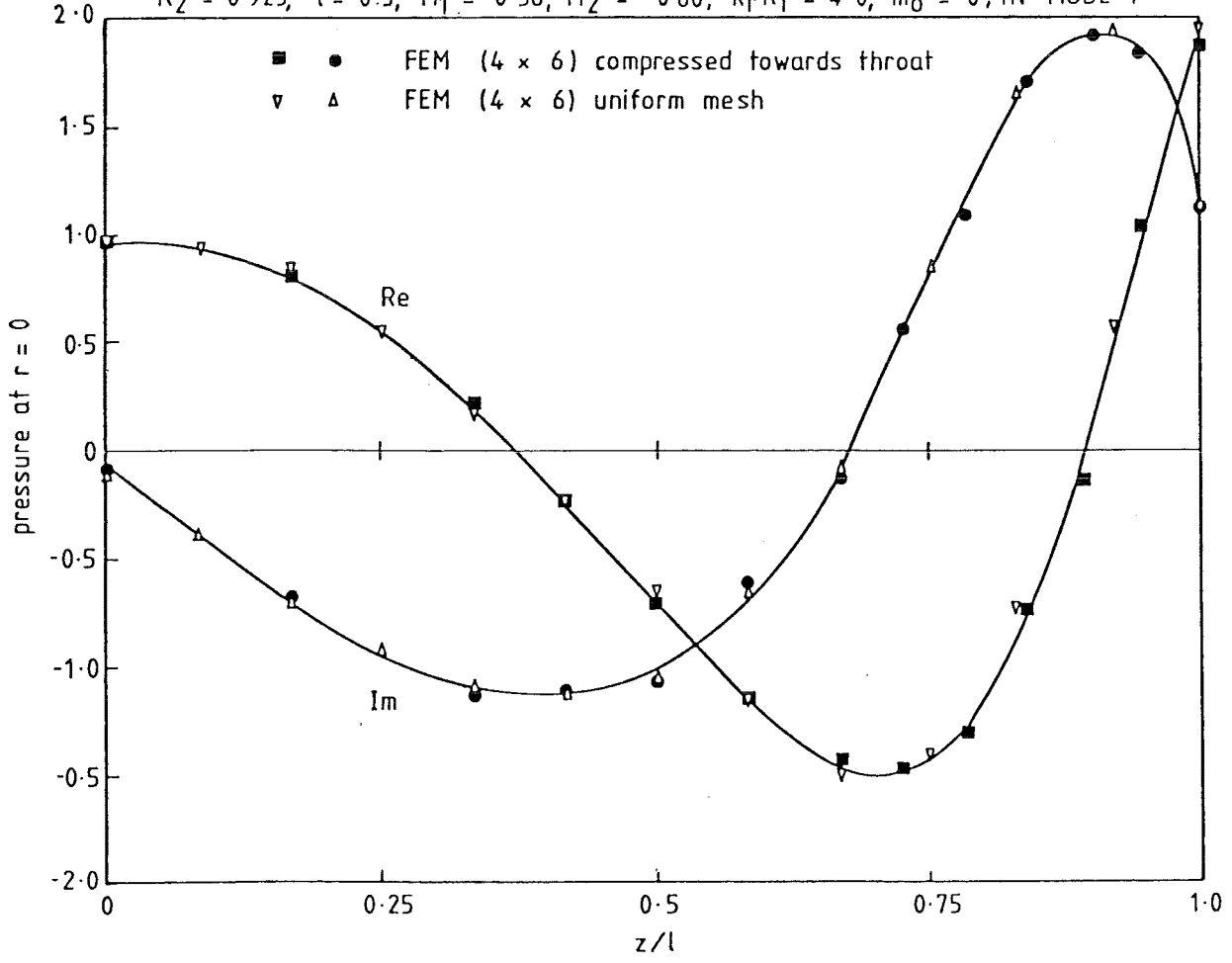

FIG. 8·51 AXIAL PRESSURE VARIATION IN COSINE-CONVERGING HARDWALLED DUCT; $R_1 = 1{\cdot}0$, $R_2 = 0{\cdot}925$, $l = 0{\cdot}5$, $M_1 = -0{\cdot}58$, $M_2 = -0{\cdot}80$, $k_r R_1 = 4{\cdot}0$, $m_o = 0$, IN MODE 2

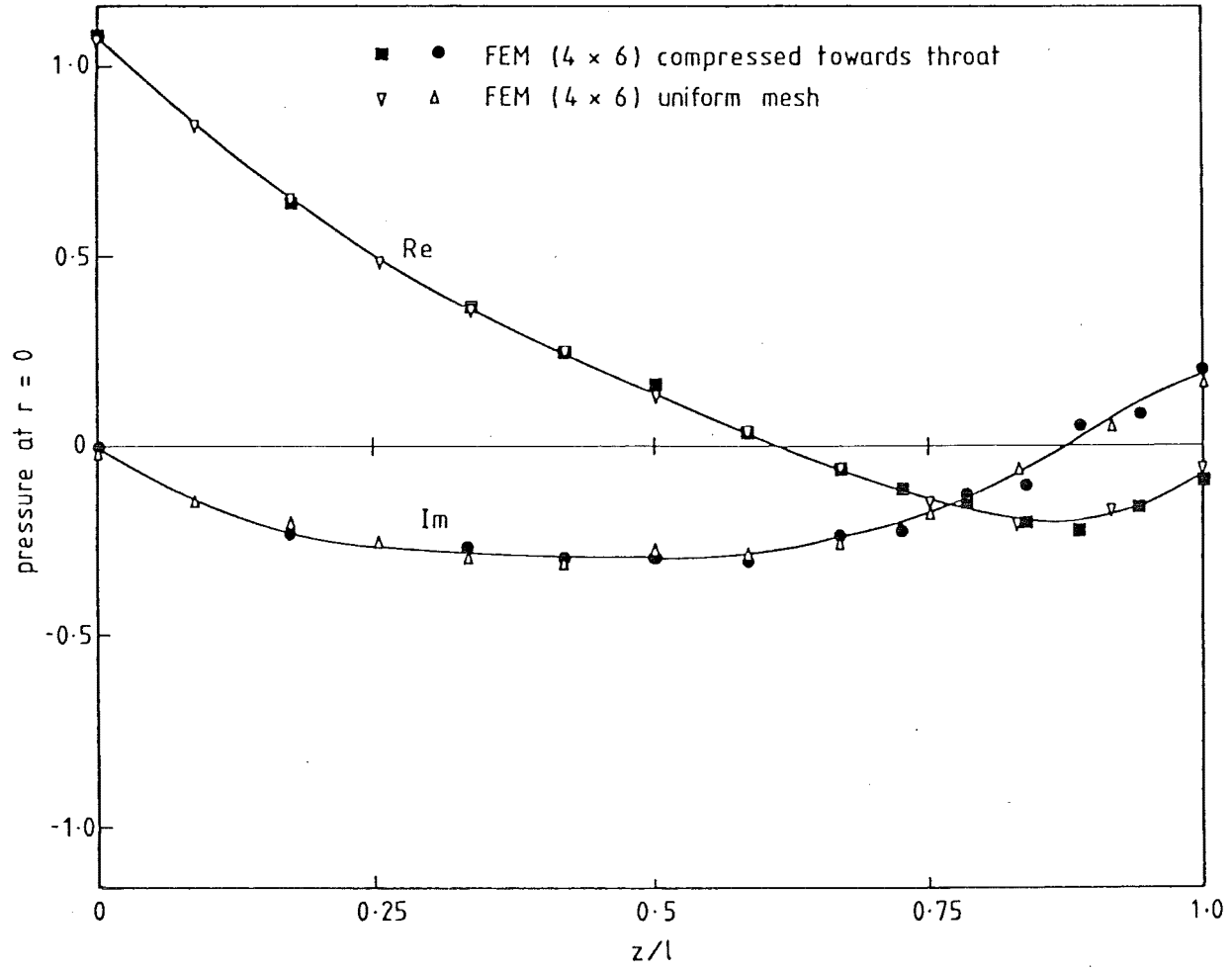

FIG. 8·52 AXIAL PRESSURE VARIATION IN COSINE-CONVERGING HARDWALLED DUCT; $R_1 = 1{\cdot}0$, $R_2 = 0{\cdot}925$, $l = 0{\cdot}5$, $M_1 = -0{\cdot}58$, $M_2 = -0{\cdot}80$, $k_r R_1 = 4{\cdot}0$, $m_o = 0$, IN MODE 1

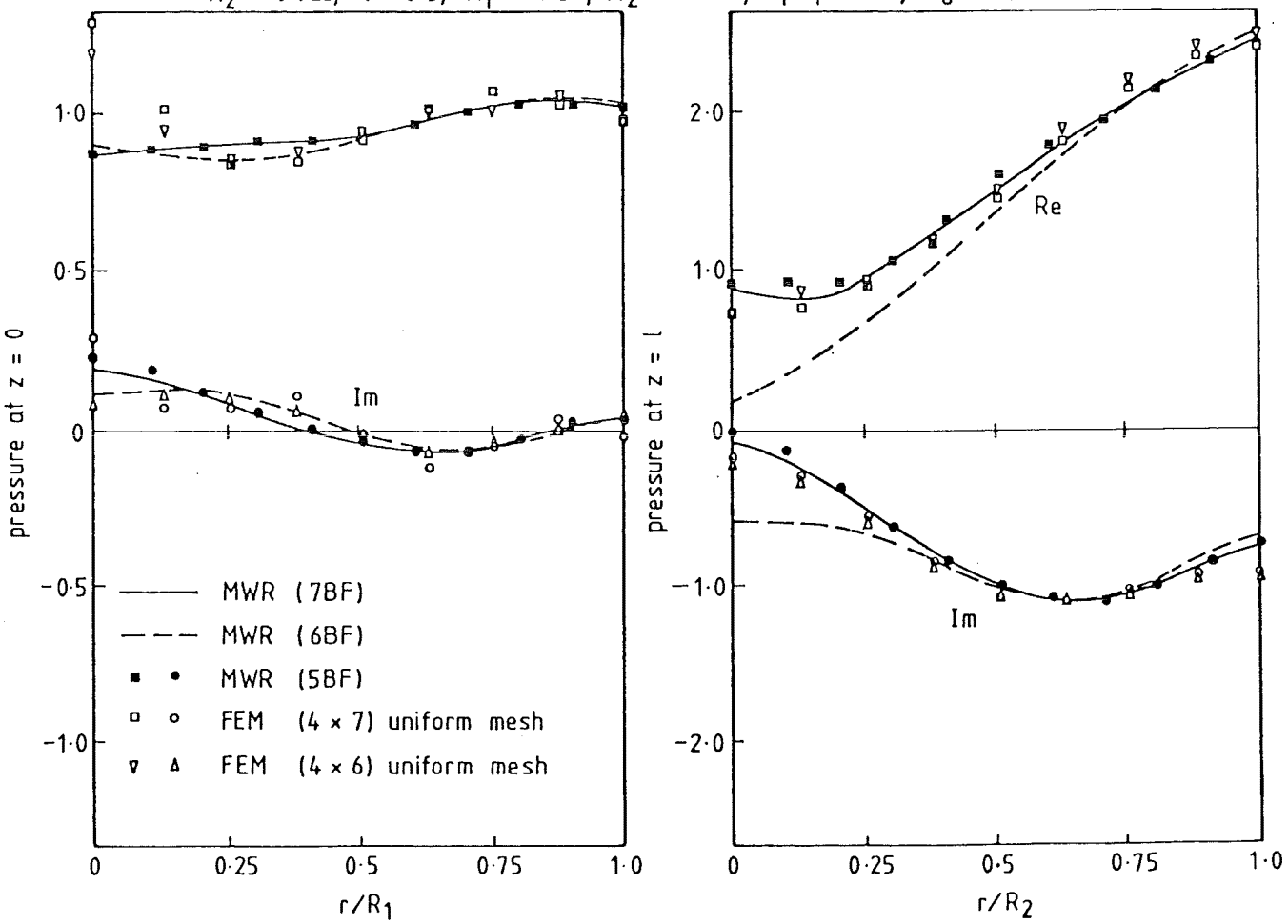

FIG. 8·53 TRANSVERSE PRESSURE VARIATIONS IN COSINE-CONVERGING HARDWALLED DUCT; $R_1 = 1{\cdot}0$, $R_2 = 0{\cdot}925$, $l = 0{\cdot}5$, $M_1 = -0{\cdot}58$, $M_2 = -0{\cdot}80$, $k_r R_1 = 4{\cdot}0$, $m_o = 0$, IN MODE 1

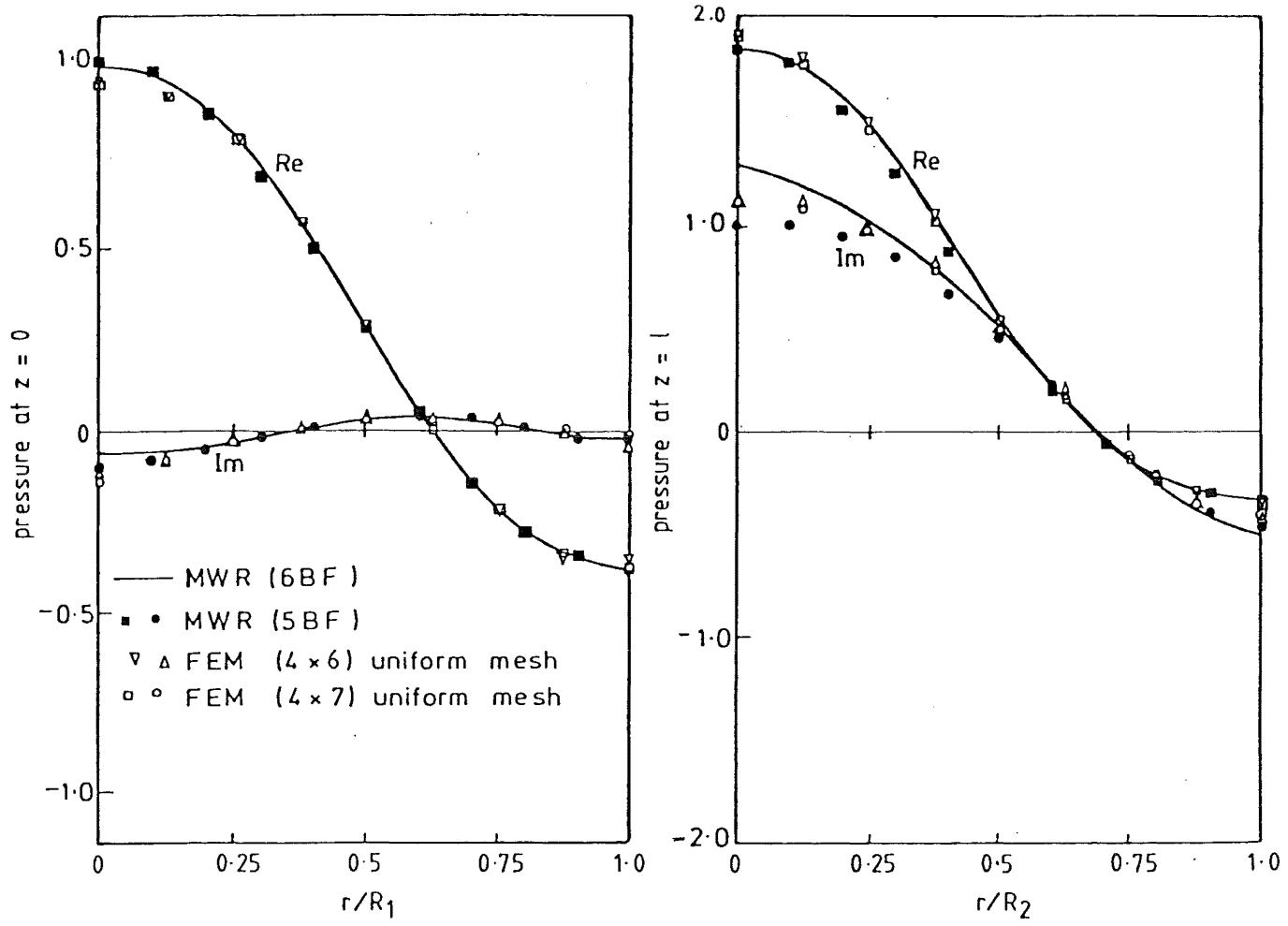

FIG. 8·54 TRANSVERSE PRESSURE VARIATIONS IN COSINE-CONVERGING HARDWALLED DUCT; $R_1 = 1{\cdot}0$, $R_2 = 0{\cdot}925, l = 0{\cdot}5$, $M_1 = -0{\cdot}58$, $M_2 = -0{\cdot}80$, $k_r R_1 = 4{\cdot}0$, $m_o = 0$, IN MODE 2

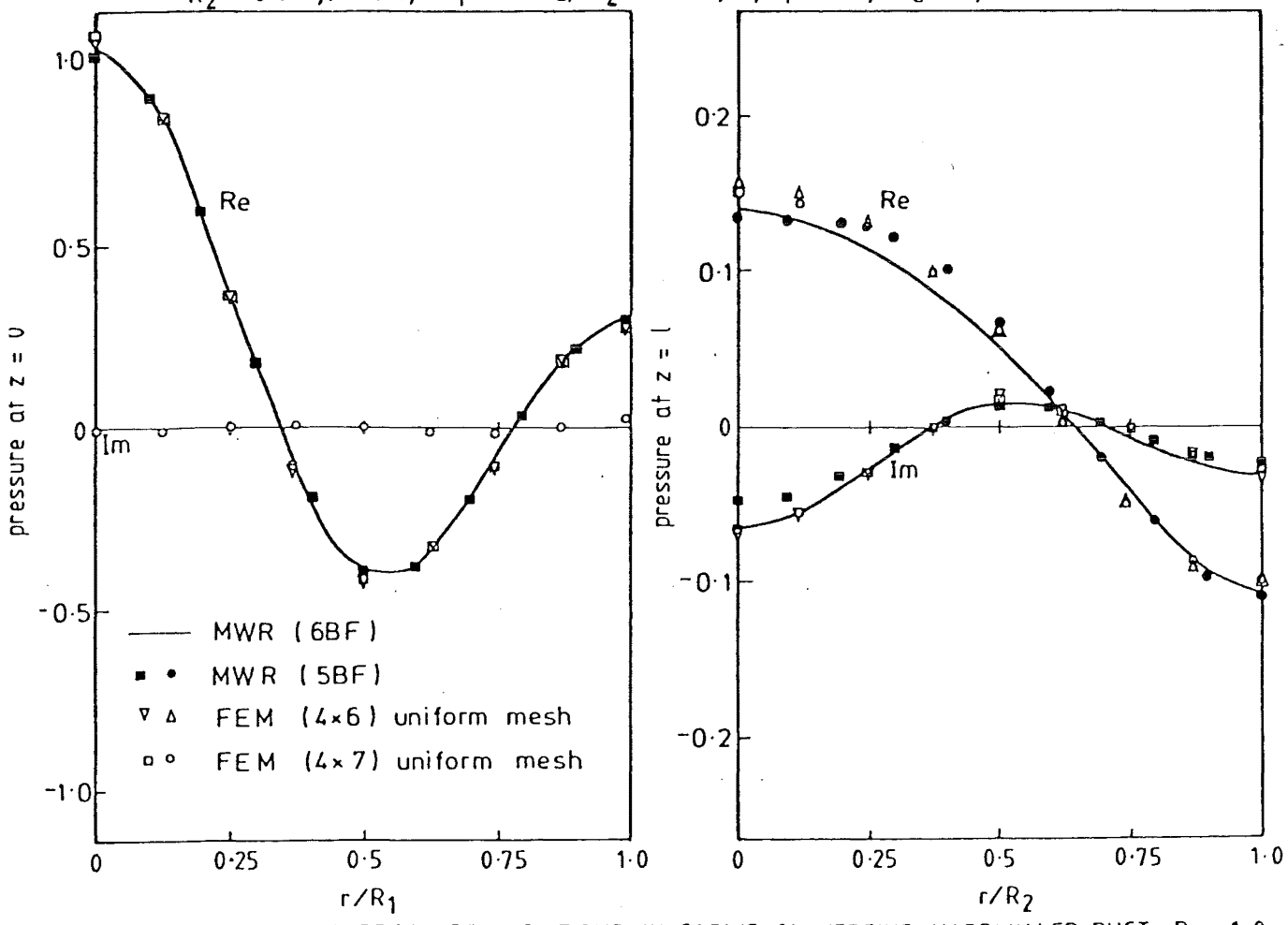

FIG. 8·55 TRANSVERSE PRESSURE VARIATIONS IN COSINE-CONVERGING HARDWALLED DUCT; $R_1 = 1{\cdot}0$, $R_2 = 0{\cdot}925, l = 0{\cdot}5$, $M_1 = -0{\cdot}58$, $M_2 = -0{\cdot}80$, $k_r R_1 = 4{\cdot}0$, $m_o = 0$, IN MODE 3

CHAPTER 9

CONCLUSIONS AND RECOMMENDATIONS

9.1 SUMMARY AND GENERAL CONCLUSIONS

The primary motivation for this study was to demonstrate the applicability of the Method of Weighted Residuals and the Finite Element Method to the solution of the multimodal sound transmission problem in circular nonuniform ducts, a problem that has not been satisfactorily solved as yet. The objective of this investigation has been achieved. The test cases with quantitative results presented in the previous chapters indicate that, in general, the two methods can provide valid and useful computational techniques in modelling acoustic problems. However, special care should be taken when the flow approaches the subsonic nonlinear regime.

The work which has been reported here can be divided into three parts : eigenproblem, no-flow case and flow case. Each part is complete and self-contained in the presentation, and represents a stage of mathematical development. Various conclusions have been made in Chapters 4 - 8. In the following one recalls briefly corner-stones and milestones in the course of study to conclude the project.

(i) The MWR and FEM solutions to eigenvalue problems for ducts with or without flow compare favourably with exact solutions, and yield particularly good agreement for the no-flow case. The MWR basis functions which are derived from the 2-D case remain useful for the axisymmetric case.

(ii) The eigenvalue scheme based on numerical integration of a non-linear differential equation derived from the transcendental equations has

been extended from the 2_D case to circular lined ducts. A proof has been given to reveal two extra modes which exist only for admittances having a positive imaginary part. These modes have no counterparts in the hardwall case.

(iii) The MWR and FEM have been fully developed for the multimodal transmission problem in ducts without flow. The FEM formulation is simpler and more efficient in general use. Extensive numerical results have been presented to substantiate the accuracy of the two methods and the validity of the matching method at the ends of the nonuniformity.

(iv) The MWR and FEM have been compared in the multimodal transmission problem involving rotational flow for several test cases. Hydrodynamic disturbances are taken into consideration, but play a trivial role in acoustic propagation. The MWR and FEM solutions to eigenproblems in uniform ducts find their use in the matching procedures. Experiments showed that the FEM formulation with natural boundary condition and point matching is most favourable. An algorithm based on the L - U decomposition method has been developed for solving a system of linear equations arising from the FEM formulation, but fails to be practical. The MWR and FEM yield comparable results for moderate Mach numbers (conservatively $|M_d| \leq 0.56$ everywhere).

(v) At high Mach numbers it becomes apparent that computational problems rapidly increase in severity. The first cut-on mode suffers the first deterioration. The FEM encounters the problem of high dimensionality and short-wavelength resolutions while the MWR shows inconsistent convergence. It is not yet possible to establish the relative reliability of the two methods.

(vi) An attempt to account for the subsonic acoustic choking phenomenon due to linear effects is inconclusive. A large transmission

loss is not an automatic consequence of high Mach number subsonic flow and other factors such as refraction due to local flow distortions and nonlinear effects must be considered.

Spinning acoustic modes (angular modes $m_o \neq 0$) of high order, which permit cut-on modes to transmit at high frequencies may be important in the acoustic choking occurrence. But the limitations of the numerical methods do not warrant further investigations.

(vii) The mean flow field solved for by the same FEM technique is compared with the approximate model employed, which is hypothesized to produce acoustic disturbance.

9.2 SUGGESTIONS AND FUTURE WORK

The MWR and FEM formulations have been restricted to circular duct configurations. Extension to the annular case is approachable in a similar way. It is believed that the annular geometry is less computationally difficult than the circular one.

The shear flow case can also be considered by the MWR with the same type of trigonometric basis functions and by the FEM with similar quadratic isoparametric element discretization. It is noted that for the shear flow, where the flow velocity vanishes at the duct walls, the conditions imposed on MWR are relaxed in the sense that the no-flow basis functions satisfy the duct-wall boundary condition. But the nonuniform flow profile would complicate the transverse solution representation and integrations at each station along the duct.

With the FEM little effort is expected in converting the present computational routines for use in the annular geometry or the shear flow. In the latter case there will be no doubt of increase in dimensionality

in the transverse direction for a compatible level of accuracy. Because the modified flow model employed in the present formulations may not be suitable for high Mach numbers, the acoustic transmission model may be enhanced if the FEM technique is used to solve for the flow field, which is subsequently incorporated into the acoustic problem. By this means the subsonic acoustic choking mechanism may be better assessed.

While the MWR is designed specifically for the particular problem and, perhaps, has advantage in regular boundary problems, the FEM has the flexibility of application to a wider class of problems. In complicated duct geometries the FEM technique may well be the only viable approach. However, trial-and-error experiments are very much a feature of the computational techniques.

In the present formulations there are several possible directions to experiment in improving the computational schemes in terms of accuracy and efficiency achievements.

(i) It is found that the success of the MWR is very much dependent upon a judicious choice of basis functions and experimentation with the class of functions may lead to improved results. Thus, to facilitate the MWR's further investigations into the nonlinear subsonic regime, it is desirable to refine the basis functions so as to increase the convergence speed at high Mach number, high frequency, and high angular mode.

(ii) In both the no-flow and flow cases numerical instability may occur in the MWR scheme if the basis functions include too many cut-off modes. This problem is most severe when low frequencies are dealt with, since in this case the MWR may require a number of heavily cut-off modes to provide enough resolution for a converged solution.

The exponential character of the cut-off solutions is believed to create the difficulty. To alleviate this problem the computational scheme can be modified to explicitly isolate the exponential behaviour so that the transfer matrix is not required to include the offending exponential factor.

(iii) For the FEM, it has been shown that if there is a degradation of accuracy it is accompanied by slope discontinuities in axial and transverse pressure variations. This suggests that the application of the FEM with elements which preserve function slope continuity at the nodes will provide increased accuracy. If the FEM is to be used to carry the range of efficient computation near the onset of nonlinear subsonic behaviour it is necessary that this type of improvement in the implementation be made.

The improvement has been demonstrated by the use of Hermitian elements in 2-D eigenproblems [104] to eliminate spurious modes and to reduce eigenmatrix dimensionality for a compatible degree of resolution. Should the four-node rectangular Hermitian elements be discretized for the acoustic transmission problem the Abrahamson's L _ U decomposition method algorithm [74] may become available, because of its simple global matrix structure in reduction of storage requirements in case too many elements are required for high Mach number resolutions.

(iv) The problem of high dimensionality in the FEM and the numerical instability in the MWR due to duct length may be alleviated if computational schemes are developed to couple various nonuniformities in succession and thus model general duct geometries. An acoustic finite element representation for a given nonuniform duct segment would be generated by accounting for left moving waves incident on the segment, and then by solving the transmission problem for successive unit values of the incident mode coefficients from the segment. This would give an influence matrix defining the reflected and transmitted modal coefficients in terms of unit incident wave coefficients. Several successive

nonuniformities could thus be joined directly without the need for a uniform duct between them. This may well be a better practical development than application of the methods to very long and complex duct nonuniformities.

BIBLIOGRAPHY

1. RAYLEIGH, J.W.S. The Theory of Sound, Dover Publications New York, N.Y. (1945).

2. MORSE, P.M. Vibration and Sound, McGraw Hill, New York, N.Y. (1948).

3. MORSE, P.M. and INGARD, U., Theoretical Acoustics, McGraw Hill Book Co., Inc. (1968).

4. MORSE, P.M. "The Transmission of Sound Inside Pipes", J. Acoust.Soc.Am., 11, 205-210, (1939).

5. CREMER, L., "Theorie der Luftschall-Damfung im Rechtekanal mit Schluckender Wand und das Sich Dabci Ergebende hochste Dampfungsmass", Acoustica, 3, 249-263, (1953).

6. INGARD, U., "On the Radiation of Sound into a Circular Tube with an Application to Resonators", J.Acoust.Soc.Am. 20, 665-682, (1948).

7. TYLER, J.M. and SOFRIN, T.G.,"Axial Flow Compressor Noise Studies", SAE Trans., 70, 309-332, (1962).

8. MORFEY, C.L. "Rotating Pressure Patterns in Ducts, Their Generation and Transmission", J.Sound & Vib., 1, 60-87 (1964).

9. RICE, E.J. "Attenuation of Sound in Soft-Walled Circular Ducts", NASA TM X-52442, (1968).

10. LAMBERT, R.F. "Acoustic Filtering in a Moving Medium", J. Acoust. Soc .Am., 28, 2054 - 2058 (1956)

11. INGARD, U., "Influence of Fluid Motion Past a Plane Boundary of Sound Reflection, Absorption and Transmission", J.Acoust. Soc.Am., 31, 1035-1036, (1959).

12. MILES, J.W., "On Reflection of Sound at an Interface of Relative Motion", J.Acoust.Soc.Am., 29, 226, (1957).

13. RIBNER, H.S. "Reflection, Transmission and Amplification of Sound by a Moving Medium", J.Acoust.Soc.Am., 29, 435, (1957).

14. MORFEY, C.L. "Sound Transmission and Generation in Ducts with Flow", J.Sound. & Vib., 14, 37-55, (1971).

15. RICE, E.J. "Propagation of Waves in an Acoustically Lined Duct with Mean Flow", NASA SP-207, 345-355, (1969).

16. KO, S.H., "Sound Attenuations in Lined Rectangular Ducts with Flow and its Application to the Reduction of Aircraft Engine Noise", J.Acoust.Soc.Am., 50, 1418-1432, (1971).

17. EVERSMAN, W., "Effect of Mach number on the Tuning of an Acoustic Lining in a Flow Duct", J.Acoust.Soc.Am., 48, 425-428, (1970).

18. TESTER, B.J., "The Optimization of Sound Attenuation in Lined Ducts Containing Uniform, Axial, Subsonic Mean Flow", Seventh International Congress on Acoustics, Budapest, Hungary, Paper20, p.7 (1967).

19. EVERSMAN, W., NELSEN, M.D., ARMSTRONG, D. and HALL, O.Jr. "Design of Acoustic Linings for Ducts with Flow", J.Aircraft, 9, 548-556, (1972).

20. PRIDMORE-BROWN, D.C. "Sound Propagation in a Fluid Flowing Through an Attenuating Duct", J.Fluid Mech.4, 393-406 (1958).

21. TACK, H.D. and LAMBERT, R.F., "Influence of Shear Flow on Sound Attenuation in a Lined Duct", J.Acoust.Soc.Am., 38, 655-666, (1965).

22. MUNGUR, P. and GLADWELL, G.M.L., "Acoustic Wave Propagation in Sheared Fluid Contained in a Duct", J.Sound & Vib., 9, 28-48 (1969).

23. MUNGUR, P, and PLUMBEE, H.E. "Propagation and Attenuation of Sound in a Soft Walled Annular Duct Containing a Sheared Flow", NASA SP-207, 305-327, (1969).

24. KURZE, U.J. and ALLEN, C.H., "Influence of Flow and High Sound Level on the Attenuation in a Lined Duct", J.Acoust. Soc.Am., 49, 1643-1654, (1971).

25. HERSH, A.S. and CATTON, L., "Effect of Shear Flow on Sound Propagation in Rectangular Duct", J.Acoust.Soc.Am., 50, 992-1003, (1971).

26. UNRUH, J.F. and EVERSMAN, W., "The Transmission of Sound in an Acoustically Treated Rectangular Duct with Boundary Layer", Report AR 72-2, Wichita State University,(1972).

27. EVERSMAN, W., "Effect of Boundary Layer on the Transmission and Attenuation of Sound in an Acoustically Treated Circular Duct", J.Acoust.Soc.Am., 49, 1372-1380, (1971).

28. KAPUR, A, and MUNGUR, P., "Sound Interaction with a Ducted Helical Flow", AIAA Paper 73-1010 (1973).

29. SAVKAR, U.J., "Propagation of Sound in Ducts with Shear Flow", J.Sound & Vib. 19, 355-372 (1971).

30. EVERSMAN, W. and BECKEMEYER, R.J., "Transmission of Sound in Ducts with Thin Shear Layers Convergence to the Uniform Flow Case", J. Acoust.Soc.Am., 52, 216-220, (1972).

31. TESTER, B.J., "Some Aspects of Sound Attenuation in Lined Ducts Containing Inviscid Mean Flows with Boundary Layers", J.Sound & Vib., 28, 217-245, (1973).

32. NAYFEH, A.H., KAISER, J.E. and SHAKER, B.S., "Effect of Mean Velocity Profile Shapes on Sound Transmission Through Rectangular Ducts", J.Sound & Vib.,34, 413-423, (1974).

33. NAYFEH, A.H., KAISER, J.E. and TELIONIS, D.P., "Acoustics of Aircraft Engine-Duct Systems", AIAA Journal, 13, 130-153, (1975).

34. KAPUR, A., CUMMINGS, A., and MUNGUR, P., "Sound Propagation in a Combustion Can with Axial Temperature and Density Gradients", J.Sound & Vib., 25, 129-138, (1972).

35. MUNGUR, P., and Tree,D., "Sound Propagation in Sheared Flow in a Duct with Transverse Temperature Gradients", Paper 24P7 Seventh International Congress on Acoustics, Vol.IV, Budapest, Hungary, 349-353, (1971).

36. NAYFEH, A.H. and SUN, J., "Effect of Transverse Velocity and Temperature Gradients on Sound Attenuation in Rectangular Ducts", J.Sound & Vib., 34, 505-517, (1974).

37. WEBSTER, A.G., "Acoustic Impedance and the Theory of Horns and of the Phonograph", Proceedings of the National Academy of Science, 5, 275-282, (1919).

38. KINSLER, L.F. and FREY, A.R., Fundamentals of Acoustics, 2nd. Ed., Wiley, N.Y., (1962).

39. PEUBE, J.L. and CHASSERIAUX, J., "Nonlinear Acoustics in Ducts with Varying Cross Section", J.Sound & Vib. 27, 533-548, (1973).

40. CUMMINGS, A., "Acoustics of a Wine Bottle", J.Sound & Vib. 31, 331-343, (1973).

41. ZORUMSKI, W.E. and CLARK, L.R. "Sound Radiation from Source in an Acoustically Treated Circular Duct", unpublished, 1971 NASA Langley Research Center, Hampton, Va.

42. ALFREDSON, R.J., "The propagation of Sound in a Circular Duct of Continuously Varying Cross Sectional Area", J.Sound & Vib. 23, 433-442, (1972).

43. MILES, J., "The Reflection of Sound due to a Change in Cross Section of a Circular Tube", J.Acoust.Soc.Am., 26, 14-19, (1954).

44. BECKEMEYER, R.J. and EVERSMAN, W., "Computational Method for Studying Acoustic Propagation in Nonuniform Wave Guides", AIAA Paper 73-1006, (1973).

45. EVERSMAN, W., COOK, E.L. and BECKEMEYER, R.J., "A Method of Weighted Residuals for the Investigation of Sound Transmission in Nonuniform Ducts Without Flow", J.Sound & Vib., 38, 105-123, (1975).

46. SCHELKUNOFF, S.A., "Generalized Telegraphist's Equations for Wave Guides", Bell System Technical Journal 31, 784-801, (1952).

47. SCHELKUNOFF, S.A., "Conversion of Maxwell's Equations into Generalized Telegraphist's Equations", Bell System Technical Journal, 39, 955-1043, (1955).

48. STEVENSON, A.F., "General Theory of Electromagnetic Horns", J.Appl.Phys. 22, 1447-1460, (1951).

49. STEVENSON, A.F., "Exact and Approximate Equations for Wave Propagation in Acoustic Horns", J.Appl.Phys. 22, 1461-1463, (1951).

50. NAYFEH, A.H. and TELIONIS, D.P., "Acoustic Propagation in Ducts with Varying Cross Sections", J.Acoust.Soc.Am., 54, 1654-1661, (1973).

51. ISAKOVITCH, M.A., "Scattering of Sound Waves on Small Irregularities in a Wave Guide", Akusticheskii Zhurnal, 3, 37-45, (1957).

52. SAMUELS, J.S., "On Propagation of Waves in Slightly Rough Ducts", J.Acoust.Soc.Am., 31, 319-325, (1959).

53. SALANT, R.F., "Acoustic Propagation in Waveguides with Sinusoidal Walls", J.Acoust.Soc.Am., 53, 504-507, (1973).

54. KING, L.S. and KARAMCHETI, K., "Propagation of Plane Waves in the Flow through a Variable Area Duct", AIAA Paper 73-1009, (1973).

55. POWELL, A., "Theory of Sound Propagation through Ducts Carrying High-Speed Flows", J.Acoust.Soc.Am., 32, 1640-1646, (1960).

56. EISENBERG, N.A. and KAO, T.W., "Propagation of Sound Through a Variable Area Duct with a Steady Compressible Flow", J. Acoust.Soc.Am., 49, 169-175, (1971).

57. HUERRE, P. and KARAMCHETI, K., "Propagation of Sound Through a Fluid Moving in a Duct of Varying Area", Proceedings of Interagency Symposium on University Research in Transportation Noise, Standford University, March 28-30, 1973.

58. DAVIS, S.S. and JOHNSON, M.L., "Propagation of Plane Waves in a Variable Area Duct Carrying a Compressible Subsonic Flow". Presented at the 87th. Meeting of the Acoustical Society of America, N.Y., 1974.

59. KOOKER, D.E., and ZINN, B.T., "Use of a Relaxation Technique in Nozzle Wave Propagation Problems", AIAA Paper 73-1011, (1973).

60. TAM, C.K.W., "Transmission of Spinning Acoustic Modes in Slightly Nonuniform Duct", J.Sound & Vib. 18, 339-351, (1971).

61. LARGE, J.B., WILBY, J.F., GRANDE, E and ANDERSON, A.O., "The Development of Engineering Practice in Jet Compressor and Boundary Layer Noise", Proc. AFOSR-UTIAS Symposium on Aerodynamic Noise, Toronto, 43-67, (1968).

62. NAYFEH, A.H., TELIONIS, D.P., and LEKOUDIS, S.G., "Acoustic Propagation in Ducts with Varying Cross Section and Sheared Mean Flow", AIAA Paper 73-1008, (1973).

63. NAYFEH, A.H., KAISER, J.E. and TELIONIS, D.P., "Transmission of Sound Through Annular Ducts of Varying Cross Sections and Sheared Mean Flow", AIAA Paper 74-58, (1974).

64. EVERSMAN, W., "A Multimodal Solution for the Transmission of Sound in Nonuniform Ducts", AIAA Paper 76-497, (1976).

65. EVERSMAN, W., ASTLEY, R.J. and VO PHU THANH, "Transmission in Nonuniform Ducts - A Comparitive Evaluation of Finite Element and Weighted Residuals Computational Schemes", AIAA Paper 77-1299, (1977).

66. KLUJBER, F., BOSCH, J.C., DEMETRICH, R.W. and ROBB, W., "Investigation of Noise Suppression by Sonic Inlets for Turbofan Engines", NASA CR 121126, (1973).

67. CHESTNUT, D., ans CLARK, L.R., "Noise Reduction by Means of Variable Geometry Inlet Guide Vanes in a Cascade Apparatus", NASA TM X-2392, (1971).

68. TAM, C.K.W., "On Finite Amplitude Spinning Acoustic Modes and Subsonic Choking", J.Sound & Vib. 16, 393-406, (1971).

69. VO, P.T. and EVERSMAN, W., "A Method of Weighted Residuals with Trigonometric Basis Functions for Sound Transmission in Circular Ducts", J.Sound & Vib., 56, 243-250, (1978).

70. KAISER, J.E., and NAYFEH, A.H., "A Wave Envelope Technique for Wave Propagation in Nonuniform Ducts", AIAA Paper 76-497, (1976).

71. BAUMEISTER, K.J., "Generalized Wave Envelope Analysis of Sound Propagation in Ducts with Variable Axial Impedance and Stepped Noise Source Profiles", AIAA Paper 75-518, (1975).

72. QUINN, D.W., "A Finite Difference Method for Computing Sound Propagation in Nonuniform Ducts", AIAA Paper 75-130, (1975).

73. SIGMAN, R.K., MAJJIGI, R.K., and ZINN, B.T., "Use of Finite Element Techniques in the Determination of the Acoustic Properties of Turbofan Inlets", AIAA Paper 77-18, (1977).

74. ABRAHAMSON, L.A., "A Finite Element Algorithm for Sound Propagation in Axisymmetric Ducts Containing Compressible Mean Flow", NASA CR-145209, (1977).

75. ASTLEY, R.J. and EVERSMAN, W., "A Finite Element Method for Transmission in Nonuniform Ducts without Flow: Comparison with the Method of Weighted Residuals", J.Sound & Vib. 57, 367-388, (1978).

76. FINLAYSON, B.A., The Method of Weighted Residuals and Variational Principles, New York: Academic Press, (1972).

77. CRANDALL, S.H., Engineering Analysis, McGraw Hill,(1956); AMR 12 (1959), Rev.1122.

78. COLLATZ, L., The Numerical Treatment of Differential Equations Springer, 1960, AMR(14) (1961), Rev. 1738.

79. POWELL, E.A. and ZINN, B.T., "Solution of Linear Instability Problems Using the Galerkin Method", Israel J. of Tech., 7 (1-2), 79-89, (1969).

80. GALERKIN, B.G."Sterzhni v plastiny. Ryady v nekotorykh voprosakh uprogogo ravnovesiya sterzhnei i plastin" Vestn. Inzhen. i Tekh. Petrograd 19, 897-908 (1915); Translation 63 - 18924. Clearinghouse Fed.Sci.Tech.Info.

81. FINLAYSON, B.A. and SCRIVEN, L.E., "The Method of Weighted Residuals - A Review", Appl.Mech.Rev., 19 (9), 735-748,(1966).

82. DUNCAN, W.J., "The Principles of Galerkin Method", Gt.Bri. Aero,Res.Council Rept. and Memo. 1848, (1938).

83. KANTOROVICH, L.V., and KRYLOV, V.I., Approximate Methods of Higher Analysis Interscience Publishers, Inc., N.Y., (1964).

84. PORITZKY, H., "The Reduction of the Solution of Certain Partial Differential Equations to Ordinary Differential Equations", in Trans. Fifth Intern.Congr.Appl.Mech. Cambridge, Mass., 700-707, (1938).

85. SHULESHKO, P., "A New Method of Solving Boundary-Value Problems of Mathematical Physics, Generalizations of Previous Methods of Solving Boundary Value Problems of Mathematical Physics" Austral.J.Appl.Sci., 10, 1-7, 8-16 (1959); AMR 13 (1960), Rev.3.

86. SNYDER, L.J., SPRIGGS, T.W. and STEWART, W.E. "Solution of the Equations of Change by Galerkin's Method", AIChE J. 10, 535-540, (1964).

87. BOLOTIN, V.V., "Nonconservative Problems of the Theory of Plastic Stability", Pergamon/Macmillan p.60 (1963); AMR 16 (1963), Rev.46.

88. MIKHLIN, S.G., "Variational Methods in Mathematical Physics", Pergamon/Macmillan (1964).

89. NORRIE, D.H. and DE VRIES, G., "The Finite Element Method" N.Y., Academic Press, (1973).

90. ZIENKIEWICZ, O.C., "The Finite Element Method in Engineering Science", McGraw Hill, London (1971).

91. HUEBNER, K.H., "The Finite Element Method for Engineers", John Wiley & Sons, Inc., New York, (1975).

92. COOK, R.D., " Concepts and Applications of Finite Element Analysis", N.Y. John Wiley & Sons, Inc., (1974).

93. TAYLOR, R.L., "On Completeness of Shape Functions for Finite Element Analysis", Int.J.Num.Meth.in Eng. Vol.(4), No.2., 201-203, (1969).

94. ZIENKIEWICZ, O.C., "Introductory Lectures on the Finite Element Method", CISM Udine, (1972).

95. DAHLQUIST, G. and BJORCK, A., "Numerical Methods", translated by Ned Anderson, Prentice Hall, 166-173, (1974).

96. EVERSMAN, W., "Computation of Axial and Transverse Wave Numbers for Uniform Two-Dimensional Ducts with Flow Using a Numerical Integration Scheme", J.Sound & Vib. 41, 252-255, (1975).

97. EVERSMAN, W., "Initial Values for the Integration Scheme to Compute the Eigenvalues for Propagation in Ducts", J.Sound & Vib. 50, 159-162, (1977).

98. BAUER, H.F., "Tables of Zeros of Cross Product Bessel Functions", Maths. of Computation 28, 128-135, (1966).

99. MÖHRING, W., "Über Schallwellen in Scherströmungen Fortschritte der Akustik, DAGA 76, VDI-Verlog, Dusseldorf, 543-546, (1976).

100. TESTER, B.J., "The Propagation and Attenuation of Sound in Lined Ducts Containing Uniform or "Plug" Flow". J. Sound & Vib. 28, 151-203, (1973).

101. EVERSMAN, W., "Energy Flow Criteria for Acoustic Propagation in Ducts with Flow", J.Acoust.Soc.Am., 49, 1717-1721, (1971).

102. TESTER, B.J., "Acoustic Energy Flow in Lined Ducts Containing Uniform or "Plug" Flow", J.Sound & Vib. 28, 205-215, (1973).

103. EVERSMAN, W., "Acoustic Energy in Ducts: Further Observations", J.Sound & Vib. 62, 517-532, (1979).

104. ASTLEY, R.J. and EVERSMAN, W., "The Application of Finite Element Techniques to Acoustic Transmission in Lined Ducts with Flow". AIAA Paper 79-0660, (1979).

105. CANDEL, S.M., "Acoustic Conservation Principles and an Application to Plane and Modal Propagation in Nozzles and Diffusers", J.Sound & Vib. 41, 207-232, (1975).

106. MORFEY, C.L., "Acoustic Energy in Nonuniform Flows", J.Sound & Vib. 14, 159-170, (1971).

107. RYSHOV, O.S. and SHEFTER, G.M., "On the Energy of Acoustic Waves Propagating in Moving Media", J.Applied Maths. and Mech. 26, 1293-1309, (1962).

108. GELDER, D., "Solution of the Compressible Flow Equations" Int.J.Num.Methods Eng. 3, 35-43, (1971).

109. O'CARROLL, M.J. and MORGAN, L.A., "Difference and Element Methods for Potential Flow", Finite Element Methods in Flow Problems 171-183, UAH Press, (1974).

APPENDIX A

DERIVATION FOR DUCT-WALL BOUNDARY CONDITION

The duct-wall boundary condition is (refer Section 2.1.2(ii))

$$\underline{v}^* \cdot \underline{\nu} = v^*_{\nu} + v^*_{o\tau} \frac{\partial}{\partial \tau} \left(\frac{v^*_{\nu}}{i\omega} \right) \tag{A.1}$$

Using subscript p to denote liner one can rewrite equation (A.1) as follows :

$$\underline{v}^* \cdot \underline{\nu} = v^*_{\nu_p} + v^*_{o\tau} \frac{\partial}{\partial \tau} \left(\frac{v^*_{\nu_p}}{i\omega} \right) \tag{A.2}$$

where $\underline{v}^*$ acoustic velocity in the flow field

$v^*_{\nu_p}$ normal acoustic velocity component in the lining.

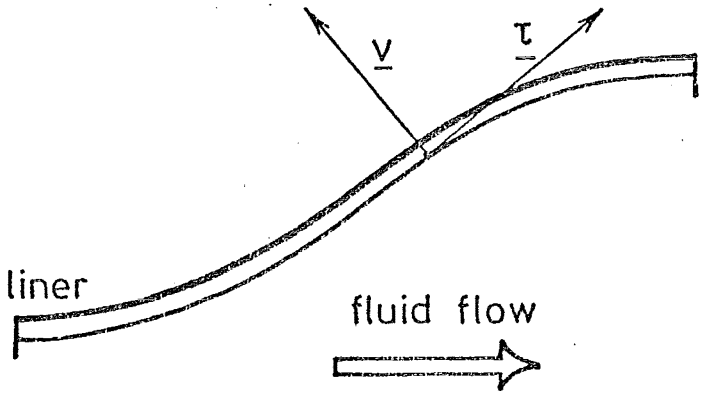

FIG. A LINING CONFIGURATION

Consider a fluid flow moving past a soft wall of an axisymmetric duct in Figure A the boundary condition is

$$\xi = \xi_p \tag{A.3}$$

where ξ is the particle displacement. The condition may be interpreted physically as follows; since the slip uniform mean flow model assumes the viscous layer is vanishingly thin, the viscous layer should be modelled as a membrane that separates the regions of uniform flow within the duct and within the porous lining. The membrane complies with waves propagating in the duct-liner configuration.

Thus, if $F(\underline{r},t)$ = constant is the equation describing the location of the membrane, where $\underline{r}$ is a position vector, the boundary condition in the flow field can be written

$$\frac{DF}{Dt} = \frac{\partial F}{\partial t} + \underline{V}' \cdot \text{grad } F = 0 \tag{A.4}$$

where $\underline{V}' = \underline{V}_o^* + \underline{V}^*$ is the total velocity (A.5)

This states that any fluid element on the boundary is on the surface $F(\underline{r},t)$ = constant. Because of the axisymmetric duct containing unwhirling flow one can choose a generalized coordinate system (ν,τ) as shown in Figure A, which is formed by the directions tangential and normal to the duct wall. In that $F(\underline{r},t)$ can take the form :

$$F(\underline{r},t) = F(\nu,\tau,t) = \nu - \xi\ (\tau,t) \tag{A.6}$$

which expresses the normal displacement ν of the membrane as a function of time t and position τ on it. So one can expand equation (A.4) in coordinates (ν,τ), using (A.5) and (A.6), as follows :

$$\frac{\partial F}{\partial t} + (\underline{V}_o^* + \underline{V}^*) \cdot \text{grad } F = 0$$

$$-\frac{\partial \xi}{\partial t} + (V_{o_\tau}^* + V_\tau^*)\left(-\frac{\partial \xi}{\partial \tau}\right) + (V_{o_\nu}^* + V_\nu^*) = 0 \tag{A.7}$$

Also $V^*_{o_\nu} = 0$ for the steady mean flow

and linearizing $V^*_{o_\tau} + V^*_\tau \approx V^*_{o_\tau}$ in equation (A.7) give

$$V^*_\nu = \underline{V}^* \cdot \underline{\nu} = \frac{\partial \xi}{\partial t} + V^*_{o_\tau} \frac{\partial \xi}{\partial \tau} \tag{A.8}$$

With the continuity of particle displacement $\xi = \xi_p$ in equation (A.3) equation (A.8) can be written

$$\underline{V}^* \cdot \underline{\nu} = \frac{\partial \xi_p}{\partial t} + V^*_{o_\tau} \frac{\partial \xi_p}{\partial \tau} \tag{A.9}$$

For a harmonic wave $e^{i\omega t}$, in the lining

$$V^*_{\nu_p} = \frac{\partial \xi_p}{\partial t} = i\,\omega\,\xi_p \tag{A.10}$$

Hence, substituting equation (A.10) into equation (A.9) one obtains :

$$\underline{V}^* \cdot \underline{\nu} = V^*_{\nu_p} + V^*_{o_\tau} \frac{\partial}{\partial \tau} \left(\frac{V^*_{\nu_p}}{i\omega} \right) \tag{A.11}$$

APPENDIX B

FEM FOR POTENTIAL FLOW FIELD

B.1 GOVERNING EQUATIONS AND POTENTIAL FUNCTION

The steady conditions for an inviscid compressible flow are stated by equations (2.2.8) - (2.2.11), which can be put in non-dimensional form with the definitions $p_o = \frac{p_o^*}{\rho_r c_r^2}$, $\underline{V}_o = \frac{\underline{V}_o^*}{c_r}$, $\rho_o = \frac{\rho_o^*}{\rho_r}$ as follows,

$$\left.\begin{aligned} &\text{Continuity} : \quad \operatorname{div}(\rho_o \underline{V}_o) = 0 \\ &\text{Momentum} : \quad \rho_o \underline{V}_o \cdot \operatorname{grad} \underline{V}_o = -\operatorname{grad} p_o \\ &\text{Energy} : \quad \underline{V}_o \cdot \operatorname{grad} p_o + \gamma p_o \operatorname{div} \underline{V}_o = 0 \\ &\text{State} : \quad p_o \gamma = \rho_o^{\gamma} \end{aligned}\right\} \qquad (B.1)$$

The duct-wall boundary condition is $\underline{V}_o \cdot \underline{\nu} = 0$ (B.2)

The appropriate velocity functional [108,109] for a potential flow in a domain D bounded by a boundary S is written in terms of nondimensional variables as follows :

$$I(\phi) = \int_D p_o \, dD + \int_{\partial D} \rho_o \phi \, dS$$

or
$$I(\phi) = \frac{1}{2} \int_D \rho_o \underline{\nabla} \phi \cdot \underline{\nabla} \phi \, dD - \int_S \phi \, \rho_o \frac{\partial \phi}{\partial \nu} \, dS \qquad (B.3)$$

where the potential function ϕ defined by

$$\nabla \phi = \underline{V}_o$$

maximizes $I(\phi)$ in equation (B.3) for the subsonic case.

B.2 Potential Flow in Axisymmetric Ducts

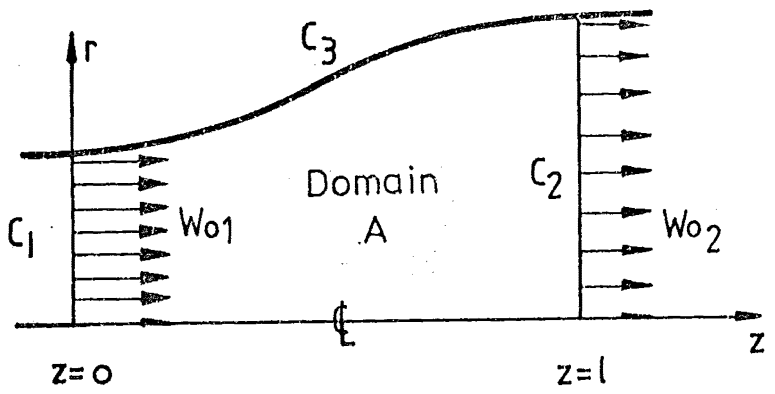

FIG. B.1 AXISYMMETRIC DUCT CONFIGURATION FOR MEAN FLOW FIELD.

In the duct configuration shown in Figure B.1 the flow is assumed to be unwhirling so that

$$\underline{V}_o = (U_o , 0 , W_o)$$

Thus, $\nabla\phi = (\frac{\partial\phi}{\partial r} , \frac{\partial\phi}{\partial z})$ in the reduced 2D domain in Figure B.1 and the functional $I(\phi)$ in equation (B.3) can be written more specifically

$$I(\phi) = \frac{1}{2} \int_A \rho_o \left[(\frac{\partial\phi}{\partial r})^2 + (\frac{\partial\phi}{\partial z})^2 \right] 2\pi r \, dr \, dz - \int_C \rho_o \frac{\partial\phi}{\partial\nu} \, 2\pi r \, ds \quad (B.4)$$

For the potential in the duct configuration considered the boundary conditions are natural conditions for the functional of equation (B.4). No special treatment is required for the duct-wall boundary condition since, from condition (B.2), there $\frac{\partial\phi}{\partial\nu}$ vanishes. Although the natural variational condition is to set $\rho_o \frac{\partial\phi}{\partial\nu}$ on the inlet and outlet boundaries the end conditions are not clear, unless a simple asymptotic form is pleaded. In any case only one distribution can be specified, not both of the velocity components (for 2-D or axisymmetric ducts), if the problem is to be well-posed.

B.3 FEM FORMULATION

The nodal FEM derived in Chapter 3 for acoustic problems is still applied here, except that a variational principle is involved. As in standard FEM techniques it is assumed that in the domain A

$$\phi = [N]\{\phi\} = [N_1 \ , \ N_2 \ \ldots . N_n] \begin{Bmatrix} \phi_1 \\ \phi_2 \\ \vdots \\ \phi_n \end{Bmatrix} \tag{B.5}$$

is defined piecewise via elements, where $\{\phi\}$ are nodal values of ϕ, components of [N] are shape functions of coordinates and n is the number of nodes in the FEM mesh.

Substituting equation (B.5) into equation (B.4) and applying the duct-wall boundary condition yield

$$I\ (\phi_j) = \frac{1}{2} \int_A \rho_o \left[\left(N_{jr}\ \phi_j\right)^2 + \left(N_{jz}\ \phi_j\right)^2 \right] 2\pi r\ dr dz + \int_{C_1} \rho_o N_j \phi_j \frac{\partial \phi_1}{\partial \nu} 2\pi r\ dr$$

$$- \int_{C_2} \rho_o\ N_j\ \phi_j\ \frac{\partial \phi_2}{\partial \nu}\ 2\pi r\ dr \tag{B.6}$$

where j = 1,2,3...n in domain A, and on boundaries C_1 and C_2 $N_j \equiv 0$ unless j corresponds to a node on C_1 or C_2. ϕ_1 and ϕ_2 are the potential function on C_1 and C_2 respectively.

The FEM formulation is formally completed when the functional $I(\phi_j)$ in equation (B.6) is maximized with respect to all ϕ_j as follows :

$$\frac{\partial I(\phi_j)}{\partial \phi_i} = \int_A \rho_o \left(N_{ir}\ N_{jr}\ \phi_j + N_{i_z}\ N_{j_z}\ \phi_j \right) 2\pi r\ dr\ dz$$

$$+ \int_{C_1} \rho_o\ N_i\ \frac{\partial \phi_1}{\partial \nu}\ 2\pi r\ dr - \int_{C_2} \rho_o\ N_i\ \frac{\partial \phi_2}{\partial \nu}\ 2\pi r\ dr = 0 \tag{B.7}$$

where i = 1,2,3...n, j = 1,2,3,...n. $N_i \equiv 0$ unless i corresponds to a node on C_1 or C_2.

B.4 IMPLEMENTATION AND RESULTS

There are two ways of treating the end boundary conditions :

(i) If a uniform flow profile is assumed on C_1 and C_2 then $\frac{\partial \phi_1}{\partial \nu} = W_{o1}$ and $\frac{\partial \phi_2}{\partial \nu} = W_{o2}$ where W_{o1} is the specified inlet condition, and W_{o2} is related to W_{o1} by an isentropic condition.

(ii) If the transverse velocity components vanish on C_1 and C_2 then ϕ_1 and ϕ_2 are constant.

In either case equation (B.7) yields a system of nonlinear equations in ϕ_i (i = 1,2,3...n) since ρ_o is dependent upon $\underline{V}_o$, hence on ϕ. Thus, an iterative solution scheme may be developed, starting with initial ρ_o values as those of the inlet condition. The criterion $\left| \frac{\rho_{oi}^{n+1} - \rho_{oi}^{n}}{\rho_{oi}^{n}} \right| \leqslant \epsilon$ may be applied to stop routines after (n+1) times of iterations.

The solution to equations (B.7) is the nodal values ϕ_i. To derive other dependent variables of equation (B.1) one has recourse to isentropic relations, and notes that $\nabla\phi = \underline{V}_o$. The extraction of derivatives $\frac{\partial \phi}{\partial r}$, $\frac{\partial \phi}{\partial z}$ gives rise to a difficulty because in this FEM formulation the slope of shape functions is not forced to be continuous at corner nodes. Consequently, for the present implementation, Lagrange interpolations and 3-point difference approximations are used to obtain the nodal derivatives.

Both of the treatments of end boundary conditions above were implemented and satisfactorily checked by comparison of flow rates across the duct at the base nodes along the duct axis. Figure B.2 presents typical results. It shows the geometry and plots velocity fields for a cosine-diverging axisymmetric duct, $R_1 = 1.0$, $R_2 = 1.268$ and $\ell = 1.6$. The end boundary conditions are forced so that $\phi_1 = 0$

at $z = 0$, $\phi_2 = 0.3$ at $z = \ell$. A mesh of 5 elements across x 10 elements along the duct was used in the FEM. The solution to the modified 1-D flow model used in the present acoustic modelling is also shown for comparisons. No rigorous discussion is offered for discrepancies between the two flow models. The FEM results simply serve to demonstrate a viable approach, which may enhance the mean flow model in the acoustic transmission in flow ducts.

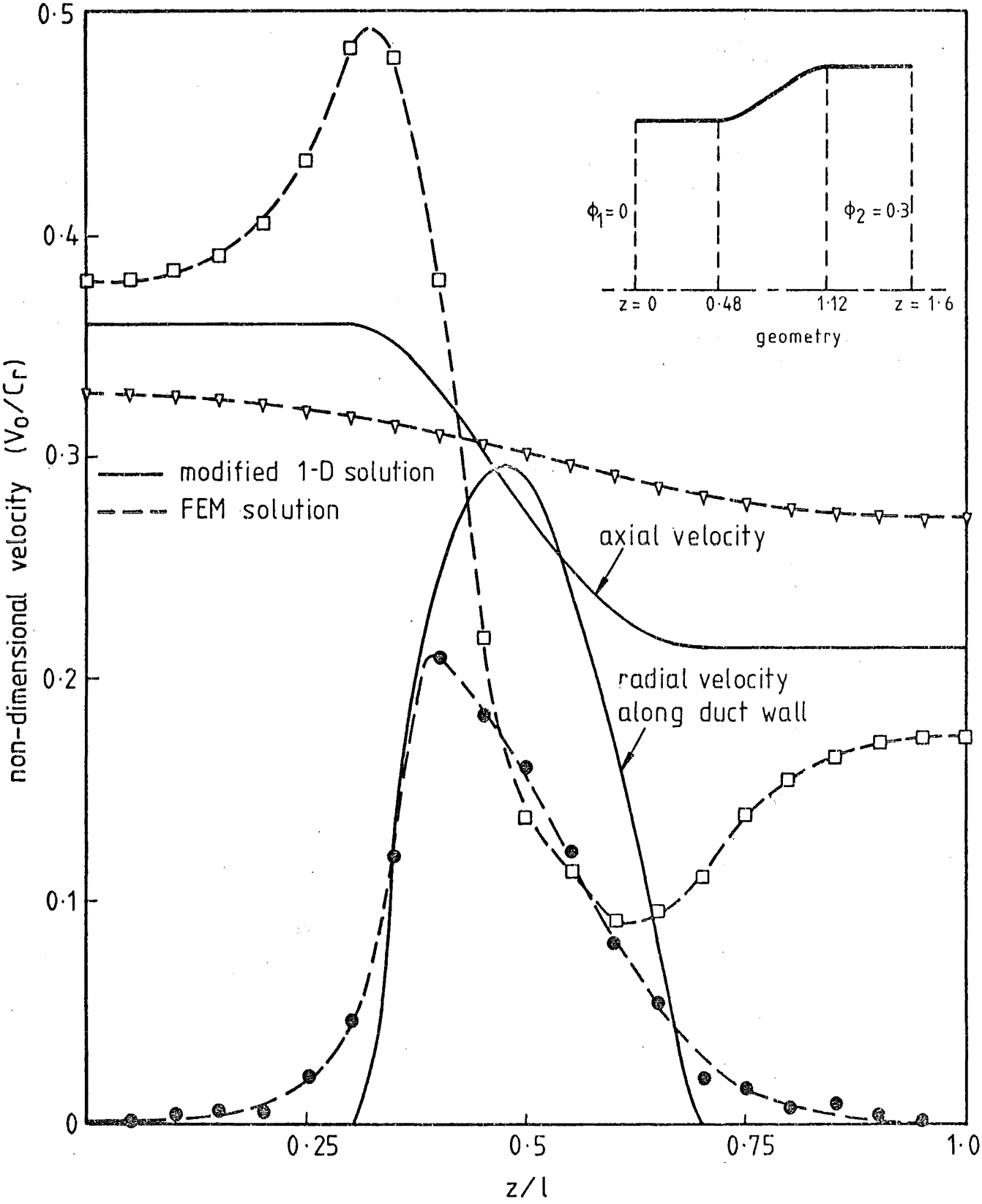

FIG. B. 2 MEAN FLOW FIELD FOR COSINE-DIVERGING AXISYMMETRIC DUCT, $R_1 = 1·0$, $R_2 = 1·268$, $l = 1·6$.

APPENDIX C

UNIFORM DUCT ACOUSTICS

There are many texts [3,38] available, which contain detailed expositions of the theory of sound propagation in uniform ducts. However, a brief review of the convected wave equation and its solution in two-dimensional and axisymmetric ducts is warranted in view of the central role played by the uniform duct eigenfunctions in the MWR procedure, and in the solution matching at the interfaces between uniform and nonuniform duct sections.

For consistency in the analysis and practical implementations the standard nondimensionalization of acoustic and mean flow variables is still retained as for nonuniform duct problems.

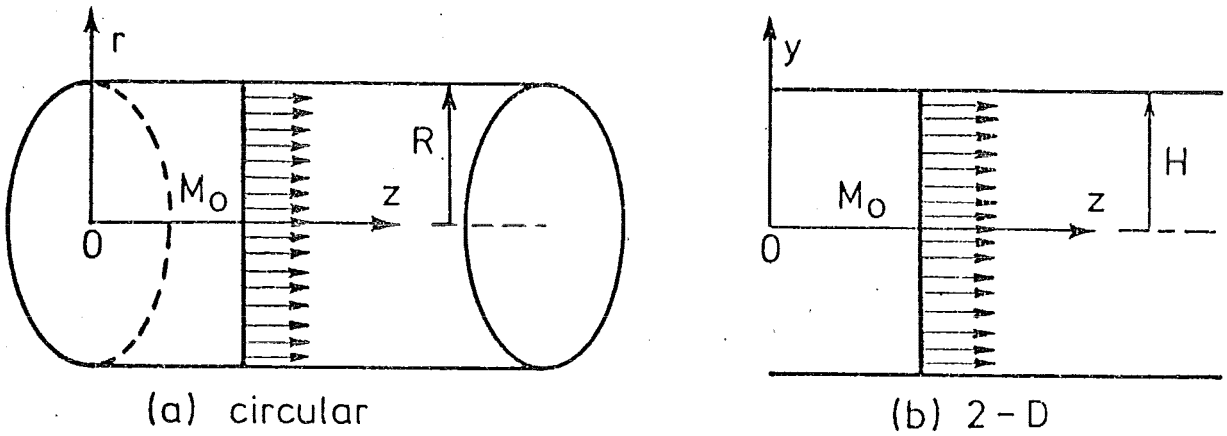

FIG. C UNIFORM DUCT GEOMETRY

C.1 AXISYMMETRIC DUCT WITH UNIFORM FLOW PROFILE

(i) Governing equations

The governing equations for acoustic perturbations in cylindrical coordinates (2.4.1) - (2.4.4) with

$$\bar{U}_o \equiv 0 \, , \quad \frac{\partial \bar{p}_o}{\partial z} \equiv 0 \, , \quad \frac{\partial \bar{W}_o}{\partial z} = 0$$

can be reduced to the nondimensional form following :

$$\bar{\rho}_o \left(ik_r u + \bar{W}_o \frac{\partial u}{\partial z} \right) = - \frac{\partial p}{\partial r} \tag{C.1}$$

$$\bar{\rho}_o \left(ikv + \bar{W}_o \frac{\partial v}{\partial z} \right) = im_o \frac{p}{r} \tag{C.2}$$

$$\bar{\rho}_o \left(ikw + \bar{W}_o \frac{\partial w}{\partial z} \right) = - \frac{\partial p}{\partial z} \tag{C.3}$$

$$ik_r p + \bar{W}_o \frac{\partial p}{\partial z} + \gamma \bar{p}_o \left[\frac{1}{r} \frac{\partial}{\partial r} (ru) - im_o \frac{v}{r} + \frac{\partial w}{\partial z} \right] = 0 \tag{C.4}$$

and the boundary condition (2.4.5) at duct walls becomes

$$\underline{V} \cdot \underline{\nu} = u = Ap - \frac{i\bar{W}_o}{k_r} A \frac{\partial p}{\partial z} \tag{C.5}$$

The relations for steady mean flow variables are reproduced here from equations (2.3.1) - (2.3.11)

$$\bar{\rho}_o = \frac{\rho_o^*}{\rho_r} = \frac{\left[1 + \frac{\gamma-1}{2} M_r^2\right]^{\frac{1}{\gamma-1}}}{\left[1 + \frac{\gamma-1}{2} M_o^2\right]^{\frac{1}{\gamma-1}}} \tag{C.6}$$

$$\bar{p}_o = \frac{p_o^*}{\rho_r c_r^2} = \frac{1}{\gamma} \frac{\left[1 + \frac{\gamma-1}{2} M_r^2\right]^{\frac{\gamma}{\gamma-1}}}{\left[1 + \frac{\gamma-1}{2} M_o^2\right]^{\frac{\gamma}{\gamma-1}}} \tag{C.7}$$

$$\bar{c}_o = \frac{c_o^*}{c_r} = \frac{\left[1 + \frac{\gamma-1}{2} M_r^2\right]^{\frac{1}{2}}}{\left[1 + \frac{\gamma-1}{2} M_o^2\right]^{\frac{1}{2}}} \tag{C.8}$$

$$\bar{W}_o = \frac{W_o^*}{c_r} = M_o \bar{c}_o = M_o \frac{\left[1 + \frac{\gamma-1}{2} M_r^2\right]^{\frac{1}{2}}}{\left[1 + \frac{\gamma-1}{2} M_o^2\right]^{\frac{1}{2}}} \tag{C.9}$$

$$k_r = \frac{\omega}{c_r} = \frac{\omega}{c_o^*} \frac{c_o^*}{c_r} = k \bar{c}_o \tag{C.10}$$

where k is the local wave number.

To derive the convected wave equation for the uniform flow model, in the present nondimensional form, one can perform differentiation of equations (C.1) and (C.3) with respect to r and z respectively, multiplication of equation (C.2) by $(-im_o/r)$; and subsequent addition of these gives

$$\bar{\rho}_o \, ik_r \left(\frac{\partial u}{\partial r} - im_o \frac{v}{r} + \frac{\partial w}{\partial z} \right) + \bar{\rho}_o \bar{W}_o \frac{\partial}{\partial z} \left(\frac{\partial u}{\partial r} - im_o \frac{v}{r} + \frac{\partial w}{\partial z} \right)$$

$$= -\left(\frac{\partial^2 p}{\partial r^2} - m_o^2 \frac{p}{r^2} + \frac{\partial^2 p}{\partial z^2} \right) \tag{C.11}$$

Equation (C.4) can be rewritten in the form

$$\left(\frac{\partial u}{\partial r} - im_o \frac{v}{r} + \frac{\partial w}{\partial z} \right) = - \frac{1}{\gamma \bar{p}_o} \left(ik_r p + \bar{W}_o \frac{\partial p}{\partial z} \right) - \frac{u}{r} \tag{C.12}$$

If equation (C.12) is substituted into equation (C.11) one obtains

$$\bar{\rho}_o \, ik_r \left(- \frac{ik_r}{\gamma \bar{p}_o} p - \frac{\bar{W}_o}{\gamma \bar{p}_o} \frac{\partial p}{\partial z} - \frac{u}{r} \right) + \bar{\rho}_o \bar{W}_o \frac{\partial}{\partial z} \left(- \frac{ik_r}{\gamma \bar{p}_o} p - \frac{\bar{W}_o}{\gamma \bar{p}_o} \frac{\partial p}{\partial z} - \frac{u}{r} \right)$$

$$= - \left(\frac{\partial^2 p}{\partial r^2} - m_o^2 \frac{p}{r^2} + \frac{\partial^2 p}{\partial z^2} \right)$$

or

$$\frac{\bar{\rho}_o}{\gamma \bar{p}_o} \left(k_r^2 p - 2 i k_r \bar{W}_o \frac{\partial p}{\partial z} - \bar{W}_o^2 \frac{\partial^2 p}{\partial z^2} \right) - \frac{\bar{\rho}_o}{r} \left(ik_r u + \bar{W}_o \frac{\partial u}{\partial z} \right)$$

$$= - \left(\frac{\partial^2 p}{\partial r^2} - m_o^2 \frac{p}{r^2} + \frac{\partial^2 p}{\partial z^2} \right) \tag{C.13}$$

The momentum equation (C.1) is to be used to eliminate the terms containing u in equation (C.13) to give

$$\frac{\bar{\rho}_o}{\gamma \bar{p}_o}\left(k_r^2 p - 2ik_r \bar{W}_o \frac{\partial p}{\partial z} - \bar{W}_o^2 \frac{\partial^2 p}{\partial z^2}\right) = -\left(\frac{\partial^2 p}{\partial r^2} + \frac{1}{r}\frac{\partial p}{\partial r} - m_o^2 \frac{p}{r^2} + \frac{\partial^2 p}{\partial z^2}\right) \quad (C.14)$$

When the relations (C.6) - (C.10) are employed equation (C.14) can be reduced to the convected wave equation in the standard form

$$\nabla^2 p + k\left(1 - i\frac{M_o}{k}\frac{\partial}{\partial z}\right)^2 p = 0 \quad (C.15)$$

where $$\nabla^2 \equiv \left(\frac{\partial^2}{\partial r^2} + \frac{1}{r}\frac{\partial}{\partial r} - \frac{m_o^2}{r^2} + \frac{\partial^2}{\partial z^2}\right)$$

To write the boundary condition(C.5) in terms of pressure p and its derivatives one can substitute equation (C.5) into momentum equation (C.1) to obtain

$$\bar{\rho}_o ik_r\left(Ap - \frac{i\bar{W}_o}{k_r} A \frac{\partial p}{\partial z}\right) + \bar{\rho}_o \bar{W}_o \frac{\partial}{\partial z}\left(Ap - \frac{i\bar{W}_o}{k_r} A \frac{\partial p}{\partial z}\right) = -\frac{\partial p}{\partial r} \text{ at } r = R$$

or

$$\bar{\rho}_o ik_r\left(Ap - 2i\frac{\bar{W}_o}{k_r}\frac{\partial p}{\partial z} - \frac{\bar{W}_o^2}{k_r^2}\frac{\partial^2 p}{\partial z^2}\right) = -\frac{\partial p}{\partial r} \text{ at } r = R \quad (C.16)$$

where $$A = \frac{\rho_r c_r}{Z} \quad \frac{\rho_o^* c_o^*}{\rho_o^* c_o^*} = \frac{\rho_r c_r}{\rho_o^* c_o^*} \quad A_o^* = \frac{A_o^*}{\bar{\rho}_o \bar{c}_o} \quad (C.17)$$

and $A_o^* = \frac{\rho_o^* c_o^*}{Z}$ is the local admittance referred to the local state in question.

With equation (C.17) and relations (C.6) - (C.10) equation (C.16) can be written

$$ik A_o^*\left(1 - i\frac{M_o}{k}\frac{\partial}{\partial z}\right)^2 p = -\frac{\partial p}{\partial r} \text{ at } r = R \quad (C.18)$$

(ii) Eigenproblem

To formulate the eigenproblem in circular uniform ducts with uniform flow the harmonic dependence of the form $e^{-ik_z z}$ is assumed in the convected wave equation (C.15) and its appropriate boundary condition (C.18) to yield

$$\frac{d^2p}{dr^2} + \frac{1}{r}\frac{dp}{dr} + \left[k^2\left(1 - 2\frac{k_z}{k} M_o - (1 - M_o^2)\left(\frac{k_z}{k}\right)^2\right) - \frac{m_o^2}{r^2}\right] p = 0 \qquad (C.19)$$

$$\text{and} \quad ik A_o^* \left[1 - 2\frac{k_z}{k} M_o + M_o^2 \left(\frac{k_z}{k}\right)^2\right] p = -\frac{dp}{dr} \quad \text{at } r = R \qquad (C.20)$$

The second-order ordinary differential equation (C.19) has the solution

$$p = a J_{m_o}(\kappa r) + b Y_{m_o}(\kappa r)$$

where J_{m_o} and Y_{m_o} are the Bessel and Newmann functions of order m_o respectively, and

$$\kappa^2 = k^2 \left[1 - 2\frac{k_z}{k} M_o - (1 - M_o^2)\left(\frac{k_z}{k}\right)^2\right]$$

$$\text{or} \qquad \frac{k_z}{k} = \frac{1}{1 - M_o^2}\left\{- M_o \pm \left[1 - (1 - M_o^2)\left(\frac{\kappa}{k}\right)^2\right]^{\frac{1}{2}}\right\} \qquad (C.21)$$

In the circular duct the pressure p must be finite at the centre-line (r = 0). This forces b to vanish. Hence

$$p = a J_{m_o}(\kappa r) \qquad (C.22)$$

To determine κ and k_z equation (C.22) is substituted into the boundary condition (C.20) to give another relation

$$\kappa R J'_{m_o}(\kappa R) + A_o^* ikR \left(1 - M_o \frac{k_z}{k}\right)^2 J_{m_o}(\kappa R) = 0 \qquad (C.23)$$

The coupled transcendental equations (C.21) and (C.23) establish the eigenproblem in circular ducts, and give an infinite number of pairs of transverse and axial eigenvalues κ_n, k_{z_n} for upstream and downstream propagation modes. Thus the general solution for the pressure in the duct can be written

$$p = \sum_{n=1}^{\infty} \left[a_n^+ J_{m_o}(\kappa_n^+ r)\, e^{-ik_{z_n}^+ z} + a_n^- J_{m_o}(\kappa_n^- r)\, e^{-ik_{z_n}^- z}\right] \qquad (C.24)$$

where subscripts + and - denote positive and negative propagating direction respectively, and κ_n, k_{z_n} are the $n^{\underline{th}}$ pair of roots κ, k_z of equations (C.21) and (C.23) corresponding to one mode of propagation in either direction.

In general, when $M_o \neq 0$, due to the coupling in the eigen-equations the eigenfunctions $J_{m_o}(\kappa_n r)$ are not orthogonal. For the no-flow case the coupling disappears to give one transcendental equation

$$\kappa_n R\, J'_{m_o}(\kappa_n R) + A_o^* \, ikR\, J_{m_o}(\kappa_n R) = 0 \qquad (C.25)$$

and $$\frac{k_{z_n}}{k} = \pm \left[1 - \left(\frac{\kappa_n}{k}\right)^2\right]^{\frac{1}{2}}$$

In this case the eigenfunctions are orthogonal over the cross-section of the duct.

To express the particle velocity components explicitly in terms of the eigenfunctions equation (C.24) are substituted into equations (C.1) - (C.3) together with the form $e^{-ik_z z}$ taken in the solution, to give the following relations :

$$w = \sum_{n=1}^{\infty} \left[\alpha_n^+ a_n^+ J_{m_o}(\kappa_n^+ r) + \alpha_n^- a_n^- J_{m_o}(\kappa_n^- r)\right] \qquad (C.26)$$

$$u = \sum_{n=1}^{\infty} \left[\beta_n^+ a_n^+ J'_{m_o}(\kappa_n^+ r) + \beta_n^- a_n^- J'_{m_o}(\kappa_n^- r)\right] \qquad (C.27)$$

$$v = \sum_{n=1}^{\infty} \left[\gamma_n^+ a_n^+ J_{m_o}(\kappa_n^+ r) + \gamma_n^- a_n^- J_{m_o}(\kappa_n^- r)\right] \qquad (C.28)$$

where

$$\alpha_n^+ = \frac{k_{z_n}^+/k_r}{\bar{\rho}_o(1-\bar{W}_o\, k_{z_n}^+/k_r)}, \quad \alpha_n^- = \frac{k_{z_n}^-/k_r}{\bar{\rho}_o(1-\bar{W}_o\, k_{z_n}^-/k_r)}$$

$$\beta_n^+ = \frac{i\,\kappa_n^+/k_r}{\bar{\rho}_o(1-\bar{W}_o\, k_{z_n}^+/k_r)}, \quad \beta_n^- = \frac{i\,\kappa_n^-/k_r}{\bar{\rho}_o(1-\bar{W}_o\, k_{z_n}^-/k_r)}$$

$$\gamma_n^+ = \frac{m_o/k_r}{\bar{\rho}_o(1-\bar{W}_o\, k_{z_n}^+/k_r)r}, \quad \gamma_n^- = \frac{m_o/k_r}{\bar{\rho}_o(1-\bar{W}_o\, k_{z_n}^-/k_r)r}$$

C.2 TWO-DIMENSIONAL DUCT WITH UNIFORM FLOW PROFILE

Consider a two-dimensional channel of height 2H with the flow in the z direction. Similar derivations in Cartesian coordinates (y,z) will give the convected wave equation in the form

$$\nabla^2 p + k^2 \left(1 - i \frac{M_o}{k} \frac{\partial}{\partial z}\right)^2 p = 0 \tag{C.29}$$

where $\nabla^2 \equiv \left(\frac{\partial^2}{\partial y^2} + \frac{\partial^2}{\partial z^2}\right)$

and the boundary condition being

$$ik A_o^* \left(1 - i \frac{M_o}{k} \frac{\partial}{\partial z}\right)^2 p = \frac{\partial p}{\partial y} \text{ at } y = H \tag{C.30}$$

The notation in Section C.1 is still applied otherwise specified.

If p is taken in the form $e^{-ik_z z}$ equations (C.29) and (C.30) become

$$\frac{d^2 p}{dy^2} + k^2 \left[1 - 2 \frac{k_z}{k} M_o - (1 - M_o^2)\left(\frac{k_z}{k}\right)^2\right] p = 0 \tag{C.31}$$

and $$ikA_o^* (1 - M_o \frac{k_z}{k})^2 p = - \frac{dp}{dy} \text{ at } y = H \tag{C.32}$$

Equation (C.31) has the solution

$$p = a \cos(\kappa y) + b \sin(\kappa y)$$

where $$\kappa^2 = k^2 \left[1 - 2 \frac{k_z}{k} M_o - (1 - M_o^2)\left(\frac{k_z}{k}\right)^2\right] \tag{C.33}$$

For symmetric modes about y = 0 b must vanish.

The boundary condition gives the relation

$$ikA_o^* (1 - M_o \frac{k_z}{k})^2 \cos(\kappa H) = \kappa \sin(\kappa H) \tag{C.34}$$

Thus, the general solution can be obtained

$$p = \sum_{n=1}^{\infty} \left[a_n^+ \cos \kappa_n^+ y \, e^{-ik_{z_n}^+ z} + a_n^- \cos \kappa_n^- y \, e^{-ik_{z_n}^- z}\right] \tag{C.35}$$

where κ_n and k_{z_n} are the n^{th} pair of roots of the transcendental

equations (C.33) and (C.34), which can be rewritten as follows :

$$\kappa_n H \tan(\kappa_n H) = ik\, H\, A_o^* \left(1 - M_o \frac{k_{z_n}}{k}\right)^2 \qquad (C.36)$$

and

$$\frac{k_{z_n}}{k} = \frac{1}{1-M_o^2} \left\{ - M_o \pm \left[1 - (1 - M_o^2)\left(\frac{\kappa_n}{k}\right)^2 \right]^{\frac{1}{2}} \right\} \qquad (C.37)$$

Conclusions on the orthogonality is similar to the case of axisymmetric ducts.

APPENDIX D

INTEGRATION SCHEME TO COMPUTE EIGENVALUES FOR PROPAGATION IN CIRCULAR DUCTS

D.1 INITIAL VALUE PROBLEM

The eigenproblem for circular ducts with or without uniform flow (Appendix C) can be written, in general :

$$\begin{cases} \kappa R\, J'_{m_o}(\kappa R) = -\, Ai\, kR \left(1 - M_o \frac{k_z}{k}\right)^2 J_{m_o}(\kappa R) & (D.1) \\ \frac{k_z}{k} = \frac{1}{1-M_o^2} \left\{ - M_o \pm \left[1 - (1 - M_o^2)\left(\frac{\kappa R}{kR}\right)^2 \right]^{\frac{1}{2}} \right\} & (D.2) \end{cases}$$

where κ, k_z are pairs of transverse and axial eigenvalues for modes of propagation.

To determine κ and k_z one can change the coupled transcendental nonlinear algebraic equations to an initial value problem involving a nonlinear ordinary differential equation by putting $A = \eta A_f$ with $0 \leqslant \eta \leqslant 1$, i.e., A is varying linearly and A_f is the wall admittance of the problem in question.

With

$$v = 1 - (1 - M_o^2)\left(\frac{\kappa R}{kR}\right)^2 \qquad (D.3)$$

$$w = \left(1 - M_o \frac{k_z}{k}\right) = \frac{1}{1-M_o^2}\left(1 \mp M_o\, v^{\frac{1}{2}}\right) \qquad (D.4)$$

$$F(\kappa R) = J'_{m_o}(\kappa R)/J_{m_o}(\kappa R) \qquad (D.5)$$

one can rewrite equations (D.1) and (D.2) as follows :

$$\kappa R\, F(\kappa R) = - ikR\, \eta A_f\, w^2 \qquad (D.6)$$

$$\frac{k_z}{k} = - \frac{1}{1-M_o^2}\left(- M_o \pm v^{\frac{1}{2}}\right) \qquad (D.7)$$

In all the development in this appendix it is noted that the sign choice is consistent provided that the principal value of the square root is

defined with positive imaginary part (i.e., in the upper half plane). This means that the upper sign is for negative propagation and the bottom one for positive propagation.

Differentiation of equation (D.6) with respect to η gives

$$\frac{d(\kappa R)}{d\eta}\left[F(\kappa R) + \kappa R\, F'(\kappa R)\right] = - i\, kR\, A_f \left[w^2 + \eta \frac{d(w^2)}{d\kappa R} \frac{d\kappa R}{d\eta}\right]$$

or

$$\frac{d(\kappa R)}{d\eta}\left[F(\kappa R) + \kappa R\, F'(\kappa R) + i\, kR\, A_f\, \eta \frac{dw^2}{d\kappa R}\right] = - ik\, R\, A_f\, w^2 \qquad (D.8)$$

But, from relations (D.3) and (D.4)

$$\frac{dw^2}{d\kappa R} = \mp \frac{M_o}{1-M_o^2}\, 2w \frac{dv^{\frac{1}{2}}}{d\kappa R}$$

$$= \pm\, 2\, M_o \frac{w}{v^{\frac{1}{2}}} \frac{\kappa R}{(kR)^2}$$

Thus, equation (D.8) can be written

$$\left[F(\kappa R) + \kappa R\, F'(\kappa R) \pm 2\, \eta\, A_f\, M_o \left(\frac{\kappa R}{kR}\right) \frac{w}{v^{\frac{1}{2}}}\right] \frac{d\kappa R}{d\eta} = - i\, kR\, A_f\, w^2$$

or

$$\frac{d\kappa R}{d\eta} = \frac{- i\, kR\, A_f\, w^2}{F(\kappa R) + \kappa R\, F'(\kappa R) \pm 2\eta\, A_f\, M_o \left(\frac{\kappa R}{kR}\right) \frac{w}{v^{\frac{1}{2}}}} \qquad (D.9)$$

The ordinary differential equation (D.9) is an initial value problem with κR as a function of a single independent variable being η $(0 \leq \eta \leq 1)$.

For the hardwall case $A = 0$ or $\eta = 0$ the transverse eigenvalues of equations (D.1) and (D.2) are known to be the roots of $J'_{m_o}(\kappa R) = 0$. If now equation (D.9) is integrated by an integration scheme such as the fourth order Runge-Kutta method from $\eta = 0$ to $\eta = 1$ with the hardwall eigenvalues being used as the initial values, then at $\eta = 1$ the solution of equation (D.9) will be the eigenvalue of coupled eigenequations (D.1) and (D.2) with $A = A_f$.

It is noted that when $m_o = 0$ the first root of $J'_{m_o}(KR)$ is zero, hence equation (D.9) becomes singular. To circumvent the singularity one can guess the root of equations (D.1) and (D.2) for η small in this case and refine it by a suitable iteration scheme such as the Newton-Raphson method, as follows :

Let $z = KR$ when $A = \eta A_f$, $\eta << 1$ and $m_o = 0$ the eigenequation (D.1) becomes

$$z\, J'_{m_o}(z) = - A\, i\, kR\, w^2\, J_{m_o}(z) \qquad (D.10)$$

with $$w = \frac{1}{(1-M_o^2)}\left(1 \mp M_o\, v^{\frac{1}{2}}\right)$$

$$v = 1 - (1 - M_o^2)\,\frac{z^2}{(kR)^2}$$

For $A = 0$ the first root of equation (D.10) is $z = 0$, for a proper problem : $A \to 0$ (i.e. $\eta << 1$) $\Rightarrow z \to 0$. So, one can make approximations :

$$\left.\begin{aligned} J_o(z) &\approx 1 - \frac{z^2}{2^2} + \frac{z^4}{2^2 4^2} - \ldots \approx 1 - \frac{z^2}{4} \\ J'_o(z) &\approx -\frac{z}{2} + \frac{z^3}{2^2 4} - \ldots \approx -\frac{z}{2} \\ w^2 &\approx \frac{1}{(1 \pm M_o)^2} \end{aligned}\right\} \qquad (D.11)$$

Substituting approximate relations (D.11) into equation (D.10) yields

$$z\left(-\frac{z}{2}\right) = i\, A\, kR\, \frac{1}{(1 \pm M_o)^2}\left(1 - \frac{z^2}{4}\right)$$

or

$$z = \pm \left[\frac{2\, i\, A\, kR\, \frac{1}{(1 \pm M_o)^2}}{1 + \frac{1}{2}\, i\, A\, kR\, \frac{1}{(1 \pm M_o)^2}} \right]^{\frac{1}{2}} \qquad (D.12)$$

Hence, there are two values to start an iteration scheme for $A = \eta\, A_f$, η is small ($\eta << 1$). Singularity can also occur for a double eigenvalue but this specific case is of no interest here.

D.2 PROOF

There exist two extra eigenvalues for $I_m(A) > 0$.

In the integration scheme above, starting with N hardwall values one can compute 2N eigenvalues for a softwalled duct in the same order because each hardwall eigenvalue on the real axis branches into two softwall eigenvalues. But, in fact, when the admittance A has a positive imaginary part there are two more starting values than can be accounted for by using hardwall values as initial conditions.

In order to prove their existence one considers the eigenequations (D.1) and (D.2) in the form :

$$\frac{z\, J'_\nu(z)}{J_\nu(z)} = -\, i\, A\, kR\, w^2 \tag{D.13}$$

$$\left.\begin{aligned} \text{where}\quad w &= \frac{1}{1-M_o^2}\left(1 \mp M_o\, v^{\frac{1}{2}}\right) \\ v &= 1 - \left(1 - M_o^2\right)\frac{z^2}{(kR)^2} \\ \nu &\equiv m_o \end{aligned}\right\} \tag{D.14}$$

When A starts from zero and branches out in a complex plane the corresponding eigenvalues z will march out from imaginary infinity as complex numbers. Therefore when A becomes vanishingly small, z becomes very large. From the asymptotic expansions of the Bessel functions :

$$\left.\begin{aligned} J_\nu(z) &= \sqrt{\frac{2}{\pi z}}\ \cos\chi \\ J'_\nu(z) &= \sqrt{\frac{2}{\pi z}}\ \left\{ -\, R(\nu,z)\sin\chi - S(\nu,z)\cos\chi \right\} \end{aligned}\right\} \tag{D.15}$$

where $\mu = 4\,\nu^2$

$$\chi = \left(z - \frac{\pi}{4} - \nu\,\frac{\pi}{2}\right)$$

$$S(\nu,z) = \frac{\mu+3}{8z}$$

$$R(\nu,z) = 1 - \frac{(\mu-1)(\mu+15)}{128z^2}$$

one can write equation (D.13) for $|z| \to \infty$ as follows:

$$\lim_{|z|\to\infty}\left(\frac{z\,J_\nu'(z)}{J(z)}\right) = \lim_{|z|\to\infty}\left(i\,A\,k\,R\,w^2\right)$$

or, from (D.15) :

$$z\,R(\nu,z)\tan\chi + z\,S(\nu,z) = A\,i\,k\,R\lim_{|z|\to\infty}(w^2) \qquad (D.16)$$

But, from (D.14)

$$\lim_{|z|\to\infty}(w^2) = -\frac{M_o^2}{1-M_o^2}\frac{z^2}{(kR)^2}$$

and for large z and enough small ν one can take

$$\chi \approx z$$

$$R(\nu,z) \approx 1$$

$$z\,S(\nu,z) \approx \frac{\mu+3}{8}$$

With these approximations, equation (D.16) can be written :

$$A\,i\,k\,R\,\frac{M_o^2}{1-M_o^2}\,\frac{z^2}{(kR)^2} + z\tan z + \frac{\mu+3}{8} = 0 \qquad (D.17)$$

Now consider the case $z = x + iy$ (x and y are real) as $|y|\to\infty$

$$\lim_{|y|\to\infty}(\tan z) = \lim_{|y|\to\infty}(\tan(x+iy))$$

$$= i\,\mathrm{sign}\,y \begin{cases} = i & y > 0 \\ = -i & y < 0 \end{cases}$$

Also put $A = a_1 + i\,a_2$ where a_1, a_2 are real.

Thus, when A is small, z has a very large imaginary part

equation (D.17) becomes

$$(a_1 + i\,a_2)\,\frac{i\,M_o^2}{(1-M_o^2)kR}\,(x+iy)^2 + (x+iy)\,i\,\mathrm{sign}\,y + \frac{\mu+3}{8} = 0 \qquad (D.18)$$

where $u = 4\nu^2 \geqslant 0$

a_1, a_2, x, y are real

With $\alpha = \dfrac{M_o^2}{(1-M_o^2)kR} \geqslant 0$, $\beta = \dfrac{\mu+3}{8} > 0$

the left-hand side of equation (D.18) can be expanded and the two real and imaginary parts are equated to zero in the following form :

$$\alpha \left[- a_2(x^2-y^2) - 2a_1xy \right] - y \text{ sign } y + \beta = 0 \qquad (D.19)$$

$$\alpha \left[a_1(x^2-y^2) - 2a_2xy \right] + x \text{ sign } y = 0 \qquad (D.20)$$

Since a_1, a_2, x are small and y is very large, now if one just considers the O(1) terms in equations (D.19) and (D.20) the approximation yields

$$\alpha a_2 y^2 - y \text{ sign } y + \beta = 0 \qquad (D.21)$$

$$- \alpha a_1 y^2 + x \text{ sign } y = 0 \qquad (D.22)$$

These result in

$$y = \frac{\text{sign } y \pm \sqrt{1 - 4a_2\alpha\beta}}{2a_2\alpha} \qquad (D.23)$$

$$x = \alpha a_1 y \frac{y}{\text{sign } y} \qquad (D.24)$$

Consider equation (D.23)

Case (i) : $a_2 < 0$

$$\Delta = 1 - 4\, a_2\alpha\beta > 1 \Rightarrow \sqrt{\Delta} > 1$$

$$y = \frac{\text{sign } y \pm \sqrt{\Delta}}{2a_2\alpha}$$

a) $y > 0$, i.e. z marches out from $+\infty$

$$y = \frac{1 \pm \sqrt{\Delta}}{2a_2\alpha}$$

only $y = \frac{1 - \sqrt{\Delta}}{2a_2\alpha}$ is acceptable

b) $y < 0$, z marches out from $-\infty$

only $y = \frac{-1 + \sqrt{\Delta}}{2a_2\alpha}$ is acceptable

Case (ii) : $a_2 > 0$

$$\Delta = 1 - 4\, a_2\alpha\beta < 1$$

and if $\quad 4\, a_2\alpha\beta < 1$, i.e. $\Delta > 0 \Rightarrow \quad 0 < \sqrt{\Delta} < 1$

then

a) $y > 0$

$$\Rightarrow y = \frac{1 \pm \sqrt{\Delta}}{2a_2\alpha} \text{ : both are acceptable}$$

b) $y < 0$

$$\Rightarrow y = \frac{-1 \pm \sqrt{\Delta}}{2a_2\alpha} \text{ : both are acceptable}$$

It is noted that, from equation (D.24)

$$(y/\text{sign}\, y) > 0 \quad \text{always}$$

Hence, another conclusion can be made that, from equation (D.24),

x,y have the same sign if $a_1 > 0$

x,y have opposite signs if $a_1 < 0$

This mathematical development serves to prove the existence of the extra roots for Im (A) > 0, therefore restrictions on parameters are rather loose because of approximations.

APPENDIX E

ALGORITHM FOR SOLVING A SYSTEM OF LINEAR EQUATIONS BY THE L-U DECOMPOSITION METHOD

The system matrix generated by the FEM formulation of Section 3.2.1 is in general unsymmetric and non-positive definite, in addition to being complex. Due to the discretization scheme described in Section 3.2.2 the system matrix contains overlapping block diagonal components. In the classical method of L-U decomposition [95,74] the decomposition of a simple block diagonal matrix is readily obtainable since the upper components of U matrix are available from the original matrix. The basic approach is still applied to the overlapping block diagonal case with appropriate modifications on the U matrix.

E.1 METHOD OF L-U DECOMPOSITION

As in Section 3.2.4 the discretization by 8-node finite elements is considered over the domain being a duct section (Figure 3.2.). The description symbols of Section 3.2.4(i) are repeated here with

n_n : the total number of nodes

n_r : the number of nodes across the duct

n_z : the number of nodes on the duct wall

n_{rm} : the number of midside nodes across the duct

n_v : the number of dependent variables per node

For the purpose of demonstrating the technique it is supposed that, in the problem of sound propagation, the least-square matching is used at the end boundary $z = 0$ and the point matching at $z = \ell$ then the system matrix [C], after assembly processes, can be recognized in the form

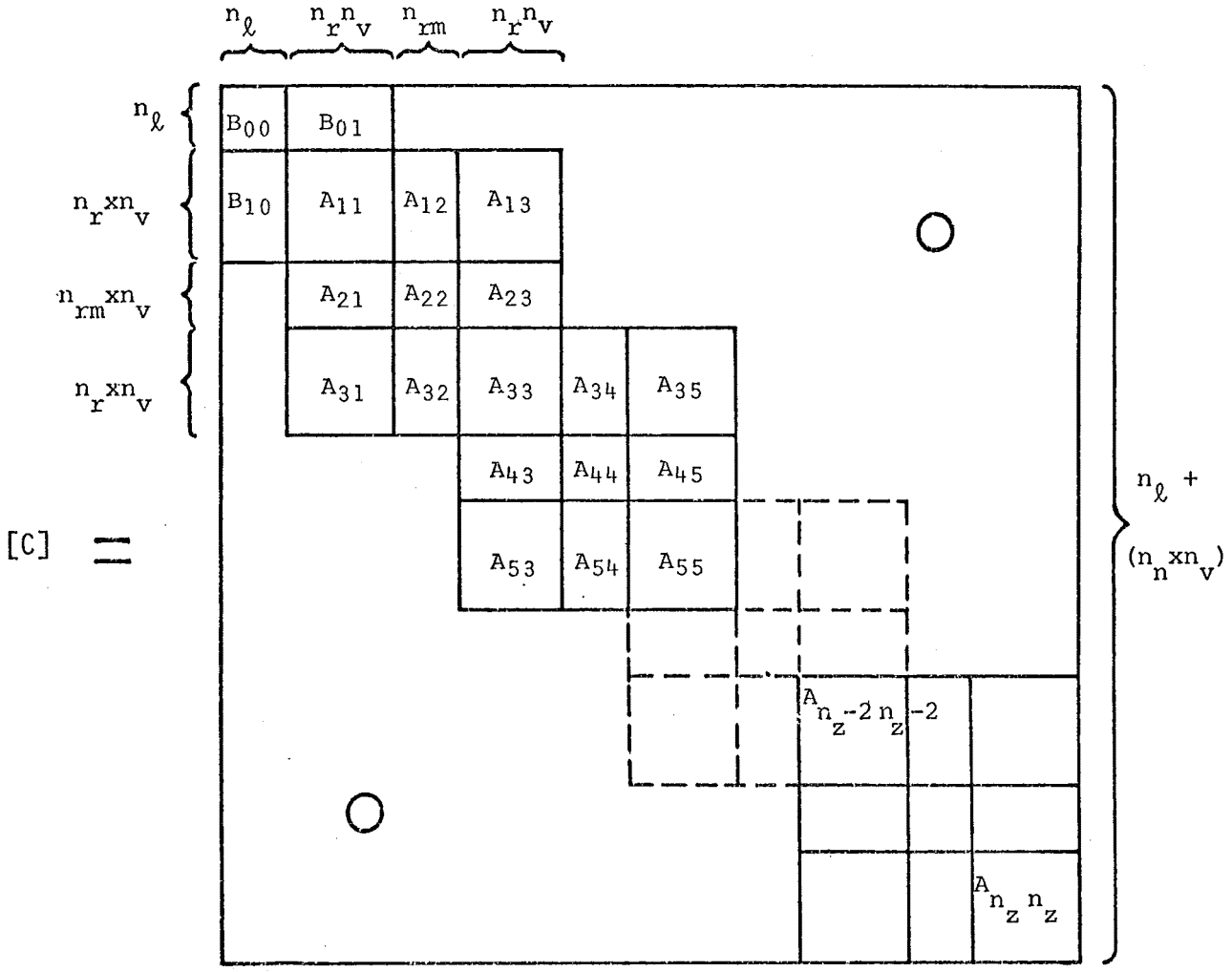

where n_ℓ depends on the number of propagation modes involved, $[B_{00}]$, $[B_{01}]$ and $[B_{10}]$ are full matrices and $[A_{ij}]$ are block diagonal matrices.

The system of simultaneous equations, given by the FEM formulation (see Section 3.2.4(ii))

$$\underset{(n_n n_v + n_\ell) \times (n_n n_v + n_\ell)}{[\ C\ ]} \quad x \quad \underset{(n_n n_v + n_\ell) x 1}{\{\ X\ \}} = \underset{(n_n n_v + n_\ell) x n_\ell}{[\ F\ ]} \qquad \text{(E.1)}$$

is to be solved for each of n_ℓ load vectors of [F] at a time. The solution can be obtained by the L-U decomposition method with forward and backward substitutions.

Thus, if $[C] = [L]\ [U]$ (E.2)

where [L] and [U] are block upper and lower triangular matrices, one can write

$$[L]\ [U]\ \{X\} = [F]$$

Inspection of the structure of matrix [C] shows that matrices [L] and [U] should take the following form :

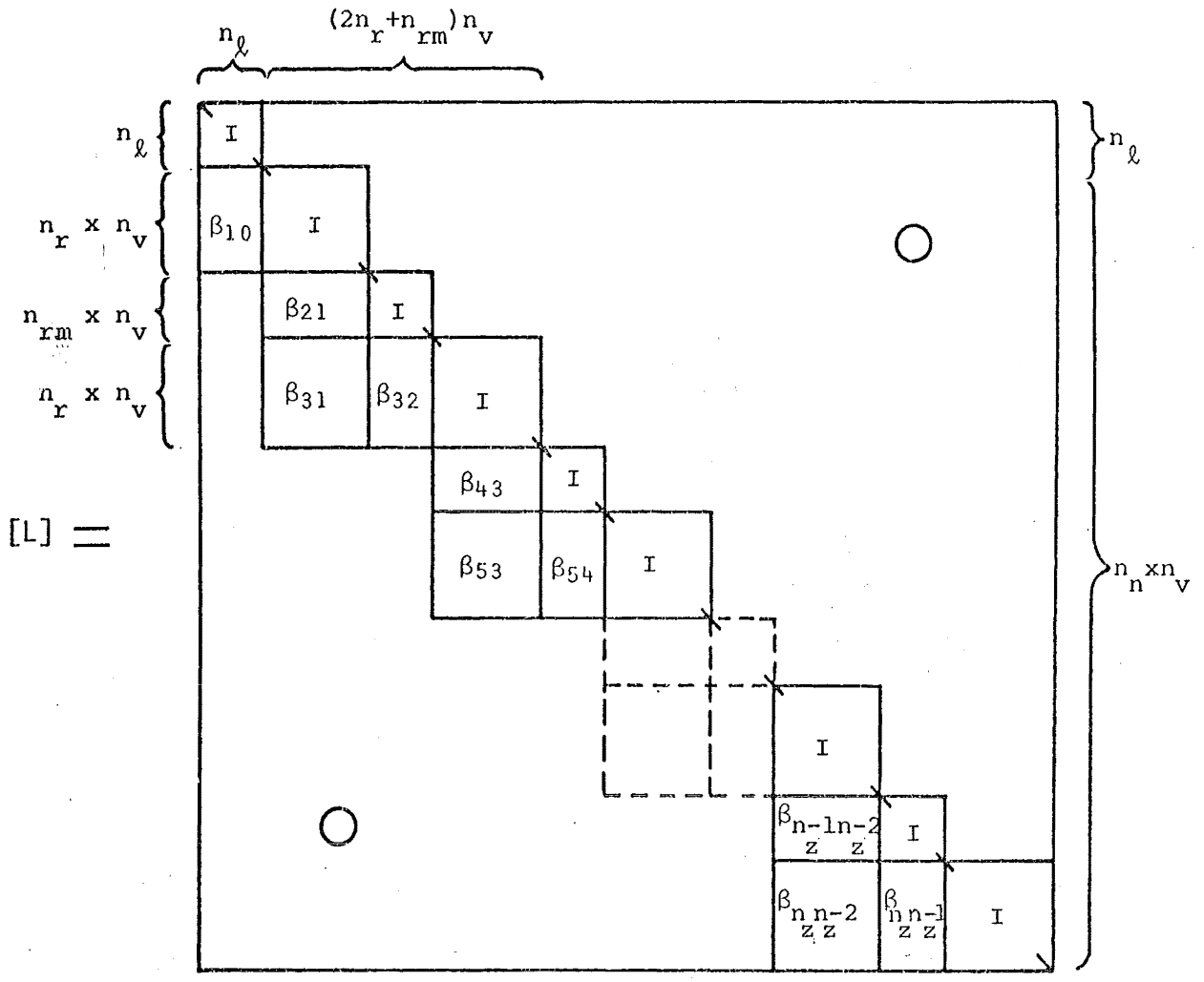
n_ℓ
$(2n_r+n_{rm})n_v$
n_ℓ
$n_r \times n_v$
$n_{rm} \times n_v$
$n_r \times n_v$
[L] =
$n_n x n_v$
I
β_{10}
β_{21}
β_{31}
β_{32}
β_{43}
β_{53}
β_{54}
β_{n-1n-2} z z
$\beta_{n\,n-2}$ z z
$\beta_{n\,n-1}$ z z

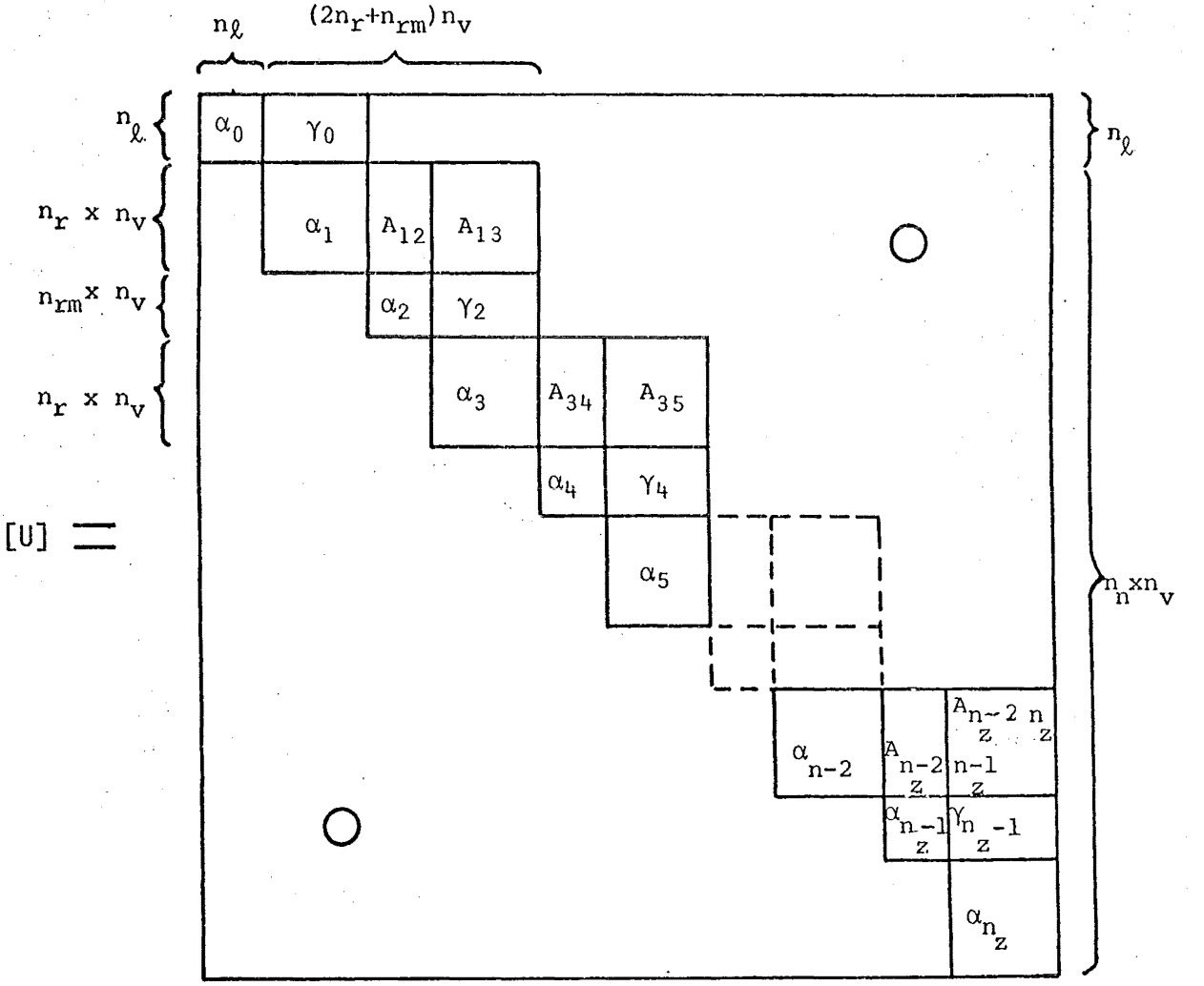
n_ℓ
$(2n_r+n_{rm})n_v$
n_ℓ
$n_r \times n_v$
$n_{rm} \times n_v$
$n_r \times n_v$
[U] =
$n_n x n_v$
α_0
γ_0
α_1
A_{12}
A_{13}
α_2
γ_2
α_3
A_{34}
A_{35}
α_4
γ_4
α_5
α_{n-2}
A_{n-2} z
$A_{n-2\,n-1}$ z z
α_{n-1} z
γ_{n-1} z
α_{n_z}

where [I] is the identity block matrix. The component matrices of [L] and [U] are given by direct substitutions to yield the following relations :

$$\left.\begin{aligned} [\alpha_0] &= [B_{00}] \\ [\gamma_0] &= [B_{01}] \\ [\beta_{10}] &= [B_{10}][\alpha_0]^{-1}, \quad [\alpha_1] = [A_{11}] - [\beta_{10}]\,[\gamma_0] \end{aligned}\right\} \tag{E.3}$$

For $k = 1,3,5\ldots n_z$ (odd integers)

$$\left.\begin{aligned} [\beta_{k+1,k}] &= [A_{k+1,k}]\,[\alpha_k]^{-1} \\ [\alpha_{k+1}] &= [A_{k+1,k+1}] - [\beta_{k+1,k}]\,[A_{k,k+1}] \\ [\gamma_{k+1}] &= [A_{k+1,k+2}] - [\beta_{k+1,k}]\,[A_{k,k+2}] \end{aligned}\right\} \tag{E.4}$$

For $k = 2,4,8\ldots n_z-1$ (even integers)

$$\left.\begin{aligned} [\beta_{k+1,k-1}] &= [A_{k+1}]\,[\alpha_{k-1}]^{-1} \\ [\beta_{k+1,k}] &= ([A_{k+1,k}] - [\beta_{k+1,k-1}]\,[A_{k-1,k}])\,[\alpha_k]^{-1} \\ [\alpha_{k+1}] &= [A_{k+1,k+1}] - [\beta_{k+1,k-1}]\,[A_{k-1,k+1}] - [\beta_{k+1,k}]\,[\gamma_k] \end{aligned}\right\} \tag{E.5}$$

It is noted that $[\gamma_k]$ arise from the interactions of midside nodes and disappears in the classical method of L-U decomposition for Abrahamson's discretization [74].

The system of linear equations (E.1) now becomes

$$[L]\,[U] = \{F\}$$

which decomposes into two triangular systems

$$[L]\,\{Y\} = \{F\} \tag{E.6}$$

and

$$[U]\,\{X\} = \{Y\} \tag{E.7}$$

which may be solved in turn by forward and backward substitutions by using the relations developed as follows :

For forward substitution, from equation (E.6)

$$\{y_0\} = \{f_0\}$$
$$\{y_1\} = \{f_1\} - [\beta_{10}]\{y_0\} \qquad \text{(E.8)}$$

$$\{y_k\} = \{f_k\} - [\beta_{k,k-1}]\{y_{k-1}\} \qquad \text{(E.9)}$$

for $k = 2,4...n_z-1$ (even integers)

$$\{y_k\} = \{f_k\} - [\beta_{k,k-2}]\{y_{k-2}\} - [\beta_{k,k-1}]\{y_{k-1}\} \qquad \text{(E.10)}$$

for $k = 3,5...n_z$ (odd integers)

For backward substitution, from equation (E.7)

$$\{x_{n_z}\} = [\alpha_{n_z}]^{-1}\{y_{n_z}\}$$
$$\{x_k\} = [\alpha_k]^{-1}(\{y_k\} - [\gamma_k]\{x_{k+1}\}) \qquad \text{(E.11)}$$

for $k = n_z - 1, n_z - 3, \ldots 0$ (even integers)

$$\{x_k\} = [\alpha_k]^{-1}(\{y_k\} - [A_{k,k+1}]\{x_{k+1}\} - [A_{k,k+2}]\{x_{k+2}\}) \qquad \text{(E.12)}$$

for $k = n_z - 2, n_z - 4, \ldots 1$ (odd integers)

where $\{F\} = \begin{Bmatrix} f_0 \\ f_1 \\ \vdots \\ f_{n_z} \end{Bmatrix}$, $\{Y\} = \begin{Bmatrix} y_0 \\ y_1 \\ \vdots \\ y_{n_z} \end{Bmatrix}$, $\{X\} = \begin{Bmatrix} x_0 \\ x_1 \\ \vdots \\ x_{n_z} \end{Bmatrix}$

and the component load vectors $\{f_k\}$, $\{y_k\}$ and $\{x_k\}$ for $k = 0, 1,...n_z$ have the dimensions which are consistent with the sizes of diagonal block matrices $[A_{kk}]$ in the system matrix [C].

E.2 PRACTICAL PROGRAMMING IMPLEMENTATION

In computer implementation the global matrix [C] is so large that programming techniques are employed to reduce the size of the storage required in direct-access memory. In view of solving the problem with a finer grid of elements an efficient packing technique is necessary. For the problem at hand a 5 x 5 element grid requires the storage of

order of more than 65,535 elements for the global system matrix even though only the block submatrices [A] are stored. (See Section 3.2.4(ii))

However, in the process of assembling the global matrix with the present system of numbering in Figure 3.2,only the coefficients corresponding to two adjacent columns of elements are required in direct-memory access at any one time. In terms of the required storage the two columns of finite elements represent two block diagonal submatrices in the global matrix [C]. These two blocks share a common portion arising from the common column of nodes.

For instance, the assembly of nodal values in the first two columns of finite elements will make contributions to coefficients of global matrix [C] in the submatrices $\left[\left(A_{ij}\right)_{\substack{i=1,3\\j=1,3}}\right]$ and $\left[\left(A_{i+2,j+2}\right)_{\substack{i=1,3\\j=1,3}}\right]$, which share the block $[A_{33}]$.

But the process of L-U decomposition of the global matrix and the forward substitution requires access to only one of such submatrices at one time. Consequently the algorithm for solving the system of linear equations by the L-U decomposition method can be envisaged by the flow chart in Figure E.

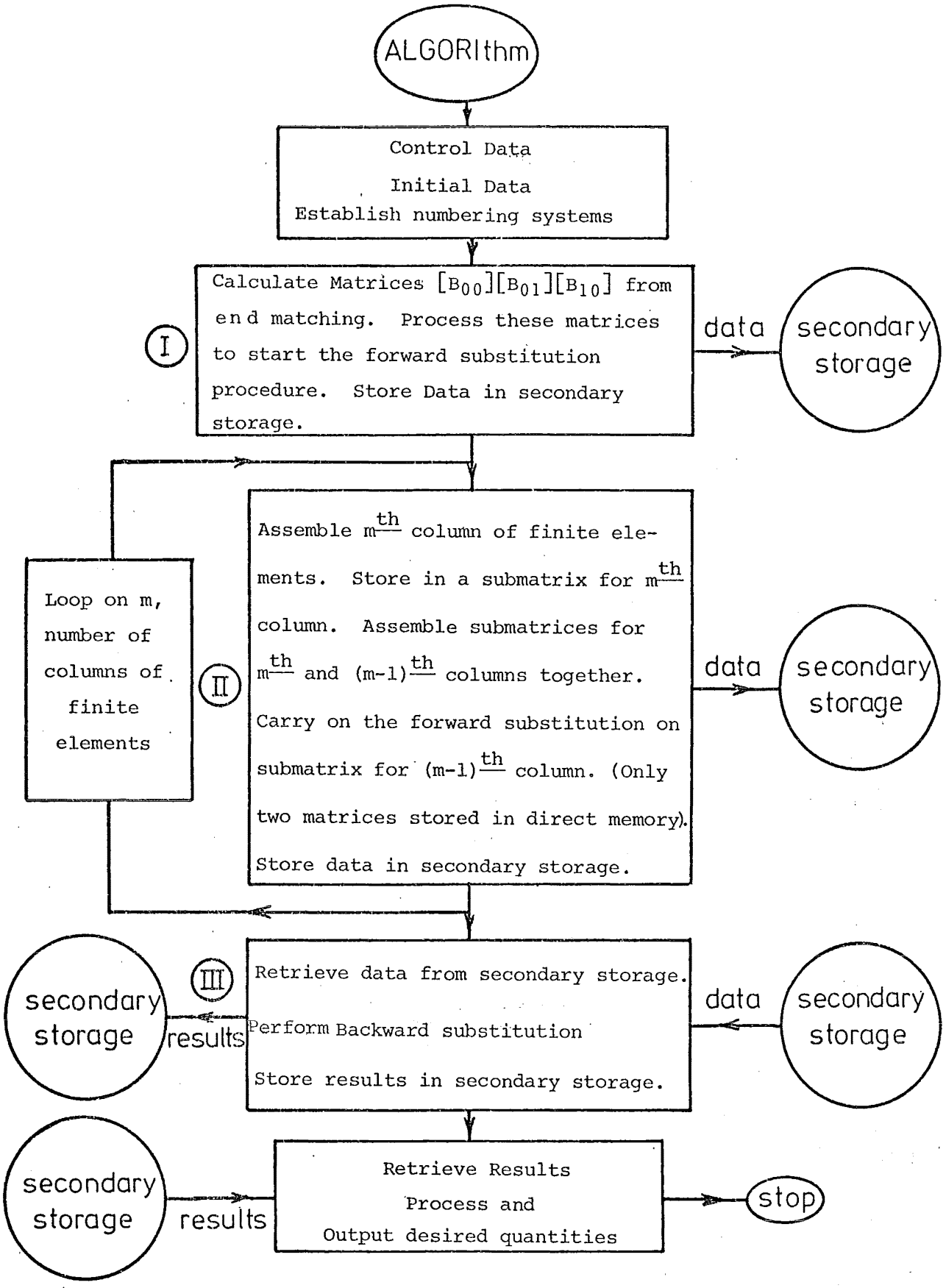

FIG. E FLOW CHART FOR L-U DECOMPOSITION METHOD

The three stages in the flow chart of Figure E: Stage (I): Data for B C, Stage (II): Assembling and forward substitution, Stage (III): Backward substitution may be elaborated in a more detailed form, using relations (E.3) - (E.5) and (E.8) - (E.12)

(I) Compute : $[B_{00}], [B_{10}], [B_{01}], \{f_o\}$

Process : $[\alpha_0]^{-1} = [B_{00}]^{-1}$

$[\gamma_0] = [B_{01}]$

$\{y_0\} = \{f_o\}$

Store : $[\alpha_0]^{-1}$, $[\gamma_0], \{y_0\}$ in that order

on a secondary storage, called FILE 1

Prepare for Stage (II)

$$[\beta_{10}] = [B_{10}]\,[\alpha_0]^{-1}$$

$$\{y_1\} = \{f_1\} - [\beta_{10}]\,\{y_0\}$$

(II) Assemble a column of elements in a matrix [A] storing it in one-dimensional array.

$$[A] = \left[\left(A_{k-1+i,k-1+j} \right)_{\substack{i=1,3 \\ j=1,3}} \right] \text{ is a block matrix}$$

Forward substitution :

Process : $[\alpha_1] = ([A_{11}] - [\beta_{10}]\,[\gamma_0])$

(1*) Invert $[\alpha_k]$ in place to obtain $[\alpha_k]^{-1}$

Store on FILE 1 in the order

$$[\alpha_k]^{-1}, [A_{k,k+1}], [A_{k,k+2}], \{y_k\}$$

Process : $[\beta_{k+1,k}] = [A_{k+1,k}][\alpha_k]^{-1}$

$$[\alpha_{k+1}]^{-1} = ([A_{k+1,k+1}] - [\beta_{k+1,k}][A_{k,k+1}])^{-1}$$

$$[\gamma_{k+1}] = [A_{k+1,k+2}] - [\beta_{k+1,k}][A_{k,k+2}]$$

$$\{y_{k+1}\} = \{f_{k+1}\} - [\beta_{k+1,k}]\{y_k\}$$

Store on FILE 1 in the order

$$[\alpha_{k+1}]^{-1}, [\gamma_{k+1}], \{y_{k+1}\}$$

Prepare for the next cycle

$$[\beta_{k+2,k}] = [A_{k+2,k}]\,[\alpha_k]^{-1}$$

$$[\beta_{k+2,k+1}] = ([A_{k+2,k+1}] - [\beta_{k+2,k}][A_{k,k+1}])[\alpha_{k+1}]^{-1}$$

$$[\alpha_{k+2}] = [A_{k+2,k+2}] - [\beta_{k+1,k}][A_{k,k+2}] - [\beta_{k+2,k+1}][\gamma_{k+1}]$$

$$\{y_{k+2}\} = \{f_{k+2}\} - [\beta_{k+1,k}]\{y_k\} - [\beta_{k+2,k+1}]\{y_{k+1}\}$$

Go back to 1* for the next cycle

($\{f_k\} \equiv 0$ except $\{f_o\}$ and $\{f_{n_z}\}$ due to B C)

$k = 1, 3, 5 \ldots\ldots n_z$

(III) Backward substitution.

Read from FILE 1 : $\alpha_{n_z}^{-1}$, y_{n_z}

Process $x_{n_z} = \alpha_{n_z}^{-1}\ y_{n_z}$

Store x_{n_z} on secondary storage FILE 2

(2*) Read from FILE 1 : α_{k-1}^{-1} , y_{k-1} , x_{k-1}

Process $\alpha_{k-1}^{-1}(y_{k-1} - \gamma_{k-1}\ x_k)$

Store x_{k-1} on FILE 2

Read from FILE 1 : α_{k-2}^{-1} , y_{k-2} , $A_{k-2,k-1}$, $A_{k-2,1}$

(Get out of the loop when k = 1)

Process $x_{k-2} = \alpha_{k-2}^{-1}\ (y_{k-2} - A_{k-2,k-1}x_{k-1} - A_{k-2,k}x_k)$

Store x_{k-2} on FILE 2

Go back to 2* for cycles for $k = n_z, n_z-2, \ldots 3, 1$

E.3 OPTIMUM STORAGE

The submatrix called [A] containing coefficients, involved in the assembly of one column of finite elements is also a sparse matrix. For instance, for the first column of 3 elements the submatrix [A] takes the form in Figure 3.9. For n_{e_1} finite elements across the duct the number of coefficients in the submatrix [A] is $(25\ n^2_{e_1} + 30\ n_{e_1} + 9) \times n^2_v$ and the number of non-zero coefficients is $(55\ n_{e_1} + 9) \times n^2_v$, assuming each $\square$ block of $n_v x n_v$ dimension in Figure 3.9 is fully occupied.

For $n_{e_1} = 5$, and $n_v = 4$ in axisymmetric duct problems, if two full-size matrices [A] are stored in direct-access memory for use in the assembly of two adjacent columns of elements about 16,000 locations become wasted for zero coefficients in the in-core storage. Five finite elements are not a high number to represent the solution across the duct for acoustics problems, especially when one considers extensions of the method to shear flow problems. Consequently in the algorithm extensive book-keeping routines have been developed to store only non-zero coefficients of [A] in one-dimensional array, called a packed matrix and retrieve them for required arithmetic operations.

Inspection of the algorithm of Section E.2 shows that a number of specialized matrix handling routines need to be used for arithmetic operations in the forward substitution stage. These include the following :

- Multiplication of a portion of a packed matrix by a full matrix and superimposing the result over the storage area of the original full matrix.

- Multiplication of a full matrix by a portion of a packed matrix and superimposing the result over the storage area of the original full matrix.

- Addition and subtraction of full matrices and portions of a packed matrix, and superimposing the result on the storage area of the original full matrix.

Once the necessity for these routines is recognized, however, their preparations are trivial.